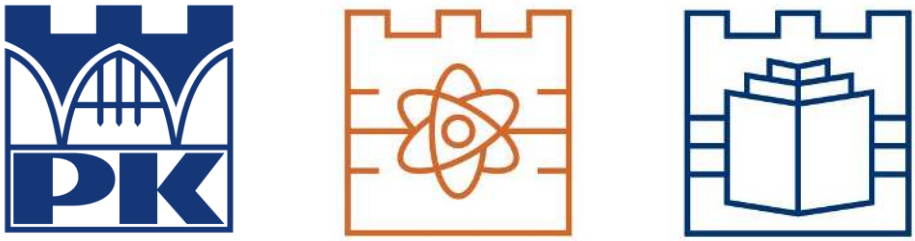

Politechnika Krakowska
im. Tadeusza Kościuszki

Wydział Inżynierii Materiałowej i Fizyki

Katedra Inżynierii Materiałowej

ROZPRAWA DOKTORSKA

Powłoka kompozytowa z kontrolowaną bioaktywnością, do zastosowań medycznych

Mgr inż. Dagmara Słota

Promotor: Prof. dr hab. inż. Agnieszka Sobczak-Kupiec

Kraków 2025

Niniejsza praca powstała w ramach projektu TEAM-NET pt. *Wielofunkcyjne kompozyty aktywne biologicznie do zastosowań w medycynie regeneracyjnej układu kostnego*, realizowanego w ramach konsorcjum, w skład którego wchodzą Politechnika Krakowska im. Tadeusza Kościuszki, Politechnika Wrocławska, Uniwersytet Łódzki oraz Sieć Badawcza Łukasiewicz, finansowanego przez Fundację na Rzecz Nauki Polskiej w ramach Programu Operacyjnego Inteligentny Rozwój (POIR.04.04.00-00-16D7/18).

Pragnę serdecznie podziękować Promotor niniejszej pracy,
Prof. dr hab. inż. Agnieszce Sobczak-Kupiec,
za wprowadzenie mnie w świat nauki i badań, za nieocenione wsparcie na każdym etapie realizacji pracy oraz rozwijania moich zainteresowań naukowych. Dziękuję za nieustający optymizm, cenne wskazówki, merytoryczne uwagi oraz zaangażowanie, które było dla mnie nie tylko wsparciem, ale i inspiracją.

*

Podziękowania za owocną współpracę oraz nieocenioną pomoc w realizacji badań in vitro i in vivo oraz analizie wyników badań biologicznych, kieruję do Zespołu z Uniwersytetu Łódzkiego, pod przewodnictwem dr Karoliny Rudnickiej, prof. UŁ.

*

Szczególne podziękowania kieruję do moich Rodziców za nieustające wsparcie, wiarę w moje możliwości oraz cierpliwość. To dzięki Wam mogłam podążać swoją drogą. Dziękuję, że zawsze mogłam na Was liczyć, niezależnie od okoliczności.

*

Dziękuję także moim Koleżankom z zespołu za wspaniałą atmosferę, życzliwość i nieocenione poczucie humoru, które sprawiało, że nawet najtrudniejsze momenty stawały się łatwiejsze do przetrwania. Wasza obecność i wsparcie były dla mnie niezwykle cenne.

I am among those who think that science has great beauty.

– Maria Skłodowska-Curie

Niniejsza rozprawa doktorska została przygotowana w formie cyklu siedmiu oryginalnych publikacji naukowych powiązanych tematycznie.

SPIS TREŚCI

Załączniki:

ZAŁĄCZNIK 1: Oświadczenia współautorów
ZAŁĄCZNIK 2: Dorobek naukowy i organizacyjny

WYKAZ NAJWAŻNIEJSZYCH OZNACZEŃ I SKRÓTÓW

ALP – fosfataza zasadowa (ang. *alkaline phosphatase*)

ASCs – komórki macierzyste z tkanki tłuszczowej (ang. *adipose-derived stem cells*)

BET – powierzchnia właściwa wyznaczona metodą Brunauera-Emmetta-Tellera (ang. *Brunauer–Emmett–Teller surface area*)

BMP-2 – białko morfogenetyczne kości typu 2 (ang. *bone morphogenetic protein-2*)

CaP/CaPs – fosforany wapnia (ang. *calcium phosphate*)

COL – kolagen (ang. *collagen*)

ECM – macierz zewnątrzkomórkowa (ang. *extracellular matrix*)

EDS – spektroskopia energii promieniowania rentgenowskiego (ang. *energy-dispersive X-ray spectroscopy*)

ESB – Europejskie Towarzystwo Biomateriałów (ang. *European Society for Biomaterials*)

FBS – surowica płodowa bydlęca (ang. *fetal bovine serum*)

FGF – czynnik wzrostu fibroblastów (ang. *fibroblast growth factor*)

FDA – Agencja Żywności i Leków (USA) (ang. *Food and Drug Administration*)

FTIR/FT-IR – spektroskopia w podczerwieni z transformacją Fouriera (ang. *Fourier-transform infrared spectroscopy*)

GSH – glutation (ang. *glutathione*)

HAp – hydroksyapatyt (ang. *hydroxyapatite*)

HPLC – wysokosprawna chromatografia cieczowa (ang. *high-performance liquid chromatography*)

IL-1β – interleukina 1β (ang. *interleukin-1β*)

IL-10 – interleukina 10 (ang. *interleukin-10*)

IPN – przenikająca się sieć polimerowa (ang. *interpenetrating polymer network*)

MIC_{99} – minimalne stężenie hamujące powodujące > 99% zahamowania wzrostu bakterii względem kontroli (ang. *minimum inhibitory concentration at 99% inhibition*)

MSC – mezenchymalne komórki macierzyste (ang. *mesenchymal stem cells*)

MTT – bromek 3-(4,5-dimetylotiazol-2-yl)2,5-difenylotetrazoliowy (ang. *3-(4,5dimethylthiazol-2-yl) - 2,5-diphenyltetrazolium bromide*)

NIH – Narodowe Instytuty Zdrowia (ang. *National Institutes of Health*)

NTC – nietraktowana kontrola (ang. *non-treated control*)

CoF – współczynnik tarcia (ang. *the coefficient of friction*)

PBS – sól fizjologiczna buforowana fosforanem (ang. *phosphate-buffered saline*)

PCL – poli(ε-kaprolakton) (ang. *polycaprolactone*)

PDGF – płytkopochodny czynnik wzrostu (ang. *platelet-derived growth factor*)

PEG – poli(glikol etylenowy) (ang. *polyethylene glycol*)

PEGDA – diakrylan poli(glikolu etylenowego) (ang. *polyethylene glycol diacrylate*)

PHB – poli-β-hydroksymaślan (ang. *poly-β-hydroxybutyrate*)

PLA – poli(kwas mlekowy) (ang. *polylactic acid*)

PVP – poliwinylopirolidon (ang. *polyvinylpyrrolidone*)

Ra – arytmetycza średnia chropowatości (ang. *arithmetic average roughness*)

ROS – reaktywne formy tlenu (ang. *reactive oxygen species*)

Rsk – współczynnik skośności profilu (ang. *skewness of the roughness profile*)

RUNX2 – czynnik transkrypcyjny Runt-related 2 (ang. *Runt-related transcription factor 2*)

SBF – sztuczny płyn ustrojowy (ang. *simulated body fluid*)

S_e – pęcznienie równowagowe (ang. *swelling equilibrium*)

SEM – skaningowa mikroskopia elektronowa (ang. *scanning electron microscopy*)

SSA – powierzchnia właściwa (ang. *specific surface area*)

TC – kontrola traktowana (ang. *treated control*)

TCP – fosforan(V) wapnia (ang. *tricalcium phosphate*)

TGF-β – transformujący czynnik wzrostu β (ang. *transforming growth factor β*)

TNF-α – czynnik martwicy nowotworów α (ang. *tumor necrosis factor α*)

WHO – Światowa Organizacja Zdrowia (ang. *World Health Organization*)

VEGF – czynnik wzrostu śródbłonka naczyniowego (ang. *vascular endothelial growth factor*)

XRD – dyfraktometria rentgenowska (ang. *X-ray diffraction*)

STRESZCZENIE

Celem niniejszej rozprawy doktorskiej było opracowanie oraz kompleksowa charakterystyka wielofunkcyjnych, kompozytowych powłok, przeznaczonych do modyfikacji powierzchni biomateriałów i implantów o niskiej bioaktywności. Postawiono tezę, że hybrydowa powłoka łącząca fazę polimerową (PVP:PEG z kolagenem) z fazą ceramiczną (HAp) oraz modyfikowana substancjami aktywnymi (klindamycyna, VEGF-165, TGF-β1) może równocześnie wspierać regenerację tkanki kostnej, ograniczać ryzyko infekcji i kształtować sprzyjające mikrośrodowisko gojenia.

W pierwszym etapie otrzymano fosforany wapnia metodą mokrego strącenia, które charakteryzowały się zróżnicowanym stosunkiem molowym Ca/P (HAp, TCP, bruszyt). Analizy XRD/FTIR/SEM+EDS potwierdziły czystość fazową i kontrolowaną morfologię. Proszki zmodyfikowano klindamycyną, której profil uwalniania był zależny od stosunku molowego Ca/P i powierzchni właściwej. Wszystkie nośniki wykazały aktywność przeciwdrobnoustrojową wobec *Staphylococcus aureus*, przy najniższym MIC_{99} dla bruszytu. Następnie opracowano kompozycję powłoki ceramiczno-polimerowej oraz dwustopniowy proces jej nakładania na podłoża (PLA, PLLA/HAp). Zaobserwowano, że zwiększenie udziału HAp podnosiło chropowatość i energię powierzchni, sprzyjając potencjalnym interakcjom komórkowym, jednak przy 15% HAp nasilało się zużycie tribologiczne. Kolagen zwiększał zdolności sorpcyjne i obniżał współczynnik tarcia. Optymalnym kompromisem właściwości mechanicznych, sorpcyjnych i tribologicznych okazała się powłoka zawierająca 5% HAp. Badania inkubacyjne w symulowanych płynach biologicznych wykazały stabilność chemiczną materiałów oraz zdolność indukowania wzrostu nowych warstw apatytowych już przy 5% HAp. Powłoki poddano modyfikacji klindamycyną, której uwalnianie zachodziło szybciej z materiałów polimerowych niż kompozytowych. Materiały z lekiem skutecznie hamowały proces tworzenia się biofilmu *Staphylococcus aureus*. Wytypowany wariant powłoki kompozytowej z 5% udziałem fazy ceramicznej poddano funkcjonalizacji przez dodatek czynników wzrostu VEGF-165 i TGF-β1, które wykazały dwufazowe, dyfuzyjnie kontrolowane uwalnianie zgodność z modelem Higuchiego. Ocena bezpieczeństwa i aktywności biologicznej obejmowała badania *in vitro* względem L929 i hFOB 1.19 oraz dwuetapowe modele *in vivo* w tym implantację podskórną oraz w defekcie czaszki. Nie stwierdzono reakcji zapalnej, poziomy cytokin prozapalnych IL-1β i TNF-α były porównywalne z kontrolą, a poziom przeciwzapalnego IL-10 był podwyższony. Analizy histologiczne i obserwacje fluorescencyjne wykazały inicjację mineralizacji w miejscach kontaktu implantu z kością, odnotowano również wzrost markera kostnienia OPN w grupach z czynnikami wzrostu i antybiotykiem.

Uzyskane wyniki potwierdzają, że zaprojektowane powłoki kompozytowe łączą bioaktywność z właściwościami przeciwdrobnoustrojowymi, oraz stymulują mineralizację nowej tkanki kostnej. Szczególnie obiecująca jest powłoka kompozytowa zawierająca 5% HAp, modyfikowana klindamycyną oraz VEGF-165 i TGF-β1. Rozwiązanie to stanowi wielofunkcyjny system dostarczania substancji aktywnych, który może zostać wykorzystany do powlekania implantów o niskiej bioaktywności, celem zapewnienia dodatkowych funkcji. Zaprezentowane wyniki potwierdzając zasadność prowadzonych badań i stanowią podstawę do dalszego rozwoju w kierunku potencjalnych zastosowań klinicznych.

ABSTRACT

The aim of this doctoral dissertation was the development and comprehensive characterization of multifunctional composite coatings intended for surface modification of biomaterials and implants with low bioactivity. It was hypothesized that a hybrid coating combining a polymer phase (PVP:PEG with collagen) with a ceramic phase (HAp) and modified with active substances (clindamycin, VEGF-165, TGF-β1) could simultaneously support bone tissue regeneration, reduce the risk of infection, and promote a favorable healing microenvironment.

In the first stage, calcium phosphates with different molar Ca/P ratios (HAp, TCP, brushite) were synthesized using the wet precipitation method. XRD/FTIR/SEM+EDS analyses confirmed phase purity and controlled morphology. The powders were modified with clindamycin, and the drug release profile was found to depend on the Ca/P molar ratio and the specific surface area. All carriers exhibited antimicrobial activity against *Staphylococcus aureus*, with the lowest MIC_{99} observed for brushite. Subsequently, a composition of a ceramic-polymer coating and a two-step deposition process on substrates (PLA, PLLA/HAp) were developed. It was observed that an increased HAp content enhanced surface roughness and surface energy, potentially promoting cell interactions; however, at 15% HAp, tribological wear intensified. Collagen increased the sorption capacity and reduced the coefficient of friction. The optimal compromise of mechanical, sorption, and tribological properties was found in the coating containing 5% HAp. Incubation studies in simulated biological fluids demonstrated chemical stability of the materials and the ability to induce the growth of new apatite layers already at 5% HAp content. The coatings were modified with clindamycin, which was released more rapidly from polymeric than composite materials. Drug-loaded materials effectively inhibited the formation of *Staphylococcus aureus* biofilm. The selected composite coating variant with 5% ceramic phase content was further functionalized with the growth factors VEGF-165 and TGF-β1, which exhibited biphasic, diffusion-controlled release, consistent with the Higuchi model. The safety and biological activity assessment included *in vitro* studies using L929 and hFOB 1.19 cell lines, as well as two-stage *in vivo* models including subcutaneous implantation and a cranial defect model. No inflammatory response was observed, the levels of pro-inflammatory cytokines IL-1β and TNF-α were comparable to control, while the level of anti-inflammatory IL-10 was elevated. Histological and fluorescence analyses confirmed the initiation of mineralization at the implant–bone interface, and increased expression of the bone formation marker OPN was noted in groups with growth factors and antibiotic.

The obtained results confirm that the designed composite coatings combine bioactivity with antimicrobial properties and stimulate the mineralization of new bone tissue. Particularly promising is the composite coating containing 5% HAp, modified with clindamycin and VEGF-165 and TGF-β1. This solution constitutes a multifunctional drug delivery system that can be used to coat implants with low bioactivity to provide additional functionalities. The presented results confirm the relevance of the conducted research and form the basis for further development towards potential clinical applications.

WYKAZ PUBLIKACJI BĘDĄCYCH PODSTAWĄ ROZPRAWY DOKTORSKIEJ

Prace przeglądowe:

P1: Dagmara Słota*, Karina Piętak, Josef Jampilek, Agnieszka Sobczak-Kupiec. *Polymeric and Composite Carriers of Protein and Non-Protein Biomolecules for Application in Bone Tissue Engineering*. Materials, 2023, 16(6), 2235. DOI: 10.3390/ma16062235.
Punkty MNiSW: 140; IF_{2023}: 3,4.

P2: Dagmara Słota*, Josef Jampilek, Agnieszka Sobczak-Kupiec. *Targeted Clindamycin Delivery Systems: Promising Options for Preventing and Treating Bacterial Infections Using Biomaterials.* International Journal of Molecular Sciences, 2024, 25(8), 4386. DOI: 10.3390/ijms25084386. Punkty MNiSW: 140; IF_{2024}: 5,6.

Prace oryginalne:

P3: Dagmara Słota*, Karina Piętak, Wioletta Florkiewicz, Josef Jampilek, Agnieszka Tomala, Mateusz M. Urbaniak, Agata Tomaszewska, Karolina Rudnicka, Agnieszka Sobczak-Kupiec. *Clindamycin-Loaded Nanosized Calcium Phosphates Powders as a Carrier of Active Substances.* Nanomaterials, 2023, 13(9), 1469. DOI: 10.3390/nano13091469.
Punkty MNiSW: 100; IF_{2023}: 4,7.

P4: Agnieszka Tomala*, **Dagmara Słota**, Wioletta Florkiewicz, Karina Piętak, Mateusz Dyląg, Agnieszka Sobczak-Kupiec. *Tribological Properties and Physiochemical Analysis of Polymer-Ceramic Composite Coatings for Bone Regeneration*. Lubricants, 2022, 10(4), 58. DOI: 10.3390/lubricants10040058. Punkty MNiSW: 70; IF_{2022}: 3,1.

P5: Dagmara Słota*, Josef Jampilek, Agnieszka Sobczak-Kupiec. *Hybrid Coatings Based on Polyvinylpyrrolidone/Polyethylene Glycol Enriched with Collagen and Hydroxyapatite: Incubation Studies and Evaluation of Mechanical and Physiochemical Properties*. Journal of Functional Biomaterials, 2024, 15(3), 62. DOI: 10.3390/jfb15030062. Punkty MNiSW: 100; IF_{2024}: 5,5.

P6: Dagmara Słota*, Mateusz M. Urbaniak, Agata Tomaszewska, Karina Niziołek, Marcin Włodarczyk, Wioletta Florkiewicz, Aleksandra Szwed-Georgiou, Agnieszka Krupa, Agnieszka Sobczak-Kupiec. *Crosslinked hybrid polymer/ceramic composite coatings for the controlled release of clindamycin*. Biomaterials Science, 2024, 12, 5253-5265. DOI: 10.1039/D4BM00055B. Punkty MNiSW: 140; IF_{2024}: 5,7.

P7: Dagmara Słota*, Aleksandra Szwed-Georgiou, Marcin Włodarczyk, Agnieszka Krupa, Karolina Rudnicka, Karina Niziołek, Bartłomiej Kryszak, Konrad Szustakiewicz, Agnieszka Sobczak-Kupiec. *Bioactive Coating with Clindamycin, VEGF-165, and TGF-β1 for Supporting Bone Tissue Regeneration*. Biomaterials Science, 2025,, DOI: 10.1039/D5BM00637F. Punkty MNiSW: 140; IF_{2025}: 5,7.

*autor korespondencyjny

Sumaryczny IF: 33,7

Sumaryczny MNiSW: 830

1. Biomateriały

Jedną z kluczowych grup materiałów stosowanych we współczesnej medycynie oraz inżynierii tkankowej są biomateriały. Zgodnie z definicją amerykańskiego National Institutes of Health (NIH) z 1982 roku, *biomateriał to dowolna substancja (z wyjątkiem leku) lub ich kombinacja, pochodzenia syntetycznego lub naturalnego, która może być stosowana przez dowolny czas, w całości lub jako część systemu, który leczy, wspomaga lub zastępuje dowolną tkankę, narząd lub funkcję organizmu* [1]. W oparciu o tę definicję, w 1986 roku European Society for Biomaterials (ESB) przedstawiło swoją wersję, zgodnie z którą jest to *materiał przeznaczony do kontaktu z systemami biologicznymi w celu oceny, leczenia, wspomagania lub zastąpienia jakiejkolwiek tkanki, narządu lub funkcji organizmu* [2]. W 1992 roku, definicja zaproponowana przez ESB została przyjęta przez Międzynarodową Organizację Normalizacyjną i stała się podstawą dla stworzenia normy ISO 10993-1, która w aktualnej formie funkcjonuje do dziś w wersji ISO 10993-1:2018 i jest podstawą dla badań i rozwoju biomateriałów [3]. Zgodnie z nią, określa się biokompatybilność, czyli główne wymaganie stawiane biomateriałom. Biokompatybilność, gwarantuje zdolność materiału do działania przy odpowiedniej reakcji gospodarza, w określonej sytuacji, bez wywoływania niepożądanych skutków lokalnych lub ogólnoustrojowych u odbiorcy. Biokompatybilne materiały muszą charakteryzować się brakiem toksyczności, nie mogą powodować zakrzepicy czy reakcji alergicznych, jak również nie powinny być kancerogenne ani mutagenne [4,5]

Z uwagi na rodzaje wiązań występujących między atomami, materiały inżynierskie klasyfikuje się na metale, polimery oraz ceramikę. W tych pierwszych, dominują wiązania metaliczne. Z uwagi na obecność elektronów swobodnych metale przewodzą ciepło i prąd elektryczny oraz charakteryzują się łatwą obróbką mechaniczną z uwagi na plastyczność. Polimery posiadają długie łańcuchy węglowe połączone wiązaniami kowalencyjnymi, ale ich właściwości kształtują także oddziaływania międzyłańcuchowe oraz gęstość usieciowania. Z kolei w ceramice występują wiązania jonowe i/lub kowalencyjne. Nie posiadają one żadnych wolnych elektronów, w związku z czym ceramika jest materiałem nieprzewodzącym zarówno prądu elektrycznego jak i ciepła [6,7]. Połączenie co najmniej dwóch, lub więcej materiałów, powoduje powstanie nowej klasy materiałów, zwanej kompozytami [8].

1.1. Rynek biomateriałów

W 2024 roku wartość rynku biomateriałów oszacowano na 69,43 miliarda USD i oczekuje się, że do 2035 roku wartość ta wzrośnie do kwoty 130,5 miliardów USD, przy założonym skumulowanym rocznym wskaźniku wzrostu (CAGR) na poziomie 5,9 % (Rysunek 1a). Głównymi czynnikami wpływającymi na rozwój rynku biomateriałowego jest wzrost liczby chorób przewlekłych, rosnące zainteresowanie

nowymi technologiami medycznymi, w tym medycyną regeneracyjną czy inżynierią tkankową oraz starzejącą się populacją [9]. Według Światowej Organizacji Zdrowia (WHO), w 2030 roku liczba osób powyżej 60 roku życia ma wynieść 1,4 miliarda, co stanowi wzrost o 40 % w porównaniu z rokiem 2020 [10].

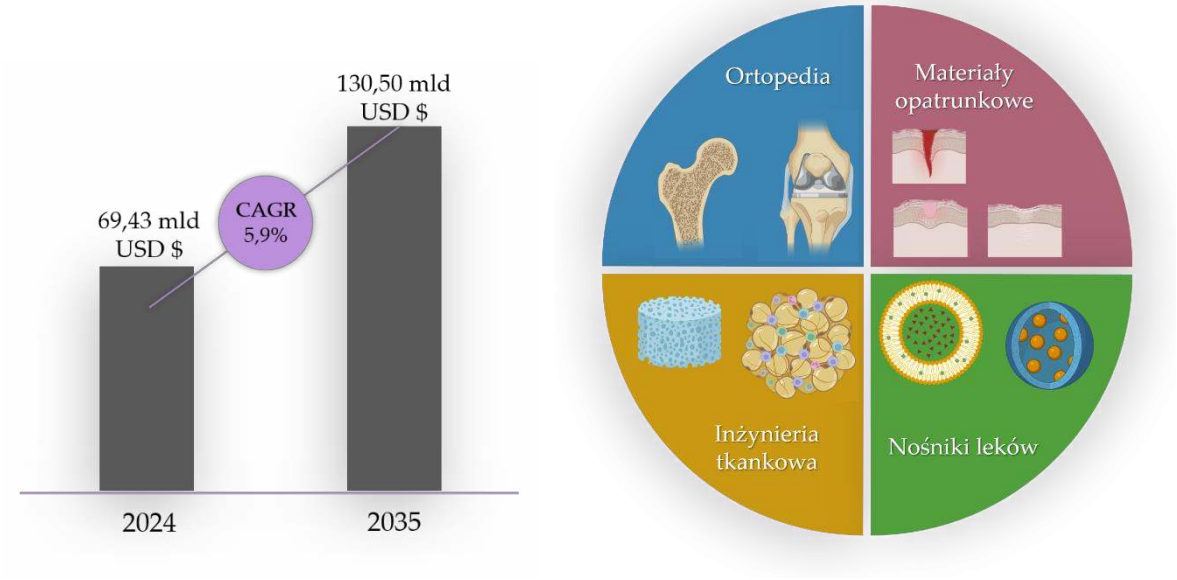

(a) (b)

Rysunek 1: (a) Prognozowany wzrost wartości rynku biomateriałów w latach 2024–2035; (b) Segmentacja rynku biomateriałów według zastosowań.

Rynek biomateriałów obejmuje szeroki zakres zastosowań medycznych i technologicznych, co znajduje odzwierciedlenie w jego podziale na liczne segmenty aplikacyjne. Główne obszary napędzające jego rozwój zaprezentowano na Rysunku 1b. Są to inżynieria tkankowa i nowe rozwiązania zaprojektowane do naprawy złożonych tkanek, ortopedia w szczególności biomateriały do wymiany stawów i naprawy złamań, systemy dostarczania leków umożliwiające terapie celowane oraz materiały opatrunkowe ułatwiające gojenie [9,11].

1.2. Biomateriały ceramiczne

W inżynierii tkanki kostnej ważne miejsce zajmują biomateriały ceramiczne, szczególnie fosforany wapnia (CaP). Składają się one z kationów wapnia oraz anionów fosforanowych. CaP są w większości słabo rozpuszczalnymi w wodzie solami trójzasadowego kwasu ortofosforowego H_3PO_4 [12]. W aplikacjach biomateriałowych najczęściej wykorzystywany jest hydroksyapatyt (HAp) o wzorze $Ca_{10}(PO_4)_6(OH)_2$ lub ortofosforan (V) wapnia (TCP) o wzorze $Ca_3(PO_4)_2$ [13]. HAp charakteryzuje się biokompatybilnością oraz bioaktywnością, wynikającą ze zdolności do stymulowania procesów osteokondukcji oraz osteointegracji [14,15]. Materiały ceramiczne wykazują niską odporność na zużycie i pękanie, a także słabą wytrzymałość na rozciąganie [16,17].

Syntetyczny HAp może być otrzymywany m.in. metodami mokrymi, suchymi, topnieniowymi czy zol-żel [18,19]. Znana jest również metoda mechanochemiczna, jednak nie znalazła ona szerokiego zastosowania [20]. Naturalnym źródłem HAp są kości zwierzęce czy koralowce [21,22]. W poniższej pracy doktorskiej do syntezy proszku HAp wykorzystano metodę mokrego strącenia zachodzącą w temperaturze wrzenia substratów zgodnie z reakcją (1).

$$6Na_2HPO_4 + 10(CH_3COO_2)Ca + 2H_2O \rightarrow Ca_{10}(PO_4)_6(OH)_2 + 8CH_3COOH + 12CH_3COONa \qquad (1)$$

HAp stanowi fazę mineralną naturalnej tkanki kostnej, a wielkość jego kryształów w kościach jest zależna od wieku. U dorosłych średnia wielkość krystalitów to około 18,1 nm, a u noworodków 8,9 nm [23]. Kształt ziaren HAp zależy od metody syntezy oraz od jego stechiometrii, i dla stechiometrycznego HAp, ze stosunkiem molowym Ca/P = 1,67 obserwuje się najczęściej kryształy igłowe lub słupkowe, podczas gdy dla HAp niestechiometrycznego, u którego stosunek molowy Ca/P jest w zakresie 1,5-1,9 na skutek np. obecności wody, deficytu jonów Ca^{2+} lub podstawień jonów zastępczych jak Mg^{2+} lub CO_3^{2-}, kształt może się różnić i przybierać formę blaszek, kłaczków czy ziaren [24–28]. Możliwość podstawień jonowych, wynika ze specyficznej budowy krystalicznej HAp, przedstawionej na Rysunku 2 [29].

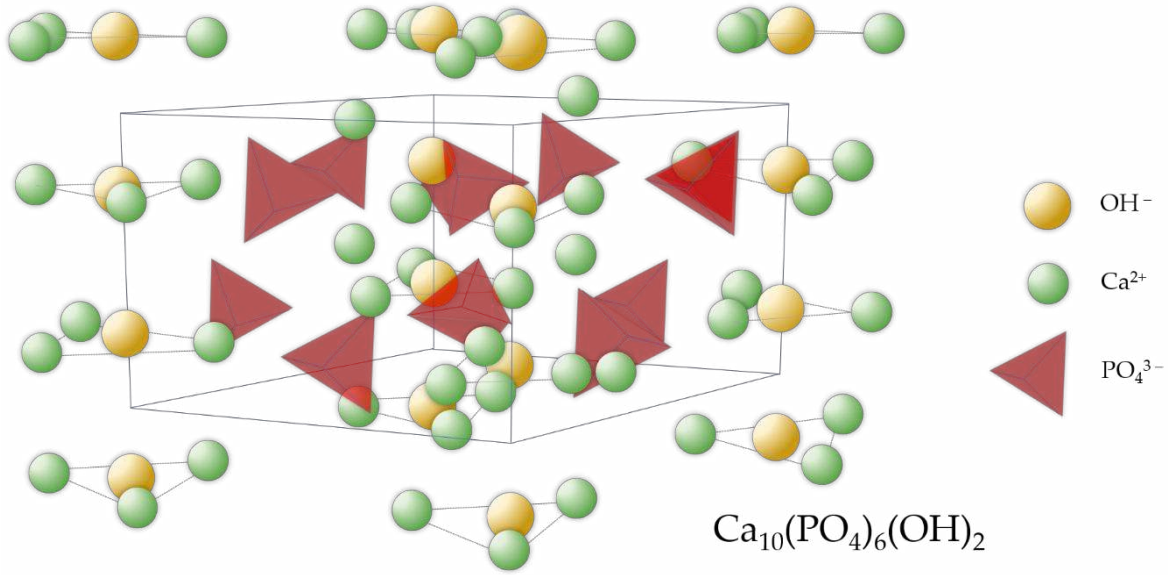

Rysunek 2: Struktura krystaliczna hydroksyapatytu $Ca_{10}(PO_4)_6(OH)_2$ w układzie heksagonalnym ($P6_3/m$). Widoczne rozmieszczenie jonów Ca^{2+}, PO_4^{3-} oraz grup OH^- w obrębie komórki elementarnej.

HAp krystalizuje w układzie heksagonalnym ($P6_3/M$), w którym jony Ca^{2+} mogą zajmować dwie różne pozycje krystalograficzne, Ca(I) tworzące kolumny wzdłuż osi c, oraz Ca(II) zlokalizowane w pobliżu kanałów anionowych OH^-. Aniony PO_4^{3-} tworzą szkielet struktury, występując w postaci tetraedrów. Taka struktura sprzyja podstawieniom jonowym zarówno w pozycjach kationowych jak i anionowych, co pozwala na modyfikację właściwości fizykochemicznych czy biologicznych HAp [30]. Z uwagi na podobieństwo strukturalne

do fazy nieorganicznej naturalnej tkanki kostnej, HAp znajduje szerokie zastosowanie w medycynie i stomatologii. W inżynierii tkanki kostnej istotną rolę odgrywa również TCP, jednak to co odróżnia go od HAp to bardziej resorbowalny charakter w środowisku fizjologicznym co sprzyja zastępowaniu go przez nową tkankę. Jednakże, wykazuje również mniejszą stabilność termodynamiczną i w praktyce często ulega przemianie do HAp [31,32]. Przemiana zachodzi zgodnie z równaniem (2).

$$3Ca_3(PO_4)_2 + Ca^{2+} + 2OH^- \rightarrow Ca_{10}(PO_4)_6(OH)_2 \qquad (2)$$

Zjawisko to, może być pożądane w niektórych aplikacjach medycznych, ponieważ bardziej resorbowalny TCP będąc fazą przejściową, może stymulować odbudowę tkanki, a następnie bardziej stabilny HAp zapewni trwałe rusztowanie oraz długotrwałą osteointegrację.

1.3. Biomateriały polimerowe

Pod pojęciem polimery, rozumie się substancje chemiczne o dużej masie cząsteczkowej, złożone z wielokrotnie powtarzających się jednostek zwanych merami [33]. Polimery wykorzystywane do projektowania biomateriałów można podzielić na dwie główne kategorie: naturalne (biopolimery) i syntetyczne [34]. Ich możliwość wykorzystania w charakterze biomateriału jest warunkowana przez spełnienie cechy biokompatybilności. Tym charakteryzują się w szczególności biopolimery, które ponadto wykazują niską immunogenność. Zaliczane są do nich polisacharydy, fibryna, keratyna, kwasy nukleinowe czy białka, w tym kolagen (COL), będący składnikiem powłoki opracowanej w ramach niniejszej rozprawy doktorskiej [35]. Struktura oraz budowa łańcuchów polimerowych umożliwia ich stosunkowo łatwą modyfikację związkami aktywnymi [36].

Pomimo zalet, stosowanie biopolimerów jako samodzielnych materiałów obarczone jest określonymi ograniczeniami funkcjonalnymi. Przede wszystkim charakteryzują się stosunkowo szybką degradacją jak również niskimi właściwościami mechanicznymi i ryzykiem zanieczyszczenia przez mikroorganizmy (bakterie, grzyby). Bezpiecznym zamiennikiem biopolimerów, są biokompatybilne polimery syntetyczne, które otrzymywane w kontrolowanych warunkach charakteryzują się powtarzalnością. Są też mniej immunogenne i cechują się lepszymi właściwościami mechanicznym [37,38].

COL stanowi około 30 % wszystkich białek występujących w organizmach kręgowców i jest kluczowym składnikiem macierzy zewnątrzkomórkowej. Największe jego ilości obecne są w skórze, kościach, więzadłach czy ścięgnach [39,40]. W inżynierii biomedycznej, COL jest stosowany jako składnik systemów dostarczania leków czy biomateriałów opatrunkowych. Jest również elementem wielu biokompozytów projektowanych do zastosowań w inżynierii tkanki kostnej.

Aplikacja COL w biomateriałach jest związana nie tylko z możliwością tworzenia biomimetyczych rozwiązań, zbliżonych do naturalnych tkanek [41,42]. Ten biopolimer wykazuje wiele cech bioaktywnych, które wpływają na regenerację. Wspomaga adhezję, migrację, proliferację oraz różnicowanie komórek, w tym komórek mezenchymalnych czy osteoblastów [43,44]. Ponadto wykazano, że ma zdolność promowania angiogenezy, zmniejszania stanów zapalnych oraz gojenia ran skóry [45].

Jednym z polimerów syntetycznych szeroko stosowanych w inżynierii materiałowej do projektowania rozwiązań jest poli(glikol etylenowy) (PEG), który cechuje się wysoką biokompatybilnością. Amerykańska Agencja ds. Żywności i Leków (FDA) uznała PEG jako bezpieczny komponent do stosowania w wyrobach medycznych [46]. Polimer ten został wykorzystany w niniejszej pracy w charakterze składnika matrycy polimerowej. W przemyśle, jest on szeroko stosowany w branży kosmetycznej oraz farmaceutycznej jako emulgator, środek utrzymujący wilgoć czy środek smarny [47]. Istotną cechą PEG kontekście zastosowań w charakterze powłok biomedycznych, jest jego zdolność do odpychania komórek bakteryjnych, najprawdopodobniej z uwagi na siły elektrostatyczne, jednak mechanizm ten nie jest jeszcze w pełni wyjaśniony [48]. Ponadto, udowodniono również, że PEG wykazuje działanie ochronne na białka cytoszkieletu aksonalnego, stanowiące wewnętrzne rusztowanie niezbędne do utrzymania struktury i funkcji neuronów [49]. Innym syntetycznym polimerem, wykorzystywanym do projektowania biomateriałów jest poliwinylopirolidon (PVP). Podobnie jak PEG, został uznany przez FDA za materiał bezpieczny w kontakcie z organizmami [50]. Pomimo swojej hydrofilowości, charakteryzuje się dobrą rozpuszczalnością w rozpuszczalnikach o różnej polarności [51]. Z tego powodu jest szeroko stosowany w przemyśle żywnościowym oraz kosmetycznym jako substancja wiążąca lub stabilizująca zawiesiny i emulsje [52,53]. Wiele doniesień literaturowych podkreśla jego potencjał wykorzystania w charakterze materiału opatrunkowego, szczególnie z uwagi na jego duże zdolności sorpcyjne [54].

1.4. Kompozyty

Ze względu na ograniczenia aplikacyjne zarówno materiałów ceramicznych, jak i polimerowych, w inżynierii tkanki kostnej istotne znaczenie zyskują materiały kompozytowe. Kompozyty, definiuje się jako układy składające się z co najmniej dwóch faz, które pozostają rozdzielone w skali makro- lub mikroskopowej, ale ich połączenie prowadzi do uzyskania materiału o innych właściwościach [55]. Ceramika wykazuje wysoką wytrzymałość na ściskanie i wysoki moduł Younga, przy jednocześnie niskiej odporności na pękanie. Z kolei faza polimerowa zapewnia elastyczność oraz podatność na modyfikacje chemiczne, co umożliwia otrzymanie materiałów nie tylko biomimetycznych, ale również funkcjonalnych [56,57].

Kość jest naturalnym kompozytem ceramiczno-polimerowym charakteryzującym się anizotropią. Faza mineralna, składa z CaP, w tym głównie z HAp, i stanowi około 65 – 70 % kości. Woda stanowi ok. 5 – 8 %, a pozostała część to faza organiczna, głównie w postaci kolagenu, który nadaje kościom elastyczność. Architektura kości jest zorganizowana w złożoną strukturę hierarchiczną, zaprezentowaną na Rysunku 3. Taka organizacja układu pozwala na połączenie dobrych właściwości mechanicznych z funkcjami biologicznymi [58,59].

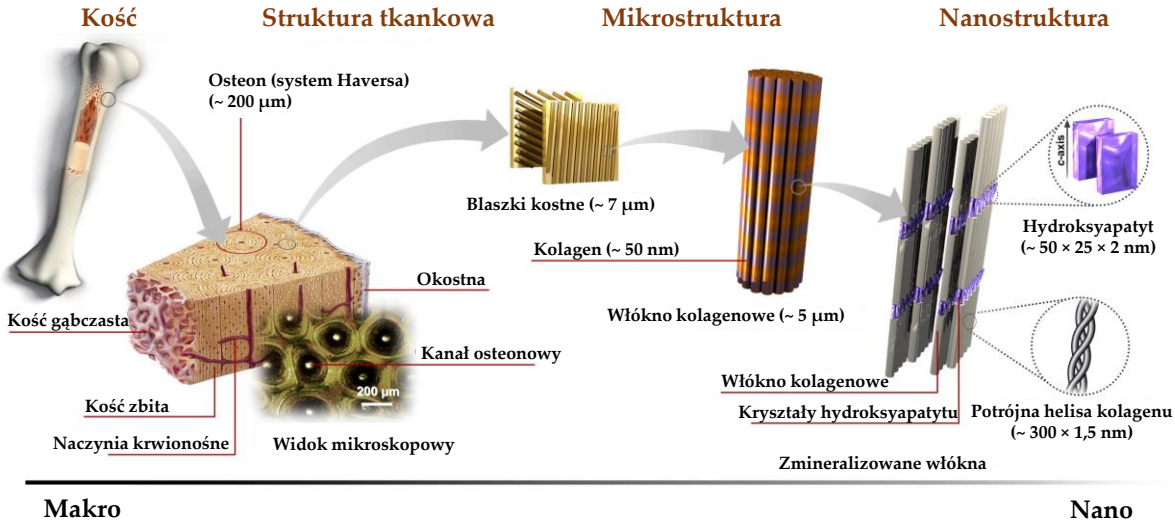

Rysunek 3: Schemat hierarchicznej organizacji strukturalnej kości [58].

Wyróżnia się kilka typów materiałów kompozytowych. Podstawowa klasyfikacja obejmuje materiały kompozytowe pochodzenia naturalnego, jak wspomniana wcześniej kość czy np. drewno, oraz syntetycznego [60]. Ponadto, klasyfikacji można dokonać również w zależności od rodzaju osnowy (ceramiczna, polimerowa, metaliczna) oraz formy fazy wzmacniającej, która może występować w postaci włókien, ziaren lub warstw [61,62]. W zależności od wybranego układu, różne typy kompozytów charakteryzować się będą odmiennymi właściwościami biologicznymi i mechanicznymi. Umożliwia to dostosowanie ich cech, do wymagań aplikacyjnych.

W przypadku tkanki kostnej i projektowanych dla niej kompozytów, doniesienia literaturowe wskazują głównie na zastosowanie polimeru jako osnowy i zawieszonej w niej fazy ceramicznej. Takie układy, w zależności od ostatecznego składu, mogą charakteryzować się biomimetyzmem i być podobne do naturalnej tkanki. Spośród biopolimerów, najczęściej w tym celu wykorzystuje się COL, chitozan, alginian sodu, kwas hialuronowy czy poli-β-hydroksymaślan (PHB). Każdy z nich jest biokompatybilny oraz wykazuje duże prawdopodobieństwo do macierzy zewnątrzkomórkowej (ECM). W praktyce wytwarza się z nich najczęściej hydrożele, rusztowania do hodowli komórkowych, powłoki czy biotusze do biodrukowania. Z kolei najczęściej wykorzystywanymi polimerami syntetycznymi są poli(kwas mlekowy) (PLA) oraz poli(ε-kaprolakton) (PCL). Z uwagi na właściwości

mechaniczne tych polimerów, kompozyty na ich bazie najczęściej otrzymywane są za pomocą technik odlewania lub druku 3D i charakteryzują się większą wytrzymałością mechaniczną niż kompozyty na bazie biopolimerów [63,64]. Opisano liczne przykłady tego typu kompozytów. W przypadku COL połączonego z HAp, wykorzystując proces liofilizacji uzyskano rusztowanie o wysokiej porowatości, sprzyjające adhezji, proliferacji oraz różnicowaniu pierwotnych komórek izolowanych z miazgi zęba [65]. W przypadku innych, porowatych rusztowań, na bazie alginianu sodu i bioszkła zaobserwowano zwiększoną proliferację ludzkich komórek osteoblastycznych MG-63 [66]. Inne podejście zaproponowano w przypadku połączenia HAp z kwasem hialuronowym, gdzie opracowano wstrzykiwalne, samonaprawiające się hydrożele. Jest to obiecujące rozwiązanie, które w krótkim czasie pozwala wypełnić ubytek tkanki, a przy tym sprzyja adhezji i proliferacji komórek [67].

Jednak wymienione porowate rusztowania czy wstrzykiwalne materiały, przeznaczone są głównie do mniejszych ubytków tkanki lub do hodowli komórkowych. Ich zaletą jest możliwość modyfikacji fazy polimerowej substancjami aktywnymi, a tym samym projektowanie nośników do kontrolowanego uwalniania biomolekuł, białek czy leków [68,69]. W przypadku większych defektów czy implantów o kontrolowanym kształcie, lepiej sprawdzają się materiały charakteryzujące się wyższymi parametrami mechanicznymi. Kompozyt wydrukowany w 3D z PCL i HAp, pomimo dużej porowatości, przy odpowiednim udziale faz, wykazuje właściwości mechaniczne porównywalne do naturalnej kości gąbczastej [70]. Podobne wyniki uzyskano dla osnowy z PLA, gdzie dodatkowo zaobserwowano indukowanie różnicowania osteogenicznego mezenchymalnych komórek macierzystych (MSC) [71]. Oprócz właściwości mechanicznych, niewątpliwą zaletą kompozytów na bazie materiałów termoplastycznych jest możliwość ich personalizacji, poprzez wydruk w dowolnym kształcie, dostosowanym do ubytków kości pacjenta [72]. Jednak struktura łańcuchowa tych materiałów polimerowych nie jest tak łatwa w modyfikacji jak struktura biopolimerów, tworzących układy hydrożelowe. Biorąc pod uwagę powyższe przykłady, wybór konkretnego układu materiałowego powinien zależeć od rodzaju ubytku i pożądanych, docelowych właściwości mechanicznych.

2. Modyfikacje powłok kompozytowych

Nowoczesne podejścia w inżynierii biomateriałów zakłada, że implant nie tylko pełni funkcję mechaniczną czy też wypełniającą, ale może również aktywnie uczestniczyć w procesach regeneracyjnych i ochronnych tkanek. Powlekanie komercyjnie dostępnych implantów bioaktywnymi powłokami stwarza możliwości funkcjonalizacji powierzchni mniej aktywnych lub inertnych materiałów [73]. W zależności od składu powłoki mogą poprawiać właściwości osteointegracyjne,

odporność na korozję, czy zapewniać działanie terapeutyczne [74]. W przypadku implantów kostnych, bioaktywne materiały ceramiczne, takie jak HAp czy inne fosforany wapnia są szczególnie interesujące, ponieważ wykazują one zdolność do tworzenia nowych warstw apatytowych na swojej powierzchni, a następnie do integracji przez nią z tkanką kostną. Utworzony apatyt cechuje się wysokim stopniem podobieństwa strukturalnego do naturalnego materiału kostnego [75,76]. Jednakże, ceramika mimo korzystnych właściwości biologicznych, wykazuje ograniczenia technologiczne wynikające z jej kruchości oraz niskiej odporności na obciążenie mechaniczne i przenoszenie naprężeń [77]. Dlatego zawieszenie jej w biokompatybilnej fazie polimerowej umożliwia otrzymanie powłok o polepszonych właściwościach. Tego typu porowata struktura może sprzyjać migracji i proliferacji komórek. Ponadto, kompozycja powłoki, w tym skład fazy polimerowej w dużym stopniu może wpłynąć również na poprawę adhezji biomateriału do podłoża [78,79]. Charakter struktury polimerowej umożliwia również modyfikację substancjami aktywnymi. Poprzez wytworzenie z substancjami aktywnymi wiązań jonowych, kowalencyjnych, kapsułkowanie w matrycy czy też wykorzystanie zjawiska sorpcji fizycznej, możliwe jest otrzymanie powłoki o zdolności do uwalniania substancji aktywnej lokalnie, bezpośrednio w miejscu gdzie wymagany jest efekt terapeutyczny. Przykładem tego typu rozwiązań są systemy dostarczania leków (DDS). Wykorzystanie DDS umożliwia działanie selektywne, zwiększa skuteczność terapii, minimalizując tym samym ryzyko toksyczności ogólnoustrojowej i przekładając się na minimalizację dawki. Samo uwalnianie może zachodzić drogą dyfuzji, degradacji lub na skutek reakcji enzymatycznych czy zmian wartości pH [80–82]. W 2024 roku globalny rynek DDS został wyceniony na 46,23 mld USD i zakłada się, że przy utrzymującej się złożonej rocznej stopie wzrostu (CAGR) na poziomie 4,1 %, wartość ta wzrośnie do 63,38 mld USD w 2032 roku [83]. W świetle przedstawionych informacji, temat ten stanowi jedno z kluczowych i dynamicznie rozwijających się zagadnień we współczesnej farmakologii i inżynierii materiałowej.

W prezentowanych badaniach zaproponowano wykorzystanie powłoki kompozytowej z kontrolowaną bioaktywnością na bazie PVP:PEG:COL:HAp, o charakterze nośnika substancji aktywnych, w tym antybiotyku i białkowych czynników wzrostu, której celem jest jednoczesna poprawa bioaktywności, regeneracja tkanek oraz zapewnienie ochrony antybakteryjnej.

2.1. Białkowe czynniki wzrostu [P1]

Pod pojęciem czynników wzrostu (GF), rozumie się białka sygnałowe lub cytokiny, które pośredniczą w funkcjach związanych z różnicowaniem oraz proliferacją komórek [84]. Ponadto mogą wpływać na gojenie ran, regulację układu odpornościowego jak również działać jako stymulatory wzrostu [85]. GF wiążą

się z receptorami błonowymi komórek docelowych, aktywując wewnątrzkomórkowe szlaki sygnałowe odpowiedzialne za przebudowę tkanek [86]. Wyróżnia się kilka głównych strategii dostarczania GF (Rysunek 4), są to: układy cząsteczkowe (np. liposomy, mikrokapsułki, nanocząstki), rusztowania, hydrożele oraz inne mniej standardowe strategie, obejmujące między innymi kompleksy supermolekularne, czy koniugaty polimerowe [87].

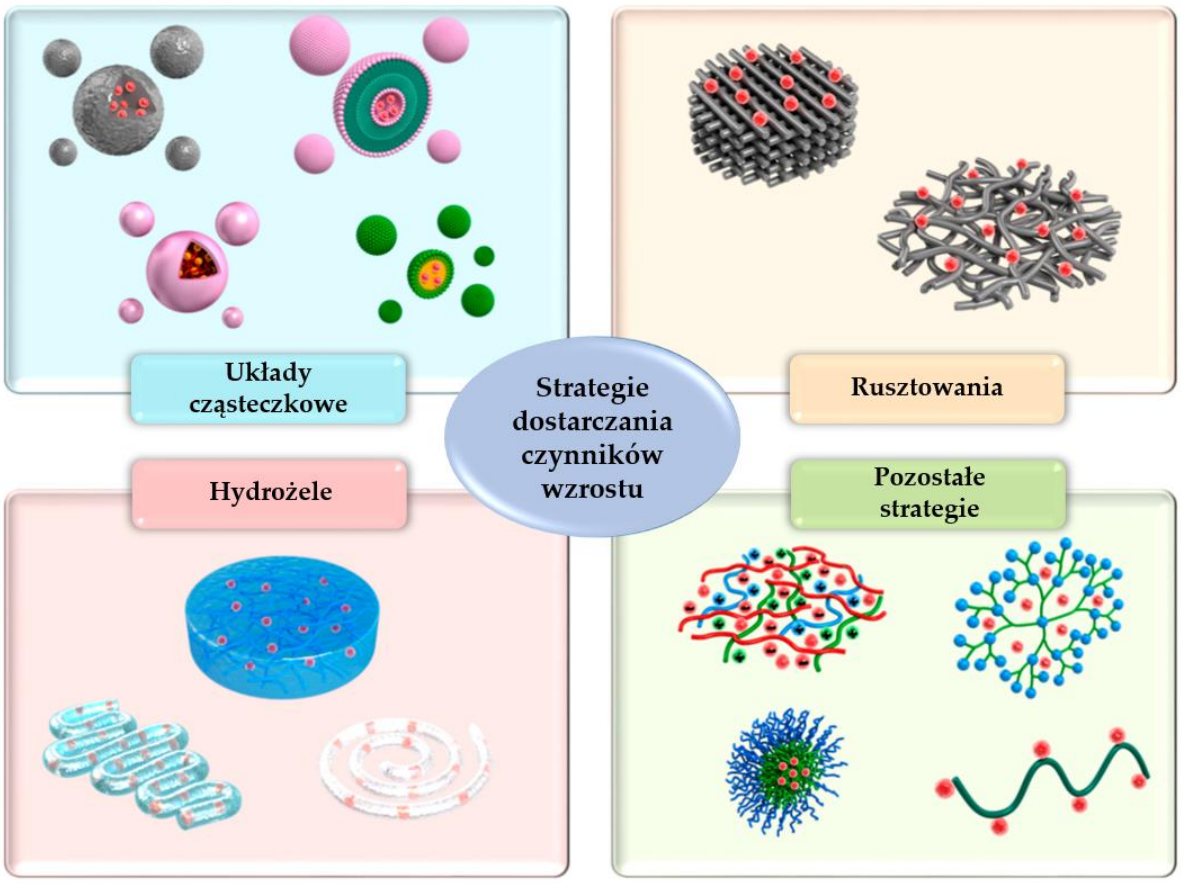

Rysunek 4: Schematyczne przedstawienie systemów dostarczania czynników wzrostu [87].

W inżynierii tkanki kostnej szczególne znaczenie przypisuje się czynnikom wspomagającym osteogenezę i angiogenezę. Stanowią one dwa procesy kluczowe dla skutecznej integracji implantu i regeneracji kości.

2.1.1. VEGF – rola w angiogenezie i potencjał terapeutyczny w integracji implantu

Czynnik wzrostu śródbłonka naczyniowego (VEGF) jest białkiem stymulującym proces angiogenezy, czyli tworzenia się naczyń włosowatych [88]. Wyróżnia się kilka izoform białka, w zależności od liczby reszt aminokwasowych które go tworzą. Najczęściej opisywanymi są VEGF-121, VEGF-165, VEGF-189 oraz VEGF-206 [89,90]. Spośród nich, izoforma -165 jest najlepiej przebadana i najczęściej opisywana w pracach naukowych. Wynika to z jej pośredniej biodostępności, polegającej

na częściowym wiązaniu się z receptorami i składnikami ECM. Zapewnia to stabilność działania, ponieważ, krótsza forma -121 jest całkowicie rozpuszczalna i szybko dyfunduje, a dłuższe formy -189 i -206 pozostają niemal całkowicie związane z ECM, co ogranicza ich biodostępność [91]. Obecność aktywnego VEGF ma kluczowe znaczenie w kontekście biomateriałów, ponieważ wspiera tworzenie odpowiedniego unaczynienia w regenerowanym miejscu. Odpowiednie ukrwienie wszczepu i otaczających tkanek sprzyja prawidłowemu procesowi gojenie kości. Ponadto, rozbudowana sieć naczyń krwionośnych dodatkowo stabilizuje implant, minimalizując ryzyko jego przesunięcia poprzez mechaniczne umocowanie w tkance [92]. Aktywność tego białka nie ogranicza się jednak tylko do stymulowania unaczynienia. Niektóre badania wykazują, że w pewnych warunkach VEGF oddziałując z komórkami MSC może pośrednio wpływać na wzrost ekspresji markerów osteogennych (RUNX2) i mineralizację [93]. W badaniach z komórkami macierzystymi wyizolowanymi z tkanki tłuszczowej (ASCs) zaobserwowano wzrost aktywności fosfatazy alkalicznej (ALP), wczesnego markera kostnienia oraz intensywniejszą mineralizację po dodaniu VEGF [94]. W celu intensyfikacji efektu działania białek lub zwiększenia aktywności biologicznej biomateriałów często stosuje się kombinację kilku GF, co pozwala uzyskać efekt synergistyczny. Przykładowo, BMP-2, jak i VEGF-165 mogą prowadzić do intensywniejszej angiogenezy i osteogenezy w porównaniu z działaniem każdego z tych czynników osobno [95,96]. Z kolei połączenie z PDGF [97] i FGF [98] sprzyja powstawaniu nie tylko większej liczby naczyń krwionośnych, ale także ich dojrzewaniu i stabilizacji poprzez stymulowanie perycytów, komórek odpowiadających za ich mechaniczne wzmocnienie i prawidłowe funkcjonowanie. Przykłady te potwierdzają zasadność łączenia różnych GF, w celu skuteczniejszego wspierania procesów regeneracji, niż w przypadku stosowania pojedynczego białka.

2.1.2. TGF-β – regulator procesów naprawczych i znaczenie w osteogenezie

Transformujący czynnik wzrostu beta (TGF-β) jest czynnikiem wzrostu kontrolującym proliferację oraz różnicowanie w większości typów komórek, oraz wykazującym działanie przeciwzapalne [99,100]. Białko to występuję w trzech izoformach, tj. TGF-β1, TGF-β2 i TGF-β3, kodowanych przez różne geny, zlokalizowane na odmiennych chromosomach [101]. TGF-β1 jest kodowany na długim ramieniu chromosomu 19 (19q13.1), TGF-β2 na chromosomie 1 (1q41), a TGF-β3 jest kodowany na chromosomie 14 (14q24) [101]. TGF-β2 odgrywa szczególną rolę w rozwoju embrionalnym i homeostazie tkankowej [102]. TGF-β3 jest związany z procesami regeneracyjnym, sprzyja gojeniu ran ograniczając widoczność blizn [103]. Z kolei TGF-β1 jest głównym regulatorem fizjologicznych. Jego występowanie jest powiązane z intensywnym stanem zapalnym występującym w procesie gojenia tkanek, jak również odgrywa kluczową rolę w procesach komórkowych,

w tym w rozwoju komórek, różnicowaniu i apoptozie [104,105]. Aktywność naprawcza tkanek związana jest z promowaniem aktywności fibroblastów i produkcją kolagenu [106]. Wykazano również, że obecność TGF-β1 zmniejsza stany zapalne poprzez regulację aktywności makrofagów i cytokin prozapalnych [107]. Jest to istotny czynnik, w dużym stopniu warunkujący powodzenie implantacji biomateriału oraz jego akceptacji przez organizm. Chociaż potwierdzono, że TGF-β moduluje różnicowanie osteoblastów [108], w zastosowaniach dotyczących tkanki kostnej, częściej projektuje się biomateriały zawierające jego kombinacje z innymi GF, co pozwala uzyskać synergistyczne działania. W połączeniu z BMP-2 zaobserwowano większą aktywność ALP, mineralizację jak również wzrost ekspresji markera kostnienia RUNX2 [109,110]. W połączeniu z FGF zaobserwowano lepsze wyniki różnicowania chondrogenicznego owczych MSC [111]. Interesującą strategią jest dostarczanie TGF-β wraz z VEGF. Wykazano, że takie połączenie sprzyja różnicowaniu osteoblastów, co dodatkowo, dzięki zdolności do wspierania angiogenezy, może zapewnić właściwe unaczynienie wszczepu [112]. Z tego powodu układ ten może być szczególnie obiecujący w kontekście regeneracji tkanki kostnej. Uwzględniając powyższe, oraz zasadność łączenia różnych GF, w niniejszej pracy doktorskiej podjęto badania z wykorzystaniem tych dwóch białek.

2.2. Klindamycyna i jej właściwości przeciwdrobnoustrojowe [P2]

Zakażenia miejsca operacji (ZMO) są jednymi z najczęściej występujących zakażeń i powikłań pooperacyjnych, które mogą wystąpić zarówno podczas hospitalizacji, jak i po wyjściu ze szpitala [113]. W Europie odsetek tych zakażeń, w zależności od rodzaju zabiegu chirurgicznego, wynosi od 0,6 % do 9,6 % [114]. Jednak globalnie, wskaźnik ZMO w chirurgii ortopedycznej wygląda różnie i w zależności od poziomu rozwoju ekonomicznego kraju wynosi 0,3 – 25 % [115]. Czynnikiem etiologicznym prowadzącym do zakażeń są najczęściej bakterie bytujące na skórze, ale mogą to być również mikroorganizmy bytujące w innych obszarach ciała lub znajdujące się w środowisku sali operacyjnej, a także na narzędziach chirurgicznych. Najczęściej występującym drobnoustrojem powodującym ZMO jest Gram-ujemna *Escherichia coli*, odpowiadająca nawet za 50 % zachorowań, oraz Gram-dodatni *Staphylococcus aureus* [116]. Infekcje bakteryjne mogą prowadzić do zapalenia kości i szpiku (*osteomyelitis*), które definiuje się jako proces zapalny spowodowany infekcją kości, który prowadzi do nadmiernej aktywacji osteoklastów, martwicy kości i może przejść w stan przewlekły [117,118]. Zgodnie z procedurą zalecaną przez WHO, antybiotykoterapia może skutecznie zapobiegać infekcjom. Z tego powodu, zasadnym jest modyfikacja biomateriałów antybiotykami, zapewniającymi właściwości przeciwdrobnoustrojowe.

W przypadku zabiegów i operacji związanych z tkanką kostną najczęściej wykorzystywanym antybiotykiem jest klindamycyna (CLD) [119]. Należy

ona do antybiotyków z grupy linkozamidów, a dzięki swoim unikalnym właściwościom i szerokiemu działaniu, jest stosowana przeciwko wielu rodzajom bakterii. CLD jest pochodną naturalnego związku – linkomycyny, uzyskiwanego z bakterii *Streptomyces lincolnensis* [120,121]. Zwykle występuje w postaci chlorowodorku klindamycyny, łatwo rozpuszczalnej w wodzie soli, ale wykorzystywana jest również forma fosforanu klindamycyny [122]. Działanie CLD polega na hamowaniu biosyntezy białek bakteryjnych. Dochodzi do niego na skutek wiązania się CLD z podjednostką 50S rybosomu bakteryjnego, dokładnie w miejscu wiązania tRNA i elongacyjnego czynnika peptydylotransferazy, czego efektem jest blokowanie tworzenie wiązań peptydowych między aminokwasami podczas translacji [123,124].

Wykorzystanie CLD w leczenie infekcji kości podyktowane jest kilkoma czynnikami. W przeciwieństwie do niektórych antybiotyków (np. gentamycyny), CLD nie wykazuje toksyczności wobec osteoblastów, czyli komórek kościotwórczych [125,126] Ponadto, charakteryzuje się wysoką zdolnością przenikania do tkanki kostnej, jak również jest aktywna wobec najczęstszych patogenów odpowiedzialnych za zapalenia kości oraz ZMO podczas operacji związanych z implantacją substytutów tkanki kostnej, takich jak *Staphylococcus aureus*, *Streptococcus spp*. oraz bakterie beztlenowe [127,128].

3. Wprowadzenie w tematykę pracy

Rozwój inżynierii materiałowej, inżynierii tkankowej oraz nowych technik wytwarzania umożliwia projektowanie innowacyjnych materiałów do zastosowań w różnych gałęziach medycyny. Jednakże wyzwaniem jest zaprojektowanie rozwiązań łączących trwałość i niezawodność z wysoką aktywnością biologiczną w miejscu implantacji. Obiecującym rozwiązaniem jest stosowanie powłok kompozytowych, które umożliwiają modyfikację wierzchniej warstwy granicznej, bezpośrednio na granicy styku materiał-tkanka, bez istotnych zmian parametrów mechanicznych implantu. Takie układy mogą pełnić również rolę nośników substancji aktywnych i leków, umożliwiając kontrolowane uwalnianie **[P1][P2]**. Co istotne, sama ceramika modyfikowana lekiem może działać jako niezależny nośnik **[P3]**, jednak zintegrowanie jej z matrycą polimerową powłoki, może prowadzić do powstania materiału kompozytowego o polepszonych właściwościach i rozszerzonym profilu działania. Hybrydowe, wielofunkcyjne powłoki kompozytowe zawierające fazę polimerową wzmocnioną fazą ceramiczną, charakteryzują się korzystnymi właściwościami fizykochemicznymi i mechanicznymi oraz zdolnością do indukowania nukleacji i wzrostu apatytu w warunkach *in vitro*, co potwierdza ich bioaktywny charakter **[P4]**. Odpowiedni dobór stosunków poszczególnych komponentów pozwala kształtować właściwości użytkowe, wpływając na parametry fizykochemiczne i tribologiczne **[P5]**. Ponadto, skład biomateriału wpływa również na profil uwalniania związków aktywnych, jak białka i leki, a tym samym na aktywność biologiczną w miejscu implantacji **[P6][P7]**.

Dotychczasowe prace badawcze, w świetle literatury przedmiotu, wskazują na istotne ograniczenia i potrzeby w zakresie poprawy bioaktywności materiałów implantacyjnych. Inertne metale, takie jak tytan czy jego stopy, choć wykazują wysoką wytrzymałość mechaniczną i dobrą biokompatybilność, nie sprzyjają bezpośredniemu wiązaniu z tkanką kostną ani nie oferują dodatkowej funkcjonalności biologicznej. Z kolei stosowane w implantologii polimery, mimo swojej wszechstronności i łatwości przetwórstwa, charakteryzują się ograniczoną wytrzymałością mechaniczną oraz niskim poziomem naturalnej bioaktywności, co znacząco ogranicza ich zdolność do integracji z tkankami twardymi. Pokrycie ich powierzchni bioaktywnymi powłokami, pozwala na zwiększenie wartości biologicznej, jak również nadanie im roli nośnika substancji aktywnych.

Na podstawie analizy najnowszych doniesień naukowo-badawczych dotyczących powłok kompozytowych oraz ich modyfikacji stwierdzono, że zasadne jest podjęcie prac nad opracowaniem nowego bioaktywnego materiału powłokowego, pełniącego funkcję nośnika substancji aktywnych. Celem tych działań było uzyskanie materiału o właściwościach przewyższających te, które charakteryzują obecnie stosowane i opisywane w literaturze powłoki. Przeprowadzone prace badawcze w tym zakresie przyniosły satysfakcjonujące wyniki, które zostały szczegółowo zaprezentowane w niniejszej rozprawie.

4. Teza i cele pracy

W prezentowanej pracy doktorskiej przedstawiono badania ukierunkowane na opracowanie innowacyjnej, kompozytowej, wielofunkcyjnej powłoki, przeznaczonej do modyfikacji powierzchni materiałów inertnych lub implantów o niskiej bioaktywności. Sformułowano następującą tezę pracy doktorskiej:

Kompozytowa powłoka, łącząca fazę polimerową z fazą ceramiczną, modyfikowana substancjami aktywnymi, może stanowić skuteczne rozwiązanie dla biomedycyny i wspomagania regeneracji tkanki kostnej. Skład takiej powłoki oraz zastosowane substancje aktywne mają wpływ na jej właściwości fizykochemiczne i biologiczne. Taki materiał może skutecznie wspierać proces regeneracji tkanki kostnej oraz ograniczać ryzyko infekcji i wystąpienia reakcji zapalnych, odpowiadając na współczesne potrzeby kliniczne w zakresie zwiększenia funkcjonalności oraz poprawę bioaktywności biomateriałów stosowanych w implantologii.

Założono, że teza ta zostanie udowodniona dzięki zaproponowaniu innowacyjnej kompozycji materiału opartej na nietoksycznych polimerach, biozgodnym hydroksyapatycie, antybiotyku o udowodnionej aktywności antybakteryjnej oraz białkowych czynnikach wzrostu stymulujących proces angiogenezy i zapewniających właściwości przeciwzapalne.

Celem naukowym pracy doktorskiej był dobór kompozycji materiałowej, oraz charakterystyka wielofunkcyjnych materiałów powłokowych otrzymanych z polimerów pochodzenia naturalnego jak również syntetycznego i hydroksyapatytu, oraz ich modyfikacja wybranymi substancjami aktywnymi. Praca miała na celu ocenę wpływu składu powłok kompozytowych na ich właściwości fizykochemiczne i biologiczne, ze szczególnym uwzględnieniem zdolności do uwalniania substancji aktywnych, działania przeciwdrobnoustrojowego oraz wspierania regeneracji tkanki kostnej.

Celem utylitarnym pracy doktorskiej było wytypowanie wielofunkcyjnej powłoki kompozytowej, która dzięki swoim właściwościom będzie zwiększać funkcjonalność oraz poprawi bioaktywność biomateriałów stosowanych w implantologii. Celem prowadzonych analiz było wykazanie, że składniki czynne wprowadzone do roztworu polimerowego nie ulegną dezaktywacji i zachowają aktywność po procesie fotosieciowania UV: klindamycyna – działanie przeciwbakteryjne, VEGF i TGF-β – zwiększenie wartości biologicznej materiału. Celem było wykazanie, że opracowana powłoka może być stosowana do powlekania innych materiałów, nadając im bioaktywny charakter, oraz że jej zastosowanie może poprawić integrację implantu z tkanką kostną.

5. Plan badań

Zakres prac badawczych prowadzonych w ramach rozprawy doktorskiej dotyczył następujących zdań:

- Przegląd literaturowy.
- Dobór warunków syntezy fazy ceramicznej – hydroksyapatytu metodą mokrego strącenia.
- Analiza fizykochemiczna i biologiczna wytypowanego proszku hydroksyapatytowego: wyznaczenie stosunku molowego Ca/P, stopnia krystaliczności, detekcja grup funkcyjnych, analiza porowatości, powierzchni właściwej, ocena morfologii powierzchni, analiza pierwiastkowa.
- Dobór warunków otrzymywania i kompozycji składników ceramiczno-polimerowej powłoki.
- Poddanie powłok analizie fizykochemicznej, mechanicznej oraz badaniom inkubacyjnym w płynach symulujących środowisko wewnętrzne organizmu: obrazowanie morfologii powierzchni, pomiary chropowatości, pomiar sił tarcia, analiza pierwiastkowa, identyfikacja grup funkcyjnych, kąt zwilżania i energia powierzchniowa, wytrzymałość na rozciąganie, twardość, zdolności sorpcyjne, potencjometria, konduktometria, ubytek masy.
- Modyfikacja hydroksyapatytu oraz powłok antybiotykiem: badanie szybkości uwalniania leku, ocena efektywności antybakteryjnej, cytozgodność, aktywność antybiofilmowa, ocena *in vivo* odpowiedzi miejscowej tkanek oraz ogólnoustrojowej na implantację biomateriałów.
- Modyfikacja powłok ceramiczno-polimerowych białkowymi czynnikami wzrostu i określenie ich biozgodności: badanie szybkości uwalniania czynników wzrostu, ocena *in vivo* biomateriałów w modelu ubytku kości czaszki szczura, w tym obrazowanie mikroskopem konfokalnym, oznaczenie poziomu cytokin zapalnych (IL-1β, TNF-α), przeciwzapalnych (IL-10) oraz osteopontyny (OPN) jako biomarkerów odpowiedzi immunologicznej i regeneracyjnej.
- Analiza otrzymanych wyników, dyskusja oraz przygotowanie publikacji naukowych.

Na Rysunku 5 przedstawiono ogólny zakres prac badawczych prowadzonych w ramach niniejszej pracy doktorskiej, z podziałem na trzy główne etapy tj. otrzymanie ceramiki hydroksyapatytowej, dobór kompozycji ceramiczno-polimerowej powłoki i jej modyfikacja, oraz przeprowadzenie obszernej analizy fizykochemicznej, mechanicznej oraz biologicznej.

Przedstawiony poniżej komentarz do cyklu publikacji wchodzących w zbiór artykułów stanowiących podstawę pracy, przedstawia główne osiągnięcia w zakresie doboru warunków syntezy hydroksyapatytu metodą mokrego strącenia, oraz doboru kompozycji i opracowania metody wytwarzania bioaktywnych

powłok o kontrolowanej aktywności. Przedstawione dalej wyniki badań zostały uzyskane na Politechnice Krakowskiej im. Tadeusza Kościuszki oraz Uniwersytecie Łódzkim. Ponadto wsparcie merytoryczne uzyskano od mentora z Comenius University na Słowacji.

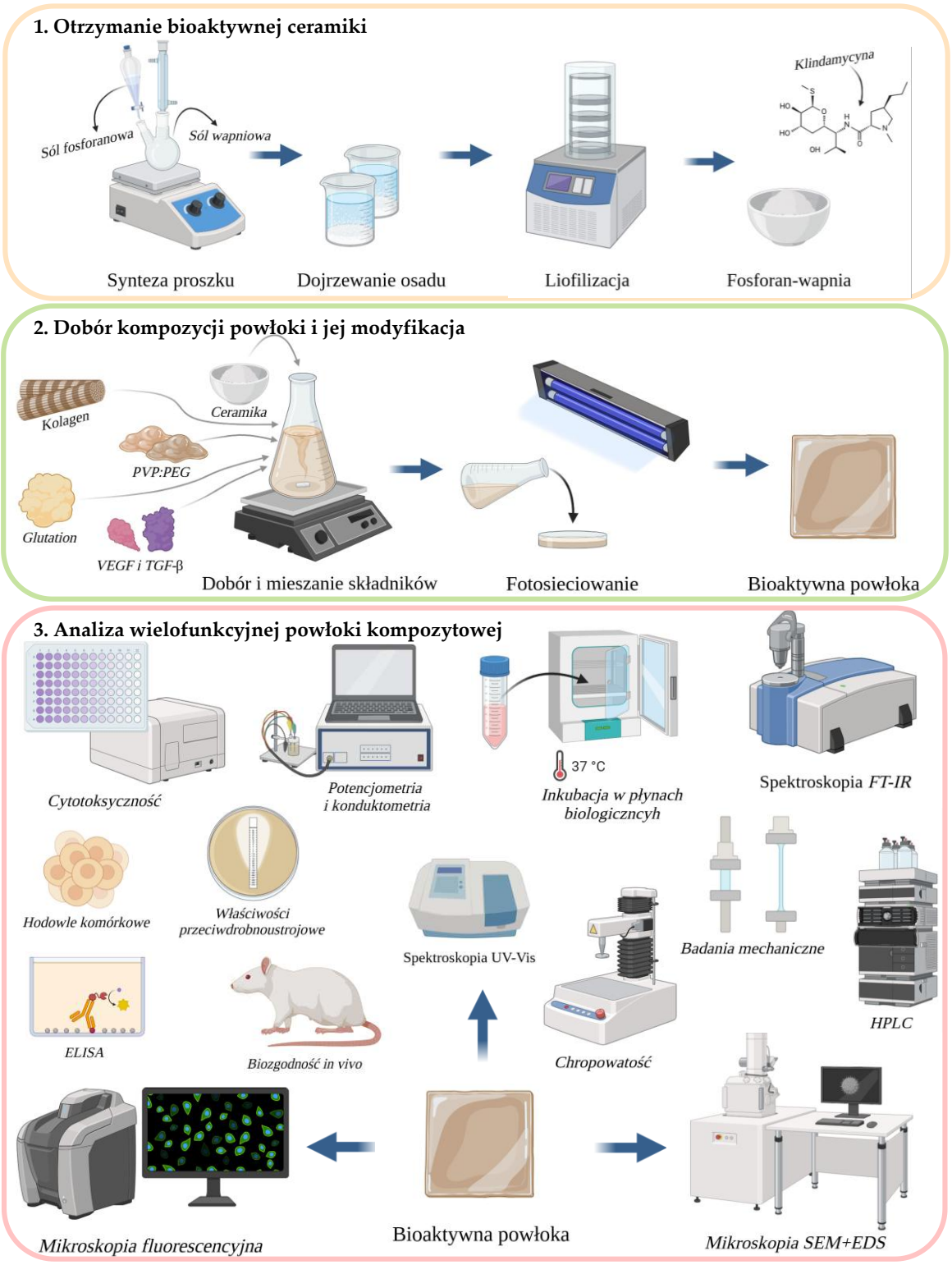

Rysunek 5: Schemat zakresu prac badawczych prowadzonych w ramach pracy doktorskiej. Grafikę utworzono za pomocą BioRender.com.

6. Rezultaty badań

6.1. Nośniki substancji aktywnej w postaci proszków fosforanowo-wapniowych modyfikowanych klindamycyną [P3]

Biorąc pod uwagę stale rosnące zainteresowanie wykorzystania CaP w inżynierii tkanki kostnej oraz możliwości jej modyfikacji w celu wytworzenia nośnika substancji aktywnej, celem bada było wytworzenie proszków CaP o różnych stosunkach molowych Ca/P do kontrolowanego uwalniania klindamycyny. Wykorzystując metodę mokrego strącenia w podwyższonej temperaturze, przy zmiennych stosunkach reagentów Na_2HPO_4 oraz $(CH_3COO)_2Ca$ otrzymano dwa proszki oznaczone kolejno jako s-1.67 (syntetyczny HAp) i 1.5 (syntetyczny TCP). Proszek 1.0 (bruszyt) otrzymano również metodą mokrego strącenia z soli Na_2HPO_4 oraz $Ca(NO_3)_2 \cdot 4H_2O$. Jako materiał odniesienia służył c-1.67 (komercyjny HAp).

Wyznaczony stosunek molowy Ca/P nie odbiegał znacznie od założonych wartości teoretycznych i odpowiadał wartościom literaturowym (Tabela 1). Analiza dyfrakcyjna XRD potwierdziła, że wszystkie próbki były czyste fazowo, a także wykazywały częściową krystaliczność. Dla proszków s-1.67 i c-1.67 dyfraktogramy wykazały obecność refleksów charakterystycznych dla heksagonalnej struktury HAp, w przypadku proszku 1.5 refleksy były typowe dla romboedrycznej struktury β-TCP, a dla proszku 1.0 zidentyfikowano występowanie monoklinicznej struktury bruszytu. Różnice w intensywności refleksów na dyfraktogramach potwierdziły zróżnicowany stopień uporządkowania struktury otrzymanych proszków. Badanie spektroskopowe FTIR umożliwiło uzyskanie widm typowych dla HAp, TCP i bruszytu, a ich analiza wykazała obecność grup funkcyjnych charakterystycznych dla każdego z proszków. Powyższe analizy potwierdziły, że zastosowane metody mokrego strącanie umożliwiają otrzymanie fazowo czystych proszków. W wyniku obrazowania SEM, zaobserwowano wpływ metody syntezy na morfologię proszków CaP. Najbardziej jednorodną morfologię w postaci zwartych, regularnych aglomeratów o porównywalnej wielkości zaobserwowano w przypadku proszku oznaczonego jako 1.5. W przypadku proszku s-1.67 również zaobserwowano tendencję do tworzenia aglomeratów, jednak pomimo zastosowania tych samych reagentów i warunków syntezy, miały one postać zbliżoną bardziej do proszku 1.0.

Tabela 1: Wyznaczona zawartość wapnia i fosforu oraz stosunek molowy Ca/P w otrzymanych proszkach.

Próbka	Zawartość Ca [wag. %]	Zawartość P [wag. %]	Stosunek molowy Ca/P
s-1.67	37,51 ± 0,65	17,26 ± 0,19	1,67
c-1.67	37,46 ± 0,38	17,27 ± 0,12	1,67
1.5	36,93 ± 0,32	18,87 ± 0,23	1,51
1.0	37,81 ± 0,41	27,91 ± 0,34	1,04

Wykorzystując zjawisko sorpcji fizycznej, proszki CaP zmodyfikowano następnie CLD i oznaczono jako C/1.0, C/1.5, C/s-1.67 i C/c-1.67. W celu detekcji sygnałów pochodzących od atomów chloru, świadczących o obecności antybiotyku przeprowadzono analizę rozkładu pierwiastków metodą EDS sprzężoną z mikroskopią SEM. Ilość uwolnionego leku określano za pomocą HPLC. Analiza profilu uwalniania klindamycyny wykazała najwyższe i najszybsze uwalnianie leku dla próbki C/1.0, a następnie C/s-1.67 i C/1.5 (Rysunek 6a).

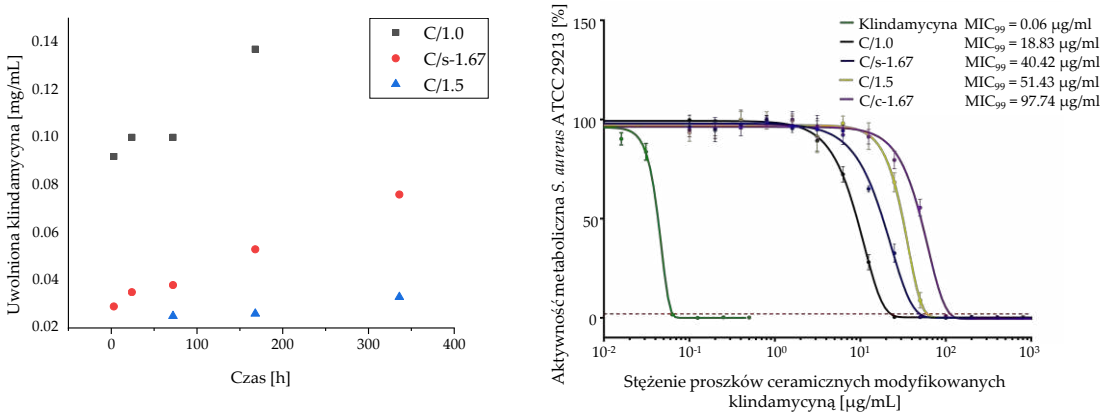

(a) (b)

Rysunek 6: (a) Profil uwalniania klindamycyny z modyfikowanych proszków ceramicznych; (b) Zależna od dawki odpowiedź modyfikowanych klindamycyną proszków względem Staphylococcus aureus ATCC 29213 i wartości MIC_{99}. Zielona linia przedstawia krzywą referencyjną hamowania metabolizmu bakteryjnego przez klindamycynę. Punkt przecięcia krzywych z czerwoną linią odpowiada 99 % redukcji aktywności metabolicznej bakterii i jest określany jako wartość MIC_{99}.

Interesującym jest, że wyniki te są w odwrotnej korelacji do zmierzonej powierzchni właściwej (SSA) proszków (Tabela 2), ponieważ materiały o mniejszej powierzchni uwalniały lek szybciej. Próbka 1.0 (SSA = 32 m^2/g), wykazała najszybsze uwalnianie, co może być spowodowane płytszą lokalizacją zaadsorbowanych cząstek leku, a tym samym krótszą drogą dyfuzji. Ponadto, niższy stosunek molowy Ca/P determinuje wyższą rozpuszczalność samej fazy ceramicznej, w porównaniu do pozostałych proszków. W przypadku próbek s-1.67 (SSA = 61 m^2/g) oraz 1.5 (SSA = 53 m^2/g), charakteryzujących się większą powierzchnią właściwą, wolniejsze tempo uwalniania może wynikać z głębszej penetracji leku do wnętrza struktury. W rezultacie zaobserwowana kolejność szybkości uwalniania klindamycyny (C/1.0 > C/s-1.67 > C/1.5) była zgodna z rosnącą całkowitą powierzchnią właściwą nośników.

W testach biologicznych (Rysunek 6b) wykonanych z użyciem bakterii szczepu *Staphylococcus aureus*, wszystkie proszki zmodyfikowane klindamycyną wykazały aktywność antybakteryjną. Najlepsze działanie przeciwbakteryjne, wyznaczone jako MIC_{99}, czyli minimalne stężenie hamujące wzrost 99 % populacji bakterii, zaobserwowano w przypadku C/1.0 (18,83 µg/ml), co pokrywało się z jego najwyższą efektywnością w zakresie uwalniania leku. Wartość MIC_{99} dla wszystkich syntezowanych proszków była niższa niż dla materiału referencyjnego.

Tabela 2: Powierzchnia właściwa i porowatość badanych proszków fosforanowo-wapniowych.

Próbka	SSA [m²/g]	Porowatość		
		Rozkład wielkości porów DFT [nm]	Objętość makroporów [cm³/g]	Powierzchnia mikroporów [m²/g]
s-1.67	53	4, 10, 11, 13	0.345	3.52
c-1.67	64	11, 13, 17, 20, 22, 24, 28	0.27	0
1.5	61	8, 10, 11, 13	0.304	0
1.0	32	4, 7, 8, 10	0.21	4.94

W efekcie opisanych wyżej prac badawczych, wykorzystując metodę mokrego strącenia, otrzymano materiały ceramiczne o różnej morfologii. Przeprowadzone analizy fizykochemiczne pozwoliły stwierdzić, że wybrane metody syntezy umożliwiają uzyskanie proszków ceramicznych o założonych stosunkach molowych Ca/P. Wszystkie proszki mogą stanowić biomateriał do zastosowań biomedycznych, zwłaszcza w regeneracji tkanki kostnej i zapobieganiu infekcjom.

6.2. Hybrydowe powłoki kompozytowe: właściwości tribologiczne i analiza fizykochemiczna [P4]

Rozwój nauki o biomateriałach umożliwia nadawanie implantom nowych właściwości poprzez modyfikacje powierzchni. Jedną z obiecujących strategii jest funkcjonalizacja powierzchni poprzez stosowanie bioaktywnych powłok. Kolejny etap badań obejmował dobór kompozycji powłok kompozytowych oraz weryfikację ich właściwości fizykochemicznych, mechanicznych i ocenę zachowania w sztucznym środowisku biologicznym, symulującym warunki

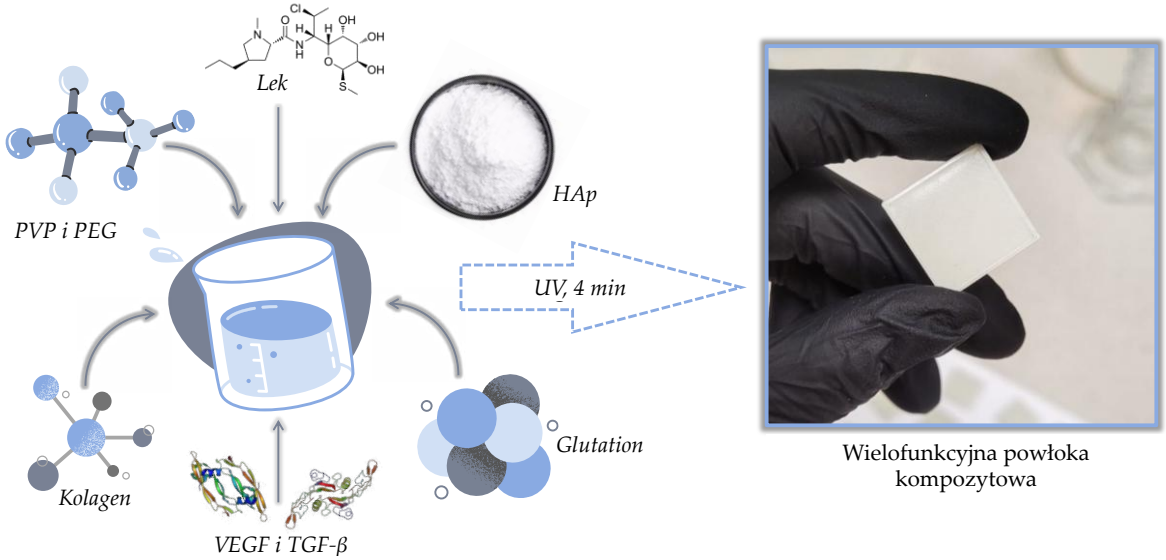

Rysunek 7: Kompozycja powłoki oraz usieciowana powłoka PVP:PEG:COL:HAp z 5 % ceramiki naniesiona na płytkę PLA.

organizmu. W oparciu o analizy wyników uzyskanych dla proszków ceramicznych, jako ceramiczną fazę kompozytowej powłoki wybrano proszek s-1.67. Chociaż docelowo lek uwalniał się szybciej z bruszytu, jako fazę wzmacniającą powłok wybrano HAp, biorąc pod uwagę potencjalną większą stabilność w środowisku biologicznym wynikającą z wyższego stosunku molowy Ca/P oraz podobieństwo struktury HAp do fazy mineralnej naturalnej tkanki kostnej.

Opracowane powłoki nanoszono na płytki PLA wydrukowane 3D o strukturze plastra miodu. W celu zwiększenia adhezji powłoki do materiału bazowego, opracowano warstwę pośrednią łączącą materiał bazowy z docelową powłoką oraz dwuetapową procedurę jej nanoszenia. W pierwszym etapie na PLA nałożono mieszaninę wodnego roztworu PVP z rozpuszczonym glutationem (GSH), którą poddano procesowi fotosieciowania przez 2 minuty. Otrzymano lepką warstwę na którą następnie nakładano docelowe powłoki tj. mieszaninę polimerową PVP:PEG, polimerową wzbogaconą kolagenem, PVP:PEG:COL oraz dwie warstwy kompozytowe PVP:PEG:COL:HAp kolejno o udziale 5 % i 15 % ceramiki. Tę warstwę sieciowano 4 minuty w świetle UV. Otrzymaną powłokę PVP:PEG:COL:HAp z 5 % udziałem ceramiki wraz z kompozycją zaprezentowano na Rysunku 7. Proces sieciowania powłok oraz odpowiedni dobór stosunków reagentów, umożliwił otrzymanie jednolitych, dobrze uformowanych powłok o strukturze pozbawionej defektów takich jak pofalowania, wybrzuszenia, spękania czy niedosieciowane obszary. Ostateczne kompozycje zewnętrznych powłok wraz z odpowiadającymi im symbolami oraz ilościami poszczególnych składników zaprezentowano w Tabeli 3.

W celu określenia potencjału opracowanych powłok do wykorzystania w charakterze nośnika substancji aktywnej przeprowadzono badanie kinetyki pęcznienia materiałów w wodzie destylowanej. Wyznaczona równowaga pęcznienia (S_e) odnosi się do maksymalnej, ustabilizowanej zdolności absorpcji płynu, wyrażonej jako procentowy przyrost masy. Parametr szybkości τ wyznaczono na podstawie dopasowania danych do modelu Voigta, w celu określenia szybkości procesu pęcznienia. Powłoki polimerowe bez HAp osiągnęły S_e na poziomie 115.8 ± 5.0 dla PVP:PEG (A) i 118,8 ± 5,1 PVP:PEG:COL (B) przy wartości parametru szybkości τ równych kolejno 30,4 ± 8,1 min oraz 29,7 ± 8,0. Dodatek fazy ceramicznej skutkował obniżeniem zarówno zdolności sorpcyjnych jak również szybkości absorpcji płynu. Ziarna HAp poprzez zajmowanie wolnych przestrzeni pomiędzy łańcuchami polimerowymi, ograniczały penetrację cząstek wody. Większy udział fazy ceramicznej korelował z niższym poziomem pęcznienia oraz większą wartością parametru τ równym 41,14 ± 10,9 dla powłoki C oraz 47,3 ± 9,2 dla powłoki D. Interesującym jest wyższa zdolność sorpcyjna powłoki PVP:PEG:COL w porównaniu do matrycy bez kolagenu (A). Dzieję się tak prawdopodobnie za sprawą dodatku kolagenu i jego zdolności do wiązania cząsteczek wody.

Tabela 3: Kompozycja opracowanych powłok.

Próbka	PVP [ml]	PEG [ml]	GSH [g]	COL [g]	HAp [% w/v]	PEGDA [ml]	Fotoinicjator [µl]
A	5	5	2	-	-	1,8	50
B				0,04	-		
C					5		
D					15		

Przeprowadzono analiza morfologia powierzchni, badana metodą profilometrii konfokalnej i mikroskopii 3D, ujawniła wzrost chropowatości (Ra) wraz ze wzrostem zawartości HAp. Najniższą wartość Ra = 1,41 ± 0,38 µm zaobserwowano w próbce powłoki bazowej A, a w materiale z 15 % udziałem fazy ceramicznej wartość ta była ponad 4-krotnie wyższa i wynosiła Ra = 6,10 ± 0,87 µm. W przypadku próbki o 5 % udziale HAp, zaobserwowano ujemny wskaźnik Rsk, co z kolei sprzyjało wyższemu energetycznie korzystnemu profilowi powierzchni (free surface energy) wynoszącym 57,04 mJ/m². Pomiar kąta zwilżania określono dla cieczy polarnej i niepolarnej. Wykazano, że obecność ceramiki zwiększa całkowitą energię powierzchni. Taka topografia może sprzyjać interakcjom biologicznym jak adhezja komórek czy osseointegracja. W testach tribologicznych (Rysunek 8) wykorzystujących nanotribometr z kulką Al_2O_3 (500 mN, 1 cm/s, czas 1 h), bazowa matryca polimerowa PVP:PEG wykazała najwyższy współczynnik tarcia i największe zużycie, wynikający ze zbyt miękkiej struktury. Dodanie kolagenu PVP:PEG:COL poprawiło właściwości tribologiczne, zaobserwowano obniżenie współczynnika tarcia CoF. Próbka zawierająca 5 % HAp wykazywała najkorzystniejsze parametry, natomiast powłoka z 15 % HAp charakteryzowała się znacznym zużyciem powierzchni. Wynikało to z wykruszania się cząstek ceramiki na skutek ruchu kulki Al_2O_3 podczas pomiaru, a wykruszona ceramika działała jak ścierniwo dla powłoki. Późniejsza analiza śladów zużycia potwierdziła najmniejsze uszkodzenia dla PVP:PEG:COL i PVP:PEG:COL:HAp 5 %, a największe dla bazy PVP:PEG i PVP:PEG:COL:HAp 15 %.

Przeprowadzone badania twardości metodą Shore A wykazały, wzrost twardości wraz z dodatkiem fazy ceramicznej. Jednak biorąc pod uwagę grubość powłok (od 548 ± 5 µm do 700 ± 8 µm) zakłada się, że twardość zdeterminowana jest głównie przez podłoże, na którym znajduje się powłoka. W ramach prowadzonych badań poddano analizie również widma spektroskopowe FTIR dla każdej powłoki po procesie sieciowania jak również dla substratów wyjściowych. Zidentyfikowano główne grupy funkcyjne, co potwierdza czystość substratów bazowych.

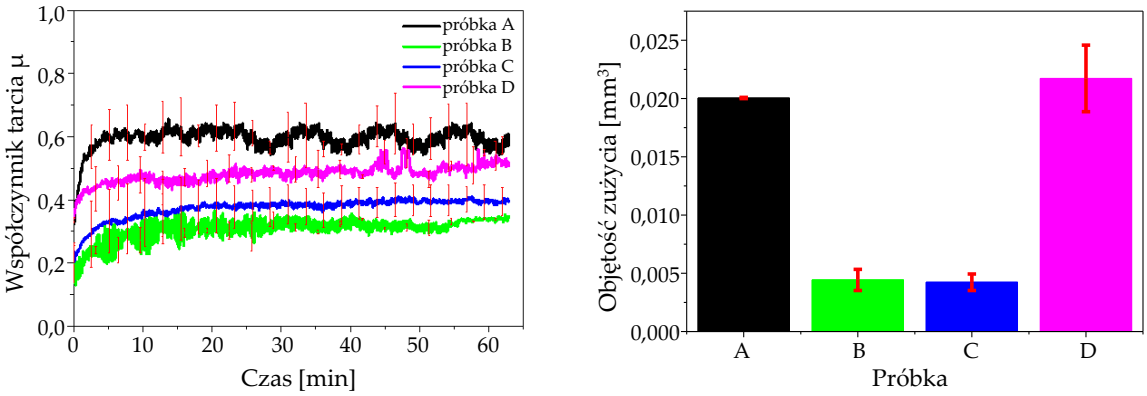

(a) (b)

Rysunek 8: Charakterystyka tribologiczna powłoka kompozytowych. (a) zmiana współczynnika tarcia w czasie; (b) objętość zużycia.

W wyniku prowadzonych prac badawczych stwierdzono, że powłoka z 5 % HAp wydaje się być optymalnym kompromisem między zapewnieniem ulepszonych właściwości tribologicznych poprzez niskie tarcie i zużycie, poprzez dobrą chropowatość powierzchni sprzyjającą interakcjom z komórkami, odpowiednią energię powierzchni i zdolność sorpcji oraz elastyczność. Wykazano, że zbyt wysoki udział HAp chociaż w teorii może przyczynić się do zwiększenia bioaktywności, w przypadku opracowanych powłok kompozytowych zwiększał kruchość i negatywnie wpływał na ścieralność.

6.3. Hybrydowe powłoki kompozytowe: badania inkubacyjne oraz ocena właściwości mechanicznych i fizykochemicznych [P5]

Kolejne prace badawcze dotyczące wielofunkcyjnej powłoki kompozytowej, obejmowały dalszą analizę fizykochemiczną, ocenę właściwości mechanicznych jak również analizę zachowania materiału podczas inkubacji, w płynach symulujących warunki wewnętrzne organizmu (tj. SBF, sztuczna ślina, płyn Ringera). Przeprowadzono analizę kinetyki pęcznienia do opisu której wykorzystano model Voigta, określając parametry S_e oraz τ. Płyny otrzymano zgodnie z przepisem zamieszczonym w publikacji. Celem badań było określenie zachowania się powłok w środowiskach o różnej wartości pH. Badania inkubacyjne prowadzono przez okres 40 dni. Analiza pH wykazała stabilność powłok w SBF przez cały okres 40-dniowej inkubacji, co sugeruje dobrą zgodność z warunkami fizjologicznymi. Podobnie, przewodnictwo jonowe było stabilne i porównywalne pomiędzy powłokami polimerowymi oraz kompozytowymi. Jednak zmiany wartości przewodnictwa świadczą o pewnych interakcjach materiałów z płynami. Największe zmiany zarówno potencjometryczne jak i konduktometryczne zaobserwowano w sztucznej ślinie, której początkowe pH było niższe niż dla SBF czy PBS. W tym płynie zaszła również największa zmiana masy próbek na skutek degradacji matrycy polimerowej od 36,19 % do 39,79 % ubytku masy. W wyniku

degradacji, na dnie naczynia inkubacyjnego zaobserwowano cząstki HAp. Podczas badań inkubacyjnych mierzono także zdolności sorpcyjne materiałów, jako że jest to jeden z parametrów determinujących potencjał wykorzystania danego materiału w charakterze nośnika substancji aktywnej. Zaobserwowano, że wraz z rosnącą zawartością HAp następował spadek zdolności sorpcyjnych powłok. Zjawisko to spowodowane było zajmowaniem wolnych przestrzeni pomiędzy łańcuchami polimerowymi przez ziarna ceramiki. W efekcie zmniejszała się objętość przestrzeni zdolnych do pochłaniania płynów. Po procesie inkubacji w SBF (Rysunek 9) przeprowadzono analizę morfologii powierzchni powłok za pomocą mikroskopii SEM, oraz wykonano mikroanalizę składu pierwiastkowego EDS (Tabela 4) w wybranych punktach. Wybrane punkty pomiarowe zaznaczono na Rysunku 9 żółtymi punkorami z numeracją 1 i 2.

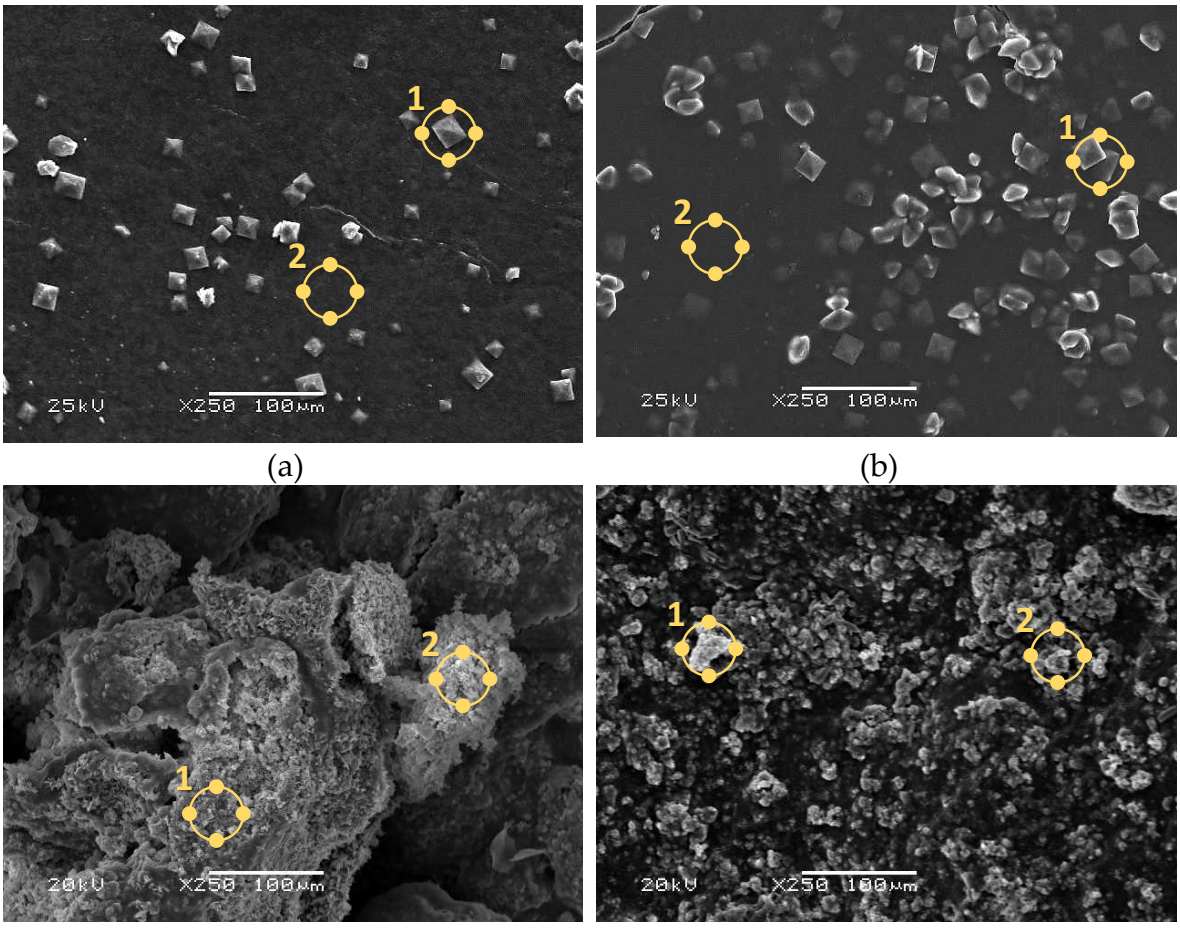

Rysunek 9: Analiza morfologiczna powłok po inkubacji w SBF ze wskazanym miejscem mikroanalizy EDS: (a) powłoka A; (b) powłoka B; (c) powłoka C; (d) powłoka D.

Zaobserwowano, że już przy 5 % zawartości HAp na powierzchni powłoki pojawiły się nowe warstwy apatytowe, co potwierdziło jej zdolność do inicjowania i wspierania procesów mineralizacji w warunkach imitujących środowisko organizmu.

Analiza mechaniczna w postaci pomiarów twardości metodą Shore'A stanowiła uzupełnienie do wcześniej opublikowanych wyników, gdzie parametr ten mierzono dla powłoki naniesionej na podkładkę polimerową. Tym razem analizie poddano sam otrzymany materiał. Powłoka bazowa z PVP:PEG osiągnęła wartość 5,8 °Sh, a dla materiału z 15 % udziałem fazy ceramicznej wartość ta wzrosła dwukrotnie do 11,6 °Sh. W przypadku wytrzymałości na rozciąganie, wraz z ilością dodanego HAp moduł Younga wzrastał, chociaż powłoki te były mniej elastyczne, co jest spójne z wykazanym wcześniej faktem, że stawały się również twardsze.

Tabela 4: Analiza punktowa EDS prezentująca skład pierwiastkowy badanych powłok po inkubacji w SBF.

Próbka	Udział atomowy [at. %]
A	1. C: 21,08; O: 54,13; Na: 3,61; Mg: 0,18; P: 0,40; Cl: 4,51; K: 0,12; Ca: 15,99 2. C: 67,64; O: 22,49; Na: 3,52; Mg: 0,28; P: 0,92; Cl: 4,47; K: 0,26; Ca: 0,43
B	1. C: 52,94; O: 25,89; Na: 2,05; Mg: 0,32; P: 0,90; Cl: 5,53; K: 0,40; Ca: 11,97 2. C: 69,37; O: 18,79; Na: 2,31; Mg: 0,14; P: 2,64; Cl: 5,49; K: 0,39; Ca: 0,88
C	1. C: 34,78; O: 33,51; Na: 3,08; Mg: 0,49; P: 10,84; Cl: 3,82; K: 0,10; Ca: 13,40 2. C: 33,93; O: 34,20; Na: 2,57; Mg: 0,29; P: 7,93; Cl: 2,14; K: 0,10; Ca: 10,85
D	1. C: 38,52; O: 32,41; Na: 0,77; Mg: 0,13; P: 8,94; Cl: 1,09; K: 0,13; Ca: 18,02 2. C: 36,92; O: 38,72; Na: 1,09; Mg: 0,33; P: 8,06; Cl: 0,93; K: 0,06; Ca: 13,89

W świetle powyższych wyników wykazano, że niewielkie zmiany kompozycji materiałowej wpływają na parametry fizykochemiczne oraz mechaniczne powłok. Potwierdzono zdolność do mineralizacji w warunkach laboratoryjnych, jak również potencjał oraz potrzebę dalszych badań nad opracowanymi w ramach pracy doktorskiej powłokami kompozytowymi, w tym badań cytotoksyczności w celu wyeliminowania ewentualnego negatywnego wpływu na tkanki oraz modyfikację substancjami aktywnymi.

6.4. Bioaktywna powłoka kompozytowa o właściwościach przeciwbakteryjnych: analiza fizykochemiczna i biologiczna [P6]

W kolejnym etapie badań dla opracowanych powłok przeprowadzono analizę kinetyki pęcznienia w buforze PBS. Na podstawie zmian masy materiałów w czasie wyznaczono zdolność sorpcyjną. Do opisu kinetyki procesu wykorzystano model Voigta, określając parametry S_e oraz τ.

Bazowe powłoki polimerowe bez dodatku HAp (A i B) charakteryzowały się S_e na poziomie odpowiednio 108,97 ± 4,68 % i 115,23 ± 5,10 %, a czas osiągnięcia równowagi τ wynosił kolejno 32,72 ± 8,39 min oraz 30,06 ± 8,01 min. Wprowadzenie do kompozycji HAp w ilości 5 % (próbka C) skutkowało obniżeniem S_e do 100,44 ± 4,35 % i wydłużeniem τ do 43,24 ± 11,27 min. Wyniki te potwierdziły wcześniejsze obserwacje, zgodnie z którymi zwiększenie udziału fazy ceramicznej

ogranicza zdolność do absorpcji płynu oraz spowalnia proces jego penetracji do wnętrza materiału. Efekt ten jest związany z obecnością ziaren ceramiki, które zajmują przestrzeń między łańcuchami polimerowymi, ograniczając tym samym przestrzenie mogące zostać zapełnione przez cząsteczki płynu. Zdolność do absorpcji płynów, jest istotnym parametrem z punktu widzenia potencjalnego zastosowania w charakterze nośnika substancji aktywnych, ponieważ wpływa na efektywność uwalniania substancji aktywnych z wnętrza materiałów. Z tego powodu, i biorąc pod uwagę uzyskane wcześniej wyniki, materiały powłokowe A-C zmodyfikowano antybiotykiem – klindamycyną (Tabela 5). Otrzymano powłoki gdzie lek został związany z matrycą polimerową lub z HAp, oraz kompozycję w których antybiotyk znajdował się zarówno w fazie ceramicznej jak i polimerowej.

Tabela 5: Kompozycja powłok modyfikowanych lekiem.

Powłoka	Kompozycja
1	Powłoka A z lekiem w matrycy polimerowej
2	Powłoka B z lekiem w matrycy polimerowej
3	Powłoka C z HAp modyfikowanym lekiem
4	Powłoka C z lekiem w matrycy polimerowej
5	Powłoka C z lekiem w matrycy polimerowej i z HAp modyfikowanym lekiem

Profil uwalniania klindamycyny analizowano metodą HPLC (Rysunek 10). Po 24 h powłoki polimerowe 1 i 2 uwolniły 35,0 % oraz 36,8 % leku. Zaobserwowana wyższa wartość dla powłoki 2 pozostała w korelacji z wyższymi zdolnościami sorpcyjnymi. Dla powłoki kompozytowej z lekiem w fazie polimerowej lub dwóch, zaobserwowano niewielkie zmiany w ilości uwolnionego leku, na poziomie ok. 1 % po 24 h. Dla wszystkich badanych powłok uzyskano dobrą

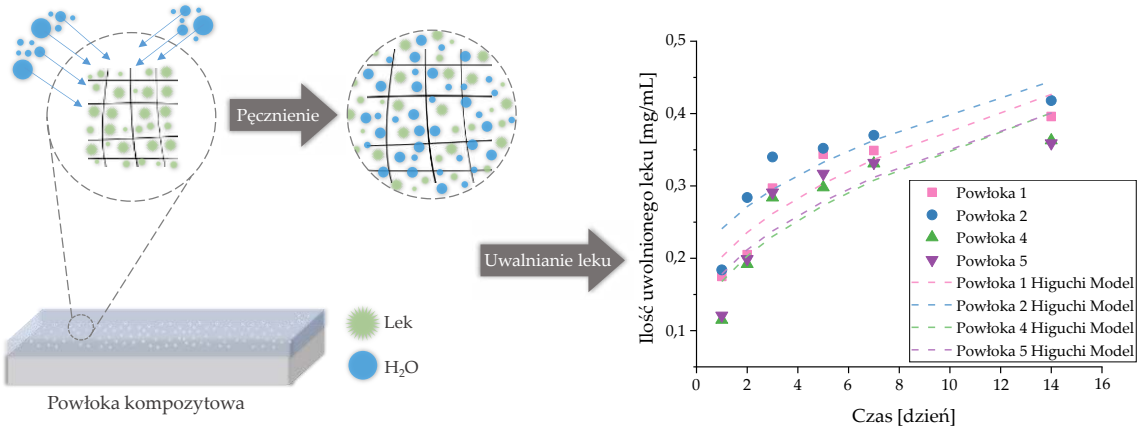

Rysunek 10: Schemat pęcznienia materiału w wyniku penetracji roztworu wodnego oraz szybkość uwalniania antybiotyku z powłok do roztworu PBS.

zgodność z modelem Higuchiego, co wskazuje, że głównym mechanizmem uwalniania klindamycyny była dyfuzja, zgodna z pierwszym prawem Ficka.

Ponadto po procesie inkubacji w PBS przeprowadzono obrazowanie SEM oraz EDS w celu oceny morfologii powierzchni i składu pierwiastkowego (Rysunek 11a). Szczególnie interesujące wyniki uzyskano dla powłoki C, na której powierzchni pojawiły się wytrącenia wtórnych warstw apatytowych, co potwierdza wysoką bioaktywność i potencjał do indukowania procesu mineralizacji.

Przeprowadzona analiza biozgodności badanych biomateriałów obejmowała ocenę działania przeciwbakteryjnego, zdolności hamowania wzrostu biofilmu bakteryjnego, cytokompatybilność oraz odpowiedź organizmu (*in vivo*) na implantację. Aktywność przeciwbakteryjną testowano wobec szczepu *Staphylococcus aureus ATCC 29213*. Badaniu poddano materiały nie zawierające klindamycyny, oznaczone jako A i C stanowiące referencję, oraz powłoki zawierające lek oznaczone numerami: 1, 3, 4 i 5. Powłoki zawierające antybiotyk powodowały znaczną redukcję metabolicznej aktywności bakterii, obniżając ją do poziomu 2,2–2,9 % w porównaniu z kontrolą ($p < 0,001$). Takiego efektu nie zaobserwowano dla materiałów bazowych. Analiza zdolności do tworzenia biofilmu przy użyciu mikroskopii konfokalnej wykazała, że powłoki z antybiotykiem hamowały wzrost struktur biofilmu już w pierwszej dobie inkubacji, a efekt ten utrzymywał się w kolejnych dniach, co świadczy o skutecznym, długotrwałym działaniu przeciwdrobnoustrojowym.

Cytotoksyczność oceniano z użyciem fibroblastów myszy linii L929 oraz ludzkich komórek osteoblastopodobnych hFOB 1.19, zgodnie z normą ISO-10993-5-2009. Aktywność metaboliczna komórek dla wszystkich materiałów mieściła się w przedziale 90-100 %, czyli powyżej minimalnego progu 70 % wymaganego przez normę ISO. Uzyskane wyniki potwierdziły bezpieczeństwo materiałów oraz brak negatywnego wpływu modyfikacji lekiem na cytozgodność.

Prowadzona analiza biologiczna *in vitro* stanowiła podstawę do przeprowadzenia badania *in vivo* z użyciem modelu zwierzęcego, polegającego na implantacji podskórnej biomateriałów u dorosłych szczurów rasy Wistar (łac. *Rattus norvegicus*) (Rysunek 11b). W świetle dotychczas uzyskanych wyników do badania *in vivo* wybrano powłokę kompozytową referencyjną - C, niemodyfikowaną klindamycyną i zawierającą 5 % HAp, oraz powłokę modyfikowaną lekiem - 4. Badanie przeprowadzono zgodnie z normą PN-EN ISO 10993-6:2017 dotyczącą oceny miejscowej reakcji zapalnej po 7 i 30 dniach od implantacji. W badaniu nie stwierdzono występowania miejscowych czy ogólnoustrojowych objawów stanu zapalnego u zwierząt. Co więcej, w surowicach zwierząt oznaczano stężenia cytokin prozapalnych (IL-1β, TNF-α) oraz przeciwzapalnej (IL-10) metodą ELISA. Uzyskane wartości były porównywalne z tymi uzyskanymi dla grupy kontrolnej zwierząt, co potwierdza brak reakcji zapalnej i dobrą tolerancję implantu przez organizm. Zgoda na przeprowadzenie eksperymentów *in vivo* została wydana przez Lokalną Komisję

Etyki ds. Doświadczeń na Zwierzętach przy Uniwersytecie Medycznym w Łodzi (nr 42/LB 192-UZ-A/2021).

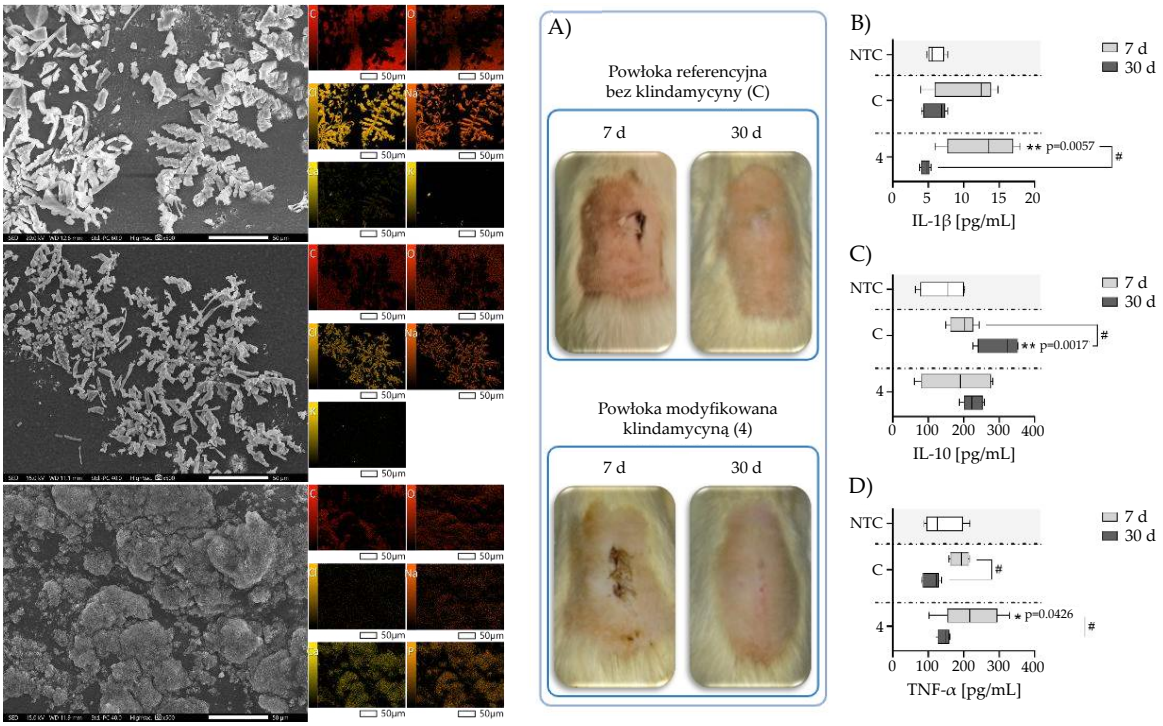

*Rysunek 11: (a) Analiza morfologii powierzchni powłok modyfikowanych klindamycyną po inkubacji w PBS; powłoka 1 (góra), powłoka 2 (środek) powłoka 4 (dół) wraz z mapowaniem pierwiastków; (b) Reprezentatywne zdjęcia przedstawiające miejsca implantacji biomateriałów: Powłoka referencyjna bez klindamycyny (C) oraz kompozyt modyfikowany klindamycyną (powłoka 4) po 7 i 30 dniach od implantacji. Stężenie interleukiny 1 beta - IL-1β (B), interleukiny 10 - IL-10 (C) oraz czynnika martwicy nowotworu α - TNF-α (D) w próbkach surowicy pobranych od zwierząt po 7 i 30 dni od implantacji. NTC - kontrola niepoddana implantacji (szczury, którym nie wszczepiono biomateriałów). Liczba zwierząt n = 3. * - Istotność statystyczna względem grupy NTC w danym punkcie czasowym, wartość p podana po „*"; # - Istotność statystyczna (p<0,05) w odniesieniu do punktów czasowych w grupie. Dane przedstawiono jako wartości minimalne i maksymalne oznaczone linią.*

Przeprowadzone badania potwierdziły, że opracowane wielofunkcyjne powłoki kompozytowe modyfikowane antybiotykiem, mogą łączyć w sobie zdolność do uwalniania leku, bioaktywność oraz właściwości przeciwdrobnoustrojowe, przy zachowaniu wysokiej biokompatybilności.

6.5. Wielofunkcyjna, bioaktywna powłoka kompozytowa o charakterze nośnika substancji aktywnych: analiza fizykochemiczna i ocena bezpieczeństwa *in vivo* [P7]

W kolejnym etapie prac kontynuowano badania nad możliwością funkcjonalizacji biologicznej opracowanych powłok kompozytowych, w kierunku materiałów zdolnych do aktywnego wspierania procesów regeneracji poprzez modulowanie mikrośrodowiska tkankowego, ograniczanie infekcji i stymulację osteogenezy oraz angiogenezy. Wybrane czynniki wzrostu tj. VEGF-165 i TGF-β1,

będącymi związkami ukierunkowanymi na indukcję procesów angiogenezy i osteogenezy, zawieszono w matrycy polimerowej. Powłoki nanoszono na podłoża kompozytowe PLLA/HAp, a następnie sieciowano promieniowaniem UV (czas 4 min, dawka 0,8 J/cm²). W oparciu o dotychczas otrzymane wyniki, do modyfikacji GF wytypowano powłokę zawierającą 5 % fazy ceramicznej oznaczoną symbolem C. Decyzja ta była podyktowana w oparciu o rezultaty analizy trybologicznej, mechanicznej oraz zdolności sorpcyjnych.

Przeprowadzono analizę fizykochemiczną określającą szybkość sedymentacji ziaren HAp w mieszaninie polimerowe PVP:PEG. Badanie to pozwoliło zoptymalizować czas procesu fotosieciowania materiałów w świetle UV, który pozwolił uniknąć nadmiernej sedymentacji fazy (Rysunek 12a). Analiza FTIR polimerów bazowych oraz czynnika sieciującego potwierdziła skuteczny mechanizm fotosieciowania. Wykazano obecność nowych wiązań kowalencyjnych, których obecność wskazuje na powstanie wzajemnie przenikającej się sieci polimerowych (IPN). Powstanie nowych wiązań i sieć IPN, umożliwia modyfikację materiałów związkami aktywnymi, poprzez zamknięcie ich w strukturze oraz ich stopniowe uwalnianie w warunkach fizjologicznych. Przeprowadzono również analizę FTIR dla powłoki zawierającej czynniki wzrostu oraz CLD, które wykazały obecność grup charakterystycznych dla poszczególnych składników. Ocena morfologii SEM ukazała chropowatą strukturę. Przeprowadzona analiza EDX wykazała, że w próbkach z antybiotykiem widoczna była obecność jonów chloru pochodzących od leku, natomiast w powłokach zawierających czynniki wzrostu odnotowano sygnały siarki, związane z obecnością mostków disiarczkowych białek VEGF i TGF-β1. Wyniki te potwierdzają obecność substancji aktywnych w materiałach.

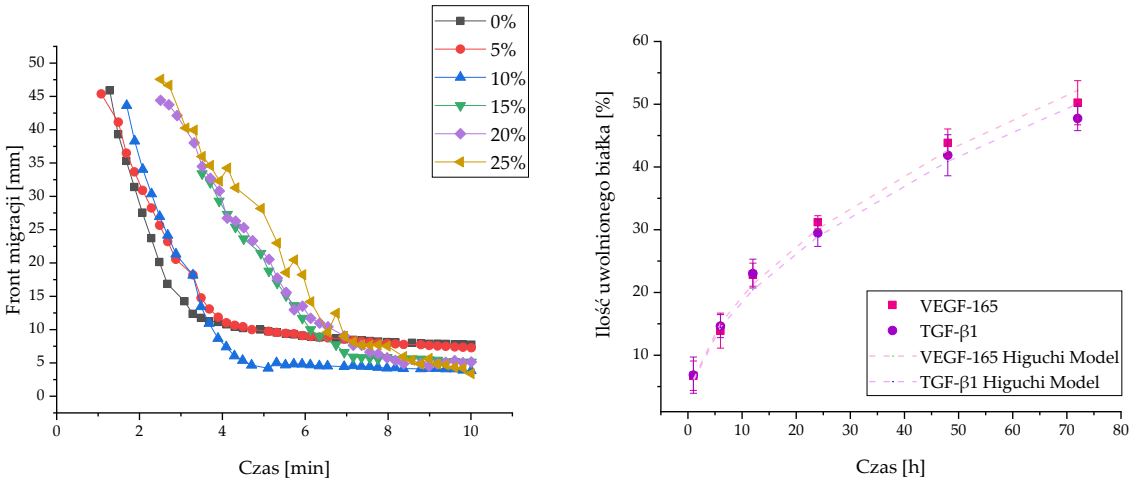

Rysunek 12: (a) Front migracji w funkcji czasu dla proszków HAp w roztworach wodnych PVP:PEG o różnych stężeniach; (b) Skumulowane profile uwalniania VEGF-165 i TGF-β1 z powłoki C/GF po 72 godzinach inkubacji w płynie PBS. Linie przerywane przedstawiają dopasowanie modelu Higuchi, wskazujące na mechanizm uwalniania kontrolowany dyfuzją.

Celem uzupełnienia poprzednio przeprowadzonych badań dotyczących uwalniania klindamycyny, przeprowadzono ocenę kinetyki uwalniania czynników wzrostu w PBS (Rysunek 12b). Zaobserwowano charakterystyczny profil dwufazowy, wskazujący na intensywne początkowe uwalnianie GF w ciągu pierwszych 24 h, podczas którego do medium uwolniło się 31,2 % VEGF-165 i 29,5 % TGF-β1, a następnie fazę dyfuzyjną, kontrolowaną mechanizmem Fickowskim. Po 72 godzinach łączna ilość uwolnionych czynników wzrostu osiągnęła 50,2 % dla VEGF-165 oraz 47,7 % dla TGF-β1. Analiza kinetyki uwalniania wykazała dobrą zgodność z modelem Higuchiego, co potwierdziło, że proces przebiega w sposób kontrolowany dyfuzją w matrycy polimerowej, a tempo elucji zależy od przenikania cząsteczek przez sieć polimerową powstałą na skutek uprzedniej ekspozycji na UV.

W wyniku przeprowadzonych dotychczas badań fizykochemicznych oraz oceny bezpieczeństwa *in vitro* i *in vivo*, materiały skierowano na kolejny etap badań obejmujący ocenę bioefektywności, stosując model *in vivo* – zarastania ubytku kości czaszki dorosłego szczura rasy Wistar (łac. *Rattus norvegicus*), masa ≥220 g, wiek ≥10 tygodni. Monitorowano zarówno reakcję miejscową (miejsce implantacji), jak i systemową organizmu, w celu wykluczenia wystąpienia patologicznej reakcji zapalnej. Ocenę reakcji ogólnoustrojowej przeprowadzono oznaczając stężenia wybranych cytokin w surowicach zwierząt metodą ELISA. Wyniki jednoznacznie wskazały na brak patologicznej reakcji zapalnej, a stężenia cytokin prozapalnych IL-1β i TNF-α pozostawały na poziomie porównywalnym do kontroli. Również stężenie IL-10 mierzonej w surowicach świadczyło o utrzymaniu równowagi immunologicznej i modulacji w kierunku procesów regeneracyjnych (Rysunek 13a). Co istotne, u zwierząt, którym implementowano materiał z czynnikami wzrostu oraz klindamycyną stwierdzono podwyższony poziom OPN, białka zaangażowanego w przebudowę kości (Rysunek 13b). Obserwacje mikroskopowe (fluorescencja) fragmentów czaszki z zaimplementowanym kompozytem wykazały mineralizację kości w miejscach powstawania nowej tkanki kostnej, czyli w miejscach kontaktu implantu z kością. Obserwacja ta dotyczyła szczególnie zwierząt otrzymujących kompozyty zawierające czynniki wzrostu VEGF-165 i TGF-β1, co potwierdza ich rolę w stymulowaniu angiogenezy i wspieraniu osteogenezy (Rysunek 13b). Zgoda na przeprowadzenie eksperymentów *in vivo* została wydana przez Lokalną Komisję Etyki ds. Doświadczeń na Zwierzętach przy Uniwersytecie Medycznym w Łodzi (nr 34/LB240/2022).

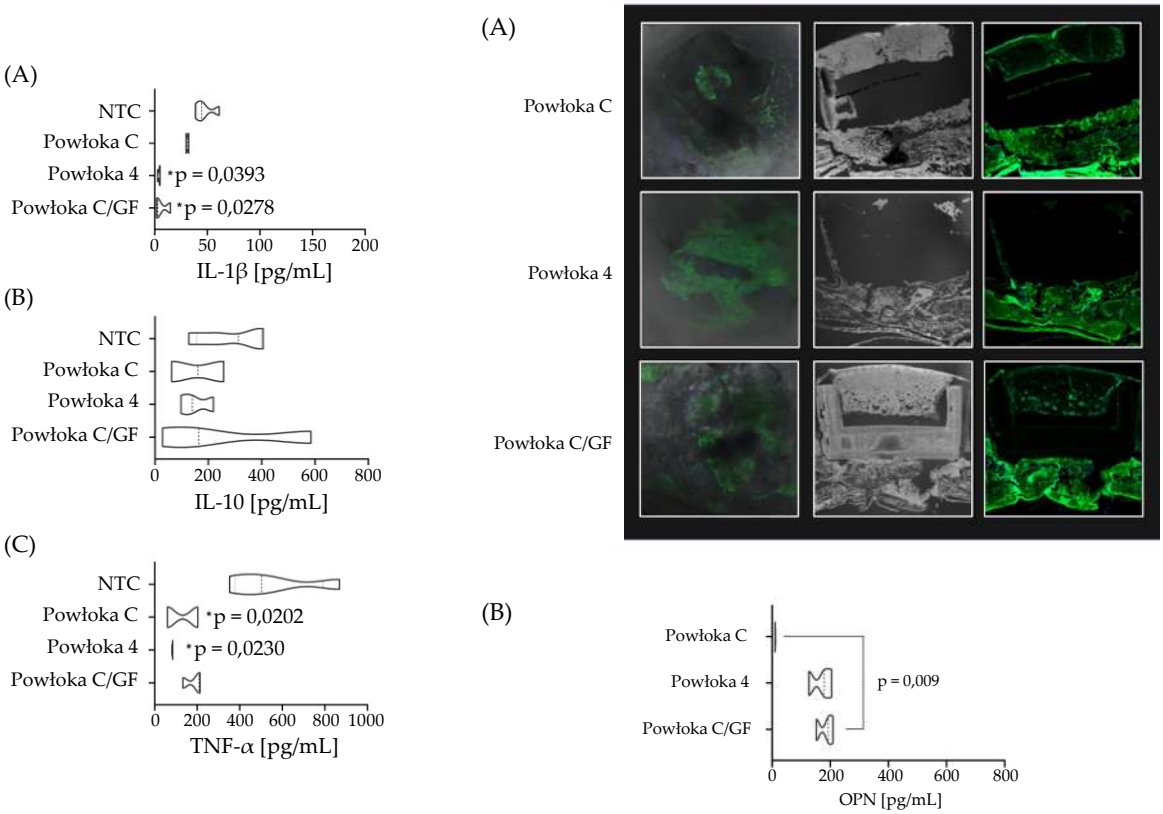

Rysunek 13: (a) Stężenie IL-1β (A), IL-10 (B) i TNF-α (C) w surowicach pobranych od zwierząt po wszczepieniu biomateriałów. NTC – kontrola, zwierzęta, którym nie wszczepiono biomateriałów; (b) Reprezentatywne zdjęcia przedstawiające przekroje czaszki szczura, zawierające wszczepiony biomateriał i przedstawiające procesy mineralizacji kości po 8 tygodniach od implantacji. Sygnał fluorescencji (zielony) odzwierciedla wbudowanie barwnika Xylenol orange, podanego *in vivo* na 72 godziny przed eutanazją i wskazuje na miejsca aktywnej mineralizacji kości (A). Poziom osteopontyny (OPN) w surowicach zwierząt (B).

Opisane w pracy wielofunkcyjne, bioaktywne powłoki kompozytowe wykazują wysoką aktywność biologiczną, wspierającą regenerację tkanki kostnej co potwierdzono dotychczas przeprowadzonymi badaniami. Materiał działa przeciwdrobnoustrojowo dzięki obecności klindamycyny, za sprawą obecności GF stymuluje angiogenezę oraz osteogenezę, jak również wykazuje bioaktywność wynikającą z charakteru HAp. Potwierdzona eksperymentalnie zdolność do kontrolowanego uwalniania wybranych substancji aktywnych w symulowanym środowisku biologicznym potwierdza ich potencjał do pełnienie roli systemu DDS. Wyniki uzyskane zarówno w badaniach *in vitro*, jak i na modelu zwierzęcym, potwierdzają wysoką biokompatybilność, brak reakcji zapalnych oraz potencjał regeneracyjny w warunkach *in vivo*, czyniąc opracowaną technologię obiecującą strategią dla dalszego rozwoju implantów kostnych nowej generacji.

7. Wnioski końcowe

W wyniku prac przeprowadzonych w ramach niniejszej rozprawy doktorskiej opracowano wielofunkcyjne, powłokowe materiały kompozytowe o charakterze nośnika substancji aktywnych, które poddano kompleksowej analizie. Na podstawie otrzymanych wyników sformułowano następujące wnioski:

- Zaproponowana metoda mokrego strącenia, przeprowadzona w temperaturze wrzenia odczynników pozwala na uzyskanie fosforanu wapnia o strukturze HAp, charakteryzującego się czystością fazową, rozwiniętą powierzchnią właściwą oraz stosunkiem molowym Ca/P zbliżonym do HAp stechiometrycznego.
- Zmiana stosunków reagentów oraz pH środowiska reakcyjnego w którym prowadzona jest synteza fosforanów wapnia, skutkuje zmianą właściwości fizykochemicznych proszków ceramicznych, w tym zmianą stopnia krystaliczności.
- Proces sorpcji fizycznej proszków fosforanowo-wapniowych w roztworze klindamycyny umożliwia otrzymanie nośników leków wykazujących właściwości przeciwdrobnoustrojowe wobec bakterii *Staphylococcus aureus*.
- Uwalnianie leku z ceramicznych nośników jest zależne od rozwinięcia powierzchni właściwej proszku.
- Powłoki kompozytowe bazujące na matrycy PVP:PEG, zawierające HAp, otrzymywane metodą fotosieciowania w świetle UV, wykazują stabilność, biokompatybilność oraz korzystną kinetykę pęcznienia, potwierdzającą potencjał do zastosowania jako nośnik substancji czynnych.
- Wprowadzenie HAp do matrycy polimerowej powoduje zmianę właściwości powłok, w tym obniżenie zdolności sorpcyjnych, zwiększenie twardości oraz modułu sprężystości, przy jednoczesnym obniżeniu zdolności do odkształcalności. Dodatek HAp na poziomie 15 % powoduje większe zużycie tribologiczne powłoki.
- Wprowadzenie kolagenu do matrycy polimerowej powoduje zwiększenie zdolności sorpcyjnych oraz obniżenie współczynnika tarcia i zużycia.
- Modyfikacja powłok kompozytowych klindamycyną umożliwia uzyskanie systemów do kontrolowanego uwalniania leku, przy czym uwalnianie leku zachodzi szybciej z fazy polimerowej niż z fazy ceramicznej. Opracowane nośniki są biozgodne i wykazują właściwości przeciwdrobnoustrojowe wobec bakterii *Staphylococcus aureus*.
- Zarówno powłoki z antybiotykiem jak i bez antybiotyku nie generują stanów zapalnych u zwierząt co potwierdziła analiza *in vivo*. Stężenia cytokin prozapalnych IL-1β i TNF-α oraz przeciwzapalnej IL-10 potwierdzają brak reakcji zapalnej i dobrą tolerancję implantu przez organizm.
- Modyfikacja powłok kompozytowych czynnikami wzrostu VEGF-165 i TGF- β1 umożliwia uzyskanie nośników substancji aktywnych,

które uwalniane lokalnie wspierają mineralizację nowej tkanki, co potwierdzono badaniami *in vivo* na modelu zwierzęcym.

Cel naukowy oraz utylitarny niniejszej rozprawy doktorskiej został w pełni zrealizowany, a uzyskane wyniki potwierdzają zasadność postawionej tezy badawczej. Opracowana, wielofunkcyjna powłoka kompozytowa składająca się z fazy polimerowej i ceramicznej, modyfikowana substancjami aktywnymi wykazywała korzystne właściwości fizykochemiczne, mechaniczne oraz biologiczne, istotne dla wspierania procesu regeneracji tkanki kostnej oraz ograniczenia ryzyka infekcji i reakcji zapalnych. Szczególnie obiecująca okazała się kompozycja zawierająca polimery syntetyczne, kolagen, glutation oraz 5 % hydroksyapatytu, dodatkowo modyfikowana klindamycyną i czynnikami wzrostu VEGF-165 oraz TGF- β1. Tak opracowana bioaktywna powłoka może pełnić rolę nośnika substancji czynnych, zapewniając równocześnie działanie przeciwdrobnoustrojowe i stymulację mineralizacji nowej tkanki kostnej. Może zostać zaaplikowana na inne, komercyjnie wykorzystywane inertne biomateriały lub implanty o niskiej bioaktywności, jak również stanowić samodzielne rozwiązanie materiałowe.

Uzyskane w ramach niniejszej rozprawy doktorskiej wyniki badań wykazały, że dzięki kontroli składu oraz kierunkowej funkcjonalizacji, możliwe jest racjonalne projektowanie wielofunkcyjnych powłok kompozytowych, co stwarza nowe możliwości rozwoju materiałów stosowanych do regeneracji tkanki kostnej. Uzyskane rezultaty badań stanowią solidną podstawę do optymalizacji procesu nanoszenia powłok, a także do badań przedklinicznych oraz translacyjnych, których celem będzie potwierdzenie skuteczności i bezpieczeństwa biomateriałów w warunkach zbliżonych do praktyki klinicznej. Takie podejście umożliwia ścieżkę wdrożenia zaproponowanych powłok kompozytowych do zastosowań medycznych, w szczególności leczeniu i wspomaganiu regeneracji tkanki kostnej przy zabiegach obarczonych wysokim ryzykiem infekcji.

LITERATURA

(1) Meier, M. A. R.; Tam, M. K. C. Shaping Effective Practices for Incorporating Sustainability Assessment in Manuscripts Submitted to ACS Sustainable Chemistry & Engineering: Biomaterials. *ACS Sustainable Chemistry and Engineering* 2021, *9* (22), 7400–7402. https://doi.org/10.1021/acssuschemeng.1c03382.

(2) Kumar, N.; Kumar, V.; Gangwar, A. K.; Shrivastava, S.; Saxena, S.; Khangembam, S. D.; Maiti, S. K.; Udehiya, R. K.; Mishra, M.; Raghuvanshi, P. D. S.; Singh, N. K. *An Introduction to Biomaterials*; 2024. https://doi.org/10.1016/B978-0-443-26470-2.00001-6.

(3) Thangaraju, P.; Varthya, S. B. ISO 10993: Biological Evaluation of Medical Devices. *Medical Device Guidelines and Regulations Handbook* 2022, 163–183. https://doi.org/10.1007/978-3-030-91855-2_11.

(4) Huzum, B.; Puha, B.; Necoara, R.; Gheorghevici, S.; Puha, G.; Filip, A.; Sirbu, P.; Alexa, O. Biocompatibility Assessment of Biomaterials Used in Orthopedic Devices: An Overview (Review). *Experimental and Therapeutic Medicine* 2021, *22* (5), 1–9. https://doi.org/10.3892/etm.2021.10750.

(5) Series, B.; Alerts, C. Advances in Ceramics - Electric and Magnetic Ceramics, Bioceramics, Ceramics and Environment. *Advances in Ceramics - Electric and Magnetic Ceramics, Bioceramics, Ceramics and Environment* 2012, 1–21. https://doi.org/10.5772/726.

(6) Bose, S.; Bandyopadhyay, A. *Introduction to Biomaterials*; Elsevier, 2013. https://doi.org/10.1016/B978-0-12-415800-9.00001-2.

(7) Chong, E. T. J.; Ng, J. W.; Lee, P.-C. Classification and Medical Applications of Biomaterials–A Mini Review. *BIO Integration* 2022, *4* (2), 54–61. https://doi.org/10.15212/bioi-2022-0009.

(8) John Cuppoletti. *Metal, Ceramic and Polymeric Composites for Various Uses*; 2011.

(9) *Market Research Future. Biomaterials Market Research Report By Application (Medical Devices, Tissue Engineering, Drug Delivery, Orthopedics, Wound Care), By Type (Natural Biomaterials, Synthetic Biomaterials, Modified Biomaterials), By Source (Plant-Based*; 2025; Vol. MRFR/1489-. https://www.marketresearchfuture.com/reports/biomaterial-market-2021.

(10) World Health Organization. *Ageing and health*. Ageing and health. https://www.knowledge-action-portal.com/en/content/ageing-and-health.

(11) Markets and Markets Research. *Biomaterials Market: Growth, Size, Share and Trends, Report Code: BT 1556*; 2024. https://www.marketsandmarkets.com/Market-Reports/biomaterials-393.html.

(12) Braga, R. R. Calcium Phosphates as Ion-Releasing Fillers in Restorative Resin-Based Materials. *Dental Materials*. 2019. https://doi.org/10.1016/j.dental.2018.08.288.

(13) de Groot, K. *Bioceramics of Calcium Phosphate*; 2018. https://doi.org/10.1201/9781351070133.

(14) Hassan, M. N.; Eltawila, A. M.; Mohamed-Ahmed, S.; Amin, W. M.; Suliman, S.;

Kandil, S.; Yassin, M. A.; Mustafa, K. Correlation between Ca Release and Osteoconduction by 3D-Printed Hydroxyapatite-Based Templates. *ACS Applied Materials and Interfaces* 2024, *16* (22), 28056–28069. https://doi.org/10.1021/acsami.4c01472.

(15) Duraisamy, R.; Ganapathy, D.; Shanmugam, R.; Thangavelu, L. Systematic Review on Hydroxyapatite and Chitosan Combination-Coated Titanium Implants on Osseointegration. *World Journal of Dentistry* 2024, *15* (1), 79–86. https://doi.org/10.5005/jp-journals-10015-2358.

(16) Abere, D. V.; Ojo, S. A.; Oyatogun, G. M.; Paredes-Epinosa, M. B.; Niluxsshun, M. C. D.; Hakami, A. Mechanical and Morphological Characterization of Nano-Hydroxyapatite (NHA) for Bone Regeneration: A Mini Review. *Biomedical Engineering Advances* 2022, *4* (October), 100056. https://doi.org/10.1016/j.bea.2022.100056.

(17) Osuchukwu, O. A.; Salihi, A.; Abdullahi, I.; Abdulkareem, B.; Nwannenna, C. S. Synthesis Techniques, Characterization and Mechanical Properties of Natural Derived Hydroxyapatite Scaffolds for Bone Implants: A Review. *SN Applied Sciences* 2021, *3* (10). https://doi.org/10.1007/s42452-021-04795-y.

(18) Anandan, D.; Kumar, A.; Jaiswal, A. K. Comparative Study of Hydroxyapatite Synthesized Using Schiff Base and Wet Chemical Precipitation Methods. *Journal of the Mechanical Behavior of Biomedical Materials* 2023, *148* (October), 106200. https://doi.org/10.1016/j.jmbbm.2023.106200.

(19) Catauro, M.; Ciprioti, S. V. Characterization of Hybrid Materials Prepared by Sol-Gel Method for Biomedical Implementations. A Critical Review. *Materials* 2021, *14* (7). https://doi.org/10.3390/ma14071788.

(20) Makarova, S. V; Borodulina, I. A.; Prosanov, I. Y.; Borisenko, T. A.; Logutenko, O. A.; Natalia, V.; Ishchenko, A. V. Silver-Substituted Hydroxyapatite : Mechanochemical Mechan. *Ceramics International* 2025, *49* (23), 37957–37966.

(21) Oktar, F. N.; Unal, S.; Gunduz, O.; Nissan, B. Ben; Macha, I. J.; Akyol, S.; Duta, L.; Ekren, N.; Altan, E.; Yetmez, M. Marine-Derived Bioceramics for Orthopedic, Reconstructive and Dental Surgery Applications. *Journal of the Australian Ceramic Society* 2023, *59* (1), 57–81. https://doi.org/10.1007/s41779-022-00813-3.

(22) Okpe, P. C.; Folorunso, O.; Aigbodion, V. S.; Obayi, C. Hydroxyapatite Synthesis and Characterization from Waste Animal Bones and Natural Sources for Biomedical Applications. *Journal of Biomedical Materials Research Part B Applied Biomaterials* 2024, *112* (7), e35440. https://doi.org/10.1002/jbm.b.35440.

(23) Mavrych, V.; Bolgova, O.; Abuzubida, A. Comparative X-Ray Diffraction Analysis of the Hydroxyapatite Crystal Structure in Developing and Mature Lumbar Vertebrae. *Cureus* 2025, *17* (5). https://doi.org/10.7759/cureus.84669.

(24) Zhang, H.; Darvell, B. W. Morphology and Structural Characteristics of Hydroxyapatite Whiskers: Effect of the Initial Ca Concentration, Ca/P Ratio and PH. *Acta Biomaterialia* 2011, *7* (7), 2960–2968. https://doi.org/10.1016/j.actbio.2011.03.020.

(25) Agbeboh, N. I.; Oladele, I. O.; Daramola, O. O.; Adediran, A. A.; Olasukanmi, O. O.; Tanimola, M. O. Environmentally Sustainable Processes for the Synthesis of Hydroxyapatite. *Heliyon* 2020, *6* (4), e03765. https://doi.org/10.1016/j.heliyon.2020.e03765.

(26) Fu, Q. Materials Science and Engineering : A Microstructure and Mechanical Properties of SiC Nanowires Reinforced Hydroxyapatite Coating on Carbon / Carbon Composites. 2025, *563* (February 2013), 10–13.

(27) Ma, G. Three Common Preparation Methods of Hydroxyapatite. *IOP Conference Series: Materials Science and Engineering* 2019, *688* (3), 10–13. https://doi.org/10.1088/1757-899X/688/3/033057.

(28) Sobczak-Kupiec, A.; Drabczyk, A.; Florkiewicz, W.; Głąb, M.; Kudłacik-Kramarczyk, S.; Słota, D.; Tomala, A.; Tyliszczak, B. Review of the Applications of Biomedical Compositions Containing Hydroxyapatite and Collagen Modified by Bioactive Components. *Materials* 2021, *14* (9). https://doi.org/10.3390/ma14092096.

(29) Sobczak-Kupiec, A.; Wzorek, Z. Właściwości Fizykochemiczne Ortofosforanów Wapnia Istotnych Dla Medycyny - TCP i HAp. *Chemia - Czasopismo Techniczne* 2010.

(30) Heimann, R. B. Structure, Properties, and Biomedical Performance of Osteoconductive Bioceramic Coatings. *Surface and Coatings Technology* 2013, *233* (August), 27–38. https://doi.org/10.1016/j.surfcoat.2012.11.013.

(31) Du, W.; Guo, X.; Zheng, Q.; Wang, L.; Su, H. Development of a Biodegradable α-TCP/PLA/NMgO Composite for Enhanced Guided Bone Regeneration. *Scientific Reports* 2025, *15* (1), 1–14. https://doi.org/10.1038/s41598-025-03426-5.

(32) Monma, H.; Kanazawa, T. The Hydration of A-Tricalcium Phosphate. 1976.

(33) Patil, S. V.; Shelake, S. S.; Patil, S. S. 11 - Polymeric Materials for Targeted Delivery of Bioactive Agents and Drugs. In *Fundamental Biomaterials: Polymers*; 2018; pp 249–266. https://doi.org/10.1016/B978-0-08-102194-1.00011-6.

(34) Sionkowska, A. Current Research on the Blends of Natural and Synthetic Polymers as New Biomaterials: Review. *Progress in Polymer Science (Oxford)* 2011, *36* (9), 1254–1276. https://doi.org/10.1016/j.progpolymsci.2011.05.003.

(35) Biswal, T. Biopolymers for Tissue Engineering Applications: A Review. *Materials Today: Proceedings* 2019, *41* (xxxx), 397–402. https://doi.org/10.1016/j.matpr.2020.09.628.

(36) Sung, Y. K.; Kim, S. W. Recent Advances in Polymeric Drug Delivery Systems. *Biomaterials Research* 2020, *24* (12), 1–12. https://doi.org/10.1016/j.jconrel.2021.11.025.

(37) Kalirajan, C.; Dukle, A.; Nathanael, A. J.; Oh, T. H.; Manivasagam, G. A Critical Review on Polymeric Biomaterials for Biomedical Applications. *Polymers* 2021, *13* (17), 1–27. https://doi.org/10.3390/polym13173015.

(38) Reddy, M. S. B.; Ponnamma, D.; Choudhary, R.; Sadasivuni, K. K. A Comparative Review of Natural and Synthetic Biopolymer Composite Scaffolds. *Polymers* 2021, *13*

(7). https://doi.org/10.3390/polym13071105.

(39) Salvatore, L.; Gallo, N.; Natali, M. L.; Campa, L.; Lunetti, P.; Madaghiele, M.; Blasi, F. S.; Corallo, A.; Capobianco, L.; Sannino, A. Marine Collagen and Its Derivatives: Versatile and Sustainable Bio-Resources for Healthcare. *Materials Science and Engineering C* 2020, *113* (April), 110963. https://doi.org/10.1016/j.msec.2020.110963.

(40) Shenoy, M.; Abdul, N. S.; Qamar, Z.; Bahri, B. M. Al; Al Ghalayini, K. Z. K.; Kakti, A. Collagen Structure, Synthesis, and Its Applications: A Systematic Review. *Cureus* 2022, *14* (5). https://doi.org/10.7759/cureus.24856.

(41) Porter, J. R.; Ruckh, T. T.; Popat, K. C. Bone Tissue Engineering: A Review in Bone Biomimetics and Drug Delivery Strategies. *Biotechnology Progress* 2009, *25* (6), 1539–1560. https://doi.org/10.1002/btpr.246.

(42) Kusnadi, K.; Herdiana, Y.; Rochima, E.; Putra, O. N.; Gazzali, A. M.; Muchtaridi, M. Collagen-Based Nanoparticles as Drug Delivery System in Wound Healing Applications. *International Journal of Nanomedicine* 2024, *19* (November), 11321–11341. https://doi.org/10.2147/IJN.S485588.

(43) Jafary, F.; Hanachi, P.; Gorjipour, K. Osteoblast Differentiation on Collagen Scaffold with Immobilized Alkaline Phosphatase. *International Journal of Organ Transplantation Medicine* 2017, *8* (4), 195–202.

(44) He, Q.; Feng, T.; Xie, Y.; Swamiappan, S.; Zhou, Y.; Zhou, Y.; Zhou, H.; Peng, X. Recent Advances in the Development and Application of Cell-Loaded Collagen Scaffolds. *International Journal of Molecular Sciences* 2025, *26*, 4009. https://doi.org/10.1039/c6an01285j.

(45) La Monica, F.; Campora, S.; Ghersi, G. Collagen-Based Scaffolds for Chronic Skin Wound Treatment. *Gels* 2024, *10* (2). https://doi.org/10.3390/gels10020137.

(46) Cao, C.; Huang, P.; Prasopthum, A.; Parsons, A. J.; Ai, F.; Yang, J. Characterisation of Bone Regeneration in 3D Printed Ductile PCL/PEG/Hydroxyapatite Scaffolds with High Ceramic Microparticle Concentrations. *Biomaterials Science* 2022, *10* (1), 138–152. https://doi.org/10.1039/d1bm01645h.

(47) Ibrahim, M.; Ramadan, E.; Elsadek, N. E.; Emam, S. E.; Shimizu, T.; Ando, H.; Ishima, Y.; Elgarhy, O. H.; Sarhan, H. A.; Hussein, A. K.; Ishida, T. Polyethylene Glycol (PEG): The Nature, Immunogenicity, and Role in the Hypersensitivity of PEGylated Products. *Journal of Controlled Release* 2022, *351* (November 2022), 215–230. https://doi.org/10.1016/j.jconrel.2022.09.031.

(48) Heuberger, M.; Drobek, T.; Spencer, N. D. Interaction Forces and Morphology of a Protein-Resistant Poly(Ethylene Glycol) Layer. *Biophysical Journal* 2005, *88* (1), 495–504. https://doi.org/10.1529/biophysj.104.045443.

(49) Asghari Niari, S.; Rahbarghazi, R.; Salehi, R.; Kazemi, L.; Fathi Karkan, S.; Karimipour, M. Fabrication, Characterization and Evaluation of the Effect of PLGA and PLGA–PEG Biomaterials on the Proliferation and Neurogenesis Potential of Human Neural SH-SY5Y Cells. *Microscopy Research and Technique* 2022, *85* (4), 1433–1443.

https://doi.org/10.1002/jemt.24006.

(50) Bianchi, M.; Pegoretti, A.; Fredi, G. An Overview of Poly(Vinyl Alcohol) and Poly(Vinyl Pyrrolidone) in Pharmaceutical Additive Manufacturing. *Journal of Vinyl and Additive Technology* 2023, *29* (2), 223–239. https://doi.org/10.1002/vnl.21982.

(51) Franco, P.; De Marco, I. The Use of Poly(N-Vinyl Pyrrolidone) in the Delivery of Drugs: A Review. *Polymers* 2020, *12* (5), 18–21. https://doi.org/10.3390/POLYM12051114.

(52) Schwartz, W. *A Critical Review of the Kinetics and Toxicology of Polyvinylpyrrolidone (Povidone)*; 2018.

(53) Zhao, C.; Cheng, H.; Jiang, P.; Yao, Y.; Han, J. Preparation of Lutein-Loaded Particles for Improving Solubility and Stability by Polyvinylpyrrolidone (PVP) as an Emulsion-Stabilizer. *Food Chemistry* 2014, *156* (August 2014), 123–128. https://doi.org/10.1016/j.foodchem.2014.01.086.

(54) Waresindo, W. X.; Luthfianti, H. R.; Hapidin, D. A.; Edikresnha, D.; Aimon, A. H.; Suciati, T.; Khairurrijal, K. PVA/PVP-Based Hydrogel with Good Swelling Ability for Potential Wound Dressing Applications. *AIP Conference Proceedings* 2025, *3197* (1), 9–13. https://doi.org/10.1063/5.0242515.

(55) Krings, W.; Gorb, S. N. Editorial: Composite Materials in Biological and Bioinspired Systems. *Interface Focus* 2024, *14* (2), 1–7. https://doi.org/10.1098/rsfs.2024.0008.

(56) Abbas, M.; Alqahtani, M. S.; Alhifzi, R. Recent Developments in Polymer Nanocomposites for Bone Regeneration. *International Journal of Molecular Sciences* 2023, *24* (4). https://doi.org/10.3390/ijms24043312.

(57) Li, X.; Guo, Z.; Huang, Q.; Yuan, C. Research and Application of Biomimetic Modified Ceramics and Ceramic Composites: A Review. *Journal of the American Ceramic Society* 2024, *107* (2), 663–697. https://doi.org/10.1111/jace.19490.

(58) Sadat-Shojai, M.; Khorasani, M. T.; Dinpanah-Khoshdargi, E.; Jamshidi, A. Synthesis Methods for Nanosized Hydroxyapatite with Diverse Structures. *Acta Biomaterialia* 2013, *9* (8), 7591–7621. https://doi.org/10.1016/j.actbio.2013.04.012.

(59) Senra, M. R.; Vieira Marques, M. de F. Synthetic Polymeric Materials for Bone Replacement. *Journal of Composites Science* 2020, *4* (4). https://doi.org/10.3390/jcs4040191.

(60) Vaz, M. F.; Canhao, H.; Fonseca, J. E. Bone: A Composite Natural Material. In *Advances in Composite Materials: Analysis of Natural and Man-Made Materials*; Web Of Science, 2011; pp 195-.

(61) Braszczyńska-Malik, K.; Pędzich, Z.; Pietrzak, K.; Rosłaniec, Z.; Sterzyński, T.; Szweycer, M. Problemy Terminologii W Kompozytach. *Kompozyty (Composites)* 2005, *5* (1), 19–24.

(62) Sumithra, G.; Reddy, R. N.; Dheeraj Kumar, G.; Ojha, S.; Jayachandra, G.; Raghavendra, G. Review on Composite Classification, Manufacturing, and

Applications. *Materials Today: Proceedings* 2023, No. May 2023, 2023–2025. https://doi.org/10.1016/j.matpr.2023.04.637.

(63) Ielo, I.; Calabrese, G.; De Luca, G.; Conoci, S. Recent Advances in Hydroxyapatite-Based Biocomposites for Bone Tissue Regeneration in Orthopedics. *International Journal of Molecular Sciences* 2022, *23* (17). https://doi.org/10.3390/ijms23179721.

(64) Pramanik, S.; Kharche, S.; More, N.; Ranglani, D.; Singh, G.; Kapusetti, G. Natural Biopolymers for Bone Tissue Engineering: A Brief Review. *Engineered Regeneration* 2023, *4* (2), 193–204. https://doi.org/10.1016/j.engreg.2022.12.002.

(65) Xie, H.; Ruan, S.; Zhao, M.; Long, J.; Ma, X.; Guo, J.; Lin, X. Preparation and Characterization of 3D Hydroxyapatite/Collagen Scaffolds and Its Application in Bone Regeneration with Bone Morphogenetic Protein-2. *RSC Advances* 2023, *13* (33), 23010–23020. https://doi.org/10.1039/d3ra03034b.

(66) Guagnini, B.; Medagli, B.; Zumbo, B.; Cannillo, V.; Turco, G.; Porrelli, D.; Bellucci, D. Alginate-Sr/Mg Containing Bioactive Glass Scaffolds: The Characterization of a New 3D Composite for Bone Tissue Engineering. *Journal of Functional Biomaterials* 2024, *15* (7). https://doi.org/10.3390/jfb15070183.

(67) Tan, Y.; Ma, L.; Chen, X.; Ran, Y.; Tong, Q.; Tang, L.; Li, X. Injectable Hyaluronic Acid/Hydroxyapatite Composite Hydrogels as Cell Carriers for Bone Repair. *International Journal of Biological Macromolecules* 2022, *216* (September 2022), 547–557. https://doi.org/10.1016/j.ijbiomac.2022.07.009.

(68) Do, N. H. N.; Truong, Q. T.; Le, P. K.; Ha, A. C. Recent Developments in Chitosan Hydrogels Carrying Natural Bioactive Compounds. *Carbohydrate Polymers* 2022, *294* (March), 119726. https://doi.org/10.1016/j.carbpol.2022.119726.

(69) Dreiss, C. A. Hydrogel Design Strategies for Drug Delivery. *Current Opinion in Colloid & Interface Science* 2020, *48*, 1–17. https://doi.org/10.1016/J.COCIS.2020.02.001.

(70) Wang, F. Z.; Liu, S.; Gao, M.; Yu, Y.; Zhang, W. B.; Li, H.; Peng, X. 3D-Printed Polycaprolactone/Hydroxyapatite Bionic Scaffold for Bone Regeneration. *Polymers* 2025, *17* (7). https://doi.org/10.3390/polym17070858.

(71) Bernardo, M. P.; da Silva, B. C. R.; Hamouda, A. E. I.; de Toledo, M. A. S.; Schalla, C.; Rütten, S.; Goetzke, R.; Mattoso, L. H. C.; Zenke, M.; Sechi, A. PLA/Hydroxyapatite Scaffolds Exhibit *in Vitro* Immunological Inertness and Promote Robust Osteogenic Differentiation of Human Mesenchymal Stem Cells without Osteogenic Stimuli. *Scientific Reports* 2022, *12* (1), 1–15. https://doi.org/10.1038/s41598-022-05207-w.

(72) Safali, S.; Berk, T.; Makelov, B.; Acar, M. A.; Gueorguiev, B.; Pape, H. C. The Possibilities of Personalized 3D Printed Implants—A Case Series Study. *Medicina (Lithuania)* 2023, *59* (2), 1–12. https://doi.org/10.3390/medicina59020249.

(73) Liu, S.; Yu, J. M.; Gan, Y. C.; Qiu, X. Z.; Gao, Z. C.; Wang, H.; Chen, S. X.; Xiong, Y.; Liu, G. H.; Lin, S. E.; McCarthy, A.; John, J. V.; Wei, D. X.; Hou, H. H. Biomimetic Natural Biomaterials for Tissue Engineering and Regenerative Medicine: New Biosynthesis Methods, Recent Advances, and Emerging Applications. *Military Medical*

Research 2023, *10* (1), 1–30. https://doi.org/10.1186/s40779-023-00448-w.

(74) Thakur, A.; Kumar, A. Recent Advancements in the Surface Treatments for Enhanced Biocompatibility and Corrosion Resistance of Titanium-Based Biomedical Implants. *Applied Chemical Engineering* 2024, *7* (1). https://doi.org/10.24294/ace.v7i1.2042.

(75) Liao, J.; Li, X.; Xuan, S.; Zhang, W.; Li, G.; Li, H. Modulating the Corrosion Performance of Magnesium Alloys through Hydroxyapatite Coating. *Chemical Engineering Journal* 2024, *495* (September 2024), 1–11. https://doi.org/10.1016/j.cej.2024.153550.

(76) Wang, B.; Zhang, Z.; Pan, H. Bone Apatite Nanocrystal: Crystalline Structure, Chemical Composition, and Architecture. *Biomimetics* 2023, *8* (1). https://doi.org/10.3390/biomimetics8010090.

(77) Su, L.; Niu, M.; Li, M.; Lu, D.; Guo, P.; Zhuang, L.; Peng, K.; Wang, H. Engineering the Mechanical Properties of Resilient Ceramic Aerogels. *Journal of the American Ceramic Society* 2024, *107* (3), 1468–1480. https://doi.org/10.1111/jace.19318.

(78) K R C, S. R.; R, S.; K, S. R. Ceramic–Polymer Hybrid Coatings for Diverse Applications. *Frontiers in Coatings, Dyes and Interface Engineering* 2024, *2* (August), 1–20. https://doi.org/10.3389/frcdi.2024.1386920.

(79) Hernandez, J. L.; Woodrow, K. A. Medical Applications of Porous Biomaterials: Features of Porosity and Tissue-Specific Implications for Biocompatibility. *Advanced Healthcare Materials* 2022, *11* (9), 1–25. https://doi.org/10.1002/adhm.202102087.

(80) Bose, A.; Burman, D. R.; Sikdar, B.; Patra, P. Nanomicelles: Types, Properties and Applications in Drug Delivery. *IET Nanobiotechnology* 2021, *15* (1), 19–27. https://doi.org/10.1049/nbt2.12018.

(81) Thang, N. H.; Chien, T. B.; Cuong, D. X. Polymer-Based Hydrogels Applied in Drug Delivery: An Overview. *Gels* 2023, *9* (7), 1–38. https://doi.org/10.3390/gels9070523.

(82) Kasza, K.; Gurnani, P.; Hardie, K. R.; Cámara, M.; Alexander, C. Challenges and Solutions in Polymer Drug Delivery for Bacterial Biofilm Treatment: A Tissue-by-Tissue Account. *Advanced Drug Delivery Reviews* 2021, *178* (November 2021). https://doi.org/10.1016/j.addr.2021.113973.

(83) *Drug Delivery Systems Market Size, Share & Industry Analysis, By Type (Inhalation, Transdermal, Injectable, and Others), By Device Type (Conventional and Advanced), By Distribution Channel (Hospital Pharmacies, Retail Pharmacies, and Others), and Regional*; 2025. https://www.fortunebusinessinsights.com/drug-delivery-systems-market-103070.

(84) Mindur, J. E.; Swirski, F. K. Growth Factors as Immunotherapeutic Targets in Cardiovascular Disease. *Arteriosclerosis, Thrombosis, and Vascular Biology* 2019, *39* (7), 1275–1287. https://doi.org/10.1161/ATVBAHA.119.311994.

(85) Toosi, S.; Behrava, J. Osteogenesis and Bone Remodeling: A Focus on Growth Factors and Bioactive Peptides. *Biofactors* 2020, *46* (3), 326–340.

https://doi.org/10.1002/biof.1598.

(86) Perona, R. Cell Signalling: Growth Factors and Tyrosine Kinase Receptors. *Clinical and Translational Oncology* 2006, *8* (2), 77–82. https://doi.org/10.1007/s12094-006-0162-1.

(87) Park, J. W.; Hwang, S. R.; Yoon, I. S. Advanced Growth Factor Delivery Systems in Wound Management and Skin Regeneration. *Molecules* 2017, *22* (8), 1–20. https://doi.org/10.3390/molecules22081259.

(88) Shaw, P.; Dwivedi, S. K. D.; Bhattacharya, R.; Mukherjee, P.; Rao, G. VEGF Signaling: Role in Angiogenesis and Beyond. *Biochimica et Biophysica Acta - Reviews on Cancer* 2024, *1879* (2), 1–52. https://doi.org/10.1016/j.bbcan.2024.189079.

(89) Montemagno, C.; Durivault, J.; Gastaldi, C.; Dufies, M.; Vial, V.; He, X.; Ambrosetti, D.; Kamenskaya, A.; Negrier, S.; Bernhard, J. C.; Borchiellini, D.; Cao, Y.; Pagès, G. A Group of Novel VEGF Splice Variants as Alternative Therapeutic Targets in Renal Cell Carcinoma. *Molecular Oncology* 2023, *17* (7), 1379–1401. https://doi.org/10.1002/1878-0261.13401.

(90) Nemashkalova, E. L.; Shevelyova, M. P.; Machulin, A. V.; Lykoshin, D. D.; Esipov, R. S.; Deryusheva, E. I. Heparin-Induced Changes of Vascular Endothelial Growth Factor (VEGF165) Structure. *Biomolecules* 2023, *13* (1), 1–11. https://doi.org/10.3390/biom13010098.

(91) Peach, C. J.; Mignone, V. W.; Arruda, M. A.; Alcobia, D. C.; Hill, S. J.; Kilpatrick, L. E.; Woolard, J. Molecular Pharmacology of VEGF-A Isoforms: Binding and Signalling at VEGFR2. *International Journal of Molecular Sciences* 2018, *19* (4). https://doi.org/10.3390/ijms19041264.

(92) Dreyer, C. H.; Kjaergaard, K.; Ding, M.; Qin, L. Vascular Endothelial Growth Factor for *in Vivo* Bone Formation: A Systematic Review. *Journal of Orthopaedic Translation* 2020, *24* (September 2020), 46–57. https://doi.org/10.1016/j.jot.2020.05.005.

(93) Murakami, J.; Ishii, M.; Suehiro, F.; Ishihata, K.; Nakamura, N.; Nishimura, M. Vascular Endothelial Growth Factor-C Induces Osteogenic Differentiation of Human Mesenchymal Stem Cells through the ERK and RUNX2 Pathway. *Biochemical and Biophysical Research Communications* 2017, *484* (3), 710–718. https://doi.org/10.1016/j.bbrc.2017.02.001.

(94) Clark, D.; Wang, X.; Chang, S.; Czajka-Jakubowska, A.; Clarkson, B. H.; Liu, J. VEGF Promotes Osteogenic Differentiation of ASCs on Ordered Fluorapatite Surfaces. *Journal of Biomedical Materials Research - Part A* 2015, *103* (2), 639–645. https://doi.org/10.1002/jbm.a.35215.

(95) Wang, L.; Chen, L.; Wang, J.; Wang, L.; Gao, C.; Li, B.; Wang, Y.; Wu, J.; Quan, C. Bioactive Gelatin Cryogels with BMP-2 Biomimetic Peptide and VEGF: A Potential Scaffold for Synergistically Induced Osteogenesis. *Chinese Chemical Letters* 2022, *33* (4), 1956–1962. https://doi.org/10.1016/j.cclet.2021.10.070.

(96) Geng, Y.; Duan, H.; Xu, L.; Witman, N.; Yan, B.; Yu, Z.; Wang, H.; Tan, Y.; Lin, L.; Li, D.; Bai, S.; Fritsche-Danielson, R.; Yuan, J.; Chien, K.; Wei, M.; Fu, W. BMP-2 and

VEGF-A ModRNAs in Collagen Scaffold Synergistically Drive Bone Repair through Osteogenic and Angiogenic Pathways. *Communications Biology* 2021, *4* (1), 1–14. https://doi.org/10.1038/s42003-020-01606-9.

(97) Brudno, Y.; Ennett-Shepard, A. B.; Chen, R. R.; Aizenberg, M.; Mooney, D. J. Enhancing Microvascular Formation and Vessel Maturation through Temporal Control over Multiple Pro-Angiogenic and pro-Maturation Factors. *Biomaterials* 2013, *34* (36), 9201–9209. https://doi.org/10.1016/j.biomaterials.2013.08.007.

(98) Kim, S. K.; Lee, J.; Song, M.; Kim, M.; Hwang, S. J.; Jang, H.; Park, Y. Combination of Three Angiogenic Growth Factors Has Synergistic Effects on Sprouting of Endothelial Cell/Mesenchymal Stem Cell-Based Spheroids in a 3D Matrix. *Journal of Biomedical Materials Research - Part B Applied Biomaterials* 2016, *104* (8), 1535–1543. https://doi.org/10.1002/jbm.b.33498.

(99) Batlle, E.; Massagué, J. Transforming Growth Factor-β Signaling in Immunity and Cancer. *Immunity* 2019, *50* (4), 924–940. https://doi.org/10.1016/j.immuni.2019.03.024.

(100) Zhang, Y.; Alexander, P. B.; Wang, X. F. TGF-β Family Signaling in the Control of Cell Proliferation and Survival. *Cold Spring Harbor Perspectives in Biology* 2017, *9* (4), 1–38. https://doi.org/10.1101/cshperspect.a022145.

(101) Krawczak-Wójcik, K.; Mazurkiewicz, A.; Petr, M. TGF-B Isoforms: TGF-B1, TGF-B2 and TGF-B3 in Ligament and Tendon Healing. *Polish Journal of Sport and Tourism* 2024, *31* (2), 3–10. https://doi.org/10.2478/pjst-2024-0008.

(102) Duan, M.; Wang, Q.; Liu, Y.; Xie, J. The Role of TGF-B2 in Cartilage Development and Diseases. *Bone and Joint Research* 2021, *10* (8), 474–487. https://doi.org/10.1302/2046-3758.108.BJR-2021-0086.

(103) Li, M.; Qiu, L.; Hu, W.; Deng, X.; Xu, H.; Cao, Y.; Xiao, Z.; Peng, L.; Johnson, S.; Alexey, L.; Kingston, P. A.; Li, Q.; Zhang, Y. Genetically-Modified Bone Mesenchymal Stem Cells with TGF-β 3 Improve Wound Healing and Reduce Scar Tissue Formation in a Rabbit Model. *Experimental Cell Research* 2018, *367* (1), 24–29. https://doi.org/10.1016/j.yexcr.2018.02.006.

(104) Lodyga, M.; Hinz, B. TGF-B1 – A Truly Transforming Growth Factor in Fibrosis and Immunity. *Seminars in Cell and Developmental Biology* 2020, *101* (December), 123–139.

(105) Su, C.; Miao, J.; Guo, J. *The Relationship between TGF-B1 and Cognitive Function in the Brain*; 2023; Vol. 205. https://doi.org/10.1016/j.brainresbull.2023.110820.

(106) Liu, Y.; Li, Y.; Li, N.; Teng, W.; Wang, M.; Zhang, Y.; Xiao, Z. TGF-B1 Promotes Scar Fibroblasts Proliferation and Transdifferentiation via up-Regulating MicroRNA-21. *Scientific Reports* 2016, *6* (August), 1–9. https://doi.org/10.1038/srep32231.

(107) Li, M. O.; Wan, Y. Y.; Sanjabi, S.; Robertson, A. K. L.; Flavell, R. A. Transforming Growth Factor-β Regulation of Immune Responses. *Annual Review of Immunology* 2006, *24*, 99–146. https://doi.org/10.1146/annurev.immunol.24.021605.090737.

(108) Yamamoto, M.; Tabata, Y.; Hong, L.; Miyamoto, S.; Hashimoto, N.; Ikada, Y. Bone

Regeneration by Transforming Growth Factor B1 Released from a Biodegradable Hydrogel. *Journal of Controlled Release* 2000, *64* (1–3), 133–142. https://doi.org/10.1016/S0168-3659(99)00129-7.

(109) Wang, Y.; He, T.; Liu, J.; Liu, H.; Zhou, L.; Hao, W.; Sun, Y.; Wang, X. Synergistic Effects of Overexpression of BMP-2 and TGF-B3 on Osteogenic Differentiation of Bone Marrow Mesenchymal Stem Cells. *Molecular Medicine Reports* 2016, *14* (6), 5514–5520. https://doi.org/10.3892/mmr.2016.5961.

(110) Rahman, M. S.; Akhtar, N.; Jamil, H. M.; Banik, R. S.; Asaduzzaman, S. M. TGF-β/BMP Signaling and Other Molecular Events: Regulation of Osteoblastogenesis and Bone Formation. *Bone Research* 2015, *3* (January). https://doi.org/10.1038/boneres.2015.5.

(111) Stamnitz, S.; Krawczenko, A.; Klimczak, A. Combined TGF-B3 and FGF-2 Stimulation Enhances Chondrogenic Potential of Ovine Bone Marrow-Derived MSCs. *Cells* 2025, *14* (13). https://doi.org/10.3390/cells14131013.

(112) Kuroda, S.; Sumner, D. R.; Virdi, A. S. Effects of TGF-B1 and VEGF-A Transgenes on the Osteogenic Potential of Bone Marrow Stromal Cells *in Vitro* and *in Vivo*. *Journal of Tissue Engineering* 2012, *3* (1), 1–12. https://doi.org/10.1177/2041731412459745.

(113) Mengistu, D. A.; Alemu, A.; Abdukadir, A. A.; Mohammed Husen, A.; Ahmed, F.; Mohammed, B.; Musa, I. Global Incidence of Surgical Site Infection Among Patients: Systematic Review and Meta-Analysis. *Inquiry (United States)* 2023, *60*, 1–4. https://doi.org/10.1177/00469580231162549.

(114) Control, E. C. for D. P. and. Healthcare-Associated Infections: Surgical Site Infections. Annual Epidemiological Report for 2017. *Ecdc* 2019, No. October.

(115) Sane, R. M.; Samant, P. D. Incidence of Surgical Site Infections and Associated Risk Factors in Clean Orthopaedic Surgeries. *Journal of Research and Practice on the Musculoskeletal System* 2021, *05* (03), 88–92. https://doi.org/10.22540/jrpms-05-088.

(116) Taherpour, N.; Mehrabi, Y.; Seifi, A.; Eshrati, B.; Hashemi Nazari, S. S. Epidemiologic Characteristics of Orthopedic Surgical Site Infections and Under-Reporting Estimation of Registries Using Capture-Recapture Analysis. *BMC Infectious Diseases* 2021, *21* (1), 1–7. https://doi.org/10.1186/s12879-020-05687-z.

(117) Jin, L.; Liu, X.; Zheng, Y.; Li, Z.; Zhang, Y.; Zhu, S.; Jiang, H.; Cui, Z.; Chu, P. K.; Wu, S. Interface Polarization Strengthened Microwave Catalysis of MoS2/FeS/Rhein for the Therapy of Bacteria-Infected Osteomyelitis. *Advanced Functional Materials* 2022, *32* (33), 1–14. https://doi.org/10.1002/adfm.202204437.

(118) Gimza, B. D.; Cassat, J. E. Mechanisms of Antibiotic Failure During Staphylococcus Aureus Osteomyelitis. *Frontiers in Immunology* 2021, *12* (February), 1–8. https://doi.org/10.3389/fimmu.2021.638085.

(119) Huzum, B.; Aprotosoaie, A. C.; Alexa, O.; Sîrbu, P. D.; Puha, B.; Veliceasa, B.; Huzum, R. M. Antimicrobials in Orthopedic Infections: Overview of Clinical Perspective and Microbial Resistance. *Medicina (Lithuania)* 2024, *60* (12), 1–19. https://doi.org/10.3390/medicina60121988.

(120) Spížek, J.; Řezanka, T. Lincosamides: Chemical Structure, Biosynthesis, Mechanism of Action, Resistance, and Applications. *Biochemical Pharmacology*. 2017, pp 20–28. https://doi.org/10.1016/j.bcp.2016.12.001.

(121) Spížek, J.; Řezanka, T. Lincomycin, Clindamycin and Their Applications. *Applied Microbiology and Biotechnology* 2004, *64* (4), 455–464. https://doi.org/10.1007/s00253-003-1545-7.

(122) Egle, K.; Skadins, I.; Grava, A.; Micko, L.; Dubniks, V.; Salma, I.; Dubnika, A. Injectable Platelet-Rich Fibrin as a Drug Carrier Increases the Antibacterial Susceptibility of Antibiotic— Clindamycin Phosphate. *International Journal of Molecular Sciences* 2022, *23* (13). https://doi.org/10.3390/ijms23137407.

(123) Krawczyk, S. J.; Leśniczak-Staszak, M.; Gowin, E.; Szaflarski, W. Mechanistic Insights into Clinically Relevant Ribosome-Targeting Antibiotics. *Biomolecules* 2024, *14* (10), 1–13. https://doi.org/10.3390/biom14101263.

(124) Del Rosso James Q.; Armillei Maria K.; Lomakin Ivan D.; Grada Ayman; Bunick Christopher G. Clindamycin: A Comprehensive Status Report with Emphasison Use in Dermatology. *Journal of Clinical and Aesthetic Dermatology* 2024, *17* (8), 29–40.

(125) Manzano-Moreno, F. J.; Gónzalez-Acedo, A.; de Luna-Bertos, E.; García-Recio, E.; Ruiz, C.; Reyes-Botella, C. Effect of Amoxicillin and Clindamycin on the Gene Expression of Markers Involved in Osteoblast Physiology. *Journal of Dental Sciences* 2024, *19* (2), 990–997. https://doi.org/10.1016/j.jds.2023.07.015.

(126) Beuttel, E.; Bormann, N.; Pobloth, A. M.; Duda, G. N.; Wildemann, B. Impact of Gentamicin-Loaded Bone Graft on Defect Healing in a Sheep Model. *Materials* 2019, *12* (7), 1–9. https://doi.org/10.3390/ma12071116.

(127) Baird, P.; Hughes, S.; Sullivan, M.; Willmot, I. Penetration into Bone and Tissues of Clindamycin Phosphate. *Postgraduate Medical Journal* 1978, *54* (628), 65–67. https://doi.org/10.1136/pgmj.54.628.65.

(128) Zelmer, A. R.; Nelson, R.; Richter, K.; Atkins, G. J. Can Intracellular Staphylococcus Aureus in Osteomyelitis Be Treated Using Current Antibiotics? A Systematic Review and Narrative Synthesis. *Bone Research* 2022, *10* (1), 1–18. https://doi.org/10.1038/s41413-022-00227-8.

SPIS TABEL

SPIS RYSUNKÓW

ARTYKUŁY NAUKOWE WCHODZĄCE W SKŁAD CYKLU PUBLIKACJI

materials

MDPI

Review

Polymeric and Composite Carriers of Protein and Non-Protein Biomolecules for Application in Bone Tissue Engineering

Dagmara Słota [1,*], Karina Piętak [1], Josef Jampilek [2,3] and Agnieszka Sobczak-Kupiec [1]

[1] Department of Materials Science, Faculty of Materials Engineering and Physics, Cracow University of Technology, 37 Jana Pawła II Av., 31-864 Krakow, Poland
[2] Department of Analytical Chemistry, Faculty of Natural Sciences, Comenius University, Ilkovicova 6, 842 15 Bratislava, Slovakia
[3] Department of Chemical Biology, Faculty of Science, Palacky University Olomouc, Slechtitelu 27, 783 71 Olomouc, Czech Republic
* Correspondence: dagmara.slota@doktorant.pk.edu.pl

Abstract: Conventional intake of drugs and active substances is most often based on oral intake of an appropriate dose to achieve the desired effect in the affected area or source of pain. In this case, controlling their distribution in the body is difficult, as the substance also reaches other tissues. This phenomenon results in the occurrence of side effects and the need to increase the concentration of the therapeutic substance to ensure it has the desired effect. The scientific field of tissue engineering proposes a solution to this problem, which creates the possibility of designing intelligent systems for delivering active substances precisely to the site of disease conversion. The following review discusses significant current research strategies as well as examples of polymeric and composite carriers for protein and non-protein biomolecules designed for bone tissue regeneration.

Keywords: biomolecules; hormones; flavonoids; lipids; growth factors; protein amino acids; osteopontin; bone sialoprotein; osteocalcin; osteonectin

Citation: Słota, D.; Piętak, K.; Jampilek, J.; Sobczak-Kupiec, A. Polymeric and Composite Carriers of Protein and Non-Protein Biomolecules for Application in Bone Tissue Engineering. *Materials* **2023**, *16*, 2235. https://doi.org/10.3390/ma16062235

Academic Editor: Roman Perez Antoñanzas

Received: 30 January 2023
Revised: 2 March 2023
Accepted: 8 March 2023
Published: 10 March 2023

1. Introduction

Drug carriers are biologically safe tools for transporting molecules for nutraceutical, pharmaceutical, and cosmetic applications, i.e., in fields of high industrial and scientific interest. According to the report Drug Delivery Systems Market Size, Share and COVID-19 Impact Analysis (Report ID: FBI103070), the global drug delivery systems market size was valued at USD 39.33 billion in 2022 and is projected to grow to USD 71.75 billion by 2029, exhibiting a compound annual growth rate of 9.0%. Only in North America, this market was valued at USD 14.15 billion in 2021. These costs are associated with the need for high financial outlays for research and investment. An estimated 10,000 molecules are generally rejected before one is selected as marketable [1,2]. In recent years, increasing emphasis has been given to using polymeric or composite materials as carriers for active substances, attempting to develop a biomaterial that will carry a therapeutic effect at a specific location in the organism. The reason for this is that the total therapeutic benefit of a drug or other active substance is not proportional to its potency in vitro. Under physiological conditions, active substances meet several barriers, such as aggregation, insolubility, degradation, or impermeability of vascular endothelial cell layers, which are responsible for the drug's short half-life in vivo as well as non-specific distribution in tissues or poor tissue penetration. Consequently, there is a risk of adverse effects, such as immunogenicity and off-target toxicity [3,4]. The main goal of designing biomaterials for active substance delivery is to release pharmacologically active biomolecules for specific drug action at an optimal rate and dose. Thus, it is possible to personalize such a system, adapting it to the needs of a particular patient (taking into account his/her gender, height, and age) [5]. There are many methods of delivering drugs and active biomolecules, not only orally, but also

transdermally or inhaled (Figure 1). However, in the case of bone regeneration, the subject of this review, innovative composites and matrices (i.e., implants) or injectable delivery systems have the most significant potential [6].

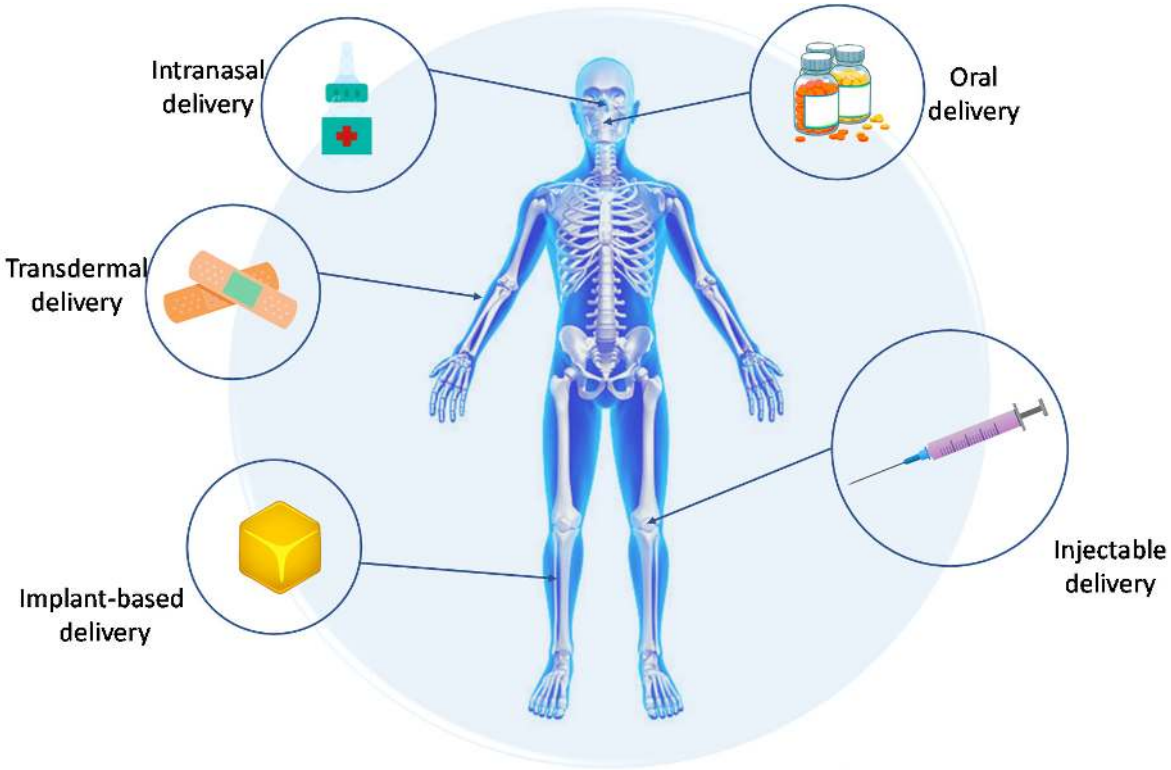

Figure 1. Strategies for delivery of biomolecules.

However, it is important to consider that drug carriers can be classified by their specific properties, including their shape, dimensions, application, and especially the way the drug content is delivered [1]. The oral administration system is the conventional and most commonly used method of drug supply. It is based on the oral dissolution and/or diffusion process. However, this method can adversely affect cellular pH and microflora in the stomach and involves the systemic distribution of the substance throughout the body and low absorption [7,8]. Other types of administration are passive or active delivery. In the first case, the release of the drug and thus the delivery of the therapeutic dose at the targeted site is a result of the natural response of the cells. In active delivery, an external stimulus must be added to the system to release a dose of the active substance exactly when it is required. These instances regard the case in which the carrier has already been administrated to the target tissue [9]. Delivery by injection involves delivering the product subcutaneously using a needle. However, a major limitation is possible infection and trauma caused by needles used in syringes [10,11]. Biomolecules and drugs are also delivered transdermally. It is a painless method of delivery by applying a drug formulation onto healthy and intact skin. From such a carrier, a substance can penetrate the body passively, through gradient diffusion, or actively, through artificially induced penetration by means of an electric field, heat, or ultrasound [12,13]. Delivery can also be provided via the intranasal route. Such administration of active substances is characterized by rapid delivery considering the large surface area and rapid systemic adsorption [14].

There are several types of drug carriers. These include nanoparticles, nanotubes, liposomes, dendrimers, and hydrogels. They differ in shape and production method [1]. Nanoparticles have been extensively used as carriers for the delivery of chemicals and biomolecular drugs, such as anticancer drugs and therapeutic proteins [15]. They are divided into two groups, nanocapsules and nanospheres, and have many different applications [16]. Due to their small size, nanoparticles can quickly dissolve in the bloodstream

and reach a specific site, transporting insoluble drugs. Nanoparticles based on biopolymers, such as proteins, are often used. Not only do they exhibit low toxicity and biodegradability, but they also are easily subjected to surface modification and are not immunogenic [17,18]. However, it is important to mention that metallic nanoparticles are the subject of intense research due to their potential health risks, given the danger of metal accumulation in the organism [19]. Another type of carrier with a significantly small size is nanotubes. They assume a cylindrical shape and are hollow inside. Nanotubes are filled with drugs or other active substances usually by functionalizing the carbon skeleton. Most often, they are used in anticancer therapy. However, information about their cytotoxicity still needs in-depth research [20,21]. On the other hand, hydrogels are a safe alternative to drug delivery systems with high application potential. Depending on the substrates selected for their synthesis, it is relatively easy to control their physicochemical properties or degradation rates. In general, these systems are constructed from distilled water and a polymeric gelling agent. They exhibit a high capacity to absorb liquids into their polymer network. Hydrogels have the ability to protect loaded drugs from the external environment, such as the acidic pH during oral administration [22–24]. Other typical polymeric carriers are dendrimers, characterized by a branched, three-dimensional structure. Their shapes can be hexagonal or cubic. The peculiar structure of dendrimers is the reason for the presence of free spaces, so-called cavities, in their molecules; such cavities can be used as specific pockets, in which various molecules can be placed by encapsulation. After fulfilling its role and releasing the active substance, it is usually excreted in the urine and/or biodegraded [25–27]. However, the most widely known and used carriers are liposomes. They are small spherical structures made of one or more phospholipid double layers. They exhibit great biocompatibility, but the main advantages of using liposomes are their increased stability and reduced toxicity of the encapsulated drug. Since the layers of liposomes are very similar to cell membranes, they are also characterized by the possibility of direct fusion [28].

Polymers are proving to be increasingly important in the carriers of various drugs. One such active substance is doxorubicin (DOX), which has been encapsulated in polymer micelles based on PEG-*b*-poly(DPA-co-DTM) or PEG-*b*-poly(DBA-co-DTM) copolymer. The micelle size increased after antibiotic loading by about 30% for the first copolymer and by about 21% for the second copolymer. The release kinetics indicate accelerated drug release at lower pH values, which may have potential applications in biomedical therapy [29]. The same active ingredient was also encapsulated into amphiphilic star copolymers with a HyperMacs core, which was prepared from disulfide-bond-containing AB2 polycaprolactone (PCL) macromonomers and then grafted with polyethylene glycol (PEG). As a result of the self-organization of the copolymers, the resulting spherical micelles in an aqueous medium were characterized by their ability to be reduction-cleavable in a reductive environment. In addition, in vitro studies showed a slow release of DOX in PBS, but a rapid release in a reducing medium, providing the possibility of using the resulting micelles for the triggered release of the anticancer drug [30]. Furthermore, doxorubicin was also used to form a magnetically reactive multifunctional magnetic vortex of Fe_3O_4@PVP@DOX with a unique domain structure. Interestingly, in vivo animal studies demonstrate that the resulting magnetic vortex nanoplatform can successfully perform magnetic demand response of heat therapy and magnetic-field-induced release of the DOX drug. This results in a synergistic effect in inhibiting tumor growth without any side effects, which is a highly desirable feature when developing this type of material [31]

The presented review demonstrates various methods of delivering selected protein biomolecules (such as growth factors, amino acids, osteopontin, osteocalcin, and osteonectin) and non-protein biomolecules (such as hormones, flavonoids, and lipids), using polymeric and composite biomaterials designed for bone tissue regeneration. The composition of the materials and their test results are discussed. Table 1 summarizes the protein biomolecules discussed in this review, and Table 2 summarizes the non-protein biomolecules.

2. Protein Biomolecules

2.1. Growth Factors

Naturally occurring substances capable of stimulating cell proliferation, wound healing, and sometimes also cell differentiation are growth factors (GFs). Usually, they are secreted proteins or cytokines that are important for regulating various cellular processes [32]. They act as signaling molecules by creating a complex signaling network between cells [33]. GFs mediate a variety of regulatory functions. They affect wound healing, cell proliferation, and migration as well as local regulation of the immune system. In addition, they can also bind to receptors in the cell membrane and act as stimulators of cell growth and metabolic functions [34]. A single GF may have to regulate different cell types, inducing a range of cellular functions in different tissues. There are three classes of tasks for GFs:

- Autocrine tasks: a specific GF affects a cell of its own origin or cells of identical phenotype. In this case, a GF produced by an osteoblast can influence the activity of another osteoblast;
- Paracrine tasks: a specific GF influences neighboring cells;
- Endocrine tasks: a specific GF floats on phenotypically different, distant cells. In this case, the GF secreted in the nervous tissue of the central nervous system can induce osteoblast activity [35,36].

GFs have important applications in wound healing, skin tissue engineering, cartilage tissue engineering, and bone tissue engineering. There are numerous classes of these biomolecules. They are characterized by different specific biological features, so their clinical applications also vary [32]. This part of the review will focus on different delivery methods of specific growth factors used in the bone healing process.

2.1.1. TGF-β

The transforming growth factor-β (TGF-β) superfamily includes a diverse range of proteins, such as TGF-β1–3, and one of the major proteins in skeletal system regeneration—bone morphogenetic proteins (BMPs) [37]. Different types of ceramics are used to provide biomimetics. Mesoporous calcium phosphate ceramics prepared by soft and hard templating were loaded with TGF-β1, and kinetic release in vitro was studied. The ceramic phase was modified by the adsorption process. Based on the results, from 0 to 50% of the initial TGF-β1 loading was released in a culture medium after 3 to 6 days [38]. Using the cryogenic 3D printing technique, bi-layered osteochondral scaffolds were designed. Osteogenic peptide/β-TCP/poly(lactic-co-glycolic acid) water-in-oil composite emulsions were printed into a hierarchically porous subchondral layer, and poly(lactic acid-co-trimethylene carbonate) water-in-oil emulsions were printed into thermal-responsive cartilage frame on top of the subchondral layer. To form the cartilage module, scaffolds were dispensed with TGF-β1 loaded type I collagen (Col) hydrogel [39]. TGF was likewise used to compose three-dimensional (3D) scaffolds based on silk fibroin (SF) and chitosan (CS) (TGF-β1-SF-CS) [40]. Proliferation and chondrogenic differentiation of rat bone marrow-derived mesenchymal stem cells (MSCs) were also evaluated in relation to gelatin (Gel) hydrogel microspheres. Gel was dehydrothermally cross-linked in different conditions in a water-in-oil emulsion state to obtain Gel hydrogel microspheres with different water content. Microspheres were then loaded with TGF-β1. The obtained results suggest that the designed biomaterial functions well both as the scaffold of MSC and the matrix of TGF-β1 release [41]. To increase the bioactivity of the biomaterial, TGF-β1 was combined with vascular endothelial growth factor (VEGF). The proteins were loaded into the reservoir fabricated from nanocrystalline calcium sulfate hemihydrate (nCaS), hydroxyapatite (HAp), and calcium sulfate hemihydrate (CaS) (nCaS/HAp/CS/TGF-1/VEGF). In vitro studies on the release of growth factors from the nCaS/HAp/CS cement were conducted for 28 days [42]. Applications combining two or more growth factors are more favorable due to their additive or synergistic effects on bone formation. TGF-β1 and insulin-like growth factor 1 (IGF-1) are particularly interesting, as they are highly expressed during bone growth [43]. Thus, TGF-β1 and IGF-1 were incorporated into a hydrogel Gel scaf-

fold and evaluated in a rat tibia segmental defect model. The release of growth factors resulted from hydrogel biodegradation [44]. Cylindrical plasma-sprayed porous-coated implants made of titanium alloy (Ti_6Al_4V) were modified with the addition of TGF-β1 and IGF-1 by incubating them in polylactic acid (PLA) solution with dissolved growth factors. Locally delivered growth factors enhance mechanical fixation and osseointegration; however, the release kinetics was not investigated [45]. The same biomaterial was later enriched with a plasma-sprayed HAp coating. As a result, due to the ceramic phase in the biomaterial, bone growth was 3-fold higher, and the local release of TGF-β1 and IGF-1 stimulated gap healing during in vivo studies [46]. Similar studies involved the use of HAp coating modified with TGF-β1 and IGF-1, which was investigated as a fusion cage to improve the results of cervical intervertebral fusion and to treat the goat cervical spine, an interbody fusion model. The obtained results suggest that such coating can enhance bone fusion [47]. Another protein that TGF was coupled with is stromal-derived factor-1α (SDF-1α). It was loaded into a silk fibroin-porous Gel scaffold. The sustained release of biomolecules occurred through in vitro degradation of the polymer matrix [48]. Although TGF-β1 is the most commonly used growth factor of the TGF family, there are also links to other variants. TGF-β2 and growth/differentiation factor 5 (GDF5) as well as their combinations were loaded into silk-fibroin scaffolds, and human primary adipose-derived MSCs were cultured on them [49]. Biodegradable poly(ether carbonate urethane)-urea (PECUU) was used to culture TGF-β3-mediated bone marrow stem cells, and their gene expression profile was investigated [50]. Another polymer matrix used as a TGF-β3 carrier is an electrospun CS-coated PCL fiber scaffold. However, the release kinetics of TGF–β3 in vivo is not known [51].

2.1.2. Combination of TGF-β and BMP-2

An interesting combination is the inclusion of TGF and bone morphogenetic protein-2 (BMP-2) in one biomaterial, as BMP is a growth factor, a protein that induces bone formation and osteoblast differentiation. A conically graded scaffold of CS-Gel hydrogel/poly(lactic-co-glycolide) (PLGA) was facilely prepared and loaded with GFs. The CS-Gel hydrogel phase was modified with TGF–β1 to promote chondrogenesis, whereas the PLGA scaffold was loaded with BMP-2 for osteogenesis. The release rate of GFs and the behavior of the obtained materials in vitro and in vivo were determined. The results show that the conically graded transition from the hydrogel to the PLGA scaffold and graded variation in the amount of growth factors from TGF-β1 to BMP-2 benefited the cartilage–bone interface reconstruction [52]. Another way was to combine PLA with PEG and HA to investigate this composition as a carrier for BMP-2. ELISA investigated the release kinetics of BMP-2 from the composites. Thirty-six male Sprague Dawley rats underwent posterolateral spinal fusion on L4–L5 with three different doses of BMP-2. ELISA demonstrated the sustained release of BMP-2 until day 21 [53]. As PLGA and Gel demonstrate good properties as drug carriers, they have also been combined with collagen to create PLGA-Col-Gel electrospun nanofiber membranes loaded with E7-BMP-2. E7-BMP-2 is a bone morphogenetic protein-2-mimicking peptide providing a better economic substitute for human protein [54]. However, the effect of a membrane made out of clear type I Col soaked with BMP-2 for the treatment of the bone system was also determined [55]. To achieve a more biomimetic and bone-like structure, biomaterials containing the ceramic phase are created. Therefore, calcium-deficient hydroxyapatite (CDHAp) was used to create a CDHAp/COL-based bio-ceramic scaffold as a BMP-2 carrier. It was evaluated in vivo in a rat calvarial critical-sized bone defect model. A sustained release of protein was observed for 35 days [56]. However, combinations with stoichiometric HAp of micro- as well as nanometric diameter are more frequent. HAp nanoparticles were soaked in BMP-2 and then suspended in a Col matrix to form a scaffold [57]. Although more frequently, HAp/Col scaffolds are first created, which are then modified with protein by immersing it in its solution. Protein then binds to both components. Scaffolds may be composed of nHAp [58] as well as ceramics of a larger diameter [59–62] and also enriched with CS microspheres loaded with BMP-2 [63].

Besides scaffolds, organic-nonorganic biomaterials such as membranes [64], coatings [65], and pastes [66] are also developed. In all cases, the release of biomolecules was possible due to the specific polymer structure of Col as well as the porous nature of HAp.

2.1.3. Combination of BMP-2 and FGF

As mentioned, applying two or more GFs can provide a better therapeutic effect due to the synergy. An example is the cooperation of BMP-2 with fibroblast growth factor (FGF), as they both regulate the spontaneous repair of bone defects. Therefore, HAp/Col scaffold discs were prepared as previously, enriched not only with BMP-2 but also with FGF-2. The obtained in vivo results confirmed that this combination has the potential to increase bone healing in old mice [67]. An interesting project is a coating composed of a biomimetic calcium phosphate layer that is applied to a synthetic bone graft covered with a poly-L-lysine/poly-L-glutamic acid polyelectrolyte multilayer (PEM) film and GFs [68]. Another type of biomaterial binding these two GFs is poly-L-lactic acid (PLLA) core–PLGA shell double-walled microspheres loaded with BMP-2 and FGF-2. It was demonstrated that they enable the release of multiple growth factors according to specific requirements [69].

2.1.4. Combination of BMP-2 and PIGF-2

Also relatively common is the combination of BMP-2 with placental growth factor-2 (PlGF-2), a member of the VEGF subfamily [70]. They were used to create PlGF-2/BMP-2-loaded heparin–*N*-(2-hydroxyl)propyl-3-trimethyl ammonium CS chloride (HTCC) nanocomplexes which have been analyzed to determine the osteogenic effect. Figure 2 illustrates schematically the mechanism of fabrication and in vitro osteogenic effect of the nanocomplexes. Dual delivery of PlGF-2 and BMP-2 could be used to improve osteoregeneration [71].

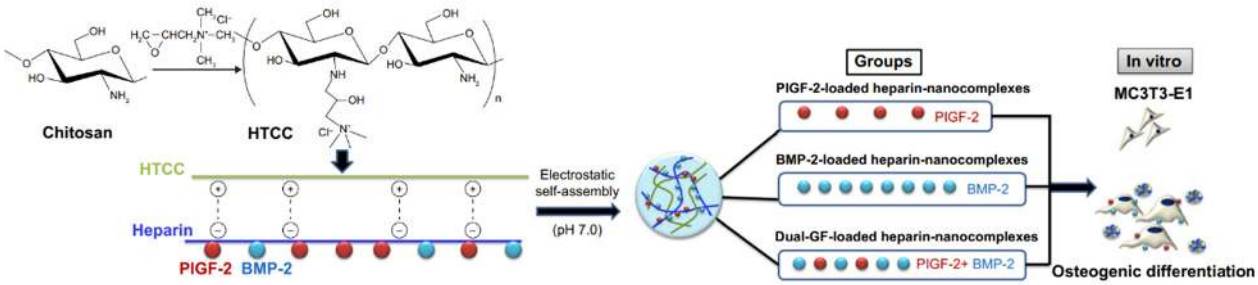

Figure 2. Schematic illustration of the fabrication mechanism and in vitro osteogenic effect of PlGF-2-/BMP-2 nanocomplexes loaded with heparin-HTCC. Reprinted from [71], Copyright 2016 Dove Medical Press Limited.

2.1.5. Combination of BMP-2 and VEGF

However, most commonly, to increase therapeutic effect, BMP is combined with VEGF. VEGFs are responsible for the regulation of vascular development, angiogenesis, and lymphangiogenesis by binding to several receptors [72]. The use of polymer carriers alone and their composites with ceramics has been reported in the literature. An example of the first group is the material consisting of PLGA microspheres loaded with BMP-2 embedded in a poly(propylene) scaffold surrounded by a Gel hydrogel loaded with VEGF for sequential release [73]. Another project incorporated Gel using PLGA/Gel electrospun nanofibers scaffolds combined with BMP-2/VEGF. The quantity of the final release of GFs in an in vitro environment was relatively high, around 80%. However, the release of GFs was not the same and was slower for BMP-2 [74]. Similar results were obtained for GFs delivered by PLA-PEG-PLA block copolymers. The BMP-2/VEGF modification was carried out by soaking, and the release of the substance occurred as a result of polymer degradation [75]. Combinations with bioactive HAp include microspheres of *O*-carboxymethyl CS used as a drug carrier to construct a compound sustained-release system loaded into HAp/Col scaffold [76]. The nanoform of ceramic is presented as a Col-nanoHAp (nHAp) scaffold, where GFs are transported in the Col matrix [77]. Another case includes the production

of SF-nHAp biomaterial, where GFs are encapsulated in SF. The modification with BMP-2/VEGF took place via chemical covalent bonding and physical adsorption. However, there is a significant difference between the release kinetics of VEGF and BMP-2 [78]. The mixture of HAp and β-tricalcium phosphate is a specific kind of ceramic and is called biphasic calcium phosphate (BCP). It was combined with nanocellulose loaded with GFs to create sponge-like scaffolds.

Interestingly, the sustained dual release of GFs was less than in previous cases, although it did not show a satisfactory effect on bone formation [79]. Equally curious is the use of calcium phosphate cement (CPC) scaffolds which consist of a mixture of β-tricalcium phosphate, dicalcium phosphate anhydrous, precipitated HAp, and nHAp. They were enriched with PLGA microspheres loaded with GFs. This project has been evaluated for avascular necrosis of the femoral head, and the research suggests that BMP and VEGF in this combination may slow or even reverse the pathological process of femoral head necrosis [80].

2.1.6. VEGF

Nonetheless, VEGF provides a remarkable therapeutic effect in targeted therapy, both in synergy with BMP and on its own, as evidenced by many published studies. It can be supplied with a carrier from a biodegradable PLGA scaffold enriched with GF. The freeze-drying technique mainly obtains this kind of porous foam. Such a structure ensures a sustainable release of substances [81]. A similar study with biomimetic PLGA microsphere scaffolds loaded with VEGF led to similar results [82]. Another more sophisticated polymeric solution to control the growth factor release is an alginate/CS/PLA system. In this material, VEGF was first encapsulated in alginate microspheres via the emulsification method and then combined with freeze-dried scaffolds. GF releases through the degradation of the polymer under in vivo conditions [83]. As shown previously, the ceramic phase in biomaterials for bone regeneration improves biomimetic properties. Hence, it is often added as one of the substrates. The foam casting method produced a high porous β-TCP coated with a thin layer of PLGA containing an encapsulated growth factor [84]. A more extensive project with a VEGF delivery system consisting of PLGA microspheres involved a 3D Gel/alginate/β-TCP scaffold. During the in vitro study, a 50% increase in alkaline phosphatase activity was observed due to VEGF release, which is a promising result [85]. Another type of ceramics used is bioactive glass. It was used to cover PLGA scaffolds with incorporated VEGF. In this case, substrate coating with this bioactive glass offers an inductive component through material degradation [86].

Nevertheless, among all types of ceramics, the most attractive is HAp. Polymers of natural origin include Col and Gel, representing a denatured form of Col. Using Col and nHAp, a porous scaffold was produced, and the freeze-drying method was used for this purpose. The entire scaffold, including the ceramic phase, was decorated with VEGF [87]. A comparable solution was employed for a ceramic-polymer cryogel composite, where the polymer phase was represented by Gel. The biomaterial was enriched with GF by the microinjection method. However, the release kinetics were not investigated [88]. Silicon-substituted HAp microporous scaffolds were prepared via robocasting. GF was modified through non-covalent binding via incubation in a specific solution. The bone regeneration capability of this biomaterial has been evaluated in vivo using an osteoporotic sheep model, and the obtained results confirmed that they represent suitable bone grafts [89]. An attractive solution using the metallic phase combines Ti_6Al_4V-ELI macroporous scaffolds coated with silicon-substituted HAp and enriched with VEGF. For this purpose, electron beam melting and dip coating methods were used. Adsorption and immobilization of vascular endothelial growth factor on scaffold surfaces were carried out through non-covalent binding by incubation. However, a deficient level of GF was observed after the initial time [90]. The development of tissue and material engineering has led to the formulation of three strategies for immobilizing GFs in biomaterials (Figure 3). The simplest method of encapsulating GFs is physical encapsulation (Figure 3(a1)), which involves incorporating

GFs into a 3D polymer matrix by mixing factors inside the polymers before the gelation or solidification process. Physical adsorption (Figure 3(a2)) has attracted a lot of attention in recent years; however, this method is associated with poor control of the active substance delivered and inefficient retention of stable soluble proteins. A layer-by-layer (Figure 3(a3)) technique is an alternative to direct adsorption, as it provides better control over the spatial as well as temporal distribution of the active ingredient. This method most often relies on electrostatic interactions between oppositely charged polyelectrolytes and GFs to deposit functional polymer coatings on surfaces of different shapes and compositions. The technique involves chemical/enzymatic reactions between proteins and functionalized surfaces, offering significant control over the amount, orientation, retention, and distribution of GFs on the carrier. When a GF is chemically bound to biomaterials, its desorption rate is controlled by enzymatic or hydrolytic cleavage of the chemical bond. Carbodiimide coupling immobilization (Figure 3(b1)) is most commonly used due to its simplicity of execution, low cost, and mild reaction conditions. Polydopamine layers are also used (Figure 3(b2)), exhibiting strong adhesion properties to nearly all types of surfaces. However, depending on the type of GF and the carrier, other compounds are also used (Figure 3(b3)), such as dextran or streptavidin. The last approach is extracellular matrix (ECM)-inspired immobilization of GFs. In these techniques, taking into consideration natural interactions between ECM and GFs, heparin-based binding, adhesive protein-binding and ECM component and hierarchical structure-based binding are distinguished [91].

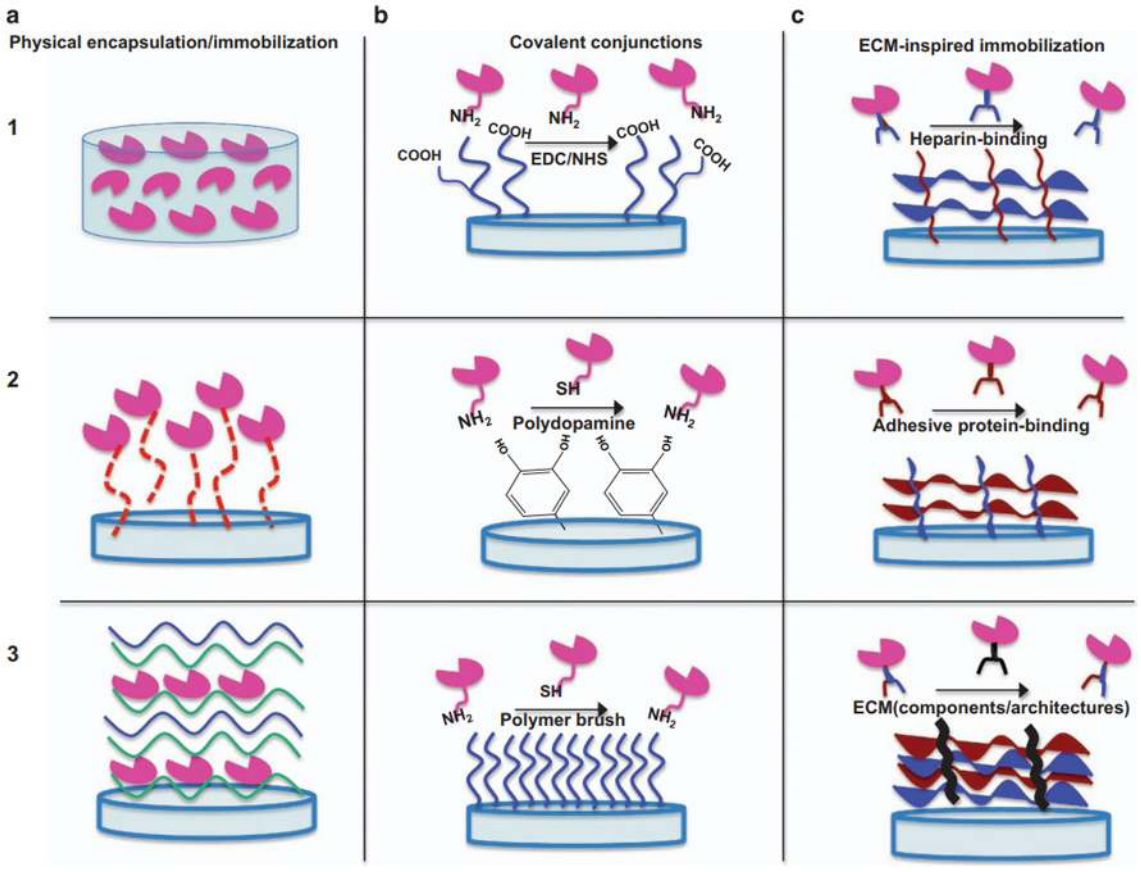

Figure 3. Approaches for the immobilization/encapsulation of growth factors (GFs) to biomaterials. (**a1**–**a3**) Physical immobilization techniques. (**b1**–**b3**) Non-selective covalent immobilization of GFs through their functional residues. (**c1**–**c3**) Extracellular matrix (ECM)-inspired immobilization reactions used for the orientation of GFs on the surfaces of biomaterials. Reprinted from [91], Copyright 2017 Springer Nature Limited.

2.1.7. Combination of VEGF and PDGF

Other synergistic effects were investigated between VEGF and platelet-derived growth factors (PDGFs). PDGFs are a family of homo- or heterodimeric growth factors, responsible for enhancing the proliferation of fibroblasts and the production of extracellular matrix by these cells [92,93]. However, they are also involved in the process of bone regeneration; thus, a brushite–CS system with incorporated VEGF and PDGF was designed. PDGF was incorporated in the liquid phase during scaffold formation, and VEGF was encapsulated in alginate microspheres and pre-included in small cylindrical CS sponges. The kinetic release was investigated in both in vitro and in vivo conditions in relation to male New Zealand rabbits [94].

2.1.8. PGDF

PDGF-BB on its own was applied in CS sponges. Modification occurred via soaking in GF solution, and the structure was freeze-dried. The release of the active substance occurred because of matrix degradation and, as a result, induced new bone formation [95]. In the more extended model, the CS sponge was enriched with chondroitin-4-sulfate (ChoS) to ensure steady release. The obtained results confirmed that the release of PDGF-BB from the ChoS–CS sponge significantly enhanced osteoblast proliferation [96]. Recombinant human platelet-derived growth factor was combined with Col matrix to ensure guided bone regeneration in in vivo conditions. The results suggest the accuracy of this project; however, the release kinetics have not been presented [97]. The method was also successfully applied to the functionalization of silk fibers (SF). These 3D textile implants were manufactured via an additive manufacturing approach [98]. Last but not least, SFs were combined with bioglass, PDGF, and the above-mentioned BMP-7 to create a mesoporous scaffold. Once again, the synergistic effect resulted in satisfactory results thanks to the sustained release of GFs [99].

2.1.9. FGF

The family of fibroblast growth factors (FGFs) is especially involved in the process of angiogenesis and wound healing but also in embryo development. A defining property of FGFs is that they bind to heparin and heparan sulfate [100]. Apart from the connection to BMP-2 described above, FGF was also utilized as the only protein modifying a HAp/Col scaffold. Abundant bone and cartilage regeneration were observed; however, the release kinetics has not been studied due to the rapid degradation of the biomaterial in in vivo conditions [101]. Other carriers assumed no use of the ceramic phase, focusing only on the properties of polymers. Therefore, the capacity of the hydrogel matrix of poly(2-hydroxyethyl methacrylate) copolymerized with 2-vinyl pyrrolidone to release FGF-2 was evaluated. The release of protein from the copolymer occurred during the swelling process. After this process, FGF-2 was active, which means it was not damaged during polymerization and sterilization [102]. Other polymers, such as PLA, are also used to design scaffolds [103] or manufacture nanosheets [104]. An alternative to solid biomaterials that degrade in a biological environment is injection materials that demonstrate a better cavity fit and allow easy application by injection compared to traditional scaffolds. Therefore, an interesting solution was designed to use a hydrogel composite of chitin/PLGA loaded with FGF-18 and $CaSO_4$ for guided bone regeneration as well as enhancing the ability to support osteogenic differentiation [105].

2.1.10. NGF

Furthermore, nerve growth factor (NGF) was experimentally used in targeted skeletal therapy, although it is responsible mainly for the development and survival of certain sympathetic as well as sensory neurons in both the central and peripheral nervous systems [106]. For targeted skeletal therapy, NGF was supplied in Col/nHAp/κ-carrageenan gel in the rabbit model of mandibular distraction osteogenesis [107].

2.2. Protein Amino Acids

Although amino acids (AA) are not strictly classified as protein biomolecules, they constitute a broad group of organic compounds, among which protein amino acids are distinguished, i.e., those that are part of proteins and are connected by peptide bonds [108,109]. For this reason, this part of the review will describe the delivery system of the protein amino acids that were experimentally used and described in the regeneration of the skeletal system.

2.2.1. RGD Peptide

One of the most commonly used peptides to functionalize biomaterials is an arginine-glycine-aspartic acid sequence called RGD peptide (Arg–Gly–Asp) (Figure 4). It is present in several proteins essential for bone regeneration, such as Col, fibronectin, bone sialoprotein, and osteopontin [110,111]. It is a cell adhesive peptide. Furthermore, various studies have demonstrated that RGD is a promoter of osteogenic differentiation in in vitro conditions and is able to stimulate in vivo bone formation [112]. Therefore, this specific sequence is experimentally combined with other biomaterials to enhance the therapeutic effect. An example is the modification of a ceramic-polymer composite, where the polymer phase was composed of Col and the ceramic phase of bone cement powder, which is a mixture of 58 wt% α-TCP and 24 wt% dicalcium phosphate (DCPA). The biomaterial was enriched with the RGD sequence by impregnation after the subsequent phosphoserine/RGD merger. The kinetics of compound release have not been studied, although under in vivo conditions, RGD appears to lead to increased bone formation around HA/Coll composite cement [113]. Another two-phase project involved creating bioresorbable PLGA/nHAp porous scaffolds decorated with this AA. The scaffold was modified via immersion in RGD solution, and obtained scaffolds were implanted into rabbits to observe preliminary application in the regeneration of mandibular defect [114]. Moreover, biphasic calcium phosphate was used to create BCP/CS scaffolds. These were modified with Arg–Gly–Asp and the aforementioned BMP-2 to evaluate their synergistic effect. RGD was covalently immobilized on the composite scaffold via EDC/NHS reaction. GF was first enclosed in bovine serum albumin nanoparticles and then immobilized on the scaffold surface [115]. For comparison, an example of soft biomaterial providing the RGD sequence is oligoPEG fumarate hydrogel. The presented study investigated the differentiation and mineralization effect of marrow stromal cells (MSCs) cultured in media [116]. Another good candidate material for cartilage tissue regeneration is poly(propylene fumarate) (PPF) due to its excellent mechanical properties during its degradation. Using micro-stereolithography, 3D printing PPF bioinks with immobilized RGD were created. The amino acid sequence's release depended on the PPF degradation rate [117]. Another soft material is cell–polymer constructs, created out of PEG hydrogel with encapsulated human mesenchymal stem cells (hMSCs) enriched with RGD sequence. In this case, an additional function of the peptide is to increase cell survival [118]. A similar model included encapsulating human embryonic stem cells (hESCs) into RGD-loaded PEGDA hydrogels. As before, the release of the active substance and cells occurred due to the degradation of the polymer matrix [119]. In another study, osteogenic precursor cells (OPC) were placed on PLA films and scaffolds decorated with RGD. However, PLA was firstly surface treated with NH_3 plasma. The obtained results suggest that this material with RGD significantly enhanced osteogenic cell attachment and differentiation into bone cells [120]. An example of another biomaterial is nanofibers. Arg-Gly-Asp was immobilized onto the electrospun PLGA nanofiber mesh surface to mimic an extracellular matrix structure. Sustained release of AA occurred via the biodegradation of polymer fibers [121]. Polydopamine (PDA) is a polymer that also undergoes degradation in a biological environment. It was used to compose hybrid ZnO/PDA/arginine-glycine-aspartic acid-cysteine (RGDC) nanorods prepared on titanium (Ti) implants. In this case, the RGD sequence was additionally enriched with cysteine amino acid, which also belongs to protein amino acids. These combinations not only enhance osteoinductivity but also have antibacterial properties [122]. For comparison, cysteine was incorporated into the PEG/HAp coating

on a titanium alloy. The degradation of the polymer allowed the release of the amino acid from the material [123]. However, *N*-acetyl-L-cysteine, which is an L-cysteine derivative, is used in such biomaterials instead.

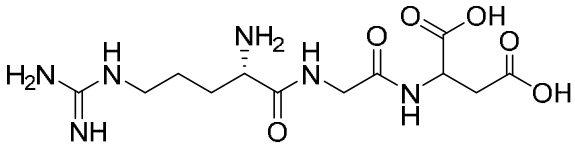

Figure 4. Structure of RGD (Arg–Gly–Asp) peptide.

2.2.2. Arginine

Since arginine (Figure 5) belongs to protein amino acids, it is used not only in the form of RGD sequence but also by itself, especially since it encourages cell attachment, proliferation, and differentiation on HAp surfaces. Therefore, composites similar to those already mentioned are created. A bone-like nanostructure was obtained by using nHAp and Col. The nanostructure was then enriched with L-arginine [124].

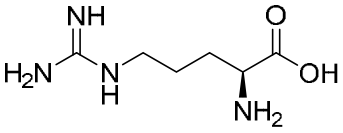

Figure 5. Structure of L-arginine.

An example of soft materials without ceramic reinforcement is a controlled-release system slowly releasing arginine–CS/plasmid DNA nanoparticles encoding the aforementioned BMP-2 gene (Arg-CS/pBMP-2 NPs). The Arg-CS/pBMP-2 nanoparticles were then encapsulated into PELA microspheres which work as the controlled-release carrier [125]. An interesting aspect is the application of magnetism and the integration of magnetic nanoarchitectures into synthetic/natural scaffolds. Thus, CS-based scaffolds containing dextran-grafted maghemite nanoarchitectures (DM) and functionalized with L-arginine were manufactured. The obtained results suggest that the simultaneous release of DMs and arginine conferred interesting properties toward osteoblast-like hMSCs, differentially stimulating their proliferation [126]. To promote osteoinductivity, a bioactive hydrogel on the basis of arginine-based unsaturated poly(ester amide) and methacrylated hyaluronic acid (HA) was developed via the photo-crosslinking method. Research has indeed confirmed the stimulation of bone formation processes; however, the kinetics of release has not been studied [127].

2.2.3. Polylysine

The last protein amino acid worth mentioning is homopolypeptide—polylysine (PL) (Figure 6). PL is utilized in biomaterials due to its high safety, water-solubility, stability, as well as antibacterial properties. It is reported that this AA may also be used to induce embryonic signaling processes during chondrogenesis in cartilage tissue engineering [128]. However, there are no many published studies on its application to cure skeletal system problems. One example is a polymer carrier from PLGA used to deliver this specific biomolecule in the targeted therapy. The surface of PLGA microspheres was first modified by introducing carboxyl groups, and this way, amino acids could be immobilized. Its release in vitro in the presence of MG63 human osteoblast-like cells positively influenced their adhesion and proliferation [129]. Another variant was the modification of poly(3-hydroxybutyrate-co-3-hydroxyvalerate)-HAp/bredigite nanofibrous composite scaffolds. The functionalization of the material was carried out by two methods, the use of the sorption process and covalent attachment. The kinetics of release has not been studied; however, the results suggest the possibility of using such connections in bone tissue regeneration [130].

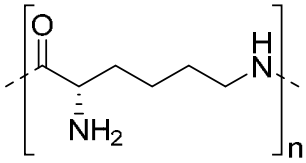

Figure 6. Schematic structure of polylysine.

2.3. Osteopontin (Bone Sialoprotein)

Osteopontin is a protein encoded in humans by the SPP1 gene and is also known as bone sialoprotein (BSP). It plays a role in apoptosis processes, cell activation, and chemotaxis. However, it is primarily a potential nucleator of HAp, responsible for biomineralization and bone remodeling [131]. An interesting fact is that with the assistance of osteopontin or appropriate antibodies, it is possible to treat specific human pathologies, e.g., autoimmune disease, cancer metastasis, immune organ atrophy, and also, primarily important in this review, bone remodeling [132]. Therefore, the osteoconductive tissue response of a biomaterial composed of a PLA matrix functionalized with HAp nanoparticles and bone sialoprotein was investigated. As a result of in vivo testing, a localized satisfied effect caused by protein release was observed. The presence of osteopontin improved the activation of bone-forming cells [133]. Another type of ceramics used to bind BSP is calcium silicate. An osteopontin-sequenced polypeptide SVVYGLR was grafted into mesoporous calcium silicate and 3D-printed into scaffolds that positively stimulated VEGF expression to improve angiogenesis during in vivo tests [134]. As in natural conditions, HAp crystals are deposited onto the type I Col; this protein was utilized to create bone sialoprotein-Col-guided materials. These display an increase in nucleation potency, yet the effect in both cases was minimal [135,136]. Col type I was also used to create carbonate-containing apatite/Col sponges decorated with BSP. The modification occurred via immersion technique. In vivo studies showed that one week after implantation into a tissue defect in rat tibia, the migration of numerous vascular endothelial cells inside the graft was observed [137]. Other functionalization of polymer matrix includes PCL/poly(2-hydroxyethyl methacrylate) surface treatment in regulating osseous tissue formation. Immobilizing BSP enhanced the attachment of osteoblastic cells [138]. However, in other studies, in order to determine protein-specific properties, different polymer-based porous scaffolds, with the absence of a mineral component, were modified via the sorption method. The obtained results suggest that chosen non-bioactive surfaces of biomaterials, e.g., polystyrene plates, β-tricalcium phosphate coated polystyrene discs, and poly(ethylene glycol terephthalate)/poly(butylene terephthalate) films with BSP, are not sufficient to prime bone marrow stromal cells for functional osteoblastic differentiation in vivo [139]. BSP, on the other hand, works effectively as a modifier of metallic surfaces. Titanium alloys are one of the most frequently used metallic biomaterials in bone problems. A Ti femoral implant was coated with protein by the physisorption method. As a result of in vivo as well as in vitro investigations, the observed increase in calcium deposition and the stimulation of cell differentiation induced by bone sialoprotein highlight its potential as a surface modifier that could enhance the osseointegration of orthopedic implants [140].

2.4. Osteocalcin

In recent years, evidence has been gathered that bone functions not only as a static structural organ that supports movement but also as an endocrine organ. One of the factors released by the skeleton is osteocalcin (Figure 7) [141].

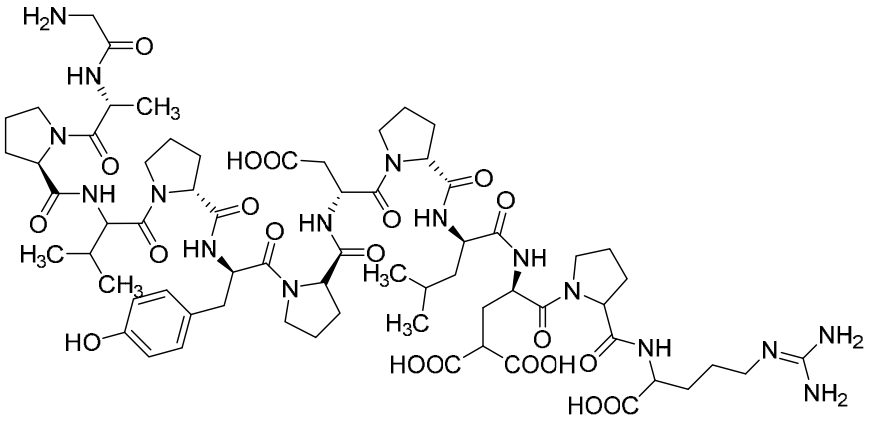

Figure 7. Chemical structure of osteocalcin.

It is an osteoblast-specific secreted protein that acts as a hormone by stimulating insulin production but also demonstrates an impact on bone mineralization and density [142]. The protein has been combined with ceramic/polymer materials featuring different structures, either pastes or cylindrical implants. In the first case, the bone cement was mixed with mineralized Col, and then osteocalcin was added to the cement paste during the setting [143]. In another one, calcium phosphate cement, containing various types of ceramic, was used as a starting material as well as a base for the whole implant. After combining with Col, a fiber-reinforced material was obtained and loaded with protein [144]. Although the release kinetics have not been studied in either case, both results suggest that osteocalcin activates osteoblasts as well as osteoclasts during early bone formation.

2.5. Osteonectin

Osteonectin is a non-collagenous protein of bone matrix that works as a calcium-binding matricellular factor in skeletal tissue [145]. The bone skeleton function refers to the differentiation of bone cells, remodeling control, and maintenance of bone mass [146]. An effect of osteonectin-derived glutamic acid sequence on the viscoelastic properties of poly(lactide ethylene oxide-fumarate) (PLEOF)/HAp composite was investigated. This way, a model of degradable material in bone regeneration was created [147]. Another connection with HAp involves the utilization of mineralized type I Col nanofibers. During synthesis, the protein was added to the polymer solution. As a result of in vivo studies, the formation of new mineralized fibers was observed in the presence of osteonectin. This could provide new insights into the novel mineralization function of this protein for bone development in in vivo conditions [148].

Table 1. Summary of the discussed protein biomolecule references.

Protein Biomolecule	References
Growth factors—TGF-β	[38–42,44–71]
Growth factors—IGF	[44–47]
Growth factors—SDF	[48]
Growth factors—BMP	[52–67,69,71,73–80,99]
Growth factors—FGF	[67,69,101–105]
Growth factors—VEGF	[42,74,74–90,94]
Growth factors—PGDF	[94–99]
Growth factors—NGF	[107]
Protein AA—RGD	[113–122]
Protein AA—Arg	[124–127]
Protein AA—PL	[129,130]
Osteopontin (bone sialoprotien)	[133–140]
Osteocalcin	[143,144]
Osteonectin	[147,148]

3. Non-Protein Biomolecules

3.1. Hormones

Hormones play a significant role in the proper functioning of the body. They are natural chemical messengers synthesized from a specific cell group. They constitute an excellent communication system from one tissue/cell to others in the body, participate in dynamic control of biochemical and physiological functions, and coordinate many processes in biological systems (neuroendocrine and immunological control). Hormonal imbalances cause disorders of regulatory mechanisms and thus disturb the homodynamic balance [149]. Therefore, the presence of hormones in implants increases the material's bioactivity, while the local delivery can provide a better as well as faster therapeutic effect. Based on the available literature, systems of local hormone delivery are presented.

3.1.1. Parathyroid Hormone

Parathyroid hormone (PTH) is produced by the glands adjacent to the thyroid gland, which control the calcium level in blood. When calcium concentration drops, the secretion of PTH increases, as it is responsible for stimulating the formation and resorption of bone tissue. The sporadic injection of small amounts determined bone formation causing bones to become stronger. Human trials have proved these abilities, and PTH itself is already used in the therapy of osteoporosis [150,151]. Biodegradable PLGA nanoparticles containing human parathyroid hormone, prepared by a modified double emulsion-solvent diffusion-evaporation method, were loaded into porous freeze-dried CS-Gel scaffolds. In vitro tests confirmed that the released PTH was biologically active during incubation and did not lose its properties due to binding to PLGA. The controlled release was observed for 28 days [152]. PLGA was also used to produce microspheres by double emulsion technique. PTH has been encapsulated and then analyzed in vitro and in vivo in relation to laboratory mice to determine the kinetics of its release and to induce a biological reaction in the bone [153]. As polymeric matrices can easily be modified with active substances, a hydrogel matrix with PEG and RGD peptides containing covalently bound peptides of PTH was designed. The study aimed to investigate the synergic effect of the released hormone and RGD on bone tissue regeneration processes [154]. A highly porous 3D nanofibrous scaffolds made of PLLA have been used to determine the optimal kinetics of release of PTH depending on the method of administration in a local bone regeneration model. The pulse method, in which a sandwich-like composite consisting of alternate alginate-PTH layers and polyanhydride (PA) insulating layers in a PCL sealant matrix, was compared with the continuous release method. In the second model, also in the PCL sealant matrix, PA microspheres loaded with PTH were charged. The difference between these two types of devices is in PTH distribution, where PTH is distributed in a layered structure to achieve pulsatile release or more uniformly in the matrix within microspheres to achieve continuous release. The kinetics was tested in vivo on a mice model [155]. Another way of pulsed PTH administration was applying a cylindrical device fabricated with a biodegradable PLLA, using a reverse solid free-form fabrication technique. On the supplied equipment, alternating isolation layers of sebacic acid, 1,3-bis(*p*-carboxyphenoxy)propane, PEG, and layers of PTH-loaded alginate were placed. The lag time was modulated by layer composition and film thickness [156]. In order to enhance the biomimetics of the carriers, biomaterials with ceramics demonstrating bioactivity are designed. A hybrid scaffold was manufactured by immobilizing polyphosphate-functionalized nHAp (PP-nHAp) on the porous surface, followed by PTH loading on the polyphosphates of nHAp surfaces. The hormone was sustainably released for up to 50 days. The results suggest a synergistic effect of using PTH and nHAp to enhance bone healing in the animal model [157]. Bioactive ceramic is not only HAp; therefore, β-tricalcium phosphate was also used to create such biomaterial. A ceramic-polymer composite of β-TCP and Col (β-TCP/Col) was created and then combined with PTH. Obtained results demonstrate that a combination of single-dose local administration of PTH and β-TCP/Col had an additive effect on local bone formation in osteoporosis rats [158]. As hydrogels display structural similarity to natural tissues,

PTH was loaded in a thiol-ene hydrogel at several concentrations and polymerized in and around an osteoconductive poly(propylene fumarate) (PPF) scaffold. The obtained biomaterial allowed the release of 80% of the hormone within 4 days, which showed bioactivity for 3 weeks [159]. PTH is only adequate when dosed by injection, because it has no oral bioavailability; therefore, a particularly interesting project was that describing the oral absorbtion of PTH in rats and monkeys facilitated by a delivery agent, 8-[(2-hydroxy-4-methoxybenzoyl)amino]caprylic acid (4-MOAC). In this study, dosing solutions were prepared by adding PTH to an aqueous solution of 4-MOAC in water. The obtained data suggest that 4-MOAC facilitates the gastrointestinal absorption of biologically active PTH in oral dosing of a 4 MOAC/PTH aqueous solution [160].

There are known combinations of biomaterials based on parathyroid hormone-related protein (PTHrP). It is used in bone-related therapy as it has been shown to induce bone anabolic actions in rodents and humans upon daily systemic administration. For this reason, an implant was created based on Gel-glutaraldehyde biopolymer-coated nanocrystalline HAp. These macroporous foams were then modified with PTHrP and biologically tested [161]. Osteostatin (OSN) is a fragment of PTHrP. ONS was chemically immobilized on a Col–HAp scaffold. The chemical attachment method via crosslinking ensures controlled continuous release in time. The in vitro and in vivo results confirmed that such a system may be adopted for a range of different proteins and thus offers the potential for treating various complex pathologies that require localized mediation drug delivery [162]. Apart from pure PTH, biomedicine also uses a PTH-derived peptide, PTHdP. Its potential as a bone growth factor for bone tissue engineering and bioactivity in the biological environment after being incorporated into the nHAp/CS scaffold was evaluated. It was demonstrated that PTHdP could significantly promote or inhibit osteogenesis when exposed intermittently or continuously to MC3T3-E1 cell culture. Moreover, sustained and controlled release of the bioactive molecule was achieved [163].

3.1.2. Vitamin D3

It is well known that vitamin D3 (cholecalciferol, Figure 8) plays a crucial role in remodeling and maintaining proper bone condition [164]. The active form of vitamin D3 (VitD3) used in biomedicine is calcitriol (Cal), produced by its hydroxylation in the liver by 25-hydroxycalciferol hydroxylase [165].

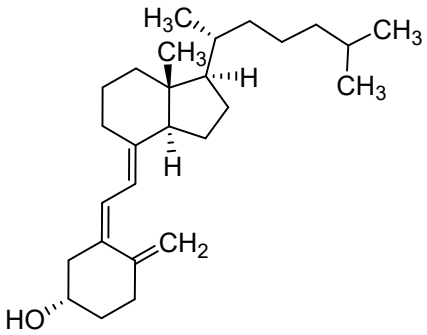

Figure 8. Structure of cholecalciferol.

The biomolecular-enabled coating was designed to improve osteogenic capabilities in bone tissue engineering. Polyelectrolyte multilayered (PEM) film coating with local immobilization of Cal in BCP scaffolds to promote osteoporotic bone regeneration by targeting the calcium-sensing receptor was designed [166]. Another ceramic/polymer material is a nanocomposite scaffold manufactured by electrospinning. The polymer scaffold, forming matrices, was made of PCL/Gel, reinforced by nHAp, and subsequently modified with VitD3. MG-63 cell line was cultured on the manufactured composite scaffolds, and the results confirmed a positive influence on the proliferation of cells with this form of Cal [167]. Subsequent studies of the same scaffold confirmed the possibility of a smooth release of VitD3in time [168]. As the main limitation of Cal is the short half-life in the bloodstream,

new therapeutic strategies and solutions are being sought to overcome this barrier. Using the single emulsion solvent evaporation method, VitD3 was encapsulated in PLGA nanoparticles. As a result, the nanoparticles remained stable under storage conditions for several weeks, and they were successfully lyophilized to increase their shelf-life using a cryoprotectant [169]. Porous scaffolds made from PLGA loaded with Cal were designed using the same components. These fully absorbable osteogenic biomaterials were prepared using the solvent casting/salt leaching method [170]. Specific scaffolds were used to investigate the influence of Cal on osteoinduction following local administration into mandibular bone defects. Hormone-loaded absorbable Col membrane scaffolds were prepared by the polydopamine coating method. Following in vivo implantation, Cal-loaded composite scaffolds underwent rapid degradation compared to materials without hormones, with pronounced replacement by new bone layers [171]. Absorbable Col fleece was soaked in Cal solution and then implanted in bone defects in the maxilla and mandible of rats. There was no significant difference between the control and research groups; moreover, the kinetics of hormone release was not investigated [172]. In order to improve the bioavailability of VitD3, it was essential to increase its solubility in water. Therefore, oleoyl alginate ester (OAE) hydrophobic nanoparticles served as hormone carriers and were prepared by acid chloride reaction. This resulted in oral carriers penetrating through cell walls and demonstrating the permanent release of the biomolecules [173].

3.1.3. Calcitonin

The hormone with an important role in the treatment of osteoporosis is calcitonin. It is produced by the thyroid gland and influences the inhibition of bone resorption, and the reduction of osteoclast formation has been proven [174]. A biomaterial was designed in which salmon calcitonin (sCT) was combined with pentapeptide-decorated silica nanoparticles (SiO_2 PepsCT). The purpose of the biomaterial was to improve therapeutic effectiveness. In vivo studies showed that the material also affects the extension of the sCT half-life [175]. Another sophisticated project was a complex of sCT and oxidized calcium alginate (sCT-OCA) loaded into a thermosensitive copolymer hydrogel. A polymer matrix consisted of PLGA-*b*-poly(ethylene glycol)-*b*-PLGA (PLGA-PEG-PLGA). Due to the nature and properties of the biomaterial, the sustained release of sCT was determined by the degradation of the hydrogel as well as the decomposition of the sCT-OCA complex [176]. In a ceramic-polymer carrier, PLGA and cement with calcium phosphate (CPC) were used. In order to obtain such a composite, microspheres with PLGA were loaded sCT and then incorporated into CPC. The hormone's release rate depended on the amount of the polymer phase [177]. A ceramic mixture containing 70% HAp and 30% β-TCP was modified with calcitonin by immersion in a hormone solution. As a result of in vitro and in vivo studies, an increase in the degree of osteogenesis was observed [178]. A similar method involving the modification of ceramic by sorption was used to produce nHAp loaded with sCT to obtain sCT-HAp-NPs [179]. Apart from the described hormone, there are connections with calcitonin gene-related peptides (CGRP). It was used as an osteogenic factor to modify a hydrogel scaffold composed of HAp and sodium alginate (SA), manufactured by the 3D printing method. Materials displayed active proliferation and differentiation in vitro and in vivo, highlighting osteoinductive abilities [180].

3.1.4. Estrogen and Testosterone

Not only the hormones responsible for regulating calcium levels are essential in controlling skeletal growth and maintaining bone mass as well as strength, but also sex hormones. Both female estrogen and male testosterone (Figure 9) affect the bone in men and women [181]. The relation between changes in bone density and estrogen level is well known. Changes in hormonal economy after menopause, particularly in estrogen expression, are the leading cause of osteoporosis [182]. However, the quantity of testosterone is equally crucial for a healthy skeleton, as it has been shown to directly affect bone cells and bone metabolism [183]. The ability to improve osteogenic differentiation of human

bone marrow mesenchymal stromal cells in the presence of estrogen was investigated by introducing this hormone on biodegradable PLGA microparticles. They ensured the intracellular release of biomolecules for seven days, which enabled the effective regulation of MSCs [184]. Estradiol, a primary natural estrogen, has been loaded into PCL/SF microfibers obtained by the electrospun method. The addition of SF increased the bioactivity of the polymer matrix. The sustained release of the hormone from the biomaterial lasted for about three weeks [185]. Its encapsulation provided impressive results regarding estrogen release in PLGA nanoparticles produced via an emulsion-diffusion-evaporation method. Hormone-loaded PLGA NPs were then placed in macroporous HAp-CS scaffolds. The nanoparticles were bonded to the scaffolds in two ways. The first method using embedding ensured the release of biomolecules for 55 days, whereas in scaffolds loaded during manufacture, the controlled release behavior of estradiol was observed for over 135 days [186]. The interesting idea was to use nanodiamond (ND) particles as a carrier. The estrogen-ND complex was then loaded into a photo–crosslinkable methacrylate glycol CS hydrogel (G). The prepared estradiol/ND/G platform increased the beneficial impact of estrogen through extended release with the highest efficiency and safety at a local level [187].

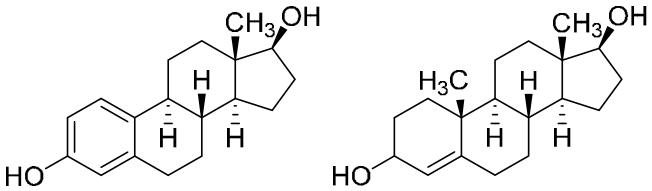

Figure 9. Structure of estradiol and testosterone.

Porous biomaterials were obtained from mesoporous bioactive glass modified with testosterone. In order to obtain these scaffolds, the solutions of both components were thoroughly mixed and then freeze-dried. Sustained-release testosterone was confirmed by the results obtained [188]. A load-bearing biodegradable scaffold made of polypropylene fumarate/tricalcium phosphate composites was modified by adding testosterone, bone morphogenetic protein-2 (BMP-2), or their combination in order to promote bone regeneration. The obtained results demonstrated that testosterone is as effective as BMP-2 in promoting the healing of critical-size segmental bone defects and that combination therapy with testosterone and BMP-2 is superior to single therapy. However, the kinetics of the release of the compounds has not been investigated [189]. The influence of the male sex hormone on cell proliferation and differentiation has been examined in relation to ceramic-polymer scaffolds based on PCL/BCP. These materials were modified with the addition of PLGA as well as testosterone (T) resulting in two types of composites, PCL/BCP/T and PLGA/PCL/BCP/T. Both scaffolds were associated with desirable characteristics for bone tissue applications; however, alkaline phosphatase levels expressed by osteoblasts were significantly greater with PLGA/PCL/BCP/T [190].

3.1.5. Insulin

Clinical and experimental studies show that insulin (Figure 10), a peptide hormone produced by the pancreatic islands, is closely related to bone density. Using it as an anabolic agent can preserve and increase bone strength through its effects on bone formation [191]. Different types of biomaterials are designed for the local supply of this biomolecule. In a biomimetic one, insulin was chemically grafted onto the surface of HAp nanorods (nHA). The insulin-grafted nHAs (nHA-I) were dispersed in PLGA polymer solution, which was electrospun to prepare PLGA/nHA-I composite nanofiber scaffolds. The obtained results suggest that the PLGA/nHA-I composite nanofiber scaffold can enhance osteoblastic cell growth, as more cells were proliferated and differentiated. However, the carrier's hormone release rate has not been studied [192]. Similar organic/inorganic materials enriched with Col have been manufactured. Insulin-loaded PLGA particles were incorporated into porous nHAp/Col scaffolds. In vitro and in vivo studies confirmed that the bioactive hormone

was successfully released from the PLGA particles within the scaffold, and the size of the particles as well as the release kinetics of the insulin could be efficiently controlled. Furthermore, the biomaterials significantly accelerated bone healing [193,194]. Scaffolds containing systematic gradients mimicking the significant gradients observed in native tissues were designed. Nanoparticles of insulin and β-glycerophosphate (β-GP) were incorporated into a non-woven mat of PCL. Human adipose-derived stromal cells (hADSCs) were cultured on these graded non-woven mats to probe their effects on the development of cellularity and mineralization. The obtained results showed that the differentiation of the stem cells increased at insulin-rich locations [195]. Instead of pure insulin, insulin-like growth factor I (IGF-I) is also often used in research. It is entrapped in the mineralized matrix of the bone during formation and affects cell proliferation by stimulating growth in various progenitor cell types. Thus, controlled IGF-I-releasing SF scaffolds were designed [196]. Another biomimetic project involving the use of ceramics consisted of the manufacture of scaffolds from alginate, tricalcium phosphate (TCP) granules, and PLGA microspheres (MS) loaded with osteoinductive IGF-I. Controlled and sustainable IGF-I release was observed for 28 days [197]. In another study, to accelerate the deposition of bone-like minerals (BLM) on the surface of the designed biomaterial, three-dimensional (3D) PLGA porous scaffolds have been modified by applying surface treatments. PLGA was incubated in an SBF solution enriched with IGF-I. Obtained mineralized scaffolds demonstrated slow controlled release over a 30-day period when they were incubated in phosphate-buffered saline (PBS) at 37 °C. Increased proliferation of bone marrow stromal cells was observed in in vitro as well as in vivo studies [198].

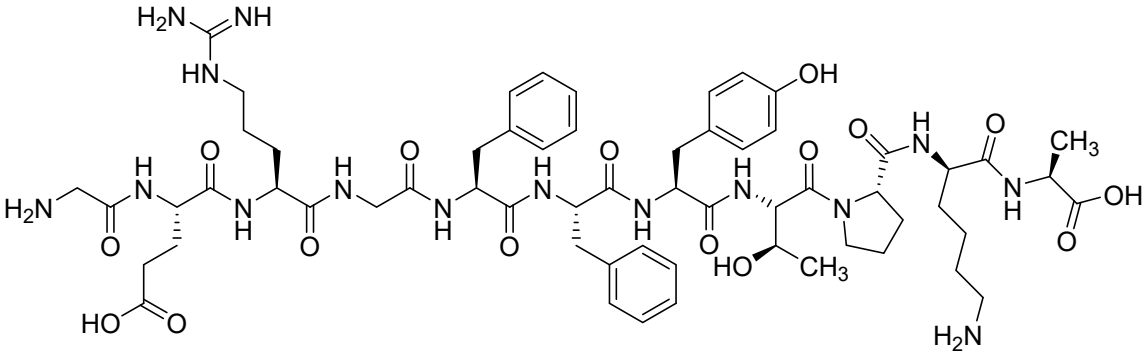

Figure 10. Schematic illustration of the chemical structure of insulin.

3.2. Flavonoids

Flavonoids are a broad group of organic chemicals found in plants. They serve as dyes, antioxidants, and natural insecticides as well as fungicides, protecting against insect and fungal attacks [199]. However, due to their specific nature, they also demonstrate interesting biochemical and antioxidant effects associated with many diseases, such as cancer, arteriosclerosis, and Alzheimer's disease [200]. They are components of many pharmaceuticals and cosmetics, considering their interesting anti-carcinogenic, antioxidative, anti-inflammatory, and anti-mutagenic properties [201]. In the regeneration of the skeletal system, these non-protein biomolecules are particularly important in stimulating the osteoblastogenesis process, which leads to the formation of new bone layers by supporting the differentiation of MSCs into osteoblasts [202]. Based on the available literature, this part of the review will briefly discuss approaches to the delivery of selected flavonoids, such as icariin, resveratrol, quercetin, and others (structures presented in Figure 11) that have been proven to be proregenerative in bone tissue.

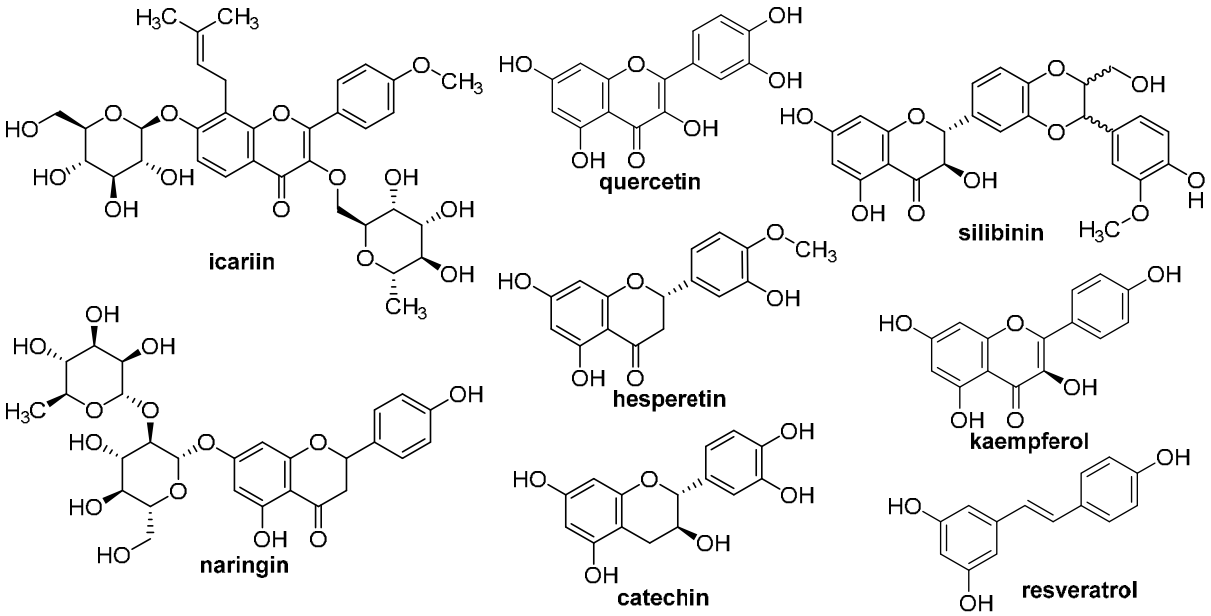

Figure 11. Chemical structure of discussed flavonoid-based compounds.

3.2.1. Icariin

In the regeneration of bone tissue with proven osteogenic and angiogenic effects, icariin (ICA) is an essential flavonoid. Several reports have shown that ICA (Figure 11) can inhibit osteoclast differentiation and increase osteogenic differentiation of mesenchymal bone stem cells (BMSCs) [203]. In order to provide the implants with the greatest possible biomimetics, they are bound to ceramics, which makes the resulting structure relatively similar to natural bone tissue. Bioactive scaffolds strengthening bone repair were developed by loading ICA into porous scaffolds with tricalcium phosphate (TCP), and the obtained porous Ica/TCP composites were then investigated for treating osteonecrosis of the femoral head (ONFH) in a rabbit model [204]. A bioactive PLGA/calcium phosphate/ICA (PTI) scaffold was fabricated by an innovative low-temperature 3D printing technology. Potentially, the main use of this biomaterial is to treat steroid-associated osteonecrosis. The obtained and presented results based on in vitro and in vivo tests against rabbit models suggest that the scaffolds are a promising potential strategy for bone tissue engineering and regeneration in patients with challenging bone cancer [205]. HAp ceramics was also used to create composites with this flavonoid. Micro/nHAp granules were modified with ICA by sorption process, consisting of immersing them in a flavonoid solution and freeze-drying [206]. Similar systems containing additional CS, a natural, degradable polymer that increases the ability of bone precursor cells to differentiate and promotes the formation of new bone tissue, are also known. The scaffolds were generated by thoroughly mixing ICA and CS/HAp in micro- as well as nanoscale (ICA-CS/HA) using the freeze-drying technique. In all cases, the drug release behavior has demonstrated that the ICA loading CS/HA scaffolds can achieve the basic effect of the permanent release of the drug simultaneously with a satisfactory effect on the bone tissue regeneration processes [207–209]. More advanced systems have also been described. Composite biomaterials were designed via the electrospun method, using Col, PCL, and HAp, additionally containing CS microspheres in which the ICA was encapsulated [210]. Combining a natural polymer, water-soluble carboxymethyl CS (CMCS) with a synthetic oil-soluble PLGA, nHAp-reinforced hybrid scaffolds loaded with ICA (ICA-loaded nHAP/CMCS/PLGA) were developed. As a result, an implant with a topological structure similar to natural bone was created. Based on in vivo and in vitro results, scaffolds effectively promoted the osteoblasts' adhesion, proliferation, and differentiation, thus having great potential and providing a unique strategy for bone repair and regeneration [211]. Another biopolymer

known to be used in drug and cell delivery systems is alginate. In its spheres, ICA was enclosed with and then combined with HAp. The freeze-drying method was used to obtain a HAp/alginate (HAA) porous composite scaffold loaded with flavonoids. The obtained data suggest its promising application in biomedicine as it mediates the processes of coupling of osteogenesis induction and inhibits osteoclast activity [212]. Bioglass-based materials are also manufactured. Using the foam replication technique, the Gel-coated 3D sponge-like scaffolds based on 45S5 bioactive glass were created. The prepared implants exhibited slightly different properties and the kinetics of flavonoid release, depending on the crosslinking agent applied, caffeic acid or EDC/NHS ((3-dimethylaminopropyl)-*N*′-ethylcarbodiimide hydrochloride/*N*-hydroxysuccinimide) [213]. Hybrid porous ICA-loaded hollow bioglass/CS (ICA/HBG/CS) therapeutic scaffolds were developed to treat critical-sized bone defects [214]. Carriers without a ceramic phase mainly focus on using the characteristic polymer structure to deliver the active substance. Mg^{2+} ions were used as a carrier. Hydrophobic ICA was preloaded on $MgO/MgCO_3$ molecules and then enclosed in microspheres made out of PLGA, which is biodegradable in the biological environment. Such a degradable system allows double-controlled release [215]. PLLA was used to create fibrous membranes using the electrospinning method. An intermediate layer of PDA was then applied to them in order to obtain increased cytocompatibility as well as osteogenic activity. The membrane was functionalized with ICA to obtain PLLA-PDA-ICA biomaterial [216]. The fibrous membrane, which simulates the artificial periosteum, was made by the electrospun method. For this purpose, ICA was introduced into PCL/Gel nanofibers [217]. Increased bone cell proliferation was achieved by using porous scaffolds. Biomaterials were made by combining the solvent casting and salt leaching techniques from poly(3-hydroxybutyrate-co-3-hydroxyvalerate) (PHBV). This way, novel ICA delivery porous PHBV scaffolds (IDPPSs) were fabricated [218]. HA is used in tissue engineering and biomaterials due to its high hydrophilicity as well as a positive effect on chondrogenesis of stem cells and chondrocytes, cartilage formation, and the integration of the neocartilage with the surrounding native cartilage. These properties are significant for the regeneration of bone and cartilage tissue. An HA-ICA hydrogel was designed. Methacrylic anhydride (MA) was combined with flavonoid and then dissolved in a solution of MA-modified HA, which resulted in obtaining the hydrogel [219]. The three-component system, enriched with Gel, was made by an emulsion-coagulation method using glutaraldehyde (GA) as a crosslinking substance. Composite microspheres of Gel/hyaluronic acid (Gel/HA) loaded with ICA as a controlled release system were presented. The study showed that the rate of release of ICA from the microspheres can be relatively easily modified by changing the GA content and crosslinking time [220]. Similarly, hydrogel materials were obtained from ICA conjugated with HA/Col (Ica-HA/Col) to promote osteochondral interface restoration [221]. Due to the impressive properties of nanomaterials and nanoparticles, there is a growing interest in their use in biomedicine. TiO_2 nanotubes were used in the study, as they are an interesting component in biomaterials for bone tissue regeneration. It was demonstrated that the surface morphology of TiO_2 nanotubes could improve the adhesion, proliferation, and differentiation of osteoblast cells and MSCs. Therefore, an ICA-functionalized coating composed of ICA and PLGA on the TiO_2 nanotube surface (NT-ICA-PLGA) to promote osteoblast cell activity and early osseointegration was designed [222]. A composite structure consisting of ICA-loaded and CS-Gel-sealed TiO_2 nanotubes was created to control the drug release profile and improve the biocompatibility of Ti substrates. Firstly, the flavonoid was placed in the TiO_2 nanotube space and then sealed with CS-Gel multilayer coatings. Based on obtained results, it is suggested that such a nanotube structure can modulate the bioactivity of primary osteoblasts [223]. A small intestine submucosa (SIS) was used as an excellent, natural biological carrier. However, SIS provides a different microenvironment than bone tissue; thus, its structure was modified with ICA. This has resulted in a permanent SIS scaffold with improved osteoinductivity and controlled local delivery of ICA. Implants were in vivo tested in a mouse calvarial

defect model, and the results of this study suggest that the SIS scaffold has the potential as an ICA delivery carrier for the enhancement of bone regeneration [224].

3.2.2. Quercetin

A particularly important place in the regeneration of the skeletal system is occupied by quercetin (QU, Figure 11). It was demonstrated that compared with other flavonoids, for example, kaempferol, it has a better stimulating effect on osteogenic differentiation of hADSC and is helpful for in vivo bone engineering [225].

As QU is poorly absorbed during oral administration, QU-loaded phytosome nanoparticles (QPs) have been prepared using the thin film hydration method. QP exhibited very high encapsulation efficiency (98.4%), and the results confirmed its superiority over free QU at the same doses as a promising hormone replacement therapy [226]. The scaffold, demonstrating a very beneficial effect on the proliferation and attachment of MC3T3-E1 cells and promoting the expression of related genes and osteogenic proteins, was made with 3D-printed PLLA. The polymer was functionalized by QU with a layer of PDA and then analyzed biologically in relation to MC3T3-E1, an osteoblast precursor cell line derived from mouse calvaria. As a result, the potential of the 3D-printed QU/PD-PLLA scaffolds with a certain amount of flavonoid as a bone-repair material was confirmed [227]. With good effects, it was decided to modify the obtained QU/PD-PLLA scaffold with CS to give it specific properties. In this way, PLLA/CS-D/QU was obtained. First, the 3D-printed PLLA scaffold was incubated in a CS solution and then freeze-dried to obtain PLLA/CS scaffolds with micro/nano-fiber hierarchical structure [228]. In order to imitate the natural bone in the best possible way, QU was also combined with ceramics. A simple two-component nHAp/QU composite was proposed. Vacuum freeze-drying technology was used to fabricate the drug delivery system. The flavonoid was mixed with the nHA bioceramic microspheres, and modification occurred through the sorption process [229]. A more advanced three-component structure built of an SF/HAp scaffold inlaid with QU (QU/SF/HAp) at different concentrations promoted osteogenesis, mainly focusing on QU's ability to enhance bone health. QU was loaded on the SF/HAp scaffolds using freeze drying [230]. Composites containing various biomaterials of natural origin were also proposed. Col obtained from duck feet was used as a polymer phase of the scaffold composed of QU and HAp (QU/DC/Hap), improving osteoconductive properties. Obtained QU/DC/HAp sponges were tested in vitro in relation to BMSCs as well as in vivo against rat calvarial bone defects. The results confirmed that these bioengineered sponges could improve bone tissue regeneration [231]. Another material of natural origin used for the biometric scaffold was goat lung fabricated by decellularization of lung tissue. After appropriate treatment, it was modified by crosslinking with QU and nHAp and characterized to evaluate the suitability of the QU crosslinked nHAp-modified scaffold for the regeneration of bone tissue [232].

3.2.3. Naringin

Naringin (Figure 11) is a flavonoid demonstrating therapeutic effects in diseases related to bone metabolism [233].

Modifying a biodegradable composite with this flavonoid determined its potential to repair bone defects. A porous composite containing genipin crosslinked Gel and β-tricalcium phosphate (GGT) was fabricated by the salt-leaching method to carry naringin (GGTN). The ability to regenerate bone tissue in vivo was assessed using the biological response of the rabbit calvary bone to these materials. Higher growth of new apatite layers at the site of GGTN implantation than of simultaneous GGT implantation was demonstrated; therefore, GGTN is promising as a bone substitute [234]. Naringin has also been supplied by incorporation into electrospun nanoscaffold containing PCL and PEG-*b*-PCL. This allowed for the creation of PCL/PEG-*b*-PCL/naringin nanoscaffolds. Based on the critical size defect (CSD) model of mouse calvarial bone and the presented results, it was shown that the scaffolds strengthen osteoblast functions and suppress

osteoclast formation [235]. The electrospinning method was also used to create naringin-loaded microsphere/sucrose acetate isobutyrate (Ng-m-SAIB) hybrid depots to improve osteogenesis in the calvarial defects of SD rats. Demonstrated results confirmed that Ng-m-SAIB hybrid depots might have promise in bone regeneration applications [236].

3.2.4. Silymarin

Silymarin (a standardized extract from the seeds of *Silybum marianum*) is composed of many compounds, with silibinin (Figure 11) being its main active ingredient. Silymarin (SIL) supports osteoblast proliferation, inhibits osteoclast proliferation, and positively affects bone regeneration. It was combined with HAp with good osteoclastic properties. For this purpose, titanium plates were covered with ceramics and then incubated in modified SBF with SIL to be absorbed. This way, titanium implants with SIL-loaded HA coatings were obtained and then implanted in twelve-week-old female Sprague Dawley rats. The results suggest that the local incorporation of coatings with SIL is helpful in improving new bone formation around the surface of titanium rods [237]. Another combination of SIL with HAp presupposed the formation of Col sponges from the Col of natural origin from duck feet (DC) by freeze-drying. The in vitro results against rabbit bone marrow stem cells and in vivo results in a rat calvarial defect model confirmed that Smn/DC/HAp grafts support cell adhesion, proliferation, and osteogenicity [238].

3.2.5. Hesperetin

Hesperetin (Figure 11) was supplied by a Gel sponge in the rat model hMSC using a scaffold combined with hesperetin/Gel. This model has influenced the rate of healing of tibial fractures in rats, speeding up the process [239].

3.2.6. Kaempferol

The kaempferol (Figure 11) was delivered in a layered composite LBL (layer by layer)-kaempferol composed of alternating layers of sodium alginate and protamine sulfate on the $CaCO_3$ core. The drug release rate was determined by its concentration in the biomaterial and layer thickness. However, it was shown that the demonstrated method enhanced drug delivery and improved pharmacokinetics [240].

3.2.7. Catechin

The influence of catechin (CC, Figure 11) on osteogenesis and mineralization has been investigated based on coatings modified with catechin hydrate. As this flavonoid is a simple multifunctional material-independent coating compound, its modification was performed by the dip-coating method. The selected media were polystyrene, silicon oxide, titanium oxide, PCL nanofiber, glass coverslip, gold, polytetrafluoroethylene, and polydimethylsiloxane. In vitro tests were performed on human adipose-derived stem cells (hADSCs) and human umbilical vein endothelial cells (HUVECs), and in vivo on a mouse calvarial defect model. As a result, it was concluded that CC-based media not only improved cell adhesion and proliferation but also significantly improved osteogenesis of hADSCs in vitro and in vivo due to the intrinsic biochemical properties of CC, including antioxidant and high calcium binding affinity [241]. Taking into account the impressive properties of CC and the effect of selenium on bone strength, a nanocomposite was formed by modifying the nHAp with this element and then combining them with CC/SE-HAp. The addition of the flavonoid was intended to improve the anticancer activity of Se-HAp nanoparticles against osteosarcoma. Studies were carried out on two lines of human cells, normal bone marrow stem cells (hBMSCs) and human osteosarcoma cell lines (MNNG/HOS). The study showed that combining a natural biomaterial (i.e., CC) with Se and HAp may be a practical therapeutic approach in bone cancer therapy [242]. The combination of CC and mesoporous HAp (mHAp) was possible through a stable amide connection resulting from the previous modification with (3-aminopropyl)triethoxysilane. Then the short- and long-term responses of cultured MSCs, osteosarcoma cells (Saos-2), and doxorubicin-resistant cells

(RSaos-2/Dox) on the surface of the prepared Cat@MHAp biomaterials were investigated. Based on the results, it was found that Cat@MHAP decreases the proliferation of Saos2 and RSaos-2/Dox cells in a time-dependent manner. At the same time, it supports the growth of MSCs, indicating the ability of Cat@MHAP to distinguish tumor cells from normal ones [243]. Epigallocatechin gallate (EGCG) is a type of the most abundant green tea CC [244]. The effect of the combination of EGCG and α-TCP on the bone regeneration capacity in a bilateral rat calvarial bone defect model was investigated. Modifying ceramics with the flavonoid was performed by sorption, possibly due to the porous nature of α-TCP. This study demonstrated the bone-promoting effect of the local application of EGCG using the obtained biomaterial [245]. The potential of three-component epigallocatechin gallate/duck feet Col/HAp (EGCG/DC/HAp) composite sponges obtained by freeze-drying for bone repair has been investigated. In vitro results against bone marrow-derived mesenchymal stromal cells as well as in vivo results in nude mice confirmed that EGCG/DC/Hap is able to direct osteogenic differentiation; thus, it could be applied to the human body substitute as a natural material for bone regeneration [246].

3.2.8. Resveratrol

Resveratrol (RSV) is an antioxidant and anti-inflammatory polyphenol, whose beneficial therapeutic effects in type II diabetes, cardiovascular diseases, and hypertension have been proved [247].

However, more and more studies are focusing on its potential use in skeletal as well as cartilage therapy. A biodegradable RSV-loading synthetic polymer (PLA) and biopolymer (Gel) composite 3D nanoscaffold was designed to support the treatment of cartilage defects. During in vivo and in vitro research, primary chondrocytes and cartilaginous tissue cells were successfully cultured on the scaffold [248]. A bioactive RSV-PLA-Gel porous nanoscaffold was designed using the same compounds and electrospinning, freeze-drying, and uniform dispersion techniques to repair articular cartilage defects. As a result, it was found that the biomaterial promotes the repair of cartilage injury as a whole and might function via activation of the PI3K/AKT intracellular signal path [249]. The osteogenic effect of an RSV-conjugated PCL scaffold was evaluated in mesenchymal cell culture and a rat calvarial defect model. A flavonoid was coupled through a hydrolysable covalent bond with the carboxylic acid groups in a porous PCL surface grafted with acrylic acid. It was found that the incorporation of RSV caused increased alkaline phosphatase activity of rat bone marrow stromal cells and enhanced mineralization of the cell–scaffold composites in vitro [250]. In order to optimize the therapeutic effect of the flavonoid, it was inoculated into polyacrylic acid to obtain a macromolecular drug, PAA-RSV, which was then incorporated into atelocollagen hydrogels (Coll) to produce Coll/Res scaffolds. Coll/PAA-RSV scaffold was implanted into the osteochondral defect of rabbits, and, after a certain time, exhibited anti-inflammatory activity. The biomaterial was also able to remove free radicals and thus protect chondrocytes and BMSC from damage; thus, it represents a potentially significant advancement in clinical options for osteochondral damage repair [251]. Col scaffolds and human adipose tissue stem cells were combined with regenerating oral mucosa and calvarial bone with RSV. The effect of these Col/RSV scaffolds in vitro and in vivo on healing and bone regeneration was evaluated. Obtained results suggest that Col/RSV scaffolds can provide helpful biological cues that stimulate craniofacial tissue formation [252]. In order to compose the most biomimetic material possible, hydrogel reinforced with a ceramic phase was used. Based on the crosslinking reaction, a hydrogel with 3,6-anhydro-α-L-galacto-β-D-galactane modified with nHAp and RSV was obtained. Based on the physiochemical and biological analysis, it was demonstrated that the designed hydrogel is a material of biological relevance and great pharmacological potential as a carrier for bioactive compound delivery [253].

3.3. Lipids

It is well known that some lipids are able to influence the molding of HAp under in vivo conditions [254]. They work as in vitro and in vivo promoters of ceramic layer formation [255]. Moreover, when administered locally, they may also cause a therapeutic effect on surrounding tissues. Therefore, they are used as a part of implants as well as biomaterials that work as carriers of biomolecules. Phosphatidylserine (PS) is a quantitatively minor membrane phospholipid that plays a crucial role in cell cycle signaling, specifically in relation to apoptosis [256]. The potential of bone repair in rat calvarial defects using a combination of HAp with phosphatidylserine liposomes was investigated. The positive effect of PS on osteogenesis processes was confirmed by in vitro and in vivo studies. Mineralization occurred faster in the presence of a two-component (HAp-PS) system [257]. To imitate biological conditions similar to natural bone, phosphatidylserine was combined with Col solution, and then nHAp was added. The freeze-drying method was used to produce a porous, organic-inorganic (nHAp-Col-PS) scaffold [258]. Based on in vitro results, the release kinetics of PS correlated with the material structure [259]. The ceramic phase was also used as bioactive glass in combination with Col microspheres loaded with phosphatidylserine to receive porous scaffolds. Obtained in vivo results demonstrate the usefulness of PS for inducing enhanced bone formation in relation to Sprague Dawley rats [260] and rabbits [261]. In another similar project, such a three-component system was additionally enriched with steroidal saponins, which were also loaded in Col microparticles. A gradient, porous scaffold was obtained, and the release rate of the biomolecule was gradient-dependent [262]. Another implantological approach was to use titanium rods. Porous Ti foam was obtained by the plasma-sprayed method, and HAp coatings on its surface were also applied by plasma spraying. The layout was modified with PS by dip-coating into phospholipid solutions in chloroform [263]. Titanium was also used to create coated discs. On Ti discs, an organic matrix containing Col and phospholipid was deposited by the Langmuir-Blodgett technique. The selected phospholipid was 1,2-dipalmitoyl-sn-glycero-3-phosphatidylcholine (DPPC), because phosphatidylcholine groups are abundant in the natural cell membrane. The obtained results suggest that Col incorporation into DPPC induced the formation of biomimetic HAp nanoparticles that resembled the HAp nanoparticles found in natural bone [264]. DPPC was also used to modify mica, a mineral classified as a silicate. The film layers were composed using the commercial Langmuir–Blodgett method. Phospholipid was released in an artificial biological environment, and after a certain time, it was found that calcium phosphate minerals may precipitate on the mica surface placed in SBF [265]. A biomaterial composed of the same components was also enriched with phospholipase A2 [266]. A valuable multi-modal platform in bone tissue therapy was designed by a combination of nHap and lipid membrane mimetic coatings (LMm); the platform consisted of 69.3% phosphatidylcholine, 9.8% phosphatidylethanolamine, 2.1% lysophosphatidylcholine, and 18.8% fatty acid. Multilamellar vesicles (MUVs) were made to provide a higher therapeutic effect using the thin-film hydration method. Lipid vesicles were the carrier for the local transport of ibuprofen and ciprofloxacin. [267].

However, not only one lipid can be used to compose such biomaterials. HAp/Col scaffolds were modified with liposomes, which were prepared from a mixture of cholesterol, 1,2-distearoyl-sn-glycero-3-phosphatidylcholine (DSPC), 1,2-distearoyl-sn-glycero-3-phosphoethanolamine-n-[methoxy(polyethylene glycol) (DSPE-PEG), and a bone-binding bisphosphonate (BP) attached. The scaffold was modified with biomolecules by incubating them in a solution containing liposomes. The release rate of PEG-liposomes and BP-liposomes from the scaffolds was investigated for 7 days. Furthermore, the interior of created liposomes worked well during in vivo examination as a drug carrier [268].

Table 2. Summary of the discussed non-protein biomolecule references.

Non-Protein Biomolecule	References
Hormones—PTH	[152–160]
Hormones—PTHrP	[161,162]
Hormones—PTHdP	[163]
Hormones—vitamin D	[166–173]
Hormones—calcitonin	[175–180]
Hormones—sex hormones	[184–190]
Hormones—insulin	[192–195]
Flavonoids—icariin	[204–224]
Flavonoids—quercetin	[226–232]
Flavonoids—naringin	[234–236]
Flavonoids—silymarine	[237,238]
Flavonoids—hesperetin	[239]
Flavonoids—kaempferol	[240]
Flavonoids—catechin	[241–246]
Flavonoids—resveratrol	[248–253]
Lipids	[257–267]
Liposomes	[268]

4. Conclusions and Perspectives

This review constitutes a collection of papers representing approaches in which tissue engineering seeks to solve problems involving bone tissue. A wide range of protein and non-protein biomolecules as active components of ceramic and polymer biomaterials are discussed in detail. According to the presented benefits of the biomolecules summarized in this review, it can be concluded that they have the potential to be adapted to the patient's specific condition. Both the type, the dose, and the delivery method of the selected molecules will affect bone regeneration and, most importantly, the patient's condition. It is important to emphasize that biocompatible polymeric materials or polymer-based composites are most widely used as active substance carriers. These materials are generally relatively cost-effective and easy to modify, and considering their physicochemical nature, they can be easily adapted to perform specific functions (i.e., by selecting hardness, degree of cross-linking, or mass). There is no single substance, protein, or drug designed strictly for bone tissue regeneration. For this reason, the review describes many biomolecules of both protein and non-protein origin. Although osteopontin, osteocalcin, or BMP-2 by their actions definitely contribute to bone regeneration, by far the better antioxidant properties are exhibited by flavonoids. Therefore, depending on the specific action of the carrier and therapeutic effect, carriers modified with the most equal biomolecules are studied, as they exhibit various effects and impacts on the body.

This article focuses primarily on the use of drug-delivery systems for bone tissue regeneration. However, biomolecule delivery systems are also used in the treatment of heart diseases and cancer as well as in the creation of new tissues. As science advances in the field of biomaterials, it is possible to design increasingly advanced next-generation materials. The systems described in this review have great potential to be used as carriers of active substances. Nevertheless, it should be emphasized that a collaboration of chemistry, biology, physics, and medical experts is needed to perfect them. In this way, the ultimate goal of improving the health and well-being of society will be achieved.

Author Contributions: Conceptualization, D.S., J.J. and A.S.-K.; writing—original draft preparation, D.S., K.P., and A.S.-K.; writing—review and editing, D.S., J.J and A.S.-K.; visualization, D.S., K.P., and A.S.-K.; supervision, A.S.-K.; project administration, J.J. and A.S.-K.; funding acquisition, J.J. and A.S.-K. All authors have read and agreed to the published version of the manuscript.

Funding: This research was funded by Foundation for Polish Science, grant number POIR.04.04.00-00-16D7/18. This work was also supported by the project APVV-17-0373.

Institutional Review Board Statement: Not applicable.

Informed Consent Statement: Not applicable.

Data Availability Statement: Not applicable.

Acknowledgments: The "Multifunctional biologically active composites for applications in bone regenerative medicine" project is carried out within the TEAM-NET program of the Foundation for Polish Science financed by the European Union under the European Regional Development Fund. The authors gratefully acknowledge financial support.

Conflicts of Interest: The authors declare no conflict of interest.

References

1. Trucillo, P. Drug Carriers: Classification, Administration, Release Profiles, and Industrial Approach. *Processes* **2021**, *9*, 470. [CrossRef]
2. Llah, H.; Santos, H.A.; Khan, T. Applications of bacterial cellulose in food, cosmetics and drug delivery. *Cellulose* **2016**, *23*, 2291–2314. [CrossRef]
3. Varanko, A.; Saha, S.; Chilkoti, A. Recent trends in protein and peptide-based biomaterials for advanced drug delivery. *Adv. Drug Deliv. Rev.* **2020**, *156*, 133–187. [CrossRef]
4. Fenton, O.S.; Olafson, K.N.; Pillai, P.S.; Mitchell, M.J.; Langer, R. Advances in Biomaterials for Drug Delivery. *Adv. Mater.* **2018**, *30*, 1705328. [CrossRef] [PubMed]
5. Singh, S.; Pandey, V.K.; Tewari, R.P.; Agarwal, V. Nanoparticle based drug delivery system: Advantages and applications. *Indian J. Sci. Technol.* **2011**, *4*, 177–180. [CrossRef]
6. Salamanna, F.; Gambardella, A.; Contartese, D.; Visani, A.; Fini, M. Nano-Based Biomaterials as Drug Delivery Systems Against Osteoporosis: A Systematic Review of Preclinical and Clinical Evidence. *Nanomaterials* **2021**, *11*, 530. [CrossRef]
7. Santos, G.B.; Ganesan, A.; Emery, F.S. Oral Administration of Peptide-Based Drugs: Beyond Lipinski's Rule. *ChemMedChem* **2016**, *11*, 2245–2251. [CrossRef]
8. Parodi, A.; Buzaeva, P.; Nigovora, D.; Baldin, A.; Kostyushev, D.; Chulanov, V.; Savvateeva, L.V.; Zamyatnin, A.A. Nanomedicine for increasing the oral bioavailability of cancer treatments. *J. Nanobiotechnol.* **2021**, *19*, 354. [CrossRef] [PubMed]
9. Attia, M.F.; Anton, N.; Wallyn, J.; Omran, Z.; Vandamme, T.F. An overview of active and passive targeting strategies to improve the nanocarriers efficiency to tumour sites. *J. Pharm. Pharmacol.* **2019**, *71*, 1185–1198. [CrossRef] [PubMed]
10. Whitby, M.; McLaws, M.L.; Slater, K. Needlestick injuries in a major teaching hospital: The worthwhile effect of hospital-wide replacement of conventional hollow-bore needles. *Am. J. Infect. Control* **2008**, *36*, 180–186. [CrossRef]
11. McLennan, D.N.; Porter, C.J.H.; Charman, S.A. Subcutaneous drug delivery and the role of the lymphatics. *Drug Discov. Today Technol.* **2005**, *2*, 89–96. [CrossRef]
12. Alkilani, A.Z.; McCrudden, M.T.C.; Donnelly, R.F. Transdermal drug delivery: Innovative pharmaceutical developments based on disruption of the barrier properties of the stratum corneum. *Pharmaceutics* **2015**, *7*, 438–470. [CrossRef]
13. Han, T.; Das, D.B. Potential of combined ultrasound and microneedles for enhanced transdermal drug permeation: A review. *Eur. J. Pharm. Biopharm.* **2015**, *89*, 312–328. [CrossRef] [PubMed]
14. Djupesland, P.G.; Messina, J.C.; Mahmoud, R.A. Breath powered nasal delivery: A new route to rapid headache relief. *Headache* **2013**, *53*, 72–84. [CrossRef]
15. Hong, S.; Choi, D.W.; Kim, H.N.; Park, C.G.; Lee, W.; Park, H.H. Protein-based nanoparticles as drug delivery systems. *Pharmaceutics* **2020**, *12*, 604. [CrossRef] [PubMed]
16. Bazylińska, U.; Lewińska, A.; Lamch, Ł.; Wilk, K.A. Polymeric nanocapsules and nanospheres for encapsulation and long sustained release of hydrophobic cyanine-type photosensitizer. *Colloids Surf. A: Physicochem. Eng. Asp.* **2014**, *442*, 42–49. [CrossRef]
17. Jacob, J.; Haponiuk, J.T.; Thomas, S.; Gopi, S. Biopolymer based nanomaterials in drug delivery systems: A review. *Mater. Today Chem.* **2018**, *9*, 43–55. [CrossRef]
18. Langer, K.; Balthasar, S.; Vogel, V.; Dinauer, N.; Von Briesen, H.; Schubert, D. Optimization of the preparation process for human serum albumin (HSA) nanoparticles. *Int. J. Pharm.* **2003**, *257*, 169–180. [CrossRef]
19. Jamkhande, P.G.; Ghule, N.W.; Bamer, A.H.; Kalaskar, M.G. Metal nanoparticles synthesis: An overview on methods of preparation, advantages and disadvantages, and applications. *J. Drug Deliv. Sci. Technol.* **2019**, *53*, 101174. [CrossRef]
20. Prato, M.; Kostarelos, K. Functionalized Carbon Nanotubes in Drug. *Acc. Chem. Res.* **2008**, *41*, 60–68. [CrossRef]
21. Yang, Z.; Zhang, Y.; Yang, Y.; Sun, L.; Han, D.; Li, H.; Wang, C. Pharmacological and toxicological target organelles and safe use of single-walled carbon nanotubes as drug carriers in treating Alzheimer disease. *Nanomed. Nanotechnol. Biol. Med.* **2010**, *6*, 427–441. [CrossRef]
22. Wu, C.; Wang, Z.; Zhi, Z.; Jiang, T.; Zhang, J.; Wang, S. Development of biodegradable porous starch foam for improving oral delivery of poorly water soluble drugs. *Int. J. Pharm.* **2011**, *403*, 162–169. [CrossRef]
23. Li, J.; Mooney, D.J. Designing hydrogels for controlled drug delivery. *Nat. Rev. Mater.* **2016**, *1*, 16071. [CrossRef]
24. Ooi, S.Y.; Ahmad, I.; Amin, M.C.I.M. Cellulose nanocrystals extracted from rice husks as a reinforcing material in gelatin hydrogels for use in controlled drug delivery systems. *Ind. Crops Prod.* **2016**, *93*, 227–234. [CrossRef]

25. Svenson, S.; Tomalia, D.A. Dendrimers in biomedical applications-reflections on the field. *Adv. Drug Deliv. Rev.* **2012**, *64*, 102–115. [CrossRef]
26. Ziemba, B.; Janaszewska, A.; Ciepluch, K.; Krotewicz, M.; Fogel, W.A.; Appelhans, D.; Voit, B.; Bryszewska, M.; Klajnert, B. In vivo toxicity of poly(propyleneimine) dendrimers. *J. Biomed. Mater. Res. Part A* **2011**, *99A*, 261–268. [CrossRef] [PubMed]
27. Mahdavijalal, M.; Ahmad Panahi, H.; Niazi, A.; Tamaddon, A. Near-infrared light responsive dendrimers facilitate the extraction of bicalutamide from human plasma and urine. *Biotechnol. J.* **2021**, *16*, 2100299. [CrossRef] [PubMed]
28. Saraf, S.; Jain, A.; Tiwari, A.; Verma, A.; Panda, P.K.; Jain, S.K. Advances in liposomal drug delivery to cancer: An overview. *J. Drug Deliv. Sci. Technol.* **2020**, *56*, 101549. [CrossRef]
29. Bai, T.; Shao, D.; Chen, J.; Li, Y.; Xu, B.B.; Kong, J. pH-responsive dithiomaleimide-amphiphilic block copolymer for drug delivery and cellular imaging. *J. Colloid Interface Sci.* **2019**, *552*, 439–447. [CrossRef] [PubMed]
30. Zhang, S.; Hou, Y.; Chen, H.; Liao, Z.; Chen, J.; Xu, B.B.; Kong, J. Reduction-responsive amphiphilic star copolymers with long-chain hyperbranched poly(ε-caprolactone) core and disulfide bonds for trigger release of anticancer drugs. *Eur. Polym. J.* **2018**, *108*, 364–372. [CrossRef]
31. Wang, X.; Qi, Y.; Hu, Z.; Jiang, L.; Pan, F.; Xiang, Z.; Xiong, Z.; Jia, W.; Hu, J.; Lu, W. Fe3O4@PVP@DOX magnetic vortex hybrid nanostructures with magnetic-responsive heating and controlled drug delivery functions for precise medicine of cancers. *Adv. Compos. Hybrid Mater.* **2022**, *5*, 1786–1798. [CrossRef]
32. Badiu, D.; Vasile, M.; Teren, O. Regulation of wound healing by growth factors and cytokines. *Wound Heal. Process Phases Promot.* **2011**, *83*, 73–93.
33. Barrientos, S.; Stojadinovic, O.; Golinko, M.S.; Brem, H.; Tomic-Canic, M. Growth factors and cytokines in wound healing. *Wound Repair Regen.* **2008**, *16*, 585–601. [CrossRef] [PubMed]
34. Toosi, S.; Behrava, J. Osteogenesis and bone remodeling: A focus on growth factors and bioactive peptides. *Biofactors* **2020**, *46*, 326–340. [CrossRef] [PubMed]
35. Barnes, G.L.; Kostenuik, P.J.; Gerstenfeld, L.C.; Einhorn, T.A. Growth factor regulation of fracture repair. *J. Bone Miner. Res.* **1999**, *14*, 1805–1815. [CrossRef]
36. Liberman, J.R.; Daluiski, A.; Einhorn, T.A. The role of growth factors in the repair of bone. Biology and clinical applications. *J Bone Jt. Surg. Am.* **2002**, *84*, 1032–1044. [CrossRef]
37. Massague, J. The transforming growth factor-beta family. *Structure* **1990**, *6*, 597–641. [CrossRef]
38. Möller-Siegert, J.; Parmentier, J.; Laquerrière, P.; Ouadi, A.; Raisslé, O.; Jallot, E.; Nedelec, J.M.; Vix-Guterl, C.; Anselme, K. Physicochemical regulation of TGF and VEGF delivery from mesoporous calcium phosphate bone substitutes. *Nanomedicine* **2017**, *12*, 1835–1850. [CrossRef]
39. Wang, C.; Yue, H.; Huang, W.; Lin, X.; Xie, X.; He, Z.; He, X.; Liu, S.; Bai, L.; Lu, B.; et al. Cryogenic 3D printing of heterogeneous scaffolds with gradient mechanical strengths and spatial delivery of osteogenic peptide/TGF-β1 for osteochondral tissue regeneration. *Int. Soc. Biofabricatio* **2020**, *12*, 025030. [CrossRef]
40. Tong, S.; Xu, D.P.; Liu, Z.M.; Du, Y.; Wang, X.K. Synthesis of and in vitro and in vivo evaluation of a novel TGF-1-SF-CS three-dimensional scaffold for bone tissue engineering. *Int. J. Mol. Med.* **2016**, *38*, 367–380. [CrossRef]
41. Ogawa, T.; Akazawa, T.; Tabata, Y. In vitro proliferation and chondrogenic differentiation of rat bone marrow stem cells cultured with gelatin hydrogel microspheres for TGF-β1 release. *J. Biomater. Sci. Polym. Ed.* **2010**, *21*, 609–621. [CrossRef] [PubMed]
42. Chiang, Y.C.; Chang, H.H.; Wong, C.C.; Wang, Y.P.; Wang, Y.L.; Huang, W.H.; Lin, C.P. Nanocrystalline calcium sulfate/hydroxyapatite biphasic compound as a TGF-β1/VEGF reservoir for vital pulp therapy. *Dent. Mater.* **2016**, *32*, 1197–1208. [CrossRef]
43. Kveiborg, M.; Flyvbjerg, A.; Eriksen, E.F.; Kassem, M. Transforming growth factor-β1 stimulates the production of insulin-like growth factor-I and insulin-like growth factor-binding protein-3 in human bone marrow stromal osteoblast progenitors. *J. Endocrinol.* **2001**, *169*, 549–561. [CrossRef]
44. Srouji, S.; Blumenfeld, I.; Rachmiel, A.; Livne, E. Bone defect repair in rat tibia by TGF-beta1 and IGF-1 released from hydrogel scaffold. *Cell Tissue Bank.* **2004**, *5*, 223–230. [CrossRef]
45. Lamberg, A.; Schmidmaier, G.; Søballe, K.; Elmengaard, B. Locally delivered TGF-β1 and IGF-1 enhance the fixation of titanium implants: A study in dogs. *Acta Orthop.* **2006**, *77*, 799–805. [CrossRef]
46. Lamberg, A.; Bechtold, J.E.; Baas, J.; Søballe, K.; Elmengaard, B. Effect of local TGF-β1 and IGF-1 release on implant fixation: Comparison with hydroxyapatite coating: A paired study in dogs. *Acta Orthop.* **2009**, *80*, 499–504. [CrossRef]
47. Gu, Y.; Zhang, F.; Lineaweaver, W.C.; Zhang, J.; Jia, L.; Qi, J.; Wang, J.; Zhen, X. In Vivo Study of Hydroxyapatite-coated Hat Type Cervical Intervertebral Fusion Cage Combined with IGF-I and TGF-b1 in the Goat Model. *Clin. Spine Surg.* **2016**, *29*, E267–E275. [CrossRef] [PubMed]
48. Chen, Y.; Wu, T.; Huang, S.; Suen, C.W.W.; Cheng, X.; Li, J.; Hou, H.; She, G.; Zhang, H.; Wang, H.; et al. Sustained Release SDF-1α/TGF-β1-Loaded Silk Fibroin-Porous Gelatin Scaffold Promotes Cartilage Repair. *ACS Appl. Mater. Interfaces* **2019**, *11*, 14608–14618. [CrossRef]
49. Font Tellado, S.; Chiera, S.; Bonani, W.; Poh, P.S.P.; Migliaresi, C.; Motta, A.; Balmayor, E.R.; van Griensven, M. Heparin functionalization increases retention of TGF-β2 and GDF5 on biphasic silk fibroin scaffolds for tendon/ligament-to-bone tissue engineering. *Acta Biomater.* **2018**, *72*, 150–166. [CrossRef] [PubMed]

50. Guo, Q.; Liu, C.; Li, J.; Zhu, C.; Yang, H.; Li, B. Gene expression modulation in TGF-β3-mediated rabbit bone marrow stem cells using electrospun scaffolds of various stiffness. *J. Cell. Mol. Med.* **2015**, *19*, 1582–1592. [CrossRef] [PubMed]
51. Reifenrath, J.; Wellmann, M.; Kempfert, M.; Angrisani, N.; Welke, B.; Gniesmer, S.; Kampmann, A.; Menzel, H.; Willbold, E. TGF–β3 loaded electrospun polycaprolacton fibre scaffolds for rotator cuff tear repair: An in vivo study in rats. *Int. J. Mol. Sci.* **2020**, *21*, 1046. [CrossRef] [PubMed]
52. Han, F.; Zhou, F.; Yang, X.; Zhao, J.; Zhao, Y.; Yuan, X. A pilot study of conically graded chitosan-gelatin hydrogel/PLGA scaffold with dual-delivery of TGF-β1 and BMP-2 for regeneration of cartilage-bone interface. *J. Biomed. Mater. Res. Part B Appl. Biomater.* **2015**, *103*, 1344–1353. [CrossRef]
53. Bal, Z.; Korkusuz, F.; Ishiguro, H.; Okada, R.; Kushioka, J.; Chijimatsu, R.; Kodama, J.; Tateiwa, D.; Ukon, Y.; Nakagawa, S.; et al. A novel nano-hydroxyapatite/synthetic polymer/bone morphogenetic protein-2 composite for efficient bone regeneration. *Spine J.* **2021**, *21*, 865–873. [CrossRef]
54. Boda, S.K.; Almoshari, Y.; Wang, H.; Wang, X.; Reinhardt, R.A.; Duan, B.; Wang, D.; Xie, J. Mineralized nanofiber segments coupled with calcium-binding BMP-2 peptides for alveolar bone regeneration. *Acta Biomater.* **2019**, *85*, 282–293. [CrossRef] [PubMed]
55. Sun, Y.K.; Cha, J.K.; Thoma, D.S.; Yoon, S.R.; Lee, J.S.; Choi, S.H.; Jung, U.W. Bone Regeneration of Peri-Implant Defects Using a Collagen Membrane as a Carrier for Recombinant Human Bone Morphogenetic Protein-2. *BioMed Res. Int.* **2018**, *2018*, 5437361. [CrossRef] [PubMed]
56. Han, S.H.; Lee, J.U.J.H.; Lee, K.M.; Jin, Y.Z.; Yun, H.S.; Kim, G.H.; Lee, J.U.J.H. Enhanced healing of rat calvarial defects with 3D printed calcium-deficient hydroxyapatite/collagen/bone morphogenetic protein 2 scaffolds. *J. Mech. Behav. Biomed. Mater.* **2020**, *108*, 103782. [CrossRef]
57. Schuster, L.; Ardjomandi, N.; Munz, M.; Umrath, F.; Klein, C.; Rupp, F.; Reinert, S.; Alexander, D. Establishment of collagen: Hydroxyapatite/BMP-2 mimetic peptide composites. *Materials* **2020**, *13*, 1203. [CrossRef] [PubMed]
58. Cai, Y.; Tong, S.; Zhang, R.; Zhu, T.; Wang, X. In vitro evaluation of a bone morphogenetic protein-2 nanometer hydroxyapatite collagen scaffold for bone regeneration. *Mol. Med. Rep.* **2018**, *17*, 5830–5836. [CrossRef]
59. Murphy, C.M.; Schindeler, A.; Gleeson, J.P.; Yu, N.Y.C.; Cantrill, L.C.; Mikulec, K.; Peacock, L.; O'Brien, F.J.; Little, D.G. A collagen-hydroxyapatite scaffold allows for binding and co-delivery of recombinant bone morphogenetic proteins and bisphosphonates. *Acta Biomater.* **2014**, *10*, 2250–2258. [CrossRef]
60. Quinlan, E.; Thompson, E.M.; Matsiko, A.; O'Brien, F.J.; López-Noriega, A. Long-term controlled delivery of rhBMP-2 from collagen-hydroxyapatite scaffolds for superior bone tissue regeneration. *J. Control. Release* **2015**, *207*, 112–119. [CrossRef] [PubMed]
61. Walsh, D.P.; Raftery, R.M.; Chen, G.; Heise, A.; O'Brien, F.J.; Cryan, S.A. Rapid healing of a critical-sized bone defect using a collagen-hydroxyapatite scaffold to facilitate low dose, combinatorial growth factor delivery. *J. Tissue Eng. Regen. Med.* **2019**, *13*, 1843–1853. [CrossRef]
62. Linh, N.T.B.; Abueva, C.D.G.; Jang, D.W.; Lee, B.T. Collagen and bone morphogenetic protein-2 functionalized hydroxyapatite scaffolds induce osteogenic differentiation in human adipose-derived stem cells. *J. Biomed. Mater. Res. Part B Appl. Biomater.* **2020**, *108*, 1363–1371. [CrossRef] [PubMed]
63. Wang, H.; Wu, G.; Zhang, J.; Zhou, K.; Yin, B.; Su, X.; Qiu, G.; Yang, G.; Zhang, X.; Zhou, G.; et al. Osteogenic effect of controlled released rhBMP-2 in 3D printed porous hydroxyapatite scaffold. *Colloids Surf. B Biointerfaces* **2016**, *141*, 491–498. [CrossRef] [PubMed]
64. Cha, J.K.; Lee, J.S.; Kim, M.S.; Choi, S.H.; Cho, K.S.; Jung, U.W. Sinus augmentation using BMP-2 in a bovine hydroxyapatite/collagen carrier in dogs. *J. Clin. Periodontol.* **2014**, *41*, 86–93. [CrossRef]
65. Lee, S.W.; Hahn, B.D.; Kang, T.Y.; Lee, M.J.; Choi, J.Y.; Kim, M.K.; Kim, S.G. Hydroxyapatite and collagen combination-coated dental implants display better bone formation in the peri-implant area than the same combination plus bone morphogenetic protein-2-coated implants, hydroxyapatite only coated implants, and uncoated implants. *J. Oral Maxillofac. Surg.* **2014**, *72*, 53–60. [CrossRef]
66. Wei, X.; Egawa, S.; Matsumoto, R.; Yasuda, H.; Hirai, K.; Yoshii, T.; Okawa, A.; Nakajima, T.; Sotome, S. Augmentation of fracture healing by hydroxyapatite/collagen paste and bone morphogenetic protein-2 evaluated using a rat femur osteotomy model. *J. Orthop. Res.* **2018**, *36*, 129–137. [CrossRef]
67. Charles, L.F.; Woodman, J.L.; Ueno, D.; Gronowicz, G.; Hurley, M.M.; Kuhn, L.T. Effects of low dose FGF-2 and BMP-2 on healing of calvarial defects in old mice. *Exp. Gerontol.* **2015**, *64*, 62–69. [CrossRef]
68. Gronowicz, G.; Jacobs, E.; Peng, T.; Zhu, L.; Hurley, M.; Kuhn, L.T. Calvarial bone regeneration is enhanced by sequential delivery of fgf-2 and bmp-2 from layer-by-layer coatings with a biomimetic calcium phosphate barrier layer. *Tissue Eng. Part A* **2017**, *23*, 1490–1501. [CrossRef] [PubMed]
69. Wang, S.; Ju, W.; Shang, P.; Lei, L.; Nie, H. Core-shell microspheres delivering FGF-2 and BMP-2 in different release patterns for bone regeneration. *J. Mater. Chem. B* **2015**, *3*, 1907–1920. [CrossRef]

70. Khalil, A.; Muttukrishna, S.; Harrington, K.; Jauniaux, E. Effect of antihypertensive therapy with alpha methyldopa on levels of angiogenic factors in pregnancies with hypertensive disorders. *PLoS ONE* **2008**, *3*, e2766. [CrossRef]
71. Liu, Y.; Deng, L.Z.; Sun, H.P.; Xu, J.Y.; Li, Y.M.; Xie, X.; Zhang, L.M.; Deng, F.L. Sustained dual release of placental growth factor-2 and bone morphogenic protein-2 from heparin-based nanocomplexes for direct osteogenesis. *Int. J. Nanomed.* **2016**, *11*, 1147–1158. [CrossRef] [PubMed]
72. Holmes, K.; Roberts, O.L.; Thomas, A.M.; Cross, M.J. Vascular endothelial growth factor receptor-2: Structure, function, intracellular signalling and therapeutic inhibition. *Cell. Signal.* **2007**, *19*, 2003–2012. [CrossRef]
73. Kempen, D.H.R.; Lu, L.; Heijink, A.; Hefferan, T.E.; Creemers, L.B.; Maran, A.; Yaszemski, M.J.; Dhert, W.J.A. Effect of local sequential VEGF and BMP-2 delivery on ectopic and orthotopic bone regeneration. *Biomaterials* **2009**, *30*, 2816–2825. [CrossRef] [PubMed]
74. An, G.; Zhang, W.B.; Ma, D.K.; Lu, B.; Wei, G.J.; Guang, Y.; Ru, C.H.; Wang, Y.S. Influence of VEGF/BMP-2 on the proliferation and osteogenetic differentiation of rat bone mesenchymal stem cells on PLGA/gelatin composite scaffold. *Eur. Rev. Med. Pharmacol. Sci.* **2017**, *21*, 2316–2328.
75. Eğri, S.; Eczacıoğlu, N. Sequential VEGF and BMP-2 releasing PLA-PEG-PLA scaffolds for bone tissue engineering: I. Design and in vitro tests. *Artif. Cells Nanomed. Biotechnol.* **2017**, *45*, 321–329. [CrossRef] [PubMed]
76. Dou, D.D.; Zhou, G.; Liu, H.W.; Zhang, J.; Liu, M.L.; Xiao, X.F.; Fei, J.J.; Guan, X.L.; Fan, Y.B. Sequential releasing of VEGF and BMP-2 in hydroxyapatite collagen scaffolds for bone tissue engineering: Design and characterization. *Int. J. Biol. Macromol.* **2019**, *123*, 622–628. [CrossRef]
77. Curtin, C.M.; Tierney, E.G.; Mcsorley, K.; Cryan, S.A.; Duffy, G.P.; O'Brien, F.J. Combinatorial gene therapy accelerates bone regeneration: Non-viral dual delivery of VEGF and BMP2 in a collagen-nanohydroxyapatite scaffold. *Adv. Healthc. Mater.* **2015**, *4*, 223–227. [CrossRef]
78. Wang, Q.; Zhang, Y.; Li, B.; Chen, L. Controlled dual delivery of low doses of BMP-2 and VEGF in a silk fibroin-nanohydroxyapatite scaffold for vascularized bone regeneration. *J. Mater. Chem. B* **2017**, *5*, 6963–6972. [CrossRef]
79. Sukul, M.; Linh, N.T.B.; Min, Y.-K.; Lee, S.-Y.; Lee, B.-T. Effect of local sustainable release of BMP2-VEGF from nano-cellulose loaded in sponge biphasic calcium phosphate (BCP) on bone regeneration. *Tissue Eng.—Part A* **2015**, *21*, 1822–1836. [CrossRef]
80. Zhang, H.X.; Zhang, X.P.; Xiao, G.Y.; Hou, Y.; Cheng, L.; Si, M.; Wang, S.S.; Li, Y.H.; Nie, L. In vitro and in vivo evaluation of calcium phosphate composite scaffolds containing BMP-VEGF loaded PLGA microspheres for the treatment of avascular necrosis of the femoral head. *Mater. Sci. Eng. C* **2016**, *60*, 298–307. [CrossRef]
81. Kaigler, D.; Wang, Z.; Horger, K.; Mooney, D.J.; Krebsbach, P.H. VEGF scaffolds enhance angiogenesis and bone regeneration in irradiated osseous defects. *J. Bone Miner. Res.* **2006**, *21*, 735–744. [CrossRef]
82. Jabbarzadeh, E.; Deng, M.; Lv, Q.; Jiang, T.; Khan, Y.M.; Nair, L.S.; Laurencin, C.T. VEGF-incorporated biomimetic poly(lactide-co-glycolide) sintered microsphere scaffolds for bone tissue engineering. *J. Biomed. Mater. Res. Part B Appl. Biomater.* **2012**, *100*, 2187–2196. [CrossRef] [PubMed]
83. De la Riva, B.; Nowak, C.; Sánchez, E.; Hernández, A.; Schulz-Siegmund, M.; Pec, M.K.; Delgado, A.; Évora, C. VEGF-controlled release within a bone defect from alginate/chitosan/PLA-H scaffolds. *Eur. J. Pharm. Biopharm.* **2009**, *73*, 50–58. [CrossRef]
84. Khojasteh, A.; Fahimipour, F.; Eslaminejad, M.B.; Jafarian, M.; Jahangir, S.; Bastami, F.; Tahriri, M.; Karkhaneh, A.; Tayebi, L. Development of PLGA-coated β-TCP scaffolds containing VEGF for bone tissue engineering. *Mater. Sci. Eng. C* **2016**, *69*, 780–788. [CrossRef] [PubMed]
85. Fahimipour, F.; Rasoulianboroujeni, M.; Dashtimoghadam, E.; Khoshroo, K.; Tahriri, M.; Bastami, F.; Lobner, D.; Tayebi, L. 3D printed TCP-based scaffold incorporating VEGF-loaded PLGA microspheres for craniofacial tissue engineering. *Dent. Mater.* **2017**, *33*, 1205–1216. [CrossRef] [PubMed]
86. Kent Leach, J.; Kaigler, D.; Wang, Z.; Krebsbach, P.H.; Mooney, D.J. Coating of VEGF-releasing scaffolds with bioactive glass for angiogenesis and bone regeneration. *Biomaterials* **2006**, *27*, 3249–3255. [CrossRef]
87. Li, B.; Wang, H.; Zhou, G.; Zhang, J.; Su, X.; Huang, Z.; Li, Q.; Wu, Z.; Qiu, G. VEGF-loaded biomimetic scaffolds: A promising approach to improve angiogenesis and osteogenesis in an ischemic environment. *RSC Adv.* **2017**, *7*, 4253–4259. [CrossRef]
88. Ozturk, B.Y.; Inci, I.; Egri, S.; Ozturk, A.M.; Yetkin, H.; Goktas, G.; Elmas, C.; Piskin, E.; Erdogan, D. The treatment of segmental bone defects in rabbit tibiae with vascular endothelial growth factor (VEGF)-loaded gelatin/hydroxyapatite "cryogel" scaffold. *Eur. J. Orthop. Surg. Traumatol.* **2013**, *23*, 767–774. [CrossRef]
89. Casarrubios, L.; Gómez-Cerezo, N.; Sánchez-Salcedo, S.; Feito, M.J.; Serrano, M.C.; Saiz-Pardo, M.; Ortega, L.; de Pablo, D.; Díaz-Güemes, I.; Fernández-Tomé, B.; et al. Silicon substituted hydroxyapatite/VEGF scaffolds stimulate bone regeneration in osteoporotic sheep. *Acta Biomater.* **2019**, *101*, 544–553. [CrossRef] [PubMed]
90. Izquierdo-Barba, I.; Santos-Ruiz, L.; Becerra, J.; Feito, M.J.; Fernández-Villa, D.; Serrano, M.C.; Díaz-Güemes, I.; Fernández-Tomé, B.; Enciso, S.; Sánchez-Margallo, F.M.; et al. Synergistic effect of Si-hydroxyapatite coating and VEGF adsorption on Ti6Al4V-ELI scaffolds for bone regeneration in an osteoporotic bone environment. *Acta Biomater.* **2019**, *83*, 456–466. [CrossRef]
91. Wang, Z.; Wang, Z.; Lu, W.W.; Zhen, W.; Yang, D.; Peng, S. Novel biomaterial strategies for controlled growth factor delivery for biomedical applications. *NPG Asia Mater.* **2017**, *9*, e435. [CrossRef]

92. Heldin, C.H.; Westermark, B. Mechanism of action and in vivo role of platelet-derived growth factor. *Physiol. Rev.* **1999**, *79*, 1283–1316. [CrossRef] [PubMed]
93. Heldin, C.H.; Eriksson, U.; Östman, A. New members of the platelet-derived growth factor family of mitogens. *Arch. Biochem. Biophys.* **2002**, *398*, 284–290. [CrossRef] [PubMed]
94. De la Riva, B.; Sánchez, E.; Hernández, A.; Reyes, R.; Tamimi, F.; López-Cabarcos, E.; Delgado, A.; Évora, C. Local controlled release of VEGF and PDGF from a combined brushite-chitosan system enhances bone regeneration. *J. Control. Release* **2010**, *143*, 45–52. [CrossRef] [PubMed]
95. Jeong Park, Y.; Moo Lee, Y.; Nae Park, S.; Yoon Sheen, S.; Pyoung Chung, C.; Lee, S.J. Platelet derived growth factor releasing chitosan sponge for periodontal bone regeneration. *Biomaterials* **2000**, *21*, 153–159. [CrossRef]
96. Park, Y.J.; Lee, Y.M.; Lee, J.Y.; Seol, Y.J.; Chung, C.P.; Lee, S.J. Controlled release of platelet-derived growth factor-BB from chondroitin sulfate-chitosan sponge for guided bone regeneration. *J. Control. Release* **2000**, *67*, 385–394. [CrossRef]
97. Al-Hazmi, B.A.; Al-Hamdan, K.S.; Al-Rasheed, A.; Babay, N.; Wang, H.-L.; Al-Hezaimi, K. Efficacy of Using PDGF and Xenograft with or Without Collagen Membrane for Bone Regeneration Around Immediate Implants With Induced Dehiscence-Type Defects: A Microcomputed Tomographic Study in Dogs. *J. Periodontol.* **2013**, *84*, 371–378. [CrossRef]
98. Wöltje, M.; Brünler, R.; Böbel, M.; Ernst, S.; Neuss, S.; Aibibu, D.; Cherif, C. Functionalization of silk fibers by PDGF and bioceramics for bone tissue regeneration. *Coatings* **2020**, *10*, 8. [CrossRef]
99. Zhang, Y.; Cheng, N.; Miron, R.; Shi, B.; Cheng, X. Delivery of PDGF-B and BMP-7 by mesoporous bioglass/silk fibrin scaffolds for the repair of osteoporotic defects. *Biomaterials* **2012**, *33*, 6698–6708. [CrossRef]
100. Burgess, W.H.; Maciag, T. The Heparin—Binding (Fibroblast) Growth Factor Family of Proteins. *Ann. Rev. Biochem.* **1989**, *58*, 575–606. [CrossRef]
101. Maehara, H.; Sotome, S.; Yoshii, T.; Torigoe, I.; Kawasaki, Y.; Sugata, Y.; Yuasa, M.; Hirano, M.; Mochizuki, N.; Kikuchi, M.; et al. Repair of large osteochondral defects in rabbits using porous hydroxyapatite/collagen (HAp/Col) and fibroblast growth factor-2 (FGF-2). *J. Orthop. Res.* **2010**, *28*, 677–686. [CrossRef]
102. Mabilleau, G.; Aguado, E.; Stancu, I.C.; Cincu, C.; Baslé, M.F.; Chappard, D. Effects of FGF-2 release from a hydrogel polymer on bone mass and microarchitecture. *Biomaterials* **2008**, *29*, 1593–1600. [CrossRef] [PubMed]
103. Gómez, G.; Korkiakoski, S.; González, M.M.; Länsman, S.; Ellä, V.; Salo, T.; Kellomäki, M.; Ashammakhi, N.; Arnaud, E. Effect of FGF and polylactide scaffolds on calvarial bone healing with growth factor on biodegradable polymer scaffolds. *J. Craniofacial Surg.* **2006**, *17*, 935–942. [CrossRef] [PubMed]
104. Murahashi, Y.; Yano, F.; Nakamoto, H.; Maenohara, Y.; Iba, K.; Yamashita, T.; Tanaka, S.; Ishihara, K.; Okamura, Y.; Moro, T.; et al. Multi-layered PLLA-nanosheets loaded with FGF-2 induce robust bone regeneration with controlled release in critical-sized mouse femoral defects. *Acta Biomater.* **2019**, *85*, 172–179. [CrossRef] [PubMed]
105. Sivashanmugam, A.; Charoenlarp, P.; Deepthi, S.; Rajendran, A.; Nair, S.V.; Iseki, S.; Jayakumar, R. Injectable Shear-Thinning CaSO4/FGF-18-Incorporated Chitin-PLGA Hydrogel Enhances Bone Regeneration in Mice Cranial Bone Defect Model. *ACS Appl. Mater. Interfaces* **2017**, *9*, 42639–42652. [CrossRef]
106. Lewin, G.R.; Mendell, L.M. Nerve growth factor and nociception. *Trends Neurosci.* **1993**, *16*, 353–359. [CrossRef] [PubMed]
107. Wang, L.; Lei, D.L.; Cheng, X.B.; Cao, J.; Tian, L.; Cui, F.Z. Effects of nerve growth factor delivery via a collagen/nano-hydroxyapatite gel to mandibular distraction osteogenesis in a rabbit model. *Int. J. Oral Maxillofac. Surg.* **2009**, *38*, 557–558. [CrossRef]
108. Ambrogelly, A.; Palioura, S.; Söll, D. Natural expansion of the genetic code. *Nat. Chem. Biol.* **2007**, *3*, 29–35. [CrossRef]
109. Lobanov, A.V.; Turanov, A.A.; Hatfield, D.L.; Gladyshev, V.N. Dual functions of codons in the genetic code. *Crit. Rev. Biochem. Mol. Biol.* **2010**, *45*, 257–265. [CrossRef]
110. Rezania, A.; Healy, K.E. The effect of peptide surface density on mineralization of a matrix deposited by osteogenic cells. *J. Biomed. Mater. Res.* **2000**, *52*, 595–600. [CrossRef]
111. Hoesli, C.A.; Garnier, A.; Juneau, P.M.; Chevallier, P.; Duchesne, C.; Laroche, G. A fluorophore-tagged RGD peptide to control endothelial cell adhesion to micropatterned surfaces. *Biomaterials* **2014**, *35*, 879–890. [CrossRef] [PubMed]
112. Bilem, I.; Chevallier, P.; Plawinski, L.; Sone, E.D.; Durrieu, M.C.; Laroche, G. RGD and BMP-2 mimetic peptide crosstalk enhances osteogenic commitment of human bone marrow stem cells. *Acta Biomater.* **2016**, *36*, 132–142. [CrossRef]
113. Schneiders, W.; Reinstorf, A.; Pompe, W.; Grass, R.; Biewener, A.; Holch, M.; Zwipp, H.; Rammelt, S. Effect of modification of hydroxyapatite/collagen composites with sodium citrate, phosphoserine, phosphoserine/RGD-peptide and calcium carbonate on bone remodelling. *Bone* **2007**, *40*, 1048–1059. [CrossRef] [PubMed]
114. Huang, Y.; Ren, J.; Ren, T.; Gu, S.; Tan, Q.; Zhang, L.; Lv, K.; Pan, K.; Jiang, X. Bone marrow stromal cells cultured on poly (lactide-co-glycolide)/nano- hydroxyapatite composites with chemical immobilization of Arg-Gly-Asp peptide and preliminary bone regeneration of mandibular defect thereof. *J. Biomed. Mater. Res. Part A* **2010**, *95*, 993–1003. [CrossRef] [PubMed]
115. Gan, D.; Liu, M.; Xu, T.; Wang, K.; Tan, H.; Lu, X. Chitosan/biphasic calcium phosphate scaffolds functionalized with BMP-2-encapsulated nanoparticles and RGD for bone regeneration. *J. Biomed. Mater. Res. Part A* **2018**, *106*, 2613–2624. [CrossRef]

116. Shin, H.; Temenoff, J.S.; Bowden, G.C.; Zygourakis, K.; Farach-Carson, M.C.; Yaszemski, M.J.; Mikos, A.G. Osteogenic differentiation of rat bone marrow stromal cells cultured on Arg-Gly-Asp modified hydrogels without dexamethasone and β-glycerol phosphate. *Biomaterials* **2005**, *26*, 3645–3654. [CrossRef]
117. Ahn, C.B.; Kim, Y.; Park, S.J.; Hwang, Y.; Lee, J.W. Development of arginine-glycine-aspartate-immobilized 3D printed poly(propylene fumarate) scaffolds for cartilage tissue engineering. *J. Biomater. Sci. Polym. Ed.* **2018**, *29*, 917–931. [CrossRef] [PubMed]
118. Salinas, C.N.; Cole, B.B.; Kasko, A.M.; Anseth, K.S. Chondrogenic differentiation potential of human mesenchymal stem cells photoencapsulated within poly(ethylene glycol)-arginine-glycine-aspartic acid-serine thiol-methacrylate mixed-mode networks. *Tissue Eng.* **2007**, *13*, 1025–1034. [CrossRef]
119. Hwang, S.N.; Vargheses, S.; Zhang, Z.; Elisseeff, J. Chondrogenic Differentiation of Human Embryonic Stem Cell–Derived Cells in Arginine-Glycine-Aspartate—Modified Hydrogels. *Tissue Eng.* **2006**, *12*, 2695–2705. [CrossRef]
120. Hu, Y.; Winn, S.R.; Krajbich, I.; Hollinger, J.O. Porous polymer scaffolds surface-modified with arginine-glycine-aspartic acid enhance bone cell attachment and differentiation in vitro. *J. Biomed. Mater. Res. Part A* **2003**, *64*, 583–590. [CrossRef] [PubMed]
121. Kim, T.G.; Park, T.G. Biomimicking Extracellular Matrix: Cell Adhesive RGD Peptide Modified Electrospun Poly(D,L-lactic-co-glycolic acid) Nanofiber Mesh. *Tissue Eng.* **2006**, *12*, 221–233. [CrossRef]
122. Li, J.; Tan, L.; Liu, X.; Cui, Z.; Yang, X.; Yeung, K.W.K.; Chu, P.K.; Wu, S. Balancing Bacteria-Osteoblast Competition through Selective Physical Puncture and Biofunctionalization of ZnO/Polydopamine/Arginine-Glycine-Aspartic Acid-Cysteine Nanorods. *ACS Nano* **2017**, *11*, 11250–11263. [CrossRef] [PubMed]
123. Słota, D.; Florkiewicz, W.; Sobczak-Kupiec, A. Ceramic-polymer coatings on Ti-6Al-4V alloy modified with L-cysteine in biomedical applications. *Mater. Today Commun.* **2020**, *25*, 101301. [CrossRef]
124. Brasinika, D.; Tsigkou, O.; Tsetsekou, A.; Missirlis, Y.F. Bioinspired synthesis of hydroxyapatite nanocrystals in the presence of collagen and L-arginine: Candidates for bone regeneration. *J. Biomed. Mater. Res. Part B Appl. Biomater.* **2016**, *104*, 458–469. [CrossRef]
125. Xu, X.; Qiu, S.; Zhang, Y.; Yin, J.; Min, S. PELA microspheres with encapsulated arginine–chitosan/pBMP-2 nanoparticles induce pBMP-2 controlled-release, transfected osteoblastic progenitor cells, and promoted osteogenic differentiation. *Artif. Cells Nanomed. Biotechnol.* **2017**, *45*, 330–339. [CrossRef]
126. Scialla, S.; Barca, A.; Palazzo, B.; D'Amora, U.; Russo, T.; Gloria, A.; De Santis, R.; Verri, T.; Sannino, A.; Ambrosio, L.; et al. Bioactive chitosan-based scaffolds with improved properties induced by dextran-grafted nano-maghemite and l-arginine amino acid. *J. Biomed. Mater. Res. Part A* **2019**, *107*, 1244–1252. [CrossRef]
127. Zhou, Y.; Gu, Z.; Liu, J.; Huang, K.; Liu, G.; Wu, J. Arginine based poly (ester amide)/ hyaluronic acid hybrid hydrogels for bone tissue Engineering. *Carbohydr. Polym.* **2020**, *230*, 115640. [CrossRef]
128. Lam, J.; Clark, E.C.; Fong, E.L.S.; Lee, E.J.; Lu, S.; Tabata, Y.; Mikos, A.G. Evaluation of cell-laden polyelectrolyte hydrogels incorporating poly(L-Lysine) for applications in cartilage tissue engineering. *Biomaterials* **2016**, *83*, 332–346. [CrossRef] [PubMed]
129. Yuan, Y.; Shi, X.; Gan, Z.; Wang, F. Modification of porous PLGA microspheres by poly-L-lysine for use as tissue engineering scaffolds. *Colloids Surf. B Biointerfaces* **2018**, *161*, 162–168. [CrossRef] [PubMed]
130. Kouhi, M.; Fathi, M.; Prabhakaran, M.P.; Shamanian, M.; Ramakrishna, S. Poly L lysine-modified PHBV based nanofibrous scaffolds for bone cell mineralization and osteogenic differentiation. *Appl. Surf. Sci.* **2018**, *457*, 616–625. [CrossRef]
131. Ganss, B.; Kim, R.H.; Sodek, J. Bone sialoprotein. *Crit. Rev. Oral Biol. Med.* **1999**, *10*, 79–98. [CrossRef] [PubMed]
132. Wang, K.X.; Denhardt, D.T. Osteopontin: Role in immune regulation and stress responses. *Cytokine Growth Factor Rev.* **2008**, *19*, 333–345. [CrossRef] [PubMed]
133. Jensen, T.; Baas, J.; Dolathshahi-Pirouz, A.; Jacobsen, T.; Singh, G.; Nygaard, J.V.; Foss, M.; Bechtold, J.; Bünger, C.; Besenbacher, F.; et al. Osteopontin functionalization of hydroxyapatite nanoparticles in a PDLLA matrix promotes bone formation. *J. Biomed. Mater. Res. Part A* **2011**, *99A*, 94–101. [CrossRef] [PubMed]
134. Zhu, M.; He, H.; Meng, Q.; Zhu, Y.; Ye, X.; Xu, N.; Yu, J. Osteopontin sequence modified mesoporous calcium silicate scaffolds to promote angiogenesis in bone tissue regeneration. *J. Mater. Chem. B* **2020**, *8*, 5849–5861. [CrossRef]
135. Baht, G.S.; Hunter, G.K.; Goldberg, H.A. Bone sialoprotein-collagen interaction promotes hydroxyapatite nucleation. *Matrix Biol.* **2008**, *27*, 600–608. [CrossRef]
136. França, C.M.; Thrivikraman, G.; Athirasala, A.; Tahayeri, A.; Gower, L.B.; Bertassoni, L.E. The influence of osteopontin-guided collagen intrafibrillar mineralization on pericyte differentiation and vascularization of engineered bone scaffolds. *J. Biomed. Mater. Res. Part B Appl. Biomater.* **2019**, *107*, 1522–1532. [CrossRef] [PubMed]
137. Hamada, Y.; Egusa, H.; Kaneda, Y.; Hirata, I.; Kawaguchi, N.; Hirao, T.; Matsumoto, T.; Yao, M.; Daito, K.; Suzuki, M.; et al. Synthetic osteopontin-derived peptide SVVYGLR can induce neovascularization in artificial bone marrow scaffold biomaterials. *Dent. Mater. J.* **2007**, *26*, 487–492. [CrossRef]
138. Chan, W.D.; Goldberg, H.A.; Hunter, G.K.; Dixon, S.J.; Rizkalla, A.S. Modification of polymer networks with bone sialoprotein promotes cell attachment and spreading. *J. Biomed. Mater. Res. Part A* **2010**, *94*, 945–952. [CrossRef]
139. Schaeren, S.; Jaquiéry, C.; Wolf, F.; Papadimitropoulos, A.; Barbero, A.; Schultz-Thater, E.; Heberer, M.; Martin, I. Effect of bone sialoprotein coating of ceramic and synthetic polymer materials on in vitro osteogenic cell differentiation and in vivo bone formation. *J. Biomed. Mater. Res. Part A* **2010**, *92*, 1461–1467. [CrossRef]

140. Baranowski, A.; Klein, A.; Ritz, U.; Ackermann, A.; Anthonissen, J.; Kaufmann, K.B.; Brendel, C.; Götz, H.; Rommens, P.M.; Hofmann, A. Surface functionalization of orthopedic titanium implants with bone sialoprotein. *PLoS ONE* **2016**, *11*, e0153978. [CrossRef]
141. Moser, S.C.; van der Eerden, B.C.J. Osteocalcin—A versatile bone-derived hormone. *Front. Endocrinol.* **2019**, *10*, 4–9. [CrossRef] [PubMed]
142. Mizokami, A.; Kawakubo-Yasukochi, T.; Hirata, M. Osteocalcin and its endocrine functions. *Biochem. Pharmacol.* **2017**, *132*, 1–8. [CrossRef] [PubMed]
143. Knepper-Nicolai, B.; Reinstorf, A.; Hofinger, I.; Flade, K.; Wenz, R.; Pompe, W. Influence of osteocalcin and collagen I on the mechanical and biological properties of Biocement D. *Biomol. Eng.* **2002**, *19*, 227–231. [CrossRef] [PubMed]
144. Rammelt, S.; Neumann, M.; Hanisch, U.; Reinstorf, A.; Pompe, W.; Zwipp, H.; Biewener, A. Osteocalcin enhances bone remodeling around hydroxyapatite/collagen composites. *J. Biomed. Mater. Res. Part A* **2005**, *73*, 284–294. [CrossRef] [PubMed]
145. Ciceri, P.; Elli, F.; Cappelletti, L.; Tosi, D.; Savi, F.; Bulfamante, G.; Cozzolino, M. Osteonectin (SPARC) Expression in Vascular Calcification: In Vitro and Ex Vivo Studies. *Calcif. Tissue Int.* **2016**, *99*, 472–480. [CrossRef]
146. Delany, A.M.; Hankenson, K.D. Thrombospondin-2 and SPARC/osteonectin are critical regulators of bone remodeling. *J. Cell Commun. Signal.* **2009**, *3*, 227–238. [CrossRef]
147. Sarvestani, A.S.; He, X.; Jabbari, E. Effect of Osteonectin-Derived Peptide on the Viscoelasticity of Hydrogel/Apatite Nanocomposite Scaffolds. *Biopolymers* **2007**, *85*, 392–406. [CrossRef]
148. Liao, S.; Ngiam, M.; Chan, C.K.; Ramakrishna, S. Fabrication of nano-hydroxyapatite/collagen/osteonectin composites for bone graft applications. *Biomed. Mater.* **2009**, *4*, 025019. [CrossRef]
149. Rattan, S.; Sharma, R. Hormones in Ageing and Logevity. *J. Chem. Inf. Model.* **2019**, *53*, 1689–1699. [CrossRef]
150. Rubin, M.R.; Bilezikian, J.P. The anabolic effects of parathyroid hormone therapy. *Clin. Geriatr. Med.* **2003**, *19*, 415–432. [CrossRef]
151. Arrighi, I.; Mark, S.; Alvisi, M.; von Rechenberg, B.; Hubbell, J.A.; Schense, J.C. Bone healing induced by local delivery of an engineered parathyroid hormone prodrug. *Biomaterials* **2009**, *30*, 1763–1771. [CrossRef] [PubMed]
152. Gentile, P.; Nandagiri, V.K.; Pabari, R.; Daly, J.; Tonda-Turo, C.; Ciardelli, G.; Ramtoola, Z. Influence of parathyroid hormone-loaded plga nanoparticles in porous scaffolds for bone regeneration. *Int. J. Mol. Sci.* **2015**, *16*, 20492–20510. [CrossRef]
153. Wei, G.; Pettway, G.J.; McCauley, L.K.; Ma, P.X. The release profiles and bioactivity of parathyroid hormone from poly(lactic-co-glycolic acid) microspheres. *Biomaterials* **2004**, *25*, 345–352. [CrossRef]
154. Jung, R.E.; Cochran, D.L.; Domken, O.; Seibl, R.; Jones, A.A.; Buser, D.; Hammerle, C.H.F. The effect of matrix bound parathyroid hormone on bone regeneration. *Clin. Oral Implant. Res.* **2007**, *18*, 319–325. [CrossRef] [PubMed]
155. Dang, M.; Koh, A.J.; Jin, X.; McCauley, L.K.; Ma, P.X. Local pulsatile PTH delivery regenerates bone defects via enhanced bone remodeling in a cell-free scaffold. *Biomaterials* **2017**, *114*, 1–9. [CrossRef] [PubMed]
156. Liu, X.; Pettway, G.J.; McCauley, L.K.; Ma, P.X. Pulsatile release of parathyroid hormone from an implantable delivery system. *Biomaterials* **2007**, *28*, 4124–4131. [CrossRef] [PubMed]
157. Koo, A.N.; Ohe, J.Y.; Lee, D.W.; Chun, J.; Lee, H.J.; Kwon, Y.D.; Lee, S.C. Bone-regenerative activity of parathyroid hormone-releasing nano-hydroxyapatite/poly(L-lactic acid) hybrid scaffolds. *Macromol. Res.* **2015**, *23*, 1168–1173. [CrossRef]
158. Tao, Z.S.; Zhou, W.S.; Wu, X.J.; Wang, L.; Yang, M.; Xie, J.B.; Xu, Z.J.; Ding, G.Z. Single-dose local administration of parathyroid hormone (1–34, PTH) with β-tricalcium phosphate/collagen (β-TCP/COL) enhances bone defect healing in ovariectomized rats. *J. Bone Miner. Metab.* **2019**, *37*, 28–35. [CrossRef] [PubMed]
159. Wojda, S.J.; Marozas, I.A.; Anseth, K.S.; Yaszemski, M.J.; Donahue, S.W. Thiol-ene Hydrogels for Local Delivery of PTH for Bone Regeneration in Critical Size defects. *J. Orthop. Res.* **2020**, *38*, 536–544. [CrossRef]
160. Leone-Bay, A.; Sato, M.; Paton, D.; Hunt, A.H.; Sarubbi, D.; Carozza, M.; Chou, J.; McDonough, J.; Baughman, R.A. Oral delivery of biologically active parathyroid hormone. *Pharm. Res.* **2001**, *18*, 964–970. [CrossRef]
161. Lozano, D.; Sánchez-Salcedo, S.; Portal-Núñez, S.; Vila, M.; López-Herradón, A.; Ardura, J.A.; Mulero, F.; Gómez-Barrena, E.; Vallet-Regí, M.; Esbrit, P. Parathyroid hormone-related protein (107-111) improves the bone regeneration potential of gelatin-glutaraldehyde biopolymer-coated hydroxyapatite. *Acta Biomater.* **2014**, *10*, 3307–3316. [CrossRef] [PubMed]
162. Quinlan, E.; Thompson, E.M.; Matsiko, A.; O'Brien, F.J.; López-Noriega, A. Functionalization of a Collagen-Hydroxyapatite Scaffold with Osteostatin to Facilitate Enhanced Bone Regeneration. *Adv. Healthc. Mater.* **2015**, *4*, 2649–2656. [CrossRef]
163. Yang, L.; Huang, J.; Yang, S.; Cui, W.; Wang, J.; Zhang, Y.; Li, J.; Guo, X. Bone Regeneration Induced by Local Delivery of a Modified PTH-Derived Peptide from Nanohydroxyapatite/Chitosan Coated True Bone Ceramics. *ACS Biomater. Sci. Eng.* **2018**, *4*, 3246–3258. [CrossRef] [PubMed]
164. Meier, C.; Woitge, H.W.; Witte, K.; Lemmer, B.; Seibel, M.J. Supplementation with oral vitamin D3 and calcium during winter prevents seasonal bone loss: A randomized controlled open-label prospective trial. *J. Bone Miner. Res.* **2004**, *19*, 1221–1230. [CrossRef]
165. Barton, M. Primum Non Nocere: Why Calcitriol («Vitamin» D) Hormone Therapy Is Not a Magic Bullet. *Arterioscler. Thromb. Vasc. Biol.* **2019**, *39*, 117–120. [CrossRef] [PubMed]
166. Tang, Q.; Hu, Z.; Jin, H.; Zheng, G.; Yu, X.F.; Wu, G.; Liu, H.; Zhu, Z.; Xu, H.; Zhang, C.; et al. Microporous polysaccharide multilayer coated BCP composite scaffolds with immobilised calcitriol promote osteoporotic bone regeneration both in vitro and in vivo. *Theranostics* **2019**, *9*, 1125–1143. [CrossRef]

167. Sattary, M.; Khorasani, M.T.; Rafienia, M.; Rozve, H.S. Incorporation of nanohydroxyapatite and vitamin D3 into electrospun PCL/Gelatin scaffolds: The influence on the physical and chemical properties and cell behavior for bone tissue engineering. *Polym. Adv. Technol.* **2018**, *29*, 451–462. [CrossRef]
168. Sattary, M.; Rafienia, M.; Kazemi, M.; Salehi, H.; Mahmoudzadeh, M. Promoting effect of nano hydroxyapatite and vitamin D3 on the osteogenic differentiation of human adipose-derived stem cells in polycaprolactone/gelatin scaffold for bone tissue engineering. *Mater. Sci. Eng. C* **2019**, *97*, 141–155. [CrossRef]
169. Ramalho, M.J.; Loureiro, J.A.; Gomes, B.; Frasco, M.F.; Coelho, M.A.N.; Pereira, M.C. PLGA nanoparticles for calcitriol delivery. In Proceedings of the IEEE 4th Portuguese Meeting on Bioengineering, ENBENG 2015, Porto, Portugal, 26–28 February 2015; pp. 26–28. [CrossRef]
170. Sun, J.Y.; Ki, S.P.; Moon, S.K.; Rhee, J.M.; Khang, G.; Hai, B.L. Repair of diaphyseal bone defects with calcitriol-loaded PLGA scaffolds and marrow stromal cells. *Tissue Eng.* **2007**, *13*, 1125–1133. [CrossRef]
171. Liu, H.; Cui, J.; Feng, W.; Lv, S.; Du, J.; Sun, J.; Han, X.; Wang, Z.; Lu, X.; Oda, K.; et al. Local administration of calcitriol positively influences bone remodeling and maturation during restoration of mandibular bone defects in rats. *Mater. Sci. Eng. C* **2015**, *49*, 14–24. [CrossRef]
172. Fügl, A.; Gruber, R.; Agis, H.; Lzicar, H.; Keibl, C.; Schwarze, U.Y.; Dvorak, G. Alveolar bone regeneration in response to local application of calcitriol in vitamin D deficient rats. *J. Clin. Periodontol.* **2015**, *42*, 96–103. [CrossRef]
173. Sun, F.; Ju, C.; Chen, J.; Liu, S.; Liu, N.; Wang, K.; Liu, C. Nanoparticles based on hydrophobic alginate derivative as nutraceutical delivery vehicle: Vitamin D3 loading. *Artif. Cells Blood Substit. Biotechnol.* **2012**, *40*, 113–119. [CrossRef] [PubMed]
174. Chesnut, C.H.; Silverman, S.; Andriano, K.; Genant, H.; Gimona, A.; Harris, S.; Kiel, D.; Leboff, M.; Maricic, M.; Miller, P.; et al. A randomized trial of nasal spray salmon calcitonin in postmenopausal women with established osteoporosis: The prevent recurrence of osteoporotic fractures study. *Am. J. Med.* **2000**, *109*, 267–276. [CrossRef]
175. Yu, P.; Chen, Y.; Wang, Y.; Liu, Y.; Zhang, P.; Guo, Q.; Li, S.; Xiao, H.; Xie, J.; Tan, H.; et al. Pentapeptide-decorated silica nanoparticles loading salmon calcitonin for in vivo osteoporosis treatment with sustained hypocalcemic effect. *Mater. Today Chem.* **2019**, *14*, 100189. [CrossRef]
176. Liu, Y.; Chen, X.; Li, S.; Guo, Q.; Xie, J.; Yu, L.; Xu, X.; Ding, C.; Li, J.; Ding, J. Calcitonin-Loaded Thermosensitive Hydrogel for Long-Term Antiosteopenia Therapy. *ACS Appl. Mater. Interfaces* **2017**, *9*, 23428–23440. [CrossRef] [PubMed]
177. Wu, R.; Ma, B.; Zhou, Q.; Tang, C. Salmon calcitonin-loaded PLGA microspheres/calcium phosphate cement composites for osteoblast proliferation. *J. Appl. Polym. Sci.* **2017**, *134*, 45486. [CrossRef]
178. Mohammadi, F.; Beshkar, M.; Meibodi, A.A.; Shirani, G. The effect of calcitonin on increasing the effectivness of hydroxyapatite and β-tricalcium phosphate in bone regeneration. *J. Craniomaxillofacial Res.* **2014**, *1*, 8–10.
179. Kotak, D.J.; Devarajan, P.V. Bone targeted delivery of salmon calcitonin hydroxyapatite nanoparticles for sublingual osteoporosis therapy (SLOT). *Nanomed. Nanotechnol. Biol. Med.* **2020**, *24*, 102153. [CrossRef]
180. Liang, T.; Wu, J.; Li, F.; Huang, Z.; Pi, Y.; Miao, G.; Ren, W.; Liu, T.; Jiang, Q.; Guo, L. Drug-loading three-dimensional scaffolds based on hydroxyapatite-sodium alginate for bone regeneration. *J. Biomed. Mater. Res. Part A* **2020**, *109*, 219–231. [CrossRef]
181. Falahati-Nini, A.; Riggs, B.L.; Atkinson, E.J.; O'Fallon, W.M.; Eastell, R.; Khosla, S. Relative contributions of testosterone and estrogen in regulating bone resorption and formation in normal elderly men. *J. Clin. Investig.* **2000**, *106*, 1553–1560. [CrossRef]
182. Lufkin, E.G.; Wahncr, H.W.; Otallon, W.M.; Hodgsoti, S.F.; Kotowicz, M.A.; Lane, A.W.; Judd, H.L.; Caplan, R.H.; Riggs, B.L. Annals of Internal Medicine Treatment of Postmenopausal Osteoporosis with Transdermal Estrogen. *Ann. Intern. Med.* **1992**, *117*, 1–9. [CrossRef] [PubMed]
183. Tuck, S.P.; Francis, R.M. Testosterone, bone and osteoporosis. *Front. Horm. Res.* **2009**, *37*, 123–132. [CrossRef]
184. Hong, L.; Krishnamachari, Y.; Seabold, D.; Joshi, V.; Schneider, G.; Salem, A.K. Intracellular release of 17-β estradiol from cationic polyamidoamine dendrimer surface-modified poly (lactic-co-glycolic acid) microparticles improves osteogenic differentiation of human mesenchymal stromal cells. *Tissue Eng. Part C: Methods* **2011**, *17*, 319–325. [CrossRef] [PubMed]
185. Steffi, C.; Wang, D.; Kong, C.H.; Wang, Z.; Lim, P.N.; Shi, Z.; San Thian, E.; Wang, W. Estradiol-Loaded Poly(ϵ-caprolactone)/Silk Fibroin Electrospun Microfibers Decrease Osteoclast Activity and Retain Osteoblast Function. *ACS Appl. Mater. Interfaces* **2018**, *10*, 9988–9998. [CrossRef]
186. Irmak, G.; Demirtaş, T.T.; Altindal, D.Ç.; Çaliş, M.; Gumusderelioglu, M. Sustained release of 17β-estradiol stimulates osteogenic differentiation of adipose tissue-derived mesenchymal stem cells on chitosan-hydroxyapatite scaffolds. *Cells Tissues Organs* **2014**, *199*, 37–50. [CrossRef] [PubMed]
187. Hong, C.; Song, D.; Lee, D.K.; Lin, L.; Pan, H.C.; Lee, D.; Deng, P.; Liu, Z.; Hadaya, D.; Lee, H.L.; et al. Reducing posttreatment relapse in cleft lip palatal expansion using an injectable estrogen–nanodiamond hydrogel. *Proc. Natl. Acad. Sci. USA* **2017**, *114*, E7218–E7225. [CrossRef]
188. Gao, K.; Wang, X.; Liu, Q.; Chen, W.; Wang, G.; Zhang, D.; Liu, L. Evaluation of osteoblast differentiation and function when cultured on mesoporous bioactive glass adsorbed with testosterone. *J. Cell. Biochem.* **2018**, *119*, 5222–5232. [CrossRef]
189. Cheng, B.H.; Chu, T.M.G.; Chang, C.; Kang, H.Y.; Huang, K.E. Testosterone Delivered with a Scaffold Is as Effective as Bone Morphologic Protein-2 in Promoting the Repair of Critical-Size Segmental Defect of Femoral Bone in Mice. *PLoS ONE* **2013**, *8*, e70234. [CrossRef]

190. Da Costa, K.J.R.; Passos, J.J.; Gomes, A.D.M.; Sinisterra, R.D.; Lanza, C.R.M.; Cortes, M.E. Effect of testosterone incorporation on cell proliferation and differentiation for polymer-bioceramic composites. *J. Mater. Sci. Mater. Med.* **2012**, *23*, 2751–2759. [CrossRef]
191. Thrailkill, K.M.; Lumpkin, C.K.; Bunn, R.C.; Kemp, S.F.; Fowlkes, J.L. Is insulin an anabolic agent in bone? Dissecting the diabetic bone for clues. *Am. J. Physiol. Endocrinol. Metab.* **2005**, *289*, E735–E745. [CrossRef]
192. Haider, A.; Gupta, K.C.; Kang, I.K. PLGA/nHA hybrid nanofiber scaffold as a nanocargo carrier of insulin for accelerating bone tissue regeneration. *Nanoscale Res. Lett.* **2014**, *9*, 1–12. [CrossRef] [PubMed]
193. Wang, X.; Wu, X.; Xing, H.; Zhang, G.; Shi, Q.; Lingling, E.; Liu, N.; Yang, T.; Wang, D.; Qi, F.; et al. Porous Nanohydroxyapatite/Collagen Scaffolds Loading Insulin PLGA Particles for Restoration of Critical Size Bone Defect. *ACS Appl. Mater. Interfaces* **2017**, *9*, 11380–11391. [CrossRef] [PubMed]
194. Wang, X.; Zhang, G.; Qi, F.; Cheng, Y.; Lu, X.; Wang, L.; Zhao, J.; Zhao, B. Enhanced bone regeneration using an insulin- loaded nano-hydroxyapatite / collagen / PLGA composite scaffold. *Int. J. Nanomed.* **2018**, *13*, 117–127. [CrossRef]
195. Erisken, C.; Kalyon, D.M.; Wang, H.; Örnek-Ballanco, C.; Xu, J. Osteochondral tissue formation through adipose-derived stromal cell differentiation on biomimetic polycaprolactone nanofibrous scaffolds with graded insulin and beta-glycerophosphate concentrations. *Tissue Eng. Part A* **2011**, *17*, 1239–1252. [CrossRef]
196. Uebersax, L.; Merkle, H.P.; Meinel, L. Insulin-like growth factor I releasing silk fibroin scaffolds induce chondrogenic differentiation of human mesenchymal stem cells. *J. Control. Release* **2008**, *127*, 12–21. [CrossRef]
197. Luginbuehl, V.; Wenk, E.; Koch, A.; Gander, B.; Merkle, H.P.; Meinel, L. Insulin-like Growth Factor I–Releasing Alginate-Tricalciumphosphate Composites for Bone Regeneration. *Pharm. Res.* **2011**, *28*, 1233–1235. [CrossRef]
198. Jayasuriya, A.C.; Shah, C. Controlled release of insulin-like growth factor-1 and bone marrow stromal cell function of bone-like mineral layer- coated poly(lactic-co-glycolicacid) scaffolds. *J. Tissue Eng. Regen. Med.* **2008**, *2*, 43–49. [CrossRef]
199. Al Aboody, M.S.; Mickymaray, S. Anti-fungal efficacy and mechanisms of flavonoids. *Antibiotics* **2020**, *9*, 45. [CrossRef] [PubMed]
200. Panche, A.N.; Diwan, A.D.; Chandra, S.R. Flavonoids: An overview. *J. Nutr. Sci.* **2016**, *5*, e47. [CrossRef]
201. Metodiewa, D.; Kochman, A.; Karolczak, S. Evidence for antiradical and antioxidant properties of four biologically active N,N-diethylamioethyl ethers of flavanone oximes: A comparison with natural polyphenolic flavonoid (rutin) action. *Biochem. Mol. Biol. Int.* **1997**, *41*, 1067–1075. [CrossRef]
202. Preethi Soundarya, S.; Sanjay, V.; Haritha Menon, A.; Dhivya, S.; Selvamurugan, N. Effects of flavonoids incorporated biological macromolecules based scaffolds in bone tissue engineering. *Int. J. Biol. Macromol.* **2018**, *110*, 74–87. [CrossRef]
203. Wu, Y.; Cao, L.; Xia, L.; Wu, Q.; Wang, J.; Wang, X.; Xu, L.; Zhou, Y.; Xu, Y.; Jiang, X. Evaluation of Osteogenesis and Angiogenesis of Icariin in Local Controlled Release and Systemic Delivery for Calvarial Defect in Ovariectomized Rats. *Sci. Rep.* **2017**, *7*, 5077. [CrossRef]
204. Xie, X.; Pei, F.; Wang, H.; Tan, Z.; Yang, Z.; Kang, P. Icariin: A promising osteoinductive compound for repairing bone defect and osteonecrosis. *J. Biomater. Appl.* **2015**, *30*, 290–299. [CrossRef]
205. Lai, Y.; Cao, H.; Wang, X.; Chen, S.; Zhang, M.; Wang, N.; Yao, Z.; Dai, Y.; Xie, X.; Zhang, P.; et al. Porous composite scaffold incorporating osteogenic phytomolecule icariin for promoting skeletal regeneration in challenging osteonecrotic bone in rabbits. *Biomaterials* **2018**, *153*, 1–13. [CrossRef] [PubMed]
206. Wu, Y.; Xia, L.; Zhou, Y.; Ma, W.; Zhang, N.; Chang, J.; Lin, K.; Xu, Y.; Jiang, X. Evaluation of osteogenesis and angiogenesis of icariin loaded on micro/nano hybrid structured hydroxyapatite granules as a local drug delivery system for femoral defect repair. *J. Mater. Chem. B* **2015**, *3*, 4871–4883. [CrossRef] [PubMed]
207. Wu, T.; Nan, K.; Chen, J.; Jin, D.; Jiang, S.; Zhao, P.; Xu, J.; Du, H.; Zhang, X.; Li, J.; et al. A new bone repair scaffold combined with chitosan/hydroxyapatite and sustained releasing icariin. *Chin. Sci. Bull.* **2009**, *54*, 2953–2961. [CrossRef]
208. Fan, J.; Bi, L.; Wu, T.; Cao, L.; Wang, D.; Nan, K.; Chen, J.; Jin, D.; Jiang, S.; Pei, G. A combined chitosan/nano-size hydroxyapatite system for the controlled release of icariin. *J. Mater. Sci. Mater. Med.* **2012**, *23*, 399–407. [CrossRef] [PubMed]
209. Li, Y.; Liu, T.; Zheng, J.; Xu, X. Glutaraldehyde-crosslinked chitosan/hydroxyapatite bone repair scaffold and its application as drug carrier for icariin. *J. Appl. Polym. Sci.* **2013**, *130*, 1539–1547. [CrossRef]
210. Zhao, H.; Tang, J.; Zhou, D.; Weng, Y.; Qin, W.; Liu, C.; Lv, S.; Wang, W.; Zhao, X. Electrospun icariin-loaded core-shell collagen, polycaprolactone, hydroxyapatite composite scaffolds for the repair of rabbit tibia bone defects. *Int. J. Nanomed.* **2020**, *15*, 3039–3056. [CrossRef]
211. Hu, Y.; Cao, S.; Chen, J.; Zhao, Y.; He, F.; Li, Q.; Zou, L.; Shi, C. Biomimetic fabrication of icariin loaded nano hydroxyapatite reinforced bioactive porous scaffolds for bone regeneration. *Chem. Eng. J.* **2020**, *394*, 124895. [CrossRef]
212. Xie, Y.; Sun, W.; Yan, F.; Liu, H.; Deng, Z.; Cai, L. Icariin-loaded porous scaffolds for bone regeneration through the regulation of the coupling process of osteogenesis and osteoclastic activity. *Int. J. Nanomed.* **2019**, *14*, 6019–6033. [CrossRef] [PubMed]
213. Reiter, T.; Panick, T.; Schuhladen, K.; Roether, J.A.; Hum, J.; Boccaccini, A.R. Bioactive glass based scaffolds coated with gelatin for the sustained release of icariin. *Bioact. Mater.* **2019**, *4*, 1–7. [CrossRef] [PubMed]
214. Xu, H.; Ge, Y.W.; Lu, J.W.; Ke, Q.F.; Liu, Z.Q.; Zhu, Z.A.; Guo, Y.P. Icariin loaded-hollow bioglass/chitosan therapeutic scaffolds promote osteogenic differentiation and bone regeneration. *Chem. Eng. J.* **2018**, *354*, 285–294.
215. Yuan, Z.; Wan, Z.; Wei, P.; Lu, X.; Mao, J.; Cai, Q.; Zhang, X.; Yang, X. Dual-Controlled Release of Icariin/Mg2+ from Biodegradable Microspheres and Their Synergistic Upregulation Effect on Bone Regeneration. *Adv. Healthc. Mater.* **2020**, *9*, 2000211. [CrossRef] [PubMed]

216. Liu, H.; Li, W.; Luo, B.; Chen, X.; Wen, W.; Zhou, C. Icariin immobilized electrospinning poly(L-lactide) fibrous membranes via polydopamine adhesive coating with enhanced cytocompatibility and osteogenic activity. *Mater. Sci. Eng. C* **2017**, *79*, 399–409. [CrossRef]
217. Gong, M.; Chi, C.; Ye, J.; Liao, M.; Xie, W.; Wu, C.; Shi, R.; Zhang, L. Icariin-loaded electrospun PCL/gelatin nanofiber membrane as potential artificial periosteum. *Colloids Surf. B Biointerfaces* **2018**, *170*, 201–209. [CrossRef]
218. Xia, L.; Li, Y.; Zhou, Z.; Dai, Y.; Liu, H.; Liu, H. Icariin delivery porous PHBV scaffolds for promoting osteoblast expansion in vitro. *Mater. Sci. Eng. C* **2013**, *33*, 3545–3552. [CrossRef]
219. He, L.; Yang, J.; Lu, J.; Xiao, Y.; Fan, Y.; Zhang, X. Preparation and characterization of a novel hyaluronic acid-icariin conjugate hydrogel. *Mater. Lett.* **2014**, *136*, 41–44. [CrossRef]
220. Yan, H.; Zhou, Z.; Huang, T.; Peng, C.; Liu, Q.; Zhou, H.; Zeng, W.; Liu, L.; Ou, B.; He, S.; et al. Controlled release in vitro of icariin from gelatin/hyaluronic acid composite microspheres. *Polym. Bull.* **2016**, *73*, 1055–1066. [CrossRef]
221. Yang, J.; Liu, Y.; He, L.; Wang, Q.; Wang, L.; Yuan, T.; Xiao, Y.; Fan, Y.; Zhang, X. Icariin conjugated hyaluronic acid/collagen hydrogel for osteochondral interface restoration. *Acta Biomater.* **2018**, *74*, 156–167. [CrossRef]
222. Ability, O.; Vivo, I.; Ma, A.; Shang, H.; Song, Y.; Chen, B.; You, Y.; Han, W.; Zhang, X. Icariin-functionalized coating on TiO_2 nanotubes surface to improve osteoblast activity in vitro and osteogenesis ability in vivo. *Coatings* **2019**, *9*, 327.
223. Zhang, Y.; Chen, L.; Liu, C.; Feng, X.; Wei, L.; Shao, L. Self-assembly chitosan/gelatin composite coating on icariin-modified TiO_2 nanotubes for the regulation of osteoblast bioactivity. *Mater. Des.* **2016**, *92*, 471–479. [CrossRef]
224. Li, M.; Gu, Q.; Chen, M.; Zhang, C.; Chen, S.; Zhao, J. Controlled delivery of icariin on small intestine submucosa for bone tissue engineering. *Mater. Sci. Eng. C* **2017**, *71*, 260–267. [CrossRef] [PubMed]
225. Kim, Y.J.; Bae, Y.C.; Suh, K.T.; Jung, J.S. Quercetin, a flavonoid, inhibits proliferation and increases osteogenic differentiation in human adipose stromal cells. *Biochem. Pharmacol.* **2006**, *72*, 1268–1278. [CrossRef]
226. Abd El-Fattah, A.I.; Fathy, M.M.; Ali, Z.Y.; El-Garawany, A.E.R.A.; Mohamed, E.K. Enhanced therapeutic benefit of quercetin-loaded phytosome nanoparticles in ovariectomized rats. *Chem. Biol. Interact.* **2017**, *271*, 30–38. [CrossRef]
227. Chen, S.; Zhu, L.; Wen, W.; Lu, L.; Zhou, C.; Luo, B. Fabrication and Evaluation of 3D Printed Poly(l -lactide) Scaffold Functionalized with Quercetin-Polydopamine for Bone Tissue Engineering. *ACS Biomater. Sci. Eng.* **2019**, *5*, 2506–2518. [CrossRef]
228. Zhu, L.; Chen, S.; Liu, K.; Wen, W.; Lu, L.; Ding, S.; Zhou, C.; Luo, B. 3D poly (L-lactide)/chitosan micro/nano fibrous scaffolds functionalized with quercetin-polydopamine for enhanced osteogenic and anti-inflammatory activities. *Chem. Eng. J.* **2020**, *391*, 123524. [CrossRef]
229. Zhou, Y.; Wu, Y.; Ma, W.; Jiang, X.; Takemra, A.; Uemura, M.; Xia, L.; Lin, K.; Xu, Y. The effect of quercetin delivery system on osteogenesis and angiogenesis under osteoporotic conditions. *J. Mater. Chem. B* **2017**, *5*, 612–625. [CrossRef] [PubMed]
230. Song, J.E.; Tripathy, N.; Lee, D.H.; Park, J.H.; Khang, G. Quercetin Inlaid Silk Fibroin/Hydroxyapatite Scaffold Promotes Enhanced Osteogenesis. *ACS Appl. Mater. Interfaces* **2018**, *10*, 32955–32964. [CrossRef]
231. Song, J.E.; Tian, J.; Kook, Y.J.; Thangavelu, M.; Choi, J.H.; Khang, G. A BMSCs-laden quercetin/duck's feet collagen/hydroxyapatite sponge for enhanced bone regeneration. *J. Biomed. Mater. Res. Part A* **2020**, *108*, 784–794. [CrossRef]
232. Gupta, S.K.; Kumar, R.; Mishra, N.C. Influence of quercetin and nanohydroxyapatite modifications of decellularized goat-lung scaffold for bone regeneration. *Mater. Sci. Eng. C* **2017**, *71*, 919–928. [CrossRef]
233. Kuang, M.J.; Zhang, W.H.; He, W.W.; Sun, L.; Ma, J.X.; Wang, D.; Ma, X.L. long Naringin regulates bone metabolism in glucocorticoid-induced osteonecrosis of the femoral head via the Akt/Bad signal cascades. *Chem. Biol. Interact.* **2019**, *304*, 97–105. [CrossRef]
234. Chen, K.; Lin, K.; Chen, Y.; Yao, C. A Novel Porous Gelatin Composite Containing Naringin for Bone Repair. *Evid. Based Complement. Altern. Med.* **2013**, *2013*, 283941. [CrossRef]
235. Ji, Y.; Wang, L.; Watts, D.C.; Qiu, H.; You, T.; Deng, F.; Wu, X. Controlled-release naringin nanoscaffold for osteoporotic bone healing. *Dent. Mater.* **2014**, *30*, 1263–1273. [CrossRef]
236. Yang, X.; Almassri, H.N.S.; Zhang, Q.; Ma, Y.; Zhang, D.; Chen, M.; Wu, X. Electrosprayed naringin-loaded microsphere/SAIB hybrid depots enhance bone formation in a mouse calvarial defect model. *Drug Deliv.* **2019**, *26*, 137–146. [CrossRef] [PubMed]
237. Tao, Z.S.; Wu, X.J.; Yang, M.; Xu, H.G. Local administration with silymarin could increase osseointegration of hydroxyapatite-coated titanium implants in ovariectomized rats. *J. Biomater. Appl.* **2019**, *34*, 664–672. [CrossRef]
238. Song, J.E.; Jeon, Y.S.; Tian, J.; Kim, W.K.; Choi, M.J.; Carlomagno, C.; Khang, G. Evaluation of silymarin/duck's feet-derived collagen/hydroxyapatite sponges for bone tissue regeneration. *Mater. Sci. Eng. C* **2019**, *97*, 347–355. [CrossRef] [PubMed]
239. Xue, D.; Chen, E.; Zhang, W.; Gao, X.; Wang, S.; Zheng, Q.; Pan, Z.; Li, H.; Liu, L. The role of hesperetin on osteogenesis of human mesenchymal stem cells and its function in bone regeneration. *Oncotarget* **2017**, *8*, 21031–21043. [CrossRef]
240. Gupta, G.K.; Kumar, A.; Khedgikar, V.; Kushwaha, P.; Gautam, J.; Nagar, G.K.; Gupta, V.; Verma, A.; Dwivedi, A.K.; Misra, A.; et al. Osteogenic efficacy enhancement of kaempferol through an engineered layer-by-layer matrix: A study in ovariectomized rats. *Nanomedicine* **2013**, *8*, 757–771. [CrossRef]
241. Lee, J.S.; Lee, J.S.; Lee, M.S.; An, S.; Yang, K.; Lee, K.; Yang, H.S.; Lee, H.; Cho, S.W. Plant Flavonoid-Mediated Multifunctional Surface Modification Chemistry: Catechin Coating for Enhanced Osteogenesis of Human Stem Cells. *Chem. Mater.* **2017**, *29*, 4375–4384. [CrossRef]

242. Khan, S.; Ullah, M.W.; Siddique, R.; Liu, Y.; Ullah, I.; Xue, M.; Yang, G.; Hou, H. Catechins-modified selenium-doped hydroxyapatite nanomaterials for improved osteosarcoma therapy through generation of reactive oxygen species. *Front. Oncol.* **2019**, *9*, 499. [CrossRef]
243. Sistanipour, E.; Meshkini, A.; Oveisi, H. Catechin-conjugated mesoporous hydroxyapatite nanoparticle: A novel nano-antioxidant with enhanced osteogenic property. *Colloids Surf. B Biointerfaces* **2018**, *169*, 329–339. [CrossRef] [PubMed]
244. Waltner-Law, M.E.; Wang, X.L.; Law, B.K.; Hall, R.K.; Nawano, M.; Granner, D.K. Epigallocatechin gallate, a constituent of green tea, represses hepatic glucose production. *J. Biol. Chem.* **2002**, *277*, 34933–34940. [CrossRef] [PubMed]
245. Rodriguez, R.; Kondo, H.; Nyan, M.; Hao, J.; Miyahara, T.; Ohya, K.; Kasugai, S. Implantation of green tea catechin α-tricalcium phosphate combination enhances bone repair in rat skull defects. *J. Biomed. Mater. Res. Part B Appl. Biomater.* **2011**, *98B*, 263–271. [CrossRef]
246. Kook, Y.J.; Tian, J.; Jeon, Y.S.; Choi, M.J.; Song, J.E.; Park, C.H.; Reis, R.L.; Khang, G. Nature-derived epigallocatechin gallate/duck's feet collagen/hydroxyapatite composite sponges for enhanced bone tissue regeneration. *J. Biomater. Sci. Polym. Ed.* **2018**, *29*, 984–996. [CrossRef]
247. Csiszar, A. Anti-inflammatory effects of resveratrol: Possible role in prevention of age-related cardiovascular disease. *Ann. New York Acad. Sci.* **2011**, *1215*, 117–122. [CrossRef]
248. Ming, L.; Zhipeng, Y.; Fei, Y.; Feng, R.; Jian, W.; Baoguo, J.; Yongqiang, W.; Peixun, Z. Microfluidic-based screening of resveratrol and drug-loading PLA/Gelatine nano-scaffold for the repair of cartilage defect. *Artif. Cells Nanomed. Biotechnol.* **2018**, *46*, 336–346. [CrossRef]
249. Yu, F.; Li, M.; Yuan, Z.; Rao, F.; Fang, X.; Jiang, B.; Wen, Y.; Zhang, P. Mechanism research on a bioactive resveratrol– PLA–gelatin porous nano-scaffold in promoting the repair of cartilage defect. *Int. J. Nanomed.* **2018**, *13*, 7845–7858. [CrossRef] [PubMed]
250. Li, Y.; Dnmark, S.; Edlund, U.; Finne-Wistrand, A.; He, X.; Norgrd, M.; Blomén, E.; Hultenby, K.; Andersson, G.; Lindgren, U. Resveratrol-conjugated poly—Caprolactone facilitates in vitro mineralization and in vivo bone regeneration. *Acta Biomater.* **2011**, *7*, 751–758. [CrossRef]
251. Wang, W.; Sun, L.; Zhang, P.; Song, J.; Liu, W. An anti-inflammatory cell-free collagen/resveratrol scaffold for repairing osteochondral defects in rabbits. *Acta Biomater.* **2014**, *10*, 4983–4995. [CrossRef]
252. Wang, C.C.; Wang, C.H.; Chen, H.C.; Cherng, J.H.; Chang, S.J.; Wang, Y.W.; Chang, A.; Yeh, J.Z.; Huang, Y.H.; Liu, C.C. Combination of resveratrol-containing collagen with adipose stem cells for craniofacial tissue-engineering applications. *Int. Wound J.* **2018**, *15*, 660–672. [CrossRef]
253. Marycz, K.; Smieszek, A.; Trynda, J.; Sobierajska, P.; Targonska, S.; Grosman, L.; Wiglusz, R.J. Nanocrystalline hydroxyapatite loaded with resveratrol in colloidal suspension improves viability, metabolic activity and mitochondrial potential in human adipose-derived mesenchymal stromal stem cells (hASCs). *Polymers* **2019**, *11*, 92. [CrossRef]
254. Raggio, C.L.; Boyan, B.D.; Boskey, A.L. In vivo hydroxyapatite formation induced by lipids. *J. Bone Miner. Res.* **1986**, *1*, 409–415. [CrossRef] [PubMed]
255. Boskey, A.L. Hydroxyapatite formation in a dynamic collagen gel system: Effects of type I collagen, lipids, and proteoglycans. *J. Phys. Chem.* **1989**, *93*, 1628–1633. [CrossRef]
256. Vance, J.E.; Stenbergen, R. Metabolism and functions of phosphatidylserine. *Prog. Lipid Res.* **2005**, *44*, 207–234. [CrossRef] [PubMed]
257. Hatakeyama, J.; Anan, H.; Hatakeyama, Y.; Matsumoto, N.; Takayama, F.; Wu, Z.; Matsuzaki, E.; Minakami, M.; Izumi, T.; Nakanishi, H. Induction of bone repair in rat calvarial defects using a combination of hydroxyapatite with phosphatidylserine liposomes. *J. Oral Sci.* **2019**, *61*, 111–118. [CrossRef]
258. Yang, C.R.; Wang, Y.J.; Chen, X.F. Preparation and evaluation of biomimetric nano-hydroxyapatite-based composite scaffolds for bone-tissue engineering. *Chin. Sci. Bull.* **2012**, *57*, 2787–2792. [CrossRef]
259. Yang, C.; Fang, C. Microporous nano-hydroxyapatite/collagen/phosphatidylserine scaffolds embedding collagen microparticles for controlled drug delivery in bone tissue engineering. *Mater. Res.* **2015**, *18*, 1077–1081. [CrossRef]
260. Xu, C.; Su, P.; Chen, X.; Meng, Y.; Yu, W.; Xiang, A.P.; Wang, Y. Biocompatibility and osteogenesis of biomimetic Bioglass-Collagen-Phosphatidylserine composite scaffolds for bone tissue engineering. *Biomaterials* **2011**, *32*, 1051–1058. [CrossRef] [PubMed]
261. Yang, C.R.; Wang, Y.J.; Chen, X.F. Mineralization regulation and biological influence of bioactive glass-collagen-phosphatidylserine composite scaffolds. *Sci. China Life Sci.* **2012**, *55*, 236–240. [CrossRef]
262. Yang, C.; Wu, H.; Chen, S.; Kang, G. Three-dimensional bioglass-collagen-phosphatidylserine scaffolds designed with functionally graded structure and mechanical features. *Biomed. Tech.* **2018**, *63*, 255–259. [CrossRef]
263. Merolli, A.; Bosetti, M.; Giannotta, L.; Lloyd, A.W.; Denyer, S.P.; Rhys-Williams, W.; Love, W.G.; Gabbi, C.; Cacchioli, A.; Leali, P.T.; et al. In vivo assessment of the osteointegrative potential of phosphatidylserine-based coatings. *J. Mater. Sci. Mater. Med.* **2006**, *17*, 789–794. [CrossRef] [PubMed]
264. Ruiz, G.C.M.; Cruz, M.A.E.; Faria, A.N.; Zancanela, D.C.; Ciancaglini, P.; Ramos, A.P. Biomimetic collagen/phospholipid coatings improve formation of hydroxyapatite nanoparticles on titanium. *Mater. Sci. Eng. C* **2017**, *77*, 102–110. [CrossRef]
265. Szcześ, A. Phosphate mineral formation on the supported dipalmitoylphosphatidylcholine (DPPC) layers. *Mater. Sci. Eng. C* **2014**, *40*, 373–381. [CrossRef]

266. Szcześ, A. Effect of the enzymatically modified supported dipalmitoylphosphatidylcholine (DPPC) bilayers on calcium carbonate formation. *Colloid Polym. Sci.* **2016**, *294*, 409–419. [CrossRef] [PubMed]
267. Placente, D.; Benedini, L.A.; Baldini, M.; Laiuppa, J.A.; Santillán, G.E.; Messina, P.V. Multi-drug delivery system based on lipid membrane mimetic coated nano-hydroxyapatite formulations. *Int. J. Pharm.* **2018**, *548*, 559–570. [CrossRef]
268. Wang, G.; Babadağli, M.E.; Uludağ, H. Bisphosphonate-derivatized liposomes to control drug release from collagen/hydroxyapatite scaffolds. *Mol. Pharm.* **2011**, *8*, 1025–1034. [CrossRef] [PubMed]

International Journal of
Molecular Sciences

MDPI

Review

Targeted Clindamycin Delivery Systems: Promising Options for Preventing and Treating Bacterial Infections Using Biomaterials

Dagmara Słota [1,*], Josef Jampilek [2,3,*] and Agnieszka Sobczak-Kupiec [1]

[1] Department of Materials Science, Faculty of Materials Engineering and Physics, KrakowUniversity of Technology, 37 Jana Pawła II Av., 31-864 Krakow, Poland; agnieszka.sobczak-kupiec@pk.edu.pl
[2] Department of Analytical Chemistry, Faculty of Natural Sciences, Comenius University, Ilkovicova 6, 842 15 Bratislava, Slovakia
[3] Department of Chemical Biology, Faculty of Science, Palacky University, Slechtitelu 27, 783 71 Olomouc, Czech Republic
* Correspondence: dagmara.slota@doktorant.pk.edu.pl (D.S.); josef.jampilek@gmail.com (J.J.)

Abstract: Targeted therapy represents a real opportunity to improve the health and lives of patients. Developments in this field are confirmed by the fact that the global market for drug carriers was worth nearly $40 million in 2022. For this reason, materials engineering and the development of new drug carrier compositions for targeted therapy has become a key area of research in pharmaceutical drug delivery in recent years. Ceramics, polymers, and metals, as well as composites, are of great interest, as when they are appropriately processed or combined with each other, it is possible to obtain biomaterials for hard tissues, soft tissues, and skin applications. After appropriate modification, these materials can release the drug directly at the site requiring a therapeutic effect. This brief literature review characterizes routes of drug delivery into the body and discusses biomaterials from different groups, options for their modification with clindamycin, an antibiotic used for infections caused by aerobic and anaerobic Gram-positive bacteria, and different methods for the final processing of carriers. Examples of coating materials for skin wound healing, acne therapy, and bone tissue fillers are given. Furthermore, the reasons why the use of antibiotic therapy is crucial for a smooth and successful recovery and the risks of bacterial infections are explained. It was demonstrated that there is no single proven delivery scheme, and that the drug can be successfully released from different carriers depending on the destination.

Keywords: clindamycin; drug delivery systems; antibiotic; surgical site infection; biomaterials

Citation: Słota, D.; Jampilek, J.; Sobczak-Kupiec, A. Targeted Clindamycin Delivery Systems: Promising Options for Preventing and Treating Bacterial Infections Using Biomaterials. *Int. J. Mol. Sci.* **2024**, *25*, 4386. https://doi.org/10.3390/ijms25084386

Academic Editor: Filipa Mascarenhas-Melo

Received: 20 March 2024
Revised: 11 April 2024
Accepted: 13 April 2024
Published: 16 April 2024

1. Introduction

Controlling the kinetics of drug release by using drug delivery systems (DDSs) brings a number of benefits to patient health. First and foremost, they allow the delivery of the active ingredient to the exact site affected by the disease. Moreover, DDSs improve the effectiveness of the drugs, reduce the severity of side effects, and allow the use of a lower dose of the substance [1,2]. Given the above, this is one of the hottest topics in modern pharmacology or materials engineering. According to a Fortune Business Insights report, the global drug delivery systems market size was valued at $39.55 billion in 2022. It is assumed that at a sustained compound annual growth rate (CAGR) of 9.1%, the value will grow to $78.76 billion in 2030. North America holds the largest share of the market, more than 40% [3]. The DDSs market continues to grow. The main drivers are an increase in patient awareness of advanced systems that allow the selective delivery of a specific drug to a certain site with improved accuracy. This enables faster onset of the effect and reduces the risk of side effects. Also, advances in medicine and science have increased the availability of new systems and improved patient comfort.

This brief review discusses various routes of drug administration into the body, pointing out their advantages and disadvantages. The focus was placed on ceramic, polymeric,

and composite clindamycin delivery systems presented in the literature for biomedical applications such as bone tissue replacement, wound healing, and acne treatment. In order to conduct the presented literature review, a search of the Google Scholar and Science Direct databases was performed. Only publications discussing the methods of manufacturing of clindamycin carriers were considered. The results of papers published between 2008 and 2024 were found, with the largest number of literature reports on the subject being between 2020 and 2022. The databases were searched based on keywords such as clindamycin; ceramic; polymer; composite; drug carrier; DDS.

The aim of this review is to identify the potential for the development and application of a specific drug in targeted therapies. Clindamycin is a broad-spectrum antibiotic; however, until now, no other literature reviews on this topic have been found, as most of the available reviews focus on a general group of drugs/active ingredients rather than on a single specific one. This brief literature review will introduce the reader to the world of clindamycin carriers, indicating the possibility of producing new multifunctional biomaterials for both hard and soft tissues.

2. Routes of Drug Administration and Drug Delivery

There are many ways to conventionally administer drugs and active substances into the body. This can be performed using syrups, tablets, suppositories, or ointments. The dosage form is chosen depending on the physicochemical properties of the drug as well as the body part being treated, the mechanism of action of the drug, and the solubility and permeability of the substance. Conventional methods of drug administration do not allow patients to fully benefit from the therapeutic potential of the drug. This is caused by the overall distribution of the drug throughout the body. This reduces the probability of a large amount of the dose reaching its destination, requiring a higher dose to be used, which increases the risk of toxicity. Figure 1 presents conventional drug delivery methods and their main disadvantages [4].

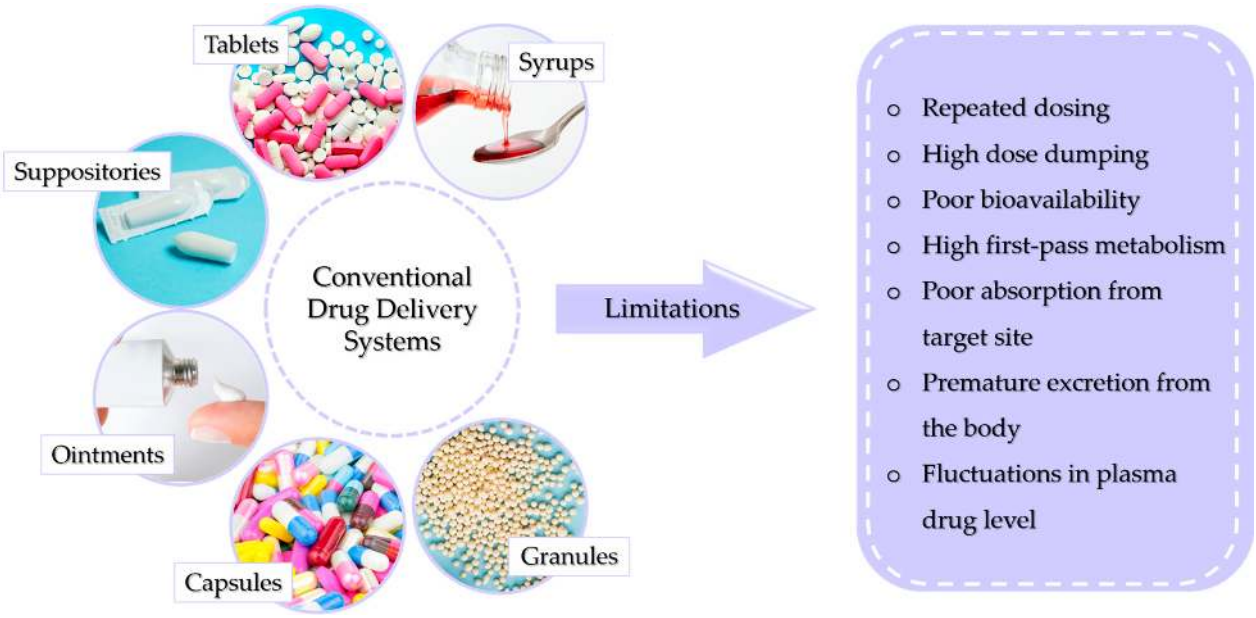

Figure 1. Possible limitations of conventional drug delivery systems.

The most popular is the oral route through which capsules, tablets, syrups, or granules are administered. This way is relatively inexpensive, the substance can be administered easily, without pain, and the absorption of the substance can occur through the entire length of the digestive tract [5,6]. However, this way is also fraught with the risk of drug destruction by stomach acid or digestive juices. The drug can also irritate the gastric mucosa and cause nausea or vomiting [7,8]. The first-pass effect, by which orally absorbed

substances are initially transported to the liver via the portal vein, is also important, as it reduces drug activity [9]. In the case of ointments, the main limitation of their application is insufficient skin permeability of drugs, which reduces the therapeutic effect. Another limitation associated with ointments is that prolonged perfusion can cause membrane degradation, which can cause skin irritation [10]. In contrast, DDSs exhibit a number of advantages over conventional intake, allowing a lower dosage, providing a longer duration of action, maintaining more uniform plasma levels, or reducing the frequency of dosing [11].

Controlled drug delivery systems for targeted therapy offer the use of multiple carriers depending on the nature of the substance being delivered or the site of action. This type of therapy, also called molecularly targeted therapy, is one of the main cancer treatments since it can be applied directly to tumor cells. However, the term is also used in the case of the targeted delivery of other drugs [12]. Depending on the need and location, this process can be based on the mechanism of active and passive targeting. The first focuses on the precise targeting of diseased cells (e.g., cancerous cells) by appropriate ligands, while in contrast, in passive targeting, the drug or other substance is delivered within the perimeter of the site requiring a therapeutic effect [13]. The release of the substance from the carrier itself can occur as a result of external impulses like an electrical signal, but also as a result of a change in the pH value or swelling [14,15].

Polymers, ceramics, and composites can be used as DDSs; however, they require appropriate processing and combination with the active substance. They include micelles, nanocapsules, microcapsules, liposomes, dendrimers, and hydrogels. The drug can be absorbed on the carrier, encapsulated in it, or bound by a chemical bond. Accordingly, the release can occur at different rates [16,17]. The drug release profile is usually expressed as the plasma drug concentration as a function of time. Figure 2 illustrates two important limits indicating the minimum and maximum concentrations.

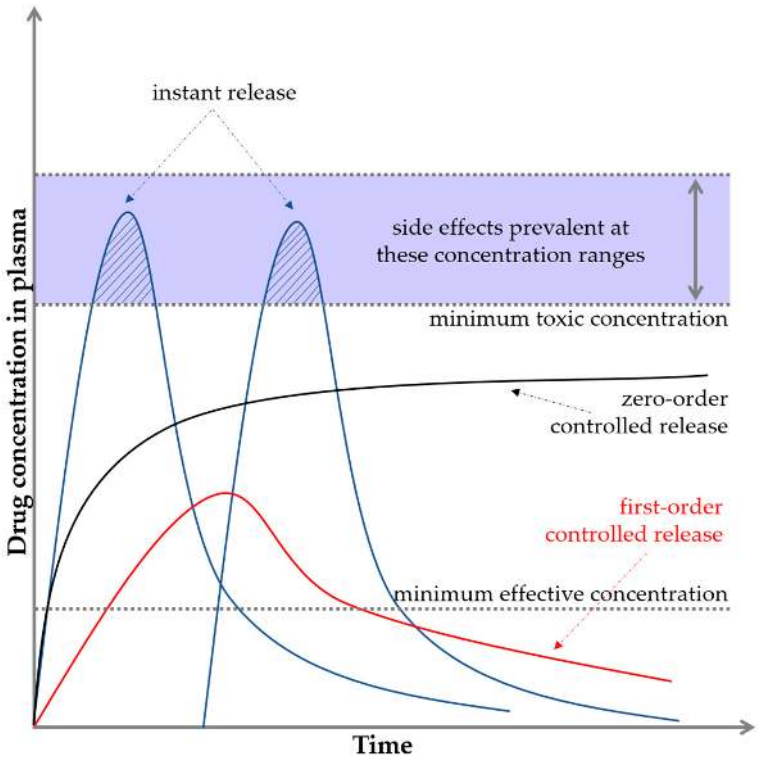

Figure 2. Basic pharmacological/biopharmaceutical profiles and levels.

If the drug concentration is too low, no therapeutic effect is observed, and this level is referred to as the minimum effective concentration. If the drug concentration is too high, toxicity problems may occur, and this level is known as the minimum toxic concentra-

tion [18,19]. In the case of conventional drug delivery, e.g., in tablet form, a sinusoidal shape of the graph is observed, where for a while, the limit of the maximum concentration is exceeded. This fact often causes the appearance of side effects. Then, the concentration drops sharply down below the minimum limit. The ideal situation is to keep the release of active substances in the interval between the minimum effective and minimum toxic concentrations, that is, in the so-called therapeutic window (black curve on the graph). This is crucial for maintaining the safety but also the effectiveness of the substance or drug. This is an example of zero-order drug release kinetics, which means that a constant amount of the active ingredient/drug is released per unit time; however, the rate itself does not depend on the concentration. This means that the drug is released at a constant rate [4,20–22].

3. Delivery of Antibiotics

The delivery of antibiotics in targeted therapy is critical to the risk of bacterial infections including surgical site infections (SSIs). In fact, SSIs are one of the most common infections that can occur both during hospitalization and after hospital discharge [23]. The etiologic agent leading to the infections is most often bacteria residing on the skin, but they can also be microorganisms residing in other areas of the body or found in the operating room environment as well as on surgical instruments [24–26]. Furthermore, bacterial infections can lead to soft tissue inflammation or osteomyelitis, which is defined as an inflammatory process caused by a bone infection that leads to bone destruction, bone necrosis, and can progress to a chronic condition [27,28]. In the case of the skin, bacteria can cause irritation, aggravate acne, or inhibit the healing process of open wounds [29]. According to the procedure recommended by the World Health Organization, antibiotic therapy can effectively prevent infections and thus problems in soft and hard tissue regeneration. For this reason, biomaterials are being developed to deliver the drug directly to the site requiring a therapeutic effect. Depending on the type of bacterial strain, different antibiotics may be used [30,31].

Clindamycin

Clindamycin (CLD) (Figure 3) is an antibiotic from the lincosamide group used against many types of bacteria thanks to its unique properties and broad effect [32,33]. It is usually available either as a readily water-soluble salt (clindamycin hydrochloride) or as a lipophilic ester (clindamycin phosphate). This ester is a prodrug of clindamycin, which is rapidly hydrolyzed by esterases to active clindamycin after application [34,35].

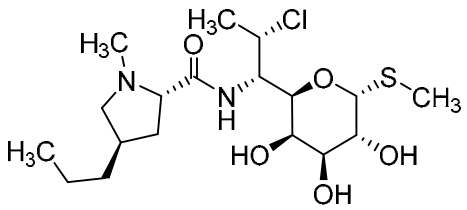

Figure 3. Chemical structure of clindamycin.

The mechanism of action of CLD is based on blocking the 23S ribosomal RNA of the 50S subunit by the inhibition of peptide bond formation, which leads to the inhibition of bacterial protein synthesis [36]. For this reason, CLD is effective in treating infections caused by Gram-positive bacteria, such as *Staphylococcus aureus* and *Streptococcus pneumoniae* [37,38]. The first of them is one of the most common causes of morbidity and mortality from an infectious agent worldwide and is often associated with SSIs [39,40]. The second one is particularly dangerous for children and can cause otitis media, pneumonia, rhinosinusitis, bacteremia, and even meningitis [41].

One of the distinctive features of CLD is its ability to penetrate tissues and body fluids [42]. This makes it highly effective in the treatment of bone disorders. It not only

combats infections at the superficial level, but also penetrates into areas where other antibiotics may be less effective [43,44]. For this reason, it is often used during bone transplants or other surgeries involving this tissue [45]. Additionally, CLD easily crosses the human placenta, but does not cross the blood–brain barrier [46,47]. However, it can cause side effects such as loss of appetite, abdominal discomfort, diarrhea, and nausea [32]. It is worth mentioning that clindamycin has relatively good stability under acidic conditions, which allows it to function effectively in the acidic environment of the stomach. This is important, especially when treating gastrointestinal infections, where substances can be exposed to stomach acid [48,49]. This means that in the case of this drug, conventional ingestion of CLD in tablet form is possible, as the substance will not be degraded/decomposed. Another issue is the above-mentioned limitations related to systemic distribution, which may reduce its effect [50,51]. The most significant benefits and negative effects associated with CLD administration are summarized in Table 1 [32,36,52,53].

Table 1. Advantages and disadvantages of using clindamycin.

Advantages	Disadvantages
• Can be administered both systemically and locally; • Diet has no effect on efficacy; • Active against most aerobic and anaerobic Gram-positive bacteria; • Increases intracellular killing of susceptible organisms, reduces bacterial adhesion to host cells; • Has a positive effect on the overall recovery outcome, as it does not block pro-angiogenic activity.	• Side effects such as allergic reactions, colitis, nausea, vomiting, and diarrhea; • Can cause esophagitis, taste disorders, and changes in hematological parameters; • Poor permeability of the outer cell envelope, thus not working well against aerobic Gram-negative bacilli.

4. Targeted Clindamycin Delivery Systems

4.1. Ceramic Carriers of Clindamycin

In order to achieve an appropriate biological effect, it is extremely important to choose the right materials for biomedical applications. In the aspect of biomaterials for bone tissue, the most commonly used are calcium phosphates, belonging to the family of biocompatible apatites. Several ceramics can be distinguished among them, which differ in their Ca/P molar ratio and thus in their properties [54–56]. The most popular is hydroxyapatite (HAp, $Ca_{10}(PO_4)_6(OH)_2$), which is the ceramic material most similar to the mineral phase of natural bone tissue. It has a Ca/P ratio of 1.67 and is bioactive and osteoconductive [57,58]. Another structure of calcium phosphate is calcium triphosphate (TCP, $Ca_3(PO_4)_2$), which has osteoinductive properties and the ability to resorb under body conditions. Its molar ratio of Ca/P is 1.5. TCP and HAp are the most commonly used ceramic materials in biomaterials with the potential to regenerate or fill bone tissue [59,60]. However, brushite (DCPD—dicalcium phosphate dihydrate, $CaHPO_4 \cdot 2H_2O$) or monethite (DCPA—dicalcium phosphate anhydrous, $CaHPO_4$), which have the same Ca/P molar ratio of 1.0, are also used for this purpose, but differ in the amount of bound water [61,62]. Nevertheless, they are all able to provide suitable conditions for the ingrowth of bone-forming elements.

The amount of drug adsorbed in the ceramic material depends on a number of factors, e.g., the concentration of the drug and the size of the carrier. However, one of the most important factors is porosity, which determines the specific surface area and affects the diffusion of the drug [63,64]. The active substance can be bound to the drug by physical sorption or by forming a covalent bond (Figure 4). The release process for most substances and porous ceramic carriers will be similar. As a result of the penetration of the liquid medium deep into the pores of the material, a systematic release of the drug into the medium occurs [56,65–67].

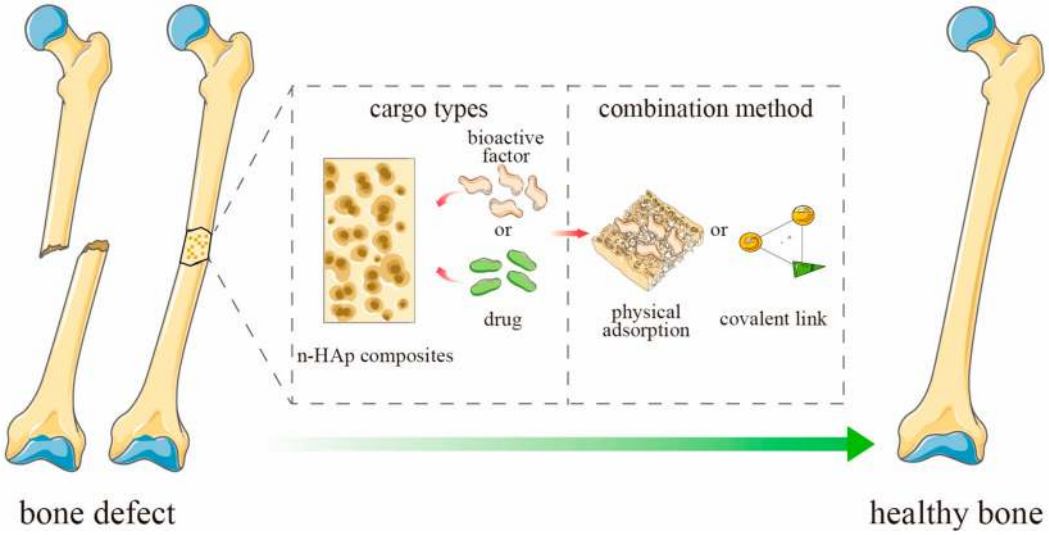

Figure 4. Schematic representation of ceramics-based scaffold loaded with active substances for bone defect. Adapted from [65], MDPI, 2023 (n-HAp = nano-hydroxyapatite).

The effect of the drug release rate was compared depending on the type of ceramic. HAp and amorphous calcium phosphate (ACP) were used for this purpose. The authors compared material modified with a range of antibiotics including ampicillin, kanamycin, oxacillin, vancomycin, and clindamycin. ACP and HAp demonstrated similar levels of activity against Gram-negative organisms; however, ACP proved to be more effective against Gram-positive organisms. This suggests that the degree of crystallinity may be one of the key factors influencing antibiotic activity [68]. An example of Gram-positive bacteria against which other carriers have been tested is *S. aureus*, which infected an osteoblastic line. HAp and DCPA were subjected to drug modification through a process of physical sorption and particle aggregation induced by drying, which led to the formation of microscopic blocks. In this study, not only was the antimicrobial nature of the carrier observed, but also the fact that it is stronger for the whole carrier than for the drug itself. This effect was likely due to the relationship occurring between HAp or DCPA and osteoblastic cells, thus confirming the highly osteoconductive nature of these calcium phosphates [69]. The influence of the physicochemical parameters of calcium phosphates on the rate of drug release was also demonstrated. Two types of HAp were subjected to physical sorption in CLD solution; one was freeze-dried initially, and the other was oven-dried at a high temperature. This resulted in changes in the surface morphology, and more drug was released over time from the oven-dried material, where larger agglomerates of grains were observed [70]. In another paper, TCP, HAp, and DCPD were also compared and subjected to CLD modification by a physical sorption process. It was demonstrated that they have a similar potential to be used as DDSs, and that the rate of drug release is affected not only by the porosity, but also by the degree of crystallinity [71]. In each case, the physical sorption process was sufficient to observe CLD release for a minimum of seven days. An interesting solution has been proposed through the use of halloysite, which has applications mainly in catalysis or environmental sciences; however, an increasing number of papers on its biomedical nature have been appearing for some time [72,73]. In this case, the mineral was subjected to CLD modification by intensive stirring and lowering the pressure, which resulted in the migration of drug particles deeper into the material. Experimentally, the carrier was subjected to etching in acetic acid, which did not affect the morphology of the ceramic, but caused an enlargement of its lumen, which resulted in an increased amount of released drug [74]. Table 2 presents a summary of the aforementioned ceramic CLD carriers.

Table 2. Ceramic carriers of clindamycin with indication of material type and applications.

Material	Applications	Refs.
ACP	NPs as intrinsic inorganic antimicrobials	[68]
HAp	NPs as intrinsic inorganic antimicrobials DDSs in form of powders and disks for hard tissue engineering	[68,69,71]
DCPA	NPs powders for hard tissue engineering	[69]
DCPD	DDSs for hard tissue engineering	[71]
TCP	DDSs for hard tissue engineering	[71]
Halloysite	Nanotubes with antibacterial properties	[74]

ACP = amorphous calcium phosphate, HAp = hydroxyapatite, DCPA = dicalcium phosphate anhydrous, DCPD = dicalcium phosphate dihydrate, DDSs = drug delivery systems, NPs = nanoparticles, TCP = calcium triphosphate.

4.2. Polymeric Carriers of Clindamycin

Modern medicine is unable to avoid polymers. They can be of natural origin or produced synthetically. Depending on the type, structure, and nature, they can exhibit a number of similar but also different, unique properties. Polymers can also be characterized by high chemical resistance or low moisture absorption. Polymers can be lightweight and very strong but also resistant to stretching. An important fact is that they can be easily molded [75–77]. By subjecting polymers to appropriate modifications, they might be further adapted to the demanding environment that is the human body. Polymers can be used to produce surgical threads, prostheses, or heart valves and can be applied as DDSs [78–80]. A drug can be transported by the polymer carrier in two ways: it can be encapsulated in the structure of the polymer between its chains or bound by a covalent bond directly to the chain or through a suitable ligand [81]. The release of the active ingredient can then occur by the degradation of the polymer, leaching of CLD, or by stimulation by various factors such as the temperature, pH, humidity, and electric or magnetic fields. The three main mechanisms of drug release from the polymer matrix, presented in Figure 5, include hydrogel swelling, material erosion, and diffusion [82].

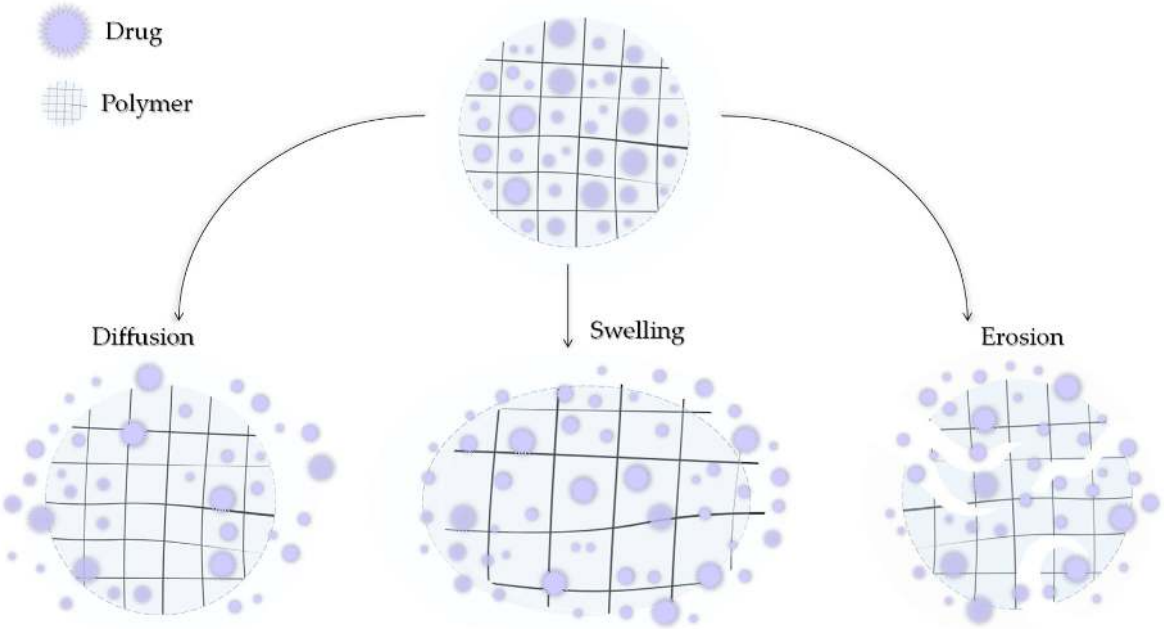

Figure 5. Three main mechanisms of drug release by diffusion, swelling, and erosion.

An extremely popular polymer of natural origin used in DDSs, especially in the design of dressing materials, is alginate (ALG). This linear, anionic polysaccharide is derived from brown algae and consists of repeating units of β-1,4-linked D-mannuronic acid (M) and L-guluronic acid (G) in various proportions. It is non-immunogenic, biodegradable,

non-toxic, and demonstrates rapid and cell-friendly gelation characteristics [83,84]. Calcium alginate nanoparticles were dispersed in ethanol and a solution of phosphorylated polyalamine containing CLD. The mixture was centrifuged and dried to obtain a precipitate of ALG with the drug. As a result of the centrifugal force generated, the CLD particles were forced deep into the material. Such an arrangement was tested against MG63 cells (line isolated from the bone of a Caucasian, 14-year-old male patient with osteosarcoma [85]) and *S. aureus* strain. Differences were observed due to variations in the pH of the environment in which the analyses were conducted. The system met expectations and demonstrated an antimicrobial effect while not inhibiting the viability of the MG63 cells [86]. An interesting solution was proposed for solid lipid nanoparticles (SLNs) constructed from ALG. They were obtained using an emulsion congealing technique with cold high-pressure homogenization. An oil phase composed of stearic acid and an aqueous phase composed of a CLD solution and a polymer solution were proposed. Analogous SLNs were obtained by replacing ALG with dextrin sulfate. It was observed that it reduced the drug release rate by about 50%, which was probably caused by the higher charge density, lower molecular weight, and lower branching density of the ionic polymer [87]. This confirms that the rate of drug release is dependent on the type of polymer. Other studies proposed a combination of ALG with other biopolymers including chitosan (CHT). The thin films are expected to have applications in skin treatments for acne and for local periodontal therapy. The proportion of individual biopolymers has been proven to affect the physicochemical properties, including the thickness and sorption capacity, and these determine the rate as well as the amount of CLD released [88,89]. CHT is a biocompatible and biodegradable cationic linear polysaccharide composed of *N*-acetyl-D-glucosamine and D-glucosamine, produced by chitin deacetylation [90]. It can be used as a hydrogel itself. Hyperbranched poly((2-(diisopropylamino)ethylmethacrylate)-*b*-(4-formyl-2-methoxyphenyl methacrylate-co-methyl ether poly(ethylene glycol)methacrylate)) nanoparticles were combined with CLD solution by centrifugation and then in a vial with CHT nanoparticles. An injectable gel was thus obtained, from which the drug was released by the pH factor, which caused the imine bonds to break. Not only did it demonstrate antimicrobial properties against *Escherichia coli* and *S. aureus*, but the viability of mouse fibroblast cell line NIH3T cells was higher than 90% [91]. The wide range of manufacturing and material processing methods means that even based on the same starting ingredients, it is ultimately possible to obtain biomaterials for different applications. The combination of gelatin (GE) and ALG can be used to produce materials for bone tissue, soft tissue, and the skin for the treatment of acne vulgaris. Colonization of *Cutibacterium* (*Propionibacterium*) *acnes* is one of the causes of skin deterioration that requires local drug therapy; however, drug particles are usually too large to penetrate the skin. (The *stratum corneum*, the uppermost layer of the skin, acts as a barrier to larger particles.) It has been proposed to create a transdermal patch containing micro-needles composed of ALG and GE (Figure 6). The needles did not pierce the dermis, but penetrated deep enough that the released CLD was able to inhibit the bacterial growth of *C. acnes* in the treated area [92].

Tissue adhesives made of these two polymers have been proposed for the treatment of traumatic wounds, including lacerated skin. Materials containing an antimicrobial agent can protect such a site from SSIs. GE and ALG solutions were mixed with NGC and ECP crosslinking agents. CLD was also added at various concentrations. The addition of the drug was found to improve the adhesive's bonding strength. When tested against *Staphylococcus albus* and *S. aureus*, complete elimination of the strain was observed within 48 h [93]. As for materials to stimulate bone regeneration processes, ALG was combined with GE nanoparticles. Firstly, the GE nanoparticles were combined with bone morphogenic protein 2 (BMP-2) and CLD in a water bath with homogenization, and then mixed with ALG. BMP-2 itself is a very potent growth factor that induces the rapid differentiation of mesenchymal stem cells into osteoblasts [94]. A functional carrier of the drug and of the active ingredient in the form of BMP-2 protein was obtained and exhibited a dual release of the components over a period of four weeks. The presence of the drug did not

interfere with the function of the protein [95]. Alginate hydrogel dressings with pectin and CLD, which were modified with the addition of hyaluronic acid, were developed. The dressings were subjected to in vivo analysis on animal models against male ICR mice, which confirmed the wound healing effect. However, it was observed that the process occurred faster in dressings containing hyaluronic acid. No significant differences were observed in the amount of antibiotic released. The materials themselves were obtained using the solvent casting method [96]. Dressing materials were also obtained by combining a biopolymer with a synthetic polymer such as polyvinyl alcohol (PVA), where solutions of ALG, PVA, and CLD were mixed, subjected to three freezing–thawing cycles, and dried. This simple method yielded flexible carriers that accelerated skin healing [97]. Additional combination with polyvinylpyrrolidone (PVP) and the solvent casting technique resulted in a peel-off mask for acne [98]. The combination with glyceryl monooleate ensures the sustained release of the antibiotic, even after oral administration [99].

Figure 6. Proposed alginate- and gelatin-based micro-needle solution for the transdermal local delivery of clindamycin. Reprinted with permission from Ref. [92], Elsevier B.V., 2022.

The aforementioned PVA can mimic human tissue and is non-toxic, biocompatible, and easy to fabricate [100]. For this reason, this synthetic polymer is often used in tissue engineering alone as well as in combination with other materials. Masks made from an aqueous solution of PVA and CLD obtained by electrospinning or electrospray technique can be used to treat skin wounds [101,102]. PVA mixed with carboxymethylated gum allowed to obtain a patch with very high absorbency, higher than that demonstrated by pure PVA, which resulted in a material for skin oozing wounds, which will be protected from microbial infection by CLD. Electrohydrodynamic atomization was used to obtain the patch from an aqueous solution of the ingredients [103]. Microsponges with ethyl cellulose for the sustained release of CLD have also been proven to be suitable for acne [104]. PVA itself has no use for hard tissue considering its hydrogel nature, which makes it very flexible. Its combination with slightly harder poly(lactic-co-glycolic acid) (PLGA) allowed the production of a DDS for the bone tissue surrounding the teeth. Drug release was observed for as long as three months [105].

PVP was described above in combination with ALG and PVA. Overall, this synthetic polymer appears in many literature reports thanks to its properties. It is not only used to produce carriers and implant materials, but also contact lenses and medical device components [106]. Antimicrobial coatings formulated from PVA and PVP designed to coat catheter surfaces have been proposed to limit the growth of undesirable microorganisms. Thus, the patient would not need to take medication to protect the body, and would be protecting himself from urinary tract infections [107]. PVP was combined with CHT, lactic acid, and CLD to form a carrier ointment for drugs administered vaginally in cases of pregnancies with symptoms of preterm labor, a condition that can be caused by bacterial vaginitis. Clinical evaluation demonstrated that the CLD cream was an effective treatment

in this case and enabled permanently maintaining a normal vaginal pH. It also exhibited physicochemical properties similar to those of physiological mucus, thereby proving to be ideal for the vaginal administration of the drug [108].

Another synthetic polymer with potential in biomedical applications is polycaprolactone (PCL). It is a semi-crystalline ester polymer characterized by biodegradability, high strength, and biocompatibility [109]. From solutions of PCL and CLD in dimethylformamide and chloroform, as well as silk fibroin in formic acid, nanofibers were prepared by electrospinning. The addition of fibroin reduced the amount of CLD released [110]. A combination of PCL and GE can be used for both bone and skin applications. The final properties of the carrier will depend on the processing method as well as component ratios. Using electrospinning, dressing materials were produced that released CLD for 6 days. They also demonstrated hydrophilicity and antibacterial properties against a Gram-positive (89%) and a Gram-negative (98%) bacteria [111]. Hard tissue materials were also developed using electrospinning, but the system was further modified by the presence of graphene oxide [112]. Polylactide (PLA) is a polymer with similar characteristics to PCL. It is not soluble in water, so 2,2,2-trifluoroethanol was used as a solvent. It was then mixed with GE and elastin in 1,1,1,3,3,3-hexafluoro- 2-propanol. Patches for skin wound therapy were produced in this way. The antimicrobial effect was confirmed against *S. aureus*, and a biosafety of 87% was validated against human umbilical vein endothelial/vascular endothelium cells. The materials released the CLD and were safe to apply, despite the use of such solvents [113]. By mixing GE with polyethylene glycol dibenzaldehyde using a vortex, a stiff gel was obtained with the formation of imine bonds. The system was crosslinked after 20 s, thus yielding a gel for in situ administration. The addition of CLD did not affect the rate of binding. It was proved that the addition of as little as 2% of the drug was able to kill the entire *S. aureus* colony [114]. Table 3 presents a summary of the aforementioned polymeric CLD carriers.

Table 3. Polymeric carriers of clindamycin with indication of material type and applications.

Material	Application	Refs.
ALG	Materials for osteomyelitis treatment	[79,80]
ALG, CHT	Skin treatments for acne and for local periodontal therapy	[81,82]
CHT	Soft hydrogel, in form of injectable gel	[84]
ALG, GE	Transdermal patch containing micro-needles for the treatment of acne vulgaris	[85]
ALG, GE	Materials for the treatment of traumatic wounds, lacerated skin	[86]
ALG, GE, BMP-2	Drug delivery systems for hard tissue engineering	[87]
ALG, pectin, hyaluronic acid	Dressing materials for wound healing	[89]
ALG, PVA	Dressing materials for wound healing	[90]
ALG, PVA, PVP	Hydrogel peel-off mask for acne	[91]
PVA	Hydrogel mask to treat skin wounds	[94,95]
PVA, carboxymethylated gum	Material for skin oozing wounds	[96]
PVA, ethyl cellulose	Microsponge for acne	[97]
PVA, PLGA	Bone tissue surrounding the teeth	[98]
PVA, PVP	Materials for urinary tract infections	[100]
PVP, CHT, lactid acid	Ointment for drugs administered vaginally	[101]
PCL, fibroin	Biocompatible nanofibers with core–shell structures for multiple applications as tissue engineering scaffolds	[103]
PCL, GE	Bone and skin applications	[104,105]
PLA, GE, elastin	Patches for skin wound therapy	[106]
GE, polyethylene glycol	Self-healing, injectable hydrogels	[107]

ALG = alginate, BMP-2 = bone morphogenic protein 2, CHT = chitosan, GE = gelatin, PCL = polycaprolactone, PLA = polylactide, PLGA = poly(lactic-co-glycolic acid), PVA = polyvinyl alcohol, PVP = polyvinylpyrrolidone.

4.3. Composite Carriers of Clindamycin

The basic division of materials into groups includes metals, ceramics, and polymers. Unfortunately, none of them meet all the requirements for implant biomaterials for bone tissue [115]. Metals are often too stiff relative to natural tissue and are associated with the risk of corrosion. This can lead to inflammation and health hazards. Polymers are a broad group of synthetic and natural materials; however, they often have low strength relative to mineralized bone tissue and too high elasticity. Ceramic materials exhibit great brittleness and susceptibility to fracture, but at the same time are often bioactive and can stimulate bone-forming cells to proliferate. For this reason, in order to maintain adequate mechanical, biological, and physicochemical properties, composites, materials formed from more than one phase, are created. Most often, the matrix is a polymer phase providing flexibility, which is reinforced by a dispersed phase in the form of ceramics providing hardness and strength. Developing new composites and combining phases makes it possible to develop biomimetic materials resembling natural tissue, which can create the right microenvironment to promote osteoblast proliferation and osteogenesis. In addition, composites are also good materials for the controlled and sustained release of active substances directly to the site where the therapeutic effect is needed [116–118].

In the context of composites for bone tissue regeneration, the most promising combinations are ceramics with polymers. An example is an ALG hydrogel with GE reinforced with a ceramic phase in the form of β-TCP. The materials were obtained by crosslinking based on water solutions. The antimicrobial potential was tested on an ex vivo human bone infection organ model [119,120]. The electrospinning method made it possible to obtain tough composite layers based on a mixture of GE, a natural polymer, and PCL, a synthetic polymer. The surface was modified with graphene oxide, which later attached DCPD through ionic interactions. The CLD was encapsulated in a polymer phase. Nanofibers obtained in this way demonstrated good biocompatibility with human osteosarcoma cells as well as no cell toxicity. Slow and controlled release of CLD but also DCPD was observed in vitro [112]. Another composite combination, whose polymer phase consists of a biological component and a synthetic one, is CHT with PLGA. It was reinforced with HAp in the form of suspended nanocrystals. CLD was combined with the polymer phase, and the composite was obtained by freeze-drying the mixture. The final form analyzed was films. The release of the antibiotic occurred by the slow degradation of CHT/PLGA and by swelling [121]. Despite the degradability exhibited by CHT, sustained release of CLD was observed for three weeks for composites based on only this biopolymer and nano-HAp. However, it was observed that with the addition of CHT, the antimicrobial efficacy of this DDS against *S. aureus* decreased. The reduced proliferation of MC3T3-E1 osteoblastic cells as well as mitochondrial dehydrogenase activity was also observed, which may suggest that CHT, despite its rather good biocompatibility properties, is not entirely suitable for such applications [122]. Of all biocompatible ceramics, it is HAp that is most commonly used in biomedical applications. Combined with PVP and betaine, again a combination of synthetic and biological components, it was used for the creation of a platform in the form of a flexible composite obtained by photocrosslinking, which exhibited good physicochemical properties. Sustained release of CLD was observed for 7 days, which proved that the increased ceramics phase reduced the amount of the drug released in vitro. The UV crosslinking process did not lead to drug degradation [123]. PVP was also used to develop bone cement composites modified with CLD, triclosan, or gentamicin as DDS materials for arthroplasty. The drugs were bonded to the cements, and PVP was intended to increase their leaching from the cement. However, for CLD and gentamicin, no difference was observed between the amount of drug released from the cement alone and from the cement with the polymer. This difference was observed only for triclosan and may be due to the difference in the chemical structure and origin of the three drugs, because triclosan comes from the chlorinated phenol group [124,125].

PLA is widely used in biomedicine to print bone defects; however, its melting point is high enough, so active compounds could degrade [126]. For this reason, to use it as a

DDS, a printing technique cannot be applied; however, such a polymer can be dissolved in suitable solvents and processed appropriately. PLA was dissolved in acetonitrile, and CLD and HAp were then added to the solution. Ultrasonic radiation was used to disintegrate the agglomerates, and finally, microcapsules were obtained. The ceramic phase was of natural origin, from crocodile bone. The loading efficiency of the CLD composite was demonstrated to increase with the proportion of HAp [127]. PLGA was also dissolved in acetonitrile. As before, CLD solution was added to the polymer; ultrasound was used. In this case, HAp and other calcium phosphate powders were also modified with CLD. Antimicrobial properties against *S. aureus* were demonstrated, and biosafety against osteoblast-like cells was confirmed despite the use of acetonitrile, a solvent that is toxic to the organism [128].

Acetone is also used as a solvent for PLGA. Therefore, PLGA in acetone was combined with a solution of CLD and HAp powder. Nanospheres capable of releasing the drug, the amount of which was determined by the content of the ceramic phase, were obtained. A schematic of this carrier formulation mechanism is presented in Figure 7. The nanoparticles were obtained by using ultrasound. The drug and ceramic grains were encapsulated in a polymer network. It was confirmed that CLD influenced the degradation of the polymer matrix, which also affected the amount of released antibiotic. A high level of cytocompatibility was observed against mouse L929 and human lung MRC-5 fibroblasts [129–132]. Not only popular bioactive ceramics in the form of TCP or HAp can be used as a reinforcing phase in the composite as the literature mentions the use of, for example, montmorillonite clay or bentonite. The first one is often used as an ingredient in skin care masks for its purifying and absorbing properties [133]. It was mixed with an aqueous solution of PVA and CLD. A crosslinking method by cyclic freeze–thaw was used. The resulting wound healing dressings exhibited antimicrobial properties due to the presence of the drug and the clay [134]. Bentonite was combined with PVP and carboxymethylcellulose (CMC) to obtain a DDS [135]. In order to ensure the flexibility of composites, they were enriched with the addition of xanthan gum and guar gum. This non-obvious combination resulted in obtaining a CLD carrier using the Petri dish casting method [136]. CMC is a derivative of cellulose, and its main area of application is in the food industry. It belongs to the group of emulsifiers or thickening agents and is labeled as E466 [137]. Its combination with halloysite, previously modified with CLD, and keratin gave nanocomposites with antimicrobial properties for skin wound healing. Drug release occurred according to the Fickian diffusion mechanism [138]. The last non-obvious combination discussed in this review is a coating composed of CMC and ALG. Naturally, drug molecules were encapsulated in the polymer network. The coating was applied by electrospinning to TiAlV and 316LVM sheets. A sandwich composite was thus obtained, where the layers of the individual materials were arranged on top of each other, rather than suspended in each other as in the previously discussed composites. CLD was released into a fluid simulating a biological environment, and the release occurred by the degradation process of the polymer phase [139]. Table 4 presents a summary of the aforementioned composites for CLD delivery.

Table 4. Composite materials for delivery of clindamycin with indication of material type and applications.

Material	Application	Refs.
PCL, GE, DCPD, graphene oxide	Microcapsules for local drug delivery and for bone regeneration	[112]
PLA, GE, TCP	Composites for bone regeneration	[113]
GE, PCL, DCPD	Nanofibers for application in bone tissue engineering	[114]
PLGA, CHT, HAp	Composite films with antimicrobial properties	[115]
CHT, HAp	Biodegradable materials for bone tissue	[116]

Table 4. *Cont.*

Material	Application	Refs.
PVP, betaine, HAp	Elastic materials for hard tissue replacement	[117]
PVP, ceramic cements	Materials for treatment in two-stage arthroplasty revisions	[119]
PLGA, HAp	Nanospheres capable of releasing the drug locally	[121–125]
PVA, montmorillonite	Wound healing dressings	[127]
PVP, CMC, bentonite	Biodegradable hydrogel films for biomedical application	[128]
CMC, keratin, halloysite	Nanocomposites with antimicrobial properties for skin wound	[131]
CMC, ALG, TiAlV/316LVM	Sandwich composite for bone tissue	[132]

ALG = alginate, GE = gelatin, CHT = chitosan, CMC = carboxymethylcellulose, DCPD = dicalcium phosphate dehydrate, HAp = hydroxyapatite, PCL = polycaprolactone, PLA = polylactide, PLGA = poly(lactic-co-glycolic acid), PVA = polyvinyl alcohol, PVP = polyvinylpyrrolidone, TCP = calcium triphosphate.

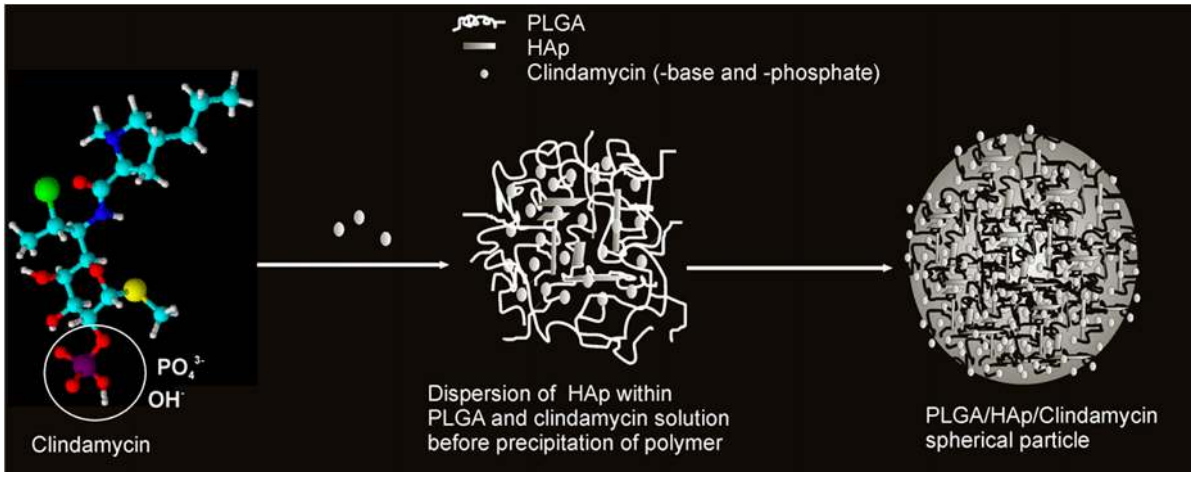

Figure 7. Proposed mechanism for the formation of spherical CLD-based poly(lactic-co-glycolic acid)/hydroxyapatite (PLGA/HAp) core–shell nanoparticles. Reprinted with permission from ref. [129], Elsevier B.V., 2011.

5. Conclusions and Future Challenges

New biomaterials can indeed transform modern medicine and therapy, providing relief to suffering and needy patients. Smart biomaterials are essential for this purpose. In the current situation, as demonstrated above, newly emerging ceramic, polymeric, and composite materials are exhibiting many advantages for their application as controlled DDSs. Materials from each group, synthetic as well as natural, are all being used in the design of new DDSs. As demonstrated in this review, depending on the purpose and target site of the implantation or application of the biomaterial, different phases are used. In the case of bone tissue, ceramics and ceramic–polymer composites are mainly investigated. It was observed that the most common ceramics of choice were bioactive calcium phosphates, such as HAp, which stimulate the activity of bone-forming cells. In the case of composites, polymers in which ceramics in the form of fine grains were homogeneously suspended in the material accounted for the greatest share. Mostly, these were synthetic polymers like PLGA or PVP. However, in the case of soft tissue or skin, biopolymers of natural origin are most often used. The most reported are ALG and GE. Physical sorption in a solution or mixing with an aqueous CLD solution was the most common method for the modification of individual phases with the drug.

However, despite enormous advances in targeted therapy and the controlled delivery of active substances, there are still many issues to be solved and improved. Unfortunately,

the release of the drug often occurs too fast and does not fit into the idea of controlled sustained release. This is likely the reason why the simple phenomenon of sorption and not chemical bonding is used. The challenge is to create a carrier that will release the drug at an appropriate rate, while exhibiting a range of characteristics and properties ideally similar to those of the tissue being replaced. At present, it seems that one of the main goals in relation to DDS biomaterials is to develop a material with adequate mechanical parameters while maintaining a sustained release of the active substance. Biomimeticism is also being considered to ensure that the new materials mimic natural tissues as closely as possible. Targeted therapy represents the future of medicine by providing faster and more effective treatment directly at the site that requires it. Thus, further development in this field is essential and important for the life of society and improving the quality of life of those in need.

Author Contributions: Conceptualization, D.S.; writing—original draft preparation, D.S.; writing—review and editing, J.J. and A.S.-K.; visualization, D.S.; supervision, J.J. and A.S.-K.; project administration, A.S.-K. and J.J.; funding acquisition, A.S.-K. and J.J. All authors have read and agreed to the published version of the manuscript.

Funding: This research was funded by the Foundation for Polish Science, grant number POIR.04.04.00-00-16D7/18. This work was also supported by project APVV-22-0133.

Institutional Review Board Statement: Not applicable.

Informed Consent Statement: Not applicable.

Data Availability Statement: Not applicable.

Acknowledgments: The "Multifunctional biologically active composites for applications in bone regenerative medicine" project is carried out within the TEAM-NET program of the Foundation for Polish Science financed by the European Union under the European Regional Development Fund. The authors gratefully acknowledge financial support.

Conflicts of Interest: The authors declare no conflicts of interest.

References

1. Ghanem, A.M. Recent advances in transdermal drug delivery systems: A review. *Int. J. Appl. Pharm.* **2024**, *16*, 28–33. [CrossRef]
2. Singh, S.; Pandey, V.K.; Tewari, R.P.; Agarwal, V. Nanoparticle based drug delivery system: Advantages and applications. *Ind. J. Sci. Technol.* **2011**, *4*, 177–180. [CrossRef]
3. Drug Delivery Systems Market Size, Share & COVID-19 Impact Analysis, by Type (Inhalation, Transdermal, Injectable, and Others), by Device Type (Conventional and Advaced), by Distribution Channel (Hospital, Pharmacies, Retail Pharmacies, and Others). Available online: https://www.fortunebusinessinsights.com/drug-delivery-systems-market-103070 (accessed on 11 March 2024).
4. Adepu, S.; Ramakrishna, S. Controlled drug delivery systems: Current status and future directions. *Molecules* **2021**, *26*, 5905. [CrossRef] [PubMed]
5. Dash, T.R.; Verma, P. Matrix tablets: An approach towards oral extended release drug delivery. *Int. J. Pharma Res. Rev.* **2013**, *2*, 12–24.
6. Pinto, J.F. Site-specific drug delivery systems within the gastro-intestinal tract: From the mouth to the colon. *Int. J. Pharm.* **2010**, *395*, 44–52. [CrossRef] [PubMed]
7. Reddy, D.; Pillay, V.; Choonara, Y.E.; Du Toit, L.C. Rapidly disintegrating oramucosal drug delivery technologies Rapidly disintegrating oramucosal drug delivery technologies. *Pharm. Develop. Technol.* **2009**, *14*, 588–601. [CrossRef]
8. Anderson, G.D.; Saneto, R.P. Current oral and non-oral routes of antiepileptic drug delivery. *Adv. Drug Deliv. Rev.* **2012**, *64*, 911–918. [CrossRef] [PubMed]
9. Matsuda, Y.; Konno, Y.; Hashimoto, T.; Nagai, M.; Taguchi, T.; Satsukawa, M.; Yamashita, S. Quantitative assessment of intestinal first-pass metabolism of oral drugs using portal-vein cannulated rats. *Pharm. Res.* **2015**, *32*, 604–616. [CrossRef]
10. Riviere, J.E.; Papich, M.G. Potential and problems of developing transdermal patches for veterinary applications. *Adv. Drug Deliv. Rev.* **2001**, *50*, 175–203. [CrossRef]
11. Escobar-Chavez, J.J.; Diaz-Torres, R.; Rodriguez-Cruz, I.M.; Dominguez-Delgado, C.L.; Sampere-Morales, R.; Angeles-Anguiano, E.; Melgoza-Contreras, L.M. Nanocarriers for transdermal drug delivery. *Res. Rep. Transdermal Drug Deliv.* **2012**, *1*, 3–17. [CrossRef]
12. Păduraru, D.N.; Niculescu, A.-G.; Bolocan, A.; Andronic, O.; Grumezescu, A.M.; Bîrlă, R. An updated overview of cyclodextrin-based drug delivery systems for cancer therapy. *Pharmaceutics* **2022**, *14*, 1748. [CrossRef]

13. Spoială, A.; Ilie, C.-I.; Motelica, L.; Ficai, D.; Semenescu, A.; Oprea, O.-C.; Ficai, A. Smart magnetic drug delivery systems for the treatment of cancer. *Nanomaterials* **2023**, *13*, 876. [CrossRef]
14. Rizwan, M.; Yahya, R.; Hassan, A.; Yar, M.; Azzahari, A.D.; Selvanathan, V.; Sonsudin, F.; Abouloula, C.N. pH Sensitive hydrogels in drug delivery: Brief history, properties, swelling, and release mechanism, material selection and applications. *Polymers* **2017**, *9*, 137. [CrossRef] [PubMed]
15. Ayran, M.; Karabulut, H.; Deniz, K.I.; Akcanli, G.C.; Ulag, S.; Croitoru, A.-M.; Tihăuan, B.-M.; Sahin, A.; Ficai, D.; Gunduz, O.; et al. Electrically triggered quercetin release from polycaprolactone/bismuth ferrite microfibrous scaffold for skeletal muscle tissue. *Pharmaceutics* **2023**, *15*, 920. [CrossRef] [PubMed]
16. Silindir Gunay, M.; Yekta Ozer, A.; Chalon, S. Drug delivery systems for imaging and therapy of Parkinson's disease. *Curr. Neuropharm.* **2015**, *14*, 376–391. [CrossRef]
17. Huang, X.; Ma, Y.; Li, Y.; Han, F.; Lin, W. Targeted drug delivery systems for kidney diseases. *Front. Bioeng. Biotechnol.* **2021**, *9*, 683247. [CrossRef]
18. Paolini, M.S.; Fenton, O.S.; Bhattacharya, C.; Andresen, J.L.; Langer, R.S. Polymers for extended-release administration. *Biomed. Microdevices* **2019**, *21*, 45. [CrossRef]
19. Kleiner, L.W.; Wright, J.C.; Wang, Y. Evolution of implantable and insertable drug delivery systems. *J. Control. Release* **2014**, *181*, 1–10. [CrossRef] [PubMed]
20. Van Tran, T.T.; Tayara, H.; Chong, K.T. Artificial intelligence in drug metabolism and excretion prediction: Recent advances, challenges, and future perspectives. *Pharmaceutics* **2023**, *15*, 1260. [CrossRef] [PubMed]
21. Hardenia, A.; Maheshwari, N.; Hardenia, S.S.; Dwivedi, S.K.; Maheshwari, R.; Tekade, R.K. Scientific rationale for designing controlled drug delivery systems. In *Basic Fundamentals of Drug Delivery—Advances in Pharmaceutical Product Development and Research*; Tekade, R.K., Ed.; Academic Press & Elsevier: London, UK, 2019; pp. 1–28.
22. Paarakh, M.P.; Jose, P.A.N.I.; Setty, C.M.; Peter, G.V. Release Kinetics—Concepts and applications. *Int. J. Pharm. Res. Technol.* **2019**, *8*, 12–20. [CrossRef]
23. Wiseman, J.T.; Fernandes-Taylor, S.; Barnes, M.L.; Saunders, R.S.; Saha, S.; Havlena, J.; Rathouz, P.J.; Craig Kent, K. Predictors of surgical site infection after hospital discharge in patients undergoing major vascular surgery. *J. Vasc. Surg.* **2015**, *62*, 1023–1031.e5. [CrossRef] [PubMed]
24. Ibrahimi, O.A.; Sharon, V.; Eisen, D.B. Surgical-Site infections and routes of bacterial transfer: Which ones are most plausible? *Dermatol. Surg.* **2011**, *37*, 1709–1720. [CrossRef] [PubMed]
25. Ali, K.M.; Al-Jaff, B.M.A. Source and antibiotic susceptibility of Gram-negative bacteria causing superficial incisional surgical site infections. *Int. J. Surg. Open* **2021**, *30*, 100318. [CrossRef]
26. Daeschlein, G.; Napp, M.; Layer, F.; von Podewils, S.; Haase, H.; Spitzmueller, R.; Assadian, O.; Kasch, R.; Werner, G.; Jünger, M.; et al. Antimicrobial efficacy of preoperative skin antisepsis and clonal relationship to postantiseptic skin-and-wound flora in patients undergoing clean orthopedic surgery. *Eur. J. Clin. Microbiol. Inf. Dis.* **2015**, *34*, 2265–2273. [CrossRef] [PubMed]
27. Brady, R.A.; Leid, J.G.; Costerton, J.W.; Shirtliff, M.E. Osteomyelitis: Clinical overview and mechanisms of infection persistence. *Clin. Microbiol. Newslet.* **2006**, *28*, 65–72. [CrossRef]
28. Rimashevskiy, D.V.; Akhtyamov, I.F.; Fedulichev, P.N.; Zaalan, W.; Ustazov, K.A.; Basith, A.; Moldakulov, J.M.; Zinoviev, M.P. Pathogenetic features of chronic osteomyelitis treatment. *Genij Ortopedii* **2021**, *27*, 628–635. [CrossRef]
29. Lam, M.; Hu, A.; Fleming, P.; Lynde, C.W. The impact of acne treatment on skin bacterial microbiota: A systematic review. *J. Cut. Med. Surg.* **2022**, *26*, 93–97. [CrossRef] [PubMed]
30. Wang, C.; Huttner, B.D.; Magrini, N.; Cheng, Y.; Tong, J.; Li, S.; Wan, C.; Zhu, Q.; Zhao, S.; Zhuo, Z.; et al. Pediatric antibiotic prescribing in China according to the 2019 World Health Organization access, watch, and reserve (AWaRe) antibiotic categories. *J. Pediatr.* **2020**, *220*, 125–131.e5. [CrossRef] [PubMed]
31. Vekemans, J.; Hasso-Agopsowicz, M.; Kang, G.; Hausdorff, W.P.; Fiore, A.; Tayler, E.; Klemm, E.J.; Laxminarayan, R.; Srikantiah, P.; Friede, M.; et al. Leveraging Vaccines to reduce antibiotic use and prevent antimicrobial resistance: A World Health Organization action framework. *Clin. Inf. Dis.* **2021**, *73*, E1011–E1017. [CrossRef]
32. Luchian, I.; Goriuc, A.; Martu, M.A.; Covasa, M. Clindamycin as an alternative option in optimizing periodontal therapy. *Antibiotics* **2021**, *10*, 814. [CrossRef]
33. Álvarez, L.A.; Van de Sijpe, G.; Desmet, S.; Metsemakers, W.J.; Spriet, I.; Allegaert, K.; Rozenski, J. Ways to Improve insights into clindamycin pharmacology and pharmacokinetics tailored to practice. *Antibiotics* **2022**, *11*, 701. [CrossRef] [PubMed]
34. Chaiwarit, T.; Rachtanapun, P.; Kantrong, N.; Jantrawut, P. Preparation of clindamycin hydrochloride loaded de-esterified low-methoxyl mango peel pectin film used as a topical drug delivery system. *Polymers* **2020**, *12*, 1006. [CrossRef] [PubMed]
35. Egle, K.; Skadins, I.; Grava, A.; Micko, L.; Dubniks, V.; Salma, I.; Dubnika, A. Injectable platelet-rich fibrin as a drug carrier increases the antibacterial susceptibility of antibiotic—clindamycin phosphate. *Int. J. Mol. Sci.* **2022**, *23*, 7407. [CrossRef] [PubMed]
36. Spížek, J.; Řezanka, T. Lincosamides: Chemical structure, biosynthesis, mechanism of action, resistance, and applications. *Biochem. Pharmacol.* **2017**, *133*, 20–28. [CrossRef]

37. Assefa, M. Inducible clindamycin-resistant *Staphylococcus aureus* strains in Africa: A systematic review. *Int. J. Microbiol.* **2022**, *2022*, 1835603. [CrossRef] [PubMed]
38. Cherazard, R.; Epstein, M.; Doan, T.-L.; Salim, T.; Bharti, S.; Smith, M.A. Antimicrobial resistant *Streptococcus pneumoniae*: Prevalence, mechanisms, and clinical implications. *Am. J. Ther.* **2017**, *24*, e361–e369. [CrossRef] [PubMed]
39. Cheung, G.Y.C.; Bae, J.S.; Otto, M. Pathogenicity and virulence of *Staphylococcus aureus*. *Virulence* **2021**, *12*, 547–569. [CrossRef]
40. Mohamed, N.; Wang, M.Y.; Le Hue, J.-C.; Liljenqvist, U.; Scully, I.L.; Baber, J.; Begier, E.; Jansen, K.U.; Gurtman, A.; Anderson, A.S. Vaccine development to prevent *Staphylococcus aureus* surgical-site infections. *Brit. J. Surg.* **2017**, *104*, e41–e54. [CrossRef] [PubMed]
41. Li, L.; Ma, J.; Yu, Z.; Li, M.; Zhang, W.; Sun, H. Epidemiological characteristics and antibiotic resistance mechanisms of *Streptococcus pneumoniae*: An updated review. *Microbiol. Res.* **2023**, *266*, 127221. [CrossRef]
42. Wade, K.C.; Benjamin, D.K. Clinical pharmacology of anti-infective drugs. In *Infectious Diseases of the Fetus and Newborn*, 7th ed.; Remington, J.S., Klein, J.O., Wilson, C.B., Nizet, V., Maldonado, Y.A., Eds.; Saunders: Philadelphia, PA, USA, 2011; pp. 1160–1211.
43. Rezahosseini, O.; Roed, C.; Holler, J.G.; Frimodt-Møller, N. Adjunctive antibiotic therapy with clindamycin or linezolid in patients with group A *Streptococcus* (GAS) *meningitis*. *Inf. Dis.* **2023**, *55*, 751–753. [CrossRef]
44. Arteagoitia, I.; Sánchez, F.R.; Figueras, A.; Arroyo-Lamas, N. Is clindamycin effective in preventing infectious complications after oral surgery? Systematic review and meta-analysis of randomized controlled trials. *Clin. Oral Investig.* **2022**, *26*, 4467–4478. [CrossRef] [PubMed]
45. Peeters, A.; Putzeys, G.; Thorrez, L. Current insights in the application of bone grafts for local antibiotic delivery in bone reconstruction surgery. *J. Bone Jt. Infect.* **2019**, *4*, 245–253. [CrossRef] [PubMed]
46. Allegaert, K.; Muller, A.E.; Russo, F.; Schoenmakers, S.; Deprest, J.; Koch, B.C.P. Pregnancy-related pharmacokinetics and antimicrobial prophylaxis during fetal surgery, cefazolin and clindamycin as examples. *Prenat. Diagn.* **2020**, *40*, 1178–1184. [CrossRef] [PubMed]
47. Eda, T.; Okada, M.; Ogura, R.; Tsukamoto, Y.; Kanemaru, Y.; Watanabe, J.; On, J.; Aoki, H.; Oishi, M.; Takei, N.; et al. Novel repositioning therapy for drug-resistant glioblastoma: In vivo validation study of clindamycin treatment targeting the mTOR pathway and combination therapy with temozolomide. *Cancers* **2022**, *14*, 770. [CrossRef] [PubMed]
48. Yang, S.H.; Lee, M.G. Dose-independent pharmacokinetics of clindamycin after intravenous and oral administration to rats: Contribution of gastric first-pass effect to low bioavailability. *Int. J. Pharm.* **2007**, *332*, 17–23. [CrossRef]
49. Lemaire, S.; Van Bambeke, F.; Pierard, D.; Appelbaum, P.C.; Tulkens, P.M. Activity of fusidic acid against extracellular and intracellular *Staphylococcus aureus*: Influence of ph and comparison with linezolid and clindamycin. *Clin. Inf. Dis.* **2011**, *52*, S493–S503. [CrossRef]
50. Hua, S. Advances in oral drug delivery for regional targeting in the gastrointestinal tract—Influence of physiological, pathophysiological and pharmaceutical factors. *Front. Pharmacol.* **2020**, *11*, 524. [CrossRef]
51. Vellonen, K.S.; Soini, E.M.; Del Amo, E.M.; Urtti, A. Prediction of ocular drug distribution from systemic blood circulation. *Mol. Pharm.* **2016**, *13*, 2906–2911. [CrossRef] [PubMed]
52. Thornhill, M.H.; Dayer, M.J.; Durkin, M.J.; Lockhart, P.B.; Baddour, L.M. Risk of adverse reactions to oral antibiotics prescribed by dentists. *J. Dent. Res.* **2019**, *98*, 1081–1087. [CrossRef]
53. Dubey, N.; Xu, J.; Zhang, Z.; Nör, J.E.; Bottino, M.C. Comparative evaluation of the cytotoxic and angiogenic effects of minocycline and clindamycin: An in vitro study. *J. Endod.* **2019**, *45*, 882–889. [CrossRef]
54. Eliaz, N.; Metoki, N. Calcium phosphate bioceramics: A review of their history, structure, properties, coating technologies and biomedical applications. *Materials* **2017**, *10*, 334. [CrossRef] [PubMed]
55. Canillas, M.; Pena, P.; De Aza, A.H.; Rodríguez, M.A. Calcium phosphates for biomedical applications. *Bol. Soc. Esp. Ceram. Vidr.* **2017**, *56*, 91–112. [CrossRef]
56. Lara-Ochoa, S.; Ortega-Lara, W.; Guerrero-Beltrán, C.E. Hydroxyapatite nanoparticles in drug delivery: Physicochemistry and applications. *Pharmaceutics* **2021**, *13*, 1642. [CrossRef] [PubMed]
57. Harb, S.V.; Bassous, N.J.; de Souza, T.A.C.; Trentin, A.; Pulcinelli, S.H.; Santilli, C.V.; Webster, T.J.; Lobo, A.O.; Hammer, P. Hydroxyapatite and β-TCP modified PMMA-TiO_2 and PMMA-ZrO_2 coatings for bioactive corrosion protection of Ti_6Al_4V implants. *Mat. Sci. Eng. C* **2020**, *116*, 111149. [CrossRef] [PubMed]
58. Shalini, B.; Kumar, A.R. A comparative study of hydroxyapatite ($Ca_{10}(PO_4)_6(OH)_2$) using sol-gel and co-precipitation methods for biomedical applications. *J. Indian Chem. Soc.* **2019**, *96*, 25–28.
59. Damerau, J.M.; Bierbaum, S.; Wiedemeier, D.; Korn, P.; Smeets, R.; Jenny, G.; Nadalini, J.; Stadlinger, B. A systematic review on the effect of inorganic surface coatings in large animal models and meta-analysis on tricalcium phosphate and hydroxyapatite on periimplant bone formation. *J. Biomed. Mat. Res. B* **2022**, *110*, 157–175. [CrossRef] [PubMed]
60. Jeong, J.; Kim, J.H.; Shim, J.H.; Hwang, N.S.; Heo, C.Y. Bioactive calcium phosphate materials and applications in bone regeneration. *Biomater. Res.* **2019**, *23*, 4. [CrossRef]
61. Wagner, M.; Hess, T.; Zakowiecki, D. Studies on the pH-dependent solubility of various grades of calcium phosphate-based pharmaceutical excipients. *J. Pharm. Sci.* **2022**, *111*, 1749–1760. [CrossRef] [PubMed]
62. El Hazzat, M.; El Hamidi, A.; Halim, M.; Arsalane, S. Complex evolution of phase during the thermal investigation of Brushite-type calcium phosphate $CaHPO_4 \cdot 2H_2O$. *Materialia* **2021**, *16*, 101055. [CrossRef]

63. Gbureck, U.; Vorndran, E.; Barralet, J.E. Modeling vancomycin release kinetics from microporous calcium phosphate ceramics comparing static and dynamic immersion conditions. *Acta Biomat.* **2008**, *4*, 1480–1486. [CrossRef]
64. Zamoume, O.; Thibault, S.; Regnié, G.; Mecherri, M.O.; Fiallo, M.; Sharrock, P. Macroporous calcium phosphate ceramic implants for sustained drug delivery. *Mat. Sci. Eng. C* **2011**, *31*, 1352–1356. [CrossRef]
65. Mo, X.; Zhang, D.; Liu, K.; Zhao, X.; Li, X.; Wang, W. Nano-hydroxyapatite composite scaffolds loaded with bioactive factors and drugs for bone tissue engineering. *Int. J. Mol. Sci.* **2023**, *24*, 1291. [CrossRef] [PubMed]
66. Wang, L.; Hou, X.; Feng, L.; Zhou, Y.; Liu, X.; Tian, C. Drug delivery properties of three—Dimensional ordered macroporous zinc—Doped hydroxyapatite. *J. Mat. Res.* **2022**, *37*, 2314–2321. [CrossRef]
67. Munir, M.U.; Salman, S.; Javed, I.; Bukhari, S.N.A.; Ahmad, N.; Shad, N.A.; Aziz, F. Nano-hydroxyapatite as a delivery system: Overview and advancements. *Artif. Cells Nanomed Biotechnol.* **2021**, *49*, 717–727. [CrossRef] [PubMed]
68. Wu, V.M.; Tang, S.; Uskoković, V. Calcium phosphate nanoparticles as intrinsic inorganic antimicrobials: The antibacterial effect. *ACS Appl. Mater. Interfaces* **2018**, *10*, 34013–34028. [CrossRef] [PubMed]
69. Uskoković, V.; Desai, T.A. Simultaneous bactericidal and osteogenic effect of nanoparticulate calcium phosphate powders loaded with clindamycin on osteoblasts infected with *Staphylococcus aureus*. *Mat. Sci. Eng. C* **2014**, *37*, 210–222. [CrossRef] [PubMed]
70. Niziołek, K.; Słota, D.; Sadlik, J.; Łachut, E.; Florkiewicz, W.; Sobczak-Kupiec, A. Influence of drying technique on physicochemical properties of synthetic hydroxyapatite and its potential use as a drug carrier. *Materials* **2023**, *16*, 6431. [CrossRef] [PubMed]
71. Słota, D.; Piętak, K.; Florkiewicz, W.; Jampílek, J.; Tomala, A.; Urbaniak, M.M.; Tomaszewska, A.; Rudnicka, K.; Sobczak-Kupiec, A. Clindamycin-loaded nanosized calcium phosphates powders as a carrier of active substances. *Nanomaterials* **2023**, *13*, 1469. [CrossRef]
72. Massaro, M.; Noto, R.; Riela, S. Past, present and future perspectives on halloysite clay minerals. *Molecules* **2020**, *25*, 4863. [CrossRef]
73. Danyliuk, N.; Tomaszewska, J.; Tatarchuk, T. Halloysite nanotubes and halloysite-based composites for environmental and biomedical applications. *J. Mol. Liq.* **2020**, *309*, 113077. [CrossRef]
74. Machowska, A.; Klara, J.; Ledwójcik, G.; Wójcik, K.; Dulińska-Litewka, J.; Karewicz, A. Clindamycin-loaded halloysite nanotubes as the antibacterial component of composite hydrogel for bone repair. *Polymers* **2022**, *14*, 5151. [CrossRef] [PubMed]
75. Cywar, R.M.; Rorrer, N.A.; Hoyt, C.B.; Beckham, G.T.; Chen, E.Y.-X. Bio-based polymers with performance-advantaged properties. *Nat. Rev. Mat.* **2022**, *7*, 83–103. [CrossRef]
76. Zhao, J.; Wang, G.; Wang, C.; Park, C.B. Ultra-lightweight, super thermal-insulation and strong PP/CNT microcellular foams. *Compos. Sci. Technol.* **2020**, *191*, 108084. [CrossRef]
77. Kraft, U.; Molina-Lopez, F.; Son, D.; Bao, Z.; Murmann, B. Ink development and printing of conducting polymers for intrinsically stretchable interconnects and circuits. *Adv. Electron. Mater.* **2020**, *6*, 1900681. [CrossRef]
78. Hart, L.F.; Hertzog, J.E.; Rauscher, P.M.; Rawe, B.W.; Tranquilli, M.M.; Rowan, S.J. Material properties and applications of mechanically interlocked polymers. *Nat. Rev. Mat.* **2021**, *6*, 508–530. [CrossRef]
79. Rezvova, M.A.; Klyshnikov, K.Y.; Gritskevich, A.A.; Ovcharenko, E.A. Polymeric heart valves will displace mechanical and tissue heart valves: A new era for the medical devices. *Int. J. Mol. Sci.* **2023**, *24*, 3963. [CrossRef] [PubMed]
80. Bărăian, A.-I.; Iacob, B.-C.; Bodoki, A.E.; Bodoki, E. In vivo applications of molecularly imprinted polymers for drug delivery: A pharmaceutical perspective. *Int. J. Mol. Sci.* **2022**, *23*, 14071. [CrossRef]
81. Hartl, N.; Adams, F.; Merkel, O.M. From Adsorption to Covalent Bonding: Apolipoprotein E Functionalization of polymeric nanoparticles for drug delivery across the blood–brain barrier. *Adv. Ther.* **2021**, *4*, 2000092. [CrossRef]
82. Priya James, H.; John, R.; Alex, A.; Anoop, K.R. Smart polymers for the controlled delivery of drugs—A concise overview. *Acta Pharm. Sin. B* **2014**, *4*, 120–127. [CrossRef]
83. Gao, Q.; Kim, B.-S.; Gao, G. Advanced strategies for 3D bioprinting of tissue and organ analogs using alginate hydrogel bioinks. *Mar. Drugs* **2021**, *19*, 708. [CrossRef]
84. Zhang, M.; Zhao, X. Alginate hydrogel dressings for advanced wound management. *Int. J. Biol. Macromol.* **2020**, *162*, 1414–1428. [CrossRef] [PubMed]
85. Wagener, N.; Di Fazio, P.; Böker, K.O.; Matziolis, G. Osteogenic effect of pregabalin in human primary mesenchymal stem cells, osteoblasts and osteosarcoma cells. *Life* **2022**, *12*, 496. [CrossRef] [PubMed]
86. Gowri, M.; Latha, N.; Suganya, K.; Rajan, M. Calcium alginate nanoparticle crosslinked phosphorylated polyallylamine to the controlled release of clindamycin for osteomyelitis treatment controlled release of clindamycin for osteomyelitis treatment. *Drug Dev. Ind. Pharm.* **2021**, *47*, 280–291. [CrossRef] [PubMed]
87. Abbaspour, M.; Makhmalzadeh, B.S.; Arastoo, Z.; Jahangiri, A.; Shiralipour, R. Effect of anionic polymers on drug loading and release from clindamycin phosphate solid lipid nanoparticles. *Trop. J. Pharm. Res.* **2013**, *12*, 477–482. [CrossRef]
88. Kilicarslan, M.; Ilhan, M.; Inal, O.; Orhan, K. Preparation and evaluation of clindamycin phosphate loaded chitosan/alginate polyelectrolyte complex film as mucoadhesive drug delivery system for periodontal therapy. *Eur. J. Pharm. Sci.* **2018**, *123*, 441–451. [CrossRef] [PubMed]
89. Zanganeh, S.M.; Tahvildari, K.; Nozari, M. Preparation and characterization of chitosan-alginate biopolymer loaded by clindamycin phosphate as an effective drug delivery system for the treatment of acne. *Polym. Bull./Res. Sq.* **2023**, 1–20. [CrossRef]

90. Do, N.H.N.; Truong, Q.T.; Le, P.K.; Ha, A.C. Recent developments in chitosan hydrogels carrying natural bioactive compounds. *Carbohydr. Polym.* **2022**, *294*, 119726. [CrossRef] [PubMed]
91. Wei, S.; Liu, X.; Zhou, J.; Zhang, J.; Dong, A.; Huang, P.; Wang, W.; Deng, L. Dual-crosslinked nanocomposite hydrogels based on quaternized chitosan and clindamycin-loaded hyperbranched nanoparticles for potential antibacterial applications. *Int. J. Biol. Macromol.* **2020**, *155*, 153–162. [CrossRef]
92. Tiraton, T.; Suwantong, O.; Chuysinuan, P.; Ekabutr, P.; Niamlang, P.; Khampieng, T.; Supaphol, P. Biodegradable microneedle fabricated from sodium alginate-gelatin for transdermal delivery of clindamycin. *Mater. Today Commun.* **2022**, *32*, 104158. [CrossRef]
93. Foox, M.; Raz-Pasteur, A.; Berdicevsky, I.; Krivoy, N.; Zilberman, M. In vitro microbial inhibition, bonding strength, and cellular response to novel gelatin-alginate antibiotic-releasing soft tissue adhesives. *Polym. Adv. Technol.* **2014**, *25*, 516–524. [CrossRef]
94. Dirzu, N.; Lucaciu, O.; Dirzu, D.S.; Soritau, O.; Cenariu, D.; Crisan, B.; Tefas, L.; Campian, R.S. BMP-2 delivery through liposomes in bone regeneration. *Appl. Sci.* **2022**, *12*, 1373. [CrossRef]
95. Schrade, S.; Ritschl, L.; Süss, R.; Schilling, P.; Seidenstuecker, M. Gelatin Nanoparticles for targeted dual drug release out of alginate-di-aldehyde-gelatin gels. *Gels* **2022**, *8*, 365. [CrossRef]
96. Hasan, N.; Cao, J.; Lee, J.; Kim, H.; Wook, J. Development of clindamycin—Loaded alginate/pectin/hyaluronic acid composite hydrogel film for the treatment of MRSA—infected wounds. *J. Pharm. Investig.* **2021**, *51*, 597–610. [CrossRef]
97. Kim, J.O.; Choi, J.Y.; Park, J.K.; Kim, J.H.; Jin, S.G.; Chang, S.W.; Li, D.X.; Hwang, M.R.; Woo, J.S.; Kim, J.A.; et al. Development of clindamycin-loaded wound dressing with polyvinyl alcohol and sodium alginate. *Biol. Pharm. Bull.* **2008**, *31*, 2277–2282. [CrossRef] [PubMed]
98. Morakul, B.; Wongrakpanich, A.; Teeranachaidekul, V.; Washiradathsathien, K.; Gamolvate, A. Clindamycin peel-off mask film, an effective formulation for *C. acnes* treatment: Characterization and microbiological activity. *Indonesian J. Pharm.* **2023**, *34*, 128–139. [CrossRef]
99. Mohamed, A.I.; Ahmed, O.A.; Amin, S.; Elkadi, O.A.; Kassem, M.A. In-vivo evaluation of clindamycin release from glyceryl monooleate-alginate microspheres by NIR spectroscopy. *Int. J. Pharm.* **2015**, *494*, 127–135. [CrossRef] [PubMed]
100. Jalageri, M.B.; Mohan Kumar, G.C. Hydroxyapatite reinforced polyvinyl alcohol/polyvinyl pyrrolidone based hydrogel for cartilage replacement. *Gels* **2022**, *8*, 555. [CrossRef] [PubMed]
101. Nadem, S.; Ziyadi, H.; Hekmati, M.; Baghali, M. Cross—linked poly(vinyl alcohol) nanofibers as drug carrier of clindamycin. *Polym. Bull.* **2020**, *77*, 5615–5629. [CrossRef]
102. Mandegari, M.; Ghasemi-Mobarakeh, L.; Varshosaz, J. Fabrication and characterization of a novel wound dressing with clindamycin loaded PVA nanoparticles for acne treatment. *Fiber. Polym.* **2022**, *23*, 3369–3379. [CrossRef]
103. Sangnim, T.; Limmatvapirat, S.; Nunthanid, J.; Sriamornsak, P.; Sittikijyothin, W.; Wannachaiyasit, S.; Huanbutta, K. Design and characterization of clindamycin-loaded nanofiber patches composed of polyvinyl alcohol and tamarind seed gum and fabricated by electrohydrodynamic atomization. *Asian J. Pharm. Sci.* **2018**, *13*, 450–458. [CrossRef]
104. Khattab, A.; Nattouf, A. Optimization of entrapment efficiency and release of clindamycin in microsponge based gel. *Sci. Rep.* **2021**, *11*, 23345. [CrossRef]
105. Ilhan, M.; Kilicarslan, M.; Orhan, K. Effect of process variables on in vitro characteristics of clindamycin phosphate loaded PLGA nanoparticles in dental bone regeneration and 3D characterization studies using nano-CT. *J. Drug Deliv. Technol.* **2022**, *76*, 103710. [CrossRef]
106. Kurakula, M.; Rao, G.S.N.K. Pharmaceutical assessment of polyvinylpyrrolidone (PVP): As excipient from conventional to controlled delivery systems with a spotlight on COVID-19 inhibition. *J. Drug Deliv. Technol.* **2020**, *60*, 102046. [CrossRef]
107. Borowska, M.; Glinka, M.; Filipowicz, N.; Terebieniec, A.; Szarlej, P. Polymer biodegradable coatings as active substance release systems for urological applications. *Monatsh. Chem.* **2019**, *150*, 1697–1702. [CrossRef]
108. Hirnle, L.; Heimrath, J.; Woytoń, J.; Kłósek, A.; Hirnle, G.; Małolepsza-Jarmołowska, K. Application of 2% clindamycin cream in the treatment of bacterial vaginosis and valuation of methylcellulose gel containing the complex of chitosan F and PVP k-90 with lactic acid as carrier for intravaginally adhbited medicines in the cases of pregnancie. *Ginekol. Polska* **2002**, *72*, 1096–1100.
109. Ilyas, R.A.; Zuhri, M.Y.M.; Norrrahim, M.N.F.; Misenan, M.S.M.; Jenol, M.A.; Samsudin, S.A.; Nurazzi, N.M.; Asyraf, M.R.M.; Supian, A.B.M.; Bangar, S.P.; et al. Natural fiber-reinforced polycaprolactone green and hybrid biocomposites for various advanced applications. *Polymers* **2022**, *14*, 182. [CrossRef]
110. Tanha, N.R.; Nouri, M. Core-shell nanofibers of silk fibroin/polycaprolactone-clindamycin: Study on nanofibers structure and controlled release behavior. *Polym. Sci. Ser. A* **2019**, *61*, 85–95. [CrossRef]
111. Mohamadi, P.; Mirmoeini, G.; Bahrami, H.; Mohsenzadeh, E.; Cochrane, C.; Koncar, V. Electrospinning of poly(caprolactone)/gelatin/clindamycin nanocomposites as an antibacterial wound dressing. *Mat. Sci. Forum* **2022**, *1063*, 71–81. [CrossRef]
112. Setia, H.; Javed, M.; Abdalkareem, S.; Abdelbasset, K.; Bokov, D.; Fakri, Y.; Najm, M.A.A.; Kazemnejadi, M. Preparation of antibacterial gel/PCL nanofibers reinforced by dicalcium phosphate-modified graphene oxide with control release of clindamycin for possible application in bone tissue engineering. *Inorg. Chem. Commun.* **2022**, *139*, 109336. [CrossRef]
113. Castillo-Ortega, M.M.; López-Peña, I.Y.; Rodríguez-Félix, D.E.; Del Castillo-Castro, T.; Encinas-Encinas, J.C.; Santacruz-Ortega, H.; Cauich-Rodríguez, J.V.; Quiroz-Castillo, J.M.; Chan-Chan, L.H.; Leyva-Verduzco, I.; et al. Clindamycin-loaded nanofibers of polylactic acid, elastin and gelatin for use in tissue engineering. *Polym. Bull.* **2022**, *79*, 5495–5513. [CrossRef]

114. Vahedi, M.; Barzin, J.; Shokrolahi, F.; Shokrollahi, P. Self-Healing, injectable gelatin hydrogels cross-linked by dynamic Schiff base linkages support cell adhesion and sustained release of antibacterial drugs. *Macromol. Mater. Eng.* **2018**, *303*, 1800200. [CrossRef]
115. Shekhawat, D.; Singh, A.; Bhardwaj, A.; Patnaik, A. A short review on polymer, metal and ceramic based implant materials. In Proceedings of the IOP Conference Series: Materials Science and Engineering, Jaipur, India, 5–6 November 2020; p. 1017. [CrossRef]
116. Janmohammadi, M.; Nazemi, Z.; Salehi, A.O.M.; Seyfoori, A.; John, J.V.; Nourbakhsh, M.S.; Akbari, M. Cellulose-based composite scaffolds for bone tissue engineering and localized drug delivery. *Bioactive Mat.* **2023**, *20*, 137–163. [CrossRef] [PubMed]
117. Kołodziejska, B.; Kaflak, A.; Kolmas, J. Biologically inspired collagen/apatite composite biomaterials for potential use in bone tissue regeneration—A review. *Materials* **2020**, *13*, 1748. [CrossRef] [PubMed]
118. Yue, S.; He, H.; Li, B.; Hou, T. Hydrogel as a biomaterial for bone tissue engineering: A review. *Nanomaterials* **2020**, *10*, 1511. [CrossRef] [PubMed]
119. Ritschl, L.; Schilling, P.; Wittmer, A.; Bohner, M.; Bernstein, A.; Schmal, H.; Seidenstuecker, M. Composite material consisting of microporous beta-TCP ceramic and alginate-dialdehyde-gelatin for controlled dual release of clindamycin and bone morphogenetic protein 2. *J. Mater. Sci. Mater. Med.* **2023**, *34*, 39. [CrossRef]
120. Kuehling, T.; Schilling, P.; Bernstein, A.; Mayr, H.O.; Serr, A.; Wittmer, A.; Bohner, M.; Seidenstuecker, M. A human bone infection organ model for biomaterial research. *Acta Biomater.* **2022**, *144*, 230–241. [CrossRef] [PubMed]
121. Xin, L. Preparation and characteristics of drug loaded PLGA chitosan/nano-hydroxyapatite membrane for guided periodontal tissue regeneration in surgical implanting. *Acad. J. Second Mil. Med. Univ.* **2017**, *12*, 194–200.
122. Uskoković, V.; Desai, T.A. In vitro analysis of nanoparticulate hydroxyapatite/chitosan composites as potential drug delivery platforms for the sustained release of antibiotics in the treatment of osteomyelitis. *J. Pharm. Sci.* **2014**, *103*, 567–579. [CrossRef]
123. Słota, D.; Florkiewicz, W.; Piętak, K.; Pluta, K.; Sadlik, J.; Miernik, K.; Sobczak-Kupiec, A. Preparation of PVP and betaine biomaterials enriched with hydroxyapatite and its evaluation as a drug carrier for controlled release of clindamycin. *Ceram. Int.* **2022**, *48*, 35467–35473. [CrossRef]
124. Ben, W.; Sun, P.; Huang, C.H. Effects of combined UV and chlorine treatment on chloroform formation from triclosan. *Chemosphere* **2016**, *150*, 715–722. [CrossRef]
125. Bayston, R.; Ashraff, W. Preventing infection on antimicrobial. *Orthop. Proc.* **2012**, *94*, 58.
126. Antoniac, I.; Popescu, D.; Zapciu, A.; Antoniac, A.; Miculescu, F.; Moldovan, H. Magnesium filled polylactic acid (PLA) material for filament based 3D printing. *Materials* **2019**, *12*, 719. [CrossRef]
127. Pradid, J.; Keawwatana, W.; Boonyang, U.; Tangbunsuk, S. Biological properties and enzymatic degradation studies of clindamycin-loaded PLA/HAp microspheres prepared from crocodile bones. *Polym. Bull.* **2017**, *74*, 5181–5194. [CrossRef]
128. Uskoković, V.; Hoover, C.; Vukomanović, M.; Uskoković, D.P.; Desai, T.A. Osteogenic and antimicrobial nanoparticulate calcium phosphate and poly-(D,L-lactide-co-glycolide) powders for the treatment of osteomyelitis. *Mat. Sci. Eng C* **2013**, *33*, 3362–3373. [CrossRef] [PubMed]
129. Vukomanović, M.; Škapin, S.D.; Jančar, B.; Maksin, T.; Ignjatović, N.; Uskoković, V.; Uskoković, D. Poly(D,L-lactide-co-glycolide)/hydroxyapatite core-shell nanospheres. Part 1: A multifunctional system for controlled drug delivery. *Colloids Surf. B* **2011**, *82*, 404–413. [CrossRef] [PubMed]
130. Vukomanović, M.; Škapin, S.D.; Poljanšek, I.; Žagar, E.; Kralj, B.; Ignjatović, N.; Uskoković, D. Poly(D,L-lactide-co-glycolide)/hydroxyapatite core-shell nanosphere. Part 2: Simultaneous release of a drug and a prodrug (clindamycin and clindamycin phosphate). *Colloids Surf. B* **2011**, *82*, 414–421. [CrossRef] [PubMed]
131. Vukomanović, M.; Zavašnik-Bergant, T.; Bračko, I.; Škapin, S.D.; Ignjatović, N.; Radmilović, V.; Uskoković, D. Poly(D,L-lactide-co-glycolide)/hydroxyapatite core-shell nanospheres. Part 3: Properties of hydroxyapatite nano-rods and investigation of a distribution of the drug within the composite. *Colloids Surf. B* **2011**, *87*, 226–235. [CrossRef] [PubMed]
132. Vukomanović, M.; Šarčev, I.; Petronijević, B.; Škapin, S.D.; Ignjatović, N.; Uskoković, D. Poly(D,L-lactide-co-glycolide)/hydroxyapatite core-shell nanospheres. Part 4: A change of the surface properties during degradation process and the corresponding in vitro cellular response. *Colloids Surf. B* **2012**, *91*, 144–153. [CrossRef] [PubMed]
133. Chen, K.; Guo, B.; Luo, J. Quaternized carboxymethyl chitosan/organic montmorillonite nanocomposite as a novel cosmetic ingredient against skin aging. *Carbohydr. Polym.* **2017**, *173*, 100–106. [CrossRef] [PubMed]
134. Delir, S.; Sirousazar, M.; Kheiri, F. Clindamycin releasing bionanocomposite hydrogels as potential wound dressings for the treatment of infected wounds. *J. Biomat. Sci.* **2020**, *31*, 1489–1514. [CrossRef]
135. Muhammad, N.; Siddiqua, S. Calcium bentonite vs sodium bentonite: The potential of calcium bentonite for soil foundation. *Mat. Today Proc.* **2022**, *4*, 822–827. [CrossRef]
136. Idris, S.A.S.; Yucel, O. Influence of bentonite nanoparticles on properties of PVP-CMC-gums hydrogel films for biomedical applications. *Int. J. Eng. Sci. Technol.* **2022**, *6*, 81–98. [CrossRef]
137. Bampidis, V.; Azimonti, G.; de Lourdes Bastos, M.; Christensen, H.; Dusemund, B.; Kos Durjava, M.; Kouba, M.; López-Alonso, M.; López Puente, S.; Marcon, F.; et al. Safety and efficacy of sodium carboxymethyl cellulose for all animal species. *EFSA J.* **2020**, *18*, e06211. [CrossRef] [PubMed]

138. Sadeghi, S.; Nourmohammadi, J.; Ghaee, A.; Soleimani, N. Carboxymethyl cellulose-human hair keratin hydrogel with controlled clindamycin release as antibacterial wound dressing. *Int. J. Biol. Macromol.* **2019**, *147*, 1239–1247. [CrossRef]
139. Maver, T.; Mastnak, T.; Mihelic, M.; Maver, U.; Finšgar, M. Clindamycin-based 3D-printed and electrospun coatings for treatment of implant-related infections. *Materials* **2021**, *14*, 1464. [CrossRef] [PubMed]

nanomaterials

MDPI

Article

Clindamycin-Loaded Nanosized Calcium Phosphates Powders as a Carrier of Active Substances

Dagmara Słota [1,*], Karina Piętak [1], Wioletta Florkiewicz [1], Josef Jampílek [2,3], Agnieszka Tomala [1], Mateusz M. Urbaniak [4,5], Agata Tomaszewska [4,5], Karolina Rudnicka [4] and Agnieszka Sobczak-Kupiec [1,*]

1 Department of Materials Engineering, Faculty of Materials Engineering and Physics, Cracow University of Technology, 37 Jana Pawła II Av., 31 864 Krakow, Poland
2 Department of Analytical Chemistry, Faculty of Natural Sciences, Comenius University, Ilkovičova 6, 842 15 Bratislava, Slovakia
3 Department of Chemical Biology, Faculty of Science, Palacky University Olomouc, Slechtitelu 27, 783 71 Olomouc, Czech Republic
4 Department of Immunology and Infectious Biology, Faculty of Biology and Environmental Protection, University of Łódź, 90-237 Łódź, Poland
5 Bio-Med-Chem Doctoral School, University of Lodz and Lodz Institutes of the Polish Academy of Sciences, 90-237 Łódź, Poland
* Correspondence: dagmara.slota@doktorant.pk.edu.pl (D.S.); agnieszka.sobczak-kupiec@pk.edu.pl (A.S.-K.)

Abstract: Bioactive calcium phosphate ceramics (CaPs) are one of the building components of the inorganic part of bones. Synthetic CaPs are frequently used as materials for filling bone defects in the form of pastes or composites; however, their porous structure allows modification with active substances and, thus, subsequent use as a drug carrier for the controlled release of active substances. In this study, four different ceramic powders were compared: commercial hydroxyapatite (HA), TCP, brushite, as well as HA obtained by wet precipitation methods. The ceramic powders were subjected to physicochemical analysis, including FTIR, XRD, and determination of Ca/P molar ratio or porosity. These techniques confirmed that the materials were phase-pure, and the molar ratios of calcium and phosphorus elements were in accordance with the literature. This confirmed the validity of the selected synthesis methods. CaPs were then modified with the antibiotic clindamycin. Drug release was determined on HPLC, and antimicrobial properties were tested against *Staphylococcus aureus*. The specific surface area of the ceramic has been demonstrated to be a factor in drug release efficiency.

Keywords: calcium phosphates; ceramics; hydroxyapatite; brushite; drug delivery system; antibiotic; clindamycin

Citation: Słota, D.; Piętak, K.; Florkiewicz, W.; Jampílek, J.; Tomala, A.; Urbaniak, M.M.; Tomaszewska, A.; Rudnicka, K.; Sobczak-Kupiec, A. Clindamycin-Loaded Nanosized Calcium Phosphates Powders as a Carrier of Active Substances. *Nanomaterials* **2023**, *13*, 1469. https://doi.org/10.3390/nano13091469

Academic Editors: Jose L. Arias, Nikolaos Dimitratos, Diego Cazorla-Amorós and Miriam Navlani-García

Received: 27 March 2023
Revised: 19 April 2023
Accepted: 20 April 2023
Published: 25 April 2023

1. Introduction

The ability to achieve targeted therapy as well as sustained and controlled release of the drug is possible through the use of drug delivery systems (DDSs). It is a hot spot in the medical field understood as a combination of drug and carrier, where the drug is loaded inside or on the surface of the carrier by chemical or physical methods [1]. In general, drug carriers are understood as safe tools for transporting molecules for nutraceutical, pharmaceutical, and cosmetic applications [2]. In recent years, many inorganic nanomaterials such as gold nanoparticles [3–5], carbon nanotubes [6–8], and quantum dots [9–11] have been extensively studied for drug delivery. In the context of bone tissue regeneration, ceramic carriers based on bioactive calcium phosphates (CaPs) are of great interest. One of the advantages of ceramic carriers is their low toxicity. Most CaPs have good biocompatibility, biodegradability, as well as biological stability [12]. Furthermore, the variety of ceramic materials as well as the methods of their synthesis make it possible to adjust the size and structure of the grains. It is therefore possible to adjust these parameters for drug loading, for example, in the nanometer size [13]. Figure 1 presents the principle of ceramic drug carrier operation. The diffusion of drugs and other active substances through the pores of

ceramics depends on their concentration gradient and solubility. The porosity of the ceramic carrier itself, as well as the specific surface area and size, affect drug diffusion [14,15].

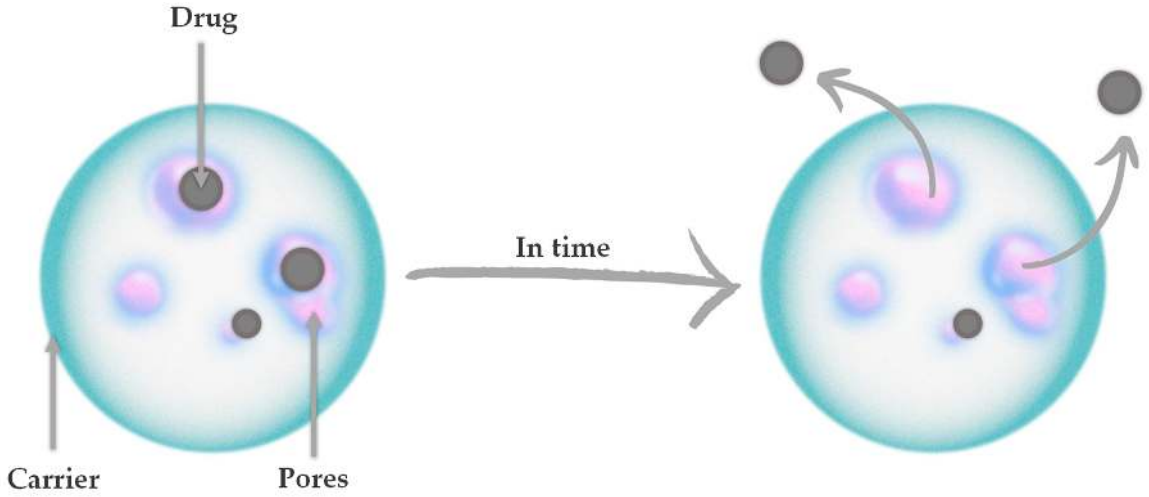

Figure 1. The principle of ceramic drug carrier operation.

The existence of CaPs in bones was discovered in 1769, and since 1900 active research has been carried out to synthesize them for medical applications such as bone defect fillers, apatite pastes, and composite materials for implants [16–19]. In the structure of CaPs are present PO_4^{3-} and HPO_4^{2-} ions found in bone and tooth-building minerals, and $H_2PO_4^-$ ions, which are formed only in acidic reaction environments. They are mostly poorly water-soluble salts of the tri-basic orthophosphoric acid H_3PO_4 and dissolve well in acids [20]. There are several types of CaP, which differ in the molar ratio of calcium and phosphorus (Ca/P). This also influences the properties of these ceramic materials. A lower Ca/P ratio corresponds to more acidic and relatively water-soluble phases [21]. Calcium phosphates occur in the $CaO–P_2O_5$ arrangement or, if they contain OH^- ions, in the arrangement $CaO–P_2O_5–H_2O$. Table 1 summarizes synthetic CaPs relevant to medical applications, along with their names, Ca/P molar ratio, and chemical formulae [22,23].

Table 1. Synthetic calcium phosphates relevant to medical applications.

Calcium Phosphates in the $CaO-P_2O_5$ Arrangement				
Abbreviation	**Systematic Name**	**Mineralogical Name**	**Chemical Formula**	**Molar Ratio Ca/P**
CP	Calcium metaphosphate	–	$Ca(PO_3)_2$	0.5
C_2P	Calcium pyrophosphate	–	$Ca_2P_2O_7$	1.0
C_3P, TCP	Tricalcium phospahte	Whitlockite	$Ca_3(PO_4)_2$	1.5
C_4P, TTCP	Tetracalcium phosphate	–	$Ca_4(PO_4)_2O$	2.0
Calcium Phosphates in the $CaO-P_2O_5-H_2O$ Arrangement				
Abbreviation	**Systematic Name**	**Mineralogical Name**	**Chemical Formula**	**Molar Ratio Ca/P**
MCPA	Calcium dihydrogenphosphate	–	$Ca(H_2PO4)_2$	0.5
MCPM	Calcium dihydrogenphosphate monohydrate	–	$Ca(H_2PO_4)_2 \cdot H_2O$	0.5
DCPD	Dicalcium phosphate dihydrate	Brushite	$CaHPO_4 \cdot 2\,H_2O$	1.0
DCPA	Dicalcium phosphate anhydrous	Monethite	$CaHPO_4$	1.0
OCP	Octacalcium phosphate	–	$Ca_8H_2(PO_4)_6 \cdot 5\,H_2O$	1.333
HA, HAp, OHAp	Pentacalcium hydroxide triphosphate	Hydroxyapatite	$Ca_{10}(PO_4)_6 \cdot 2\,H_2O$	1.667

Currently, hydroxyapatite (HA) and tricalcium phosphate (TCP) are widely used as implant materials [24,25]. HA is the most well-known and widespread phase and has a Ca/P ratio of 1.67. It represents the mineral part of natural bone, which consists of 70% of just this inorganic material [26]. TCP has a Ca/P ratio of 1.5 and occurs in two polymorphic varieties (high-temperature α-TCP and low-temperature β-TCP). α-TCP is produced at temperatures above 1125 °C, while β-TCP is formed at temperatures below 1125 °C [27]. In contrast to α-TCP, β-TCP is thermodynamically stable in biological environments and within the normal temperature range. α-TCP exhibits better and faster solubility than β-TCP, and for this reason, the low-temperature variety has found wider application in medicine and dentistry [28,29]. Furthermore, also of interest in the context of applications where the implant is to be replaced by newly formed bone over time is brushite (DCPD). The main difference between DCPD and HA is its solubility in body fluids, in which DCPD is 100 times more soluble than HA. For this reason, brushite biomaterials are resorbable in vivo and will start faster, and this aspect also affects the increase in porosity of such a biomaterial over time, which allows surrounding tissues to grow into it [30,31]. An undeniable advantage of CaPs in the context of their use as biomaterials, including drug carriers, is their biocompatibility, as they do not induce inflammation or other negative reactions. Moreover, some of them exhibit bioactivity (e.g., HA), affecting the proliferation and adhesion of bone-forming cells—osteoblasts [32–34]. The bioactivity of ceramics is related to the processes of degradation and release of ions from the material. As a result of this phenomenon, the local concentration of Ca and P ions increases, which stimulates the formation of new apatite layers and bone minerals on the surface of the material. They also affect the expression of osteoblast differentiation markers, such as BMPs, COL1, ALP, BSP, and OCN [29–32]. The interaction between ceramics and osteoblasts depends on the geometry of the material and is improved if the surface of the phosphate–calcium is charged or polarized. Therefore, for the successful application of the materials, attention should also be paid to their resistance to both ultraviolet and X-rays. The application of the materials depends on their resistance to aging, including but not limited to radiation [35–39]. X-rays promote the decarboxylation of the collagen side chain, which in turn negatively affects the electrostatic bonding between the phosphate groups in CaP and the carboxylate groups of the protein side chains [40].

In the following work, four calcium phosphate ceramic powders were modified with clindamycin using the physical sorption method. Clindamycin is an antibiotic of the lincosamide group [41]. It has a broad spectrum of activity that includes both Gram-positive bacteria (including many strains of MRSA) and anaerobic bacteria. The function of this drug antibiotic is to block the synthesis of bacterial proteins [42]. Clindamycin is most often used in complaints of bacterial infection of the oral cavity or teeth or bacterial infection of bones [43,44]. Hence, the authors decided to select this specific drug for ceramic phase modification in this study. Considering the properties of this drug, it is significant that the authors have also previously used it to modify hydroxyapatite-reinforced hydrogel materials [45]. In this study, using high-performance liquid chromatography (HPLC), the drug release rate was determined, and the antimicrobial properties of the carriers against *Staphylococcus aureus* ATCC 29213 were determined. The clean powders were subjected to physicochemical analysis, including X-Ray diffraction analysis (XRD), Fourier-transform infrared spectroscopy (FTIR), or Ca/P molar ratio determination. No other literature describing identical ceramic-drug combinations was found.

2. Materials and Methods

2.1. Materials

All reagents used for ceramics s-1.67 and 1.5 syntheses, i.e., the sodium phosphate dibasic (Na_2HPO_4), calcium acetate monohydrate ($Ca(CH_3CO_2)_2 \cdot H_2O$), and ammonia water ($NH_4OH$, 25%) were purchased from Sigma-Aldrich (Darmstadt, Germany). The commercial hydroxyapatite identified in the publication as c-1.67 was also from Sigma-Aldrich (Darmstadt, Germany). The reagents for the brushite ceramics, i.e., dis-

odium hydrogen phosphate dihydrate ($Na_2HPO_4 \cdot 2H_2O$) and calcium nitrate tetrahydrate ($Ca(NO_3)_2 \cdot 4H_2O$), were purchased from Sigma-Aldrich (Darmstadt, Germany). The mobile phase in the HPLC was a combination of acetonitrile from Honeywell (Seelze, Germany) and KH_2PO_4 from DOR-CHEM (Krakow, Poland). The reagents necessary for the determination of the Ca/P molar ratio were HNO_3 and HCl from Stanlab (Lublin, Poland), $Bi(NO_3)_3$, triethanolamine, as well as KOH from Sigma-Aldrich (Darmstadt, Germany), and disodium edetate from Warchem (Warsaw, Poland). The drug selected for powder modification was clindamycin hydrochloride from Sigma-Aldrich (Darmstadt, Germany). Demineralized water purified with Hydrolab model HLP 5sp was used for all solutions.

For biological research, the bacteria *Staphylococcus aureus* ATCC 29213 (American Type Culture Collection, Manassas, VA, USA) was purchased. Bacteria were cultured in Mueller–Hinton Broth from Merck (Darmstadt, Germany). Resazurin was from Merck (Darmstadt, Germany), and phosphate-buffered saline (PBS) was from Oxoid (Basingstoke, UK).

2.2. Ceramic Synthesis

Four nanopowders were selected for this study. Three of them were obtained by wet precipitation methods with different Ca/P molar ratios in the range of 1.0–1.67, and a commercial hydroxyapatite designated as c-167 was selected as a reference powder. The material synthesis methods are described below.

The hydroxyapatite-structured powder, designated as s-1.67, was synthesized by wet precipitation at boiling temperature. Firstly, solutions of Na_2HPO_4 (0.32 mol/L) and $(CH_3COO)_2Ca$ (0.128 mol/L) were prepared. Distilled water and a specified volume of Na_2HPO_4 were poured into a three-necked flask. Then, using 25% ammonia water, the pH of the system was brought to 11. After the entire system was brought to the boiling point of the ingredients, $(CH_3COO)_2Ca$ was dropped in at a rate of 1 drop/sec. After the synthesis was completed, the ceramic suspension was cooled and allowed to stand for 24 h. After this time, the precipitate was washed thoroughly with distilled water, brought to neutral pH, and freeze-dried. This method was also described in a previous paper [46,47].

The ceramic powder, marked as 1.5, was obtained in an analogous manner to s-1.67 by reducing the volume of the added acetate salt accordingly. The ratios of salt solutions were calculated to obtain a Ca/P ratio of 1.5.

The brushite powder, designated as 1.0, was synthesized using the wet precipitation method. In the first step, 500 mL each of aqueous solutions of $Na_2HPO_4 \cdot 2H_2O$ and $Ca(NO_3)_2 \cdot 4H_2O$ were prepared, where the concentration of both solutions was 0.5 mol/L. The $Na_2HPO_4 \cdot 2H_2O$ solution was placed on a magnetic stirrer, and the prepared $Ca(NO_3)_2 \cdot 4H_2O$ solution was dropped in at a rate of 1 drop per second. The pH of the solution was maintained between 6 and 6.5 with 25% ammonia water. The resulting ceramic suspension was aged for 24 h, washed thoroughly with distilled water to a neutral pH, and freeze-dried.

2.3. Determination of Calcium and Phosphorus Content

The molar ratio of Ca and P (Ca/P) plays a crucial role in the formation of the calcium phosphate phase. Furthermore, the value of the ratio is one of the indicators suggesting which ceramic material the powder under examination belongs to [48]. The determinations were conducted in accordance with the Polish standard for phosphorus based on PN-80/C-87015 for calcium based on PN-97/R-64803 [49,50].

Phosphorus content (wt. %) was determined according to Formula (1):

$$\%P = \frac{\left(\frac{M_1 \cdot V_1 \cdot 100\%}{m \cdot V_2 \cdot 1000}\right)}{2.29} \quad (1)$$

where M_1 is a P_2O_5 content in the analyzed sample determined from the standard curve [mg/mL]; V_1—volume of volumetric flask used for phosphorus extraction [mL]; m—sample

mass used for extraction [g]; V_2—volume of solution collected for analysis [mL]; and 2.29—conversion factor from P_2O_5 to P.

Calcium content (wt. %) was determined according to Formula (2):

$$\%Ca = \left(\frac{0.04008 \cdot V_1 \cdot c \cdot V_2}{m \cdot V_3}\right) \cdot 100 \quad (2)$$

where V_1 is a volume of EDTA solution consumed during calcium titration [mL].; c—titer of EDTA solution set to calcium standard solution [mol/L]; V_2—volume of sample solution [mL]; m—sample mass used for extraction [g]; and V_3—volume of solution collected for calcium titration [mL].

Calcium and phosphorus determinations were repeated for all powders. Each measurement was performed in triplicate.

2.4. X-ray Diffraction Analysis

In order to perform structural characterization of the ceramic powders obtained, X-ray diffraction analysis was performed using a Malvern Panalytical Aeris X-ray diffractometer with PIXcel1D-Medipix3 detector (Malvern, UK) with Cu Kα radiation. All measurements were carried out at a step size of 0.0027166° 2θ over a range of 2θ from 10 to 100° with a time per step of 340.425 s.

2.5. Fourier-Transform Infrared Spectroscopy Analysis

Individual functional groups in ceramic powders were identified using Fourier-transform infrared spectroscopy (FT-IR). The analysis was carried out under room conditions using a Nicolet iS5 91 FT-IR spectrometer equipped with an iD7 ATR attachment (Thermo Scientific, Loughborough, UK) in the range 4000–400 cm^{-1} (32 scans at 4.0 cm^{-1} resolution).

2.6. Specific Surface Area and Porosity Studies

Specific surface area (SSA) and porosity studies were performed using Auto-sorb-1 Quantachrome flow apparatus, with nitrogen as an adsorbate, at −196 °C. Prior to the measurements, all samples were preheated and degassed under vacuum at 200 °C for 18 h. The specific surface area of the samples was determined with the multipoint Brunauer–Emmett–Teller (BET) analysis method. The Brunauer–Emmett–Teller (BET) theory explains the physical adsorption–desorption of gas molecules on a solid surface and represents the basis for the analysis of measured data. Micropore pore volume and micropore surface were determined with the t-plot method, while the mesopore pore volume and mesopore surface were determined with the Barret–Joyner–Halenda (BJH) and density-functional theory (DFT) methods. DFT methods allow one to obtain reliable pore size distributions over the complete range of micro- and mesopores (for a recent review on the application of DFT methods for pore size analysis). Methods for pore size analysis based on DFT and molecular simulation are now widely used and are commercially available for many important adsorptive or adsorbent systems and are featured in a standard by the International Organization for Standardization (ISO). The calculation of the pore size distribution function f(W) is based on a solution of the general adsorption isotherm (GAI) equation, which correlates the experimental adsorption isotherm N(p/p 0) with the kernel of the theoretical adsorption or desorption isotherms N(p/p 0,W).

2.7. Preparation of Ceramic Powders with Drug

The antibiotic selected for powder modification by physical sorption was clindamycin hydrochloride. Ceramic weights of 0.5 g each were inserted into 40 mL of the drug solution at a concentration of 2 mg/mL for 5 days. The samples were stored in tightly closed containers at 4 °C. After this time, the samples were centrifuged with a laboratory centrifuge (MPW Med. Instruments MPW—260R) for 15 min, at 4 °C with a speed of 5500 rpm, and then the solution was decanted from the precipitate. The remaining powders

were dried and submitted for release kinetics studies. Samples of ceramic powders after drug modification were similarly marked as C/1.0, C/1.5, C/c-1.67, and C/s-1.67.

2.8. Kinetic Release Studies of Antibiotic

The prepared drug-modified ceramic powders were submitted for release kinetics studies. Powder samples of 0.5 g each were incubated in 15 mL PBS over a period of 14 days. To examine the amount of clindamycin released from the samples, the collected incubation fluids were analyzed by high-performance liquid chromatography (HPLC). The principle of HPLC for the determination of released clindamycin is schematically presented in Figure 2.

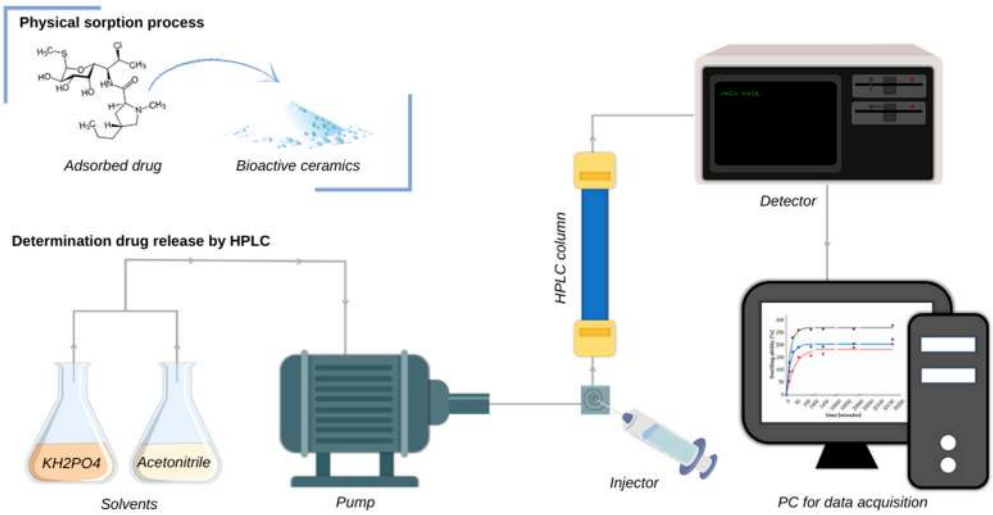

Figure 2. Principle of HPLC for the determination of clindamycin.

Determination of drug released from the powders was carried out on a Shimadzu HPLC system (Kyoto, Japan) consisting of an SPD-M20A UV-Vis photodiode array detector, a CTO-20AC column oven, and an LC-20AD pump. The antibiotic was separated on a C18 reversed-phase Kinetex® column (250 mm × 4.6 mm) with a pore size of 100 Å and a particle size of 5 µm. The system was operated isocratically with a mobile phase consisting of a mixture of acetonitrile and KH_2PO_4 (45:55 *v*/*v*) at pH = 7.5 at a flow rate of 1.0 mL/min (30 °C). The sample was injected through a 20 µL sampling loop. The experiment was conducted with the detector set at 210 nm. Each time, prior to measurement, 1 mL of the collected incubation fluid was centrifuged at 18,000 rpm at 4 °C using an MPW-260R (Warsaw, Poland).

2.9. Morphology Analysis

Scanning electron microscopy (SEM) imaging was performed using a Jeol 5510LV with an EDS IXRF system detector (Freising, Germany) to determine the structure of the powders and their shape. The powders were attached to a carbon tape and then coated with nano-gold. EDS microanalysis was also performed for clindamycin-modified C/s-1.67, determining elements such as Au, Ca, P, and Cl.

2.10. Antimicrobial Activity of Clindamycin-Modified Ceramic Powders

The antimicrobial activity of clindamycin-modified ceramic powders against *Staphylococcus aureus* ATCC 29213 was assessed by the determination of the minimum inhibitory concentration (MIC) by classic broth microdilution and resazurin reduction assay [51]. The bacteria were cultured in Mueller–Hinton Broth to mid-log phase, and the inoculum was standardized to 0.5 McFarland (5×10^5 CFU/mL) as recommended by EUCAST guidelines [52]. The clindamycin-modified ceramic powders were distributed into wells of a 96-well plate (Nunc, Rochester, NY, USA) containing 100 µL Mueller–Hinton

Broth (MHB) to form a series of 2-fold dilution. Then the bacterial suspension (100 µL) was added to each well, and plates were incubated for 24 h at 37 °C. Control wells contained bacterial culture alone (positive control of bacterial growth), and wells with MHB alone (negative control) were included. In addition, a reference antibiotic, clindamycin, in the range of 256–0.001 µg/mL was included. Four independent experiments were performed in triplicate. Then in the classic method, the MIC was read manually as the lowest concentration of antimicrobial agent that completely inhibits the growth of the organism as detected by the unaided eye. Whereas to assess the MIC_{99} on the basis of microbial metabolic activity prior to reading, the 20 µL of 0.02% resazurin in sterile PBS was added to each well and left for 3 h. Fluorescence was measured at an excitation wavelength of 560 nm and emission wavelength of 590 nm using a SpectraMax® i3x Multi-Mode Microplate Reader (Molecular Devices, San Jose, CA, USA).

3. Results

3.1. Determination of Calcium and Phosphorus Content

The Ca/P molar ratios for the powders and the determined elemental contents of calcium and phosphorus (wt. %) are presented in Table 2. The determined Ca/P molar ratios differ slightly from the assumed values. In the case of s-1.67 and c-1.67, the values obtained are very close to the stoichiometric HA, which is assigned a value of 1.67. The slight discrepancies that can be observed for all synthesized samples may be due to the incorporation of foreign cations or anions into the atomic structure of the ceramics. The reactions were carried out in an air atmosphere; hence, substitutions of, for example, phosphate groups by CO_3^{2-} ions are possible.

Table 2. Calcium and phosphorus content and Ca/P molar ratio in powders (mean ± SD).

Sample	Ca Content (wt. %)	P Content (wt. %)	Ca/P Molar Ratio
s-1.67	37.51 ± 0.65	17.26 ± 0.19	1.67
c-1.67	37.46 ± 0.38	17.27 ± 0.12	1.67
1.5	36.93 ± 0.32	18.87 ± 0.23	1.51
1.0	37.81 ± 0.41	27.91 ± 0.34	1.04

3.2. X-ray Diffraction Analysis

Figure 3 exhibits the XRD patterns of the ceramic nanopowders tested. The diffractograms of s-1.67 and c-1.67, according to International Center for Diffraction Data File Card No. 01-080-7085, were assigned to the hexagonal structure of hydroxyapatite (P63/m space group). Both samples s-1.67 and c-1.67 show the peak with the highest intensity at 31.74° of two theta (211), assigned which corresponds to the main peak of the HA hexagonal structure. The XRD results obtained demonstrate that the developed hydroxyapatite synthesis method enables the preparation of crystalline and phase-pure hydroxyapatite [50,53].

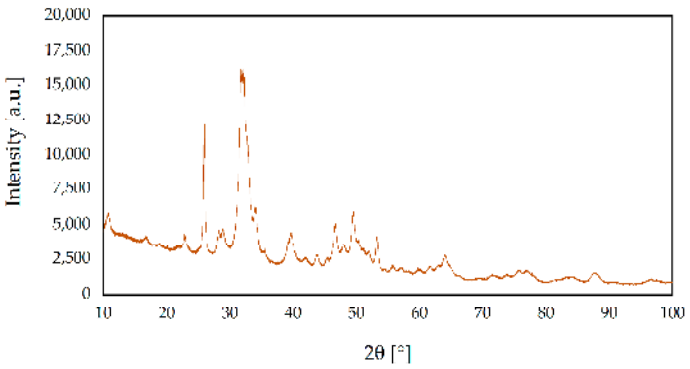

(**a**)

Figure 3. *Cont.*

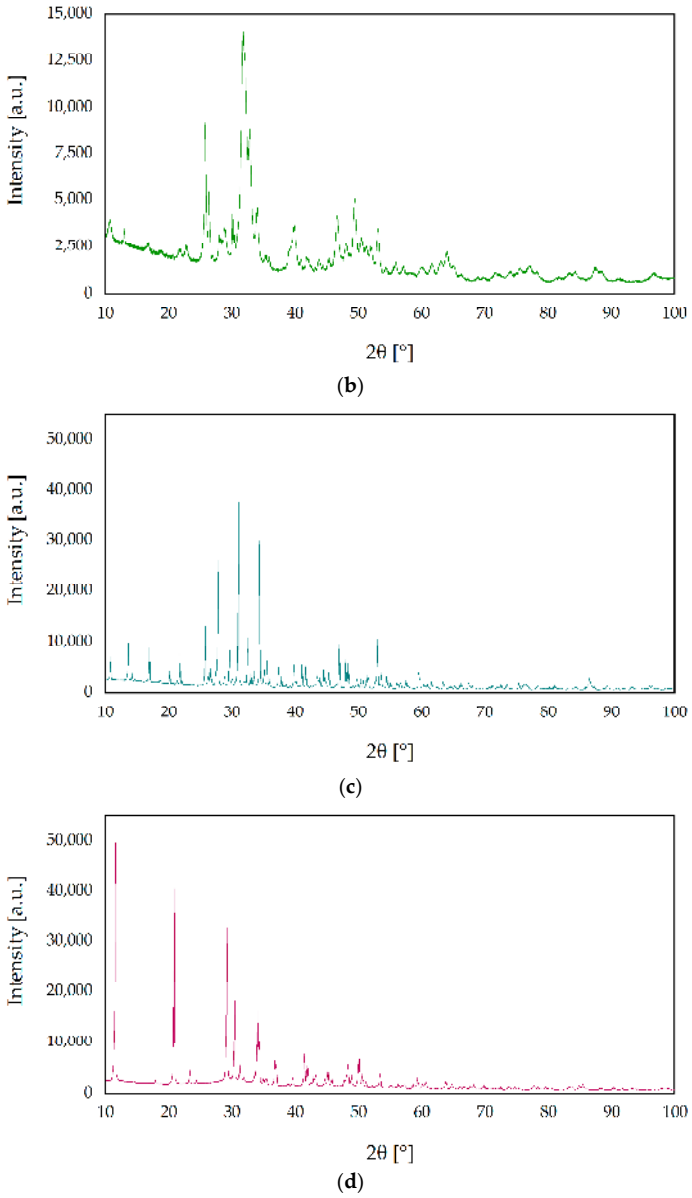

Figure 3. X-ray diffraction (XRD) patterns of ceramic nanopowders: (**a**) s-1.67, (**b**) c-1.67, (**c**) 1.5, and (**d**) 1.0.

Based on the analysis of the diffractogram of the sample labeled 1.5, the highest intensity is shown by the peak at 31.02° of two theta (0210), which is characteristic of the rhombohedral structure of β-TCP (R3c space group) [54]. The XRD result was found to be consistent with the phases listed in the ICDD database File Card No. 04-008-8714 assigned to β-TCP.

The reflections obtained for the sample designated 1.0 in the XRD study show characteristic peaks assigned to the monoclinic structure of brushite (Ia space group). Analysis of the obtained diffractogram shows characteristic peaks at two theta equal to 11.60° (020) and 23.39° (040), which are in accordance with the File Card No. 00-011-0293 in the ICDD database.

The degree of crystallinity (X_c) of samples was calculated using OriginPro 2023 software. The crystalline fraction was determined by integrating the areas under the crystalline (P_c) and amorphous (P_a) diffractions pattern and calculated in accordance with the following formula:

$$X_c = \frac{P_c}{P_a + P_c}$$

The obtained results have shown significant differences in crystallinity among samples. The degree of crystallinity of s-1.67 and c-1.67 were 41.5% and 48.6%, respectively. On the other hand, the highest crystallinity was observed for sample 1.5 (82.8%), whereas the crystallinity degree of sample 1.0 was 75.1%. On this basis, it can be concluded that the method produces phase-pure and crystalline [55,56].

3.3. Fourier Transform Infrared Spectroscopy Analysis

The comparative analysis of the FT-IR spectra of the ceramic nanopowders is shown in Figure 4. Both the spectrum of sample s-1.67 and c-1.67 show characteristic peaks for hydroxyapatite. The spectrum at 1018 cm^{-1} can be identified as asymmetric P–O stretching vibrations. The peaks at 559 cm^{-1} and 599 cm^{-1} have been attributed to triple degenerate O–P–O stretching modes in PO_4^{3-}. The peaks of the characteristic functional groups present in the synthesized hydroxyapatite overlap with the FT-IR spectrum of commercial hydroxyapatite [47,57].

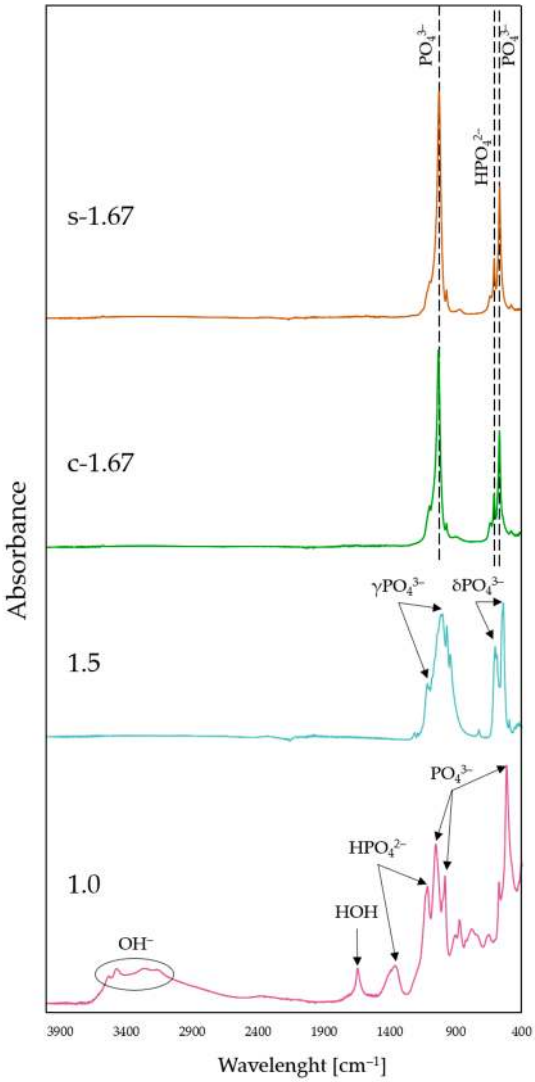

Figure 4. FT-IR spectra of nanopowders: s-1.67, c-1.67, 1.5, and 1.0.

On the FT-IR spectrum for the sample marked 1.5, peaks at a wavenumber of 541 cm^{-1} and 603 cm^{-1}, attributed to triply degenerated asymmetric bending vibrations for PO_4^{3-}, are visible. Spectral analysis revealed the presence of triply degenerated asymmetric stretching of the orthophosphate groups of PO_4^{3-}, as evidenced by distinct bands in the range 1015–1116 cm^{-1}. Furthermore, at 944 cm^{-1} and 979 cm^{-1}, symmetric stretching

is also attributed to the PO_4^{3-} group. The FT-IR spectral analysis performed indicates that the phase obtained was β-TCP [54,58–60].

FT-IR spectral analysis of sample 1.0 indicates that the vibrations at 1118 and 1203 cm^{-1}, which are characteristic of the brushite phase, can be attributed to the monohydrogen phosphate ion HPO_4^{2-}. The peaks at 572 cm^{-1}, 983 cm^{-1} and 1052 cm^{-1} correspond to the PO_4^{3-} group. Furthermore, the spectral band occurring between 3153 and 3532 cm^{-1} is attributed to the OH^- group. Moreover, the characteristic peak at 1645 cm^{-1} is assigned to HOH [56,61–63].

Based on the FT-IR spectral analysis of the ceramic nanopowders, the presence of characteristic functional groups was identified, and consequently, it was confirmed that monophasic compounds are obtained as a result of the developed methods for the synthesis of calcium phosphate ceramics.

3.4. Specific Surface Area and Porosity Studies

Importantly, the morphological properties such as high surface area, large pore volume, and narrow particle size distribution are well suited for the application of nanoencapsulation in drug delivery systems. The results obtained are presented in Table 3.

Table 3. N2 physisorption-derived parameters characterizing the obtained samples (SSA—specific surface area).

Sample	SSA [m^2/g]	Porosity		
		Pore Size Distribution DFT [nm]	Pore Volume Macropores [cm^3/g]	Pore Area Micropores Vt [m^2/g]
s-1.67	53	4, 10, 11, 13	0.345	3.52
c-1.67	64	11, 13, 17, 20, 22, 24, 28	0.27	0
1.5	61	8, 10, 11, 13	0.304	0
1.0	32	4, 7, 8, 10	0.21	4.94

Experimental adsorption and desorption isotherms of nitrogen (77 K) are presented in Figure 5b,d,f,h. The investigated powders 1.0 and s-1.67 reveal mesoporosity and microporosity structure, while samples 1.5 and c-1.67 reveal mesopore structure, while microporosity is 0 for both samples. This is supported by the shape of the isotherms, which are of type IV (according to IUPAC classification). The specific surface area is related to mesoporosity changes from 64 to 61 m^3/g for c-1.67 and powder 1.5 to 53–32 m^3/g for powder s-1.67 and sample 1.0. The higher the specific surface area, the better drug delivery systems can be developed on the basis of this powder.

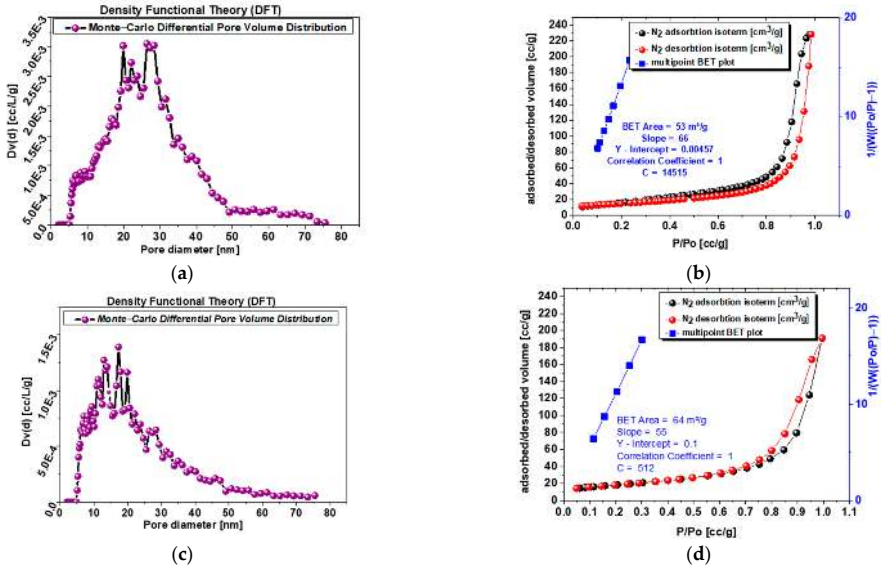

Figure 5. *Cont.*

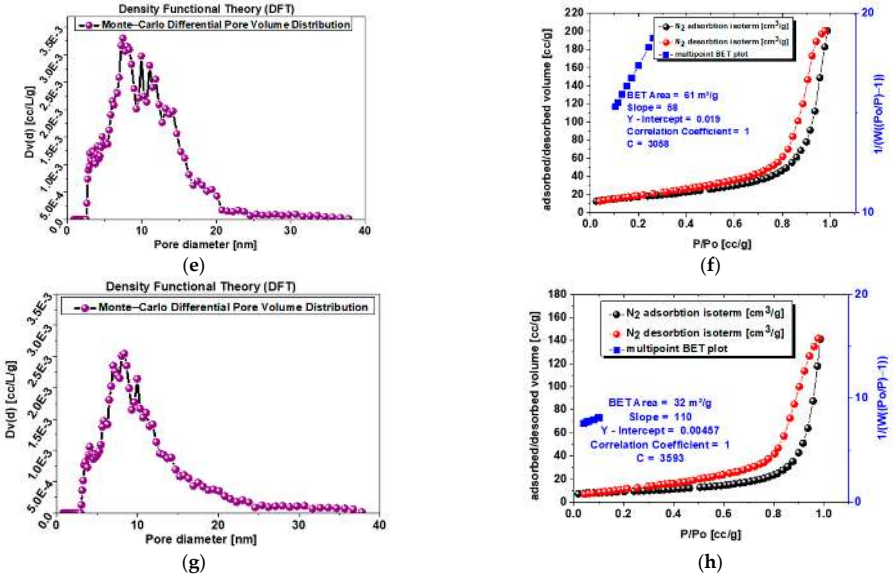

Figure 5. (**a**) Sample s-1.67 mesopore size differential distribution according to DFT (Dv(d) [cc/L/g]; (**b**) sample s-1.67 adsorption–desorption isotherms and multipoint BET plot; (**c**) sample c-1.67 mesopore size differential distribution according to DFT (Dv(d) [cc/L/g]; (**d**) sample c-1.67 adsorption–desorption isotherms and multipoint BET plot; (**e**) sample 1.5 mesopore size differential distribution according to DFT (Dv(d) [cc/L/g]l; (**f**) sample 1.5 adsorption–desorption isotherms and multipoint BET plot.; (**g**) sample 1.0 mesopore size differential distribution according to DFT (Dv(d) [cc/L/g]; (**h**) sample 1.0 adsorption–desorption isotherms and multipoint BET plot.

Analysis of Figure 5a,c,e,g with pore volume distribution profiles exhibit single narrow peaks for sample 1.0 and powder s-1.67 with a maximum at 8–12 nm, while powder 1.5 shows more broad peaks at a similar range of 8–13 nm, and the most blurred peaks at widest range represents commercial sample c-1.67 at 15–30 m.

3.5. Kinetic Release Studies of Antibiotic

The amount of clindamycin in mg/mL released from the powder samples is presented in Figure 6.

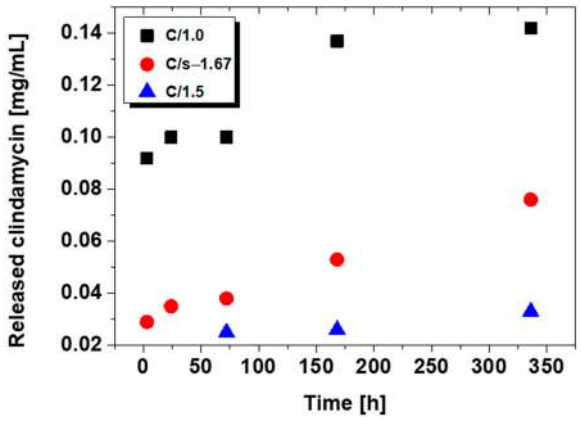

Figure 6. Release profile of clindamycin from modified ceramic powders.

The release results for C/1.0, C/1.5, and C/s-1.67 are presented. For commercial hydroxyapatite C/c-1.67, the amount of drug released was too small to be determined. As can be observed, after a 14-day immersion, the largest amount of drug is released from brushite (C/1.0), and the amount is practically double that for synthetic hydroxyapatite

(C/s-1.67). In the case of TCP (C/1.5), clindamycin was only able to be determined on day three after immersion in PBS.

Chromatograms for C/s-1.67 powder (after 24 h and 14 days) are presented in Figure 7. The peak for clindamycin was determined at retention times of 5727 (day 1) and 5604 (day 14). The results indicate that the release of clindamycin is dependent on time and type of powder. It was indicated that during incubation, clindamycin content in the liquid increased continuously for 14 days. It was also observed that the smaller the specific surface area of the powder, the faster the drug is released (see Section 3.4 Specific Surface Area and Porosity Studies).

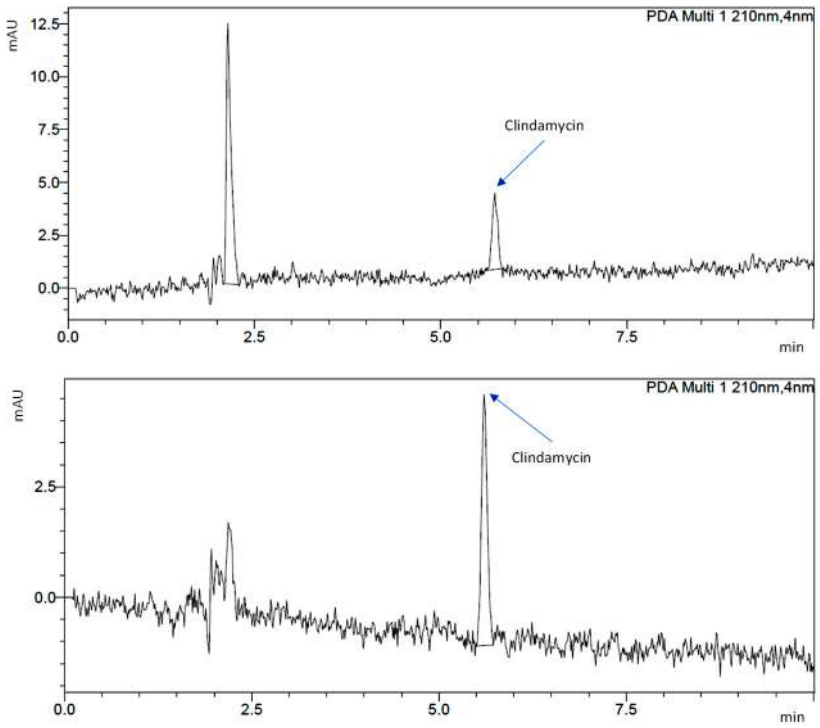

Figure 7. Chromatograms demonstrating drug release from s-1.67: (**a**) after 1 day of incubation and (**b**) after 14 days of incubation.

Finally, it is important to clarify the amount of drug selected for powder modification, a solution with a concentration of 2 mg/mL. The recommended therapeutic dose of clindamycin for an adult (about 70 kg) starts at 150 mg. However, this is the conventional amount that should be taken orally. This means that a sizable portion of the active ingredient will already be degraded in the gastrointestinal tract, and in addition, much of it will undergo general distribution throughout the body. As a result, only a small part of the drug will reach the affected area. Drug carriers being developed for targeted therapy allow the active ingredient to act directly at the site where the therapeutic effect is expected. This involves a significant reduction in the amount of antibiotic the patient should receive. The dose can be increased or decreased depending on individual needs.

3.6. Morphology Analysis

Scanning electron microscopy imaging was carried out to determine the grain shape of each powder (Figure 8). A high similarity was observed between s-1.67 and 1.0. In both cases, the powder took on a flocculent shape in small agglomerates. The flocculent structure can also be seen in the case of commercial hydroxyapatite c-1.67. The most regular, granular shape was observed for TCP 1.5.

Using EDS microanalysis, the presence of individual elements in C-s-1.67 was determined (Figure 9). Au was measured considering the necessity of sputtering the surface of

the samples with gold. Ca and P because these are the main components of the calcium phosphates prepared within this publication. Cl, on the other hand, was determined, in a manner of speaking, to validate the presence of the antibiotic in the modified powder. The molecular formula of clindamycin hydrochloride, as was used during this study, is $C_{18}H_{34}Cl_2N_2O_5S$. Hence, if chlorine ions are present on the EDS mapping, it means that they come directly from the bound drug.

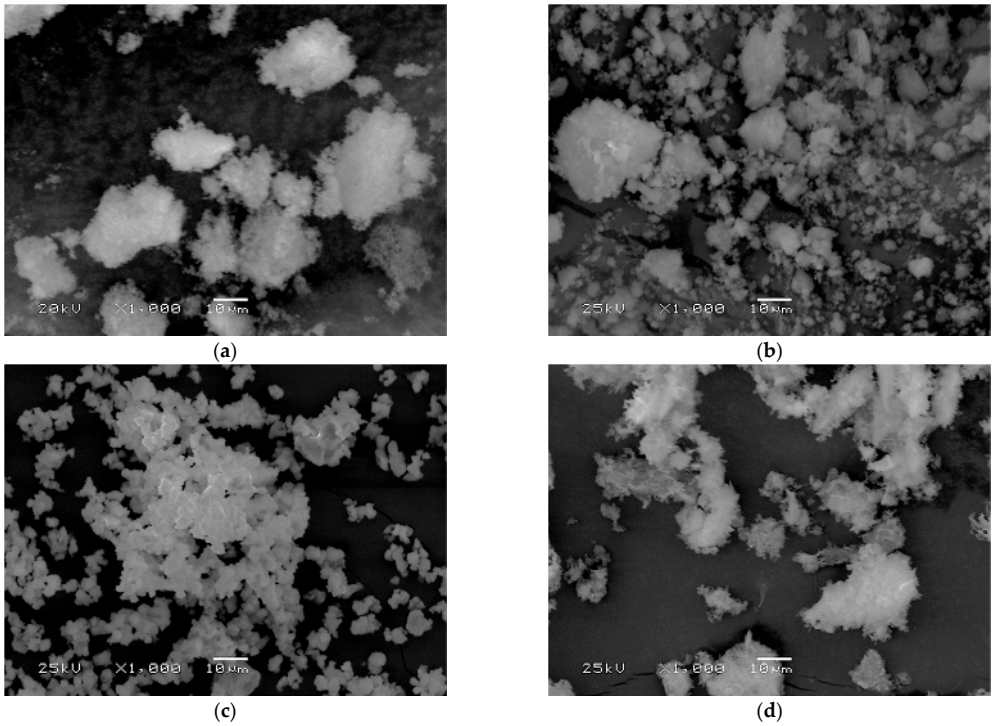

Figure 8. Powder surface morphology for (**a**) s-1.67, (**b**) c-1.67, (**c**) 1.5, and (**d**) 1.0.

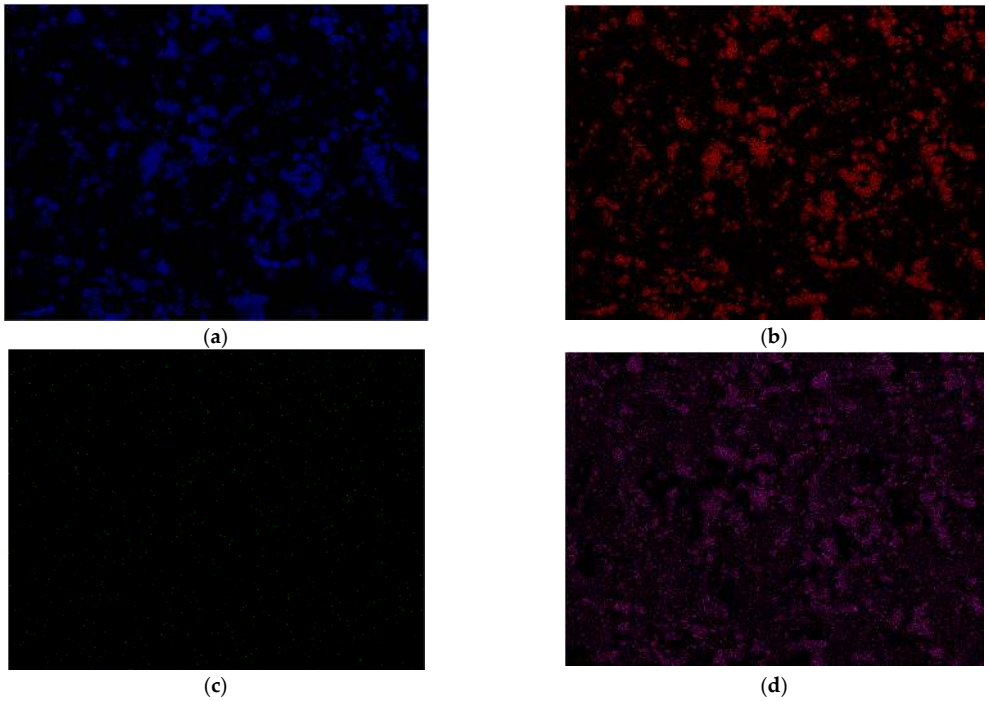

Figure 9. EDS microanalysis for C/s-1.67. Determination of elements (**a**) Ca, (**b**) P, (**c**) Cl, and (**d**) Au.

In the case of Ca and P (blue and red colors), overlapping elemental maps were observed. This is due to the connections between these elements in the structure of calcium phosphates. Small green signals from chlorine were observed, distributed fairly parallel across the entire volume of the test powder. This suggests an effective drug modification and confirms the presence of the antibiotic in the ceramics.

3.7. Antimicrobial Activity of Clindamycin-Modified Ceramic Powders

It was demonstrated that all tested ceramic powders containing clindamycin exhibited strong antibacterial activity towards *Staphylococcus aureus*, which gives evidence that the antibiotic stayed active and in the range of biologically effective concentrations. Whereas materials lacking this antibiotic did not exhibit antimicrobial activity. The MIC values (Table 4) for the C/s-1.67 and C/1.0 ceramic powders were 12.5 μg/mL, which is 100-fold higher than the MIC value of clindamycin, while the C/1.5 ceramic powder showed a higher MIC value equal to 25 μg/mL, and the highest MIC (weakest antimicrobial potential) was observed for the C/c-1.67 ceramic powder. The MIC value for the reference antibiotic, clindamycin, was 0.125 ug/mL, which confirms the susceptibility of the selected strain to clindamycin [52].

Table 4. Minimum inhibitory concentration (MIC) of ceramic powders against *Staphylococcus aureus*.

Ceramic Powder	MIC [μg/mL]
s-1.67	>25,600
C/s-1.67	12.5
c-1.67	>25,600
C/c-1.67	50
1.5	>25,600
C/1.5	25
1.0	>25,600
C/1.0	12.5
Clindamycin	0.125

To address the question of whether the obtained clindamycin-modified powders exhibit antibacterial activity, we have also evaluated MIC_{99} values, defined as a concentration that causes a 99% reduction in the metabolic activity of bacterial cells. Resazurin reduction assay is reported as a non-cytotoxic assay to monitor the metabolic activity and proliferation of live bacterial cells. Resazurin, a non-fluorescent water-soluble dye, is reduced to highly fluorescent resorufin in proportion to the metabolic activity of a bacterial cell population [51]. As illustrated in Figure 10, the lowest MIC_{99} value for all tested clindamycin-loaded ceramics was shown for C/1.0 powder (18.83 ± 1.23 μg/mL), which indicates the strongest antimicrobial activity. We have shown that C/s-1.67 (40.42 ± 5.80 μg/mL) had significantly higher antimicrobial properties compared to the C/c-1.67 (97.74 ± 15.50 μg/mL).

Statistical analyses and graphs for biological studies were performed using GraphPad Prism version 9.1.0 for Windows (GraphPad Software, San Diego, CA, USA). Data were compared using one-way ANOVA with Dunnett's post hoc test.

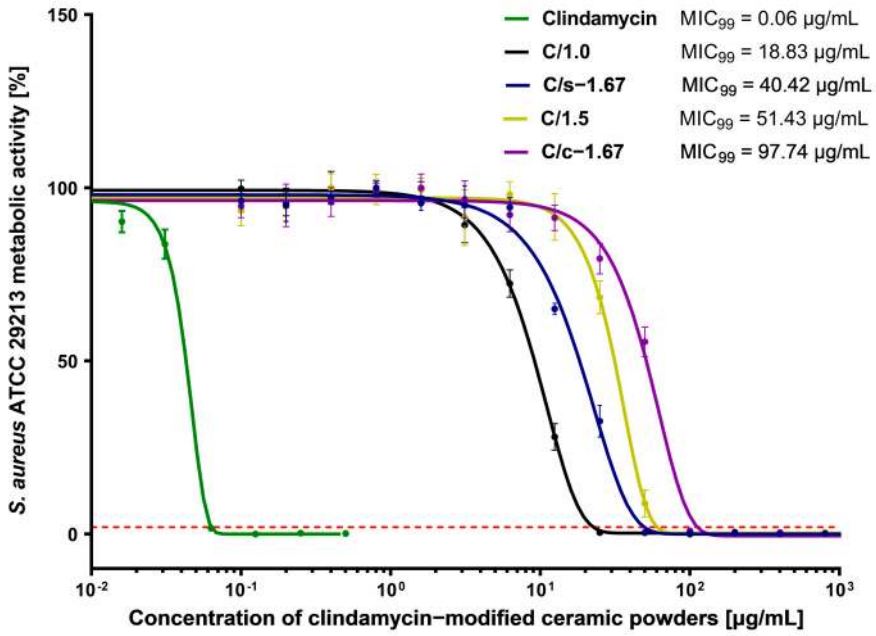

Figure 10. Dose-response curves of clindamycin-modified ceramic powders against *Staphylococcus aureus* ATCC 29213 and MIC_{99} values. The green line represents the reference curve of bacterial metabolic inhibition for clindamycin. The intersection of the dose-effect curves with the red line (the 99% reduction in bacterial metabolic activity) is identified as the MIC_{99} value. Each point represents the averages of four independent experiments in triplicate. Error bars indicate standard deviations.

4. Discussion

In conclusion, ceramic materials with different morphologies have been successfully synthesized by wet precipitation methods. A number of analyses carried out allow us to conclude that the selected methods of synthesis by the wet precipitation technique make it possible to obtain ceramic powders of TCP, brushite, and hydroxyapatite. This fact was confirmed by FTIR analysis, where the main functional groups present in the materials were assigned, as well as by XRD analysis, in which the obtained diffractograms were related to the corresponding data sheets. All powders were phase-pure; however, the observed background spectrum suggests that they are only partially crystalline and partially amorphous. In addition, hydroxyapatite s-1.67 was compared with its commercial counterpart, c-1.67. Presumably, high-temperature calcination would enable materials with a higher degree of crystallinity to be obtained. This study also confirmed that based on the same substrates, changing only their starting ratios and not changing the process conditions, it is possible to obtain both synthetic hydroxyapatite s-1.67 and TCP 1.5. This is an important fact considering the different properties of the two materials and their potential applications.

The chosen physical sorption method was successful in modifying ceramic powders. This is evidenced by the presence of chlorine ions derived from the drug as detected by SEM-EDS. However, it can be concluded that the materials, especially the commercial c-1.67, do not show high clindamycin loading efficiency. A relationship was observed between the specific surface area of the ceramic and drug release. The smaller the specific surface area, the faster the drug is released. This is in accordance with literature reports, as a larger pore surface area would result in a more efficient migration of the drug into the interior of the ceramic and, thus, a later, longer drug release [64]. Drug adsorption on ceramic powders is mainly accomplished by forming bonds between Ca^{2+} ions on the ceramic surface and oxygen atoms in the drug molecule [65]. This study exhibits that the degree of crystallinity of the tested nanopowders influences the loading capacity of the active substance, as well as the amount of drug released. For sample 1.0, with a degree of crystallinity of 75.1%, the highest concentration of clindamycin was obtained. However,

a different correlation was observed for sample 1.5, where the degree of crystallinity is the highest, while less drug was released.

Determining the pore size distribution, the smallest pores observed were for brushite, a ceramic with a Ca/P ratio of 1.0, and synthetic hydroxyapatite s-1.67. A biological correlation was observed for these powders, as these two powders demonstrated the highest antimicrobial ability. Naturally, pure clindamycin exhibited the greatest antimicrobial ability against *Staphylococcus aureus*, while the ceramic powders themselves not modified with the drug did not demonstrate it at all. A close correlation was observed between the results obtained for the biological tests on antimicrobial capacity and the results for drug release from HPLC.

The studies presented in this manuscript confirm the effect of specific surface area on the nature of modification of porous powders by physical sorption, as well as the subsequent rate of drug release. Considering that the s-1.67 and 1.5 powders were based on the same method, the same conditions were maintained during synthesis, and only the concentration of initial substrates differed, it suggests that this aspect also affects the size of the specific surface area since a slight difference was observed between the values for these powders. However, it can be concluded that ceramic porous materials have been successfully synthesized as a drug carrier for targeted therapy.

Author Contributions: Conceptualization, D.S. and K.P.; methodology, D.S., K.P., M.M.U., A.T. (Agnieszka Tomala) and A.T. (Agata Tomaszewska); software, W.F., M.M.U. and A.T. (Agnieszka Tomala); validation, W.F., A.T. (Agnieszka Tomala), K.P. and D.S.; formal analysis, D.S., K.P. and M.M.U.; investigation, D.S., K.P., W.F., A.T. (Agnieszka Tomala), M.M.U. and A.T. (Agata Tomaszewska); resources, A.S.-K., J.J. and K.R.; data curation, A.S.-K., J.J. and K.R.; writing—original draft preparation, K.P., D.S., M.M.U., A.T. (Agnieszka Tomala) and A.T. (Agata Tomaszewska); writing—review and editing, A.S.-K., J.J. and K.R.; visualization, D.S. and K.P.; supervision, A.S.-K., J.J. and K.R.; project administration, A.S.-K.; funding acquisition, A.S.-K. All authors have read and agreed to the published version of the manuscript.

Funding: This research was funded by the Foundation for Polish Science, grant number POIR.04.04.00-00-16D7/18. This work was also partially supported by the project APVV-17-0373 and by the Operation Program of Integrated Infrastructure for the project, UpScale of Comenius University Capacities and Competence in Research, Development and Innovation, ITMS2014+:313021BUZ3, co-financed by the European Regional Development Fund.

Data Availability Statement: Data that support the findings of this study are contained within the article.

Acknowledgments: The "Multifunctional biologically active composites for applications in bone regenerative medicine" project is carried out within the TEAM-NET program of the Foundation for Polish Science, financed by the European Union under the European Regional Development Fund. The authors gratefully acknowledge financial support. The research work was also carried out within the SMART-MAT Functional Materials Science Club (BioMat section) at the Faculty of Materials Engineering and Physics of the Cracow University of Technology.

Conflicts of Interest: The authors declare no conflict of interest.

References

1. Zang, S.; Chang, S.; Shahzad, M.B.; Sun, X.; Jiang, X.; Yang, H. Ceramics-based Drug Delivery System: A Review and Outlook. *Rev. Adv. Mater. Sci.* **2019**, *58*, 82–97. [CrossRef]
2. Trucillo, P. Drug Carriers: Classification, Administration, Release Profiles, and Industrial Approach. *Processes* **2021**, *9*, 470. [CrossRef]
3. Adeyemi, O.S.; Sulaiman, F.A. Evaluation of metal nanoparticles for drug delivery systems. *J. Biomed. Res.* **2015**, *29*, 145–149. [CrossRef]
4. Kong, F.Y.; Zhang, J.W.; Li, R.F.; Wang, Z.X.; Wang, W.J.; Wang, W. Unique roles of gold nanoparticles in drug delivery, targeting and imaging applications. *Molecules* **2017**, *22*, 1445. [CrossRef]
5. Singh, P.; Pandit, S.; Mokkapati, V.R.S.S.; Garg, A.; Ravikumar, V.; Mijakovic, I. Gold nanoparticles in diagnostics and therapeutics for human cancer. *Int. J. Mol. Sci.* **2018**, *19*, 1979. [CrossRef] [PubMed]
6. Jampilek, J.; Kralova, K. Advances in drug delivery nanosystems using graphene-based materials and carbon nanotubes. *Materials* **2021**, *14*, 1059. [CrossRef] [PubMed]

7. Tanaka, M.; Aoki, K.; Haniu, H.; Kamanaka, T.; Takizawa, T.; Sobajima, A.; Yoshida, K.; Okamoto, M.; Kato, H.; Saito, N. Applications of carbon nanotubes in bone regenerative medicine. *Nanomaterials* **2020**, *10*, 659. [CrossRef]
8. Anisimov, R.A.; Gorin, D.A.; Abalymov, A.A. 3D Cell Spheroids as a Tool for Evaluating the Effectiveness of Carbon Nanotubes as a Drug Delivery and Photothermal Therapy Agents. *C* **2022**, *8*, 56. [CrossRef]
9. Nair, A.; Haponiuk, J.T.; Thomas, S.; Gopi, S. Natural carbon-based quantum dots and their applications in drug delivery: A review. *Biomed. Pharmacother.* **2020**, *132*, 110834. [CrossRef]
10. Iannazzo, D.; Pistone, A.; Celesti, C.; Triolo, C.; Patané, S.; Giofré, S.V.; Romeo, R.; Ziccarelli, I.; Mancuso, R.; Gabriele, B.; et al. A smart nanovector for cancer targeted drug delivery based on graphene quantum dots. *Nanomaterials* **2019**, *9*, 282. [CrossRef]
11. Mousavi, S.M.; Hashemi, S.A.; Kalashgrani, M.Y.; Omidifar, N.; Bahrani, S.; Rao, N.V.; Babapoor, A.; Gholami, A.; Chiang, W.H. Bioactive Graphene Quantum Dots Based Polymer Composite for Biomedical Applications. *Polymers* **2022**, *14*, 617. [CrossRef]
12. Festas, A.J.; Ramos, A.; Davim, J.P. Medical devices biomaterials—A review. *Proc. Inst. Mech. Eng. Part L J. Mater. Des. Appl.* **2020**, *234*, 218–228. [CrossRef]
13. Li, H.; Li, C.; Wu, L.; Wang, H.; Li, J.; Fu, M.; Wang, C.A. In-situ synthesis and properties of porous cordierite ceramics with adjustable pore structure. *Ceram. Int.* **2020**, *46*, 14808–14815. [CrossRef]
14. Gbureck, U.; Vorndran, E.; Barralet, J.E. Modeling vancomycin release kinetics from microporous calcium phosphate ceramics comparing static and dynamic immersion conditions. *Acta Biomater.* **2008**, *4*, 1480–1486. [CrossRef] [PubMed]
15. Zamoume, O.; Thibault, S.; Regnié, G.; Mecherri, M.O.; Fiallo, M.; Sharrock, P. Macroporous calcium phosphate ceramic implants for sustained drug delivery. *Mater. Sci. Eng. C* **2011**, *31*, 1352–1356. [CrossRef]
16. Vezenkova, A.; Locs, J. Sudoku of porous, injectable calcium phosphate cements—Path to osteoinductivity. *Bioact. Mater.* **2022**, *17*, 109–124. [CrossRef]
17. Mahjoory, M.; Shahgholi, M.; Karimipour, A. The Effects of Initial Temperature and Pressure on the Mechanical Properties of Reinforced Calcium Phosphate Cement with Magnesium Nanoparticles; a Molecular Dynamics Approach. *SSRN Electron. J.* **2022**, *135*, 106067. [CrossRef]
18. Kołodziejska, B.; Kaflak, A.; Kolmas, J. Biologically inspired collagen/apatite composite biomaterials for potential use in bone tissue regeneration—A review. *Materials* **2020**, *13*, 1748. [CrossRef]
19. Motameni, A.; Alshemary, A.Z.; Evis, Z. A review of synthesis methods, properties and use of monetite cements as filler for bone defects. *Ceram. Int.* **2021**, *47*, 13245–13256. [CrossRef]
20. Braga, R.R. Calcium phosphates as ion-releasing fillers in restorative resin-based materials. *Dent. Mater.* **2019**, *35*, 3–14. [CrossRef]
21. Dorozhkin, S.V. Calcium orthophosphates ($CaPO_4$): Occurrence and properties. *Prog. Biomater.* **2015**, *5*, 9–70. [CrossRef] [PubMed]
22. Matsuya, S.; Takagi, S.; Chow, L.C. Effect of mixing ratio and pH on the reaction between $Ca_4(PO_4)_2O$ and $CaHPO_4$. *J. Mater. Sci. Mater. Med.* **2000**, *1*, 305–311. [CrossRef] [PubMed]
23. Ślósarczyk, A. *Bioceramika Hydroksyapatytowa*; Biuletyn Ceramiczny nr 13 Ceramika 51; Polskie Towarzystwo Ceramiczne: Kraków, Poland, 1997.
24. Harb, S.V.; Bassous, N.J.; de Souza, T.A.C.; Trentin, A.; Pulcinelli, S.H.; Santilli, C.V.; Webster, T.J.; Lobo, A.O.; Hammer, P. Hydroxyapatite and β-TCP modified PMMA-TiO_2 and PMMA-ZrO_2 coatings for bioactive corrosion protection of Ti6Al4V implants. *Mater. Sci. Eng. C* **2020**, *116*, 111149. [CrossRef]
25. Damerau, J.M.; Bierbaum, S.; Wiedemeier, D.; Korn, P.; Smeets, R.; Jenny, G.; Nadalini, J.; Stadlinger, B. A systematic review on the effect of inorganic surface coatings in large animal models and meta-analysis on tricalcium phosphate and hydroxyapatite on periimplant bone formation. *J. Biomed. Mater. Res. Part B Appl. Biomater.* **2022**, *110*, 157–175. [CrossRef] [PubMed]
26. Shalini, B.; Kumar, A.R. A comparative study of hydroxyapatite ($Ca_{10}(PO_4)_6(OH)_2$) using sol-gel and co-precipitation methods for biomedical applications. *J. Indian Cham. Soc.* **2019**, *96*, 25–28.
27. De Aza, P.N.; Rodríguez, M.A.; Gehrke, S.A.; Maté-Sánchez de Val, J.E.; Calvo-Guirado, J.L. A Si-αTCP scaffold for biomedical applications: An experimental study using the rabbit tibia model. *Appl. Sci.* **2017**, *7*, 706. [CrossRef]
28. Horch, H.H.; Sader, R.; Pautke, C.; Neff, A.; Deppe, H.; Kolk, A. Synthetic, pure-phase beta-tricalcium phosphate ceramic granules (Cerasorb®) for bone regeneration in the reconstructive surgery of the jaws. *Int. J. Oral Maxillofac. Surg.* **2006**, *35*, 708–713. [CrossRef]
29. Sánchez-Salcedo, S.; Arcos, D.; Vallet-Regí, M. Upgrading Calcium Phosphate Scaffolds for Tissue Engineering Applications. *Key Eng. Mater.* **2008**, *377*, 19–42. [CrossRef]
30. Mirkiani, S.; Mesgar, A.S.; Mohammadi, Z.; Matinfar, M. Synergetic reinforcement of brushite cements by monetite/apatite whisker-like fibers and carboxymethylcellulose. *Materialia* **2022**, *21*, 101329. [CrossRef]
31. Hurle, K.; Maia, F.R.; Ribeiro, V.P.; Pina, S.; Oliveira, J.M.; Goetz-Neunhoeffer, F.; Reis, R.L. Osteogenic lithium-doped brushite cements for bone regeneration. *Bioact. Mater.* **2022**, *16*, 403–417. [CrossRef]
32. Ben-Nissan, B. *Advances in Calcium Phosphate Biomaterials*; Springer: Berlin/Heidelberg, Germany, 2014.
33. Qadir, M.; Li, Y.; Wen, C. Ion-substituted calcium phosphate coatings by physical vapor deposition magnetron sputtering for biomedical applications: A review. *Acta Biomaterialia* **2019**, *89*, 14–32. [CrossRef] [PubMed]
34. Tavoni, M.; Dapporto, M.; Tampieri, A.; Sprio, S. Bioactive calcium phosphate-based composites for bone regeneration. *J. Compos. Sci.* **2021**, *5*, 227. [CrossRef]
35. Jeong, J.; Kim, J.H.; Shim, J.H.; Hwang, N.S.; Heo, C.Y. Bioactive calcium phosphate materials and applications in bone regeneration. *Biomater. Res.* **2019**, *23*, 4. [CrossRef]

36. Frank, O.; Heim, M.; Jakob, M.; Barbero, A.; Schäfer, D.; Bendik, I.; Dick, W.; Heberer, M.; Martin, I. Real-time quantitative RT-PCR analysis of human bone marrow stromal cells during osteogenic differentiation in vitro. *J. Cell. Biochem.* **2002**, *85*, 737–746. [CrossRef] [PubMed]
37. Whited, B.M.; Skrtic, D.; Love, B.J.; Goldstein, A.S. Osteoblast response to zirconia-hybridized pyrophosphate-stabilized amorphous calcium phosphate. *J. Biomed. Mater. Res. Part A* **2006**, *76A*, 596–604. [CrossRef]
38. Orimo, H. The mechanism of mineralization and the role of alkaline phosphatase in health and disease. *Nippon Med. Sch.* **2010**, *77*, 4–12. [CrossRef]
39. Bystrova, A.V.; Dekhtyar, Y.D.; Popov, A.I.; Coutinho, J.; Bystrov, V.S. Modified hydroxyapatite structure and properties: Modeling and synchrotron data analysis of modified hydroxyapatite structure. *Ferroelectrics* **2015**, *475*, 135–147. [CrossRef]
40. Hübner, W.; Blume, A.; Pushnjakova, R.; Dekhtyar, Y.; Hein, H.J. The influence of X-ray radiation on the mineral/organic matrix interaction of bone tissue: An FT-IR microscopic investigation. *Int. J. Artif. Organs* **2005**, *28*, 66–73. [CrossRef]
41. Moroi, H.; Kimura, K.; Ido, A.; Banno, H.; Jin, W.; Wachino, J.I.; Yamada, K.; Kikkawa, F.; Park, Y.J.; Arakawa, Y. Erythromycin-susceptible but clindamycin-resistant phenotype of clinical ermb-pcr-positive group b streptococci isolates with is1216e-inserted ermb. *Jpn. J. Infect. Dis.* **2019**, *72*, 420–422. [CrossRef]
42. Hu, H.; Ramezanpour, M.; Hayes, A.J.; Liu, S.; Psaltis, A.J.; Wormald, P.J.; Vreugde, S. Sub-inhibitory clindamycin and azithromycin reduce s. Aureus exoprotein induced toxicity, inflammation, barrier disruption and invasion. *J. Clin. Med.* **2019**, *8*, 1617. [CrossRef]
43. Ahmadi, H.; Ebrahimi, A.; Ahmadi, F. Antibiotic Therapy in Dentistry. *Int. J. Dent.* **2021**, *2021*, 1–10. [CrossRef] [PubMed]
44. Álvarez, L.A.; Van de Sijpe, G.; Desmet, S.; Metsemakers, W.J.; Spriet, I.; Allegaert, K.; Rozenski, J. Ways to Improve Insights into Clindamycin Pharmacology and Pharmacokinetics Tailored to Practice. *Antibiotics* **2022**, *11*, 701. [CrossRef]
45. Słota, D.; Florkiewicz, W.; Piętak, K.; Pluta, K.; Sadlik, J.; Miernik, K.; Sobczak-Kupiec, A. Preparation of PVP and betaine biomaterials enriched with hydroxyapatite and its evaluation as a drug carrier for controlled release of clindamycin. *Ceram. Int.* **2022**, *48*, 35467–35473. [CrossRef]
46. Słota, D.; Florkiewicz, W.; Piętak, K.; Szwed, A.; Włodarczyk, M.; Siwińska, M.; Rudnicka, K.; Sobczak-Kupiec, A. Preparation, Characterization, and Biocompatibility Assessment of Polymer-Ceramic Composites Loaded with Salvia officinalis Extract. *Materials* **2021**, *14*, 6000. [CrossRef] [PubMed]
47. Tomala, A.M.; Słota, D.; Florkiewicz, W.; Piętak, K.; Dyląg, M.; Sobczak-Kupiec, A. Tribological Properties and Physiochemical Analysis of Polymer-Ceramic Composite Coatings for Bone Regeneration. *Lubricants* **2022**, *10*, 58. [CrossRef]
48. Sawada, M.; Sridhar, K.; Kanda, Y.; Yamanaka, S. Pure hydroxyapatite synthesis originating from amorphous calcium carbonate. *Sci. Rep.* **2021**, *11*, 1–9. [CrossRef]
49. Słota, D.; Florkiewicz, W.; Sobczak-Kupiec, A. Ceramic-polymer coatings on Ti-6Al-4V alloy modified with L-cysteine in biomedical applications. *Mater. Today Commun.* **2020**, *25*, 101301. [CrossRef]
50. Florkiewicz, W.; Słota, D.; Placek, A.; Pluta, K.; Tyliszczak, B.; Douglas, T.E.L.; Sobczak-Kupiec, A. Synthesis and characterization of polymer-based coatings modified with bioactive ceramic and bovine serum albumin. *J. Funct. Biomater.* **2021**, *12*, 21. [CrossRef]
51. Gong, X.; Liang, Z.; Yang, Y.; Liu, H.; Ji, J.; Fan, Y. A resazurin-based, nondestructive assay for monitoring cell proliferation during a scaffold-based 3D culture process. *Regen. Biomater.* **2020**, *7*, 271–281. [CrossRef]
52. European Committee on Antimicrobial Susceptibility Testing. *Breakpoint Tables for Interpretation of MICs and Zone Diameters*, Version 13.0; European Committee on Antimicrobial Susceptibility Testing: Växjö, Sweden, 2013.
53. Bilton, M.W. Nanoparticulate Hydroxyapatite and Calcium—Based CO_2 Sorbents. Ph.D. Thesis, University of Leeds, Leeds, UK, 2012; pp. 201–282.
54. Chang, M.C. Use of Wet Chemical Method to Prepare β Tri-Calcium Phosphates having Macro- and Nano-crystallites for Artificial Bone. *J. Korean Ceram. Soc.* **2016**, *53*, 670–675. [CrossRef]
55. Nur, A.; Jumari, A.; Budiman, A.W.; Wicaksono, A.H.; Nurohmah, A.R.; Nazriati, N.; Fajaroh, F. Synthesis of nickel—Hydroxyapatite by electrochemical method. *IOP Conf. Ser. Mater. Sci. Eng.* **2019**, *543*, 012026. [CrossRef]
56. Binitha, M.P.; Pradyumnan, P.P. Dielectric Property Studies of Biologically Compatible Brushite Single Crystals Used as Bone Graft Substitute. *J. Biomater. Nanobiotechnol.* **2013**, *4*, 119–122. [CrossRef]
57. Mansour, S.F.; El-dek, S.I.; Ahmed, M.A.; Abd-Elwahab, S.M.; Ahmed, M.K. Effect of preparation conditions on the nanostructure of hydroxyapatite and brushite phases. *Appl. Nanosci.* **2016**, *6*, 991–1000. [CrossRef]
58. Ding, X.; Li, A.; Yang, F.; Sun, K.; Sun, X. B-Tricalcium Phosphate and Octacalcium Phosphate Composite Bioceramic Material for Bone Tissue Engineering. *J. Biomater. Appl.* **2020**, *34*, 1294–1299. [CrossRef]
59. Duarte Moreira, A.P.; Soares Sader, M.; De Almeida Soares, G.D.; Leão, M.H.M.R. Strontium incorporation on microspheres of alginate/β-tricalcium phosphate as delivery matrices. *Mater. Res.* **2014**, *17*, 967–973. [CrossRef]
60. Besleaga, C.; Nan, B.; Popa, A.C.; Balescu, L.M.; Nedelcu, L.; Neto, A.S.; Pasuk, I.; Leonat, L.; Popescu-Pelin, G.; Ferreira, J.M.F.; et al. Sr and Mg Doped Bi-Phasic Calcium Phosphate Macroporous Bone Graft Substitutes Fabricated by Robocasting: A Structural and Cytocompatibility Assessment. *J. Funct. Biomater.* **2022**, *13*, 123. [CrossRef] [PubMed]
61. Rojas-Montoya, I.D.; Fosado-Esquivel, P.; Henao-Holguín, L.V.; Esperanza-Villegas, A.E.; Bernad-Bernad, M.J.; Gracia-Mora, J. Adsorption/desorption studies of norfloxacin on brushite nanoparticles from reverse microemulsions. *Adsorption* **2020**, *26*, 825–834. [CrossRef]

62. Sayahi, M.; Santos, J.; El-Feki, H.; Charvillat, C.; Bosc, F.; Karacan, I.; Milthorpe, B.; Drouet, C. Brushite (Ca,M)HPO_4, $2H_2O$ doping with bioactive ions (M = Mg^{2+}, Sr^{2+}, Zn^{2+}, Cu^{2+}, and Ag^{+}): A new path to functional biomaterials? *Mater. Today Chem.* **2020**, *16*, 100230. [CrossRef]
63. Idowu, B.; Cama, G.; Deb, S.; Di Silvio, L. In vitro osteoinductive potential of porous monetite for bone tissue engineering. *J. Tissue Eng.* **2014**, *5*, 1–4. [CrossRef]
64. Ma, M.Y.; Zhu, Y.J.; Li, L.; Cao, S.W. Nanostructured porous hollow ellipsoidal capsules of hydroxyapatite and calcium silicate: Preparation and application in drug delivery. *J. Mater. Chem.* **2008**, *18*, 2722–2727. [CrossRef]
65. Zhao, Q.; Zhang, D.; Sun, R.; Shang, S.; Wang, H.; Yang, Y.; Wang, L.; Liu, X.; Sun, T.; Chen, K. Adsorption behavior of drugs on hydroxyapatite with different morphologies: A combined experimental and molecular dynamics simulation study. *Ceram. Int.* **2019**, *45*, 19522–19527. [CrossRef]

lubricants

MDPI

Article

Tribological Properties and Physiochemical Analysis of Polymer-Ceramic Composite Coatings for Bone Regeneration

Agnieszka Maria Tomala [1,*], Dagmara Słota [1], Wioletta Florkiewicz [1], Karina Piętak [1], Mateusz Dyląg [1,2] and Agnieszka Sobczak-Kupiec [1]

[1] Department of Materials Science, Faculty of Materials Engineering and Physics, Cracow University of Technology, 37 Jana Pawła II Av., 31-864 Cracow, Poland; dagmara.slota@doktorant.pk.edu.pl (D.S.); wioletta.florkiewicz@pk.edu.pl (W.F.); karina.pietak@doktorant.pk.edu.pl (K.P.); mateusz.dylag@atmat.pl (M.D.); agnieszka.sobczak-kupiec@pk.edu.pl (A.S.-K.)

[2] ATMAT Sp. z o.o., Siwka 17, 31-588 Cracow, Poland

* Correspondence: agnieszka.tomala@pk.edu.pl

Abstract: The biomaterial coatings for bone tissue regeneration described in this study promote bioactivity. The ceramic-polymer composite coatings deposited on polylactide (PLA) plates contain polymers, namely polyvinylpyrrolidone (PVP)/polyethylene glycol (PEG), while the ceramic phase is hydroxyapatite (HA). Additionally, collagen (COL) and glutathione (GSH) are components of high biological value. Bone tissue materials requires additionally demanding tribological properties, which are thoroughly described in this research. These findings, presented herein for the first time, characterize this type of highly specific composite coating material and their indicate possible application in bone regeneration implants. Implementation of the collagen in the PVP/PEG/HA composite matrix can tailor demanding tribological performance, e.g., anti-wear and friction reduction. The addition of the ceramic phase in too high a content (15%) leads to the decreased swelling ability of materials and slower liquid medium absorption by composite coatings, as well as strong surface roughening and loosening tribological properties. In consequence, small particles of HA from the very rough composite crumble, having a strong abrasive effect on the sample surface. In conclusion, sample C composed of PVP/PEG/GSH/COL/HA (5%) exhibits high bioactivity, strong mechanical and tribological properties, the highest free surface energy, porosity, and accepted roughness to be implemented as a material for bone regeneration.

Keywords: biomaterials; coatings; hydroxyapatite; tribology

Citation: Tomala, A.M.; Słota, D.; Florkiewicz, W.; Piętak, K.; Dyląg, M.; Sobczak-Kupiec, A. Tribological Properties and Physiochemical Analysis of Polymer-Ceramic Composite Coatings for Bone Regeneration. *Lubricants* **2022**, *10*, 58. https://doi.org/10.3390/lubricants10040058

Received: 2 March 2022
Accepted: 22 March 2022
Published: 2 April 2022

1. Introduction

A significant feature of medical devices including implants that has been emphasized in recent years is their multifunctionality to ensure effective and long-lasting function. One solution that can provide this involves coating the implants, thereby creating specific films [1]. The coating technique requires a layer of another biomaterial to cover the surface of the implant [2]. Coating implants is one strategy used to increase biocompatibility as well as provide additional features without changing the based material. In the case of materials developed for bone regeneration, coating can be used to add the desired feature of improved osseointegration. Furthermore, coating implants with a layer can be very useful in increasing tissue cell adhesion to the surface and inhibiting bacterial colonization [3]. The most effective osseointegration-promoting properties can be achieved by coating the materials with bioactive calcium phosphate ceramics (CaP). The presence of a bioactive CaP coating can not only help to form a stable interface between the implant and the bone, but also block the diffusion of toxic elements from the implant into the body, especially when coating metallic components [4,5].

Osseointegration itself depends on the mechanical bonding between bone and implant after surgical placement as well as the cellular response at the bone-implant interface, hence the importance of proper material selection [6]. Therefore, among the CaP, hydroxyapatite (HA) is particularly interesting in the context of bone regeneration as it exhibits osteoconductive abilities that are important in this process [7]. A better connection between the implant and natural tissue eliminates the danger of implant loosening, which has contributed to the failure of biomaterial application in the patient's body over the past two decades [8]. Frequently, HA itself is used as a coating material by applying it to the implant surface by various techniques, including plasma spraying or laser surface treatment [9,10]. Of particular interest in this aspect is the ability to provide osteoconductive conditions through which surrounding tissues can bind to HA [11]. Additionally, it can be modified with Sr and Zn ions to impart antimicrobial properties or increase wettability [12]. However, it is still difficult to eliminate the basic application limitations of HA, which are brittleness and low mechanical strength. These properties limits its potential in terms of use for load-bearing implants [13]. The solution to this problem may be to suspend the HA in a polymer matrix, as this will give flexibility [14,15].

As polymeric biomaterials, polymers that are biologically safe and do not exhibit cytotoxicity or allergic reactions are used [16]. Polyvinylopirolidone (PVPP) is a water-soluble substance approved by the U.S. Food and Drug Administration (FDA) as non-toxic and safe for body contact [17,18]. It exhibits excellent physiological biocompatibility as well as good adhesion [19,20]. Another synthetic polymer that is also characterized by high solubility, biocompatibility, as well as good tolerance is poly(ethylene glycol) (PEG). It is non-immunogenic and for this reason is suitable for medical applications, including as a carrier for active substances [21,22]. Furthermore, the FDA has approved PEG-conjugated drugs for safe use in humans [23]. An otherwise equally interesting polymeric material being considered for bone tissue regeneration is polylactic acid (PLA). Due to its properties, such as biocompatibility, biodegradability, and osteoconductive ability, it is used as a material for drug delivery systems, surgical implants, as well as tissue growth films [24–27].

The presented work describes the results of research on innovative ceramic–polymer composite coatings containing glutathione and bioactive calcium phosphate for bone tissue regeneration. The objective of this study was to obtain a highly flexible and wear-resistant composite coating for implants. The materials have great potential considering the high biological value of the components used in their synthesis, such as glutathione and hydroxyapatite, which promote osteogenesis. So far, no other solution of this type has been found.

2. Materials and Methods

2.1. Reagents

The reagents used for the synthesis of HA, i.e., the sodium phosphate dibasic (Na_2HPO_4) (7558-79-4), calcium acetate monohydrate ($Ca(CH_3CO_2)_2 \cdot H_2O$) (5743-26-0), and ammonia water (NH_4OH, 25%) (1336-21-6), as well as polymers polyvinylpyrrolidone (PVP) (9003-39-8), polyethylene glycol (PEG) (25322-68-3), poly(ethylene glycol) Mn 575 diacrylate Mn 575 (PEGDA) (26570-48-9), 2-hydroxy-2-methylpropiophenone 97% (7473-98-5), peptide l-glutathione reduced 98% (GSH) (70-18-8), collagen from bovine achilles tendon (COL) (9007-34-5), and diiodomethane 99% (75-11-6) were obtained from Sigma-Aldrich (Darmstadt, Germany). Ultra-high quality (UHQ) water was purchased from Elga Purelab UHQ (Marlow, Buckinghamshire, UK).

2.2. Preparation of Coatings

A 15% PVP solution and a 15% PEG solution were prepared to obtain mixtures for the preparation of composites. Suitable amounts of the solutions so prepared and HA powder obtained as previously in [28] were used to obtain the blends used for the preparation of coatings. In the first step, 0.25 mL of PVP 15% mixture with GSH was applied to polylactide (PLA) plates with dimensions of 2 cm × 2 cm × 2 mm, obtained by 3D printing by the fused deposition modeling technique, and crosslinked under UV light using Medilux UV 436 HF

(Medilux, Korntal-Münchingen, Germany) lamp (220 V, 60 Hz) for 2 min. Then, coatings with the composition presented in Table 1 were applied to the crosslinked layer and placed under UV light for 4 min. The obtained coatings on PLA plates are presented in Figure 1. In order to measure the thickness, the coatings were scratched/indented in a few regions of the coatings surface. The results are given in Figure 1. The surface morphologies were imaged using a VHX Series Digital Microscope (Keyence, Osaka, Japan). A high-performance camera provided the total image resolution of 4000 pixels (H) × 3000 pixels (V) with 4 K mode on. The high-resolution HDR function allows observation at magnification from 20× down to 2500× of low contrasting parts or parts with significant height variation using additional depth composition. The multi-lighting function was used in order to detect the morphology of the coatings presented in Figure 1. The 4 K CMOS Sensor of the VHZ-7000 series (Keyence, Osaka, Japan) allowed to perform 2D and 3D measurements, including measurement of the roughness profile.

Table 1. Coatings composition.

Sample Symbol	PVP (mL)	PEG (mL)	GSH (g)	COL (g)	HA [% *w*/*v*]	PEGDA (mL)	Photoinitiator (µL)
A	5	5	2	-	-	1.8	50
B				0.04	-		
C					5		
D					15		

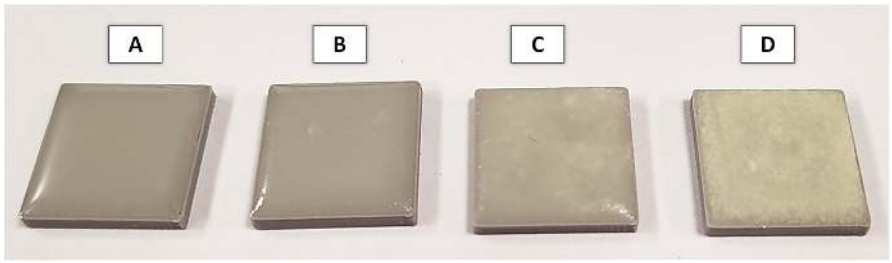

(**a**)

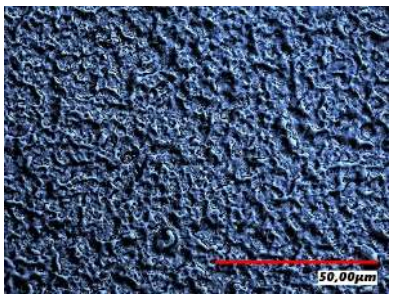

Sample A (548 ± 5 µm)

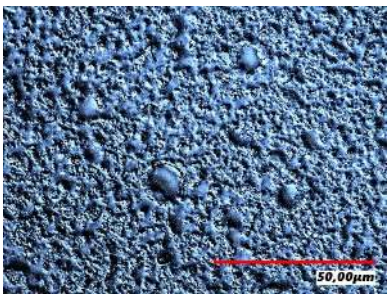

Sample B (700 ± 8 µm)

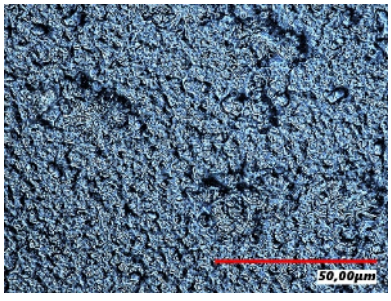

Sample C (605 ± 9 µm)

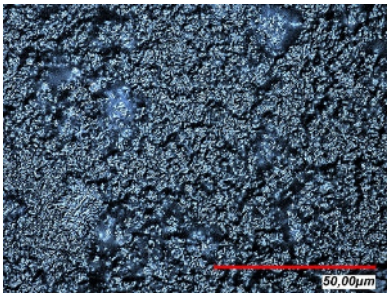

Sample D (680 ± 12 µm)

(**b**)

Figure 1. (**a**) The obtained on PLA plates; (**b**) high resolution microscope micrographs at magnification 2500×, including coatings thicknesses [µm].

2.3. Fourier-Transform Infrared Spectroscopy Analysis

Fourier transform infrared (FT-IR) spectroscopy was used to identify individual functional groups in pure components (PVP, PEG, COL, GSH, HA) and samples. The analysis was carried out under room conditions using a Nicolet iS5 FT-IR spectrometer equipped with an iD7 ATR attachment (Thermo Scientific, Loughborough, UK) in the range of 4000–400 cm^{-1} (32 scans at 4.0 cm^{-1} resolution).

2.4. Determination of Sorption Capacity

To determine the effect of coatings composition on their swelling kinetic, the prepared samples were incubated in distilled water at 36.6 °C for 7 days. The swelling ability of the coatings immersed in water was calculated in accordance with the following formula:

$$\text{Swelling ability } = \frac{m_1 - m_0}{m_0} \times 100\% \quad (1)$$

where:

m_1—the weight of immersed sample (g)
m_0—the initial weight of specimen (g)

The kinetic of coatings swelling was investigated by Voigt-based viscoelastic model Equation (2) [29]. To determine rate parameters and equilibrium swelling, Origin software was used.

$$S_t = S_e[1 - e^{-\frac{t}{\tau}}] \quad (2)$$

where:

S_t—swelling at given time t (%),
S_e—equilibrium swelling (power parameter) (%),
t—time for swelling S_t (min),
τ—the "rate parameter" (min).

2.5. Surface Topography and Roughness

The surface roughness was measured using a stylus line contact profilometer TALYSURF PGI 830 (Taylor Hobson, San Francisco, CA, USA). Phase Grating Interferometer (PGI) measurement was realized in the relationship between stylus tip movement (input) and response in the gauge head electronics (output) throughout the total measuring range. Stylus arms have a diamond tip with standard coarse tip radius of 2 µm and tip angle of 90°. Surface roughness was determined according to ISO 4287 with stylus acquisition mode from a line distance of 4 mm. The roughness profile, including parameters Ra (roughness), Rq (kurtosis), and Rsk (skewness), numerically describe the topography of the measured surfaces. Ra characterizes the departures of the roughness profile from the mean line, and Rq is the rms (root mean square) parameter corresponding to Ra. The skewness (Rsk), describing the asymmetry of the profile about the mean line, showed a tendency to be in positive or negative values. The mean value and deviation were determined from at least three repetitions of measurement at different spots on the sample. Ultra TalyMap 5.1. Platinum software (Taylor Hobson, San Francisco, CA, USA) was used for 2D profile and 3D topography analysis and to export the surface images. The composite coatings were additionally evaluated using a Taylor Hobson CCI HD non-contact 3D Optical Profiler.

2.6. Contact Angle and Surface Free Energy

The wettability of samples was measured by the sessile drop method (drop volume—2 µL) followed by image processing using a Drop Shape Analysis (DSA) system 10 Mk2 (Kruss, Germany). In the DSA system, a digital camera measures the parameters of the drop (diameter, height, etc.). In the case of the sessile drop, parameters depend on the angle which the drop forms with the surface. The obtained results are compared with the so-called dimensionless (theoretical) profiles, which are solutions of the Laplace–Young equation [30].

The contact angle was determined for a polar solvent, which was ultra-high quality (UHQ) water of resistivity 18 MΩ/cm, and non-polar diodomethane. Surface free energy was calculated according to Owens–Wendt–Rebel–Keeble approach [31]. The averaged contact angle values and the surface free energy of each tested sample was determined from at least three repetitions of measurement at different spots on the sample. The standard deviation of the surface free energy was determined according to the error propagation method.

2.7. Nanotribometer

For friction force measurements of coatings, the NTR2 Nanotribometer (CSM Instruments SA, Freiburg, Germany) was used. It can conduct both linear reciprocating and rotating modes. The device enables to control the following test parameters: speed, load, distance, time, and frequency. The motion resistance is determined during the test by measuring the deflection of the elastic arm with the ball or pin sample. The measurements were conducted for 1 h at 25 °C under a normal load of 500 mN and at an average speed of 1 cm/s (3.18 Hz). The test conditions are given in Table 2.

Table 2. Detailed parameters used for friction force measurements of coatings.

Tribological Test Set-Up	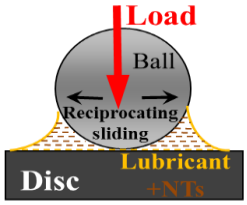
Contactconditions	Point contact at reciprocating sliding
Track length	1 mm
Speed	average 1 cm/s (3.18 Hz)
Normal Load	500 mN
Mean contact pressure	50 MPa
Temperature	25 °C
Test duration	1 h
Measured parameters	Coefficient of friction vs. time and wear volume

2.8. Hardness Measurement of Coatings

To determine the effect of the ceramic phase on the hardness of the coatings, Shore A hardness was measured using a Zwick 3130, ZwickRoell GmbH & Co. KG, Ulm, Germany. The measurement was performed with a load of 10 Newtons.

3. Results and Discussion

3.1. Fourier-Transform Infrared Spectroscopy Analysis

The FTIR analysis performed in this study was used as a qualitative investigation to confirm the identity of the pure components and the developed coatings.

Figure 2 shows FTIR absorbance spectra of pure components PVP, PEG, COL, GSH, HA, and coating compositions. The characteristic stretching and bending vibration of the functional groups are exhibited on the FTIR spectra.

Analyzing the spectra of the composites coatings clearly shows the peaks coming from the base polymers, which are PVP and PEG. This is particularly evident in the spectra of all composite coatings, where the peak at 1660 cm^{-1} is attributed to the C=O bonds originating from PVP [32]. At 1270 cm^{-1} and 2875 cm^{-1}, the CH_2 group was observed in polymers that are present in the obtained coatings [33].

The glutathione spectrum identified a -CN group at 1080 cm^{-1}, a -CH group at 1310 cm^{-1}, and a -COO group at 1624 cm^{-1} [34]. The spectrum of samples B, C, and D shows peaks of amide I at 1740 cm^{-1}, amide II at 1630 cm^{-1}, and a set of three weaker bands that represent amide III vibration modes centered at 1230 cm^{-1}, originating from

collagen [35]. It is worth noting that these peaks overlap with the peaks from the polymers. In samples C and D, spectral analysis revealed the presence of phosphate groups as evidenced by distinct bands in the 560–1023 cm^{-1} range. The peaks at 560 cm^{-1} and 575 cm^{-1} originate from triple degenerate O-P-O bending modes in PO_4^{3-}. The peak occurring at 1023 cm^{-1} is associated with asymmetric P-O stretching vibrations [36].

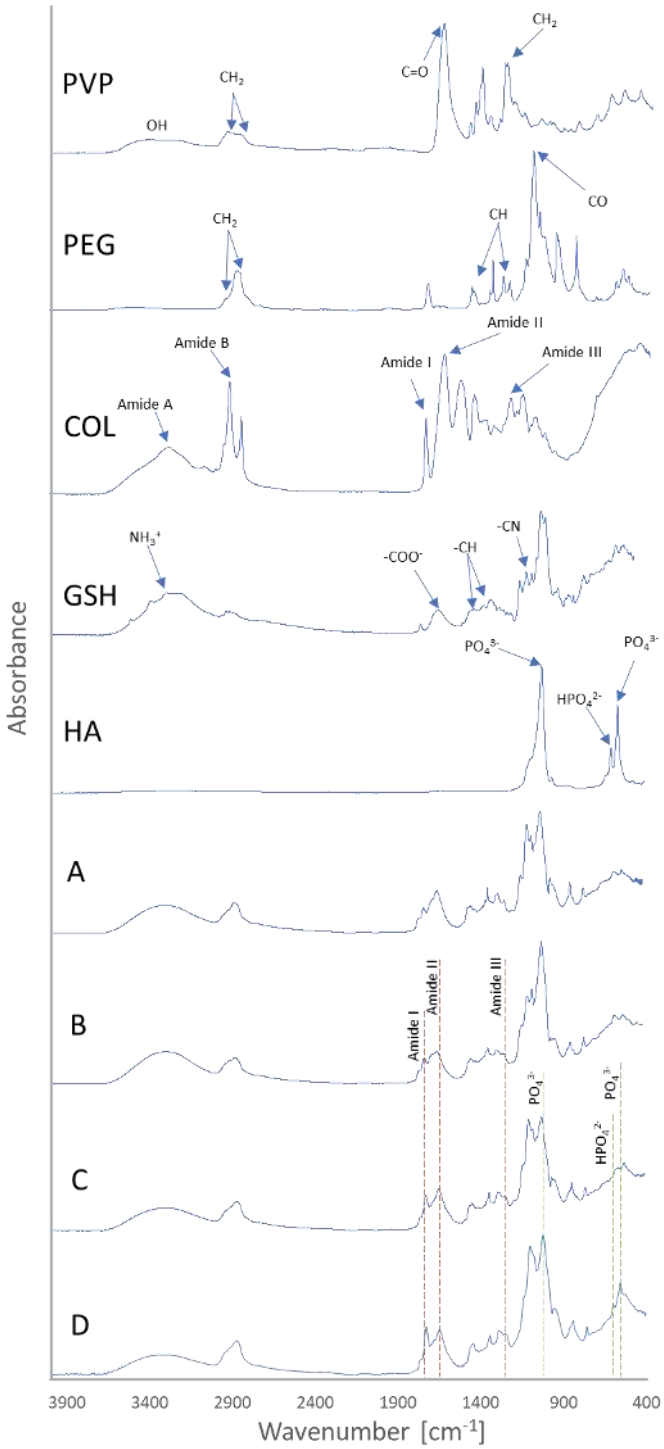

Figure 2. FTIR spectra of PVP, PEG, COL, GSH, HA and coatings.

3.2. Determination of Sorption Capacity

In Figure 3, the swelling kinetics of the tested coated materials immersed in distilled water for 7 days is presented. Equilibrium swelling and rate parameters (τ) are shown in

Table 3. The equilibrium swelling of coatings was in the range of 82.5 ± 2.8–118.8 ± 5.1%, and the lowest swelling capacity was recorded for sample D containing 15% *w/v* of HA. It can be observed that the equilibrium swelling of materials is strongly dependent on their composition. The addition of ceramic at variable contents leads to a decrease in material equilibrium swelling in comparison with the polymeric coating, as shown in Table 3. Moreover, it is shown that composite coatings (samples C and D) are also characterized with greater rate parameters (τ) as compared to polymeric coatings (samples A and B). Thus, it can be concluded that the addition of ceramic leads to the decreased swelling ability of materials and slower liquid medium absorption by composite coatings [15].

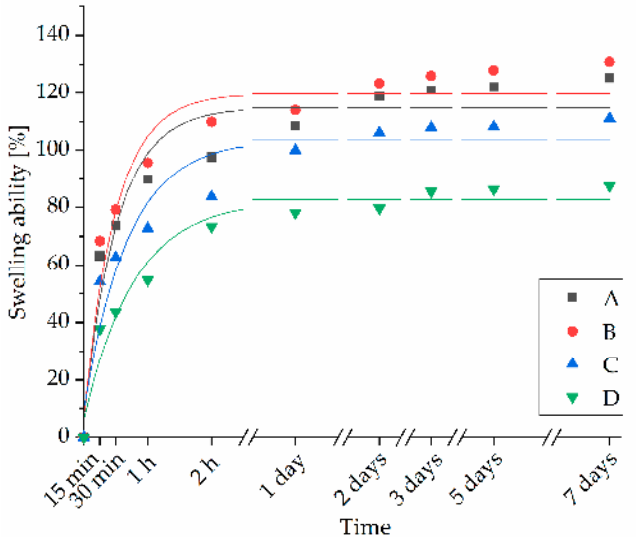

Figure 3. Swelling kinetics of coatings in distilled water. Solid lines indicate fittings for the swelling ability of individual samples.

Table 3. Rate parameter (τ) and equilibrium swelling (S_e) of tested samples.

Sample	*Se* [%]	τ
A	115.8 ± 5.0	30.41 ± 8.1
B	118.8 ± 5.1	29.7 ± 8.0
C	103.8 ± 4.5	41.14 ± 10.9
D	82.5 ± 2.8	47.3 ± 9.2

3.3. Surface Topography and Roughness

The composite coatings PVP/PEG/GSH were evaluated using a Taylor Hobson CCI HD non-contact 3D Optical Profiler. Results of the analysis of the surface topography of tested samples are presented in Figure 4. By analyzing the results, the effect of HAp addition on the surface topography can be seen. As the proportion of ceramic phase increases, the surface becomes less regular, rougher, and wavier. Results of the analysis of the surface topography of tested samples are presented in Figure 4.

Surface roughness was measured according to ISO 4287 with contact stylus acquisition mode in a line distance of 4 mm. Roughness profile and acquired roughness parameters are given in Figure 5. By comparing all the composite coatings, sample A (PVP/PEG/GSH) shows the lowest surface roughness value, R_a (1.41 ± 0.38), which indicates that it is the smoothest surface, as visible in topography image in Figure 4a. In contrast, sample D (PVP/PEG/GSH/collagen and HA 15 wt.%) shows the highest R_a (6.10 ± 0.87) value, followed by sample C (PVP/PEG/GSH/collagen and HA 5 wt.%) with an R_a value (3.76 ± 0.61). According to these results, it can be concluded that the addition of HA strongly increases the surface roughness due to the presence of grains of HA on the surface (red wide dots) visible on Figure 4c,d. The addition of collagen in comparison to the basic

matrix sample A resulted in the formation of small sharp peaks on the surface presented in surface topography Figure 4b. However, the roughness value Ra is increased marginally. Meanwhile, the presence of HA in 15% wt.% content (sample D) increased Ra and Rq values strongly when compared to the original polymer matrix, sample A (visible in Figure 5a,d). In general root mean square follows Ra values, increasing from sample A to D, following the amount of HA in the coating. Only skewness is unsimilar in describing the asymmetry, which is positive from samples A, B, and D consisting predominately of peak asperities visible in Figure 5a,b,d. Skewness for sample C is negative, representing surfaces that consist primarily of valleys, which can be clearly observed in Figure 5c. Rsk is an excellent parameter for measuring surfaces that are expected to have peaks or valleys. However, if a surface has been largely planarized such that a few peaks or valleys remain, then Rsk returns to nearly zero, which is the case for samples A, C, and D.

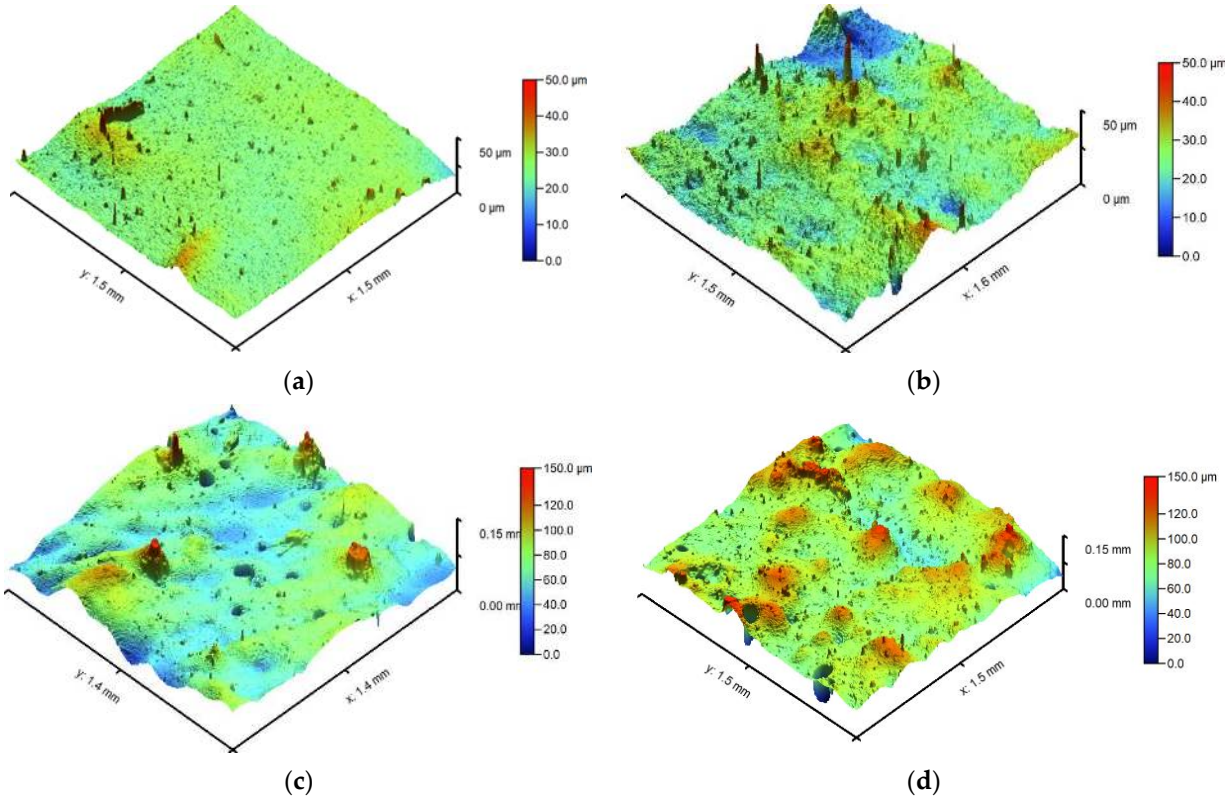

Figure 4. Surface topography of composite coatings for (**a**) sample A; (**b**) sample B; (**c**) sample C; (**d**) sample D.

3.4. Contact Angle and Surface Free Energy

In Table 4, the water contact angle and polar surface free energy calculated for it (Owens–Wendt–Kaelble approach) are listed, as well as the diiodomethane contact angle and dispersive surface free energy calculated for it. Total surface free energy is the sum of both components.

Sample A, the reference coating containing only PVP/PEG/GSH, has similar wettability for the polar component (water) to sample B, additionally containing collagen, resulting in a similar total free surface energy for both samples. This outcome can be also explained by similar roughness parameters for both samples. The presence of HA in coatings C and D decreased contact angles for polar and non-polar fluids and increased the total free surface energy when compared to samples A and B. The highest free surface energy can be noted for coating C, composed of PVP/PEG/GSH/collagen and HA 5 wt.%, which can be correlated with negative Rsk skewness for the surface that consists primarily of valleys (Figure 5c).

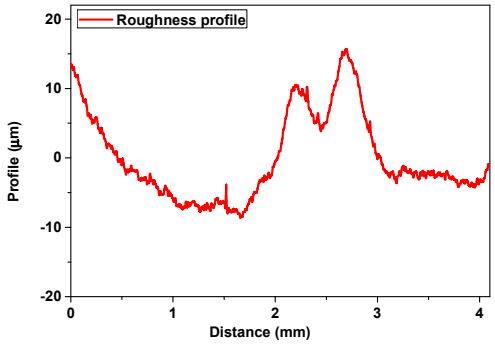

Roughness parameters according to ISO 4287		
Ra [µm]	1.41	±0.38
Rq [µm]	1.76	±0.43
Rsk [µm]	0.29	±0.54

(**a**)

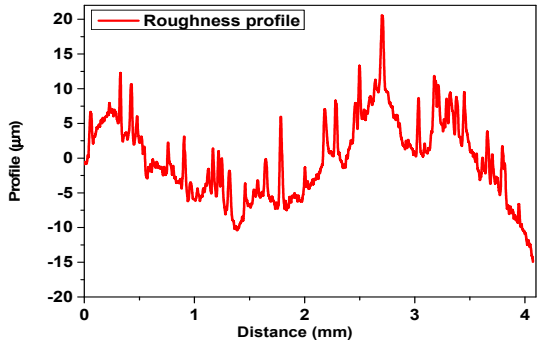

Roughness parameters according to ISO 4287		
Ra [µm]	2.14	±0.17
Rq [µm]	2.96	±0.34
Rsk [µm]	1.15	±0.25

(**b**)

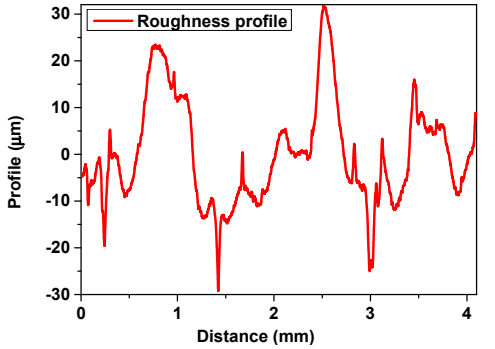

Roughness parameters according to ISO 4287		
Ra [µm]	3.76	±0.61
Rq [µm]	4.91	±0.66
Rsk [µm]	−0.08	±0.47

(**c**)

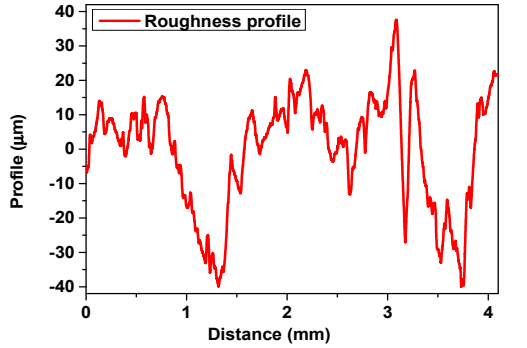

Roughness parameters according to ISO 4287		
Ra [µm]	6.10	±0.87
Rq [µm]	7.57	±0.90
Rsk [µm]	0.21	±0.18

(**d**)

Figure 5. Surface roughness profile and parameters of a composite coatings (**a**) A—PVP/PEG/GSH; (**b**) B—PVP/PEG/GSH/COL; (**c**) C—PVP/PEG/GSH/COL and HAp 5 wt.%; (**d**) D—PVP/PEG.GSH/COL and HAp 15 wt.%.

Table 4. Contact angles and surface free energies for samples A—D.

Sample Symbol and H_2O Drop Shape	θ H_2O [°]—Contact Angle for Polar Fluid	θ DJD [°]—Contact Angle for Non-Polar Fluid	δ^P_S [mJ/m^2] Surface Energy for Water	δ^D_S [mJ/m^2] Surface Energy for Djd	δ_S [mJ/m^2] Free Surface Energy
A 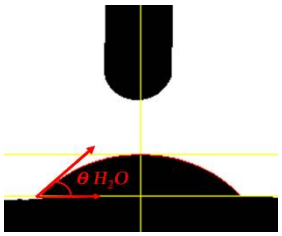	50.3 ± 1.3	35.0 ± 1.6	24.80	25.17	49.97

Table 4. *Cont.*

Sample Symbol and H_2O Drop Shape	θ H_2O [°]—Contact Angle for Polar Fluid	θ DJD [°]—Contact Angle for Non-Polar Fluid	δ^P_S [mJ/m²] Surface Energy for Water	δ^D_S [mJ/m²] Surface Energy for Djd	δ_S [mJ/m²] Free Surface Energy
B 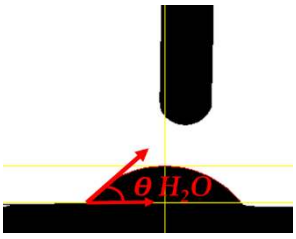	53.7 ± 2.0	26.27 ± 0.4	18.64	31.04	49.68
C 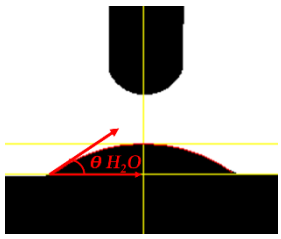	40.1 ± 1.9	28.4 ± 1.0	32.30	24.74	57.04
D 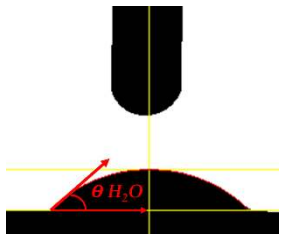	46.0 ± 1.9	27.1 ± 1.2	26.15	27.42	53.57

3.5. Nanotribometer

The coefficient of friction (CoF) of the coatings based on PVP/PEG and glutathione was investigated based on a reciprocating sliding test with a nanotribometer. The tribological performance of tested coatings was evaluated with an Al_2O_3 ball most-representative material configuration. Preliminarily, parameters were adjusted to follow ASTM standard. Unfortunately, it turned out that the conditions were too harsh. Further, the conditions were adopted for the PVP/PEG coatings and set as presented in Table 2: load of 500 mN and speed of 1 cm/s for 1 h at room temperature. The averaged friction scans as a function of time are presented in Figure 6a. The error bars visible on the friction curves represent the reproducibility of three repetitional tests. Directly after the frictional test, the wear tacks analysis on the tested samples was performed using a 3D Optical Profiler Interferometric System. The volume analysis method estimates the volume between the worn surface and a reference plane. The reference plane was set as the average height of the unworn area outside the wear track. The wear volume was calculated for the whole wear track, and only the area under the reference plane was considered.

The highest friction visible in Figure 6a was noted for reference sample A, which is related to the insufficient mechanical strength of this coating. When in contact with PBS fluid especially, the coating become too soft to perform the test. Thus, it was carried out in dry contact conditions. Moreover, as can be observed in Figure 6a, the black curve representing coating A is most unstable and oscillating, due which the error bars are also higher. As expected, high friction values lead to high wear volume, as presented in the columnar graph at Figure 6b, which is also related to poor mechanical strength. Sample B which was additionally composed of collagen in comparison to sample A presents a very low coefficient of friction, high frictional scan reproducibility, and low wear rate. The collagen component clearly has a beneficial effect on the tribological properties of the PVP/PEG coatings, also affecting an improvement of the mechanical strength. The

addition of HA ceramic at increasing contents led to a slow increase of CoF μ and wear rate. The addition of HA ceramic phase in 5% to sample C is represented by the blue frictional scan and blue column on the wear rate graph (Figure 6a,b). As presented, the CoF and wear volume are still satisfactory low. The situation changes when too much HA phase is added to the polymeric PVA/PVP compound, as is the case for sample D represented by the CoF pink curve and wear column bar. Although the COF is not the highest (Figure 6a) the wear increases evidently (Figure 6b). This behaviour can be explained by the crushing and crumbling of the small particles of HA from the very rough PVA/PVP compound coating, causing these particles to have a strong abrasive effect of on the sample D surface. This explains why the friction is not very high, as the particles by rolling in contact reduce friction, although causing surface damage.

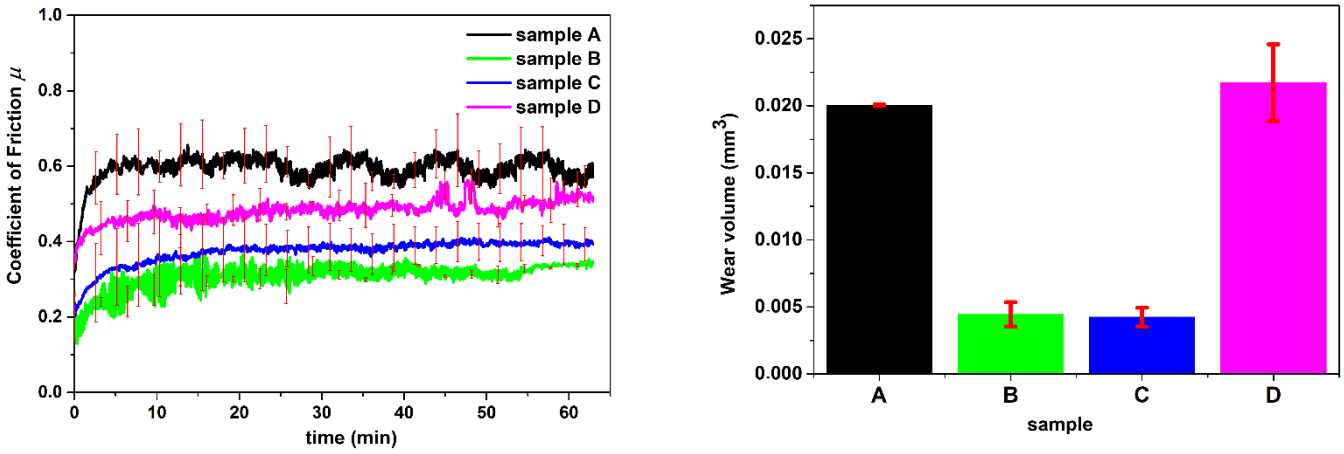

(**a**) (**b**)

Figure 6. Nanotribometer tests result represented with friction curves including error bars distribution over the curve (**a**) and wear volume bar graphs measured with 3D Optical Profiler Interferometric System (**b**).

The surfaces of the coatings based on PVP/PEG, glutathione, collagen, and HA after the reciprocating sliding test with a nanotribometer were thoroughly investigated with optical and interferometric microscopes, the results of which are presented in Figure 7a–d. The length, width, and depth of the wear scare was measured, as well as the roughness parameters inside the track. The surface height parameters measured for area (kurtosis Sq, skewness Ssk, and roughness Sa) quantitatively describe the damaged wear track. As can be observed, the rough wear zone for samples A and D (Figure 7a,d) correlates with the high wear volume in Figure 6b. The lowest wear volume and at the same time minimal damage and lowest CoF can be observed for sample B, which contains collagen and 0% HA, and for sample C, which contains collagen and 5% HA.

3.6. Hardness Measurement of Coatings

Figure 8 presents the results obtained for the Shore A hardness measurements for the obtained composite coatings. In the case of coatings without the contribution of the ceramic phase, i.e., A and B, relatively similar results oscillating around the value of 85 were obtained. However, the influence of HA on the hardness can be seen, as the value clearly increases with an increase in the contribution of HA to the materials. However, it is important to note that the hardness measurements were also influenced by PLA plates. Considering the thickness of the applied ceramic–polymer coating on the PLA, it is possible that the PLA plate had a significant impact on the measurement result.

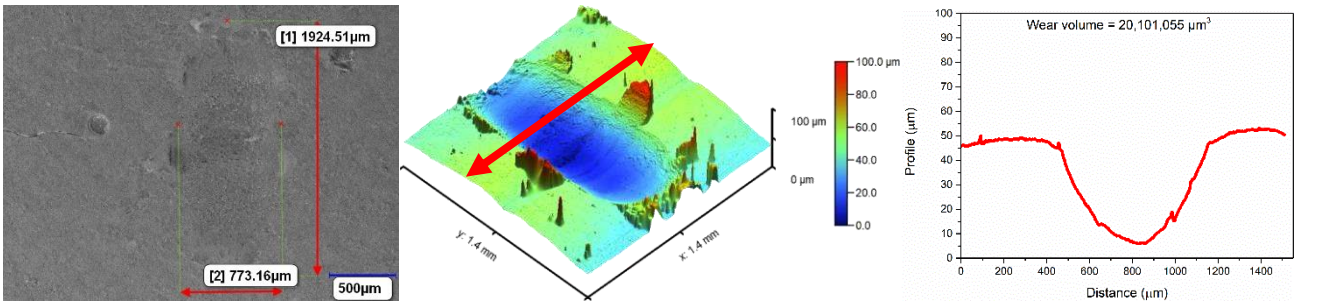

(**a**)

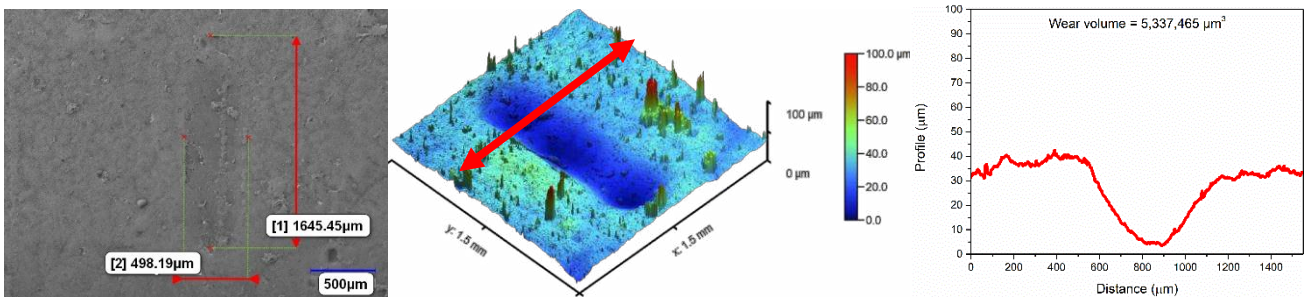

(**b**)

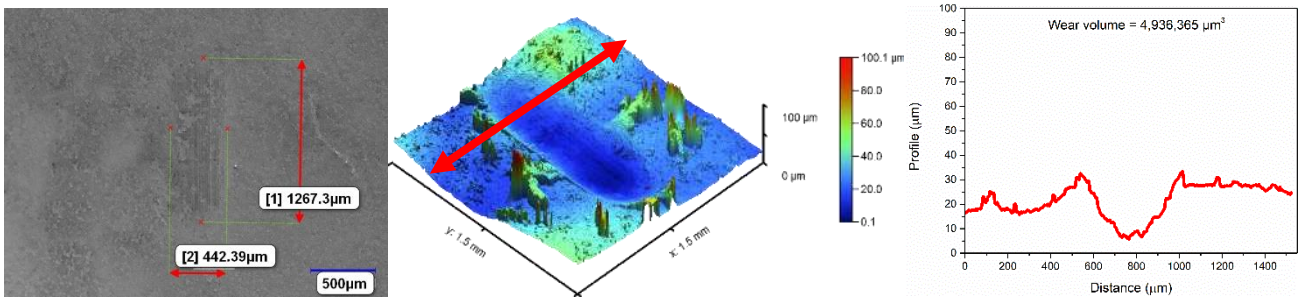

(**c**)

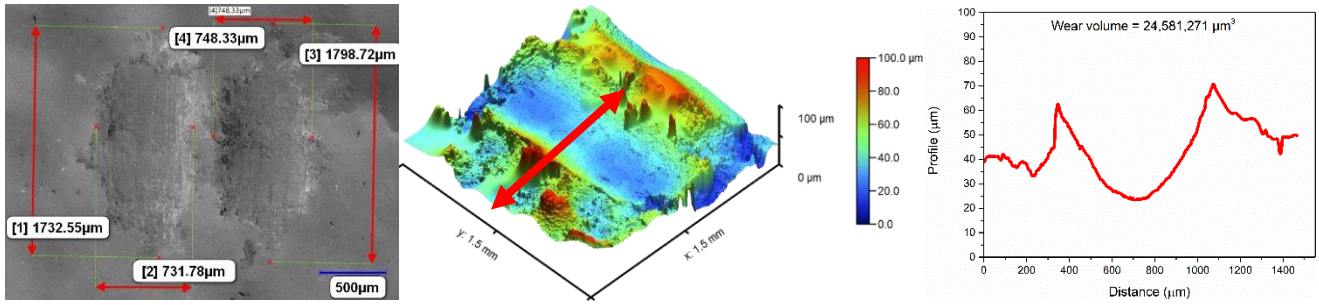

(**d**)

Figure 7. Wear tracks topography after nanotribometer tests: optical and interferometric micrographs including roughness parameters within the wear track for samples A–D (**a**–**d**). Cross section of the surface profile is marked on the interferometric image and presented as a graph. (**a**) Sample A, roughness inside the wear scare: Sa = 7.89 µm, Sq = 9.66 µm, Ssk = 0.2 µm. (**b**) Sample B, roughness inside the wear scare: Sa = 1.58 µm, Sq = 1.89 µm, Ssk = 0.4 µm. (**c**) Sample C, roughness inside the wear scare: Sa = 3.59 µm, Sq = 4.42 µm, Ssk = 0.36 µm. (**d**) Sample D, roughness inside the wear scare: Sa = 6.14 µm, Sq = 7.56 µm, Ssk = 0.46 µm.

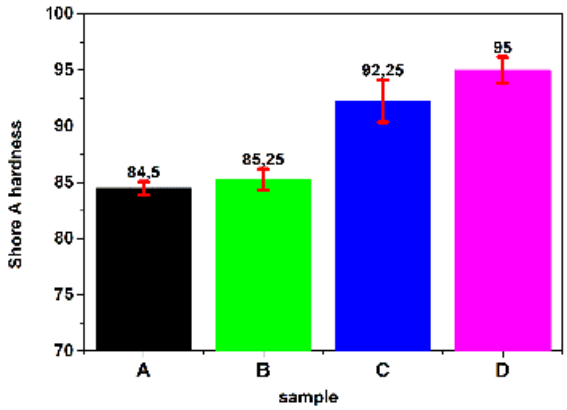

Figure 8. Hardness measurement of coatings by the shore method A.

However, the results obtained are consistent with literature reports on composites with ceramics [37,38].

4. Conclusions

We can assume that the preparation method of PVP/PEG/GSH/COL/HA coatings on PLA plates was successful. The developed technology as well as the choice of crosslinking agent and photoinitiator allowed to perform the photocrosslinking process under UV light without any by-products. Moreover, the coatings were fully crosslinked, and the ceramics did not crumble. Good integrity was also achieved, as the coating was fully continuous and uniformly crosslinked, with no significant irregularities or holes. Last but not least, high adhesion was obtained, with the coating fully and permanently adhered to the PLA wafer, and good adhesion was observed for both wet and dried coatings. Moreover, the coatings exhibited good mechanical strength and a well-developed surface morphology and topography. The nanotribometric reciprocating sliding test method showed excellent tribological properties of the composites coating containing collagen and a small amount (5%) of HA ceramic phase. Meanwhile, the ceramic phase in too high a content (15%) decreased the swelling ability of composites and slowed liquid medium absorption, additionally causing surface roughening. In consequence, during the reciprocating sliding test, small and hard particles of HA from the very rough composite are crushed, having a strong abrasive effect on the sample surface and loosening tribological properties. It can be concluded that sample C composed of PVP/PEG/GSH/COL/HA(5%) exhibits high biological value for its osteoconductivity, strong mechanical and tribological properties, highest free surface energy, as well as porosity and accepted roughness to be implemented as safe materials for bone regeneration. No such materials with the same or similar composition designed for bone tissue regeneration are available in the literature so far. Therefore, given the satisfactory results, further studies, especially physicochemical and biological, are needed to confirm the biosafety and the absence of cytotoxicity.

Author Contributions: Conceptualization, A.M.T. and D.S.; data curation, A.M.T., D.S. and M.D.; formal analysis, D.S. and A.S.-K.; funding acquisition, A.S.-K.; investigation, A.M.T.; methodology, A.M.T., D.S. and K.P.; project administration, A.S.-K.; software, W.F. and K.P.; supervision, A.M.T. and A.S.-K.; validation, A.M.T., D.S., W.F. and M.D.; visualization, D.S., W.F. and K.P.; writing—original draft, A.M.T. and D.S.; writing—review and editing, W.F. All authors have read and agreed to the published version of the manuscript.

Funding: This research was funded by Foundation for Polish Science, grant number POIR.04.04.00-00-16D7/18.

Institutional Review Board Statement: Not applicable.

Informed Consent Statement: Not applicable.

Data Availability Statement: The data that support the findings of this study are contained within the article.

Acknowledgments: The "Multifunctional biologically active composites for applications in bone regenerative medicine" project is carried out within the TEAM-NET program of the Foundation for Polish Science financed by the European Union under the European Regional Development Fund. The authors gratefully acknowledge financial support.

Conflicts of Interest: The authors declare no conflict of interest.

References

1. Djošić, M.; Janković, A.; Mišković-Stanković, V. Electrophoretic Deposition of Biocompatible and Bioactive Hydroxyapatite-Based Coatings on Titanium. *Materials* **2021**, *14*, 5391. [CrossRef]
2. Chevallier, P.; Turgeon, S.; Sarra-Bournet, C.; Turcotte, R.; Laroche, G. Characterization of Multilayer Anti-Fog Coatings. *ACS Appl. Mater. Interfaces* **2011**, *3*, 750–758. [CrossRef] [PubMed]
3. Soon, G.; Pingguan-Murphy, B.; Lai, K.W.; Akbar, S.A. Review of Zirconia-Based Bioceramic: Surface Modification and Cellular Response. *Ceram. Int.* **2016**, *42*, 12543–12555. [CrossRef]
4. Eliaz, N.; Metoki, N. Calcium Phosphate Bioceramics: A Review of Their History, Structure, Properties, Coating Technologies and Biomedical Applications. *Materials* **2017**, *10*, 334. [CrossRef] [PubMed]
5. Spraying, D. Creation of Bioceramic Coatings on the Surface of Ti–6Al–4V Detonation Spraying. *Coatings* **2021**, *11*, 1433.
6. Li, J.; Jansen, J.A.; Walboomers, X.F.; van den Beucken, J.J. Mechanical Aspects of Dental Implants and Osseointegration: A Narrative Review. *J. Mech. Behav. Biomed. Mater.* **2020**, *103*, 103574. [CrossRef]
7. Kaneko, S.; Yamamoto, Y.; Wada, K.; Kumagai, G.; Harada, Y.; Yamauchi, R.; Ishibashi, Y. Ultraviolet Irradiation Improves the Hydrophilicity and Osteo-Conduction of Hydroxyapatite. *J. Orthop. Surg. Res.* **2020**, *15*, 425. [CrossRef]
8. Bai, L.; Liu, Y.; Du, Z.; Weng, Z.; Yao, W.; Zhang, X.; Huang, X.; Yao, X.; Crawford, R.; Hang, R.; et al. Differential Effect of Hydroxyapatite Nano-Particle versus Nano-Rod Decorated Titanium Micro-Surface on Osseointegration. *Acta Biomater.* **2018**, *76*, 344–358. [CrossRef]
9. Xia, L.; Xie, Y.; Fang, B.; Wang, X.; Lin, K. In Situ Modulation of Crystallinity and Nano-Structures to Enhance the Stability and Osseointegration of Hydroxyapatite Coatings on Ti-6Al-4V Implants. *Chem. Eng. J.* **2018**, *347*, 711–720. [CrossRef]
10. Um, S.H.; Chung, Y.W.; Seo, Y.; Seo, H.; Ok, M.R.; Kim, Y.C.; Han, H.S.; Chung, J.J.; Edwards, J.R.; Jeon, H. Robust Hydroxyapatite Coating by Laser-Induced Hydrothermal Synthesis. *Adv. Funct. Mater.* **2020**, *30*, 2005233. [CrossRef]
11. Beig, B.; Liaqat, U.; Niazi, M.F.K.; Douna, I.; Zahoor, M.; Niazi, M.B.K. Current Challenges and Innovative Developments in Hydroxyapatite-Based Coatings on Metallic Materials for Bone Implantation: A Review. *Coatings* **2020**, *10*, 1249. [CrossRef]
12. Ullah, I.; Siddiqui, M.A.; Liu, H.; Kolawole, S.K.; Zhang, J.; Zhang, S.; Ren, L.; Yang, K. Mechanical, Biological, and Antibacterial Characteristics of Plasma-Sprayed (Sr,Zn) Substituted Hydroxyapatite Coating. *ACS Biomater. Sci. Eng.* **2020**, *6*, 1355–1366. [CrossRef] [PubMed]
13. Chen, Y.; Ren, J.; Liu, W.; Zhao, D. Enhanced Scratch Performance of Plasma Sprayed Hydroxyapatite Composite Coatings Reinforced with BN Nanoplatelets. *Coatings* **2020**, *10*, 652. [CrossRef]
14. Zhao, H.; Liao, J.; Wu, F.; Shi, J. Mechanical Strength Improvement of Chitosan/Hydroxyapatite Scaffolds by Coating and Cross-Linking. *J. Mech. Behav. Biomed. Mater.* **2021**, *114*, 104169. [CrossRef] [PubMed]
15. Jung, H.G.; Lee, D.; Lee, S.W.; Kim, I.; Kim, Y.; Jang, J.W.; Lee, J.H.; Lee, G.; Yoon, D.S. Nanoindentation for Monitoring the Time-Variant Mechanical Strength of Drug-Loaded Collagen Hydrogel Regulated by Hydroxyapatite Nanoparticles. *ACS Omega* **2021**, *6*, 9269–9278. [CrossRef] [PubMed]
16. Banoriya, D.; Purohit, R.; Dwivedi, R.K. Advanced Application of Polymer Based Biomaterials. *Mater. Today Proc.* **2017**, *4*, 3534–3541. [CrossRef]
17. Grant, J.J.; Pillai, S.C.; Perova, T.S.; Hehir, S.; Hinder, S.J.; McAfee, M.; Breen, A. Electrospun Fibres of Chitosan/PVP for the Effective Chemotherapeutic Drug Delivery of 5-Fluorouracil. *Chemosensors* **2021**, *9*, 70. [CrossRef]
18. Ozkan, G.; Franco, P.; Capanoglu, E.; De Marco, I. PVP/Flavonoid Coprecipitation by Supercritical Antisolvent Process. *Chem. Eng. Process.—Process Intensif.* **2019**, *146*, 107689. [CrossRef]
19. López-Calderón, H.D.; Avilés-Arnaut, H.; Galán Wong, L.J.; Almaguer-Cantú, V.; Laguna-Camacho, J.R.; Calderón-Ramón, C.; Escalante-Martínez, J.E.; Arévalo-Niño, K. Electrospun Polyvinylpyrrolidone-Gelatin and Cellulose Acetate Bi-Layer Scaffold Loaded with Gentamicin as Possible Wound Dressing. *Polymers* **2020**, *12*, 2311. [CrossRef]
20. Voronova, M.; Rubleva, N.; Kochkina, N.; Afineevskii, A.; Zakharov, A.; Surov, O. Preparation and Characterization of Polyvinylpyrrolidone/Cellulose Nanocrystals Composites. *Nanomaterials* **2018**, *8*, 1011. [CrossRef]
21. Bakaic, E.; Smeets, N.M.B.; Hoare, T. Injectable Hydrogels Based on Poly(Ethylene Glycol) and Derivatives as Functional Biomaterials. *RSC Adv.* **2015**, *5*, 35469–35486. [CrossRef]
22. Knop, K.; Hoogenboom, R.; Fischer, D.; Schubert, U.S. Poly(Ethylene Glycol) in Drug Delivery: Pros and Cons as Well as Potential Alternatives. *Angew. Chem.—Int. Ed.* **2010**, *49*, 6288–6308. [CrossRef] [PubMed]
23. Thi, T.T.H.; Pilkington, E.H.; Nguyen, D.H.; Lee, J.S.; Park, K.D.; Truong, N.P. The Importance of Poly(Ethylene Glycol) Alternatives for Overcoming PEG Immunogenicity in Drug Delivery and Bioconjugation. *Polymers* **2020**, *12*, 298. [CrossRef]

24. Chakravarty, J.; Rabbi, M.F.; Chalivendra, V.; Ferreira, T.; Brigham, C.J. Mechanical and Biological Properties of Chitin/Polylactide (PLA)/Hydroxyapatite (HAP) Composites Cast Using Ionic Liquid Solutions. *Int. J. Biol. Macromol.* **2020**, *151*, 1213–1223. [CrossRef] [PubMed]
25. Serra, T.; Mateos-Timoneda, M.A.; Planell, J.A.; Navarro, M. 3D Printed PLA-Based Scaffolds: A Versatile Tool in Regenerative Medicine. *Organogenesis* **2013**, *9*, 239–244. [CrossRef]
26. Munirah, S.; Kim, S.H.; Ruszymah, B.H.I.; Khang, G. The Use of Fibrin and Poly(Lactic-Co-Glycolic Acid) Hybrid Scaffold for Articular Cartilage Tissue Engineering: An in Vivo Analysis. *Eur. Cells Mater.* **2008**, *15*, 41–52. [CrossRef]
27. Gregor, A.; Filová, E.; Novák, M.; Kronek, J.; Chlup, H.; Buzgo, M.; Blahnová, V.; Lukášová, V.; Bartoš, M.; Nečas, A.; et al. Designing of PLA Scaffolds for Bone Tissue Replacement Fabricated by Ordinary Commercial 3D Printer. *J. Biol. Eng.* **2017**, *11*, 31. [CrossRef]
28. Słota, D.; Florkiewicz, W.; Piętak, K.; Szwed, A.; Włodarczyk, M.; Siwińska, M.; Rudnicka, K.; Sobczak-Kupiec, A. Preparation, Characterization, and Biocompatibility Assessment of Polymer-Ceramic Composites Loaded with Salvia Officinalis Extract. *Materials* **2021**, *14*, 6000. [CrossRef]
29. Kabiri, K.; Omidian, H.; Hashemi, S.A.; Zohuriaan-Mehr, M.J. Synthesis of Fast-Swelling Superabsorbent Hydrogels: Effect of Crosslinker Type and Concentration on Porosity and Absorption Rate. *Eur. Polym. J.* **2003**, *39*, 1341–1348. [CrossRef]
30. Marmur, A. Thermodynamic Aspects of Contact Angle Hysteresis. *Adv. Colloid Interface Sci.* **1994**, *50*, 121–141. [CrossRef]
31. Owens, D.K.; Wendt, R.C. Estimation of the Surface Free Energy of Polymers. *J. Appl. Polym. Sci.* **1969**, *13*, 1741–1747. [CrossRef]
32. Abdelghany, A.M.; Mekhail, M.S.; Abdelrazek, E.M.; Aboud, M.M. Combined DFT/FTIR structural studies of monodispersed PVP/Gold and silver nano particles. *J. Alloys Compd.* **2015**, *646*, 326–332. [CrossRef]
33. Deygen, I.M.; Kudryashova, E.V. New Versatile Approach for Analysis of PEG Content in Conjugates and Complexes with Biomacromolecules Based on FTIR Spectroscopy. *Colloids Surf. B Biointerfaces* **2016**, *141*, 36–43. [CrossRef] [PubMed]
34. Negishi, Y.; Nobusada, K.; Tsukuda, T. Glutathione-Protected Gold Clusters Revisited: Bridging the Gap between Gold(I)-Thiolate Complexes and Thiolate-Protected Gold Nanocrystals. *J. Am. Chem. Soc.* **2005**, *127*, 5261–5270. [CrossRef]
35. De Campos Vidal, B.; Mello, M.L.S. Collagen Type I Amide I Band Infrared Spectroscopy. *Micron* **2011**, *42*, 283–289. [CrossRef]
36. Rehman, I.; Bonfield, W. Characterization of Hydroxyapatite and Carbonated Apatite by Photo Acoustic FTIR Spectroscopy. *J. Mater. Sci. Mater. Med.* **1997**, *8*, 1–4. [CrossRef]
37. Nihmath, A.; Ramesan, M.T. Development of Hydroxyapatite Nanoparticles Reinforced Chlorinated Acrylonitrile Butadiene Rubber/Chlorinated Ethylene Propylene Diene Monomer Rubber Blends. *J. Appl. Polym. Sci.* **2021**, *138*, 50189. [CrossRef]
38. Verma, N.; Zafar, S.; Talha, M. Influence of Nano-Hydroxyapatite on Mechanical Behavior of Microwave Processed Polycaprolactone Composite Foams. *Mater. Res. Express* **2019**, *6*, 085336. [CrossRef]

Journal of
Functional
Biomaterials

MDPI

Article

Hybrid Coatings Based on Polyvinylpyrrolidone/Polyethylene Glycol Enriched with Collagen and Hydroxyapatite: Incubation Studies and Evaluation of Mechanical and Physiochemical Properties

Dagmara Słota [1,*], Josef Jampilek [2,3,*] and Agnieszka Sobczak-Kupiec [1]

[1] Department of Materials Science, Faculty of Materials Engineering and Physics, Cracow University of Technology, 37 Jana Pawła II Av., 31-864 Krakow, Poland; agnieszka.sobczak-kupiec@pk.edu.pl
[2] Department of Analytical Chemistry, Faculty of Natural Sciences, Comenius University, Ilkovicova 6, 842 15 Bratislava, Slovakia
[3] Department of Chemical Biology, Faculty of Science, Palacky University, Slechtitelu 27, 783 71 Olomouc, Czech Republic
* Correspondence: dagmara.slota@doktorant.pk.edu.pl (D.S.); josef.jampilek@gmail.com (J.J.)

Abstract: Coating materials offers an intriguing solution for imparting inert implants with additional bioactive characteristics without changing underlying parameters such as mechanical strength. Metallic implants like endoprostheses or polymeric implants can be coated with a thin layer of bioactive film capable of stimulating bone-forming cells to proliferate or release a drug. However, irrespective of the final implantation site of such a coating biomaterial, it is necessary to conduct detailed mechanical and physicochemical in vitro analyses to determine its likely behavior under biological conditions. In this study, polymeric and composite coatings with hydroxyapatite obtained under UV light underwent incubation tests in four different artificial biological fluids: simulated body fluid (SBF), artificial saliva, Ringer's fluid, and water (as the reference fluid). The potentiometric and conductometric properties, sorption capacity, and degradation rate of the coatings were examined. Furthermore, their hardness, modulus of elasticity, and deformation were determined. It was demonstrated that the coatings remained stable in SBF liquid at a pH value of around 7.4. In artificial saliva, the greatest degradation of the polymer matrix (ranging between 36.19% and 39.79%) and chipping of hydroxyapatite in the composite coatings were observed. Additionally, the effect of ceramics on sorption capacity was determined, with lower capacity noted with higher HA additions. Moreover, the evaluation of surface morphology supported by elemental microanalysis confirmed the appearance of new apatite layers on the surface as a result of incubation in SBF. Ceramics also influenced mechanical aspects, increasing hardness and modulus of elasticity. For the polymer coatings, the value was 11.48 ± 0.61, while for the composite coating with 15% ceramics, it increased more than eightfold to a value of 93.31 ± 11.18 N/mm^2. Based on the conducted studies, the effect of ceramics on the physicochemical as well as mechanical properties of the materials was determined, and their behavior in various biological fluids was evaluated. However, further studies, especially cytotoxicity analyses, are required to determine the potential use of the coatings as biomaterials.

Keywords: coatings; ceramic; polymer; hydroxyapatite; collagen; polyvinylpyrrolidone; polyethylene glycol; glutathione

Citation: Słota, D.; Jampilek, J.; Sobczak-Kupiec, A. Hybrid Coatings Based on Polyvinylpyrrolidone/Polyethylene Glycol Enriched with Collagen and Hydroxyapatite: Incubation Studies and Evaluation of Mechanical and Physiochemical Properties. *J. Funct. Biomater.* **2024**, *15*, 62. https://doi.org/10.3390/jfb15030062

Academic Editor: Nenad Ignjatovic

Received: 23 January 2024
Revised: 23 February 2024
Accepted: 28 February 2024
Published: 1 March 2024

1. Introduction

The coating technique consists of covering the surface of an implant with a layer of another biomaterial [1]. Coating modifies the surface of biomaterials and the biological response of the host tissue in the peri-implant area [2]. In the case of bone implants, bioactive ceramics, such as hydroxyapatite (HA), are of particular interest in this aspect;

they spontaneously form a bony apatite layer on their surface in a living organism and fuse with bone through this layer. These types of materials are of great clinical importance as bone-restorative materials. The formed apatite is highly similar to bone mineral in its composition and structure. Therefore, osteoblasts preferentially proliferate and differentiate to produce apatite as well as collagen on this layer of apatite. When an inert material (whether polymer or metallic) is coated with hydroxyapatite, bone cells adhere to the surface of the apatite coating without intermediate layers. Later, the hydroxyapatite matrix of bone cells becomes integrated with the coating, resulting in excellent adhesion of the coated implant to the bone [3–5].

Many biologically active compounds can be used to manufacture coatings, thereby providing some additional biological functions [6,7]. Collagen is a polymer of natural origin that has been used in medicine and cosmetology for more than 50 years. Due to its wide range of properties, it is used as a material or intermediate in wound healing dressings, dentistry, scaffold design for osteochondral engineering, otolaryngology, and aesthetic medicine [8,9]. Otolaryngology is a medical field focusing on the ears, nose, and throat. It also includes head and neck surgery [10]. Collagen is the most abundant protein in the extracellular matrix in mammals. It is a non-toxic biopolymer that is highly biodegradable. Moreover, it demonstrates poor immunogenicity and very good degradability. Currently, about 29 types of collagen proteins are known, which are characterized by their diverse and unique structures [11]. Depending on the structure and function, many types are distinguished. The most important are collagen types I and II. The first one constitutes about 70% of all collagen types, and is mainly found in ligaments, bones, and tendons. The second is the main component of vitreous cartilage and the main collagen of the vitreous body, as well as the nucleus pulposus of intervertebral discs. The presence of collagen ensures flexibility and improves tissue condition [12–14]. In biomedical and implant applications, fish collagen is most commonly used. It can take both fibrillar and non-fibrillar forms and is distinguished by lower melting and gelling temperatures than collagens extracted from mammals [15,16].

Glutathione (GSH) is an interesting biologically active tripeptide. It is a compound that demonstrates strong antioxidant properties, but beyond that, it is involved in many other functions [17]. It is responsible for recycling vitamins E and C, transporting amino acids, and producing coenzymes. Importantly, with age, GSH levels gradually decrease, so its external delivery is important [18–20].

Another biologically active ingredient that can significantly affect the acceleration of regeneration of the skeletal or cartilaginous system is the above-mentioned HA. It is a ceramic that occurs naturally in the body forming the mineral phase of bone (constituting about 70%, and the remaining 30% is mainly collagen proteins) [21,22]. Synthetic HA used in implantology can chemically bind to surrounding tissues; it has osteoconductive properties and the ability to stimulate bone-forming cells to proliferate.

Regardless of the type, due to a variety of processes occurring in the body, biomaterials must be subjected to detailed physicochemical or mechanical analysis. Different physiological fluids exhibit different chemical compositions or pH values, so they can interact differently with implanted foreign bodies. Artificial biological fluids are used to simulate the biological environment in an in vitro laboratory setting. The most common of these are simulated body fluid (SBF), artificial saliva, and Ringer's fluid, whose composition corresponds to extracellular fluid [23,24].

The study of the interaction of materials with fluids allows the monitoring of a range of parameters such as ionic conductivity, changes in pH values, degree of degradation, and swelling coefficient. They can vary depending on the composition of biomaterials. Potentiometric and conductometric tests help determine whether hazardous components are released or precipitate from the interior of the material during fluid interactions, which could negatively affect the cellular balance. Any spike in pH values to highly alkaline or acidic is a cause for concern, since cells in the implant area are unable to proliferate under such conditions [25,26]. Degradation studies provide information on how quickly a

biomaterial will disintegrate into smaller molecules or fragments and can be replaced by newly growing tissue. However, both degradation and swelling capacity are also strategies for delivering active substances including drugs in targeted therapies. As a result of gradual degradation, active substances that are physically or chemically bound to the material are released. In the case of swelling, drug delivery involves the gradual elution from polymer chains following the penetration of the liquid medium deep into the network [27–29]. Given the above, in vitro studies are recommended before proceeding to cellular or in vivo studies on animal models.

The work presented in this paper continues the study of innovative composite coatings containing polyvinylpyrrolidone (PVP), polyethylene glycol (PEG), eGSH, COL, and bioactive HA for bone tissue regeneration [30,31]. The composite coating guarantees improved properties because it combines the features of polymeric and ceramic materials. Ceramics are characterized by brittleness, so they are unable to carry loads; however, suspending them in a polymeric hydrogel matrix can overcome this problem without losing their bioactive character. The aim of the study was to evaluate the mechanical and physicochemical properties of the developed materials and to determine their potential as active substance carriers by determining the sorption capacity in selected simulated biological fluids. It should be emphasized that the developed materials have great potential due to the high biological value of the components used in their synthesis, such as glutathione and hydroxyapatite, which promote osteogenesis. No other solution of this type has been found so far. Figure 1 presents the research methodology of the study.

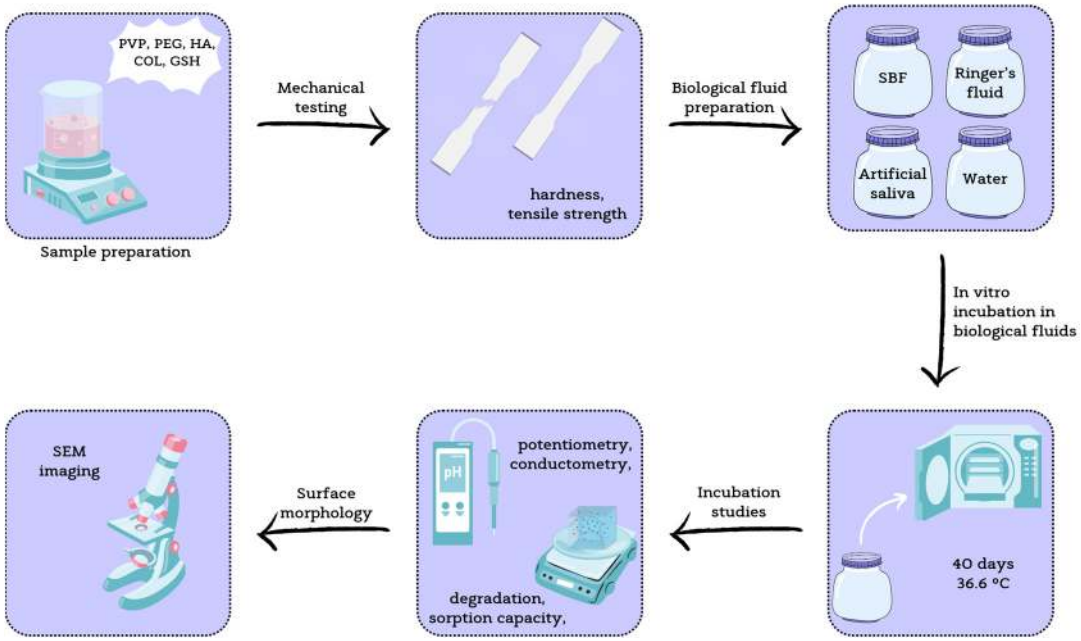

Figure 1. Workflow of the study, from sample preparation to individual analysis.

2. Materials and Methods

2.1. Reagents

The reagents used for the synthesis of HA, i.e., calcium acetate monohydrate ($Ca(CH_3CO_2)_2 \cdot H_2O$), sodium phosphate dibasic (Na_2HPO_4), and ammonia water (NH_4OH, 25%), as well as polymers, i.e., polyethylene glycol (PEG), polyvinylpyrrolidone (PVP), poly(ethylene glycol) diacrylate Mn 575 (PEGDA), collagen from bovine Achilles tendon (COL), and other reagents, such as 2-hydroxy-2-methylpropiophenone 97% and peptide L-glutathione reduced 98% (GSH), were obtained from Sigma-Aldrich (Darmstadt, Germany). For the preparation of Ringer's solution and simulated body fluid (SBF) fluid, NaCl, KCl, $CaCl_2$, and Na_2SO_4 from Eurochem BGD (Tarów, Poland) were used. Additionally, $NaHCO_3$ from DOR-CHEM (Krakow, Poland), $K_2HPO_2 \cdot 3H_2O$ and $MgCl_2 \cdot 6H_2O$ from

Chempur (Piekary Slaskie, Poland), 2-amino-2-(hydroxymethyl)- propane-1,3-diol (Tris) from POCH (Gliwice, Poland), and HCl 35–38% solution from Stanlab (Lublin, Poland) were purchased.

2.2. Preparation of Coatings

The coatings were prepared as previously described [30], and their composition is presented in Table 1. The crosslinking process was used, exposing the samples to UV light for 4 min with a lamp power of 0.8 J/cm^2, and a distance from the lamp of 5 cm.

Table 1. Coating composition.

Sample Symbol	PVP (mL)	PEG (mL)	GSH (g)	COL (g)	HA (% *w*/*v*)	PEGDA (mL)	Photoinitiator (µL)
A	5	5	2	-	-	1.8	50
B				0.04	-		
C					5		
D					15		

The developed method of coating preparation and application is a completely waste-free technique and generates no by-products. Ultraviolet light crosslinking resulted in a fully crosslinked material, and no crumbling of the ceramics was observed even at higher HA concentrations. Also, good integrity was obtained as the coatings were fully continuous and uniformly crosslinked with no significant irregularities or holes. Figure 2 demonstrates the resulting materials applied to hard polylactide (PLA) plates.

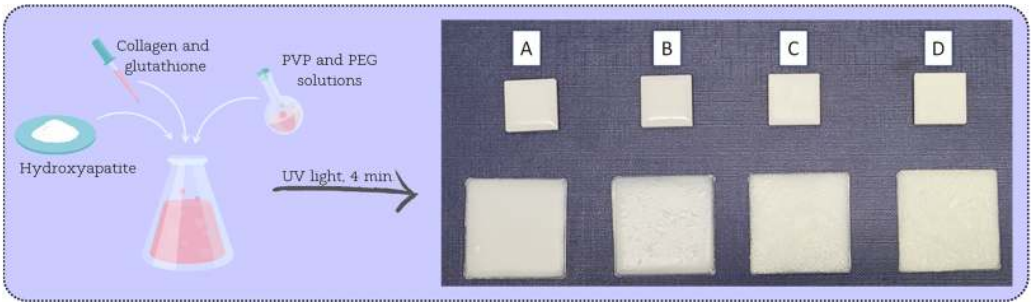

Figure 2. Coatings applied to polymer plates. Smaller squares above—PLA plates obtained by 3D printing. Larger squares below—PLA plates obtained by injection molding.

2.3. Methodology of Incubation Tests

2.3.1. Fluid Preparation

A pH-metric study of the coatings was conducted to determine their bioactivity. Three incubation fluids were selected: SBF (simulated body fluid), artificial saliva, and Ringer's solution (60 mL). These were placed in sterile sealed containers, and 1 g coating discs were immersed in them.

The purpose of this study was to confirm the interactions occurring between the sample and the incubation fluids. The molecules and ions contained in the fluids, interacting with the biomaterial, cause a change in pH value. The materials were incubated in a POL-EKO incubator, model ST 5 B SMART (Wodzisław Śląski, Poland), at 36.6 °C for 40 days. The pH values were measured using an Elmetron CX-701 multifunctional device (Zabrze, Poland).

Ringer's fluid and SBF were prepared according to the details in Tables 2–4. For all fluids, each subsequent component was added after the previous component was completely dissolved. Ringer's solution was obtained at room temperature. To prepare the SBF solution, 700 mL of distilled water was heated to 36.5 °C (±0.5 °C). One by one, all the

ingredients were added, and finally, with a solution of HCl and $(CH_2OH)_3CNH_2$, the pH was brought to 7.4–7.45. After that distilled water was added to a volume of 1000 mL.

Table 2. Reagents for preparation of artificial saliva (pH 5.5, 1 L).

Order	Reagent	Amount (g/1000 mL)
#1	NaCl	0.400
#2	KCl	0.400
#3	$CaCl_2 \cdot 2H_2O$	0.795
#4	$Na_2HPO_4 \cdot H_2O$	0.780
#5	$Na_2S \cdot 9H_2O$	0.005
#6	$CO(NH_2)_2$	1.000

Table 3. Reagents for preparation of SBF (pH 7.4–7.45, 1 L).

Order	Reagent	Amount (g/1000 mL)
#1	NaCl	8.035
#2	$NaHCO_3$	0.355
#3	KCl	0.225
#4	$K_2HPO_4 \cdot 3H_2O$	0.231
#5	$MgCl_2 \cdot 6H_2O$	0.311
#6	1 M HCl	40 mL
#7	$CaCl_2$	0.292
#8	Na_2SO_4	0.072
#9	Tris	6.118
#10	1 M HCl	Appropriate amount for adjusting pH

Table 4. Reagents for preparation of Ringer's solution (pH 6.4–6.5, 1 L).

Order	Reagent	Amount (g/1000 mL)
#1	NaCl	8.600
#2	KCl	0.300
#3	$CaCl_2 \cdot 2H_2O$	0.480

2.3.2. Electrochemical Analysis—Potentiometry

Potentiometric analysis was carried out in order to determine the change in pH values of the solutions in which the coatings were incubated. This assay enables the in vitro stability of the material to be determined in an incubation medium, which simulates conditions in a living organism by its composition. The purpose of this research was to confirm the interactions occurring between the sample and the incubation medium. The ions and molecules contained in the fluids, interfering with the biomaterial, cause a change in the pH value. The obtained dried coating samples with an initial mass of 1 g were incubated at a constant temperature of 36.6 °C in the POL-EKO incubator, model ST 5 B SMART, in prepared artificial biological fluids and distilled water (100 mL) for 40 days. Distilled water was chosen as the reference fluid. Three replicates were performed for each coating composition. The pH value of the fluids was systematically measured using the Elmetron CX-701 multifunctional device with an EPS-1 pH-metric electrode (Zabrze, Poland).

2.3.3. Electroanalytical Analysis—Conductivity

Conductometric analysis was carried out in order to evaluate the ionic conductivity in the incubation medium. The ion exchange occurring at the material/liquid interface causes changes in the conductometric value, as well as gives an indication that the material is not inert under the given conditions. The movement of ions and the appearance of their increasing number causes changes in the conductivity value. Analogous to potentiometric

measurement, dried samples of 1 g were placed in artificial biological fluids and distilled water as the reference (100 mL) and incubated in a POL-EKO incubator, model ST 5 B SMART, for 40 days at a constant temperature of 36.6 °C. Three replicates were performed for each coating composition. The conductometric value of the fluids was systematically measured using the Elmetron CX-701 multifunctional device with an ECF-1 conductivity sensor (Zabrze, Poland).

2.3.4. Determination of Sorption Capacity

One of the strategies for delivering drugs and others active ingredients in targeted therapies is to determine the swelling capacity of materials. The composition of composite materials can affect not only their structure, but also the ability of these materials to swell (to bind water within their structure). In order to investigate the relationship between composition and swelling ability, a swelling kinetics study was carried out. For this purpose, 1 g discs were placed in sterile containers filled with the selected incubation fluids, i.e., SBF, artificial saliva, Ringer's fluid, and distilled water as the reference (100 mL), at 36.6 °C. After 15 min, the samples were removed, excess liquid was collected using filter paper, and the samples were weighed. The measurement was repeated for all samples analogously after 15 min, 30 min, 45 min, 1 h, 2 h, 24 h, 7 days, and 14 days. Three replicates were performed for each coating composition.

The swelling ability of the coatings immersed in fluids was calculated in accordance with the following formula (Equation (1)):

$$\text{Swelling ability} = \frac{m_1 - m_0}{m_0} \cdot 100\% \quad (1)$$

where m_1 is the weight of the immersed sample (g) and m_0 is the initial weight of the sample (g).

The kinetics of coating swelling was investigated using the Voigt-based viscoelastic model (Equation (2)) [32].

$$S_t = S_e\left[1 - e^{-\frac{t}{\tau}}\right] \quad (2)$$

where S_t is swelling at a given time t (%), S_e is equilibrium swelling (power parameter) (%), t is time of swelling S_t (min), and τ is the rate parameter (min).

2.3.5. Degradation Studies

Depending on the purpose of the biomaterial in the body as well as the functions they are expected to take over, it is expected that they will be stable or able to degrade over time. Degradation allows biomaterials to overgrow with new, natural tissue. To determine the stability of coatings in a biological environment, a degradation study was conducted. For this purpose, discs weighing approximately 1 g were placed in sterile containers filled with selected incubation fluids, i.e., SBF, artificial saliva, Ringer's fluid (100 mL), and distilled water as the reference, at 36.6 °C. The containers remained unopened for a period of 60 days. Three replicates were performed for each coating composition. After this time, the samples were removed, dried, and weighed. Based on the equation below (Equation (3)), the degree of degradation in each liquid was determined.

$$\text{Degree of degradation} = \frac{m_t - m_{t0}}{m_{t0}} \cdot 100\% \quad (3)$$

where m_t is the weight of the dry sample after incubation time (g) and m_{t0} is the initial dry sample mass at time t_0 (g).

2.4. Surface Morphology

The imaging and observation of the structure of the materials provides information on the possible mineralization processes that may occur on the surface under the influence of interaction with the incubation medium. After a 14-day incubation in SBF, the coatings were

dried and referred for examination. To determine differences in surface morphology before and after incubation in artificial biological fluids, imaging was performed using a JEOL 5510LV (Tokyo, Japan) scanning electron microscope (SEM) with an EDS IXRF detector. Before SEM measurement, the samples were lyophilized and coated with a conductive gold nanolayer. EDS microanalysis was performed with points in order to detect specific elements on the surface of the samples.

2.5. Hardness Measurement

The composition of the materials as well as the addition of ceramics can affect the mechanical parameters of the coatings obtained. In order to determine the influence of the ceramic phase on the hardness of the coatings, Shore A hardness was measured using a ZwickRoell 3130 (Ulm, Germany). The measurement was performed at a load of 10 N. The instrument was pressed against the material. The indenter, extending from the base, was pressed into the material, as a result of which the balance between the force of the spring and the response of the material was established. Once the equilibrium is established, the pointer stops at the corresponding range of the scale represented in Shore degrees (0–100) [33]. Three replicates were performed for each coating composition. The hardness of the materials was measured by the Shore method according to the PN-ISO 868 standard, with an indenter according to the PN-93/C-04206 standard [34,35].

2.6. Static Tensile Test

Biomaterials in the environment of a living organism are subjected to various loads; hence, it is crucial to study not only their physicochemical but also mechanical parameters. Static tensile tests were carried out on a Shimadzu AGS-X 10 kN testing machine (Kyoto, Japan). The tensile test was conducted in accordance with the PN-EN ISO 527-1 standard at a crosshead speed of 1 mm/min [36]. A load value of 5 N was applied. Longitudinal paddle-shaped coating samples were prepared in order to perform the static tensile test. Three replicates were performed for each coating composition.

2.7. Statistical Analysis

The results of the experiments were subjected to statistical analysis. Statistical significance was calculated using one-way analysis of variance (ANOVA) (alpha value = 5%). The sorption capacity of the coatings and hardness measurement results were subjected to this analysis. For all other experiments, measurements were performed in triplicate and are presented as mean value and standard deviation (SD).

3. Results

3.1. Results of Incubation Tests

3.1.1. Electrochemical Analysis—Potentiometry

The greatest changes in pH value (Figure 3) were observed in artificial saliva, where the pH value increased from 5.5 all the way up to a value of 7.5 for ceramic coatings (**C** and **D**) and around 6.5 for polymer coatings (**A** and **B**). During incubation in artificial saliva, small pieces of the coating were observed on the bottom of the vessel, which may suggest partial degradation of the material. The higher pH value for coatings **C** and **D** is likely due to the leaching of hydroxyapatite, which determines a higher, even more alkaline pH. In SBF, the materials exhibited the greatest stability, with the pH ranging between 7 and 7.5, meaning safety for the body. However, SBF itself has buffering properties, which probably explains the slight changes. The coatings behaved similarly in Ringer's fluid, where an increase to a maximum value of approximately 7 was observed from the first day and the initial pH value of 6.5. This is good information, since physiological fluids in the body have a standard pH value between 7 and 7.5. Depending on diet, lifestyle, and health condition, it is about 7.35–7.45 for blood [37].

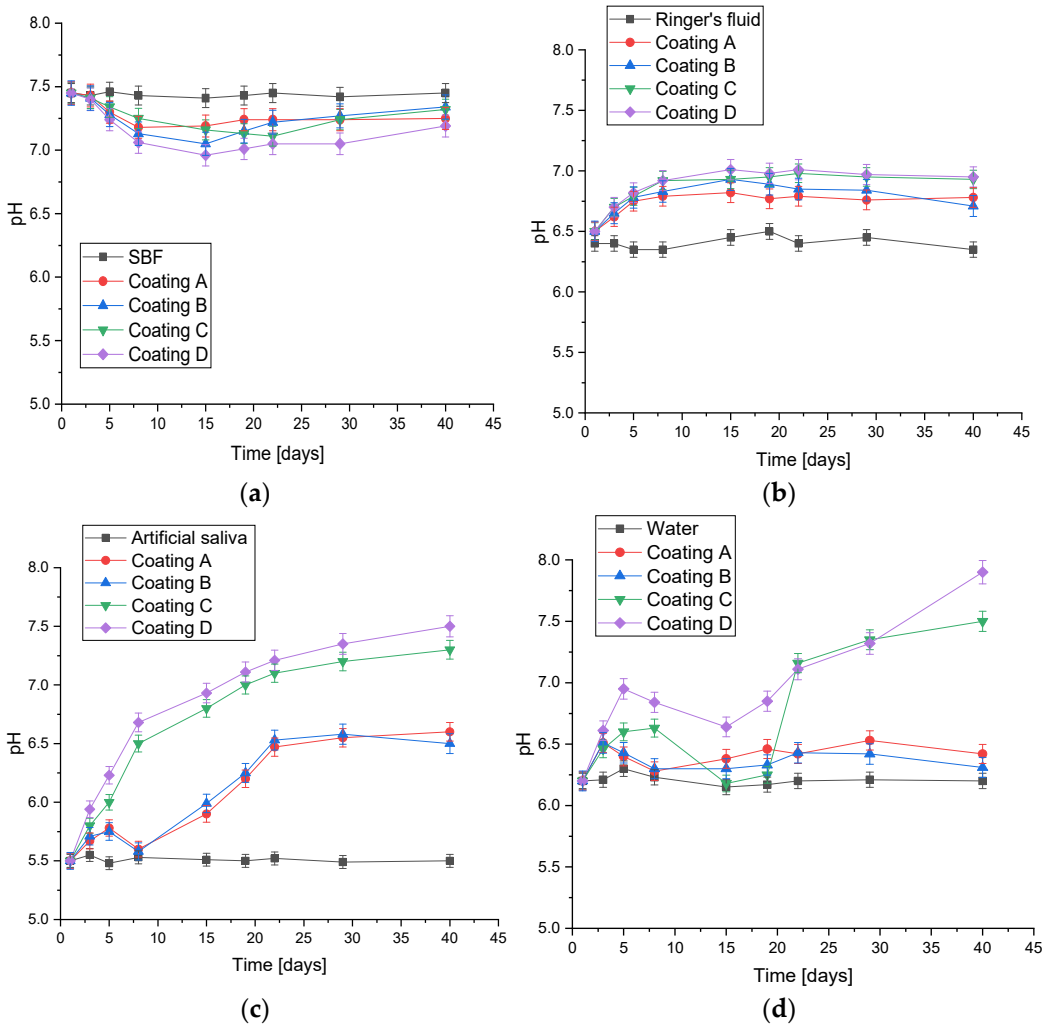

Figure 3. Potentiometric analysis of coatings during 40-day incubation in: (**a**) SBF; (**b**) Ringer's fluid; (**c**) artificial saliva; (**d**) distilled water (number of repetitions $n = 3$).

3.1.2. Electroanalytical Analysis—Conductivity

In parallel to measuring changes in pH values, the ionic conductivity of electrolytes (SBF, water, Ringer's fluid, distilled water) was monitored over time (Figure 4). The value of conductivity depends on the amount of ions present in the solution during incubation and changes with their concentration. This confirms the interactions occurring between the coatings and the medium as well as ongoing ion exchange. The smallest differences in conductivity were observed for coatings in distilled water. Pure distilled water is practically devoid of any ions that could interact with coatings; however, due to the penetration of the fluid into the material, the leaching of under-crosslinked polymer solutions or ceramic grains probably occurred, resulting in small changes. It can be concluded that, for polymer coatings, practically no changes were recorded, as the difference in value was approximately 1 mS; for **C** and **D** coatings with hydroxyapatite, the differences from the initial values were about 4 and 7 mS, respectively. The largest substitutions were observed in artificial saliva, and were caused by the observed partial degradation. The conductivity value doubled from about 110 to about 220 on the last day of measurement. In the case of SBF and Ringer's fluid, the samples behaved similarly, and the spikes in ionic conductivity values may indicate processes of continuous crystallization and recrystallization on the surface of the materials due to interaction with ions from the solutions.

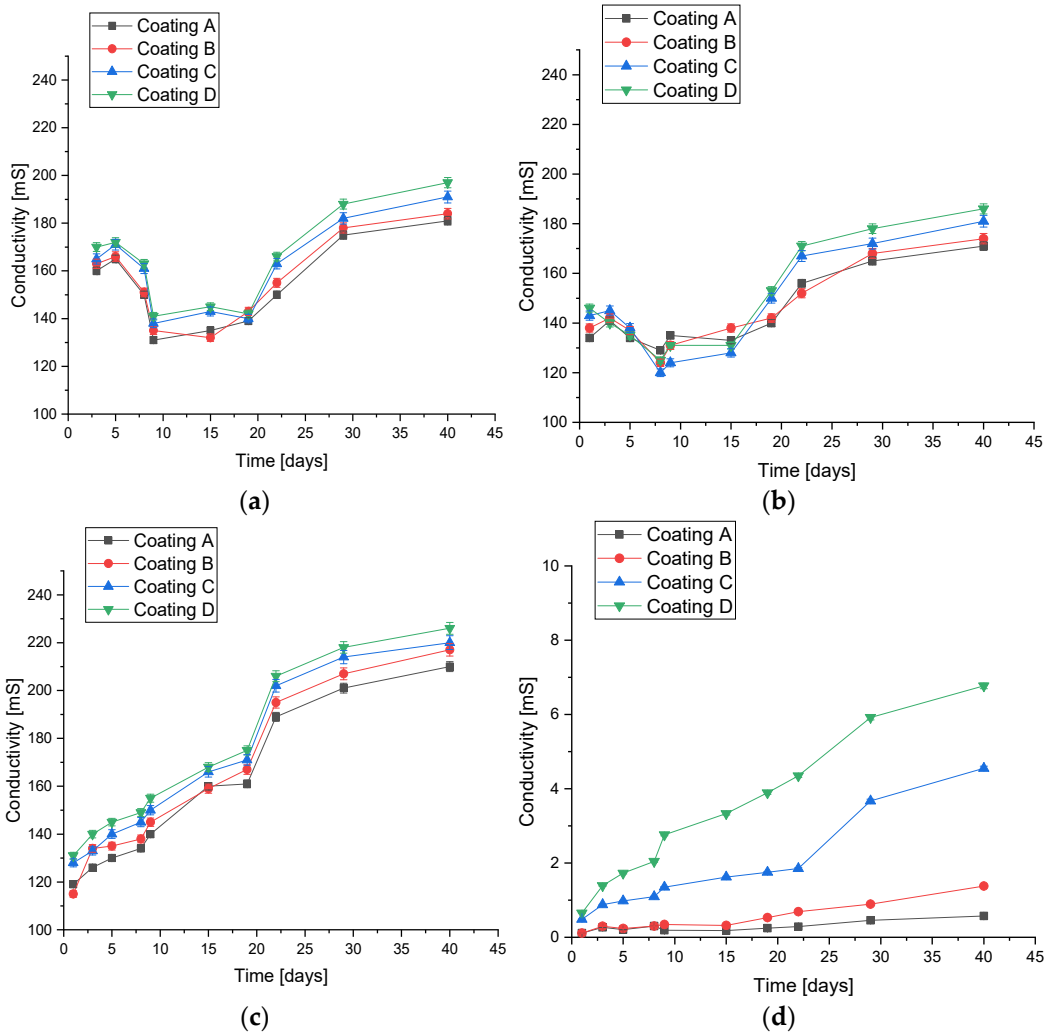

Figure 4. Conductivity analysis of coatings during 40-day incubation in (**a**) SBF; (**b**) Ringer's fluid; (**c**) artificial saliva; and (**d**) distilled water (number of repetitions n = 3).

3.1.3. Determination of Sorption Capacity

During incubation studies, swelling ability (Figure 5) and equilibrium swelling (Table 5) were determined for coatings in the four fluids: SBF, artificial saliva, Ringer's fluid, and distilled water. An increase in swelling coefficients was observed for all samples over time. The results for distilled water have been presented previously; however, in this publication, they were chosen to be compared to other fluids [30]. It was observed that in all liquids, coating **B** exhibited the highest sorption capacity. In coatings **C** and **D**, hydroxyapatite was present, the grains of which limited the possibility of swelling by occupying the free spaces between the polymer chains. This resulted in smaller amounts of fluid being able to reach deeper into the material. On the other hand, coating **A** was lacking collagen fibers that were found in coating **B**. Collagen demonstrates the ability to bind large amounts of water molecules, which probably explains the highest observed sorption capacity [38]. The rate parameter (τ) was also determined, which, for all coatings, was the highest for water. Other liquids present a much richer chemical composition and contain more ions, and as a result, ions can react with each other and crystallize on the surface, or form additional crosslinks between polymer chains [39]. This results in an increase in the crosslinking density of the polymer matrix and consequently a reduction in the amount of free space where water molecules can reach, resulting in a reduction in sorption capacity.

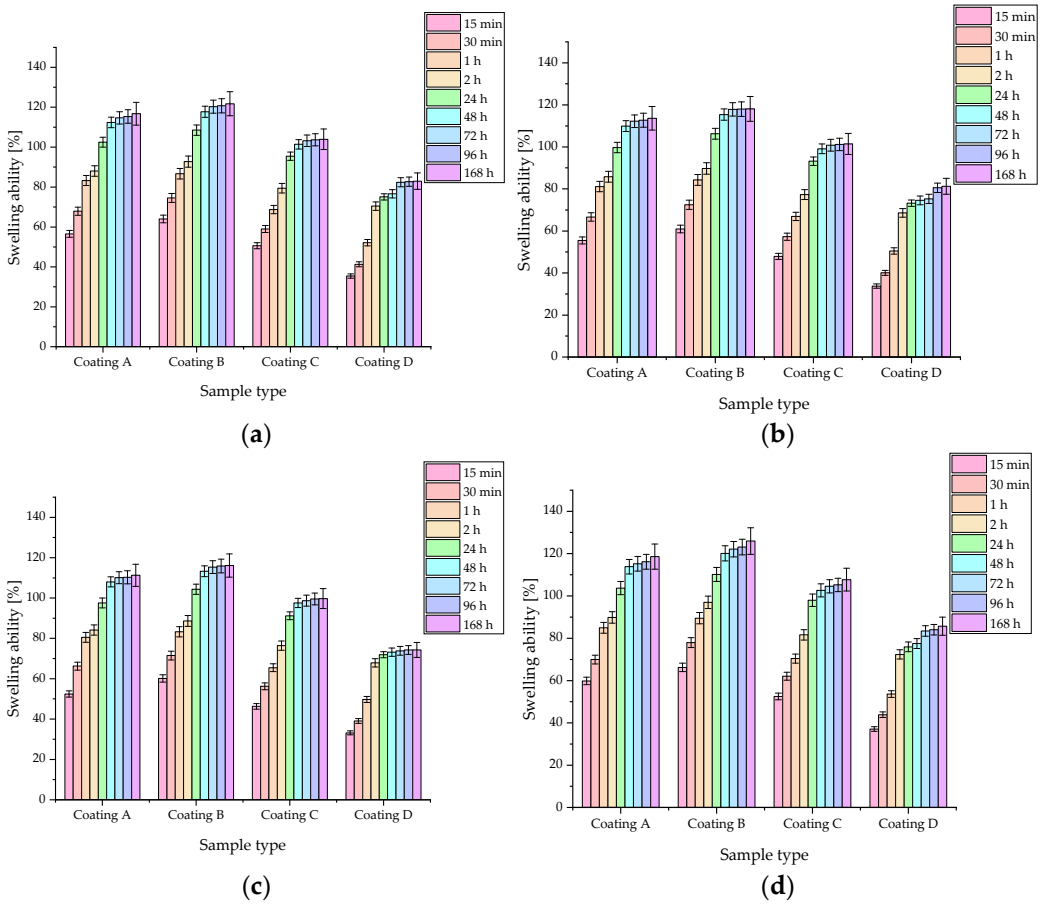

Figure 5. Sorption capacities determined by swelling ability (%) for samples in (**a**) SBF; (**b**) Ringer's fluid; (**c**) artificial saliva; and (**d**) distilled water. According to statistical analysis: SBF f-ratio = 0.08937, p = 0.965651; Ringer's fluid f-ratio = 0.2221, p = 0.880727; artificial saliva f-ratio = 0.39524, p = 0.756828; distilled water f-ratio = 0.45687, p = 0.7133633 (number of repetitions n = 3).

Table 5. Rate parameter (τ) and equilibrium swelling (Se) of tested samples in SBF, Ringer's fluid, artificial saliva, and water.

Sample Type	SBF		Ringer's Fluid		Artificial Saliva		Water	
	Se (%)	τ	Se (%)	τ	Se (%)	τ	Se (%)	τ
A	109.67 ± 4.49	23.65 ± 5.81	107.01 ± 4.44	34.45 ± 5.83	104.91 ± 4.17	23.00 ± 5.45	115.8 ± 5.00	30.41 ± 8.11
B	114.27 ± 4.93	20.79 ± 5.44	111.77 ± 4.81	21.68 ± 5.64	109.73 ± 4.65	21.17 ± 5.42	118.8 ± 5.13	29.70 ± 8.04
C	99.04 ± 4.23	30.01 ± 7.69	96.81 ± 4.02	30.86 ± 7.67	95.14 ± 3.86	31.14 ± 7.53	103.81 ± 4.52	51.14 ± 10.91
D	80.11 ± 1.52	54.16 ± 10.17	77.11 ± 1.48	51.88 ± 9.77	73.68 ± 0.86	46.84 ± 5.39	82.51 ± 2.79	47.30 ± 9.22

For all fluids, the highest sorption capacity was observed during the first 48 h when changes were dynamic. After that time, the values slowly stabilized and varied little. However, it is important to highlight that swelling abilities were exhibited by all samples, potentially confirming their applicability as carriers of active substances.

3.1.4. Degradation Studies

Degradation studies were conducted for 60 days in the four liquids. The conditions of a living organism were simulated. Each of the fluids had a slightly different initial pH value: for SBF, it was about 7.4, for Ringer's fluid about 6.5, for artificial saliva about 5.5, and for distilled water about 6.5. The difference in weight before and after the incubation period was observed for all samples (see Table 6). The largest changes were observed for coatings in artificial saliva where the difference ranged from 36.19% for coating **A** to 39.79% for coating **D**. Significantly, in artificial saliva, a greater loss was observed for composite

coatings, while in the other liquids, larger values were observed for polymer coatings **A** and **B**. This is probably caused by the low pH of saliva, which caused degradation of the polymer matrix, and eventually the ceramic began to crumble out of the coating as well. Fragments of coatings were observed on the bottom of the vessel during potentiometric measurements. The smallest changes were observed for SBF, where a value of only 8.14% was observed for coating **D**. These small differences are probably due to the continuous processes of crystallization and recrystallization on the surface of the coating due to the interaction of the biomaterials with the ions present in the liquid. It is likely that partial degradation occurs in SBF, as it occurs even in distilled water, but recrystallization processes make the loss percentages not so large.

Table 6. Degradation of materials during incubation indicated by mass difference (%).

Sample Type	Mass Difference (%)			
	SBF	Ringer's Fluid	Artificial Saliva	Distilled Water
A	12.12	22.93	36.19	16.30
B	12.46	23.65	37.41	15.58
C	10.84	20.85	37.89	15.56
D	8.14	20.25	39.79	14.18

3.2. Surface Morphology

Figure 6 presents the surface morphology of the coatings at ×250 magnification before incubation in SBF.

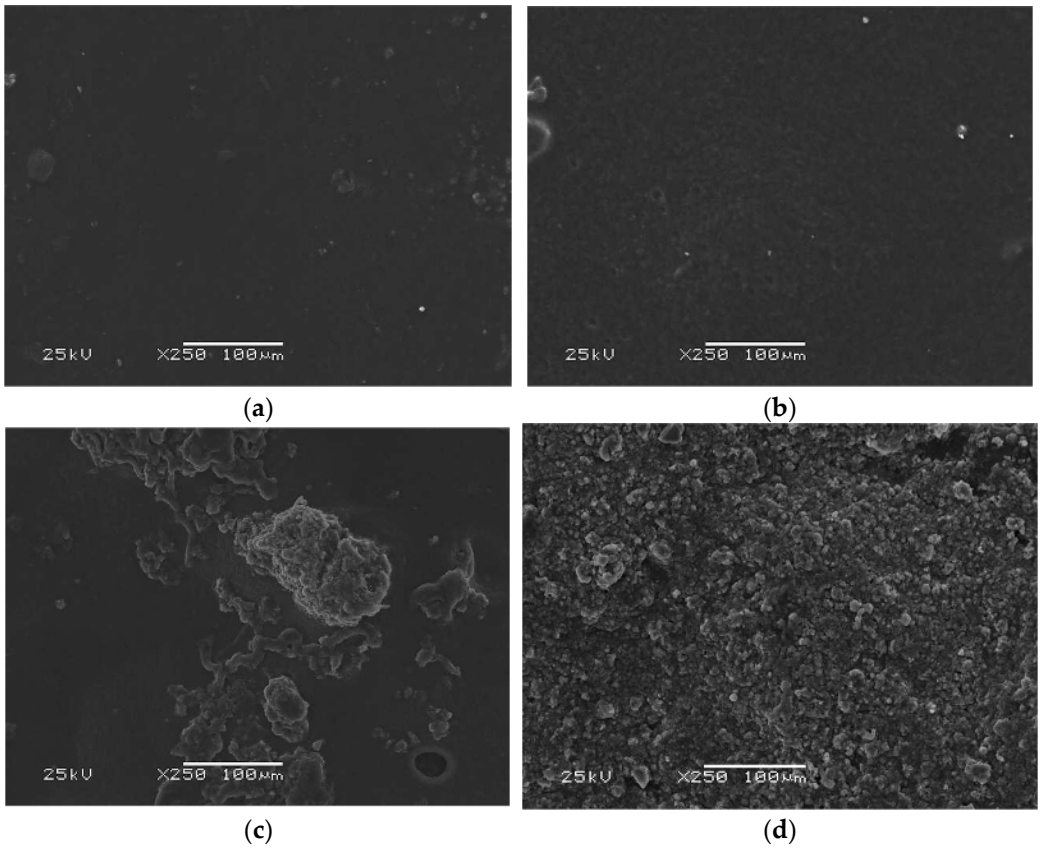

(**a**) (**b**) (**c**) (**d**)

Figure 6. Morphology analysis of the coatings before the incubation period: (**a**) SEM image of coating **A**; (**b**) SEM image of coating **B**; (**c**) SEM image of coating **C**; (**d**) SEM image of coating **D**.

Despite the presence of collagen in coating **B** and its absence in coating **A**, the surfaces of these two polymeric materials are similar and relatively smooth. Noticeably, as the

proportion of HA in the materials increases, the number of crystals observed during measurement increases. In coating **C**, it is possible to indicate a polymeric phase as well as a ceramic phase, while in the case of coating **D**, the surface of the material is practically entirely covered with HA grains, with no polymeric free spots breaking through.

The coatings were incubated in SBF liquid for a period of 14 days. Figure 7 demonstrates a microscopic image of the surface of the dried samples after this time. The precipitation of crystals with a characteristic square shape was observed on the polymer coatings. For coating **B**, there were slightly more of them, although they were still in comparable amounts. For coating **C**, comparing the image to that before the immersion period in SBF, the appearance of new crystals in the form of cauliflower-shaped efflorescence was observed, which covered the entire surface of the sample; no polymer phase was found penetrating to the surface. The **D** coating before and after the incubation period looks similar; however, after incubation, it appears to be rougher, which may be due to the precipitation of new apatite layers and crystals. The appearance of new apatite layers and crystals on the surface of incubated samples is a very desirable result. Such biomineralization is proof of the bioactivity of the coatings due to the evidence of interaction between the material and the fluid medium [39,40].

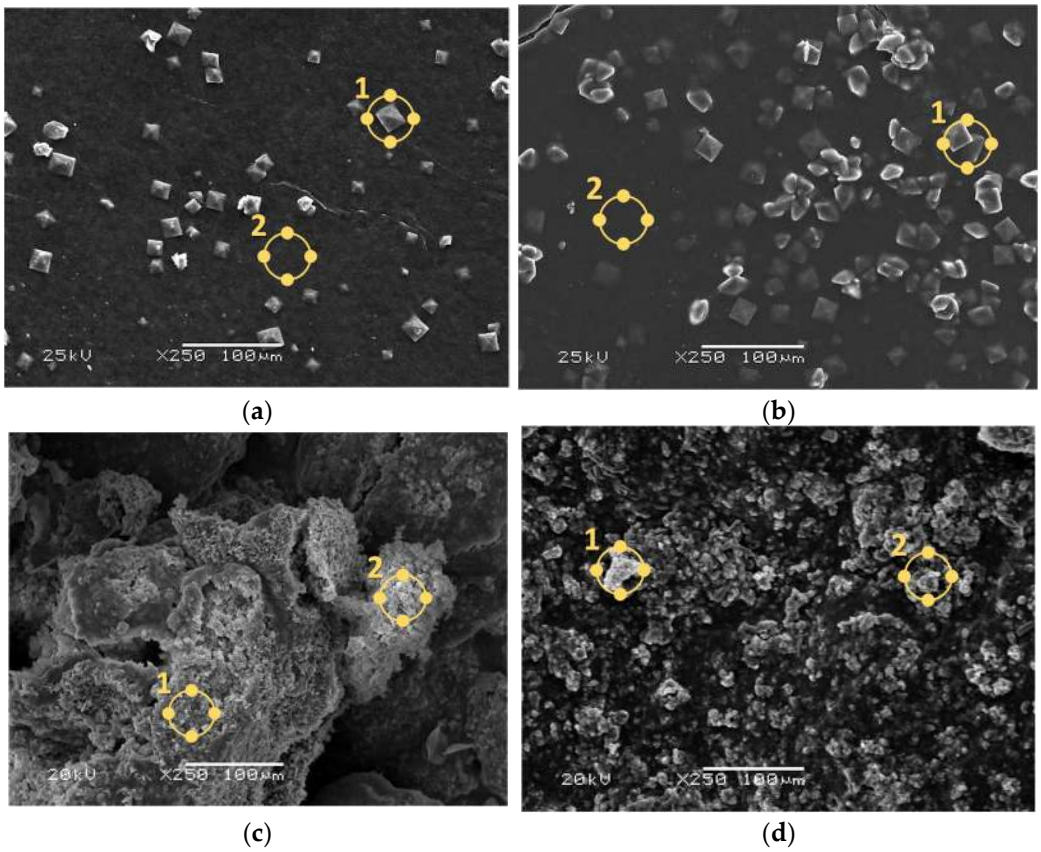

Figure 7. Morphology analysis of the coatings after the incubation period with EDS microanalysis points indicated by yellow circles: (**a**) SEM image of coating **A**; (**b**) SEM image of coating **B**; (**c**) SEM image of coating **C**; (**d**) SEM image of coating **D**.

In parallel with the analysis of surface morphology by SEM, EDS microanalysis was carried out to determine the presence of individual elements. The elements C and O derived mainly from polymers, Ca and P derived from HA, and the composition of the SBF fluid, as well as Mg, Na, K, and Cl, whose ions were also found in SBF, were determined. Au, which was sputtered onto the samples before measurement, was not quantified. The results are presented in Table 7. For each coating, two spots on the surface were inspected. In composite coatings **C** and **D**, the compositions at the two sites tested are similar. High Ca

and P contents indicate precipitated apatite layers. In the case of polymer coatings **A** and **B**, Ca ions were also observed on the surface, but the amount of P was disproportionately higher. Larger amounts of these elements are found in composite materials. It was also observed that there were more Cl ions on the surface of these coatings, which probably indicates the precipitation of sodium, potassium, or calcium chlorides from the solution on the surface. The detection of Mg, Na, and Cl after incubation indicates the desired reactions between the artificial saline fluid and the biomaterial.

Table 7. Elemental composition of tested coatings after incubation in SBF for each EDS point.

Sample Type	Atomic Percentage (%)	
A	1.	C: 21.08, O: 54.13, Na: 3.61 Mg: 0.18, P: 0.40, Cl: 4.51, K: 0.12, Ca: 15.99
	2.	C: 67.64, O: 22.49, Na: 3.52, Mg: 0.28, P: 0.92, Cl: 4.47, K: 0.26, Ca: 0.43
B	1.	C: 52.94, O: 25.89, Na: 2.05 Mg: 0.32, P: 0.90, Cl: 5.53, K: 0.40, Ca: 11.97
	2.	C: 69.37, O: 18.79, Na: 2.31, Mg: 0.14, P: 2.64, Cl: 5.49, K: 0.39, Ca: 0.88
C	1.	C: 34.78, O: 33.51, Na: 3.08, Mg: 0.49, P: 10.84, Cl: 3.82, K: 0.10, Ca: 13.40
	2.	C: 33.93, O: 34.20, Na: 2.57, Mg: 0.29, P: 7.93, Cl: 2.14, K: 0.10, Ca: 10.85
D	1.	C: 38.52, O: 32.41, Na: 0.77, Mg: 0.13, P: 8.94, Cl: 1.09, K: 0.13, Ca: 18.02
	2.	C: 36.92, O: 38.72, Na: 1.09, Mg: 0.33, P: 8.06, Cl: 0.93, K: 0.06, Ca: 13.89

Based on the obtained images and the amount of each element, it was demonstrated that the ability to form mineralized apatite layers on the surface of incubated materials is fully dependent on the presence of a ceramic phase in the coating. Therefore, a higher proportion of the ceramic phase in biomaterials is likely to increase their bioactivity through the ability to form new apatite layers. This phenomenon is related to the unique nature of SBF—more specifically, its ionic composition. Interactions between Ca^{2+} ions and negatively charged HA cause the spontaneous growth of apatite-like nuclei on the surface. In time, it is transformed into bone-like apatite through the incorporation of P ions [41].

3.3. Hardness Measurement

Figure 8 demonstrates the results of Shore A hardness measurements for the obtained composite coatings. Previously, a similar study was conducted for the same coatings, but applied to PLA plates [30].

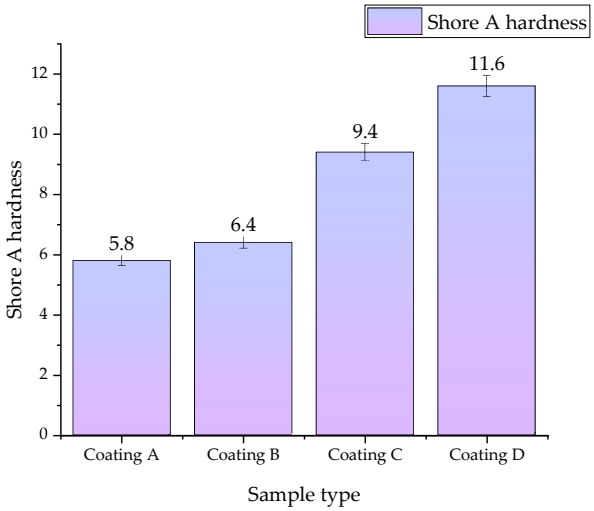

Figure 8. Hardness measurements of coatings performed by the Shore A method. According to statistical analysis, f-ratio = 91.5, $p < 0.00001$ (number of repetitions $n = 3$).

A clear effect of HA addition on hardness was observed, as the value clearly increases with the higher proportion of HA in the materials. For the coatings without the ceramic

phase, i.e., **A** and **B**, similar relatively low results were obtained. However, the influence of HA on hardness is evident, as this value clearly rises with an increase in the content of HA, reaching the highest value of 11.6 for sample **D**. Comparing the results obtained with those previously published for coatings deposited on PLA plates, it can be concluded that the coating itself does not significantly affect this parameter, and the hardness is determined by the substrate to which they are deposited (in this case, PLA).

3.4. Static Tensile Test

As a result of the study, a clear effect of the ceramic phase and thus the composition of the coatings on the parameters studied was observed. The obtained results are presented in Table 8. The addition of the ceramic phase caused an increase in the modulus of elasticity. Figure 9 demonstrates the process of preparing a sample for measurement.

Table 8. Young's modulus and maximum deformation parameters of the obtained materials (number of repetitions $n = 3$).

Sample	Modulus of Elasticity (N/mm^2)	Max. Deformation (%)
A	11.48 ± 0.61	20.51 ± 1.78
B	13.22 ± 3.46	15.71 ± 0.38
C	48.22 ± 3.87	4.63 ± 0.48
D	93.31 ± 11.18	2.15 ± 1.01

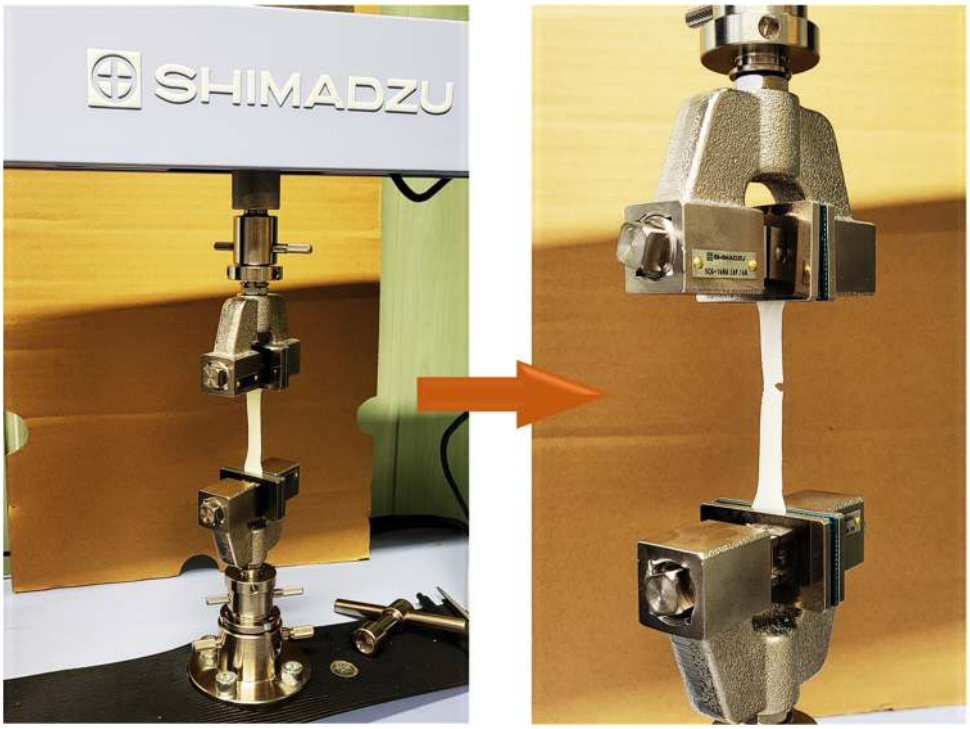

Figure 9. Coating sample during static tensile strength test measurement.

Comparing polymer samples **A** and **B** with sample **D** containing 15% ceramic phase, an almost ninefold increase in modulus values was observed. At the same time, a decrease in deformation values was observed in the presence of HA. This parameter was almost ten times lower for composite sample **D** compared to polymer sample **A**. Maximum deformation can be defined as the tendency of a material to change shape or deform when a tensile force is applied. Deformation occurs when, as a result of stretching an elastic material, internal intermolecular forces oppose the applied force [42]. Thus, it can be concluded that the presence of HA significantly affects the strength parameters of the developed coatings. No significant effect of collagen addition was observed.

4. Discussion

Polymer-based composite materials with a suspended ceramic phase are well-known and extensively studied materials in skeletal regeneration applications. However, their potential for use as coating materials represents a niche. The key is the selection of components to obtain a fully crosslinked and homogeneous material. This study presents a method for obtaining coating materials. These were subjected to in vitro incubation tests in order to determine their behavior under conditions similar to those in a living organism. The mechanical parameters of the materials were also determined. The incubation studies were conducted in four incubation fluids—SBF, artificial saliva, Ringer's fluid, and distilled water—in order to check the behavior of the coatings in environments with slightly different environmental conditions. Changes in pH value, ionic conductivity, and sorption capacity were examined. Some correlations between the first two parameters were shown. In artificial saliva where the greatest changes in pH were observed, there was the greatest increase in ionic conductivity values. Moreover, the greatest degree of degradation was also observed in this fluid. The materials demonstrated the greatest pH stability in Ringer's fluid and SBF, and in these fluids, the ionic conductivity was also similar. In all cases, the conductivity values were higher for composite coatings than for polymeric ones. The effect of the proportion of the ceramic phase on the sorption capacity was also observed. The higher the proportion of the ceramic phase, the lower the swelling capacity of the biomaterials. The swelling results were compared to a similar work dealing with the development of injectable hydrogels for hard tissue. Although the purpose was different, the chemical composition of the material was similar, consisting of PEG, nanometer-sized ceramics, and PEGDA. In this case, a significantly higher increase in swelling capacity was observed [43]. However, the cited work used PEG with a molecular weight of 35,000 g/mol, while for the coatings, PEG with a molecular weight of 10,000 g/mol was used. It can therefore be speculated that molecular weight may affect the sorption capacity. Unfortunately, the exact weight for PEGDA was not given. Significantly, the changes in conductivity values confirm the existence of interactions between the incubation fluids and the coatings, as confirmed by SEM and EDS analysis. The formation of new apatite crystals and probably chloride crystals was detected. Once again, a correlation due to the presence of HA in the material was demonstrated, as no new apatite precipitates were observed in coatings where it was absent. On the other hand, as little as 5% of HA was enough for the entire surface to be covered with new apatite layers within 14 days, which is a very desirable phenomenon, indicating the ability of the coatings to undergo biomineralization, which is needed for the target application of the developed materials: coating metallic and polymeric implants and ensuring their bioactive nature. Observations of surface changes and the biomineralization process are consistent with reports in the literature. For composites based on PVP and nano-HA, new apatite crystals were already observed after incubation in SBF at 3 and 7 days [44]. However, the origin of the hydroxyapatite should also be considered in this type of application, as its bioactivity can vary depending on whether it is natural or synthetic [45].

The analysis of mechanical properties demonstrated that the materials did not have a high modulus of elasticity despite the presence of HA, which has high strength parameters. This is probably because the coatings were relatively thin (the thickness of the coatings was previously reported in [30]). However, in this case, its influence on the measured parameter can also be clearly seen, with the modulus of elasticity being higher with more ceramics in the polymer phase. A similar relationship was observed for the measurement of hardness; relating this to previous studies, it can be concluded that once the coating is applied to the target implant/biomaterial, the mechanical strength of the entire system will not be determined by the presence of the developed coating, but by the properties of the covered material. The effect of hydroxyapatite reinforcement on polymeric and hydrogel materials has been reported in the literature, where it has been confirmed that it increases the modulus of elasticity. In other composites based on PEG or PVP and polyvinyl alcohol,

the value of modulus of elasticity was up to four times higher, and the final material was able to carry greater loads [43,46].

Nevertheless, with reference to the discussion presented above, it should be emphasized that the factors analyzed in the presented manuscript, mainly mechanical resistance and incubation fluids, are not the only ones that affect the implanted biomaterial in the body. Biological fluids, besides the considered ions, contain various types of proteins and other active components that can affect the implanted material via surface energy changes, hydrophilic/hydrophobic interactions, and charge changes through cationic/anionic binding [47].

5. Conclusions

This work describes the physicochemical and mechanical analysis of composite coatings intended for coating implants for craniofacial bone regeneration. The stability of the materials was demonstrated in incubating fluids such as SBF, with no drastic changes in pH value or material degradation observed. Moreover, sorption capacity analysis showed that the materials are able to bind fluids and swell, which enables their potential use as carriers of active substances in targeted therapy. The coatings themselves do not have high tensile strength or hardness, and this parameter is determined by the substrate that is covered with them. Analyzing the results obtained, it can be concluded that the application of coatings on an implantable material will not change its mechanical properties, but will add the desired bioactivity. This parameter is determined by the nature of HA with its ability to osteoconduct and precipitate new apatite layers, and was confirmed by SEM and EDS analysis. The results obtained confirm the need for further research on the developed composite coatings, including cytotoxicity studies to eliminate possible negative effects on tissues.

6. Patents

The results of extensive research, part of which is presented in this manuscript, are three patent applications to the Polish Patent Office: no: P.442978, application date: 29 November 2022; no: P.442979, application date: 29 November 2022; no: P.442980, application date: 29 November 2022.

Author Contributions: Conceptualization, D.S.; methodology, D.S.; software, D.S.; validation, D.S.; formal analysis, D.S.; investigation, D.S.; resources, D.S.; data curation, D.S.; writing—original draft preparation, D.S.; writing—review and editing, J.J. and A.S.-K.; visualization, D.S.; supervision, J.J. and A.S.-K.; project administration, A.S.-K.; funding acquisition, A.S.-K. and J.J. All authors have read and agreed to the published version of the manuscript.

Funding: This research was funded by the Foundation for Polish Science, grant number POIR.04.04.00-00-16D7/18. The "Multifunctional biologically active composites for applications in bone regenerative medicine" project is carried out within the TEAM-NET program of the Foundation for Polish Science financed by the European Union under the European Regional Development Fund. This work was also supported by projects APVV-17-0373 and APVV-22-0133.

Data Availability Statement: The data that support the findings of this study are contained within the article.

Acknowledgments: The authors would like to thank Stanisław Kuciel for lending the equipment to conduct the mechanical tests and Krzysztof Miernik for lending a scanning electron microscope.

Conflicts of Interest: The authors declare no conflicts of interest.

References

1. Chevallier, P.; Turgeon, S.; Sarra-Bournet, C.; Turcotte, R.; Laroche, G. Characterization of multilayer anti-fog coatings. *ACS Appl. Mater. Interfaces* **2011**, *3*, 750–758. [CrossRef] [PubMed]
2. Marco, F.; Milena, F.; Gianluca, G.; Vittoria, O. Peri-implant osteogenesis in health and osteoporosis. *Micron* **2005**, *36*, 630–644. [CrossRef] [PubMed]

3. Nouri, A.; Wen, C. Introduction to surafce coating and modification of metallic biomaterials. In *Surface Coating and Modification of Metallic Biomaterials*; Wen, C., Ed.; Elsevier: Amsterdam, The Netherlands, 2015; pp. 3–45, ISBN 978-1-78242-316-4.
4. Kokubo, T.; Himeno, T.; Kim, H.M.; Kawashita, M.; Nakamura, T. Process of bonelike apatite formation on sintered hydroxyapatite in serum-containing SBF. *Key Eng. Mater.* **2004**, *254–256*, 139–142. [CrossRef]
5. Batchelor, A.W.; Chandrasekaran, M. *Service Characteristics of Biomedical Materials and Implants*; Imperial College Press: London, UK, 2004; ISBN 978-1-78326-060-7.
6. Priyadarshini, B.; Rama, M.; Chetan; Vijayalakshmi, U. Bioactive coating as a surface modification technique for biocompatible metallic implants: A review. *J. Asian Ceram. Soc.* **2019**, *7*, 397–406. [CrossRef]
7. Kravanja, K.A.; Finšgar, M. A review of techniques for the application of bioactive coatings on metal-based implants to achieve controlled release of active ingredients. *Mater. Des.* **2022**, *217*, 110653. [CrossRef]
8. Shekhter, A.B.; Fayzullin, A.L.; Vukolova, M.N.; Rudenko, T.G.; Osipycheva, V.D.; Litvitsky, P.F. Medical applications of collagen and collagen-based materials. *Curr. Med. Chem.* **2017**, *26*, 506–516. [CrossRef] [PubMed]
9. Ghomi, E.R.; Nourbakhsh, N.; Akbari Kenari, M.; Zare, M.; Ramakrishna, S. Collagen-based biomaterials for biomedical applications. *J. Biomed. Mater. Res.—Part B* **2021**, *109*, 1986–1999. [CrossRef]
10. Alhazmi, W.; Almutairi, A.; Al-Muqbil, A.; Al-Ali, A.; Alhasson, M. Pattern of ear, nose, and throat disease seen by otolaryngologists at Qassim University outpatient clinics, Saudi Arabia. *Int. J. Med. Dev. Ctries.* **2021**, *5*, 1430–1436. [CrossRef]
11. Sionkowska, A.; Skopinska, J.; Wisniewski, M.; Leznicki, A.; Fisz, J. Spectroscopic studies into the influence of UV radiation on elastin hydrolysates in water solution. *J. Photochem. Photobiol. B Biol.* **2006**, *85*, 79–84. [CrossRef]
12. Xu, Q.; Torres, J.E.; Hakim, M.; Babiak, P.M.; Pal, P.; Battistoni, C.M.; Nguyen, M.; Panitch, A.; Solorio, L.; Liu, J.C. Collagen- and hyaluronic acid-based hydrogels and their biomedical applications. *Mater. Sci. Eng. R Rep.* **2021**, *146*, 100641. [CrossRef]
13. He, Y.; Wang, C.; Wang, C.; Xiao, Y.; Lin, W. An overview on collagen and gelatin-based cryogels: Fabrication, classification, properties and biomedical applications. *Polymers* **2021**, *13*, 2299. [CrossRef] [PubMed]
14. Ahmad, M.I.; Li, Y.; Pan, J.; Liu, F.; Dai, H.; Fu, Y.; Huang, T.; Farooq, S.; Zhang, H. Collagen and gelatin: Structure, properties, and applications in food industry. *Int. J. Biol. Macromol.* **2024**, *254*, 128037. [CrossRef] [PubMed]
15. Muralidharan, N.; Shakila, R.J.; Sukumar, D.; Jeyasekaran, G. Skin, bone and muscle collagen extraction from the trash fish, leather jacket (*Odonus niger*) and their characterization. *J. Food Sci. Technol.* **2013**, *50*, 1106–1113. [CrossRef] [PubMed]
16. Leuenberger, B.H. Investigation of viscosity and gelation properties of different mammalian and fish gelatins. *Food Hydrocoll.* **1991**, *5*, 353–361. [CrossRef]
17. Parcheta, M.; Świsłocka, R.; Orzechowska, S.; Akimowicz, M.; Choińska, R.; Lewandowski, W. Recent developments in effective antioxidants: The structure and antioxidant properties. *Materials* **2021**, *14*, 1984. [CrossRef]
18. Lim, J.C.; Grey, A.C.; Zahraei, A.; Donaldson, P.J. Age-dependent changes in glutathione metabolism pathways in the lens: New insights into therapeutic strategies to prevent cataract formation—A review. *Clin. Exp. Ophthalmol.* **2020**, *48*, 1031–1042. [CrossRef] [PubMed]
19. Gürbüz Çolak, N.; Eken, N.T.; Ülger, M.; Frary, A.; Doğanlar, S. Mapping of quantitative trait loci for antioxidant molecules in tomato fruit: Carotenoids, vitamins C and E, glutathione and phenolic acids. *Plant Sci.* **2020**, *292*, 110393. [CrossRef]
20. Aoyama, K. Glutathione in the brain. *Int. J. Mol. Sci.* **2021**, *22*, 5010. [CrossRef]
21. Bal, Z.; Kaito, T.; Korkusuz, F.; Yoshikawa, H. Bone regeneration with hydroxyapatite-based biomaterials. *Emergent Mater.* **2020**, *3*, 521–544. [CrossRef]
22. Shi, H.; Zhou, Z.; Li, W.; Fan, Y.; Li, Z.; Wei, J. Hydroxyapatite based materials for bone tissue engineering: A brief and comprehensive introduction. *Crystals* **2021**, *11*, 149. [CrossRef]
23. Schille, C.; Braun, M.; Wendel, H.P.; Scheideler, L.; Hort, N.; Reichel, H.P.; Schweizer, E.; Geis-Gerstorfer, J. Corrosion of experimental magnesium alloys in blood and PBS: A gravimetric and microscopic evaluation. *Mater. Sci. Eng. B* **2011**, *176*, 1797–1801. [CrossRef]
24. Anurag, K.P.; Avinash, K.; Rupesh, K.; Gautam, R.K.; Behera, C.K. Tribological performance of SS 316L, commercially pure titanium, and Ti6Al4V in different solutions for biomedical applications. *Mater. Today Proc.* **2023**, *78*, A1–A8. [CrossRef]
25. Vladescu, A.; Pârâu, A.; Pana, I.; Cotrut, C.M.; Constantin, L.R.; Braic, V.; Vrânceanu, D.M. In vitro activity assays of sputtered HAp coatings with SiC addition in various simulated biological fluids. *Coatings* **2019**, *9*, 389. [CrossRef]
26. Ruan, C.; Hu, N.; Ma, Y.; Li, Y.; Liu, J.; Zhang, X.; Pan, H. The interfacial pH of acidic degradable polymeric biomaterials and its effects on osteoblast behavior. *Sci. Rep.* **2017**, *7*, 6794. [CrossRef] [PubMed]
27. Reid, R.; Sgobba, M.; Raveh, B.; Rastelli, G.; Sali, A.; Santi, D.V. Analytical and simulation-based models for drug release and gel-degradation in a tetra-PEG hydrogel drug-delivery system. *Macromolecules* **2015**, *48*, 7359–7369. [CrossRef]
28. Hu, J.; Chen, Y.; Li, Y.; Zhou, Z.; Cheng, Y. A thermo-degradable hydrogel with light-tunable degradation and drug release. *Biomaterials* **2017**, *112*, 133–140. [CrossRef] [PubMed]
29. Bordbar-Khiabani, A.; Gasik, M. Smart hydrogels for advanced drug delivery systems. *Int. J. Mol. Sci.* **2022**, *23*, 3665. [CrossRef]
30. Tomala, A.M.; Słota, D.; Florkiewicz, W.; Piętak, K.; Dyląg, M.; Sobczak-Kupiec, A. Tribological properties and physiochemical analysis of polymer-ceramic composite coatings for bone regeneration. *Lubricants* **2022**, *10*, 58. [CrossRef]
31. Słota, D.; Piętak, K.; Florkiewicz, W.; Jampílek, J.; Tomala, A.; Urbaniak, M.M.; Tomaszewska, A.; Rudnicka, K.; Sobczak-Kupiec, A. Clindamycin-loaded nanosized calcium phosphates powders as a carrier of active substances. *Nanomaterials* **2023**, *13*, 1469. [CrossRef]

32. Pluta, K.; Florkiewicz, W.; Malina, D.; Rudnicka, K.; Michlewska, S.; Królczyk, J.B.; Sobczak-Kupiec, A. Measurement methods for the mechanical testing and biocompatibility assessment of polymer-ceramic connective tissue replacements. *Meas. J. Int. Meas. Confed.* **2021**, *171*, 108733. [CrossRef]
33. Bartecka, G.; Równicka-Zubik, J.; Sułkowska, A.; Moczyński, M.; Famulska, W.; Sułkowski, W.W. The influence of polyurethane component on the properties of polyurethane-rubber composites obtained from waste materials. *Mol. Cryst. Liq. Cryst.* **2014**, *603*, 27–36. [CrossRef]
34. *PN-ISO 868*; Tworzywa sztuczne i ebonite. Oznaczanie twardości metodą wciskania z zastosowaniem twardościomierza (twardość metodą Shore'A). Polski Komitet Normalizacyjny: Warszawa, Poland, 2005.
35. *PN-93/C-04206*; Guma. Oznaczanie twardości przez wgniecenie przy użyciu kieszonkowych twardościomierzy. Polski Komitet Normalizacyjny: Warszawa, Poland, 2015.
36. *PN-EN ISO 527-1*; Tworzywa sztuczne. Oznaczanie właściwości mechanicznych przy statycznym rozciąganiu. Polski Komitet Normalizacyjny: Warszawa, Poland, 2020.
37. Li, Y.; Liu, X.; Xu, X.; Xin, H.; Zhang, Y.; Li, B. Red-blood-cell waveguide as a living biosensor and micromotor. *Adv. Funct. Mater.* **2019**, *29*, 1905568. [CrossRef]
38. Madhavi, W.A.M.; Weerasinghe, S.; Fullerton, G.D.; Momot, K.I. Structure and dynamics of collagen hydration water from molecular dynamics simulations: Implications of temperature and pressure. *J. Phys. Chem. B* **2019**, *123*, 4901–4914. [CrossRef] [PubMed]
39. Slota, D.; Gląb, M.; Tyliszczak, B.; Dogulas, T.E.L.; Rudnicka, K.; Miernik, K.; Urbaniak, M.M.; Rusek-Wala, P.; Sobczak-upiec, A. Composites based on hydroxyapatite and whey protein isolate for applications in bone regeneration. *Materials* **2021**, *14*, 2317. [CrossRef]
40. Correa da Silva Braga de Melo, C.; Balestrero Cassiano, F.; Soares Bronze-Uhle, É.; de Toledo Stuani, V.; Alves Ferreira Bordini, E.; de Oliveira Gallinari, M. Mineral-induced bubbling effect and biomineralization as strategies to create highly porous and bioactive scaffolds for dentin tissue engineering. *J. Biomed. Mater. Res. Part B Appl. Biomater.* **2022**, *11*, 1757–1770. [CrossRef] [PubMed]
41. Shibata, H.; Yokoi, T.; Goto, T.; Kim, I.Y.; Kawashita, M.; Kikuta, K.; Ohtsuki, C. Behavior of hydroxyapatite crystals in a simulated body fluid: Effects of crystal face. *Nippon Seramikkusu Kyokai Gakujutsu Ronbunshi/J. Ceram. Soc. Jpn.* **2013**, *121*, 807–812. [CrossRef]
42. Saba, N.; Jawaid, M.; Sultan, M.T.H. *An Overview of Mechanical and Physical Testing of Composite Materials*; Elsevier Ltd.: Amsterdam, The Netherlands, 2018; ISBN 9780081022924.
43. Gaharwar, A.K.; Dammu, S.A.; Canter, J.M.; Wu, C.J.; Schmidt, G. Highly extensible, tough, and elastomeric nanocomposite hydrogels from poly(ethylene glycol) and hydroxyapatite nanoparticles. *Biomacromolecules* **2011**, *12*, 1641–1650. [CrossRef]
44. Suresh Kumar, C.; Dhanaraj, K.; Vimalathithan, R.M.; Ilaiyaraja, P.; Suresh, G. Hydroxyapatite for bone related applications derived from sea shell waste by simple precipitation method. *J. Asian Ceram. Soc.* **2020**, *8*, 416–429. [CrossRef]
45. Sossa, P.A.F.; Giraldo, B.S.; Garcia, B.C.G.; Parra, E.R.; Arango, P.J.A. Comparative study between natural and synthetic hydroxyapatite: Structural, morphological and bioactivity properties. *Rev. Mater.* **2018**, *23*, e-12217. [CrossRef]
46. Jalageri, M.B.; Mohan Kumar, G.C. Hydroxyapatite reinforced polyvinyl alcohol/polyvinyl pyrrolidone based hydrogel for cartilage replacement. *Gels* **2022**, *8*, 555. [CrossRef]
47. Rahmati, M.; Silva, E.A.; Reseland, J.E.; Heyward, C.A.; Haugen, H.J. Biological responses to physicochemical properties of biomaterial surface. *Chem. Soc. Rev.* **2020**, *49*, 5178–5224. [CrossRef]

Biomaterials Science

ROYAL SOCIETY OF CHEMISTRY

PAPER

View Article Online
View Journal

Cite this: DOI: 10.1039/d4bm00055b

Crosslinked hybrid polymer/ceramic composite coatings for the controlled release of clindamycin

Dagmara Słota, *[a] Mateusz M. Urbaniak, [b,c] Agata Tomaszewska,[b,d] Karina Niziołek,[a] Marcin Włodarczyk,[b] Wioletta Florkiewicz,[e] Aleksandra Szwed-Georgiou, [b] Agnieszka Krupa[b] and Agnieszka Sobczak-Kupiec[e]

A major risk associated with surgery, including bone tissue procedures, is surgical site infection. It is one of the most common as well as the most serious complications of modern surgery. A helpful countermeasure against infection is antibiotic therapy. In the present study, a methodology has been developed to obtain clindamycin-modified polymer–ceramic hybrid composite coatings for potential use in bone regenerative therapy. The coatings were prepared using a UV-light photocrosslinking method, and the drug was bound to a polymeric and/or ceramic phase. The sorption capacity of the materials in PBS was evaluated by determining the swelling ability and equilibrium swelling. The influence of the presence of ceramics on the amount of liquid bound was demonstrated. The results were correlated with the rate of drug release measured by high-performance liquid chromatography (HPLC). Coatings with higher sorption capacity released the drug more rapidly. Scanning electron microscopy (SEM) imaging was carried out comparing the surface area of the coatings before and after immersion in PBS, and the proportions of the various elements were also determined using the EDS technique. Changes in surface waviness were observed, and chlorine ions were also determined in the samples before incubation. This proves the presence of the drug in the material. The *in vitro* tests conducted indicated the release of the drug from the biomaterials. The antimicrobial efficacy of the coatings was tested against *Staphylococcus aureus*. The most promising material was tested for cytocompatibility (MTT reduction assay) against the mouse fibroblast cell line L929 as well as human osteoblast cells hFOB. It was demonstrated that the coating did not exhibit cytotoxicity. Overall, the results signaled the potential use of the developed polymer–ceramic hybrid coatings as drug carriers for the controlled delivery of clindamycin in bone applications. The studies conducted were the basis for directing samples for further *in vivo* experiments determining clinical efficacy.

Received 11th January 2024,
Accepted 24th July 2024

DOI: 10.1039/d4bm00055b

rsc.li/biomaterials-science

Introduction

In 2019, the number of new cases of bone fractures as well as injuries worldwide was estimated as 178 million, which represents an increase of 33.4% since 1990. Approximately 7% of fractures required surgical intervention and implantation of biomaterials to fill structural defects and/or restore bone tissue function. The increase in the incidence of bone injuries due to the emergence of lifestyle diseases, *i.e.* osteoporosis, has contributed to the increased investment in the development and implementation of new biomaterials. According to a report prepared by Vantage Market Research, the global market for biocomposites used in regenerative medicine was valued at $24.2 billion in 2021 and is expected to reach about $57.5 billion by 2028 at a CAGR of 15.5%.[1,2] Key factors driving this market are the increasing number of road traffic accidents, the rising incidence of acquired or congenital deformities, and technological advances in plastic surgery.[3,4]

Nowadays, a lot of attention is being given to the development of multifunctional materials, whose purpose will be not only to fill the defect, but also to provide the implant with other functions, such as being a carrier of an active substance or a drug.[5] The release of the drug at a specific lesion site can

[a]*Cracow University of Technology, CUT Doctoral School, Faculty of Materials Engineering and Physics, Department of Materials Engineering, 37 Jana Pawła II Av., 31 864 Kraków, Poland. E-mail: dagmara.slota@pk.edu.pl*
[b]*University of Lodz, Faculty of Biology and Environmental Protection, Department of Immunology and Infectious Biology, 12/16 Banacha St, 90-237 Łódź, Poland*
[c]*University of Lodz, Faculty of Chemistry, Department of Inorganic and Analytical Chemistry, 12 Tamka St, 91-403 Łódź, Poland*
[d]*Bio-Med-Chem Doctoral School of the University of Lodz and Lodz Institutes of the Polish Academy of Sciences, 12/16 Banacha St, 90-237 Łódź, Poland*
[e]*Cracow University of Technology, Faculty of Materials Engineering and Physics, Department of Materials Engineering, 37 Jana Pawła II Av., 31 864 Kraków, Poland*

effectively accelerate tissue regeneration and patient recovery.[6] This is highly important in terms of surgical site infections (SSI), such as those after bone grafts. SSI are the most common infections that can occur both during hospitalisation as well as after hospital discharge.[7] The etiologic agent leading to infections is most often bacteria residing on the skin, but can also be microorganisms residing in other areas of the body or found in the operating room environment, as well as on surgical instruments.[8] Bacterial infections are highly dangerous as they can lead to osteomyelitis, which is defined as an inflammatory process caused by a bone infection that leads to bone destruction and bone necrosis, and eventually can progress to a chronic condition.[9,10] According to the procedure recommended by the World Health Organization, antibiotic therapy can effectively prevent infection.[11] Therefore, the development of a biomaterial that is capable of releasing the drug directly at the site requiring a therapeutic effect and protection is a real opportunity to improve the health of patients.

The work presented here involves the development of hybrid composite coatings based on synthetic polymers like poly(vinylpyrrolidone) (PVP), poly(ethylene glycol) (PEG) and poly(ethylene glycol) diacrylate (PEGDA) as well as natural ones like collagen (COL). PEG especially in a hydrogel form is a well-known flexible biomaterial approved by the Food and Drug Administration (FDA), USA, for various biomedical uses. It is characterised by exceptional tunability and biocompatibility, and its softness as well as elasticity make it similar to natural tissues. Chemically, this polymer is composed of a repeating subunit of ethylene glycol ($HO–CH_2–CH_2–OH$), and its structure can be described as $H–(O–CH_2–CH_2)_n–OH$.[12,13]

Similar biological properties are demonstrated by PVP, which is biocompatible and biodegradable and has good water solubility. It also has one of the lowest cytotoxicities among synthetic polymers.[14,15] Similar to PEG, it has been approved by the FDA, USA for a wide range of applications. Commercially, the most common uses are as hydrogels for wound dressings and binders in pharmaceuticals.[16] It consists of a repeating *N*-vinylpyrrolidone monomer, and its mer structure can be expressed as $–[CH_2CH(C_4H_6NO)]–$.[17]

However, in the aspect of bone regeneration, it is COL that has the most significant properties, as it is a protein biopolymer that occurs in large quantities in the connective tissues of animal organisms, including humans. It is the main structural component of skin, bones, tendons, ligaments and other tissues, as well as being the principal ingredient in the extracellular matrix. COL is applied in bone regeneration to provide structural support, stimulate bone cell growth and restore natural bone tissue.[18,19] A typical structural element of COL is a triple helical rod-like domain composed of three polypeptide chains of glycine, proline and hydroxyproline.[20,21] So far, 29 different types of collagen have been discovered, which differ in their molecular isoforms. Most commonly used in biomedical applications are types I, II and III.[22]

Besides the aforementioned polymers, furthermore, the entire coating's structure has been enriched with glutathione (GSH) and hydroxyapatite (HAp) to increase the biological value. Glutathione is a tripeptide composed of the amino acid residues of glutamic acid, cysteine and glycine and it exhibits antioxidant properties that are manifested in the restoration of thiol (–SH) groups in proteins. It is also considered as an inhibitor of the inflammatory response involving reactive oxygen species (ROS). ROS play a significant role in the metabolism and ageing of living organisms due to the presence of an O–O bond or an oxygen atom with an unpaired electron. Reducing ROS-induced oxidative stress damage has been proved to be possible with the presence of GSH, which enhances metabolic detoxification. This tripeptide is found in all plant and animal organisms, and with age, its amount decreases.[23–25]

In this work, physicochemical as well as biological analyses were performed to determine the potential for using the developed hybrid ceramic/polymer coatings as a clindamycin carrier for targeted therapy. Such a therapy enables the drug to be released directly at the lesion site requiring a therapeutic effect. Moreover, it allows an appropriate dose of the substance to be tailored to the individual patient's needs. The study provides the basis for directing biomaterials for further *in vivo* analyses.

Materials and methods

Materials

Synthetic and natural polymers as well as the other components necessary for the synthesis of the polymer matrix, *i.e.*, polyvinylpyrrolidone (PVP), polyethylene glycol (PEG), poly (ethylene glycol) diacrylate Mn 575 (PEGDA), 2-hydroxy-2-methylpropiophenone (97%), peptide L-glutathione (reduced 98%) (GSH) and collagen from bovine Achilles tendon (COL), were purchased from Sigma-Aldrich (Darmstadt, Germany). All reagents used for hydroxyapatite (HAp) syntheses, *i.e.*, calcium acetate monohydrate ($Ca(CH_3CO_2)_2·H_2O$), sodium phosphate (dibasic) (Na_2HPO_4), and ammonia water (NH_4OH, 25%), were also obtained from Sigma-Aldrich (Darmstadt, Germany). The measurement of sorption capacity was carried out in a Phosphate Buffered Saline (PBS) solution prepared from tablets (Oxoid, United Kingdom). Clindamycin hydrochloride was the active ingredient selected for coating modification and was purchased from Sigma-Aldrich (Darmstadt, Germany). Drug release was determined by high-performance liquid chromatography (HPLC), where the mobile phase was a combination of acetonitrile from Honeywell (Seelze, Germany) and KH_2PO_4 from DOR-CHEM (Krakow, Poland).

Bacterial strain and cell lines used in biological studies. *Staphylococcus aureus* (*S. aureus*) ATCC 29213, the L929 (CCL-1™) cell line of mouse fibroblasts and the hFOB 1.19 (CRL-3602™) cell line of human fetal osteoblasts were purchased from ATCC (Manassas, VA, USA). Cell culture media RPMI-1640 and DMEM/Nutrient Mixture F-12 Ham were bought from Sigma-Aldrich (Darmstadt, Germany), fetal bovine serum (FBS) were bought from Cytogen (Lodz, Poland), antibiotics added to cell cultures (penicillin and streptomycin)

were purchased from Biowest (Nuaillé, France) and geneticin was bought from Gibco (Waltham, MA, USA). Resazurin and 3-(4,5-dimethylthiazol-2-yl)-2,5-diphenyltetrazolium bromide (MTT) were obtained from Sigma-Aldrich (Darmstadt, Germany). ELISA kits for detecting rat IL-1β, IL-10, and TNF-α were purchased from R&D Systems (Minneapolis, MN, USA).

Material preparation

Hydroxyapatite and composite coatings were prepared as previously described.[26] This work is a continuation of the research efforts on developing drug carriers. Based on previous studies on the modification of ceramic powders with clindamycin, the powder described in an earlier publication as C/s-1.67 was selected.[27]

Polymer and composite coatings based on PVP, PEG with collagen and glutathione enriched with HAp were prepared, according to the composition presented in Table 1. In order to carry out the photocrosslinking reaction under UV light, a photoinitiator, 2-hydroxy 2-methylpropiophenone, and a crosslinking agent in the form of poly(ethylene glycol) diacrylate (PEGDA) average Mn 575 were also added.

A–C coatings were modified with clindamycin by combining the drug with a polymeric and/or ceramic phase. 5 carriers were obtained, as presented in Table 2. To modify the polymer phase with the drug, a solution containing 30 mg of clindamycin was prepared. Next, appropriate amounts of PVP and PEG polymers were dissolved in the drug solution to obtain a concentration of 15%. In the next step, GSH, PEGDA and a photoinitiator were added, and the whole mixture was subjected to photocrosslinking under UV light. The steps were repeated for coatings 2 and 4, considering the respective amounts of COL and HAp. Coatings 3 and 5 contained clindamycin-enriched HAp, which was modified as described earlier.[27]

Schematically, the composition of the coating materials and the synthesis conditions as well as a picture of an example of a finished coating applied to a PLA plate are presented in Fig. 1.

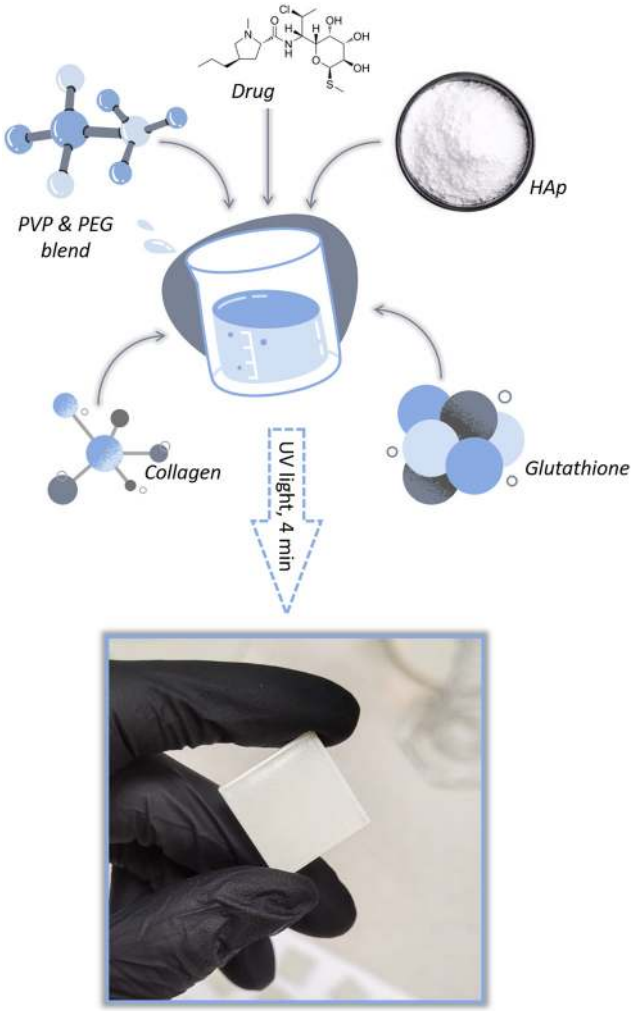

Fig. 1 Schematic of the coating material composition, the synthesis conditions and a picture of an example of a finished coating applied to a PLA plate.

Table 1 Coating composition

Coating symbol	PVP 15% [mL]	PEG 15% [mL]	GSH [g]	COL [g]	HAp [% w/v]
A	5	5	2	—	—
B	5	5	2	0.04	—
C	5	5	2	0.04	5
D	5	5	2	0.04	15

Table 2 Composition of the developed composite and polymeric clindamycin carriers

Coating symbol	Composition
1	Coating A with the drug in a polymer matrix
2	Coating B with the drug in a polymer matrix
3	Coating C with drug-modified HAp
4	Coating C with the drug in a polymer matrix
5	Coating C with drug-modified HAp and with the drug in a polymer matrix

Determination of sorption capacity

The composition of materials can affect both their structure and their swelling ability, which is understood as the ability to absorb water and/or other liquids into the polymer structure. As a result, an increase not only in the mass but also in the volume of the material occurs.

To study the swelling capacity of composite coatings, initial samples of 1 g were prepared and immersed in 100 ml of PBS, and then weighed after a specified incubation time (15 minutes, 30 minutes, 1 h, 2 h, 1 day, 2 days, 3 days or 7 days). For this purpose, after pulling the sample from the PBS solution, the excess liquid from the surface was drained with filter paper. The incubation process of the materials was carried out at 36.6 °C. The sorption capacity of the samples was then calculated according to eqn (1), where m_0 is the mass

of the dry sample and m_1 is the mass of the sample at the specified incubation time:

$$\text{Swelling ability} = \frac{m_1 - m_0}{m_0} \times 100\%. \quad (1)$$

The kinetics of composite swelling was determined by defining equilibrium swelling and the rate parameters. For this purpose, the Voigt-based viscoelastic model (eqn (2)) was used, where S_e is the equilibrium swelling [%], S_t is the swelling at time t [%], t is time [min], and τ is a rate parameter indicating the time required for the sample to absorb 0.63 of its ultimate swelling [min].[28]

$$S_t = S_e\left[1 - e^{-\frac{t}{\tau}}\right] \quad (2)$$

Incubation studies

A stability study was carried out in a PBS solution, simulating the environment of a living organism, by measuring the pH value for a period of 40 days at 36.6 °C. In parallel, the value of electrical conductivity was monitored, which provides information on the activity of ions in the incubation medium. For the measurements, an Elmetron CX-701 multifunctional device (Zabrze, Poland) with an EPS-1 pH-metric electrode and ECF-1 conductivity sensor was used.

Surface morphology

To study the surface morphology of the clindamycin-formed coatings, studies were performed using a JEOL IT200 Scanning Electron Microscope (SEM) (JEOL Ltd, MA, USA) with an EDS system detector. A comparative analysis of the clindamycin coatings before and after incubation in PBS was performed to study the changes during the incubation process. EDS examination and elemental mapping were performed after the surface testing. Before SEM measurements, the samples were coated with a gold nanolayer using a DII-29030SCTR Smart Coater sputtering machine (JEOL Ltd, MA, USA).

Drug release rate studies

To determine the rate of drug release, clindamycin-modified biomaterials were placed in sterile, sealed containers filled with 60 mL of PBS solution. The containers were then stored in an incubator (POL-EKO, Wodzisław Śląski, Poland) at 36.6 °C. The concentration of the released drug was determined by a high-performance liquid chromatography (HPLC) technique (Shimadzu, Kyoto, Japan), using the methodology described earlier.[27] Release studies were conducted over a period of 14 days.

Sterilisation and sample preparation for biological studies

Prior to biological evaluation, all tested composites were sterilised by gamma irradiation with a dose of 25 kGy with gamma rays from a ^{60}Co source at the Institute of Applied Radiation Chemistry, Lodz University of Technology in Lodz. We used 14 mm diameter discs to evaluate the antibacterial activity of the tested coatings. Tested materials of a size equal to 1/10 of the 96-well plate well surface were used in the cytocompatibility studies.

Evaluation of the antibacterial activity

The antibacterial activity of the post-incubation supernatants from the clindamycin-modified composite coatings against *S. aureus* ATCC 29213 (American Type Culture Collection, Manassas, VA, USA) was assessed using a resazurin reduction assay.[29] The percentage of metabolically active bacteria treated with the tested post-incubation supernatants of the coatings was determined in relation to the untreated culture of *S. aureus* ATCC 29213. The clindamycin-modified coatings and clindamycin-free reference samples were distributed in the wells of a 24-well plate containing 1 mL of Mueller–Hinton Broth (MHB; Sigma Aldrich, Darmstadt, Germany) and incubated for 24 h (37 °C, 5% CO_2) to obtain the post-incubation supernatants. The bacteria were cultured in MHB to a mid-log phase and the inoculum was standardised to 0.5 McFarland (5×10^5 CFU mL^{-1}) as recommended by the EUCAST guidelines.[30] The post-incubation supernatants were transferred to new wells of the 24-well plate. Then, the bacterial suspension (500 μL) was added to each well, and the plates were incubated for 24 h at 37 °C. Control wells containing the bacterial culture alone (positive control of bacterial growth) and wells with MHB alone (negative control) were included. Four independent experiments were performed in triplicate. The antibacterial activity was assessed based on the metabolic ability of the bacteria to reduce resazurin to resorufin in the milieu of the post-incubation supernatant. Prior to reading, 100 μL of 0.02% resazurin (Sigma-Aldrich, Darmstadt, Germany) in sterile PBS was added to each well and left for 3 h. Fluorescence was measured at an excitation wavelength of 560 nm and an emission wavelength of 590 nm using a SpectraMax® i3x multi-mode microplate reader (Molecular Devices, San Jose, CA, USA).

Anti-biofilm activity

S. aureus ATCC 29213 was used to evaluate the anti-biofilm activity of the tested composite coatings. The bacteria were cultured in MHB to a mid-log phase, and the inoculum was prepared at a concentration of 1×10^6 CFU ml^{-1} for the test. The clindamycin-modified coatings (1, 3, 4 and 5) and clindamycin-free reference samples (A and C) were placed in a 24-well plate, and then 1 mL of the prepared bacterial suspension was added to each well with the tested samples. The plates were incubated for one, three or seven days at 37 °C. After incubation, unbound bacteria were washed with PBS, and the formed biofilm was stained using a LIVE/DEAD™ BacLight™ kit (Thermo Fisher Scientific, Waltham, MA, USA) according to the manufacturer's protocol. After labelling, the biofilm was fixed with 80% methanol (Sigma-Aldrich, Saint Louis, MO, USA) for 15 min, and then the composite coatings were visualised using a TCS LSI Scanning Confocal Macroscope (SCM, Leica, Wetzlar, Germany).

Cytocompatibility

The composites were tested for their cytocompatibility according to the guidelines for testing components with potential

biomedical applications of The International Standard Organization (ISO-10993-5-2009) as described previously.[31,32] The research was carried out using the two cell lines: the reference line recommended by the ISO standard, mouse fibroblasts (L929), and human fetal osteoblasts (hFOB 1.19). The L929 fibroblasts were cultured in RPMI-1640 medium with 10% FBS supplemented with streptomycin (100 μg mL^{-1}) and penicillin (100 U mL^{-1}) at 37 °C and 5% CO_2 in a humidified incubator (>90% humidity). The hFOB 1.19 cell line was cultured in the DMEM/Nutrient Mixture F-12 Ham medium with the addition of 10% FBS and geneticin (0.3 mg mL^{-1}) at 34 °C with 5% CO_2 and humidity >90%. Adherent cells were detached from the culture dish using 0.25% trypsin EDTA solution. Cell suspensions at densities of 1×10^4 cells per well for L929 and 4×10^4 cells per well for hFOB 1.19 were added to the 96-well plate at a volume of 200 μL and incubated overnight under conditions appropriate for each cell line to form a monolayer. After overnight cell culture, the test materials of a size equal to 1/10 of the well surface were added to the wells with the cell monolayers. At the same time, samples containing a reference biomaterial (a medically certified peripheral venous catheter) were prepared. Cells cultured in the medium alone served as a non-treated control (NTC), while cells incubated with 0.3% H_2O_2 solution were used as a treated control (TC). The cell cultures were incubated with the test materials and the control samples for 24 h in conditions appropriate for each cell line. After incubation, the MTT (3-(4,5-dimethylthiazol-2-yl)-2,5-diphenyltetrazolium bromide) solution (5 mg mL^{-1}) was added to each well (20 μL) and incubated for 4 h. After that, the plates were centrifuged and then the supernatants were replaced with 200 μL of DMSO and mixed to dissolve the formazan crystals. The absorbance of the dissolved crystals was measured at 570 nm (Multiskan EX, Thermo Fisher Scientific, Waltham, MA, USA).

In vivo study of local tissue response and systemic response to implantation of biomaterials

The research involved using adult rats (*Rattus norvegicus*, Wistar breed) that weighed at least 220 g and were at least ten weeks old. These rats were obtained from the internal breeding facility of the Animal House of the Faculty of Biology and Environmental Protection of the University of Lodz (breeder code 048). Approval for *in vivo* experiments (42/LB 192-UZ-A/2021) was granted by the Local Animal Ethics Committee at the University of Lodz Medical School. The study included three groups with two of them containing composites (a clindamycin-free reference (C) and a modified clindamycin composite (4)) and a control group. The procedure included testing the local tissue response and the systemic response to the implantation of biomaterials. The local reaction after implantation was studied based on the PN-EN ISO 10993-6:2017 standard "Biological evaluation of medical devices/Testing of the local reaction after implantation". Since the tested composites were intended to have long-term contact with the body, observations after implantation were made at two-time points: 7 and 30 days. Briefly, 24 hours before surgery, food was withdrawn from the animals. On the day of the procedure, the skin on the rats' backs (6 × 4 cm from the angle of the scapula to the sacrum) was depilated using a shaver. During the surgical procedure, the animals were continuously anaesthetised using a mixture of isoflurane (5%) and oxygen, and the anaesthetised animals were immobilised in the abdominal position. The skin and subcutaneous tissues were incised in the midline of the spine at a length of approximately 3–4 cm, and subcutaneous pockets were created on the right and left sides of the spine. Two fragments of the same biomaterial were placed inside each pocket. Thus, each animal in the group (3 individuals per group) received two fragments of the same biomaterial (sterilised by radiation). The incised skin was sutured with single stitches and the postoperative wound was disinfected with Octenisept. To manage pain, each animal received subcutaneous injections of an analgesic drug for three consecutive days (butorphanol at a dose of 2 mg per kg body weight). After the procedure, the animals were placed individually in clean, sterile cages and their recover observed. The study involved observing the animals' behaviour (food and water intake) and general health conditions, and the healing process of postoperative wounds for 7 and 30 days.

The control group consisted of animals that had not undergone the procedure and were in good general condition, demonstrating no signs of local or systemic inflammatory reaction.

After 7 and 30 days, animals were euthanized for blood collection (to obtain the serum) and organ resection (lymph nodes, spleen, liver and kidneys).

The levels of IL-1β, IL-10, and TNF-α in the serum samples were determined using enzyme-linked immunosorbent assays (R&D Systems, Minneapolis, MN, USA) following the manufacturer's instructions.[33] The minimum detectable levels were 31.2 pg mL^{-1} for IL-1β, 62.5 pg mL^{-1} for IL-10, and 62.5 pg mL^{-1} for TNF-α. Absorbance values at 450 nm of samples and standards at serial concentrations were obtained using a Multiskan EX reader (Thermo Fisher Scientific, USA) and translated into the concentration of the evaluated biomarkers using the MyAssay Data analysis tool.

Statistical analyses

Statistical analyses and graphs for the biological studies were performed using GraphPad Prism version 9.1.0 for Windows (GraphPad Software, San Diego, CA, USA). The antibacterial activity data were compared using the Kruskal–Wallis test with Dunnett's *post hoc* test. For cytocompatibility studies and statistical analysis, the Shapiro–Wilk test was used to assess the Gaussian distribution. The Brown–Forsythe test was used to verify the equality of group variances. Data were analysed separately for each cell line using one-way ANOVA following Tukey's multiple comparison test. The Kolmogorov–Smirnov test confirmed that the *in vivo* dataset is normally distributed. Data from both within and between groups were analysed using a two-way ANOVA with Tukey's multiple comparison test. The experiments were conducted three times, with each experiment being repeated twice for technical accuracy.

A p-value of less than 0.05 was considered to be statistically significant.

Results and discussion

Polymer and composite coatings were subjected to swelling studies in order to determine their sorption capacity. The results obtained are presented in Fig. 2.

The effect of material composition on fluid binding capacity was confirmed. The smallest increment was observed for sample D, containing a 15% share of the ceramic phase, with swelling ability at 84% after 7 days in PBS. A slightly larger increase at 106% was observed for sample C, which contained a 5% share of the ceramic phase. The swelling abilities for polymer coatings A and B were significantly higher, at 117% and 124%, respectively. Thus, the sorption capacity decreased as the proportion of the ceramic phase increased. The reason for this is that the ceramic grains occupy the free spaces between the polymer chains, thus preventing fluid penetration into the material. The highest swelling ability was observed for coating B, which differed from shell A by the presence of collagen from bovine tendons. This effect is presumably caused by the properties of collagen, which has in its structure proline, an amino acid capable of binding water molecules.[34,35]

The swelling ability results are correlated with the determined equilibrium swelling (S_e), presented together with the rate (τ) parameter in Table 3. The S_e of coatings was in the range of 81.26 ± 1.63 to 108.97 ± 4.68%, reaching the highest results for polymer coating B and the lowest for composite coating D. However, composite coatings C and D presented a higher value of the τ parameter, suggesting that the presence of ceramics not only reduces the sorption capacity, but also slows down the penetration speed of the fluid inside the material.

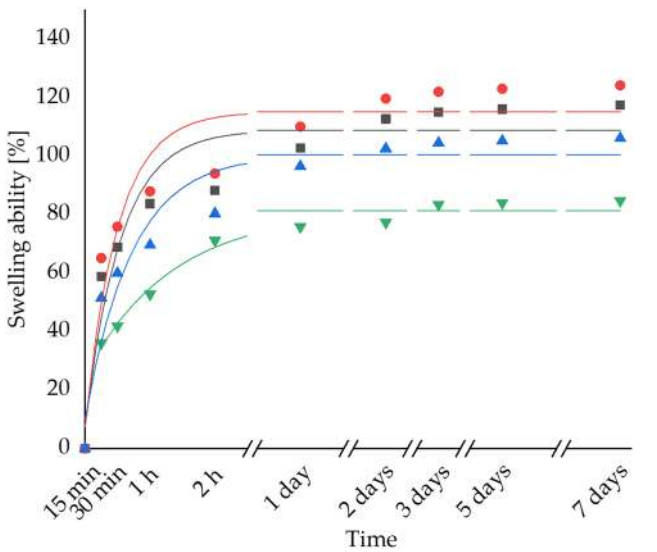

Fig. 2 Swelling kinetics of coatings A–D in PBS. The solid lines indicate fittings for the swelling ability of the individual samples.

Table 3 Rate parameter (τ) and equilibrium swelling (S_e) of the tested samples

Coating symbol	S_e [%]	τ
A	108.97 ± 4.68	32.72 ± 8.39
B	115.23 ± 5.10	30.06 ± 8.01
C	100.44 ± 4.35	43.24 ± 11.27
D	81.26 ± 1.63	79.15 ± 15.78

It is significant that even low sorption capacity and swelling of the material confirms the potential use of the biomaterial as a carrier of the active substance. It has been demonstrated that swelling of the material is one of the mechanisms of drug release, since during diffusion of liquid molecules into the interior of the material, molecules of the drug or other active substances are leached outward.[36,37] The results were the basis for modifying the coatings with clindamycin, and thus developing the carriers.

Potentiometric analysis was performed to determine the changes in the pH value of the PBS solution in which the coatings were incubated for 40 days (Fig. 3, top). This allowed to determine the stability of the materials under conditions simulating the environment of a living organism. Regardless of the composition and chemical formulation, the samples behaved relatively similarly, and the pH value oscillated between 7 and 7.5, which is safe for the organism. The subtle changes could be the result of leaching of residual polymers or ceramic particles from the interior of the materials. This phenomenon is confirmed by ionic conductivity measurements (Fig. 3, bottom). If the material was inert and did not interact with PBS, the conductivity value would remain relatively constant.[38] Changes in the range of 130–190 mS are indicative of ion exchange occurring between the sample and the fluid. In this case, slightly higher conductivity values were observed for materials with a higher proportion of the ceramic phase (coatings C and D). It is possible that individual, fine ceramic grains leached from the polymer matrix into the solution, which increased the conductivity. However, no noticeable degradation of the materials was observed.

Based on the coating compositions labelled A–D, drug loaded materials were prepared (samples 1–5) with the antibiotic bound to the ceramic and/or polymer phase. The carriers were immersed in 60 mL of PBS, into which clindamycin was released. Fig. 4 presents the percentage of the antibiotic released after 24 h. The initial hours of drug treatment are extremely important, as inhibition of bacterial growth occurs then, significantly affecting the further development of the disease. It was observed that after 1 day, the largest amounts of the drug were released from coating no. 1 and 2, *i.e.*, biomaterials based on polymers alone (without the ceramic phase), in which clindamycin was bound to PVP and PEG. The results were similar, at 35% and 36.8%, respectively. Smaller values were observed for the composite coatings. In coating 4, the

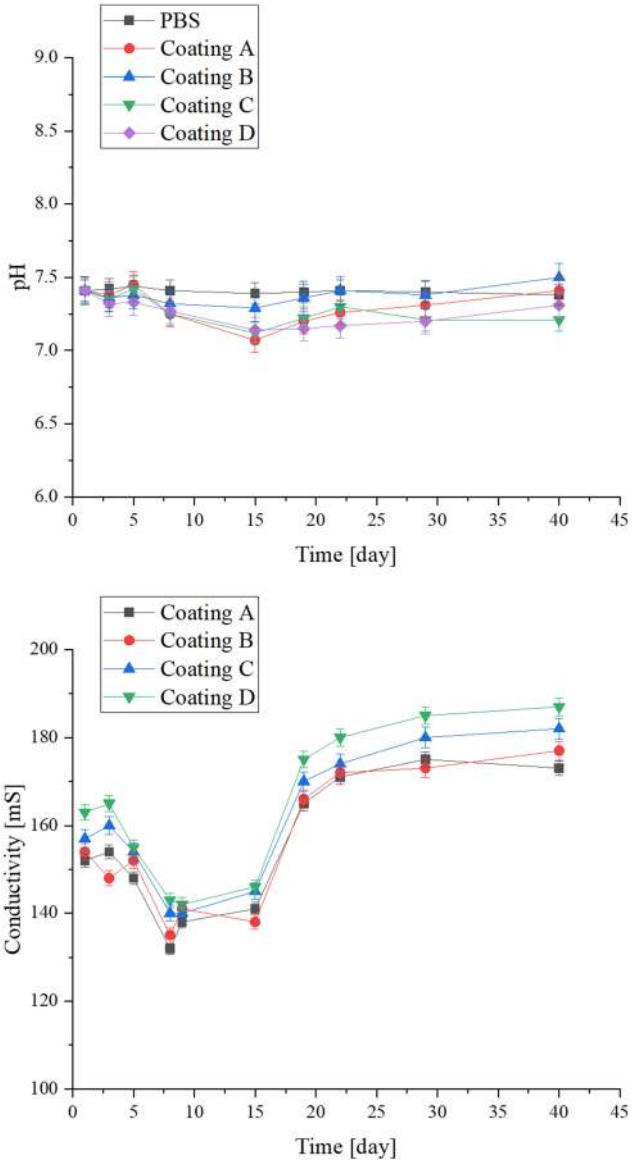

Fig. 3 Study of the behaviour of the coatings during a 40-day incubation in PBS; measured pH values (top) and ionic conductivity (bottom).

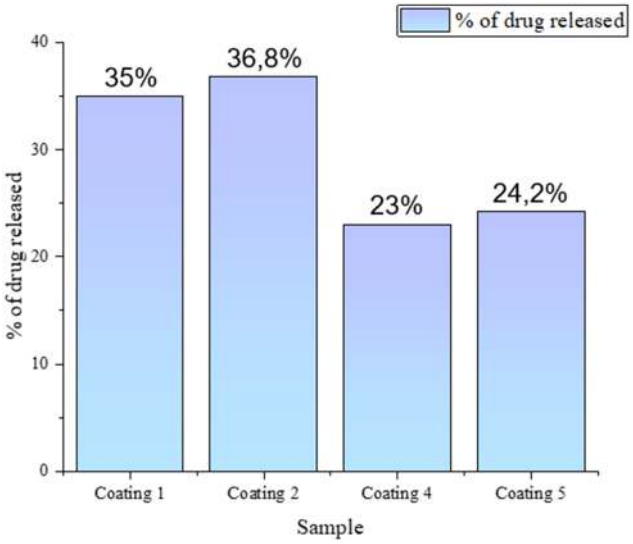

Fig. 4 Percentage of clindamycin released from coatings after 24 hours of incubation in PBS.

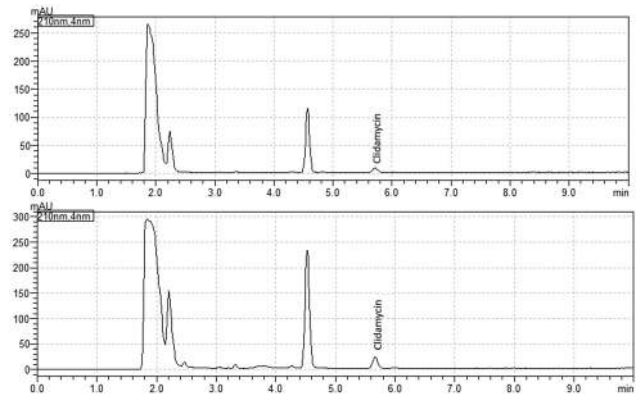

Fig. 5 Chromatograms of drug release from coating 5 after 1 day (top) and after 14 days (bottom).

drug was released from the polymer compound, and in sample 5, additionally from the interior of the drug-loaded HAp that was suspended in the matrix. However, the drug concentration values obtained were about one-third lower than those for the polymer materials at 23% and 24.2%, respectively.

The antibiotic release study was conducted for 14 days using HPLC. Fig. 5 presents chromatograms from days 1 and 14 of drug release from coating 5 into PBS and Fig. 6 presents a diagram demonstrating the amount of clindamycin in mg mL^{-1} released over time. Furthermore, the mechanism of release of the active ingredient from inside the swelling polymer matrix is presented schematically.

The trend observed as early as 24 hours continues until the end of the study, and the highest amount of drug escapes from coating 2 (PVP/PEG/COL). Finally, on the 14th day of measurement, it releases the largest amount of antibiotics, just over 25 mg, which is 83.6% of the total amount in the material. A slightly lower, although similar, value was observed for coating 1 (PVP/PEG) at 79.2%. As with the swelling results, composite materials exhibit the lowest values. Significantly, 71.6% of the drug was released from coating 4 and 72.6% from coating 5, while in the second one, clindamycin was bound to both the polymer and the ceramic phases. Such similar values suggest that the drug molecules are unable to escape from the hydroxyapatite grains and then pass through the polymer network. Presumably, this is the reason why it was not possible to determine the drug concentration for coating 3, containing clindamycin-modified hydroxyapatite, without the presence of the drug in the matrix.

Release rate studies confirm that all materials exhibit the nature of an active substance carrier. However, previous

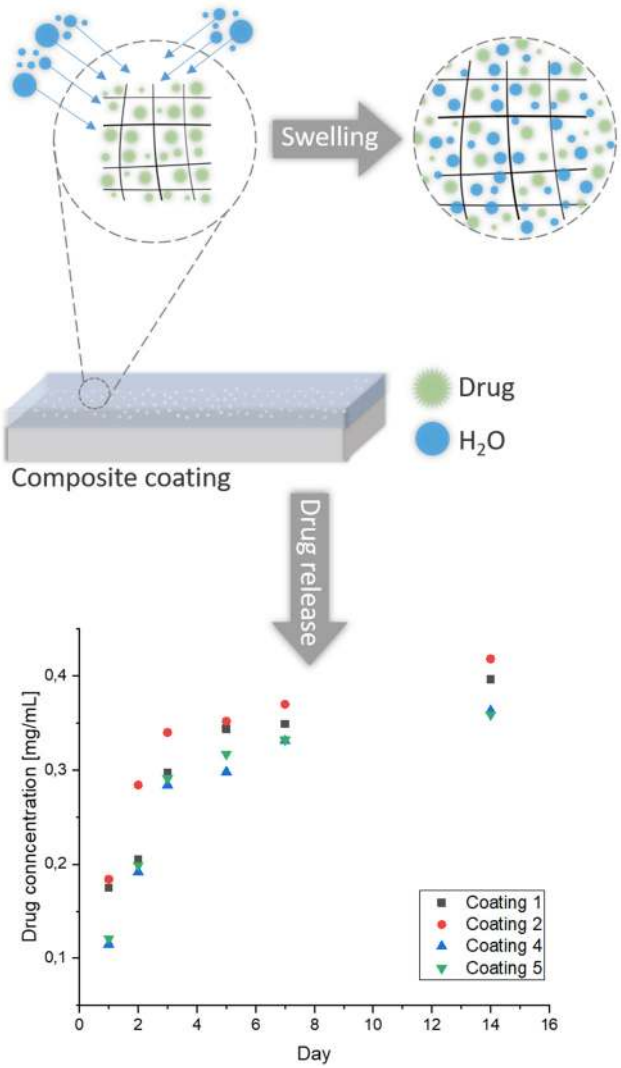

Fig. 6 Scheme of material swelling due to the penetration of aqueous solution and the rate of drug release from the polymer and composite coatings into PBS.

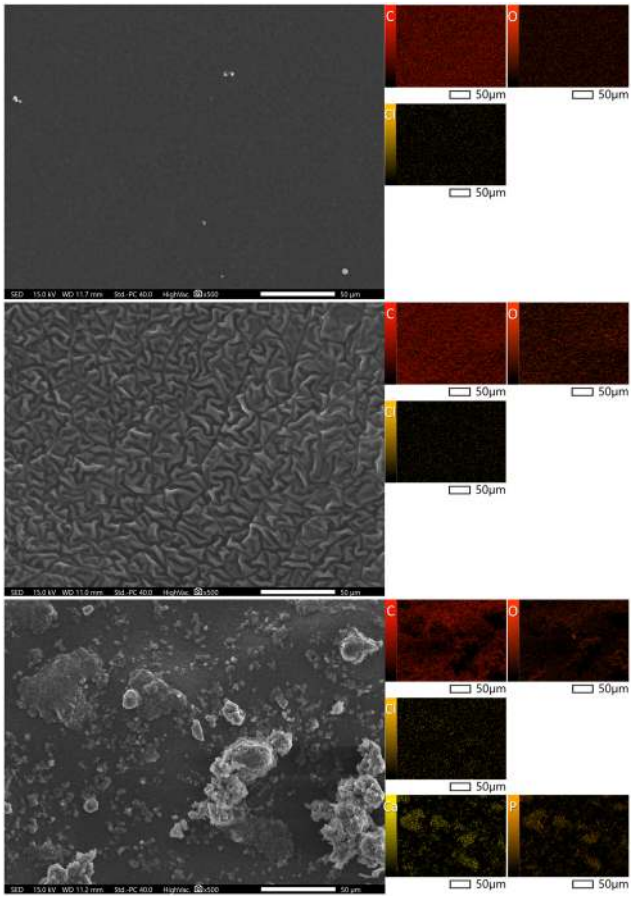

Fig. 7 Analysis of the morphology of clindamycin coatings before incubation for samples 1 (top), 2 (middle) and 4 (bottom) with mapping.

studies have suggested that in the context of bone tissue regeneration, the composite coating has the greatest potential in terms of physicochemical and tribological properties. Although polymer coatings 1 and 2 released more drug, the lack of hydroxyapatite caused them to lack bioactivity toward hard tissue regeneration. Clindamycin was determined to have a retention time of 5.7 minutes. An increase in the peak absorbance intensity with time could be observed. The other peaks detected earlier were presumably from the crosslinking agent or PVP and/or PEG polymers, as they appeared in each sample of both composite and polymer coatings. However, this requires further investigation. Considering the above results, drug release depends on time and the type of carrier as well as its composition.

The surface morphology of the obtained composite coatings before incubation in PBS solution is presented in Fig. 7. Analysing the SEM images, it can be seen that coatings 1 and 2 are characterized by a smooth surface, while EDS analysis (Table 4) confirms that carbon and oxygen are derived from the polymers. Moreover, analysis of the surface morphology of coating 4 demonstrates the presence of crystals in the polymer surface that correspond to the apatite layers, which confirm the occurrence of calcium and phosphorus in the EDS spectrum and elemental mapping.

In all three coatings, there exists clindamycin, which contains chlorine ions. Analysing the EDS spectra, it can be seen that this element is present in all the samples examined and is evenly distributed on each sample. Chlorine ions are not present in the chemical structure of any of the other components used in the development of the coating, hence it can be concluded that their presence confirms the modification with clindamycin, or more precisely clindamycin hydrochloride.

During the 14-day incubation in PBS solution, there were visible changes in the surface morphology of the obtained antibiotic composite coatings, as presented in Fig. 8. In both samples 1 and 2, characteristic crystals are visible, deposited on the polymer surface. In the EDS analysis (Table 5) and elemental mapping, ions from the composition of the incubation fluid appear. The presence of Na, Cl, K and Ca ions

Table 4 Elemental EDS analysis of coatings before the incubation period, and a summary of mass [%] and atomic [%] amounts of the individual elements

	Coating 1		Coating 2		Coating 4	
Element	Mass [%]	Atom [%]	Mass [%]	Atom [%]	Mass [%]	Atom [%]
C	65.26 ± 0.13	71.50 ± 0.14	63.93 ± 0.11	70.24 ± 0.12	57.21 ± 0.12	65.70 ± 0.14
O	34.59 ± 0.24	28.45 ± 0.20	36.06 ± 0.20	29.71 ± 0.17	37.45 ± 0.23	32.29 ± 0.20
Cl	0.15 ± 0.01	0.06 ± 0.00	0.12 ± 0.01	0.05 ± 0.00	0.06 ± 0.01	0.02 ± 0.00
Ca	—	—	—	—	3.61 ± 0.05	1.24 ± 0.02
P	—	—	—	—	1.66 ± 0.03	0.74 ± 0.01

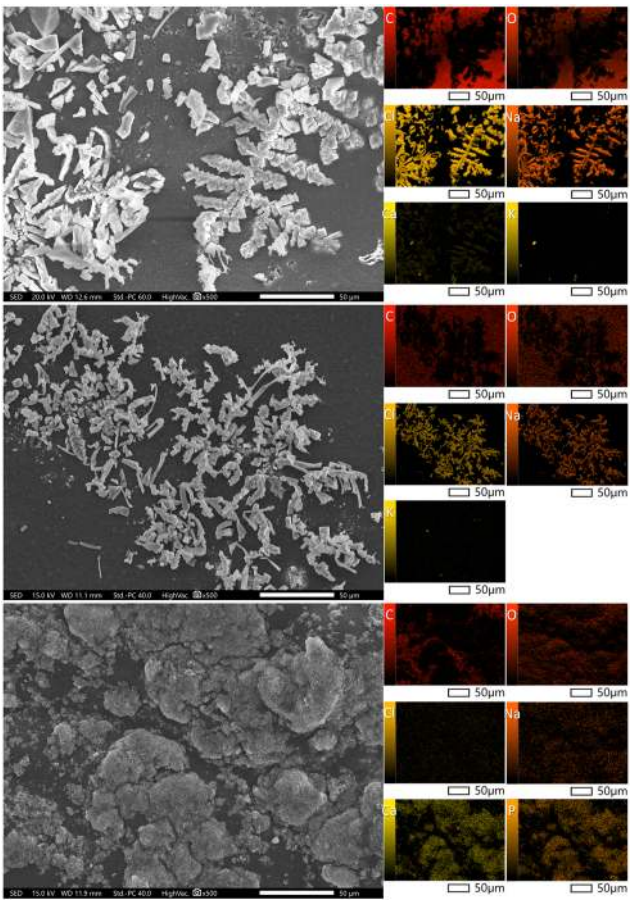

Fig. 8 Analysis of the morphology of clindamycin coatings after incubation in PBS for samples 1 (top), 2 (middle) and 4 (bottom) with mapping.

demonstrates that the biomaterial reacts with the solution in which it is incubated.

However, composition 4 exhibits the presence of ions from the incubation fluid. During the 14-day incubation period, there occurred changes visible on the surface of the obtained composite coatings of the active substance. Significant changes in the surface morphology as a result of incubation were observed for coating 4.

As a result of the interactions of bioactive hydroxyapatite with PBS, new apatite layers precipitated on the surface. This indicates the bioactivity of the coating towards apatite nucleation and suggests that not only can the coating serve as a drug carrier, but compared to the polymeric samples 1 and 2, it exhibits additional biological functions. Both changes in surface appearance and an increase in the amount of Ca and P elements during EDS microanalysis can be observed.

Clindamycin is widely used to treat bone infections caused by *Staphylococcus* due to its numerous advantages, including high bone penetration with long-lasting activity against bacterial biofilm formation and adhesion, high biodistribution, and low costs of synthesis and treatment.[39,40]

It was demonstrated that the obtained composites release clindamycin in biologically active and effective doses. The clindamycin-modified composite coatings 1, 3, 4, and 5 released the antibiotic, causing a statistically significant ($p < 0.001$) reduction in the metabolic activity of *S. aureus* ATCC 29213 to 2.3 ± 0.5%, 2.9 ± 1.4%, 2.2 ± 1.4%, and 2.7 ± 0.5%, respectively, compared to the untreated bacterial culture (Fig. 9). We have also shown that clindamycin-modified coatings do not differ with regard to their antimicrobial potential, which indicates a similar profile of the antibacterial properties of the tested com-

Table 5 Elemental EDS analysis of coatings after the incubation period in PBS, and a summary of mass [%] and atomic [%] amounts of the individual elements

	Coating 1		Coating 2		Coating 4	
Element	Mass [%]	Atom [%]	Mass [%]	Atom [%]	Mass [%]	Atom [%]
C	60.93 ± 0.17	72.96 ± 0.21	59.56 ± 0.14	70.79 ± 0.17	34.60 ± 0.12	47.17 ± 0.16
O	18.48 ± 0.15	16.62 ± 0.14	22.96 ± 0.15	20.49 ± 0.13	40.34 ± 0.23	41.29 ± 0.24
Na	9.47 ± 0.05	5.92 ± 0.03	7.73 ± 0.05	4.80 ± 0.03	0.99 ± 0.03	0.70 ± 0.02
Cl	10.80 ± 0.04	4.38 ± 0.02	9.46 ± 0.06	3.81 ± 0.02	0.36 ± 0.01	0.17 ± 0.01
K	0.21 ± 0.01	0.08 ± 0.00	0.20 ± 0.01	0.07 ± 0.00	0.27 ± 0.02	0.11 ± 0.01
Ca	0.10 ± 0.01	0.04 ± 0.00	0.09 ± 0.01	0.03 ± 0.00	15.34 ± 0.111	6.27 ± 0.04
P	—	—	—	—	8.11 ± 0.06	4.29 ± 0.03

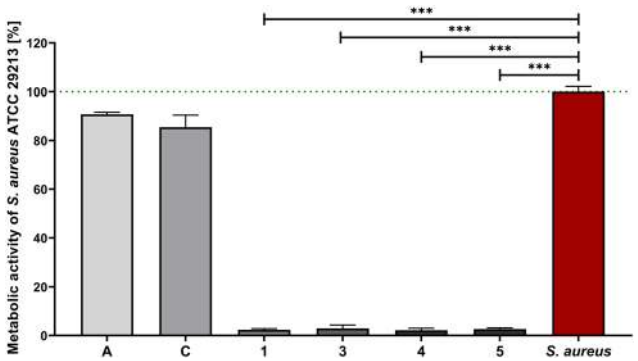

Fig. 9 Antibacterial activity of the clindamycin-modified composite coatings (1, 3, 4 and 5) and clindamycin-free references (A and C) against *S. aureus* ATCC 29213. The green line represents the reference metabolic activity of non-treated *S. aureus* (red bar). Results are shown as mean values with standard deviations (SD) of four independent experiments performed in triplicate for each experimental variant. Statistical significance – ***$p < 0.001$.

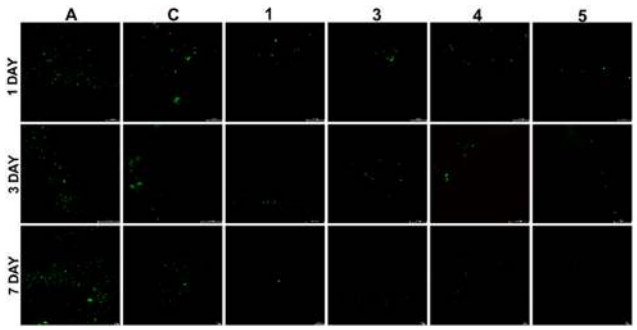

Fig. 10 Representative images of the biofilm formed by *S. aureus* on the clindamycin-modified coatings (1, 3, 4 and 5) or the control coatings (A and C) after 1, 3 or 7 days of incubation. Green fluorescence presents live bacteria on composites.

posites. Unlike coatings containing clindamycin, their reference samples (A and C) did not exhibit the ability to reduce the metabolic activity of bacteria.

A well-described technique for obtaining biodegradable composites with antibacterial properties is placing antibiotics in a ceramic phase, which is usually based on calcium sulfate or calcium phosphate. Local release of antibiotics from biodegradable and dissolving ceramic carriers increases the effectiveness of bacterial eradication after possible post-implantation infection and, therefore, results in better osseointegration of the biocomposite.[41,42] In this study, the suitability of composite coatings containing clindamycin in the ceramic or polymer phase and in both layers for eradicating *S. aureus* was demonstrated. It was revealed previously that clindamycin-loaded nanosized calcium phosphate powders have strong antistaphylococcal properties and can be considered as components of antibacterial biocomposites.[27]

S. aureus is one of the leading causes of post-implantation bone tissue infections associated with biofilm formation. The attachment of *S. aureus* to orthopaedic implants and host tissue, as well as the formation of a mature biofilm, plays an essential role in the persistence of chronic infections and the impairment of host bone regeneration mechanisms. Biofilm formation reduces susceptibility to antibacterial agents and immune system defence mechanisms, leading to a worsening prognosis of implant acceptance and the possibility of developing bacteremia.[43,44] A scanning confocal macroscope (SCM) was used to visually examine the anti-biofilm activities of clindamycin-modified coatings and clindamycin-free reference samples. To evaluate the biofilm inhibition properties, *S. aureus* ATCC 29213 was cultured with the coating samples for 1, 3, and 7 days and then observed using a SCM. As presented in Fig. 10, entirely green fluorescence of live bacteria was observed across the biofilm on the control coating groups (A and C). The presence of live bacteria throughout the experiment reached the highest degree of biofilm coverage of clindamycin-free coatings A and C after 7 days of culture with *S. aureus*. In the case of clindamycin-modified coatings (1, 3, 4 and 5), a low degree of biofilm development was observed after 1, 3 and 7 days of incubation with bacteria, resulting from the antibacterial effect of clindamycin released from the composites. The results show that adding clindamycin effectively limits biofilm formation on the first day of incubation, regardless of whether the drug is bound to the polymer or ceramic phase of the composite.

Biomaterials used in regenerative medicine must have appropriate mechanical and physicochemical properties supporting the regeneration of damaged tissues, but apart from them, one of the most important parameters they should meet is their biocompatibility and lack of cytotoxicity.[45] To address this aspect, we assessed the impact of coating C and coating 4 (sample C modified with clindamycin in the polymer matrix) on the metabolic activity of two cell lines, L929 and hFOB 1.19. These samples were selected because compared to polymer coatings, they not only served as a drug carrier, but also exhibited bioactivity toward the formation of new apatite layers during incubation in PBS. It was demonstrated that the obtained coatings remained cytocompatible for both tested cell lines. The cell viability of L929 fibroblasts remained over 90% (sample C: 91.3% ± 11.5% and sample 4: 92.7% ± 6.9%) and the presence of materials had no significant effect on cell viability compared to either the positive control (102.1% ± 4.2%) or the reference material (95.8% ± 11.8%). Similarly, none of the tested materials (coating C: 98.9% ± 17.0% and coating 4: 88.7% ± 9.8%) significantly affected the cell metabolic activity compared to the reference material (103.6% ± 4.2%) for the hFOB 1.19 cell line (Fig. 11). In both L929 and hFOB 1.19 cell lines after incubation with the tested coatings, cell viability remained over 70%, which met the ISO-10993-5-2009 criteria and proved their cytocompatibility. The presented results confirm the *in vitro* safety of the tested materials and their potential application in *in vivo* studies, in particular those aimed at bone tissue regeneration, due to their cytocompatibility with the human osteoblast cell line.

The current study's results confirm that the clindamycin-modified coatings do not cause changes in L929 cell metabolic

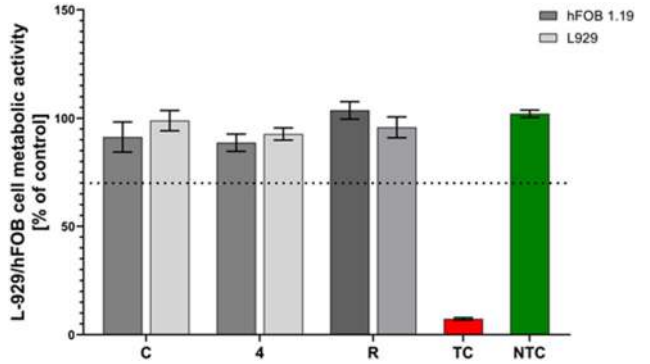

Fig. 11 The metabolic activity of mouse L929 fibroblasts and human hFOB 1.19 fetal osteoblasts after 24 h of incubation with coatings. NTC – non-treated control (green bar) and TC – treated control (red bar), in terms of cell metabolic activity; R – biomaterials derived from a medically certified peripheral venous catheter. Dotted line – 70% of the cell viability cutoff. The data are presented as mean ± SD for the three separate experiments.

activity, making them cytocompatible. The research also includes a human osteoblast cell model, confirming the safety of the composite coatings tested against hFOB 1.19 cells. These promising results indicate the potential use of the coatings for bone tissue regeneration.

The results presented in Fig. 12A indicate the lack of potentially harmful effects of the tested biomaterials in the *in vivo* system. Observation of the biomaterials' implantation sites demonstrates no local inflammatory reaction, and the healing of surgical wounds does not display any signs of inflammation. Measurement of the concentrations of pro-inflammatory cytokines (IL-1β and TNF-α) confirms the absence of a systemic inflammatory response to the implanted biomaterials. The results are then compared to the levels of cytokines found in the sera of the control animals (Fig. 12B and D). Although the concentrations of both pro-inflammatory cytokines are higher 7 days after biomaterial implantation compared to 30 days, this is related to the body's mobilisation immediately after the surgical procedure.

Measurement of the anti-inflammatory cytokine IL-10 in the animal sera indicated higher levels 30 days after the implantation of biomaterials, particularly those not modified with clindamycin (C). Elevated levels of IL-10 in the animal sera 30 days after surgery correlated in some way with the low levels of pro-inflammatory cytokines in the same samples (Fig. 12C).

Our findings align with those of Rodriguez *et al.*,[46] who observed a decrease in the levels of pro-inflammatory cytokines IL-1β and TNF-α over time (up to 14 days), following the surgical implantation of biomaterials in a rat model. Moreover, they observed that levels of anti-inflammatory cytokines, such as IL-10 and TGFβ, increased across all study groups from day 4 to day 14. Levels of anti-inflammatory cytokines are expected to rise over time as the wound healing process progresses.[47]

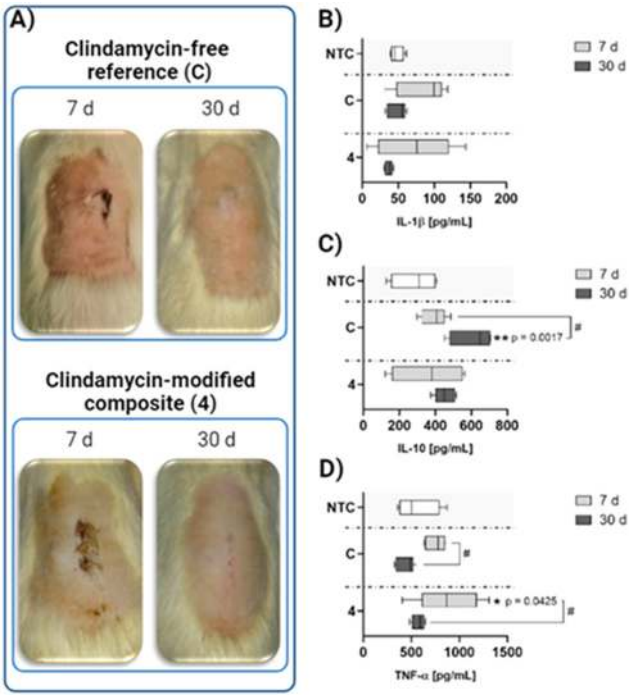

Fig. 12 Representative images demonstrating the implantation sites for biomaterials: clindamycin-free references (C) (top panel) and clindamycin-modified composite (4) at 7 and 30 days after implantation (A). The concentration of interleukin-1 beta – IL-1β (B), interleukin 10 – IL-10 (C), and tumor necrosis factor α – TNF-α (D) in the serum samples obtained from the animals at 7 and 30 days after implantation. NTC – non-treated control (rats not subjected to implantation of the biomaterials). Number of animals, $n = 3$. * – Statistical significance *vs.* the NTC within the time point; the p-value is given after the asterisk. # – Statistical significance ($p < 0.05$) with regard to the time points within the group. Data are presented as minimum and maximum values represented as a line.

Conclusions

Hybrid polymer–ceramic composite coatings have been successfully developed for the controlled release of clindamycin. The developed method of synthesis under UV light, based on a photocrosslinking procedure, enabled continuous, fully crosslinked materials without ripples or irregularities to be obtained. The coatings exhibited a lower sorption capacity as the proportion of the ceramic phase increased. Related to this phenomenon is the release of the drug, which was greater for polymeric materials without hydroxyapatite. It was also demonstrated that the coating containing the drug bound to hydroxyapatite was not able to release it in satisfactory amounts. The largest amount of clindamycin was released from the coating exhibiting the best sorption capacity. Elemental EDS analysis confirmed the presence of chlorine ions derived from the antibiotic in the material before the immersion period in PBS, and the surface morphology indicated changes in the structure after the incubation period. The *in vitro* release of clindamycin from the coatings indicated its role in developing a controlled drug delivery system. Antimicrobial properties were confirmed for all materials

against *S. aureus*. The conducted studies had a preliminary character as well as were aimed to select materials for further procedures under *in vivo* conditions. Evaluation of the local tissue response and systemic response to the *in vivo* implantation of the coatings indicates that there are no potentially harmful effects of the developed biomaterials. However, further research is required to fully determine the application potential of the hybrid polymer/ceramic composite coatings presented in this manuscript.

Author contributions

Conceptualization, D.S.; methodology, D.S. and M.M.U.; software, D.S.; validation, D.S.; formal analysis, D.S., K.N. and M. M.U.; investigation, D.S., M.M.U., W.F. and A.T.; resources, D. S.; data curation, D.S.; writing—original draft preparation, D. S., K.N. M.M.U. and A.T.; writing—review and editing, A.S.-K.; visualization, D.S.; supervision, A.S.-K.; project administration, A.S.-K.; funding acquisition, A.S.-K. and M.M.U.; planning, execution, and analysis of the *in vivo* experiments, A.S.-G., M. W., and A.K. All authors have read and agreed to the published version of the manuscript.

Ethical statement

All animal procedures were performed in accordance with the Guidelines for Care and Use of Laboratory Animals of the University of Lodz and approved by the Local Ethical Committee for Animal Experiments based at the Medical University of Lodz (Protocol No. ŁB192/2021 dated February 8, 2021).

Data availability

Data for this article, including SEM imaging, EDS microanalysis, HPLC drug release determination and incubation results, are available at the Mendeley Data repository at **https://doi.org/10.17632/jytvts9z3t.1**. Data for this article including the biosafety assessment against L929 cells, antimicrobial properties and *in vivo* evaluation are available at **https://hdl.handle.net/11089/52948**.

Conflicts of interest

There are no conflicts to declare.

Acknowledgements

The "Multifunctional biologically active composites for applications in bone regenerative medicine" project was carried out within the TEAM-NET program of the Foundation for Polish Science, financed by the European Union under the European Regional Development Fund (grant number POIR.04.04.00-00-16D7/18). The authors gratefully acknowledge the financial support.

The authors express their thanks to Karolina Rudnicka and Przemysław Płociński from the Department of Immunology and Infectious Biology, Faculty of Biology and Environmental Protection, University of Lodz, for their help with the experimental design, data analysis, and supervision. The authors would like to express their gratitude to Sylwia Michlewska and Marika Grodzicka from the Laboratory of Microscopic Imaging and Specialized Biological Techniques, Faculty of Biology and Environmental Protection, University of Lodz, for their help in visualising bacterial biofilms.

References

1 D. Arcos, A. R. Boccaccini, M. Bohner, A. Díez-Pérez, M. Epple, E. Gómez-Barrena, A. Herrera, J. A. Planell, L. Rodríguez-Mañas and M. Vallet-Regí, *Acta Biomater.*, 2014, **10**, 1793–1805.
2 C. Joe, Top Companies in Bio-Composites Market by Size, Share, Historical and Future Data & CAGR | Report by Vantage Market Research, 2023.
3 A. L. Jardini, M. A. Larosa, R. M. Filho, C. A. D. C. Zavaglia, L. F. Bernardes, C. S. Lambert, D. R. Calderoni and P. Kharmandayan, *J. Cranio-Maxillofac. Surg.*, 2014, **42**, 1877–1884.
4 S. B. Naique, M. Pearse and J. Nanchahal, *J. Bone Jt. Surg. – Ser. B*, 2006, **88**, 351–357.
5 M. Djošić, A. Janković and V. Mišković-Stanković, *Materials*, 2021, **14**, 5391.
6 Y. Zhang, Y. Xu, H. Kong, J. Zhang, H. F. Chan, J. Wang, D. Shao, Y. Tao and M. Li, *Exploration*, 2023, **3**, 20210170.
7 W. Kolasiński, *Pol. J. Surg.*, 2018, **90**, 1–7.
8 J. Parvizi, S. Barnes, N. Shohat and C. E. Edmiston, *Am. J. Infect. Control*, 2017, **45**, 1267–1272.
9 X. Lu, R. Chen, J. Lv, W. Xu, H. Chen, Z. Ma, S. Huang, S. Li, H. Liu, J. Hu and L. Nie, *Acta Biomater.*, 2019, **99**, 363–372.
10 E. A. Masters, R. P. Trombetta, K. L. de Mesy Bentley, B. F. Boyce, A. L. Gill, S. R. Gill, K. Nishitani, M. Ishikawa, Y. Morita, H. Ito, S. N. Bello-Irizarry, M. Ninomiya, J. D. Brodell, C. C. Lee, S. P. Hao, I. Oh, C. Xie, H. A. Awad, J. L. Daiss, J. R. Owen, S. L. Kates, E. M. Schwarz and G. Muthukrishnan, *Bone Res.*, 2019, **7**(1), 20.
11 WHO, World Health Organization.
12 M. B. Browning, S. N. Cereceres, P. T. Luong and E. M. Cosgriff-Hernandez, *J. Biomed. Mater. Res., Part A*, 2014, **102**, 4244–4251.
13 Z. Peng, C. Ji, Y. Zhou, T. Zhao and R. M. Leblanc, *Appl. Mater. Today*, 2020, **20**, 100677.
14 A. Kuźmińska, B. A. Butruk-Raszeja, A. Stefanowska and T. Ciach, *Colloids Surf., B*, 2020, **192**, 4–9.

15 M. S. B. Husain, A. Gupta, B. Y. Alashwal and S. Sharma, *Energy Sources, Part A*, 2018, **40**, 2388–2393.
16 E. E. Doğan, P. Tokcan, M. E. Diken, B. Yilmaz, B. K. Kizilduman and P. Sabaz, *Adv. Mater. Sci.*, 2019, **19**, 32–45.
17 P. Franco and I. De Marco, *Polymers*, 2020, **12**, 18–21.
18 L. Yu, D. W. Rowe, I. P. Perera, J. Zhang, S. L. Suib, X. Xin and M. Wei, *ACS Appl. Mater. Interfaces*, 2020, **12**, 18235–18249.
19 L. Sbricoli, R. Guazzo, M. Annunziata, L. Gobbato, E. Bressan and L. Nastri, *Materials*, 2020, **13**, 1–16.
20 A. Terzi, N. Gallo, S. Bettini, T. Sibillano, D. Altamura, M. Madaghiele, L. De Caro, L. Valli, L. Salvatore, A. Sannino and C. Giannini, *Macromol. Biosci.*, 2020, **20**, 1–18.
21 L. Ruiz-Rodriguez, P. Loche, L. T. Hansen, R. R. Netz, P. Fratzl, E. Schneck, K. G. Blank and L. Bertinetti, *MRS Bull.*, 2021, **46**, 889–901.
22 A. Sionkowska, K. Adamiak, K. Musiał and M. Gadomska, *Materials*, 2020, **13**, 4217.
23 M. Diotallevi, P. Checconi, A. T. Palamara, I. Celestino, L. Coppo, A. Holmgren, K. Abbas, F. Peyrot, M. Mengozzi and P. Ghezzi, *Front. Immunol.*, 2017, **8**, 1239.
24 C. Gaucher, A. Boudier, J. Bonetti, I. Clarot, P. Leroy and M. Parent, *Antioxidants*, 2018, **7**(5), 62.
25 L. Wang, M. Shen, Q. Hou, Z. Wu, J. Xu and L. Wang, *Int. J. Biol. Macromol.*, 2022, **222**, 1175–1191.
26 A. M. Tomala, D. Słota, W. Florkiewicz, K. Piętak, M. Dyląg and A. Sobczak-Kupiec, *Lubricants*, 2022, **10**, 58.
27 D. Słota, K. Piętak, W. Florkiewicz, J. Jampílek, A. Tomala, M. M. Urbaniak, A. Tomaszewska, K. Rudnicka and A. Sobczak-Kupiec, *Nanomaterials*, 2023, **13**(9), 1469.
28 K. Kabiri, H. Omidian, S. A. Hashemi and M. J. Zohuriaan-Mehr, *Eur. Polym. J.*, 2003, **39**, 1341–1348.
29 X. Gong, Z. Liang, Y. Yang, H. Liu, J. Ji and Y. Fan, *Regener. Biomater.*, 2020, **7**, 271–281.
30 European Committee on Antimicrobial Susceptibility Testing. Breakpoint Tables for Interpretation of MICs and Zone Diameters, Version 13.0: European Committee on Antimicrobial Susceptibility Testing, Växjö, Sweden, 2013.
31 M. Biernat, A. Szwed-Georgiou, K. Rudnicka, P. Płociński, J. Pagacz, P. Tymowicz-Grzyb, A. Woźniak, M. Włodarczyk, M. M. Urbaniak, A. Krupa, P. Rusek-Wala, N. Karska and S. Rodziewicz-Motowidło, *Int. J. Mol. Sci.*, 2022, **23**(22), 14315.
32 K. Nawrotek, M. Tylman, K. Rudnicka, J. Gatkowska and M. Wieczorek, *Carbohydr. Polym.*, 2016, **152**, 119–128.
33 P. Piszko, M. Włodarczyk, S. Zielińska, M. Gazińska, P. Płociński, K. Rudnicka, A. Szwed, A. Krupa, M. Grzymajło, A. Sobczak-Kupiec, D. Słota, M. Kobielarz, M. Wojtków and K. Szustakiewicz, *Int. J. Mol. Sci.*, 2021, **22**(16), 8587.
34 H. Susi, J. S. Ard and R. J. Carroll, *Biopolymers*, 1971, **10**, 1597–1604.
35 E. Karna, L. Szoka, T. Y. L. Huynh and J. A. Palka, *Cell. Mol. Life Sci.*, 2020, **77**, 1911–1918.
36 A. Martinac, J. Filipović-Grčić, B. Perissutti, D. Voinovich and Ž. Pavelić, *J. Microencapsulation*, 2005, **22**, 549–561.
37 G. Leyva-Gómez, M. L. Del Prado-Audelo, S. Ortega-Peña, N. Mendoza-Muñoz, Z. Urbán-Morlán, M. González-Torres, M. G. Del Carmen, G. Figueroa-González, O. D. Reyes-Hernández and H. Cortés, *Pharmaceutics*, 2019, **11**(5), 217.
38 A. Kaczmarek-Pawelska, K. Winiarczyk and J. Mazurek, *J. Achiev. Mater. Manuf. Eng.*, 2017, **81**, 35–40.
39 M. Bustamante-Torres, B. Arcentales-Vera, J. Estrella-Nuñez, H. Yánez-Vega and E. Bucio, *Macromol*, 2022, **2**, 258–283.
40 B. Agathe, V.-G. Véronique, L. Delphine, B. Odile, B. Morgane, H. Maxime, O. Xavier, D. Saidou and B.-S. Firouzé, *Diagn. Microbiol. Infect. Dis.*, 2021, **99**, 115225.
41 J. Ferguson, M. Diefenbeck and M. Mcnally, *J. Bone Jt. Infect.*, 2017, **2**, 38–51.
42 V. Kavarthapu, J. Giddie, V. Kommalapati, J. Casey, M. Bates and P. Vas, *J. Clin. Med.*, 2023, **12**(9), 3239.
43 J. L. Lister and A. R. Horswill, *Front. Cell. Infect. Microbiol.*, 2014, **4**, 1–9.
44 M. Bhattacharya, D. J. Wozniak, P. Stoodley and L. Hall-Stoodley, *Expert Rev. Anti-Infect. Ther.*, 2015, **13**, 1499–1516.
45 M. Sokolsky-Papkov, K. Agashi, A. Olaye, K. Shakesheff and A. J. Domb, *Adv. Drug Delivery Rev.*, 2007, **59**, 187–206.
46 A. Rodriguez, H. Meyerson and J. M. Anderson, *J. Biomed. Mater. Res., Part A*, 2009, **89**, 152–159.
47 K. L. Singampalli, S. Balaji, X. Wang, U. M. Parikh, A. Kaul, J. Gilley, R. K. Birla, P. L. Bollyky and S. G. Keswani, *Front. Cell Dev. Biol.*, 2020, **8**, 636.

Biomaterials Science

ROYAL SOCIETY OF CHEMISTRY

PAPER

View Article Online
View Journal

Cite this: DOI: 10.1039/d5bm00637f

Bioactive coating with clindamycin, VEGF-165, and TGF-β1 for supporting bone tissue regeneration

Dagmara Słota, *[a] Aleksandra Szwed-Georgiou, [b] Marcin Włodarczyk,[b] Agnieszka Krupa,[b] Karolina Rudnicka, [b] Karina Niziołek,[a] Bartłomiej Kryszak,[c] Konrad Szustakiewicz [c] and Agnieszka Sobczak-Kupiec[d]

The growing demand for implantable devices, implants, and plastic surgery is a major factor driving the growth of the global biomaterials market. Both new materials and opportunities to enhance the properties of existing solutions are being explored. One such approach involves coating existing materials with bioactive layers to provide additional functions. In this study, a bioactive coating was developed in an environmentally friendly and cost-effective manner, using polyethylene glycol (PEG), polyvinylpyrrolidone (PVP), hydroxyapatite (HAp), collagen (COL), and glutathione (GSH). The coating demonstrated the ability to release the antibiotic clindamycin, the vascular endothelial growth factor-165 (VEGF-165), which promotes angiogenesis, and the transforming growth factor-β1 (TGF-β1), which provides anti-inflammatory properties. The physicochemical properties of the coating were evaluated, and its *in vivo* integration with natural bone tissue was assessed using a rat skull bone defect model in adult Wistar rats (Rattus norvegicus). It was demonstrated that VEGF-165 and TGF-β1 were released within 24 hours at approximately 30% each, a dose capable of producing a therapeutic effect. The *in vivo* results suggest that incorporating growth factors into the composite coating significantly promotes mineralization at the site of injury. Our coating has the potential to support bone tissue regeneration through the synergistic effects of proteins; however, further studies are required.

Received 24th April 2025,
Accepted 31st July 2025

DOI: 10.1039/d5bm00637f

rsc.li/biomaterials-science

Introduction

The global biomaterials market continues to grow, with increases driven by growing funding for regenerative and personalized medicine, the use of biomaterials in various therapeutic areas, as well as rising demand for implantable devices or plastic surgery. Biomaterials for bone tissue include implants for defects, biocomposites, endporpotes or coatings. The last ones are particularly interesting as they can provide additional functions without changing the underlying parameters they cover, such as a personalized 3D printed defect or endoprosthesis.[1,2] Orthopaedic injuries involving the aforementioned biomaterials represent a significant public health problem worldwide and a heavy burden of disability or suffering for patients. Globally, there has been a major increase in the number of musculoskeletal disorders that require surgical interventions involving the use of permanent, temporary or biodegradable medical devices. Statistics from 1990 indicate 221 million patients affected by orthopaedic conditions, while in 2020, as many as 494 million patients were reported, which represents an increase of 123.4%. It is important to note that the success of a clinician's intervention, depends largely on the character of the chosen device and its parameters, which will determine the biological response. For this reason, more and more bioactive biocomposites are designed.[3] However, in the process of developing new materials, it is crucial to consider not only their functional properties but also their impact on the natural environment. In the face of ongoing climate change and ecosystem degradation, it is essential to employ sustainable synthesis methods that minimize raw material and energy consumption while reducing waste.[4–6]

Ceramic-polymer biocomposites are a modern group of materials dedicated to biomedical engineering applications, particularly in bone tissue implantology. They are multiphase systems combining the properties of ceramic inorganic materials, most often calcium phosphates such as hydroxyapatite (HAp), with polymers, both natural (*e.g.* collagen) and

[a]*Cracow University of Technology, CUT Doctoral School, Faculty of Materials Engineering and Physics, Department of Materials Science, 37 Jana Pawła II Av., 31-864 Krakow, Poland. E-mail: dagmara.slota@pk.edu.pl*
[b]*University of Lodz, Faculty of Biology and Environmental Protection, Department of Immunology and Infectious Biology, 12/16 Banacha St, 90-237 Łódź, Poland*
[c]*Department of Polymer Engineering and Technology, Faculty of Chemistry, Wroclaw University of Science and Technology, Wyb. Wyspianskiego 27, 50-370 Wroclaw, Poland*
[d]*Cracow University of Technology, Faculty of Materials Engineering and Physics, Department of Materials Science, 37 Jana Pawła II Av., 31-864 Krakow, Poland*

of synthetic origin (*e.g.* polyvinylpyrrolidone (PVP) or polyethylene glycol (PEG)).[7–9] The ceramic component provides bioactivity, understood as the ability to form bonds with natural bone tissue, as well as high mechanical compressive strength to the composites. Moreover, it stimulates bone-forming cells to proliferate.[10–12] On the other hand, the polymer component improves flexibility, reduces the brittleness of the ceramic, and enables controlled release of active agents such as growth factors such as vascular endothelial growth factor, transforming growth factor or drugs. As a result of these properties, ceramic-polymer biocomposites can be used in bone fillings, scaffolds and as implant coatings[13–15]

A key challenge in material design is optimizing mechanical, physicochemical as well as biocompatibility properties. It is important to achieve a balance between the durability of the material, its performance as well as its ability to promote regenerative processes.[16,17] Furthermore, it is necessary to confirm the effectiveness and safety of potential biomaterials in *in vivo* studies, which provide the necessary information on their behaviour in a complex biological environment. In the case of class III medical devices *e.g.* all implantable materials, such preclinical studies are required, as potential toxicity or other risks can be excluded.[18] *In vivo* studies enable assessment of the biocomposite's integration with natural bone tissue or the degree of induction of osteogenesis.[19,20] Thanks to such analyses, it is possible to tailor the properties of biocomposites to individual patient requirements, which are also particularly important in the context of personalizing materials in terms of the amount of active substances released, since the dose will naturally be different for an adult and a child.

In this work, a ceramic-polymer coating capable of releasing vascular endothelial growth factor (VEGF) and transforming growth factor-β (TGF-β) from between polymer chains was analysed thoroughly. These two proteins were chosen because of their biological properties. VEGF is a highly pleiotropic protein with both vascular as well as extravascular functions. Primarily, it is known as an angiogenesis factor that, has the ability to rebuild blood vessels.[21] Furthermore, it induces proliferation, migration as well as capillary morphogenesis of endothelial cells.[22] Depending on the number of amino acid residues, there are several isoforms of this protein, of which VEGF121, -165, -189 and -206 are the most dominant. Apart from their influence on the processes of angiogenesis, they also affect the development of the nervous system.[23,24] TGF-β is an anti-inflammatory factor and a key regulator of many cellular functions, including cellular immunity. It maintains immune homeostasis and prevents autoimmunity.[25] The effects of this protein on osteoblasts is also proven, resulting in increased differentiation, which includes the secretion of bone matrix proteins and subsequent mineralization.[26]

Despite numerous advances in the development of materials engineering or ceramic-polymer biomaterials, there is still a lack of bioactive coatings capable of delivering multiple biological agents in a controlled manner while maintaining adequate mechanical properties, biocompatibility and biodegradability. Furthermore, many proposed systems have not been validated *in vivo*, limiting their clinical relevance and hindering implementation. The research presented in this manuscript seeks to fill this gap by proposing a multifunctional composite coating that combines hydroxyapatite with a PVP : PEG matrix, enabling dual release of VEGF and TGF-β, the drug, and allowing direct application to solid surfaces *via* photocrosslinking, while also subscribing to the concept of sustainable production.

In this study, we present a new, previously unproposed strategy for obtaining and applying a bioactive coating for covering solid materials for the treatment of bone regeneration. The innovative character of this work lies not only in the crosslinking method itself, which has been explored in other biomedical contexts, but also in the integration of this approach into a ceramic-polymer material that supports dual growth factor as well as drug release and has been biologically validated *in vivo*. To our knowledge, this is the first report of such a coating composition, structure, and application method being tested in an animal model, thus providing a significant step toward clinical translation in bone tissue regeneration For the first time, coatings obtained by photocrosslinking with such chemical composition and biological properties are presented.

Materials and methods

Reagents

Reagents for the synthesis of ceramics phase, such as sodium phosphate dibasic (Na_2HPO_4), calcium acetate monohydrate ($Ca(CH_3CO_2)_2{\cdot}H_2O$) and ammonia solution ($NH_4OH$, 25%), were purchased from Sigma-Aldrich (Darmstadt, Germany). Medical grade poly(L-lactide) (PLLA), Resomer L210S (M_n = 304 020 g mol^{-1}, PDI = 1.96, 100% L-lactide unit fraction) from Evonik (Essen, Germany) was used for composite plates preparation. All polymers, along with other components required for the synthesis of the coatings, including polyvinylpyrrolidone (PVP), polyethylene glycol (PEG), poly(ethylene glycol) diacrylate (PEGDA) with a molecular weight of 5752-hydroxy-2-methylpropiophenone (97%), L-glutathione peptide (reduced, 98%) (GSH), and collagen derived from bovine Achilles tendon (COL), were also sourced from Sigma-Aldrich (Darmstadt, Germany). Clindamycin hydrochloride, one of the active ingredient chosen for coating modification, was also obtained from Sigma-Aldrich (Darmstadt, Germany). The active ingredients for the coating modification, *i.e.* Recombinant Human VEGF-165 and Recombinant Human TGF-β1, were purchased from Shenandoah Biotechnology (Warminster, U.S.) and Merck (Darmstadt, Germany), respectively. The Human VEGF Elisa Kit and Human TGF-β1 ELISA Kit from Invitrogen by Thermo Fisher Scientific (Vienna, Austria) were used sequentially for their determination after *in vitro* release.

PLLA/HAp plates preparation

The first stage involved preparing the materials for processing. Synthetic HAp with a Ca/P molar ratio of 1.67 was used.

Details on the preparation of HAp are provided in the SI (subsections 1–4). The post-synthetic HAp suspension was decanted. The resulting sediment was frozen at −40 °C and then freeze-dried at −53 °C under a vacuum (below 10 mbar) using a FreeZone 2.5 Liter Benchtop Freeze Dryer (Labconco, USA). The HAp powder was then calcined in an electric furnace at 600 °C for 3 hours, while the PLLA was dried at 70 °C for 24 hours. Finally, the materials were weighed, thoroughly mixed at a polymer-to-filler weight ratio of 7 : 3, and prepared for further processing.

A processing procedure was selected to ensure good dispersion of HAp in the PLLA matrix, as well as dimensional stability and product repeatability.[27] To effectively incorporate the HAp filler into the polymer, the prepared formulation was processed by co-rotating twin-screw extrusion. A Thermo Fisher Scientific (Waltham, USA) twin-screw extruder (D = 20 mm, L/D = 40) equipped with special mixing zones was used. The material was processed at a screw speed of 200 rpm and a set temperature of 200 °C across all heating zones. The extrudate was cooled on an air track, wound on a winder (Thermo Fisher Scientific, Waltham, USA) and regranulated using a Brabender (Duisburg, Germany) pelletizer. The composite granules were subsequently injection molded using a BOY XS micro-injection molding machine (Dr Boy GmbH & Co. KG, Neustadt-Fernthal, Germany). The process was performed with a barrel temperature of 220 °C, a flow channel temperature of 200 °C, an injection pressure of 250 bar, a cooling time of 15 seconds, and a cooling temperature of 50 °C. The injection molding process produced plate-shaped samples with dimensions of 35 mm × 35 mm and a thickness of 2 mm.

The final forming process was carried out using CNC milling with an ATMSolutions Basic Mill (Warsaw, Poland), controlled by Mach 3 CNC Controller software and equipped with a 1 mm diameter end mill. The cylinders, made from injection-molded plates, were 2 mm high and 3.8 mm in diameter. Each cylinder had a symmetrically oriented hole in the base, milled to a depth of 1 mm and a diameter of 3.0 mm. They provided a base in the form of plates on which the bioactive coatings were applied.

Preparation of coatings

Additional information regarding the preparation of coatings is presented in the SI (subsection 5). Fig. 1A schematically presents the process of obtaining coatings. Coatings composition is presented in Table 1. 200 µl of the mixture was deposited on a PLLA/HAp plate and crosslinked. The materials were obtained by UV photocrosslinking process using a suitable crosslinking agent and photoinitiator. The sample was irradiated for 4 minutes at an irradiation power of 0.8 J cm^{-2}. An example of the resulting coating applied to a PLLA/HAp pad, ready for implantation into an animal model is presented in Fig. 1B.

The proposed material obtaining method is environmentally friendly, does not generate by-products that would require disposal and allows for full incorporation of all reagents used during synthesis. Coatings modified with growth factors were

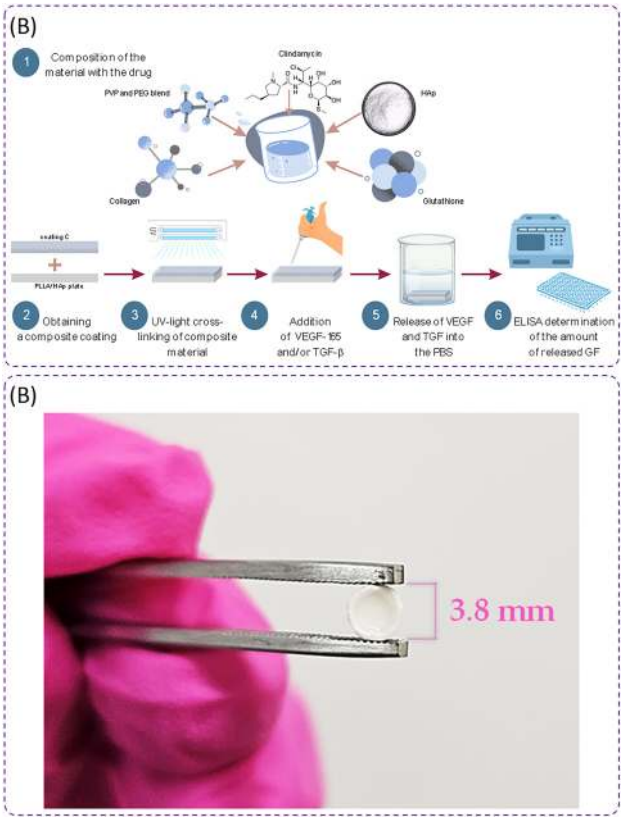

Fig. 1 (A) Schematic of the process of obtaining and modifying the coating with GF proteins. (B) Coating applied to a PLLA/HAp plate ready for *in vivo* implementation.

Table 1 Composition of coatings indicating basic differences in formulation

Coating symbol	Coating C	Coating 4	Coating C/GF
PVP 15% [µL]	100		
PEG 15% [µL]	100		
COL [mg]	0.8		
GSH [mg]	40		
HAP [mg]	10		
Clindmycin [mg]	—	0.5	—
VEGF-165 [µg]	—	—	100
TGF-β1 [µg]	—	—	100

produced as follows. An aqueous solution of VEGF-165 and an aqueous solution of TGF-β1 were prepared in order to reconstruct proteins. Solutions of VEGF-165 and/or TGF-β1 were then dripped onto the surface of the cross-linked coating so that 100 µg of the selected protein was present in the material. Based on our previous work the coating thickness in this study was assumed to be approximately 600 µm, which is considered suitable for bone tissue regeneration.[28] We acknowledge that depending on the type of implant *e.g.*, a 3D-printed material designed to fill a bone defect or a metallic endoprosthesis – some variability in coating thickness may arise due to differences in geometry and application conditions. Nevertheless,

the method enables full reagent utilization without generating by-products, supporting its environmentally responsible profile.

Determination of sedimentation rate

The process of obtaining composite coatings was carried out under UV light using a photocrosslinking process that occurred over a period of 4 minutes. In order to avoid excessive sedimentation of the powder in the aqueous solution of the polymers, an analysis of the sedimentation rate of HAp powder in different concentrations of PVP/PEG was carried out. A polymer ratio of 1 : 1 (PVP : PEG) and its aqueous concentrations of 0%, 5%, 10%, 15%, 20% and 25% were proposed. The analysis was carried out using a MultiScan MS20 DataPhysics Instruments (Filderstadt, Germany). Measurements were conducted for 10 minutes, performing 20 scans at a time interval of 12 seconds.

Fourier-transform infrared spectroscopy analysis

The composition of coating composite materials has been selected and studied previously,[28,29] however, the mechanism of the occurring photocrosslinking process has not been adequately investigated so far. In order to clarify the phenomena occurring, the base composition in the form of a PVP/PEG blend was analysed using Fourier transform infrared spectroscopy. Analysis was also performed for coatings modified with clindamycin, VEGF and TGF to determine whether the addition of the active ingredient affects the overall system. The study was performed using a Nicolet iS5 FT-IR spectrometer equipped with an iD7 ATR detector (Thermo Scientific, Loughborough, UK). The measurement was carried out at room temperature, in the range from 4000 to 400 cm^{-1}. For each sample, a total of 32 scans were carried out at a resolution of 4.0 cm^{-1}.

Morphology analysis

The coating materials were imaged by scanning electron microscopy (SEM) to determine whether additions of active ingredients affect the morphology of the biomaterials. The interior of the coatings was examined. Prior to measurement, the coatings were thoroughly dried, bonded to carbon pads for immobilization, and then coated with a layer of nano-gold using a DII-29030SCTR Smart Coater sputtering device (JEOL Ltd, MA, USA). A JEOL IT200 microscope (JEOL Ltd, MA, USA) was used for imaging. The device is equipped with an energy-dispersive X-ray spectroscopy (EDX) system detector, with which elemental analysis and mapping of elements on the surface were carried out. Elemental analysis was carried out by determining mass percentage (%M.) as well as atomic percentage (%At.). The measurements were performed at ×500 magnification.

TGF-β1 release test

The TGF-β1-modified sample was incubated in 1 mL PBS. After 24 h, a 100 μL sample of incubation fluid was collected and protein determination was performed. TGF-β1 detection was performed using the corresponding Invitrogen Thermo Fisher Scientific ELISA kit and its protocol.[30] Reconstitution of the human TGF standard to a concentration of 4 ng mL^{-1} was performed. A series of dilutions of the standards to 2000 pg mL^{-1}, 1000 pg mL^{-1}, 500 pg mL^{-1}, 250 pg mL^{-1}, 125 pg mL^{-1}, 63 pg mL^{-1} and 31 pg mL^{-1} were then prepared. Then 20 μL of the sample was mixed with 180 μL Assay Buffer and 20 μL of 1 N HCl and allowed to stand for 1 h. After this time, 20 μL of 1 N NaOH was added and the wells were washed with Wash Buffer. 60 μL Assay Buffer was added and allowed to stand at room temperature for 2 h. During this time, the plate was continuously shaken. After this time, the plate was washed and 100 μL Biotin-conjugate was added. It was again shaken for 1 h, after which it was washed and 100 μL Streptavidin-HRP was added and again shaken for 1 h. Then 100 μL TMB Substrate Solution was washed and pipetted. Then, plate was incubated for 30 minutes in the dark, monitoring periodically the optical density for standard 1 at 620 nm, using an ELISA Microplate Reader, BioTek 800 TS (Winooski, Vermont, U.S). When it reached a value above 0.9, 100 μL of stop solution was added. Absorbance was read at 450 nm using the same device as mentioned above.

VEGF release test

The VEGF-165-modified sample was incubated in 1 mL PBS. After 24 h, a 1 μL sample of incubation fluid was collected and protein determination was performed. VEGF-165 detection was performed using the corresponding Invitrogen Thermo Fisher Scientific ELISA kit and its protocol.[31] The human VEGF standard was reconstituted to a concentration of 10 000 pg mL^{-1} and then diluted sequentially to concentrations of 1500 pg mL^{-1}, 750 pg mL^{-1}, 188 pg mL^{-1}, 93.8 pg mL^{-1}, and 23.4 pg mL^{-1} to obtain a series of standards. The Streptavidin-HRP solution was then prepared. In the first step, the procedure leading to antigen binding was carried out. 50 μL of Incubation Buffer, 100 μL of appropriate standards, 50 μL of Standard Dilueted Buffer and 50 μL of sample were added to individual wells of the 96-well plate. After 2 hours, the plate was washed with Wash Buffer and 100 μl of Biotin conjugate was added. After 1 hour, the plate was rinsed again and 100 μl of Streptavidin-HRP was added. This was allowed to stand for 30 minutes and washed again using a Wash Buffer. In the next step, 100 μl of Stabilized Chromogen was added and the color of the wells was observed to change to blue. This was incubated for 30 minutes in the dark. After this time, 100 μL Stop Solution was added to each well and the color change from blue to yellow was observed. Absorbance was read at 450 nm, using a ELISA Microplate Reader, BioTek 800 TS (Winooski, Vermont, U.S). The entire procedure was conducted at room temperature.

In vivo study on the application of biomaterials in a rat skull bone defect model

Adult rats (*Rattus norvegicus*, Wistar breed), weighing at least 220 g, aged at least 10 weeks, were used for the study. The rats were from the in-house breeding facility of the Department of

Biology and Environmental Protection at the University of Lodz. Permission to perform *in vivo* experiments (34/LB240/2022) was granted by the Local Animal Ethics Committee at the Medical University of Lodz, based on the results of *in vitro* evaluation of biocomposites, with a particular emphasis on cytocompatibility testing, as presented in our previous study.[32] The experiment included three groups, one of which contained a reference composite – coating C, and two groups contained modified composites: coating 4 and coating C/GF. The control group comprised animals that did not undergo implantation of any biomaterial, serving as a baseline for physiological responses. After 8 weeks, the animals were euthanized for blood collection (obtaining serum) and isolation of skulls with implanted biomaterials. Concentrations of the cytokines: IL-1β, IL-10, TNF-α and osteopontin (OPN) in serum samples were measured by immunoenzymatic ELISA (R&D Systems, Minneapolis, MN, USA) according to the manufacturer's instructions and as described by Słota *et al.*, 2024.[32] The assay sensitivity thresholds were 31.2 pg mL^{-1} for IL-1β and 62.5 pg mL^{-1} for IL-10, TNF-α and OPN. Absorbance at 450 nm for standards nd samples across serial dilutions was measured using a Multiskan EX microplate reader (Thermo Fisher Scientific, USA), and biomarker concentrations were calculated using GainData (Arigo Biolaboratories, **https://www.arigobio.com/elisa-analysis**). Standard curve was generated by fitting the data to a 4-parameter logistic (4PL) curve. Statistical analysis was performed using GraphPad Prism. The Kruskal–Wallis test was used to assess group differences, followed by Dunn's multiple comparisons test. Differences were considered statistically significant at $p < 0.05$.

Results and discussion

In order to select the appropriate concentration of PVP/PEG solution to form the base of the final composite coatings, the stability of the HAp ceramic phase in the polymer was evaluated. For this purpose, the migration front was determined as a function of time (Fig. 2A). The results obtained demonstrate the differences between the stability of the HAp suspensions tested.

For a concentration of 5% and distilled water (0%), the curves overlap, and the flattening of the migration front occurs a little later. For the highest concentration of 25%, the obtained curve is jagged, which may suggest that the polymer mixture was not completely homogeneous and the suspended powders did not sediment uniformly in it. It is significant that already at the stage of solution preparation, some dissolution difficulties were observed for this concentration.

Fig. 2B demonstrates the procedure for measuring sedimentation rates. The segregation process was analysed by measuring light intensity with temporal and positional resolution. Fig. 2C presents vials of HAp powder at different aqueous concentrations of PVP : PEG polymers. The results of the analysis of the sedimentation rate of HAp in PVP/PEG solutions of different concentrations are presented in Table 2. Based on the given values, it can be indicated that the concentration of polymer solutions affects the sedimentation process. The value obtained for the highest polymer concentration equals −10.19 ± 1.07 mm min^{-1}, and is practically three times lower than for distilled water (0%) alone. Based on the data obtained, the concentration chosen for further study was 15%. This concen-

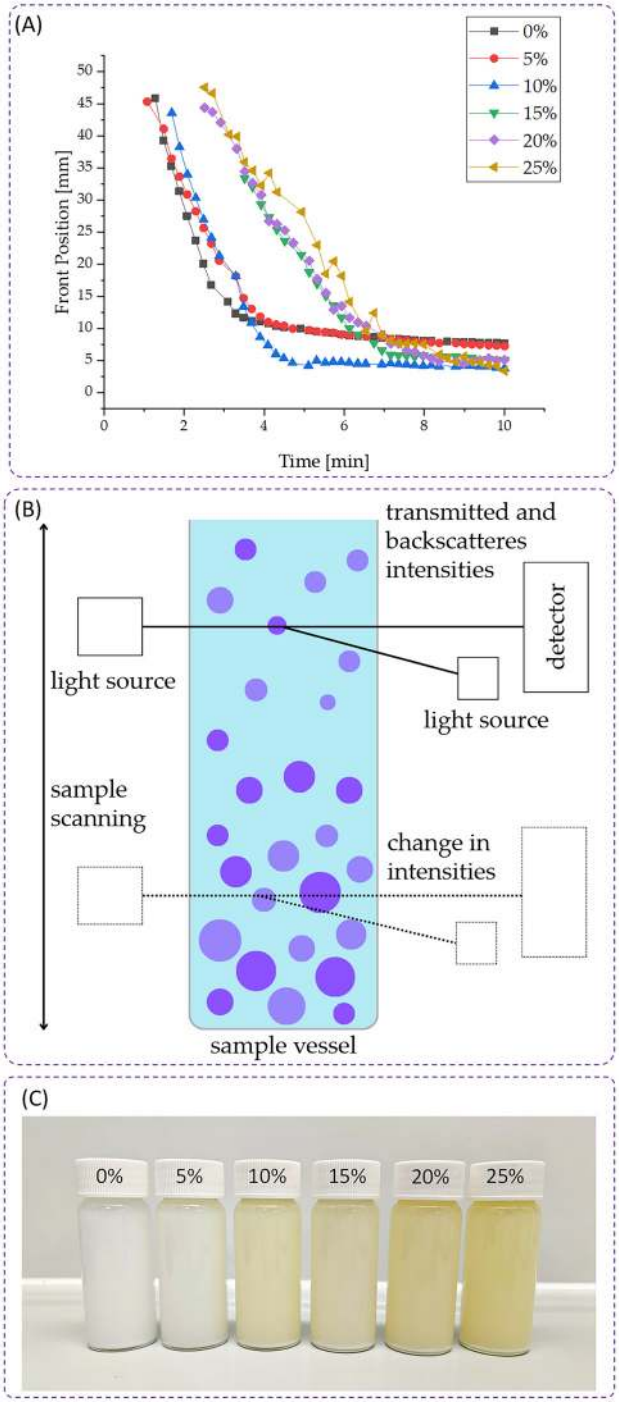

Fig. 2 (A) Migration front as a function of time for HAp powders in PVP/PEG aqueous solutions with different concentrations.(B) Schematic of the procedure for measuring the sedimentation rate. (C) Samples of ceramics in uncrosslinked polymer solution.

Table 2 Sedimentation rate of HAp powder in PVP/PEG solutions of different concentrations

PVP/PEG [%]	Sedimentation rate [mm min^{-1}]
0	−35.59 ± 7.95
5	−32.59 ± 1.07
10	−24.4 ± 0.28
15	−16.25 ± 0.07
20	−12.55 ± 4.66
25	−10.19 ± 1.07

tration was found to offer a favorable balance between stabilizing ability and practical usability. At this concentration, the PVP : PEG polymers dissolved efficiently, and the HAp particles were evenly distributed, resulting in a homogeneous suspension. In contrast, higher concentrations, 20% and particularly 25% required more time and energy to dissolve and displayed visible heterogeneities during preparation. Moreover, preliminary assessments of the final UV-crosslinked coatings indicated that formulations with 20% polymer content yielded stiffer and less flexible materials compared to the 15% ones, likely due to increased crosslink density. Considering the intended application in bone tissue engineering, where moderate elasticity is beneficial, the 15% concentration was selected for further work as a compromise between colloidal stability, processability, and mechanical suitability.

The composition of coating composite materials has been selected and studied previously.[28,29,32] However, the mechanism of the occurring photocrosslinking process has not been adequately investigated so far. In order to clarify the phenomena occurring, the base composition in the form of a PVP/PEG/PEGDA blend, at PVP and PEG concentration of 15% was analyzed using Fourier transform infrared spectroscopy.

Analysis was carried out on samples of pure polymers, as well as the crosslinking agent PEGDA in crosslinked and uncrosslinked forms. The photoinitiator used was 2-hydroxy-2-methylpropiophenone. The obtained spectra are presented in Fig. 3A. Upon exposure to UV radiation, the photoinitiator dissociates into two highly reactive radicals. These attack the –C═C– double bond, which are found in PEGDA. This is evidenced by the complete disappearance of the absorption band characteristic of this bond at 1622 cm^{-1} (marked with a circle in the Fig. 3). Thus, the –C–C– covalent bond is formed, resulting in a three-dimensional network of polymer chains[33,34] For the cross-linked PVP/PEG/PEGDA polymer blend, this phenomenon is not visible because of the presence of a very strong signal that comes from the –C═O carbonyl group from PVP at 1658 cm^{-1}.[35] For the cross-linked PVP/PEG/PEGDA sample, changes in the intensity of the bands in the 3000–3500 cm^{-1} range are also observed, while they are clearly evident for the pure components, therefore may indicate interactions between the components in the matrix. It can be concluded that the formation of the materials was carried out PEGDA radical crosslinking.

The radical crosslinking presented in this work was enabled by the use of a UV light source, which also served as

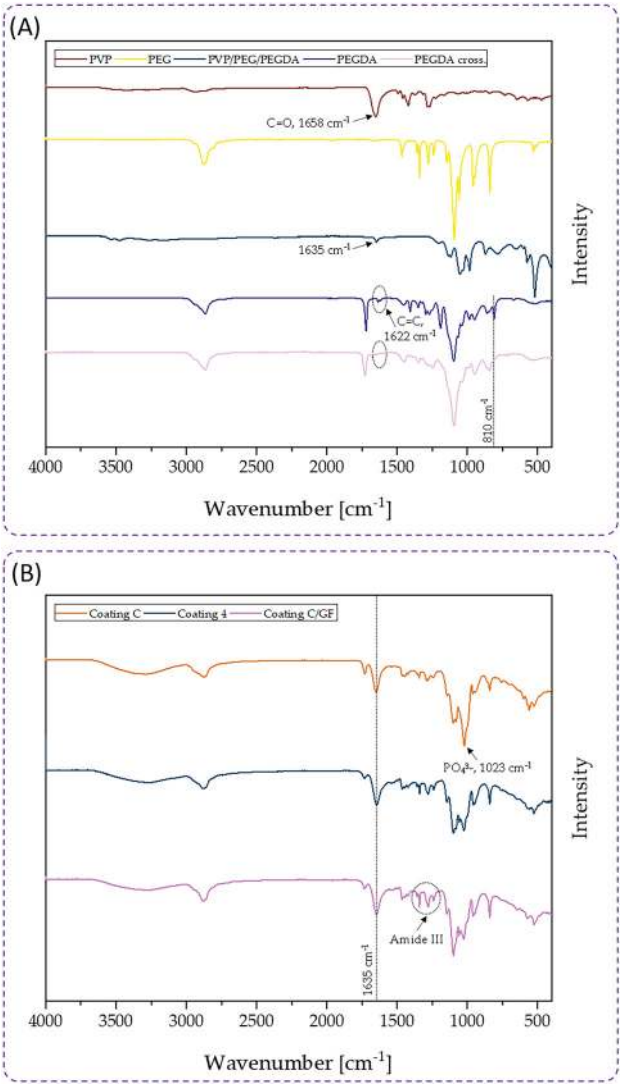

Fig. 3 (A) ATR FT-IR spectra of the individual components and the developed base polymer composition. (B) ATR FT-IR spectra of the obtained coatings.

an indicator of the process. For this reason, particular attention was given to the topic of photcrosslinking. Compared to conventional chemical crosslinking, photopolymerization offers a more sustainable approach. By significantly reducing the consumption of chemical reagents typically used in crosslinking reactions, this method contributes to the overall minimization of the carbon footprint. These advantages highlight the potential of the proposed method for biomedical applications, particularly in the development of implant coatings aimed at enhancing tissue regeneration while minimizing environmental impact.

Based on the obtained spectra, it was concluded that the resulting photocrosslinking interactions are hydrogen bonds that create an interpenetrating polymer network (IPN).[36] The occurrence of hydrogen interaction was confirmed on the basis of the peak position of the carbonyl group, which shifted gently

towards smaller values. For the PVP/PEG/PEGDA blend, the value is 1635 cm^{-1}, while for pure PVP the signal is observed at 1658 cm^{-1}. The conversion of the double bond to a single one is also confirmed by the absence of a signal at 810 cm^{-1} for PEGDA cross. Which occurs for pure PEGDA and corresponds to the –C–H bond (marked in the Fig. 3A with a dashed line).[37] Based on the above information, Fig. 4 presents the proposed polymer network formation mechanism. It is considered that the polymer networks formed in this way are a good material for carrying active substances, since they can encapsulate biomolecules in their structure between polymer chains.[38]

The spectra of the base coating and the antibiotic- and GF-modified coating are presented in Fig. 3B. The obtained spectra for coating C, coating 4 and coating C/GF appear quite similar, which suggests that the main functional groups remain the same in all samples, and the addition of active substances did not significantly affect the chemical structure of the base matrix. In the case of these multicomponent materials, the disappearance of the aforementioned band at 1635 cm^{-1} is not observed, as there is a strong signal from Amide I in this range, which comes mainly from the stretching vibrations of the C=O bond present in collagen or can be from the peptide bond from glutathione.[28] The strongly prominent peak for coating C at 1023 cm^{-1} belongs to the asymmetric stretch PO_4^{3-}, one of the main phosphate bands characteristic for Hap.[39] In the case of coating C/GF, a slight enhancement of the bands at 1285 cm^{-1} and 1340 cm^{-1} (indicated by the dashed line on the purple spectrum) was observed, which may originate from the Amide III group found in VEGF and TGF-β, a group characteristic of protein structures.[40]

Ceramic-polymer composites can be obtained in a variety of ways including chemical crosslinking, thermal crosslinking or photo-crosslinking. Also the sol–gel method.[41] Compared to these, the photocrosslinking method has some advantages, as it usually takes less time than chemical or sol–gel crosslinking, and does not require high temperatures like thermal crosslinking. However, even though photocrosslinking usually takes a few minutes, it is extremely important to avoid excessive sedimentation of the ceramic phase, therefore, to select the crosslinking and composition parameters in such a way as to obtain a continuous material quickly enough so that one of the phases does not have time to fall off, and the final material obtained shows an even distribution of phases. Determination of the migration front and sedimentation rate of ceramics in polymer solutions allowed to select a polymer composition with optimal viscosity. The results obtained for a 1 : 1 PVP/PEG blend, were consistent with reports of a similar study for PVP.[42] The use of a photocrosslinking process and the selection of the appropriate amount of components or photoinitiator and crosslinking agent, in this case PEGDA, allows control over the physicochemical parameters of the material. The amount of PEGDA affects the mechanical parameters of the material's hardness or elasticity, as well as the kinetics of the release of active substances, as the degree of crosslinking of the material affects the rate of their release.[43] The higher the degree of crosslinking, the less permeable the pores of the hydrogel become, which translates into hindering the process of particle diffusion. In the case of a lower degree of crosslinking, the materials exhibit a greater ability to swell, which facilitates particle diffusion.[44]

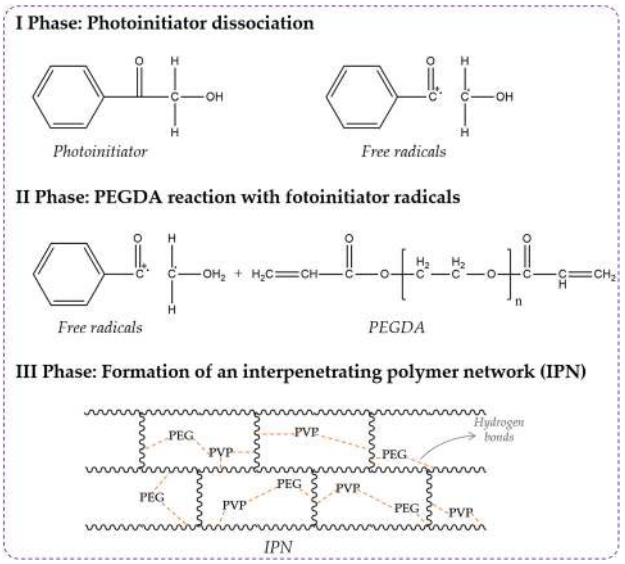

Fig. 4 The proposed mechanism for crosslinking materials.

The results of the SEM imaging are provided in Fig. 5. The surfaces appear to be similar to each other and no significant differences in structure are observed. The smoother sections in coating C/GF are likely the result of sample preparation for testing, as the coating was removed from the PLLA to examine the coating interior.

The elemental composition of the coatings was determined by EDX microanalysis and expressed as mass percent (m.%) and atomic percent (at.%). These values are presented in Table 3. The table summarizes the elemental content found on the microscopically observed materials. The content of Ca and P is similar in all materials, and their presence is a result of the composition of the HAp used in the coatings as a reinforcing phase. For coating 4, the presence of Cl ions was detected, the origin of which is related to clindamycin. Clindamycin hydrochloride was used hence its presence. The map of Cl distribution in the material confirms that the drug is evenly distributed throughout the material.[45] Also of interest is the detection of S for coating C/GF, the origin of which is probably related to the chemical structure of the VEGF and TGF-β proteins. This element is involved in the formation of disulfide bridges in proteins.[46,47] Although its % content is low relative to the other elements, its even distribution can be observed throughout the volume of the test sample. Additional information on EDX analysis of coatings is presented in the SI (subsection 6).

Fig. 6 presents the amounts of VEGF-165 and TGF-β1 released over 72 h incubation in PBS fluid. The first 24 hours after implant placement are vital for establishing the foundation of healing and integration, influencing the long-term success of biomaterial. In this initial period, a relatively fast

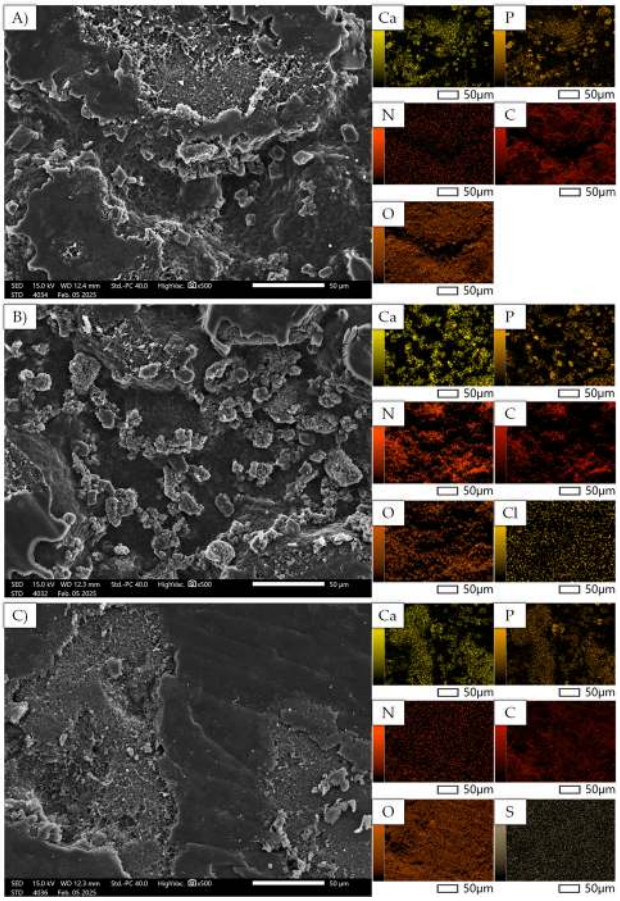

Fig. 5 SEM imaging of the morphology of the samples (A) coating C, (B) coating 4, (C) coating C/GF.

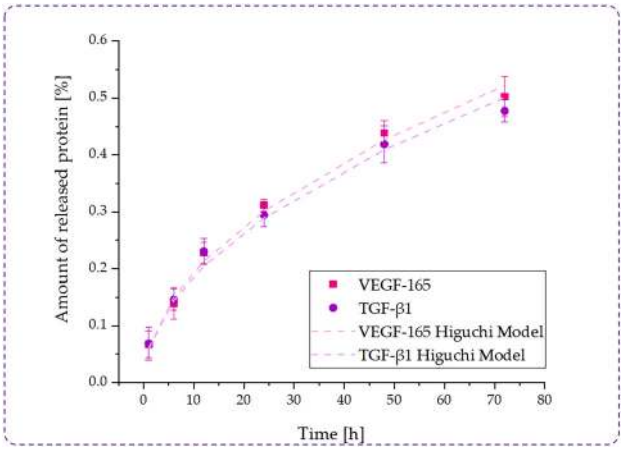

Fig. 6 Cumulative release profiles of VEGF-165 and TGF-β1 from the coating C/GF over 72 h incubation in PBS fluid. Dashed lines represent the Higuchi model fit indicating a diffusion-controlled release mechanism.

release of both incorporated growth factors was observed. The released amounts of VEGF-165 and TGF-β1 are similar and reach 31.2% and 29.5%, respectively. These similar values may be a result of the fact that despite their different properties and parameters, these proteins possess a relatively similar kDa value. TGF-β1 is a 25 kDa polypeptide that consists of two seemingly identical 12.5 kDa subunits linked by disulfide bonds.[48] On the other hand, the size of VEGF-165 is estimated at 23–22 kDa.[49] Given these values, it is likely that the two proteins were able to penetrate the polymer network in a similar manner, migrating between polymer chains.[50]

After the initial burst phase, sustained release was observed, with cumulative release reaching approximately 50.2% for VEGF-165 and 47.7% for TGF-β1 after 72 hours. This biphasic profile, consisting of a rapid initial release followed by a slower, continuous phase, is characteristic of polymer-based delivery systems. The slower phase is likely to result from the diffusion of proteins trapped deeper in the cross-linked polymer matrix and possibly interacting with the hydrogel components.

To better understand the release mechanism, the experimental data were fitted to the Higuchi model which describes drug release governed by Fickian diffusion from a homogeneous matrix.[51] The model provided a good fit to the experimental data for both growth factors, yielding release constants of k = 0.062 (VEGF-165) and k = 0.059 (TGF-β1). These values, together with the curve fit in the graph, confirm that diffusion through the polymer network is the main mechanism driving protein release.[52] Furthermore, the similar release profile for both GFs supports the concept that protein diffusion in this system is primarily influenced by polymer network structure and porosity, rather than specific differences due to protein type.

Previous work has demonstrated that as the proportion of HAp increases, the amount of clindamycin released decreases.

Table 3 Elemental EDX analysis of coatings, summary of mass [%] and atomic [%] amounts of individual elements

	Coating C		Coating 4		Coating C/GF	
Element	Mass [%]	Atom [%]	Mass [%]	Atom [%]	Mass [%]	Atom [%]
Ca	5.99 ± 0.28	2.16 ± 0.10	6.55 ± 0.31	2.38 ± 0.11	6.32 ± 0.26	2.29 ± 0.10
P	2.22 ± 0.14	1.03 ± 0.07	2.16 ± 0.15	1.02 ± 0.07	2.35 ± 0.13	1.10 ± 0.06
N	3.27 ± 0.53	3.37 ± 0.54	4.09 ± 0.59	4.27 ± 0.61	3.60 ± 0.50	3.73 ± 0.51
C	45.30 ± 0.45	54.44 ± 0.55	42.54 ± 0.47	51.70 ± 0.57	44.01 ± 0.42	53.23 ± 0.50
O	43.22 ± 0.97	38.99 ± 0.87	44.44 ± 1.02	40.55 ± 0.93	43.60 ± 0.89	39.59 ± 0.81
Cl	—	—	0.22 ± 0.05	0.09 ± 0.02	—	—
S	—	—	—	—	0.11 ± 0.05	0.74 ± 0.01

As little as 5% addition of ceramic reduced the amount of clindamycin released by about 12% after 24 h incubation in PBS.[32] Considering those reports, in this work, the material exhibiting the greatest application potential (coating C) was modified with growth factors – VEGF-165 and TGF-β1. Naturally, the amount of proteins released will also depend on the original amount used for modification. For this reason, it is rather tough to compare them to other literature reports. However, in the context of the research presented in this paper, the amount released is extremely important in terms of the effective dose of each substance. In the case of VEGF, the therapeutic effect of improving intervascular integrity was observed for doses of 0.1 mg kg^{-1} for intratissue administration and 1.0 mg kg^{-1} for intravenous injection.[53] However, these data are related to doses adjusted for improved renal health. In the case of TGF-β1, on the other hand, biological activity can already be observed at the surprisingly low dose range of 0.1–10 ng mL^{-1}. It is presumed that the reduction in damage to hippocampal CA1 neurons (responsible for cognitive function and memory processes), observed at this amount of protein, may be related to the antioxidant and anti-apoptotic effects of TGF-β1.[54] As little as 0.1 ng mL^{-1} TGF-β1 exhibited the ability to produce cartilage matrix, while material without GF did not show this ability at all.[55] VEGF at a concentration of 120 ng mL^{-1} causes an approximately twofold increase in the expression of osteoblast differentiation genes, *i.e.* alkaline phosphatase (ALP) and collagen I alpha I (COL1α1).[56] Studies conducted in this work have demonstrated that positive changes can also be observed at a much lower dose. In particular, compared to an intravenous dose, the amount of active ingredient released locally may be reduced, as systemic distribution of the compound throughout the body is then avoided.[57]

The analysis of cytokine levels presented in Fig. 7 illustrates the biocompatibility and safety of the tested biomaterials (coating C, coating 4, coating C/GF) applied to animals. Fig. 8 shows the surgical procedure for implantation of polymer-ceramic composites into cranial bone defects in a rat model. The levels of the pro-inflammatory cytokines IL-1β and TNF-α remained consistently low across all experimental groups. This suggests that the tested biomaterials do not activate acute inflammatory pathways, indicating a lack of harmful effects. The levels of IL-10, a cytokine associated with anti-inflammatory activity and tissue repair, remained comparable across groups with only slight variations, indicating that the inflammatory process was effectively modulated. Importantly, the concentrations of all tested cytokines were compared with the values measured in the sera of untreated animals (NTC).

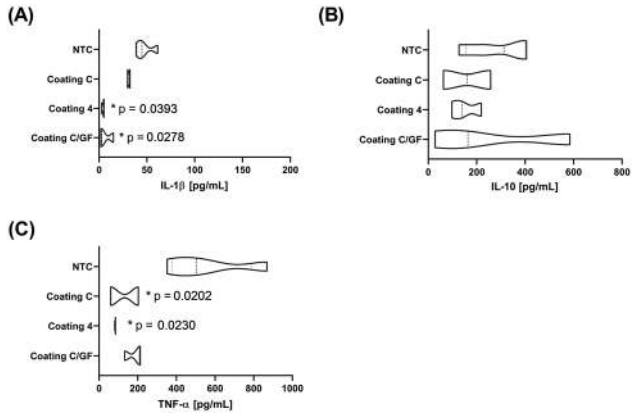

Fig. 7 The concentration of interleukin-1β – IL-1β (A), interleukin-10 – IL-10 (B) and tumor necrosis factor-α – TNF-α (C) in the serum samples obtained from animals after biomaterials implantation. NTC – non-treated control (rats not subjected to implantation of the biomaterials). Number of animals, n = 3. * – statistical significance *vs.* NTC, p value given next to "*".

The next stage of the work involved visualizing the mineralization of the animals' cranial bones at the site of the defect. For this purpose fluorescent dye – Xylenol orange (concentration 25 mg per kg body weight) was injected subcutaneously into the animals 8 weeks after implantation of the tested biomaterials, at 72 hours before euthanasia. The fluorescence signal reflects the incorporation of Xylenol orange dye indicating active bone mineralization sites. The images obtained indicate that the coating C/GF material facilitated the mineralization of the bone areas directly in contact with the implanted material (areas glowing green, Fig. 9A). Skull sections containing the implanted biomaterials were also visualized with a confocal macroscope using the following wavelengths λ = 440/570 – 610 nm for Xylenol orange. The images obtained indicate that the coating C/GF material contributed to significant bone regeneration 8 weeks after implantation compared to the reference material – coating C (area glowing green, Fig. 9A).

Significantly elevated levels of osteopontin (OPN) in the coating 4 and coating C/GF groups further confirmed the microscopic observations (Fig. 9B). OPN is a multifunctional protein crucial in bone healing, particularly in the recruitment and activation of osteoclasts and osteoblasts. Elevated OPN levels in serum indicate active bone remodeling and mineralization processes, underscoring the higher regenerative efficacy of the growth factor-enriched composite.[58–60]

In vivo results suggest that incorporating growth factors: VEGF-165 and TGF-β1 into the composite significantly promoted mineralization at the defect site as evidenced by increased osteopontin (OPN) levels in serum, measured using ELISA, and histological analysis of the explanted cranial bone defects, which revealed enhanced bone matrix deposition and mineralized tissue formation compared to the control groups. Growth factors such as VEGF-165 and TGF-β1 are crucial mediators in the process of bone regeneration and tissue healing. VEGF-165 stimulates angiogenesis by promoting the proliferation and migration of endothelial cells, which leads to the formation of new blood vessels. This is particularly important in bone repair, as an adequate blood supply is essential for delivering oxygen, nutrients, and cells involved in the healing process. In addition to its role in angiogenesis, VEGF-165 enhances osteoblast activity, facilitating the formation of new bone tissue by promoting the differentiation and mineralization of these bone-forming cells.[61,62] Also,

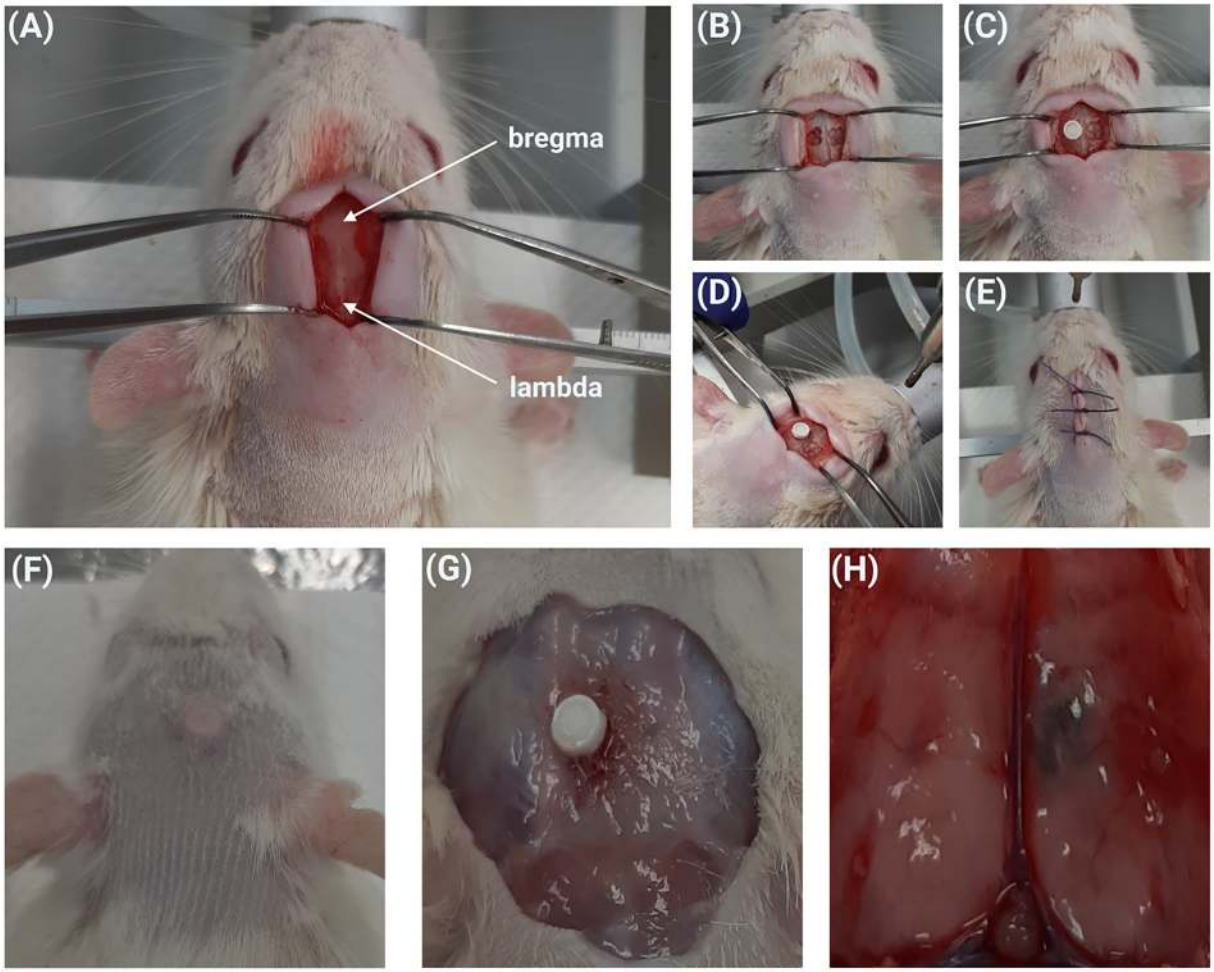

Fig. 8 Steps in the surgical procedure for implantation of polymer-ceramic composites into cranial bone defects in a rat model. (A) Exposure of the calvarial area showing anatomical landmarks (bregma and lambda) for precise defect localization. (B) Creation of a standardized circular defect in the calvarial bone using a trephine drill under sterile conditions. (C and D) Placement of the composite material into the defect site. (E) Closure of the surgical site using sutures to ensure proper healing. (F) Post-operative recovery of the animal under monitoring. (G) Inspection of the defect site during the healing period to assess implant positioning and integration. (H) Visualization of the cranial area showing spontaneous regeneration of the tissue defect without the involvement of an implant.

VEGF released from the composite can play supportive role in bone regeneration by enhancing angiogenesis, as demonstrated by increase tube formation of endothelial cells. This angiogenetic activity alongside upregulated osteogenic and angiogenic biomarkers *in vivo*, contributed to effective bone defect repair.[63] On the other hand, TGF-β1 plays a pivotal role in bone regeneration by regulating several processes in the extracellular matrix. It promotes the deposition of key components such as collagen and proteoglycans, which provide a scaffold for bone tissue development. Furthermore, TGF-β1 stimulates the recruitment and differentiation of mesenchymal stem cells (MSCs) into osteoblasts, enhancing bone formation. It also modulates the activity of osteoclasts to maintain a balanced bone remodeling process.[64–66] Together, these growth factors act synergistically to create an environment conducive to effective bone healing and regeneration.

This study confirmed that the coating contributed to significant bone regeneration 8 weeks after implantation compared to the reference material, and furthermore, the developed coating was demonstrated not to activate acute inflammatory pathways, as confirmed by determining levels of the pro-inflammatory cytokines IL-1β and TNF-α and comparing the obtained values to those of untreated animals. In the case of bone tissue regeneration, many previous studies, such as the work of Zhang *et al.* (2019) or Uskoković and Desai (2014), are often concerned with ceramic-only systems for local delivery of active ingredients.[67,68] Mainly this is HAp, the gold standard in the biomedical field due to its composition and similarity to human bone. However, it is important to consider that the use of composites can significantly improve material properties. Addition of HAp to the composite leads to a highly improved effect on MC3T3 cell differentiation and mineraliz-

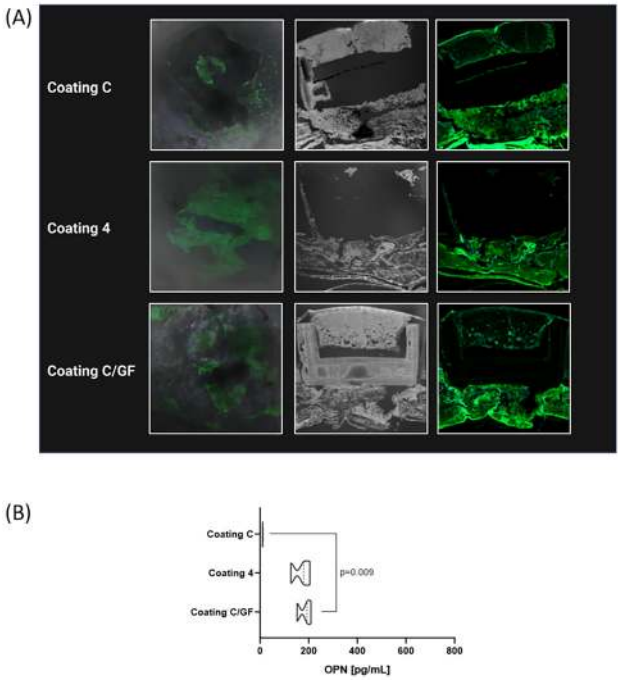

Fig. 9 Representative images of skull sections containing implanted biomaterial illustrating bone mineralization processes after 8 weeks of implantation. The fluorescence signal reflects the incorporation of Xylenol orange dye, administered *in vivo* at 72 hours prior to euthanasia, indicating active bone mineralization sites (A). Serum levels of osteopontin – OPN (B).

ation of the extracellular matrix. Cell differentiation for the ceramic materials was up to twice as high.[69]

Future perspectives

The results presented in this study have important implications for the development of materials engineering aimed at bone tissue regeneration. The developed composite coatings, with their controlled-release properties and synergistic growth factor action, offer a promising solution for bone defects of critical size. The ability to adapt the photocrosslinking process to different shapes and sizes of implants increases its versatility in personalized medicine applications, by tailoring it to individual patient needs. The coating can be used on its own as a more flexible filling, or applied to cover other implants, as demonstrated in this study with composite or polymer structures, as well as 3D-printed component. As a result, solid materials that have no, or very low, biological activity can receive additional functions and important properties. It is also important to note that this approach has the potential to reduce reliance on allo- and autografts, which are associated with donor site morbidity, limited availability, as well as being a potential ethical constraint. From an application perspective, it is also crucial to highlight the sustainable nature of the developed materials. The proposed method of obtaining these coatings is both ecological and economical, as it eliminates the need for toxic solvents and reagents while preventing the generation of hazardous by-products that would otherwise require costly disposal. Environmentally friendly methods of materials synthesis, is an important factor in the context of global sustainability efforts. Minimization of energy consumption as well as reduction of chemical waste are in line with the principles of green chemistry, promoting responsible innovation in regenerative medicine. This environmentally conscious approach not only supports sustainable material development but also have potential to enhance the feasibility of translating these findings into clinical and industrial applications. However, the results presented in the above paper have their limitations, and potential application would be possible with the appropriate steps. The presented solution in the legal sense is a class-three medical device, which must meet the relevant standards as well as regulations. The process would need to be scaled up and translated from the laboratory to a real environment. The coating material has been tested under *in vivo* conditions on animal models in the form of rats, relatively small animals, therefore the model may not fully reflect the actual bone healing process due to anatomical differences. Future studies should consider larger animal models that exhibit greater similarity to humans. The potential to expand the solution, as well as to increase its biological value, is the possibility of modifying the carrier additionally with other active agents, which, acting synergistically to the pre-applied components, could promote tissue regeneration. In the aspect of bone tissue, this could be bone morphogenetic protein (BMP).

Conclusions

The results obtained in this study highlight the significant potential of incorporating growth factors such as VEGF-165 and TGF-β1, and clindamycin into ceramic-polymer composite coatings for bone tissue regeneration. The materials can be customized into a variety of shapes and sizes which increases versatility for personalized medicine applications. The unique solution proposed in the presented work to obtain coatings was the use of a photocrosslinking process in UV light.

In conclusion, the composite coatings developed and presented in this work, obtained by crosslinking and capable of releasing clindamycin and protein growth factors, represent a novel as well as an effective strategy for promoting bone regeneration. This technology potentially may significantly impact orthopaedic and regenerative medicine clinical practice. However, while studies conducted in both *in vitro* and *in vivo* conditions have confirmed safety as well as bioactivity, further research is needed in this context.

Author contributions

Conceptualization: DS; visualization: DS; preparation of materials and material elements: DS, BK; investigation: DS, ASG, MW, AK, KN; supervision: ASK, KR; planning, execution,

and analysis of *in vivo* experiments, ASz-G, MW, and AK; writing—original draft: DS, ASG, MW, AK, BK; writing—review & editing: ASK, KR; resources: ASK, KS, KR; management: ASK, KS, KR; project administration: ASK. All authors have read and agreed to the published version of the manuscript.

Conflicts of interest

There are no conflicts to declare.

Ethical statement

All animal procedures were performed in accordance with the Guidelines for Care and Use of Laboratory Animals of University of Lodz and approved by the Local Ethical Committee for Animal Experiments based at the Medical University of Lod (Protocol No. ŁB192/2021 dated February 8, 2021).

Data availability

Supplementary information: data related to this article, including FTIR measurements, XRD measurements, GF release determination, SEM imaging, EDS microanalysis, as well as stability and sedimentation rate measurements, are available in the Mendeley Data repository at **https://data.mendeley.com/datasets/m9xh8wysc5/1** and the data including cytokine measurements (IL-1β, IL-10, TNF-α and OPN) and representative confocal images, are available in the University of Lodz repository at **https://hdl.handle.net/11089/56178**. See Supplementary information at DOI: **https://doi.org/10.1039/d5bm00637f**.

Acknowledgements

The "Multifunctional biologically active composites for applications in bone regenerative medicine" project was carried out within the TEAM-NET program of the Foundation for Polish Science, financed by the European Union under the European Regional Development Fund (grant number POIR.04.04.00-00-16D7/18). The authors gratefully acknowledge the financial support. The authors would like to express their deep thanks to PhD Wioletta Florkiewicz and PhD Michał Grzymajło for their technical support during the laboratory work. The authors also thank PhD Katarzyna Harazna for her valuable comments and suggestions.

References

1 L. A. Dobrzański, A. D. Dobrzańska-Danikiewicz and L. B. Dobrzański, *Processes*, 2021, **99**(4), DOI: **10.3390/pr9050865**.
2 G. Gautam, S. Kumar and K. Kumar, *Mater. Today: Proc.*, 2022, **50**, 2206–2217.
3 M. A. Markets, *Biomaterials Market by Type (Metallic (Gold, Magnesium), Ceramic (Aluminum Oxide, Carbon), Polymer (Polyethylene, Polyester), Natural (Hyaluronic acid, Collagen, Gelatin)), Application (Orthopedic, Dental, CVD, Ophthalmology) & Region - Global Forecast to*, 2024.
4 Z. U. Arif, M. Y. Khalid, M. F. Sheikh, A. Zolfagharian and M. Bodaghi, *J. Environ. Chem. Eng.*, 2022, **10**(4), DOI: **10.1016/j.jece.2022.108159**.
5 M. Yang, L. Chen, J. Wang, G. Msigwa, A. I. Osman, S. Fawzy, D. W. Rooney and P. S. Yap, *Environ. Chem. Lett.*, 2023, **21**, 55–80.
6 E. Asadian, S. Abbaszadeh, F. Ghorbani-Bidkorpeh, S. Rezaei, B. Xiao, H. A. Santos and M. A. Shahbazi, *Biomater. Sci.*, 2024, 9–92.
7 Z. Abbas, M. Dapporto, A. Tampieri and S. Sprio, *J. Compos. Sci.*, 2021, **5**(10), 259.
8 C. I. Idumah, *Polym. Polym. Compos.*, 2021, **29**, 509–527.
9 F. Nudelman and R. Kröger, *Science*, 2022, **376**, 137–138.
10 M. Liu, Y. Wang, X. Liu, Q. Wei, C. Bao and K. Zhang, *ACS Biomater. Sci. Eng.*, 2023, **9**, 3032–3057.
11 M. Zhang, J. Liu, T. Zhu, H. Le, X. Wang, J. Guo, G. Liu and J. Ding, *ACS Appl. Mater. Interfaces*, 2022, **14**, 1–19.
12 F. Wei, G. Liu, Y. Guo, R. Crawford, Z. Chen and Y. Xiao, *Biomater. Sci.*, 2018, **8**, 2156–2171.
13 W. Liang, X. Wu, Y. Dong, R. Shao, X. Chen, P. Zhoud and F. Xu, *Biomater. Sci.*, 2021, **6**, 1924–1944.
14 D. Qin, N. Wang, X.-G. You, A.-D. Zhang, X.-G. Chen and Y. Liu, *Biomater. Sci.*, 2022, **2**, 318–353.
15 K. Jahan and M. Tabrizian, *Biomater. Sci.*, 2016, **4**, 25–39.
16 A. Dubey, S. Jaiswal and D. Lahiri, *ACS Biomater. Sci. Eng.*, 2022, **8**, 1001–1027.
17 E. Tahmasebi, M. Alam, M. Yazdanian, H. Tebyanian, A. Yazdanian, A. Seifalian and S. A. Mosaddad, *J. Mater. Res. Technol.*, 2020, **9**, 11731–11755.
18 M. E. Brassesco, J. Cortez, V. Triacca, J. Payen and Y. Bayon, *ACS Biomater. Sci. Eng.*, 2024, **10**, 1910–1920.
19 H. A. Rather, D. Jhala and R. Vasita, *Mater. Sci. Eng. C*, 2019, **103**, 109761.
20 A. Gilarska, A. Hinz, M. Bzowska, G. Dyduch, K. Kamiński, M. Nowakowska and J. Lewandowska-Łańcucka, *ACS Appl. Mater. Interfaces*, 2021, **13**, 49762–49779.
21 C. Rastogi, H. T. Rube, J. F. Kribelbauer, J. Crocker, R. E. Loker, G. D. Martini, O. Laptenko, W. A. Freed-Pastor, C. Prives, D. L. Stern, R. S. Mann and H. J. Bussemaker, *Science*, 2021, **373**, E3692–E3701.
22 Y. Wu, R. Fu, S. Mohanty, M. Nasser, B. Guo and G. Ghosh, *ACS Appl. Bio Mater.*, 2019, **2**, 2339–2346.
23 A. Halim, H. C. Kuo and P. S. Hou, *Discover Neurosci.*, 2025, **20**, 3.
24 B. Aksan and D. Mauceri, *J. Biomed. Sci.*, 2025, **32**, 1–21.
25 E. Kardalas, E. Sakkas, M. Ruchala, D. Macut and G. Mastorakos, *Rev. Endocr. Metab. Disord.*, 2022, **23**, 431–447.

26 X. Lin, S. Patil, Y. G. Gao and A. Qian, *Front. Pharmacol.*, 2020, **11**, 1–15.
27 B. Kryszak, M. Biernat, P. Tymowicz-Grzyb, A. Junka, M. Brożyna, M. Worek, P. Dzienny, A. Antończak and K. Szustakiewicz, *Polymer*, 2023, **287**, 126428.
28 A. M. Tomala, D. Słota, W. Florkiewicz, K. Piętak, M. Dyląg and A. Sobczak-Kupiec, *Lubricants*, 2022, **10**, 58.
29 D. Słota, J. Jampilek and A. Sobczak-Kupiec, *J. Funct. Biomater.*, 2024, **15**, 1–18.
30 Thermo Fisher Scientific. *Human TGF-β1 ELISA Kit user guide (Pub. No. MAN0016624 Rev. A.0). From Thermo Fisher Scientific website*: **https://assets.thermofisher.cn/TFS-Assets%2FLSG%2Fmanuals%2FMAN0016624-249-4-Hu-TGF-beta1-ELISA-UG.pdf**.
31 Thermo Fisher Scientific. *Human VEGF ELISA Kit product information sheet (Pub. No. MAN0003960 Rev. 3.0). From Thermo Fisher Scientific website*: **https://tools.thermofisher.com/content/sfs/manuals/KHG0111_Hu_VEGF_ELISA_Rev2.pdf**.
32 D. Słota, M. M. Urbaniak, A. Tomaszewska, K. Niziołek, M. Włodarczyk, W. Florkiewicz, A. Szwed-Georgiou, A. Krupa and A. Sobczak-Kupiec, *Biomater. Sci.*, 2024, (20), 5253–5265.
33 M. Chen, R. Aluunmani, G. Bolognesi and G. T. Vladisavljević, *Molecules*, 2023, **99**(10), 2341.
34 M. Hakim Khalili, R. Zhang, S. Wilson, S. Goel, S. A. Impey and A. I. Aria, *Polymers*, 2023, **15**, 2341.
35 H. M. Zidan, E. M. Abdelrazek, A. M. Abdelghany and A. E. Tarabiah, *J. Mater. Res. Technol.*, 2019, **8**, 904–913.
36 C. Cona, K. Bailey and E. Barker, *Polymers*, 2024, **16**(14), 2050.
37 D. K. Thukral, S. Dumoga, S. Arora, K. Chuttani and A. K. Mishra, *Cancer Nanotechnol.*, 2014, **5**, 1–15.
38 F. Khan, M. Atif, M. Haseen, S. Kamal, M. S. Khan, S. Shahidc and S. A. A. Nami, *J. Mater. Chem. B*, 2022, 170–203.
39 D. K. Khajuria, V. B. Kumar, D. Gigi, A. Gedanken and D. Karasik, *ACS Appl. Mater. Interfaces*, 2018, **10**, 19373–19385.
40 M. Mitra, M. H. Sanfui, S. Roy, M. Deb, C. Roy, A. Dutta, N. N. Ghosh, M. Rahaman, P. K. Chattopadhyay, S. Roy and N. R. Singha, *Macromolecules*, 2023, **56**, 9078–9096.
41 M. Shahbazi, S. J. Ahmadi, A. Seif and G. Rajabzadeh, *Food Hydrocolloids*, 2016, **61**, 378–389.
42 M. Głab, S. Kudłacik-Kramarczyk, A. Drabczyk, J. Walter, A. Kordyka, M. Godzierz, R. Bogucki, B. Tyliszczak and A. Sobczak-Kupiec, *Molecules*, 2021, **26**(14), 4268.
43 W. X. Wu, Y. C. Huang and W. F. Lee, *Iran. Polym. J.*, 2020, **29**, 679–691.
44 M. J. L. Dantas, B. F. F. Santos, A. A. Tavarez, M. A. Maciel, B. M. Lucena, M. V. Fook and S. M. Silva, *Molecules*, 2019, **24**, 1–20.
45 P. J. Weldrick, S. San and V. N. Paunov, *ACS Appl. Nano Mater.*, 2021, **4**, 1187–1201.
46 V. Manuelli, C. Pecorari, G. Filomeni and E. Zito, *FEBS J.*, 2022, **289**, 5413–5425.
47 M. V. Lukassen, C. Scavenius, I. B. Thøgersen and J. J. Enghild, *Biochemistry*, 2016, **55**, 5610–5621.
48 Z. Deng, T. Fan, C. Xiao, H. Tian, Y. Zheng, C. Li and J. He, *Signal Transduction Targeted Ther.*, 2024, **9**(1), 61.
49 I. Inoki, T. Shiomi, G. Hashimoto, H. Enomoto, H. Nakamura, K. Makino, E. Ikeda, S. Takata, K. Kobayashi and Y. Okada, *FASEB J.*, 2001, **16**(2), 1–27.
50 Y. Tang, X. Zhang, X. Li, C. Ma, X. Chu, L. Wang and W. Xu, *Eur. Polym. J.*, 2022, **162**, 110881.
51 D. R. Paul, *Int. J. Pharm.*, 2011, **418**, 13–17.
52 J. Siepmann and N. A. Peppas, *Int. J. Pharm.*, 2011, **418**, 6–12.
53 J. P. Waller, S. P. Burke, J. Engel, A. R. Chade and G. L. Bidwell, *Sci. Rep.*, 2021, **11**, 1–15.
54 P. Henrich-Noack, J. H. M. Prehn and J. Krieglstein, *Stroke*, 1996, **27**, 1609–1615.
55 X. Ju, X. Liu, Y. Zhang, X. Chen, M. Chen, H. Shen, Y. Feng, J. Liu, M. Wang and Q. Shi, *Smart Mater. Med.*, 2022, 85–93.
56 B. Divband, M. Aghazadeh, Z. H. Al-qaim, Z. Haleem, M. Samiei, F. H. Hussein, A. Shaabani, S. Shahi and R. Sedghi, *Carbohydr. Polym.*, 2021, 118589.
57 S. G. Antimisiaris, A. Marazioti, M. Kannavou, E. Natsaridis, F. Gkartziou, G. Kogkos and S. Mourtas, *Adv. Drug Delivery Rev.*, 2021, **174**, 53–86.
58 D. E. Rodriguez, T. Thula-mata, E. J. Toro, Y. Yeh, C. Holt, S. Holliday and L. B. Gower, *Acta Biomater.*, 2014, **10**, 494–507.
59 S. Bolamperti, I. Villa and A. Rubinacci, *Bone Res.*, 2022, **10**(1), 48.
60 M. Nagao, T. N. Feinstein, Y. Ezura, T. Hayata, T. Notomi, Y. Saita, R. Hanyu, H. Hemmi, Y. Izu, S. Takeda, K. Wang, S. Rittling, T. Nakamoto, K. Kaneko, H. Kurosawa, G. Karsenty, D. T. Denhardt, J. P. Vilardaga and M. Noda, *Proc. Natl. Acad. Sci. U. S. A.*, 2011, **108**, 17767–17772.
61 K. Hu and B. R. Olsen, *Bone*, 2016, **91**, 30–38.
62 S. Tong, D. P. Xu, Z. M. Liu, Y. Du and X. K. Wang, *J. Craniofacial Surg.*, 2016, **27**, 509–515.
63 C. Huang, S. Shi, M. Qin, X. Rong, Z. Ding, X. Fu, W. Zeng, L. Luo, D. Wang, Z. Luo, Y. Li and Z. Zhou, *Adv. Sci.*, 2024, **11**, 1–18.
64 W. Mengruii, W. Shali, C. Wei and L. Yi-Ping, *Cell Res.*, 2024, **34**, 101–123.
65 M. N. Labour, M. Riffault, S. T. Christensen and D. A. Hoey, *Sci. Rep.*, 2016, **6**, 1–13.
66 S. Kasagi and W. Chen, *Cell Biosci.*, 2013, **3**, 1–7.
67 K. Zhang, Y. Zhou, C. Xiao, W. Zhao, H. Wu, J. Tang, Z. Li, S. Yu, X. Li, L. Min, Z. Yu, G. Wang, L. Wang, K. Zhang, X. Yang, X. Zhu, C. Tu and X. Zhang, *Sci. Adv.*, 2019, **5**, 1–16.
68 V. Uskoković and T. A. Desai, *Mater. Sci. Eng. C*, 2014, **37**, 210–222.
69 P. Jiang, Y. Zhang, R. Hu, X. Wang, Y. Lai, G. Rui and C. Lin, *Bioact. Mater.*, 2021, **6**, 1118–1129.

Supplementary information for:

Bioactive Coating with Clindamycin, VEGF-165, and TGF-β1 for Supporting Bone Tissue Regeneration

*Dagmara Słota *[,a], Aleksandra Szwed-Georgiou [b], Marcin Włodarczyk [b], Agnieszka Krupa [b], Karolina Rudnicka [b], Karina Niziołek [a], Bartłomiej Kryszak [c], Konrad Szustakiewicz [c], Agnieszka Sobczak-Kupiec [d]*

[a] Cracow University of Technology, CUT Doctoral School, Faculty of Materials Engineering and Physics, Department of Materials Science, 37 Jana Pawła II Av., 31-864 Krakow, Poland

[b] University of Lodz, Faculty of Biology and Environmental Protection, Department of Immunology and Infectious Biology, 12/16 Banacha St, 90-237 Łódź, Poland

[c] Department of Polymer Engineering and Technology, Faculty of Chemistry, Wroclaw University of Science and Technology, Wyb. Wyspianskiego 27, 50-370 Wroclaw, Poland

[d] Cracow University of Technology, Faculty of Materials Engineering and Physics, Department of Materials Science, 37 Jana Pawła II Av., 31-864 Krakow, Poland

1. Selection of optimal synthesis conditions of the ceramic phase

HAp powder was obtained by reacting Na_2HPO_4 and $(CH_3COO)_2Ca$. The reaction was carried out at the boiling point of the components. In order to obtain a powder with the preferable properties, the reaction was carried out at pH values of 5.5, 9 and 11. In addition, the molar concentrations of the salts were changed according to Table S1-S3. For all reactions, the procedure was analogous. First, 80 mL of Na_2HPO_4 solution was placed in a three-neck flask and a few drops of ammonia water were added (if the reaction was carried out at pH 9 and 11). Distilled water was added and brought to boiling point. When the boiling point was reached, 200 ml of $(CH_3COO)_2Ca$ was added dropwise with constant stirring at a rate of 1 drop/s. After completion of the reaction, the resulting HAp powder was aged for 24 hours at room temperature, and then the precipitate was washed thoroughly with distilled water to obtain a neutral pH and subjected to freeze-drying proses. The powder obtained at pH=11 with a label of 3.5 exhibited higher reaction efficiency.

The proposed method for synthesizing HAp powders is more environmentally friendly and sustainable compared to the conventional wet precipitation method based on the strong acid H_3PO_4 and the strong base $Ca(OH)_2$. This approach operates under milder conditions, and potential by-products, such as sodium acetate (CH_3COONa), are less environmentally problematic compared to the residues from H_3PO_4 and $Ca(OH)_2$ neutralization, which may contain undesirable ions affecting aquatic ecosystems. Additionally, this method reduces water consumption for precipitate washing, as the conventional technique often requires extensive rinsing to remove excess unreacted reagents and salts and to adjust the pH to a neutral level.

Table S1. Molar concentrations of reactants for obtaining HAp powders in pH=5.5.

Powder symbol	Reagent	
	Na_2HPO_4 [mol/L]	$(CH_3COO)_2Ca$ [mol/L]
1.1	0.16	0.064
1.2	0.2	0.08
1.3	0.24	0.096
1.4	0.28	0.112
1.5	0.32	0.128

Table S2. Molar concentrations of reactants for obtaining HAp powders in pH=9.

Powder symbol	Reagent	
	Na_2HPO_4 [mol/L]	$(CH_3COO)_2Ca$ [mol/L]
2.1	0.16	0.064
2.2	0.2	0.08
2.3	0.24	0.096
2.4	0.28	0.112
2.5	0.32	0.128

Table S3. Molar concentrations of reactants for obtaining HAp powders in pH=11.

Powder symbol	Reagent	
	Na_2HPO_4 [mol/L]	$(CH_3COO)_2Ca$ [mol/L]
3.1	0.16	0.064
3.2	0.2	0.08
3.3	0.24	0.096
3.4	0.28	0.112
3.5	0.32	0.128

2. FT-IR spectroscopy analysis

FT-IR analysis was used to analyze the obtained hydroxyapatite powders. For this purpose, a Thermo Scientific Nicolet iS5 FTIR spectrophotometer equipped with an iD7 ATR attachment (Loughborough, UK) was used. The instrument has a reflective optical system with a monolithic diamond crystal ATR, which enabled high optical contact between the sample and the diamond, leading to good resolution. The spectra were recorded at room temperature, in the wavelength range of 4000-400 cm-1.

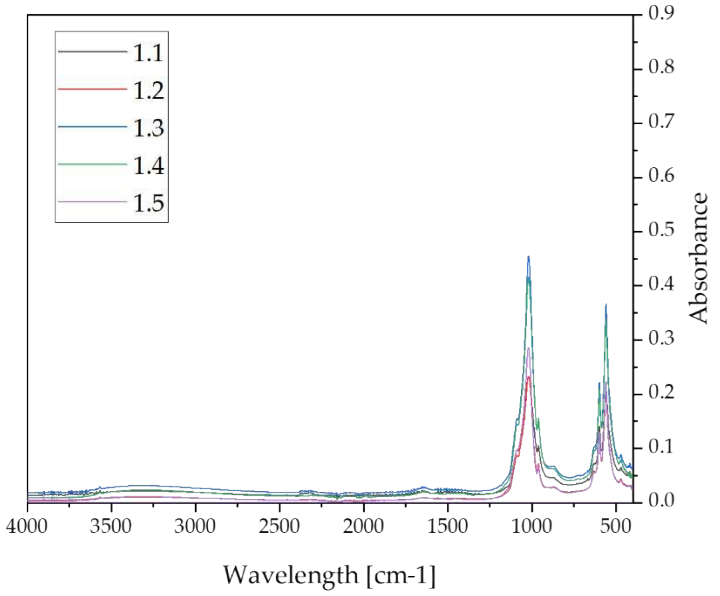

Figure S1. FTIR spectra of hydroxyapatite obtained at pH=5.5.

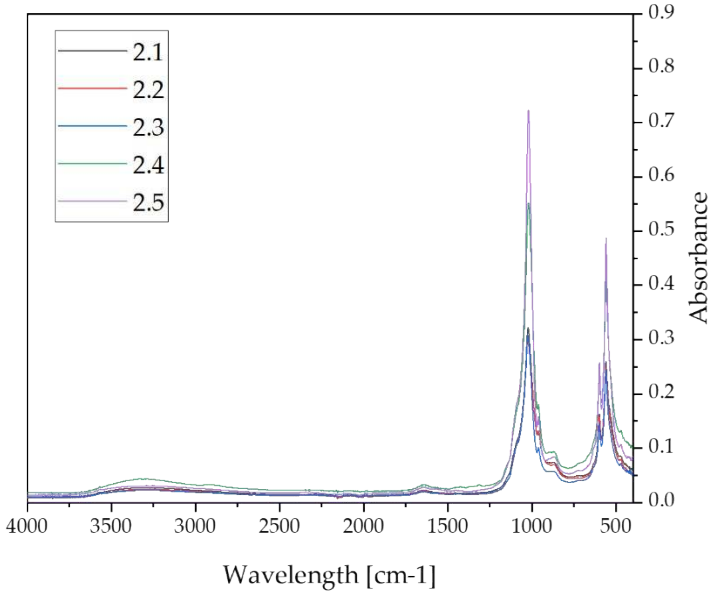

Figure S2. FTIR spectra of hydroxyapatite obtained at pH=9.

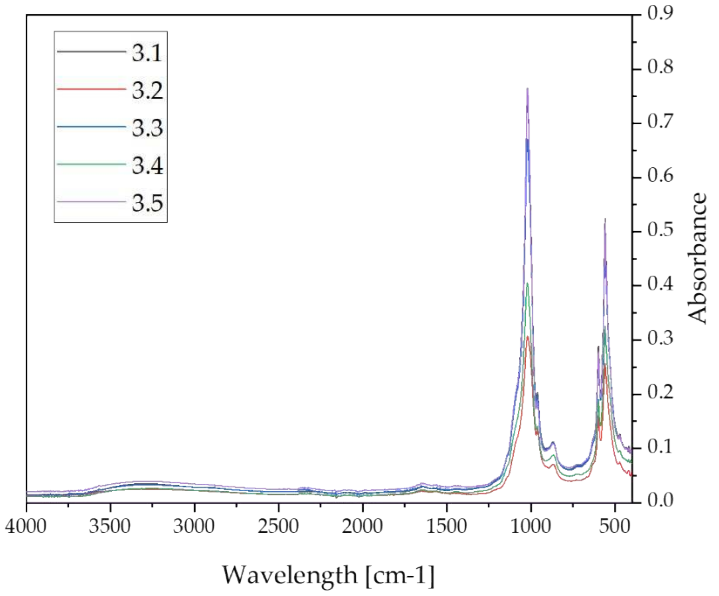

Figure S3. FTIR spectra of hydroxyapatite obtained at pH=11.

FTIR spectra of the obtained HAp powders are demonstrated in Figures S1-S3. Analysis of the obtained results confirmed that both the pH of the reaction as well as the concentrations of the reagents affect the intensity of the peaks on the spectra. Despite the difference in intensities, the spectra relatively overlap, with characteristic functional groups defined at similar locations. Characteristic stretching vibrations of the PO_4^{3-} phosphate group were identified in the wavelength range of 1000 cm^{-1} – 1100 cm^{-1}. In the case of powders obtained at environmental pH 9 and 11, small bands in the region of 870 and 1450 cm^{-1} are observed, which are probably associated with CO_3^{2-} groups. This may be the result of conducting the synthesis in an air atmosphere. A broad sweeping band at ~3570 cm^{-1} is attributed to valence vibrations of the OH-group, embedded in the HAp structure [1,2].

The powder obtained at pH=11 with a label of 3.5 exhibited highest peak intensity on the FTIR spectrum. For this reason, and because of the yield of a chemical reaction it was selected for further study.

3. X-ray diffraction analysis

X-ray diffraction (XRD) was used to determine the phase composition and crystallinity of powder 3.5. A Rigaku SmartLab X-ray diffractometer (Wilmington, MA, USA) was

used for the study. The measurement was carried out in the 2θ range of 10° – 60° and with a step size of 0.002° 2θ. Voltage 40 kV, current 30 mA.

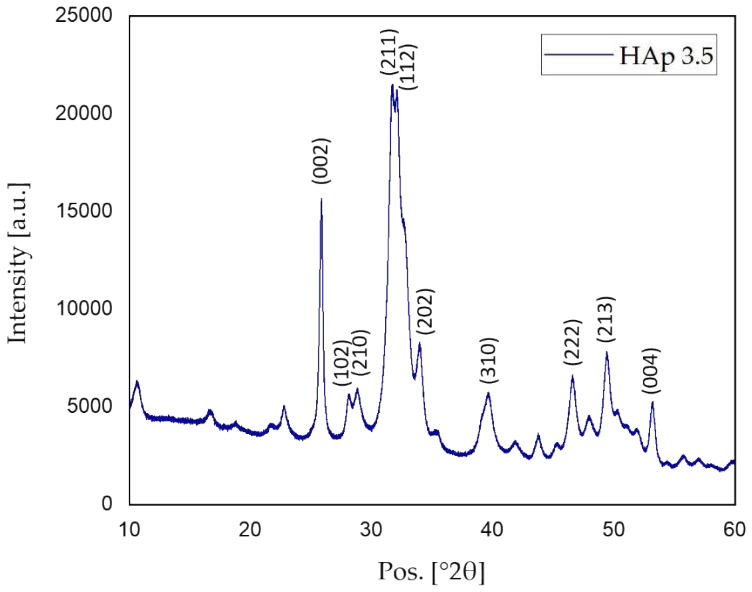

Figure S4. XRD diffractogram of HAp 3.5.

The result of XRD analysis of the 3.5 powder, along with the labeled crystallographic plots, is presented in Figure S4. The analysis confirmed that the only identified phase is HAp, and the powder itself is phase pure. The results were compared with ICDD data file card No. 01-080-7085 [3].

4. Ca/P

FT-IR and XRD analysis confirmed that the selected material 3.5 is HAp powder, however, a Ca/P molar ratio determination was carried out for additional verification. For stoichiometric, natural HAp, this ratio has a value of 1.67. The determinations were carried out in accordance with the Polish ISO standard for calcium based on PN-97/R-64803, and for phosphorus based on PN-80/C-87015.

The determinations resulted in a Ca/P value of 1.6652 ± 0.0157, which is very similar to the stoichiometric value of HAp.

5. Selection of the method of obtaining coatings and their compositions

The materials were prepared through a photopolymerization process. A polymer blend of PVP and PEG was selected as the base material, using aqueous solutions at a concentration of 15% in a 1:1 ratio. To adjust the crosslinking parameters, different amounts of the crosslinking agent PEGDA with molecular weights of 575 and 250 were used. The amount of crosslinker was set at 1.6, 1.8, and 2.0 mL per 10 mL of polymer mixture. The photoinitiator, 2-hydroxy-2-methylpropiophenone, was added in amounts of 30, 40, and 50 μL per 10 mL of the polymer mixture.

The order of component addition was crucial. First, the PVP:PEG blend was added to a beaker, followed by PEGDA, and the mixture was stirred vigorously using a magnetic stirrer. After approximately 2 minutes of mixing, the photoinitiator was introduced, followed by additional stirring. The resulting solution was then poured onto a Petri dish and placed under a UV radiation source.

The samples were crosslinked for 4 minutes. It was observed that PEGDA with a molecular weight of 250 did not form a crosslinked network regardless of the UV exposure time, or only a few gelled fragments appeared. Due to this, PEGDA 250 was discarded. For PEGDA with a molecular weight of 575, all samples underwent crosslinking, but their flexibility varied depending on the crosslinker-to-photoinitiator ratio. Samples with 1.6 mL of PEGDA were highly flexible but also fragile and prone to tearing when removed from the container. In contrast, samples with a higher PEGDA content were stiffer. The optimal composition was determined to be PEGDA = 1.8 mL and photoinitiator = 50 μL.

In the next step, the samples were mixed with active ingredients and HAp. To achieve this, 1 g of GSH, 0.04 g of COL, and either 0.5 g, 1.0 g, or 1.5 g of HAp were added to the PVP:PEG mixture. The crosslinker and photoinitiator were then introduced following the same procedure as before. The experiment was repeated with 2 g of GSH. All samples successfully crosslinked; however, the sample containing 2 g of GSH and 0.5 g of HAp exhibited the best mechanical properties. As the ceramic phase content increased, the samples became less flexible and more brittle under bending stress.

The procedure was repeated, but instead of pouring the coatings onto a Petri dish, the mixture was applied onto PLA plates. The samples underwent photopolymerization and were dried. Improved adhesion was observed for coatings with GSH at a concentration of 2 g per 10 mL. To further enhance adhesion to the PLA substrate, a mixture of 15% PVP with GSH was proposed. Coatings were applied by dispensing 0.25 mL of PVP:GSH onto a PLA plate (dimensions: 2 cm × 2 cm × 2 mm).

The coatings were subjected to photopolymerization for 2 minutes. Next, an additional layer, formulated according to Table S4, was applied onto the crosslinked surface and exposed to UV light for 4 minutes.

The developed synthesis method for coatings based on biocompatible components offers an environmentally friendly and cost-effective alternative to traditional material fabrication processes, such as chemical crosslinking. By utilizing UV light-induced photopolymerization, the materials are obtained in just 4 minutes, significantly reducing energy consumption and processing time. Moreover, the reaction proceeds without generating by-products, minimizing the need for additional purification or waste disposal processes, which would otherwise impose extra costs from an industrial perspective, and reducing environmental impact. This method aligns with the principles of green chemistry and the sustainable development of biomedical materials.

Table S4. The final composition of the coating, calculated for a PVP:PEG volume of 10 mL.

Coating	PVP 15% [mL]	PEG 15% [mL]	GSH [g]	COL [g]	HAp [g]	PEGDA [mL]	Photoinitiator [μL]
Coating A	5	5	2	-	-	1.8	50
Coating B				0.04	-		
Coating C					0.5		
Coating D					1.5		

The UV crosslinking process was conducted using a Medilux UV 436 HF lamp (Medilux, Korntal-Münchingen, Germany) (220 V, 60 Hz).

Since the proposed C coating exhibited the most satisfying properties after the crosslinking process, it was the one chosen for further analysis, including modification with growth factors and clindamycin hydrochloride.

6. EDX elemental microanalysis of coatings

Figure S5 presents the EDX spectra of the composite coatings. The analysis demonstrated some similarities in the composition of the materials. All three samples exhibit the consistent presence of the major elements carbon (C), oxygen (O), phosphorus (P) and calcium (Ca), which are derived from the basic material constituents that are invariant across all coatings. For the Coating 4 spectrum (Figure S1B), chloride (Cl) peaks appear, which are associated with the presence of the antibiotic clindamycin hydrochloride.

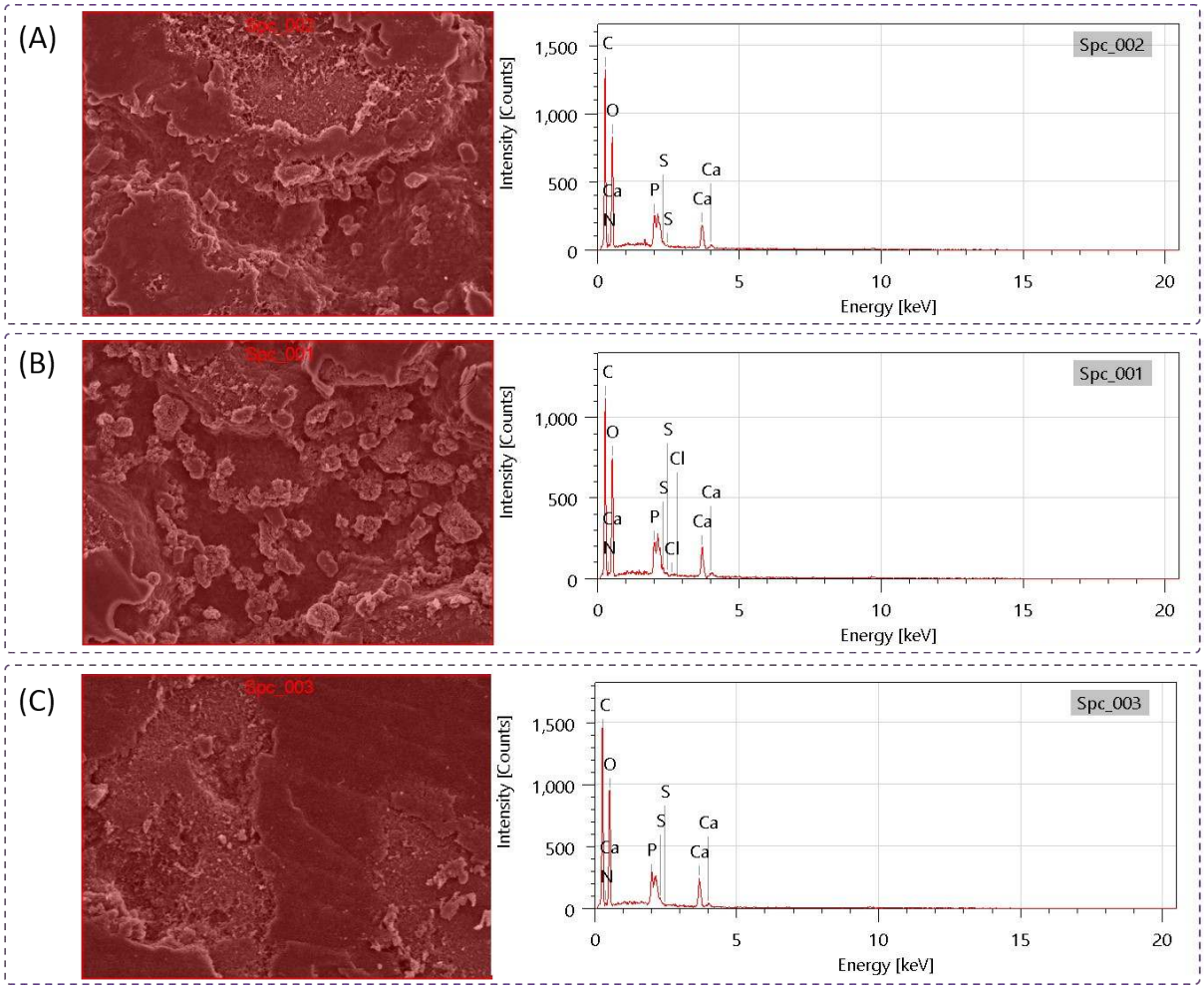

Figure S5. EDX spectrum of the bioactive coatings with identified elements measured across the surface. (A) Coating C. (B) Coating 4. (C) Coating C/GF.

7. Selection of the sterilization method

Materials for in vivo testing have been subjected to radiation sterilization in order to eliminate potential microorganisms and contaminants. This method was chosen based on the fact of deep penetration of radiation compared to sterilization with UV light, which acts mainly on the surface, as well as in view of the fact that this technique does not change the properties of materials and does not promote their degradation. To confirm this phenomenon, UV and radiation sterilization methods were compared before material implantation. For this purpose, three identical PVP:PEG base coatings were prepared under sterile conditions. Then, one of them was sterilized with UV light for 30 minutes, the second was sterilized by radiation (gamma radiation, 35 kGy, 60Co radiation source), and the third material was left unsterilized as a reference material. Surface morphologies were visualized using a VHX series digital microscope (Keyence, Osaka, Japan) at x500 magnification. In addition, a surface spectrum analysis was performed using FT-IR in an analogous manner as described in Chapter 2 of the supplement.

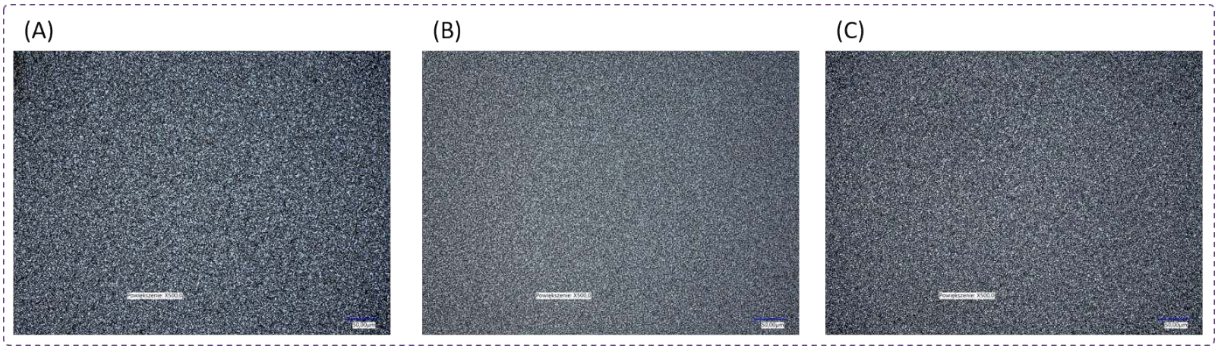

Figure S6. Comparison of PVP:PEG coating morphology (A) after exposure to UV light. (B) without sterilization. (C) after exposure to gamma radiation.

A comparison of the surfaces of the materials revealed no significant differences that could be the result of the chosen sterilization technique, as confirmed by the images presented in Figure S6. However, differences were observed on FT-IR spectra (Figure S7). In the case of the material without sterilization, as well as that subjected to radiation sterilization, the spectra completely overlap and practically no differences are observed. This confirms that exposure to radiation does not cause changes in the material. The spectrum of the material after a 30-minute UV exposure exhibits differences compared to the other two. An increase in the intensity of the bands at 841 cm^{-1}, 955 cm^{-1}, 1136 cm^{-1}, 1283 cm^{-1} and 1296 cm^{-1} is observed. At a wave number of

1727 cm^{-1} the peak decreases in intensity. These changes confirm that under the influence of UV radiation, changes occur in the material, which can affect the physicochemical properties.

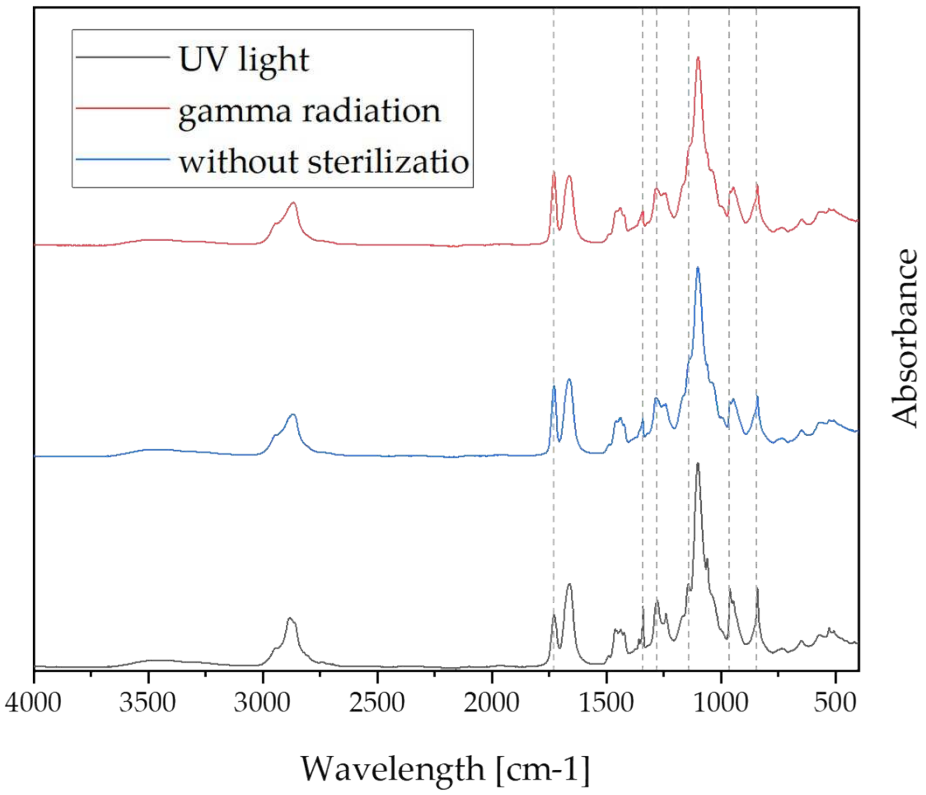

Figure S7. FT-IR spectra of PVP:PEG matrices after UV and radiation exposure, as well as material untreated by sterilization.

ZAŁĄCZNIK 1: Oświadczenia współautorów

Politechnika Krakowska
Wydział Inżynierii
Materiałowej i Fizyki

Kraków, 25.08.2025 r.

mgr inż. Karina Niziołek
Katedra Inżynierii Materiałowej
Wydział Inżynierii Materiałowej i Fizyki
Politechnika Krakowska

OŚWIADCZENIE

Jako współautor pracy naukowej pt. *Polymeric and Composite Carriers of Protein and Non-Protein Biomolecules for Application in Bone Tissue Engineering*, Materials 2023;16(6):2235, oświadczam, iż mój własny wkład merytoryczny w przygotowanie oraz przedstawienie pracy w formie publikacji wyniósł 5% i dotyczył przeglądu liteartury.

Jednocześnie wyrażam zgodę na przedłożenie ww. publikacji przez mgr inż. Dagmarę Słotę do rozprawy doktorskiej jako część spójnego tematycznie zbioru artykułów opublikowanych w czasopismach naukowych.

Oświadczam również, iż samodzielna i możliwa do wyodrębnienia część ww. pracy, stanowiąca indywidualny wkład mgr inż. Dagmary Słoty, obejmuje 85% całości i dotyczy przeglądu literatury, zaprojektowania grafik oraz przygotowania manuskryptu publikacji.

Karina Niziołek
.....

(podpis współautora)

Bratislava, 25.08.2025

Prof. Pharm Dr. Josef Jampílek, Ph.D.
Department of Analytical Chemistry
Faculty of Natural Sciences
Comenius University
Bratislava
Slovakia

STATEMENT

As a co-author of the scientific article entitled *Polymeric and Composite Carriers of Protein and Non-Protein Biomolecules for Application in Bone Tissue Engineering*, Materials 2023;16(6):2235, I hereby declare that my own substantive contribution to the preparation and presentation of the work in the form of a publication amounted to 5% and concerned the verification of the correctness, and substantive support during the preparation of the manuscript.

At the same time, I give my consent for the aforementioned publication to be included by MSc Eng. Dagmara Słota in her doctoral dissertation as part of a thematically consistent collection of articles published in scientific journals.

I also declare that the independent and identifiable part of the above-mentioned work, constituting the individual contribution of MSc Eng. Dagmara Słota, accounts for 85% of the total and covers the literature review, preparation of graphics, and preparation of the manuscript for publication.

.....

(podpis współautora)

COMENIUS UNIVERSITY BRATISLAVA
Faculty of Natural Sciences
Department of Analytical Chemistry
Mlynská dolina, Ilkovičova 6
842 15 Bratislava, Slovakia - 1 -

Politechnika Krakowska
Wydział Inżynierii
Materiałowej i Fizyki

Kraków, 25.08.2025 r.

prof. dr hab. inż. Agnieszka Sobczak-Kupiec
Katedra Inżynierii Materiałowej
Wydział Inżynierii Materiałowej i Fizyki
Politechnika Krakowska

OŚWIADCZENIE

Jako współautor pracy naukowej pt. *Polymeric and Composite Carriers of Protein and Non-Protein Biomolecules for Application in Bone Tissue Engineering*, Materials 2023;16(6):2235, oświadczam, iż mój własny wkład merytoryczny w przygotowanie oraz przedstawienie pracy w formie publikacji wyniósł 5% i dotyczył weryfikacji poprawności oraz merytorycznego wsparcia podczas przygotowywania manuskryptu.

Jednocześnie wyrażam zgodę na przedłożenie ww. publikacji przez mgr inż. Dagmarę Słotę do rozprawy doktorskiej jako część spójnego tematycznie zbioru artykułów opublikowanych w czasopismach naukowych.

Oświadczam również, iż samodzielna i możliwa do wyodrębnienia część ww. pracy, stanowiąca indywidualny wkład mgr inż. Dagmary Słoty, obejmuje 85% całości i dotyczy przeglądu literatury, zaprojektowania grafik oraz przygotowania manuskryptu publikacji.

A Sobczak-Kupiec

.....

(podpis współautora)

Bratislava, 25.08.2025

Prof. Pharm Dr. Josef Jampílek, Ph.D.
Department of Analytical Chemistry
Faculty of Natural Sciences
Comenius University
Bratislava
Slovakia

STATEMENT

As a co-author of the scientific article entitled *Targeted Clindamycin Delivery Systems: Promising Options for Preventing and Treating Bacterial Infections Using Biomaterials*, International Journal of Molecular Sciences 2024;25(8):4386, I hereby declare that my own substantive contribution to the preparation and presentation of the work in the form of a publication amounted to 5% and concerned the verification of the correctness, and substantive support during the preparation of the manuscript.

At the same time, I give my consent for the aforementioned publication to be included by MSc Eng. Dagmara Słota in her doctoral dissertation as part of a thematically consistent collection of articles published in scientific journals.

I also declare that the independent and identifiable part of the above-mentioned work, constituting the individual contribution of MSc Eng. Dagmara Słota, accounts for 90% of the total and covers the literature review, preparation of graphics, and preparation of the manuscript for publication.

.....

(podpis współautora)

COMENIUS UNIVERSITY BRATISLAVA
Faculty of Natural Sciences
Department of Analytical Chemistry
Mlynská dolina, Ilkovičova 6
842 15 Bratislava, Slovakia - 1 -

Politechnika Krakowska
Wydział Inżynierii
Materiałowej i Fizyki

Kraków, 25.08.2025 r.

prof. dr hab. inż. Agnieszka Sobczak-Kupiec
Katedra Inżynierii Materiałowej
Wydział Inżynierii Materiałowej i Fizyki
Politechnika Krakowska

OŚWIADCZENIE

Jako współautor pracy naukowej pt. *Targeted Clindamycin Delivery Systems: Promising Options for Preventing and Treating Bacterial Infections Using Biomaterials*, International Journal of Molecular Sciences 2024;25(8):4386, oświadczam, iż mój własny wkład merytoryczny w przygotowanie oraz przedstawienie pracy w formie publikacji wyniósł 5% i dotyczył weryfikacji poprawności oraz merytorycznego wsparcia podczas przygotowywania manuskryptu.

Jednocześnie wyrażam zgodę na przedłożenie ww. publikacji przez mgr inż. Dagmarę Słotę do rozprawy doktorskiej jako część spójnego tematycznie zbioru artykułów opublikowanych w czasopismach naukowych.

Oświadczam również, iż samodzielna i możliwa do wyodrębnienia część ww. pracy, stanowiąca indywidualny wkład mgr inż. Dagmary Słoty, obejmuje 90% całości i dotyczy przeglądu literatury, zaprojektowania grafik oraz przygotowania manuskryptu publikacji.

A. Sobczak-Kupiec

.....

(podpis współautora)

Politechnika Krakowska
Wydział Inżynierii
Materiałowej i Fizyki

Kraków, 25.08.2025 r.

mgr inż. Karina Niziołek
Katedra Inżynierii Materiałowej
Wydział Inżynierii Materiałowej i Fizyki
Politechnika Krakowska

OŚWIADCZENIE

Jako współautor pracy naukowej pt. *Clindamycin-Loaded Nanosized Calcium Phosphates Powders as a Carrier of Active Substances*, Nanomaterials 2023;13:1469, oświadczam, iż mój własny wkład merytoryczny w przygotowanie oraz przedstawienie pracy w formie publikacji wyniósł 5% i dotyczył wykonania części eksperymentalnej oraz interpretacji wyników.

Jednocześnie wyrażam zgodę na przedłożenie ww. publikacji przez mgr inż. Dagmarę Słotę do rozprawy doktorskiej jako część spójnego tematycznie zbioru artykułów opublikowanych w czasopismach naukowych.

Oświadczam również, iż samodzielna i możliwa do wyodrębnienia część ww. pracy, stanowiąca indywidualny wkład mgr inż. Dagmary Słoty, obejmuje 60% całości i dotyczy opracowania koncepcji badawczej, przeglądu literatury, wykonania części eksperymentalnej, interpretacji wyników, dyskusji oraz przygotowania manuskryptu publikacji.

Karina Niziołek
.....

(podpis współautora)

Kraków, 12.09.2025 r.

dr inż. Wioletta Florkiewicz

OŚWIADCZENIE

Jako współautor pracy naukowej pt. *Clindamycin-Loaded Nanosized Calcium Phosphates Powders as a Carrier of Active Substances*, Nanomaterials 2023;13:1469, oświadczam, iż mój własny wkład merytoryczny w przygotowanie oraz przedstawienie pracy w formie publikacji wyniósł 5% i dotyczył konsultacji uzyskanych wyników oraz wsparcia merytorycznego.

Jednocześnie wyrażam zgodę na przedłożenie ww. publikacji przez mgr inż. Dagmarę Słotę do rozprawy doktorskiej jako część spójnego tematycznie zbioru artykułów opublikowanych w czasopismach naukowych.

Oświadczam również, iż samodzielna i możliwa do wyodrębnienia część ww. pracy, stanowiąca indywidualny wkład mgr inż. Dagmary Słoty, obejmuje 60% całości i dotyczy opracowania koncepcji badawczej, przeglądu literatury, wykonania części eksperymentalnej, interpretacji wyników, dyskusji oraz przygotowania manuskryptu publikacji.

Wioletta Florkiewicz

(podpis współautora)

Bratislava, 25.08.2025

Prof. Pharm Dr. Josef Jampílek, Ph.D.
Department of Analytical Chemistry
Faculty of Natural Sciences
Comenius University
Bratislava
Slovakia

STATEMENT

As a co-author of the scientific article entitled *Clindamycin-Loaded Nanosized Calcium Phosphates Powders as a Carrier of Active Substances*, Nanomaterials 2023;13(9):1469, I hereby declare that my own substantive contribution to the preparation and presentation of the work in the form of a publication amounted to 5% and concerned the consultation of the obtained results, verification of the correctness of the discussion, and substantive support during the preparation of the manuscript.

At the same time, I give my consent for the aforementioned publication to be included by MSc Eng. Dagmara Słota in her doctoral dissertation as part of a thematically consistent collection of articles published in scientific journals.

I also declare that the independent and identifiable part of the above-mentioned work, constituting the individual contribution of MSc Eng. Dagmara Słota, accounts for 60% of the total and covers the development of the research concept, literature review, execution of the experimental part, interpretation of the results, discussion, and preparation of the manuscript for publication.

.....

(podpis współautora)

COMENIUS UNIVERSITY BRATISLAVA
Faculty of Natural Sciences
Department of Analytical Chemistry
Mlynská dolina, Ilkovičova 6
842 15 Bratislava, Slovakia

Politechnika Krakowska
Wydział Inżynierii
Materiałowej i Fizyki

Kraków, 25.08.2025 r.

dr inż. Agnieszka Tomala
Katedra Inżynierii Materiałowej
Wydział Inżynierii Materiałowej i Fizyki
Politechnika Krakowska

OŚWIADCZENIE

Jako współautor pracy naukowej pt. *Clindamycin-Loaded Nanosized Calcium Phosphates Powders as a Carrier of Active Substances*, Nanomaterials 2023;13:1469, oświadczam, iż mój własny wkład merytoryczny w przygotowanie oraz przedstawienie pracy w formie publikacji wyniósł 5% i dotyczył wykonania części eksperymentalnej oraz interpretacji wyników.

Jednocześnie wyrażam zgodę na przedłożenie ww. publikacji przez mgr inż. Dagmarę Słotę do rozprawy doktorskiej jako część spójnego tematycznie zbioru artykułów opublikowanych w czasopismach naukowych.

Oświadczam również, iż samodzielna i możliwa do wyodrębnienia część ww. pracy, stanowiąca indywidualny wkład mgr inż. Dagmary Słoty, obejmuje 60% całości i dotyczy opracowania koncepcji badawczej, przeglądu literatury, wykonania części eksperymentalnej, interpretacji wyników, dyskusji oraz przygotowania manuskryptu publikacji.

Agnieszka Tomala
.....
(podpis współautora)

Łódź, 07.05.2025 r.

dr Mateusz M. Urbaniak
Katedra Immunologii i Biologii Infekcyjnej
Wydział Biologii i Ochrony Środowiska
Uniwersytet Łódzki

OŚWIADCZENIE

Jako współautor pracy naukowej pt. *Clindamycin-Loaded Nanosized Calcium Phosphates Powders as a Carrier of Active Substances*, Nanomaterials 2023;13:1469, oświadczam, iż mój własny wkład merytoryczny w przygotowanie oraz przedstawienie pracy w formie publikacji wyniósł 5% i dotyczył opracowania koncepcji, przeglądu literatury, wykonania części eksperymentalnej, interpretacji wyników, dyskusji oraz przygotowania manuskryptu publikacji w zakresie badań na modelu bakteryjnym.

Jednocześnie wyrażam zgodę na przedłożenie ww. publikacji przez mgr inż. Dagmarę Słotę do rozprawy doktorskiej jako część spójnego tematycznie zbioru artykułów opublikowanych w czasopismach naukowych.

Oświadczam również, iż samodzielna i możliwa do wyodrębnienia część ww. pracy, stanowiąca indywidualny wkład mgr inż. Dagmary Słoty, obejmuje 60% całości i dotyczy opracowania koncepcji badawczej, przeglądu literatury, wykonania części eksperymentalnej, interpretacji wyników, dyskusji oraz przygotowania manuskryptu publikacji.

Mateusz M. Urbaniak

(podpis współautora)

Łódź, 07.05.2025 r.

mgr Agata Tomaszewska
Katedra Immunologii i Biologii Infekcyjnej
Wydział Biologii i Ochrony Środowiska
Uniwersytet Łódzki

OŚWIADCZENIE

Jako współautor pracy naukowej pt. *Clindamycin-Loaded Nanosized Calcium Phosphates Powders as a Carrier of Active Substances*, Nanomaterials 2023;13:1469, oświadczam, iż mój własny wkład merytoryczny w przygotowanie oraz przedstawienie pracy w formie publikacji wyniósł 5% i dotyczył wykonania części eksperymentalnej, interpretacji wyników, dyskusji oraz przygotowania manuskryptu publikacji w zakresie badań na modelu bakteryjnym.

Jednocześnie wyrażam zgodę na przedłożenie ww. publikacji przez mgr inż. Dagmarę Słotę do rozprawy doktorskiej jako część spójnego tematycznie zbioru artykułów opublikowanych w czasopismach naukowych.

Oświadczam również, iż samodzielna i możliwa do wyodrębnienia część ww. pracy, stanowiąca indywidualny wkład mgr inż. Dagmary Słoty, obejmuje 60% całości i dotyczy opracowania koncepcji badawczej, przeglądu literatury, wykonania części eksperymentalnej, interpretacji wyników, dyskusji oraz przygotowania manuskryptu publikacji.

Agata Tomaszewska

(podpis współautora)

Łódź, 07.05.2025 r.

dr Karolina Rudnicka, prof. UŁ
Katedra Immunologii i Biologii Infekcyjnej
Wydział Biologii i Ochrony Środowiska
Uniwersytet Łódzki

OŚWIADCZENIE

Jako współautor pracy naukowej pt. *Clindamycin-Loaded Nanosized Calcium Phosphates Powders as a Carrier of Active Substances*, Nanomaterials 2023;13:1469, oświadczam, iż mój własny wkład merytoryczny w przygotowanie oraz przedstawienie pracy w formie publikacji wyniósł 5% i obejmował zaplanowanie etapów badań mikrobiologicznych i komórkowych, nadzór nad realizacją prac i przygotowaniu części publikacji oraz udział w korekcie pierwszej wersji manuskryptu.

Jednocześnie wyrażam zgodę na przedłożenie ww. publikacji przez mgr inż. Dagmarę Słotę do rozprawy doktorskiej jako część spójnego tematycznie zbioru artykułów opublikowanych w czasopismach naukowych.

Oświadczam również, iż samodzielna i możliwa do wyodrębnienia część ww. pracy, stanowiąca indywidualny wkład mgr inż. Dagmary Słoty, obejmuje 60% całości i dotyczy opracowania koncepcji badawczej, przeglądu literatury, wykonania części eksperymentalnej, interpretacji wyników, dyskusji oraz przygotowania manuskryptu publikacji.

.....

(podpis współautora)

Politechnika Krakowska
Wydział Inżynierii
Materiałowej i Fizyki

Kraków, 25.08.2025 r.

prof. dr hab. inż. Agnieszka Sobczak-Kupiec
Katedra Inżynierii Materiałowej
Wydział Inżynierii Materiałowej i Fizyki
Politechnika Krakowska

OŚWIADCZENIE

Jako współautor pracy naukowej pt. *Clindamycin-Loaded Nanosized Calcium Phosphates Powders as a Carrier of Active Substances*, Nanomaterials 2023;13:1469, oświadczam, iż mój własny wkład merytoryczny w przygotowanie oraz przedstawienie pracy w formie publikacji wyniósł 5% i dotyczył konsultacji uzyskanych wyników, sprawdzenia poprawności dyskusji oraz wsparcia merytorycznego podczas opracowywania pracy.

Jednocześnie wyrażam zgodę na przedłożenie ww. publikacji przez mgr inż. Dagmarę Słotę do rozprawy doktorskiej jako część spójnego tematycznie zbioru artykułów opublikowanych w czasopismach naukowych.

Oświadczam również, iż samodzielna i możliwa do wyodrębnienia część ww. pracy, stanowiąca indywidualny wkład mgr inż. Dagmary Słoty, obejmuje 60% całości i dotyczy opracowania koncepcji badawczej, przeglądu literatury, wykonania części eksperymentalnej, interpretacji wyników, dyskusji oraz przygotowania manuskryptu publikacji.

A. Sobczak-Kupiec

.....

(podpis współautora)

Politechnika Krakowska
Wydział Inżynierii
Materiałowej i Fizyki

Kraków, 25.08.2025 r.

dr inż. Agnieszka Tomala
Katedra Inżynierii Materiałowej
Wydział Inżynierii Materiałowej i Fizyki
Politechnika Krakowska

OŚWIADCZENIE

Jako współautor pracy naukowej pt. *Tribological Properties and Physiochemical Analysis of Polymer-Ceramic Composite Coatings for Bone Regeneration,* Lubricants 2022;10(4):58, oświadczam, iż mój własny wkład merytoryczny w przygotowanie oraz przedstawienie pracy w formie publikacji wyniósł 10% i dotyczył wykonania pomiarów mikroskopowych i ich analizy.

Jednocześnie wyrażam zgodę na przedłożenie ww. publikacji przez mgr inż. Dagmarę Słotę do rozprawy doktorskiej jako część spójnego tematycznie zbioru artykułów opublikowanych w czasopismach naukowych.

Oświadczam również, iż samodzielna i możliwa do wyodrębnienia część ww. pracy, stanowiąca indywidualny wkład mgr inż. Dagmary Słoty, obejmuje 70% całości i dotyczy opracowania koncepcji badawczej, przeglądu literatury, wykonania części eksperymentalnej, interpretacji wyników, dyskusji oraz przygotowania manuskryptu publikacji.

Agnieszka Tomala
.....
(podpis współautora)

Kraków, 12.09.2025 r.

dr inż. Wioletta Florkiewicz

OŚWIADCZENIE

Jako współautor pracy naukowej pt. *Tribological Properties and Physiochemical Analysis of Polymer-Ceramic Composite Coatings for Bone Regeneration,* Lubricants 2022;10(4):58, oświadczam, iż mój własny wkład merytoryczny w przygotowanie oraz przedstawienie pracy w formie publikacji wyniósł 5% i dotyczył wykonania części eksperymentalnej.

Jednocześnie wyrażam zgodę na przedłożenie ww. publikacji przez mgr inż. Dagmarę Słotę do rozprawy doktorskiej jako część spójnego tematycznie zbioru artykułów opublikowanych w czasopismach naukowych.

Oświadczam również, iż samodzielna i możliwa do wyodrębnienia część ww. pracy, stanowiąca indywidualny wkład mgr inż. Dagmary Słoty, obejmuje 70% całości i dotyczy opracowania koncepcji badawczej, przeglądu literatury, wykonania części eksperymentalnej, interpretacji wyników, dyskusji oraz przygotowania manuskryptu publikacji.

Wioletta Florkiewicz

(podpis współautora)

Politechnika Krakowska
Wydział Inżynierii
Materiałowej i Fizyki

Kraków, 25.08.2025 r.

mgr inż. Karina Niziołek
Katedra Inżynierii Materiałowej
Wydział Inżynierii Materiałowej i Fizyki
Politechnika Krakowska

OŚWIADCZENIE

Jako współautor pracy naukowej pt. *Tribological Properties and Physiochemical Analysis of Polymer-Ceramic Composite Coatings for Bone Regeneration,* Lubricants 2022;10(4):58, oświadczam, iż mój własny wkład merytoryczny w przygotowanie oraz przedstawienie pracy w formie publikacji wyniósł 5% i dotyczył wykonania części eksperymentalnej oraz interpretacji wyników.

Jednocześnie wyrażam zgodę na przedłożenie ww. publikacji przez mgr inż. Dagmarę Słotę do rozprawy doktorskiej jako część spójnego tematycznie zbioru artykułów opublikowanych w czasopismach naukowych.

Oświadczam również, iż samodzielna i możliwa do wyodrębnienia część ww. pracy, stanowiąca indywidualny wkład mgr inż. Dagmary Słoty, obejmuje 70% całości i dotyczy opracowania koncepcji badawczej, przeglądu literatury, wykonania części eksperymentalnej, interpretacji wyników, dyskusji oraz przygotowania manuskryptu publikacji.

Karina Niziołek
.....

(podpis współautora)

Kraków, 25.08.2025 r.

dr inż. Mateusz Dyląg
Katedra Inżynierii Materiałowej
Wydział Inżynierii Materiałowej i Fizyki
Politechnika Krakowska

OŚWIADCZENIE

Jako współautor pracy naukowej pt. *Tribological Properties and Physiochemical Analysis of Polymer-Ceramic Composite Coatings for Bone Regeneration,* Lubricants 2022;10(4):58, oświadczam, iż mój własny wkład merytoryczny w przygotowanie oraz przedstawienie pracy w formie publikacji wyniósł 5% i dotyczył zaprojektowania oraz wydrukowania polimerowych kształtek.

Jednocześnie wyrażam zgodę na przedłożenie ww. publikacji przez mgr inż. Dagmarę Słotę do rozprawy doktorskiej jako część spójnego tematycznie zbioru artykułów opublikowanych w czasopismach naukowych.

Oświadczam również, iż samodzielna i możliwa do wyodrębnienia część ww. pracy, stanowiąca indywidualny wkład mgr inż. Dagmary Słoty, obejmuje 70% całości i dotyczy opracowania koncepcji badawczej, przeglądu literatury, wykonania części eksperymentalnej, interpretacji wyników, dyskusji oraz przygotowania manuskryptu publikacji.

Mateusz Dyląg

(podpis współautora)

Politechnika Krakowska
Wydział Inżynierii
Materiałowej i Fizyki

Kraków, 25.08.2025 r.

prof. dr hab. inż. Agnieszka Sobczak-Kupiec
Katedra Inżynierii Materiałowej
Wydział Inżynierii Materiałowej i Fizyki
Politechnika Krakowska

OŚWIADCZENIE

Jako współautor pracy naukowej pt. *Tribological Properties and Physiochemical Analysis of Polymer-Ceramic Composite Coatings for Bone Regeneration,* Lubricants 2022;10(4):58, oświadczam, iż mój własny wkład merytoryczny w przygotowanie oraz przedstawienie pracy w formie publikacji wyniósł 5% i dotyczył konsultacji uzyskanych wyników, sprawdzenia poprawności dyskusji oraz wsparcia merytorycznego podczas opracowywania pracy.

Jednocześnie wyrażam zgodę na przedłożenie ww. publikacji przez mgr inż. Dagmarę Słotę do rozprawy doktorskiej jako część spójnego tematycznie zbioru artykułów opublikowanych w czasopismach naukowych.

Oświadczam również, iż samodzielna i możliwa do wyodrębnienia część ww. pracy, stanowiąca indywidualny wkład mgr inż. Dagmary Słoty, obejmuje 70% całości i dotyczy opracowania koncepcji badawczej, przeglądu literatury, wykonania części eksperymentalnej, interpretacji wyników, dyskusji oraz przygotowania manuskryptu publikacji.

A. Sobczak-Kupiec
.....
(podpis współautora)

Bratislava, 25.08.2025

Prof. Pharm Dr. Josef Jampílek, Ph.D.
Department of Analytical Chemistry
Faculty of Natural Sciences
Comenius University
Bratislava
Slovakia

STATEMENT

As a co-author of the scientific article entitled *Hybrid Coatings Based on Polyvinylpyrrolidone/Polyethylene Glycol Enriched with Collagen and Hydroxyapatite: Incubation Studies and Evaluation of Mechanical and Physiochemical Propertiess*, Journal of Functional Biomaterials 2024;15(3):62, I hereby declare that my own substantive contribution to the preparation and presentation of the work in the form of a publication amounted to 5% and concerned the verification of the correctness of the discussion, and substantive support during the preparation of the manuscript.

At the same time, I give my consent for the aforementioned publication to be included by MSc Eng. Dagmara Słota in her doctoral dissertation as part of a thematically consistent collection of articles published in scientific journals.

I also declare that the independent and identifiable part of the above-mentioned work, constituting the individual contribution of MSc Eng. Dagmara Słota, accounts for 90% of the total and covers the development of the research concept, literature review, execution of the experimental part, interpretation of the results, discussion, and preparation of the manuscript for publication.

.....

(podpis współautora)

COMENIUS UNIVERSITY BRATISLAVA
Faculty of Natural Sciences
Department of Analytical Chemistry
Mlynská dolina, Ilkovičova 6
842 15 Bratislava, Slovakia - 1 -

Politechnika Krakowska
Wydział Inżynierii
Materiałowej i Fizyki

Kraków, 25.08.2025 r.

prof. dr hab. inż. Agnieszka Sobczak-Kupiec
Katedra Inżynierii Materiałowej
Wydział Inżynierii Materiałowej i Fizyki
Politechnika Krakowska

OŚWIADCZENIE

Jako współautor pracy naukowej pt. *Hybrid Coatings Based on Polyvinylpyrrolidone/Polyethylene Glycol Enriched with Collagen and Hydroxyapatite: Incubation Studies and Evaluation of Mechanical and Physiochemical Properties*, Journal of Functional Biomaterials 2024;15(3):62, oświadczam, iż mój własny wkład merytoryczny w przygotowanie oraz przedstawienie pracy w formie publikacji wyniósł 5% i dotyczył konsultacji uzyskanych wyników, sprawdzenia poprawności dyskusji oraz wsparcia merytorycznego podczas opracowywania pracy.

Jednocześnie wyrażam zgodę na przedłożenie ww. publikacji przez mgr inż. Dagmarę Słotę do rozprawy doktorskiej jako część spójnego tematycznie zbioru artykułów opublikowanych w czasopismach naukowych.

Oświadczam również, iż samodzielna i możliwa do wyodrębnienia część ww. pracy, stanowiąca indywidualny wkład mgr inż. Dagmary Słoty, obejmuje 90% całości i dotyczy opracowania koncepcji badawczej, przeglądu literatury, wykonania części eksperymentalnej, interpretacji wyników, dyskusji oraz przygotowania manuskryptu publikacji.

.....

(podpis współautora)

Łódź, 07.05.2025 r.

dr Mateusz M. Urbaniak
Katedra Immunologii i Biologii Infekcyjnej
Wydział Biologii i Ochrony Środowiska
Uniwersytet Łódzki

OŚWIADCZENIE

Jako współautor pracy naukowej pt. *Crosslinked hybrid polymer/ceramic composite coatings for the controlled release of clindamycin*, Biomaterials Science 2024;12:5253-5265, oświadczam, iż mój własny wkład merytoryczny w przygotowanie oraz przedstawienie pracy w formie publikacji wyniósł 5% i dotyczył opracowania koncepcji, przeglądu literatury, wykonania części eksperymentalnej, interpretacji wyników, dyskusji oraz przygotowania manuskryptu publikacji w zakresie badań na modelu komórkowym i bakteryjnym.

Jednocześnie wyrażam zgodę na przedłożenie ww. publikacji przez mgr inż. Dagmarę Słotę do rozprawy doktorskiej jako część spójnego tematycznie zbioru artykułów opublikowanych w czasopismach naukowych.

Oświadczam również, iż samodzielna i możliwa do wyodrębnienia część ww. pracy, stanowiąca indywidualny wkład mgr inż. Dagmary Słoty, obejmuje 60% całości i dotyczy opracowania koncepcji badawczej, przeglądu literatury, wykonania części eksperymentalnej, interpretacji wyników, dyskusji oraz przygotowania manuskryptu publikacji.

Mateusz M. Urbaniak

(podpis współautora)

Łódź, 07.05.2025 r.

mgr Agata Tomaszewska
Katedra Immunologii i Biologii Infekcyjnej
Wydział Biologii i Ochrony Środowiska
Uniwersytet Łódzki

OŚWIADCZENIE

Jako współautor pracy naukowej pt. *Crosslinked hybrid polymer/ceramic composite coatings for the controlled release of clindamycin*, Biomaterials Science 2024;12:5253-5265, oświadczam, iż mój własny wkład merytoryczny w przygotowanie oraz przedstawienie pracy w formie publikacji wyniósł 5% i dotyczył wykonania części eksperymentalnej, interpretacji wyników oraz przygotowania manuskryptu publikacji w zakresie badań na modelu komórkowym i bakteryjnym.

Jednocześnie wyrażam zgodę na przedłożenie ww. publikacji przez mgr inż. Dagmarę Słotę do rozprawy doktorskiej jako część spójnego tematycznie zbioru artykułów opublikowanych w czasopismach naukowych.

Oświadczam również, iż samodzielna i możliwa do wyodrębnienia część ww. pracy, stanowiąca indywidualny wkład mgr inż. Dagmary Słoty, obejmuje 60% całości i dotyczy opracowania koncepcji badawczej, przeglądu literatury, wykonania części eksperymentalnej, interpretacji wyników, dyskusji oraz przygotowania manuskryptu publikacji.

Agata Tomaszewska

(podpis współautora)

Politechnika Krakowska
Wydział Inżynierii
Materiałowej i Fizyki

Kraków, 25.08.2025 r.

mgr inż. Karina Niziołek
Katedra Inżynierii Materiałowej
Wydział Inżynierii Materiałowej i Fizyki
Politechnika Krakowska

OŚWIADCZENIE

Jako współautor pracy naukowej pt. *Crosslinked hybrid polymer/ceramic composite coatings for the controlled release of clindamycin*, Biomaterials Science 2024;12:5253-5265, oświadczam, iż mój własny wkład merytoryczny w przygotowanie oraz przedstawienie pracy w formie publikacji wyniósł 5% i dotyczył wykonania części eksperymentalnej.

Jednocześnie wyrażam zgodę na przedłożenie ww. publikacji przez mgr inż. Dagmarę Słotę do rozprawy doktorskiej jako część spójnego tematycznie zbioru artykułów opublikowanych w czasopismach naukowych.

Oświadczam również, iż samodzielna i możliwa do wyodrębnienia część ww. pracy, stanowiąca indywidualny wkład mgr inż. Dagmary Słoty, obejmuje 60% całości i dotyczy opracowania koncepcji badawczej, przeglądu literatury, wykonania części eksperymentalnej, interpretacji wyników, dyskusji oraz przygotowania manuskryptu publikacji.

Karina Niziołek
.....

(podpis współautora)

Łódź, 07.05.2025 r.

dr Marcin Włodarczyk
Katedra Immunologii i Biologii Infekcyjnej
Wydział Biologii i Ochrony Środowiska
Uniwersytet Łódzki

OŚWIADCZENIE

Jako współautor pracy naukowej pt. *Crosslinked hybrid polymer/ceramic composite coatings for the controlled release of clindamycin*, Biomaterials Science 2024;12:5253-5265, oświadczam, iż mój własny wkład merytoryczny w przygotowanie oraz przedstawienie pracy w formie publikacji wyniósł 5% i obejmował udział w planowaniu, przeprowadzeniu oraz opracowaniu wyników eksperymentów *in vivo*.

Jednocześnie wyrażam zgodę na przedłożenie ww. publikacji przez mgr inż. Dagmarę Słotę do rozprawy doktorskiej jako część spójnego tematycznie zbioru artykułów opublikowanych w czasopismach naukowych.

Oświadczam również, iż samodzielna i możliwa do wyodrębnienia część ww. pracy, stanowiąca indywidualny wkład mgr inż. Dagmary Słoty, obejmuje 60% całości i dotyczy opracowania koncepcji badawczej, przeglądu literatury, wykonania części eksperymentalnej, interpretacji wyników, dyskusji oraz przygotowania manuskryptu publikacji.

.....

(podpis współautora)

Kraków, 12.09.2025 r.

dr inż. Wioletta Florkiewicz

OŚWIADCZENIE

Jako współautor pracy naukowej pt. *Crosslinked hybrid polymer/ceramic composite coatings for the controlled release of clindamycin*, Biomaterials Sciences 2024;12:5253-5265, oświadczam, iż mój własny wkład merytoryczny w przygotowanie oraz przedstawienie pracy w formie publikacji wyniósł 2% i dotyczył wykonania części eksperymentalnej.

Jednocześnie wyrażam zgodę na przedłożenie ww. publikacji przez mgr inż. Dagmarę Słotę do rozprawy doktorskiej jako część spójnego tematycznie zbioru artykułów opublikowanych w czasopismach naukowych.

Oświadczam również, iż samodzielna i możliwa do wyodrębnienia część ww. pracy, stanowiąca indywidualny wkład mgr inż. Dagmary Słoty, obejmuje 60% całości i dotyczy opracowania koncepcji badawczej, przeglądu literatury, wykonania części eksperymentalnej, interpretacji wyników, dyskusji oraz przygotowania manuskryptu publikacji.

(podpis współautora)

Łódź, 07.05.2025 r.

dr Aleksandra Szwed-Georgiou
Katedra Immunologii i Biologii Infekcyjnej
Wydział Biologii i Ochrony Środowiska
Uniwersytet Łódzki

OŚWIADCZENIE

Jako współautor pracy naukowej pt. *Crosslinked hybrid polymer/ceramic composite coatings for the controlled release of clindamycin*, Biomaterials Science 2024;12:5253-5265, oświadczam, iż mój własny wkład merytoryczny w przygotowanie oraz przedstawienie pracy w formie publikacji wyniósł 5% i dotyczył planowania, wykonania oraz analizy eksperymentów *in vivo*.

Jednocześnie wyrażam zgodę na przedłożenie ww. publikacji przez mgr inż. Dagmarę Słotę do rozprawy doktorskiej jako część spójnego tematycznie zbioru artykułów opublikowanych w czasopismach naukowych.

Oświadczam również, iż samodzielna i możliwa do wyodrębnienia część ww. pracy, stanowiąca indywidualny wkład mgr inż. Dagmary Słoty, obejmuje 60% całości i dotyczy opracowania koncepcji badawczej, przeglądu literatury, wykonania części eksperymentalnej, interpretacji wyników, dyskusji oraz przygotowania manuskryptu publikacji.

Aleksandra Szwed-Georgiou
.....

(podpis współautora)

Łódź, 07.05.2025 r.

dr hab. Agnieszka Krupa, prof. UŁ
Katedra Immunologii i Biologii Infekcyjnej
Wydział Biologii i Ochrony Środowiska
Uniwersytet Łódzki

OŚWIADCZENIE

Jako współautor pracy naukowej pt. *Crosslinked hybrid polymer/ceramic composite coatings for the controlled release of clindamycin*, Biomaterials Science 2024;12:5253-5265, oświadczam, iż mój własny wkład merytoryczny w przygotowanie oraz przedstawienie pracy w formie publikacji wyniósł 10% i obejmował zaplanowanie badań z udziałem zwierząt, nadzór nad realizacją prac oraz uczestniczenie w wykonaniu doświadczeń *in vivo*. Dodatkowo brałam udział w korekcie pierwszej wersji manuskryptu.

Jednocześnie wyrażam zgodę na przedłożenie ww. publikacji przez mgr inż. Dagmarę Słotę do rozprawy doktorskiej jako część spójnego tematycznie zbioru artykułów opublikowanych w czasopismach naukowych.

Oświadczam również, iż samodzielna i możliwa do wyodrębnienia część ww. pracy, stanowiąca indywidualny wkład mgr inż. Dagmary Słoty, obejmuje 60% całości i dotyczy opracowania koncepcji badawczej, przeglądu literatury, wykonania części eksperymentalnej, interpretacji wyników, dyskusji oraz przygotowania manuskryptu publikacji.

Agnieszka Krupa
.....

(podpis współautora)

Politechnika Krakowska
Wydział Inżynierii
Materiałowej i Fizyki

Kraków, 25.08.2025 r.

prof. dr hab. inż. Agnieszka Sobczak-Kupiec
Katedra Inżynierii Materiałowej
Wydział Inżynierii Materiałowej i Fizyki
Politechnika Krakowska

OŚWIADCZENIE

Jako współautor pracy naukowej pt. *Crosslinked hybrid polymer/ceramic composite coatings for the controlled release of clindamycin*, Biomaterials Science 2024;12:5253-5265, oświadczam, iż mój własny wkład merytoryczny w przygotowanie oraz przedstawienie pracy w formie publikacji wyniósł 3% i dotyczył konsultacji uzyskanych wyników, sprawdzenia poprawności dyskusji oraz wsparcia merytorycznego podczas opracowywania pracy.

Jednocześnie wyrażam zgodę na przedłożenie ww. publikacji przez mgr inż. Dagmarę Słotę do rozprawy doktorskiej jako część spójnego tematycznie zbioru artykułów opublikowanych w czasopismach naukowych.

Oświadczam również, iż samodzielna i możliwa do wyodrębnienia część ww. pracy, stanowiąca indywidualny wkład mgr inż. Dagmary Słoty, obejmuje 60% całości i dotyczy opracowania koncepcji badawczej, przeglądu literatury, wykonania części eksperymentalnej, interpretacji wyników, dyskusji oraz przygotowania manuskryptu publikacji.

A. Sobczak-Kupiec

.....

(podpis współautora)

Łódź, 23.09.2025 r.

dr Aleksandra Szwed-Georgiou
Katedra Immunologii i Biologii Infekcyjnej
Wydział Biologii i Ochrony Środowiska
Uniwersytet Łódzki

OŚWIADCZENIE

Jako współautor pracy naukowej pt. *Bioactive coating with clindamycin, VEGF-165, and TGF-β1 for supporting bone tissue regeneration*, Biomaterials Science 2025, oświadczam, iż mój własny wkład merytoryczny w przygotowanie oraz przedstawienie pracy w formie publikacji wyniósł 8% i dotyczył udziału w doświadczeniach *in vivo*, a także opracowania wyników i przygotowania ich do publikacji.

Jednocześnie wyrażam zgodę na przedłożenie ww. publikacji przez mgr inż. Dagmarę Słotę do rozprawy doktorskiej jako część spójnego tematycznie zbioru artykułów opublikowanych w czasopismach naukowych.

Oświadczam również, iż samodzielna i możliwa do wyodrębnienia część ww. pracy, stanowiąca indywidualny wkład mgr inż. Dagmary Słoty, obejmuje 55% całości i dotyczy opracowania koncepcji badawczej, przeglądu literatury, wykonania części eksperymentalnej, interpretacji wyników, dyskusji oraz przygotowania manuskryptu publikacji.

……

(podpis współautora)

Łódź, 23.09.2025 r.

dr Marcin Włodarczyk
Katedra Immunologii i Biologii Infekcyjnej
Wydział Biologii i Ochrony Środowiska
Uniwersytet Łódzki

OŚWIADCZENIE

Jako współautor pracy naukowej pt. *Bioactive coating with clindamycin, VEGF-165, and TGF-β1 for supporting bone tissue regeneration*, Biomaterials Science 2025, oświadczam, iż mój własny wkład merytoryczny w przygotowanie oraz przedstawienie pracy w formie publikacji wyniósł 8% i dotyczył udziału w doświadczeniach *in vivo*, a także opracowania wyników i przygotowania ich do publikacji.

Jednocześnie wyrażam zgodę na przedłożenie ww. publikacji przez mgr inż. Dagmarę Słotę do rozprawy doktorskiej jako część spójnego tematycznie zbioru artykułów opublikowanych w czasopismach naukowych.

Oświadczam również, iż samodzielna i możliwa do wyodrębnienia część ww. pracy, stanowiąca indywidualny wkład mgr inż. Dagmary Słoty, obejmuje 55% całości i dotyczy opracowania koncepcji badawczej, przeglądu literatury, wykonania części eksperymentalnej, interpretacji wyników, dyskusji oraz przygotowania manuskryptu publikacji.

(podpis współautora)

Łódź, 23.09.2025 r.

dr hab. Agnieszka Krupa, prof. UŁ
Katedra Immunologii i Biologii Infekcyjnej
Wydział Biologii i Ochrony Środowiska
Uniwersytet Łódzki

OŚWIADCZENIE

Jako współautor pracy naukowej pt. *Bioactive coating with clindamycin, VEGF-165, and TGF-β1 for supporting bone tissue regeneration*, Biomaterials Science 2025, oświadczam, iż mój własny wkład merytoryczny w przygotowanie oraz przedstawienie pracy w formie publikacji wyniósł 9% i dotyczył udziału w doświadczeniach *in vivo*, a także opracowania wyników i przygotowania ich do publikacji.

Jednocześnie wyrażam zgodę na przedłożenie ww. publikacji przez mgr inż. Dagmarę Słotę do rozprawy doktorskiej jako część spójnego tematycznie zbioru artykułów opublikowanych w czasopismach naukowych.

Oświadczam również, iż samodzielna i możliwa do wyodrębnienia część ww. pracy, stanowiąca indywidualny wkład mgr inż. Dagmary Słoty, obejmuje 55% całości i dotyczy opracowania koncepcji badawczej, przeglądu literatury, wykonania części eksperymentalnej, interpretacji wyników, dyskusji oraz przygotowania manuskryptu publikacji.

Agnieszka Krupa
.....
(podpis współautora)

Łódź, 23.09.2025 r.

dr Karolina Rudnicka, prof. UŁ
Katedra Immunologii i Biologii Infekcyjnej
Wydział Biologii i Ochrony Środowiska
Uniwersytet Łódzki

OŚWIADCZENIE

Jako współautor pracy naukowej pt. *Bioactive coating with clindamycin, VEGF-165, and TGF-β1 for supporting bone tissue regeneration*, Biomaterials Science 2025, oświadczam, iż mój własny wkład merytoryczny w przygotowanie oraz przedstawienie pracy w formie publikacji wyniósł 5% i dotyczył analizy wyników i przygotowania ich do publikacji.

Jednocześnie wyrażam zgodę na przedłożenie ww. publikacji przez mgr inż. Dagmarę Słotę do rozprawy doktorskiej jako część spójnego tematycznie zbioru artykułów opublikowanych w czasopismach naukowych.

Oświadczam również, iż samodzielna i możliwa do wyodrębnienia część ww. pracy, stanowiąca indywidualny wkład mgr inż. Dagmary Słoty, obejmuje 55% całości i dotyczy opracowania koncepcji badawczej, przeglądu literatury, wykonania części eksperymentalnej, interpretacji wyników, dyskusji oraz przygotowania manuskryptu publikacji.

(podpis współautora)

Politechnika Krakowska
Wydział Inżynierii
Materiałowej i Fizyki

Kraków, 23.09.2025 r.

mgr inż. Karina Niziołek
Katedra Inżynierii Materiałowej
Wydział Inżynierii Materiałowej i Fizyki
Politechnika Krakowska

OŚWIADCZENIE

Jako współautor pracy naukowej pt. *Bioactive coating with clindamycin, VEGF-165, and TGF-β1 for supporting bone tissue regeneration,* Biomaterials Science 2025, oświadczam, iż mój własny wkład merytoryczny w przygotowanie oraz przedstawienie pracy w formie publikacji wyniósł 5% i dotyczył pomocy w oznaczaniu białek oraz przygotowaniu materiałów na eksperymenty *in vivo*.

Jednocześnie wyrażam zgodę na przedłożenie ww. publikacji przez mgr inż. Dagmarę Słotę do rozprawy doktorskiej jako część spójnego tematycznie zbioru artykułów opublikowanych w czasopismach naukowych.

Oświadczam również, iż samodzielna i możliwa do wyodrębnienia część ww. pracy, stanowiąca indywidualny wkład mgr inż. Dagmary Słoty, obejmuje 55% całości i dotyczy przeglądu literatury, zaprojektowania grafik oraz przygotowania manuskryptu publikacji.

Karina Niziołek
.....

(podpis współautora)

Wrocław, 23.09.2025 r.

dr inż. Bartłomiej Kryszak
Katedra Inżynierii i Technologii Polimerów
Wydział Chemiczny
Politechnika Wrocławska

OŚWIADCZENIE

Jako współautor pracy naukowej pt. *Bioactive coating with clindamycin, VEGF-165, and TGF-β1 for supporting bone tissue regeneration*, Biomaterials Science 2025, oświadczam, iż mój własny wkład merytoryczny w przygotowanie oraz przedstawienie pracy w formie publikacji wyniósł 5% i dotyczył przygotowania kształtek badawczych oraz opisu sposobu ich wytworzenia.

Jednocześnie wyrażam zgodę na przedłożenie ww. publikacji przez mgr inż. Dagmarę Słotę do rozprawy doktorskiej jako część spójnego tematycznie zbioru artykułów opublikowanych w czasopismach naukowych.

Oświadczam również, iż samodzielna i możliwa do wyodrębnienia część ww. pracy, stanowiąca indywidualny wkład mgr inż. Dagmary Słoty, obejmuje 55% całości i dotyczy opracowania koncepcji badawczej, przeglądu literatury, wykonania części eksperymentalnej, interpretacji wyników, dyskusji oraz przygotowania manuskryptu publikacji.

Bartłomiej Kryszak

(podpis współautora)

Wrocław, 23.09.2025 r.

dr hab. inż. Konrad Szustakiewicz
Katedra Inżynierii i Technologii Polimerów
Wydział Chemiczny
Politechnika Wrocławska

OŚWIADCZENIE

Jako współautor pracy naukowej pt. *Bioactive coating with clindamycin, VEGF-165, and TGF-β1 for supporting bone tissue regeneration*, Biomaterials Science 2025, oświadczam, iż mój własny wkład merytoryczny w przygotowanie oraz przedstawienie pracy w formie publikacji wyniósł 5% i dotyczył wytłaczania i wtrysku kompozytów PLLA-hydroksyapatyt użytych jako podłoża w w/w publikacji.

Jednocześnie wyrażam zgodę na przedłożenie ww. publikacji przez mgr inż. Dagmarę Słotę do rozprawy doktorskiej jako część spójnego tematycznie zbioru artykułów opublikowanych w czasopismach naukowych.

Oświadczam również, iż samodzielna i możliwa do wyodrębnienia część ww. pracy, stanowiąca indywidualny wkład mgr inż. Dagmary Słoty, obejmuje 55% całości i dotyczy opracowania koncepcji badawczej, przeglądu literatury, wykonania części eksperymentalnej, interpretacji wyników, dyskusji oraz przygotowania manuskryptu publikacji.

K. Szustakiewicz

.....

(podpis współautora)

Politechnika Krakowska
Wydział Inżynierii
Materiałowej i Fizyki

Kraków, 23.09.2025 r.

prof. dr hab. inż. Agnieszka Sobczak-Kupiec
Katedra Inżynierii Materiałowej
Wydział Inżynierii Materiałowej i Fizyki
Politechnika Krakowska

OŚWIADCZENIE

Jako współautor pracy naukowej pt. *Bioactive coating with clindamycin, VEGF-165, and TGF-β1 for supporting bone tissue regeneration,* Biomaterials Science 2025, oświadczam, iż mój własny wkład merytoryczny w przygotowanie oraz przedstawienie pracy w formie publikacji wyniósł 5% i dotyczył konsultacji uzyskanych wyników, sprawdzenia poprawności dyskusji oraz wsparcia merytorycznego podczas opracowywania pracy.

Jednocześnie wyrażam zgodę na przedłożenie ww. publikacji przez mgr inż. Dagmarę Słotę do rozprawy doktorskiej jako część spójnego tematycznie zbioru artykułów opublikowanych w czasopismach naukowych.

Oświadczam również, iż samodzielna i możliwa do wyodrębnienia część ww. pracy, stanowiąca indywidualny wkład mgr inż. Dagmary Słoty, obejmuje 55% całości i dotyczy przeglądu literatury, zaprojektowania grafik oraz przygotowania manuskryptu publikacji.

A. Sobczak-Kupiec
.....
(podpis współautora)

ZAŁĄCZNIK 2: Dorobek naukowy i organizacyjny

1. Aktualne wskaźniki bibliometryczne

Numer ORCID: 0000-0002-8570-3594

Źródło	Scopus	ResearchGate	Google Scholar
Wskaźnik Hirscha	9	10	10
Liczba publikacji	26	27	35
Liczba cytowań	239	278	300
Sumarycznie IF	172,2		
Sumarycznie MNiSW	3610		

(dane aktualne na dzień 28.09.2025)

2. Publikacje naukowe niewchodzące w cykl rozprawy doktorskiej

[1] **Dagmara Słota***, Karina Niziołek, Edyta Kosińska, Julia Sadlik, Agnieszka Sobczak-Kupiec: *Biocompatible Thermoplastics in Additive Manufacturing of Bone Defect Fillers: State of the Art and Future Prospect*s. Materials. 2025, 18(16), 3723. DOI: 10.3390/ma18163723, IF: 3,2

[2] Karina Niziołek*, **Dagmara Słota**, Patryk Polanowski, Julia Iwaniec: *Materiały z bioaktywnymi związkami wspomagającymi syntezę kolagenu w skórze. Przegląd i zastosowanie*. Inżyniera Materiałowa. 2025, 3, 5-12. DOI: 10.15199/28.2025.3.1

[3] Karina Niziołek*, **Dagmara Słota**, Anna Ronowska, Agnieszka Sobczak-Kupiec: *Calcium phosphate biomaterials modified with Mg2+ or Mn2+ ions: Structural, chemical, and biological characterization*. Ceramics International. 2025, 51(17), 23542-23558. DOI: 10.1016/j.ceramint.2025.03.042, IF: 5,6

[4] Dominika Träger, Katarzyna Młyniec, Katarzyna Haraźna*, **Dagmara Słota**, Karina Niziołek, Josef Jampilek, Agnieszka Sobczak-Kupiec: *Development of Glutathione Hydrogel Carriers Containing Zinc Oxide Microparticles for Skin Regeneration Processes*. International Journal of Molecular Sciences. 2025, 26(4), 1395. DOI: 10.3390/ijms26041395, IF: 4,9

[5] Julia Iwaniec, Karina Niziołek*, Patryk Polanowski, **Dagmara Słota**, Edyta Kosińska, Julia Sadlik, Krzysztof Miernik, Josef Jampilek, Agnieszka Sobczak-Kupiec: *Polyethylene Glycol/Pullulan-based carrier for silymarin delivery and its potential in biomedical applications*. International Journal of Molecular Sciences. 2024, 25(18), 9972. DOI: 10.3390/ijms25189972, IF: 5,6

[6] Kamila Lis, Joanna Szechyńska, Dominika Träger, Julia Sadlik, Karina Klaudia Niziołek, **Dagmara Słota***, Josef Jampilek, Agnieszka Sobczak-Kupiec: *Hybrid polymer–inorganic materials with hyaluronic acid as controlled antibiotic release systems*. Materials. 2024, 17(1), 58. DOI: 10.3390/ma17010058, IF: 3,4

[7] Karina Niziołek*, **Dagmara Słota**, Agnieszka Sobczak-Kupiec: *Polysaccharide-based composite systems in bone tissue engineering: A review*. Materials. 2024, 17(17), 4220. DOI: 10.3390/ma17174220, IF: 3,4

[8] Karina Niziołek, **Dagmara Słota***, Julia Sadlik, Edyta Kosińska, Klaudia Korzeń, Josef Jampilek, Agnieszka Sobczak-Kupiec: *Sideritis raeseri—modified coatings on Ti-6Al-4V as a carrier for controlled delivery systems of active substances*. Materials. 2024, 17(10), 2250. DOI: 10.3390/ma17102250, IF: 3,4

[9] Paweł J. Piszko*, **Dagmara Słota**, Agnieszka Sobczak-Kupiec, Agnieszka Tomala, Karina Klaudia Niziołek, Konrad Szustakiewicz: *Behavior of PGS/apatite foam scaffolds during incubation in SBF, PBS, Ringer's solution, artificial saliva, and distilled water*. Polimery w Medycynie. 2024, 54(2), 92-104. DOI: 10.17219/pim/196496

[10] Julia Sadlik*, Edyta Kosińska, **Dagmara Słota**, Karina Niziołek, Agnieszka Tomala, Marcin Włodarczyk, Paweł Piątek, Jakub Skibiński, Josef Jampilek, Agnieszka Sobczak-Kupiec: *Bioactive hydrogel based on collagen and hyaluronic acid enriched with freeze-dried sheep placenta for wound healing support*. International Journal of Molecular Sciences. 2024, 25(3), 1687. DOI: 10.3390/ijms25031687, IF: 5,6

[11] Katarzyna Młyniec, Dominika Träger, Karina Klaudia Niziołek*, **Dagmara Słota**: *Zastosowanie wybranych flawonoidów jako substancji aktywnych w medycynie regeneracyjnej*. Inżynieria Materiałowa. 2023, 44(6), 12-18. DOI: 10.15199/28.2023.6.2,

[12] Karina Niziołek*, **Dagmara Słota**, Julia Sadlik, Emilia Łachut, Wioletta Florkiewicz, Agnieszka Sobczak-Kupiec: *Influence of Drying Technique on Physicochemical Properties of Synthetic Hydroxyapatite and Its Potential Use as a Drug Carrier*. Materials. 2023, 16(19), 6431. DOI: 10.3390/ma16196431, IF: 3,4

[13] Paweł Piszko*, Bartłomiej Kryszak, Małgorzata Gazińska, **Dagmara Słota**, Agnieszka Sobczak-Kupiec, Marcin Włodarczyk, Aleksandra Szwed-Georgiou, Karolina Rudnicka, Konrad Szustakiewicz: *The effect of filler content on mechanical properties and cell response of elastomeric PGS/apatite foam scaffolds*. Ceramics International. 2023, 49(15), 25353-25363. DOI: 10.1016/j.ceramint.2023.05.071, IF: 4,7

[14] Julia Sadlik, **Dagmara Słota***: *Fish skin as a source of collagen. Characteristics, extraction methods and applications*. Inżynieria Materiałowa. 2023, 44(1), 20-25. DOI: 10.15199/28.2023.1.3

[15] Dominika Träger, **Dagmara Słota***, Karina Niziołek, Wioletta Florkiewicz, Agnieszka Sobczak-Kupiec: *Hybrid polymer-inorganic coatings enriched with*

carbon nanotubes on Ti-6Al-4V alloy for biomedical applications. Coatings. 2023, 13(10), 1813. DOI: 10.3390/coatings13101813, IF: 3,1

[16] Mateusz Dyląg*, Mateusz Krzysztof Góra, **Dagmara Słota**: *Materiały termoplastyczne wzmacniane włóknami o potencjalne do wykorzystania w wytwarzaniu addytywnym*. Inżynieria Materiałowa. 2022, 43(4), 13-20. DOI: 10.15199/28.2022.4.3

[17] Miloš Hricovíni*, Raymond J. Owens, Andrzej Bak, Violetta Kozik, Witold Musiał, Roberta Pierattelli, Magdaléna Májeková, Yoel Rodríguez, Robert Musioł, Aneta Slodek, Pavel Štarha, Karina Piętak, **Dagmara Słota**, Wioletta Florkiewicz, Agnieszka Sobczak-Kupiec, Josef Jampílek: *Chemistry towards biology-instruct: snapshot*. International Journal of Molecular Sciences. 2022, 23(23), 14815. DOI: 10.3390/ijms232314815, IF: 6,2

[18] Julia Sadlik, Joanna Szechyńska, Oliwia Grzywacz, **Dagmara Słota***, Karina Piętak, Wioletta Florkiewicz: *Ostatnie doniesienia na temat nanocząstek złota jako biomateriału w stomatologii i medycynie*. Inżynieria Materiałowa. 2022, 43(3), 14-19. DOI: 10.15199/28.2022.3.2

[19] **Dagmara Słota***, Wioletta Florkiewicz, Karina Piętak, Klaudia Pluta, Julia Sadlik, Krzysztof Miernik, Agnieszka Sobczak-Kupiec: *Preparation of PVP and betaine biomaterials enriched with hydroxyapatite and its evaluation as a drug carrier for controlled release of clindamycin*. Ceramics International. 2022, 48(23), Part A, 35467-35473. DOI: 10.1016/j.ceramint.2022.08.151, IF: 4,5

[20] Wioletta Florkiewicz, **Dagmara Słota***, Angelika Placek, Klaudia Pluta, Bożena Tyliszczak, Timothy E. L. Douglas, Agnieszka Sobczak-Kupiec: *Synthesis and characterization of polymer-based coatings modified with bioactive ceramic and bovine serum albumin*. Journal of Functional Biomaterials. 2021, 12(2), 21. DOI: 10.3390/jfb12020021, IF: 4,9

[21] Magdalena Głąb, **Dagmara Słota***: *Biologiczne tusze do drukowania 3D narządów i tkanek*. Inżynieria Materiałowa. 2021, 42(2-3), 24-32. DOI: 10.15199/28.2021.2-3.2

[22] **Dagmara Słota***, Magdalena Głąb, *Biodrukowanie z wykorzystaniem biotuszy na bazie alginianów*. Inżynieria Materiałowa. 2021, 42(4-5), 12-17. DOI: 10.15199/28.2021.4-5.1

[23] Paweł Piszko*, Marcin Włodarczyk, Sonia Zielińska, Małgorzata Gazińska, Przemysław Płociński, Karolina Rudnicka, Aleksandra Szwed, Agnieszka Krupa, Michał Grzymajło, Agnieszka Sobczak-Kupiec, **Dagmara Słota**, Magdalena Kobielarz, Magdalena Wojtków, Konrad Szustakiewicz: *PGS/HAp microporous composite scaffold obtained in the TIPS-TCL-SL method:*

an innovation for bone tissue engineering. International Journal of Molecular Sciences. 2021, 22(16), 8587. DOI: 10.3390/ijms22168587, IF: 6,2

[24] **Dagmara Słota***, Magdalena Głąb, Bożena Tyliszczak, Timothy E. L. Douglas, Karolina Rudnicka, Krzysztof Miernik, Mateusz M. Urbaniak, Paulina Rusek-Wala, Agnieszka Sobczak-Kupiec: *Composites based on hydroxyapatite and whey protein isolate for applications in bone regeneration*. Materials. 2021, 14(9), 2317. DOI: 10.3390/ma14092317, IF: 3,7

[25] **Dagmara Słota***, Wioletta Florkiewicz, Karina Piętak, Aleksandra Szwed, Marcin Włodarczyk, Małgorzata Siwińska, Karolina Rudnicka, Agnieszka Sobczak-Kupiec: *Preparation, characterization, and biocompatibility assessment of polymer-ceramic composites loaded with salvia officinalis extract*. Materials. 2021, 14(20), 6000. DOI: 10.3390/ma14206000, IF: 3,7

[26] Agnieszka Sobczak-Kupiec, Anna Drabczyk, Wioletta Florkiewicz, Magdalena Głąb, Sonia Kudłacik-Kramarczyk, **Dagmara Słota**, Agnieszka Tomala, Bożena Tyliszczak*: *Review of the applications of biomedical compositions containing hydroxyapatite and collagen modified by bioactive components*. Materials. 2021, 14(9), 2096. DOI: 10.3390/ma14092096, IF: 3,7

[27] Wioletta Florkiewicz*, **Dagmara Słota**, Agnieszka Makra, Bożena Tyliszczak: *In vitro investigation on calcium sulfate gypsum/hydroxyapatite composites*. Inżynieria Materiałowa. 2021, 42(4-5), 21-26. DOI: 10.15199/28.2021.4-5.3

[28] **Dagmara Słota***, Wioletta Florkiewicz, Agnieszka Sobczak-Kupiec: *Ceramic-polymer coatings on Ti-6Al-4V alloy modified with l-cysteine in biomedical applications*. Materials Today Communications. 2020, 25, 101301. DOI: 10.1016/j.mtcomm.2020.101301, IF: 3,5

3. Projekty naukowe

Kierownik projektu:

[1] Projekt LIDER pn. *Bioaktywny, kompozytowy granulat o potencjale do biodruku 3D*. Finansowany przez Narodowe Centrum Badań i Rozwoju, (LIDER14/0266/2023). 05.2024 – obecnie

Wykonawca:

[2] Projekt FutureLab PK pn. *Bioaktywne filmy hialuronowe wzbogacane ekstraktem z morwy białej oraz tlenkiem cynku jako wsparcie w niwelowaniu zmian trądzikowych*. Finansowany przez Politechnikę Krakowską. 02.2025 – obecnie

[3] Projekt OPUS pn. *Hierarchiczne podejście do inżynierii tkanki kostno-chrzęstnej*. Finansowany przez Narodowe Centrum Nauki, (UMO-2022/45/B/ST8/02557). 03.2023 – obecnie

[4] Projekt M-ERA.NET pn. *Przyszła generacja bioaktywnych, strukturyzowanych laserowo implantów na bazie Ti/HAp*. Finansowany przez Narodowe Centrum Badań i Rozwoju, (M-ERA.NET.3/2-22/48/BiLaTex/2023). 05.2024 – 08.2025

[5] Inkubator Innowacyjności TRL 4.0 pn. *Kompozytowy Nośnik Substancji Aktywnej* finansowany przez Centrum Transferu Technologii Politechniki Krakowskiej

[6] Projekt Studenckie Koła Naukowe Tworzą Innowacje pn. *Hybrydowe materiały do stymulowania produkcji kolagenu w skórze*. Finansowany przez Ministerstwo Nauki i Szkolnictwa Wyższego, (SKN/SP/602130/2024). 06.2024 – 06.2025

[7] Projekt FutureLab PK pn. *Innowacyjne materiały polimerowe i kompozytowe – maski kosmetyczne do stymulowania białek fibrylarnych*. Finansowany przez Politechnikę Krakowską. 03.2024 – 03.2025

[8] Projekt Studenckie Koła Naukowe Tworzą Innowacje pn. *Biomateriały polimerowe o charakterze nośnika substancji aktywnej do zastosowań w medycynie*. Finansowany przez Ministerstwo Nauki i Szkolnictwa Wyższego, (SKN/SP/568478/2023). 05.2023 – 05.2024

[9] Projekt FutureLab PK pn. *Biomateriały kompozytowe do zastosowań medycznych*. Finansowany przez Politechnikę Krakowską. 02.2023 – 02.2024

[10] Projekt Operacyjny Inteligentny Rozwój pn. *Opracowanie innowacyjnych rozwiązań konstruowania wielofunkcyjnych urządzeń do szybkiego prototypowania i produkcji niskoseryjnej w sposób zautomatyzowany i bezobsługowy*. Finansowany przez Narodowe Centrum Badań i Rozowju, (POIR.01.01.01-00-0124/19). 11.2021 – 12.2021

[11] Projekt TEAM-NET pn. *Wielofunkcyjne kompozyty aktywne biologicznie do zastosowań w medycynie regeneracyjnej układu kostnego*. Finansowany przez Fundację na Rzecz Nauki Polskiej, (POIR.04.04.00-00-16D7/18). 01.2020 – 12.2022

4. Patenty i zgłoszenia patentowe

[1] Zgłoszenie patentowe do UPRP pn. *„Zgłoszenie patentowe do UPRP pn. „Bioaktywny materiał kompozytowy i sposób otrzymywania bioaktywnego materiału kompozytowego”*, 28.03.2025, P.451609.

[2] Zgłoszenie patentowe do UPRP pn. „*Sposób otrzymywania hybrydowego nośnika substancji aktywnych należących do grupy leków przeciwnowotworowych i hybrydowy nośnik substancji aktywnych należących do grupy leków przeciwnowotworowych*", 22.11.2023, P.446804.

[3] Zgłoszenie patentowe w procedurze PCT pn. „*Porowate i lite elastomerowe aktywne biologicznie kompozyty polimerowo-ceramiczne*", 30.06.2023, PCT/PL2023/050048

[4] Zgłoszenie patentowe do UPRP pn. „*Lite elastomerowe aktywne biologicznie kompozyty polimerowo-ceramiczne oraz sposób ich wytwarzania*", 12.02.2023, P.443751.

[5] Zgłoszenie patentowe do UPRP pn. „*Porowate elastomerowe aktywne biologicznie kompozyty polimerowo-ceramiczne do wypełniania ubytków kostnych i regeneracji tkanki kostnej oraz sposób ich wytwarzania*", 12.02.2023, P.443750.

[6] Zgłoszenie patentowe do UPRP pn. „*Sposób otrzymywania dwuwarstwowej bioaktywnej powłoki kompozytowej i dwuwarstwowa bioaktywna powłoka kompozytowa*", data zgłoszenia 29.11.2022, P.442979.

[7] Zgłoszenie patentowe do UPRP pn. „*Sposób otrzymywania bioaktywnego kompozytu i bioaktywny kompozyt*", 29.11.2022, P.44280.

[8] Patent pn. „*Sposób otrzymywania kompozytu o osnowie polimerowej zawierającej hydroksyapatyt i kompozyt o osnowie polimerowej zawierającej hydroksyapatyt*", na podstawie zgłoszenia P.442978, z dnia 29.11.2022.

5. Staże i wyjazdy naukowo-badawcze

[1] Wizyta w European Commission - Joint Research Centre (JRC), jedna z 10 oddelegowanych naukowców z Polski, jedyna doktorantka – Ispra, Włochy, 24.06.2025 – 26.06.2025

[2] Staż w firmie DMG Sp. z o.o. – Kraków, Polska, 05.05.2022 – 25.05.2022

[3] Staż w firmie ATMAT Sp. z o.o. – Kraków, Polska, 8.11.2021 – 8.12.2021

[4] Staż naukowy pod opieką prof. Josefa Jampilka na Comenius University, Faculty of Pharmacy (staż w ramach programu mentoringowego trwającego od 01.01.2029 – 31.12.2022) – Bratysława, Słowacja, 04.10.2021 – 15.10.2021

[4] Staż naukowy pod opieką dr Karoliny Rudnickiej na Uniwersytecie Łódzkim, Wydział Biologii i Ochrony Środowiska – Łódź, Polska, 27.02.2020 – 06.03.2020

[5] Staż naukowy pod opieką dr Tiomthy Douglas na Lancaster University, Materials Science Institute – Lancaster, Anglia, 28.01.2020 – 06.02.2020

6. Nagrody i wyróżnienia

[1] Tytuł Młodego Promotora Polski, w kategorii działalność naukowa, przyznany przez Pierwszą Damę RP w ramach III Edycji konkurs.

[2] Tytuł Rising Star in Engineering podczas gali Excellence in Engineering Awards - Women in Tech Summit 2025, TOP10 Kobiet w Inżynierii w Polsce.

[3] Laureatka Nagrody zespołowej Rektora Politechniki Krakowskiej im. Tadeusza Kościuszki za szczególne osiągnięcia organizacyjne studentów i doktorantów.

[4] Zajęcie drugiego miejsca w ogólnopolskim konkursie organizowanym przez Dziennik Gazetę Prawną "Eureka. Odkrywamy Polskie Wynalazki".

[5] Nagroda Canadian Special Award podczas targów iCAN 2025 w Kanadzie za rozwiązanie „3D Printing Granulate Supporting Bone Tissue Regeneration”.

[6] Złoty medal na 10th International Invention Innovation Competition in Canada 2025 za rozwiązanie „3D Printing Granulate Supporting Bone Tissue Regeneration”.

[7] Srebrny medal na 10th International Invention Innovation Competition in Canada 2025 za rozwiązanie „Hierarchically Structured, Functional Graded Multi-Layer Polymer-Ceramic Composites for Osteochondral Tissue Engineering”.

[8] Złoty medal na 18. Międzynarodowych Targach Wynalazków i Innowacji INTARG® 2025 za rozwiązanie „Granulat do druku 3D wspierający regenerację tkanki kostnej”.

[9] Srebrny medal na 18. Międzynarodowych Targach Wynalazków i Innowacji INTARG® 2025 za rozwiązanie „Bioaktywny kompozyt do wspomagania regeneracji tkanki kostno-chrzęstnej”.

[10] Złoty medal na 18. Międzynarodowych Targach Wynalazków i Innowacji INTARG® 2025 za rozwiązanie „Funkcjonalne, bioaktywne kompozyty do konstrukcji przewodów do prowadzenia nerwów obwodowych”.

[11] Złoty medal na 18. Międzynarodowych Targach Wynalazków i Innowacji INTARG® 2025 za rozwiązanie „Biokatywna filmowa maska hydrożelowa – nowoczesna alternatywa dla wspomagania terapii zmian trądzikowych”.

[12] Złoty medal na 18. Międzynarodowych Targach Wynalazków i Innowacji INTARG® 2025 za rozwiązanie „Innowacyjna maska hydrożelowa wzbogacana astaksantyną do terapeutycznej regeneracji i poprawy integralności skóry".

[13] Laureatka Nagrody Santander dla studentów i doktorantów Politechniki Krakowskiej 2025.

[14] Złoty medal na międzynarodowych targach IPITEx2025 – Intellectual Property, Invention, Innovation and Technology Exposition (Tajlandia) za rozwiązanie "Development of an active substance carrier containing zinc oxide to promote the treatment of acne vulgaris".

[15] Nagroda specjalna od World Invention Intellectual Property associations (WIIP) podczas targów IPITEx 2025 za rozwiązanie "Development of an active substance carrier containing zinc oxide to promote the treatment of acne vulgaris".

[16] Złoty medal na międzynarodowych targach IPITEx 2025 – Intellectual Property, Invention, Innovation and Technology Exposition (Tajlandia) za rozwiązanie "Hybrid skin masks with antioxidant properties to simulate collagen production".

[17] Srebrny medal na międzynarodowych targach IPITEx 2025 – Intellectual Property, Invention, Innovation and Technology Exposition (Tajlandia) za rozwiązanie "Gradient polysaccharidebased composite biomaterials for osteochondral tissue applications".

[18] Złoty medal na międzynarodowej wystawie wynalazków ARCA za rozwiązanie „Bioactive composite materials for bone tissue engineering".

[19] Laureatka nagrody Super Mentor 2024 od FutureLab PK za wyjątkową i wykraczającą poza standardowe obowiązki pracę mentorską ze studentami.

[20] Nagroda główna podczas 17 edycji konkursu Kraków Bez Barier, w kategorii Innowacyjne technologie i innowacyjne projekty badawcze.

[21] Współtwórca rozwiązania nagrodzonego podczas XIV Ogólnopolskiego Konkursu Student-Wynalazca.

[22] Nagroda specjalna Prezesa Polskiego Związku Pracodawców Przemysłu Farmaceutycznego, w ramach XIV Ogólnopolskiego Konkursu Student-Wynalazca.

[23] Nagroda specjalna Prezesa Stowarzyszenia Polskich Wynalazców i Racjonalizatorów, w ramach XIV Ogólnopolskiego Konkursu Student-Wynalazca.

[24] Laureatka programu wizerunkowego Polski Innowator 2024, w kategorii: Osobistość Nauki.

[25] Laureatka programu wizerunkowego Naukowiec Przyszłości 2024.

[26] Złoty medal na międzynarodowej wystawie wynalazków International Warsaw Invention Show 2024 (Polska), za „Polymer-peptide mask modified with zinc nanoparticles to promote skin regeneration".

[27] Nagroda za najlepszy krajowy wynalazek zaprezentowany podczas International Warsaw Invention Show, rozwiązanie „Polymer-peptide mask modified with zinc nanoparticles to promote skin regeneration".

[28] Srebrny medal na międzynarodowej wystawie wynalazków International Warsaw Invention Show 2024 (Polska), za „Sposób otrzymywania hybrydowego nośnika substancji aktywnych należących do grupy leków przeciwnowotworowych i hybrydowy nośnik substancji aktywnych należący do grupy leków przeciwnowotworowych".

[29] Brązowy medal na międzyanrodowej wystawie wynalazków iENA - International Trade Fair "Ideas - Inventions - New Products (Niemcy), za „Method of obtaining hybrid carrier of active substances belonging to the group of anticancer drugs and hybrid carrier of active substances belonging to the group of anticancer drugs".

[30] Top 3 i nominacja do nagrody Młodego Promotora Polski, w kategorii działalność naukowa, (II Edycja), konkurs organizowany przez Pierwszą Damę RP.

[31] Złoty medal na międzynarodowej wystawie wynalazków Arca - 20th International Innovation Exhibition (Chorwacja), za "Bioactive composite materials for bone tissue engineering".

[32] Złoty medal na międzynarodowej wystawie wynalazków Invention Innovation Competition (#ICAN) (Kanada), za „Polymer-peptide mask modified with zinc nanoparticles to promote skin regeneration".

[33] Brązowy medal na międzynarodowej wystawie wynalazków 49th International Exhibition of Inventions Geneva (Szwajcaria), za „Method of obtaining a hybrid carrier of active substances belonging to the group of anticancer drugs and a hybrid carrier of active substances belonging to the group of anticancer drugs".

[34] Nagroda Specjalna od National Research Counciol of Thailand za najlepszy wynalazek i innowacje podczas 49th International Exhibition of Inventions Geneva (Szwajcaria).

[35] Złoty medal na międzynarodowej wystawie wynalazków Korea International Women's Invention Exposition (Korea), za „Hyaluronic acid-based systems for controlled release of antibiotic".

[36] Nagroda Specjalna od Vietnam Association for Intellectual Women podczas Korea International Women's Invention Exposition.

[37] Srebrny medal na międzynarodowej wystawie wynalazków 48th International Exhibition of Inventions Geneva (Szwacjaria), za „Bioactive composite materials for bone tissue engineering".

[38] Laureatka XIII Edycji Ogólnopolskiego Konkursu Student-Wynalazca.

[39] Laureatka nagrody Super Mentor 2023 od FutureLab PK za wyjątkową i wykraczającą poza standardowe obowiązki pracę mentorską ze studentami.

[40] Laureatka programu wizerunkowego Naukowiec Przyszłości 2023, w kategorii: Kobieta nauki, która zmienia świat.

[41] Złoty medal na międzynarodowej wystawie wynalazków Kaohsiung International Invention & Design EXPO 2023 (Tajwan), za „Active substance carrier for controlled delivery of selected flavonoid compounds with multidirectional effects".

[42] Złoty medal na międzynarodowej wystawie wynalazków International Warsaw Invention Show 2023 (Polska), za „Collagen-ceramic composite coatings as vancomycin carrier".

[43] Złoty medal na międzynarodowej wystawie wynalazków International Warsaw Invention Show 2023 (Polska), za „Bioactive composite materials for bone tissue engineering".

[44] Wyróżnienie za referat podczas Ogólnopolskiej Konferencji Młodych Naukowców nt. Analiza Zagadnienia, Analiza Wyników – Wystąpienie Młodego Naukowca, Edycja IV, referat pn. „Kompozytowe materiały powłokowe do regeneracji tkanki kostnej".

[45] Wyróżnienie za referat podczas Ogólnopolskiej Konferencji Młodych Naukowców nt. Nowe Trendy w Badaniach Naukowych – Wstąpienie Młodego Naukowca, Edycja V.

[46] Zajęcie III miejsca w konkursie na najlepszy poster podczas XIV Konferencji Naukowo-Technicznej Materiały Węglowe i kompozyty polimerowe Nauka – Przemysł ' 2022. Poster pn. „Hybrydowe powłoki polimerowo-nieorganiczne zawierające lek do zastosowań biomedycznych".

[47] Złoty medal na międzynarodowej wystawie wynalazków International Warsaw Invention Show 2022 (Polska), za „Antibacterial composite coatings for applications in regenerative medicine".

[48] Srebrny medal na międzynarodowej wystawie wynalazków International Warsaw Invention Show 2022 (Polska), za „Bioactive composites as biomaterials for bone regeneration".

[49] Srebrny medal na międzynarodowej wystawie wynalazków International Trade Fari Ideas-Iventions-New Products (Niemcy), za "Bioactive composites containing collagen and hydroxyapatite supporting bone defect regeneration".

[50] Złoty medal na międzynarodowej wystawie wynalazków International Warsaw Invention Show 2021 (Polska), za "Bioactive composite coatings for biomedical application".

[51] Złoty medal na mi międzynarodowej wystawie wynalazków International Warsaw Invention Show 2020 (Polska), za "Synthetic hydroxyapatite with controlled morphology".

[52] Wyróżnienie za referat podczas ogólnopolskiej konferencji naukowej Nowe Trendy w Badaniach Naukowych, Edycja I.

[53] Wyróżnienie za wygłoszony referat podczas ogólnopolskiej Konferencia Młodych Naukowców: Dokonania Naukowe Doktorantów, VIII Edycja.

7. Najważniejsze konferencje naukowe

[1] Referat naukowy „*Kompozyty przeznaczone do regeneracji tanki kostnej i chrzestnej*", 10 Forum Inteligentnego Rozwoju. Polska, Uniejów, 9-10.06.2025.

[2] Referat naukowy „*Engineering the Future of Medicine: Novel Biomaterials for Drug Delivery and Bone Regeneration*", Biotechnological innovation for a sustainable future. Polska, Kraków, 20-21.05.2025 – konferencja międzynarodowa, w ramach Prezydencji Polski w UE.

[3] Plakat naukowy „*Hybrid polymer/ceramic composite materials to support bone tissue regeneration*", 16th US-Japan symposium on drug delivery systems. Stany Zjednoczone, Lahaina, 15-19.12.2024 – konferencja międzynarodowa.

[4] Referat naukowy „*Innovative material for 3D printing of bones*", Life Science Open Space Summit 2024. Polska, Kraków, 28-29.11.2024 – konferencja międzynarodowa.

[5] Plakat naukowy „*Hybrid polymer-inorganic composites with fibrillar protein in bone tissue regeneration*", 12th World Biomaterials Congress. Korea, Daegu, 26-31.05.2024 – konferencja międzynarodowa.

[6] Referat naukowy „*Multifunctional biomaterials for targeted therapy in bone regeneration*", Life Science Open Space 2023 - Collaboration and Innovation Summit for Health and Quality of Life. Polska, Kraków, 30.11-01.12.2023 – konferencja międzynarodowa.

[7] Referat naukowy „ *Controlled release of VEGF and TGF-β growth factors from polymer/inorganic hybrid coatings*", 36th International Multidisciplinary Conference "Recent Studies and Research". Anglia, Londyn, 27-28.10.2023 – konferencja międzynarodowa.

[8] Plakat naukowy „*Biopolymeric materials enriched with silk fibroin protein*", 32nd Annual Conference "Biomaterials in Medicine and Veterinary Medicine". Polska, Rytro, 12-15.10.2023 – konferencja międzynarodowa.

[9] Plakat naukowy „*Modyfikacja fosforanów-wapnia jonami magnezu i wanadu*", V Ogólnopolska Konferencja Naukowa IMPLANTY2023; Technologie, chemia, medycyna. Polska, Gdańsk, 18-20.05.2023 – konferencja ogólnopolska.

[10] Plakat naukowy „*Incubation Studies of Ceramic-Polymer Coatings in Artificial Biological Fluids*", International Conference on Chemical and Biochemical Engineering. Szwecja, Sztokholm, 05-06.12.2022 – konferencja międzynarodowa.

[11] Referat naukowy „*Evaluation of hybrid coating materials as drug carriers*", International Conference on Medical and Biosciences. Hiszpania, Madryt, 22-23.11.2022 – konferencja międzynarodowa.

[12] Referat naukowy „*Modern composite coatings materials for medical applications"*, International Multidisciplinary Conference "Recent Studies and Ideas". Luksemburg, Luksemburg, 18-19.11.2022 – konferencja międzynarodowa.

[13] Referat naukowy „*Hybrydowe materiały powłokowe jako nośniki leków do kontrolowanego uwalniania klindamycyny*", Nowe Trendy w Badaniach Naukowych – Wystąpienie Młodego Naukowca, Edycja V Polska (online), 21-23.10.2022 – konferencja ogólnopolska.

[14] Plakat naukowy „*Hybrydowe powłoki polimerowo-nieorganiczne zawierające lek do zastosowań biomedycznych*", XIV Konferencja Naukowo-Techniczna - Materiały Węglowe i Kompozyty Polimerowe. Nauka – Przemysł'2022. Polska, Ustroń, 18-21.10.2022 – konferencja ogólnopolska.

[15] Plakat naukowy „*Physicochemical and mechanical behavior analysis of composite coatings designed for bone regeneration*", Chemistry towards Biology (CTB10) – Instruct conference. Słowacja, Bratysława, 11-14.09.2022 – konferencja międzynarodowa.

[16] Plakat naukowy „*Multifunctional composite coatings supporting bone regeneration*", Tissue Engineering and Regenerative Medicine International Society, Inc.- European Chapter. Polska, Kraków, 28.06-01.07.2022 – konferencja międzynarodowa.

[17] Plakat naukowy „*Właściwości trybologiczne i fizykochemiczne powłok kompozytowych do zastosowań implantacyjnych*", IV Ogólnopolska Konferencja Naukowa IMPLANTY2022. Polska, Gdańsk, 27-28.05.2022 – konferencja ogólnopolska.

[18] Referat naukowy „*Physiochemical analysis and tribological properties of composite coatings for bone regeneration*", 20th International Conference and Exhibition on Materials Science and Chemistry, 2nd chapter. Hiszpania, Barcelona, 25-26.04.2022 – konferencja międzynarodowa.

[19] Referat naukowy „*Development of ceramic-polymer composite coatings for hard tissue replacement with glutathione ang collagen*", 20th International Conference and Exhibition on Materials Science and Chemistry, 1st chapter. Włochy, Rzym, 21-22.03.2022 – konferencja międzynarodowa.

[20] Plakat naukowy „*Biocompatibility assessment of polymer-ceramic composites loaded with plant extract*", International Conference NanoMed 2021. Włochy, Mediolan, 20-22.10.2021 – konferencja międzynarodowa.

[21] Plakat naukowy „*Studies on kinetic of the release and antioxidant properties of plant extract applied as a modifier in polymer-ceramic composites*", Global Summit and Expo on Materials Science and Nanoscience. Portugalia, Lizbona, 06-08.09.2022 – konferencja międzynarodowa.

[22] Plakat naukowy „*Powłoki ceramiczno polimerowe do regeneracji tkanki kostnej*", III Ogólnopolska Konferencja Naukowa IMPLANTY2021. Gdańsk (online), 18.06.2021 – konferencja ogólnopolska.

[23] Referat naukowy „*Kompozyty polimerowo-ceramiczne modyfikowane wybranymi biomolekułami*", Ogólnopolska Konferencja o Kompozytach Ok!Ok!. Polska (online), 21-22.05.2021 – konferencja ogólnopolska.

[24] Referat naukowy „*Protein-based composite hydrogels for bone tissue regeneration*", International Conference UK-Poland Bioinspired Materials. Anglia (online), 23-24.11.2020 – konferencja międzynarodowa.

[25] Referat naukowy „*Hybrydowe wieloskładnikowe hydrożele na bazie WPI do regeneracji układu kostnego*”, Nowe Trendy w Badaniach Naukowych – Wystąpienie Młodego Naukowca, Edycja I. Polska (online), 20-21.06.2020 – konferencja ogólnopolska.

[26] Referat naukowy „*Fosforany wapnia wykorzystywane w biomedycynie dobór warunków syntezy i charakterystyka*”, Konferencja Młodych Naukowców: Dokonania Naukowe Doktoratów, VIII Edycja. Polska (online), 28-28.04.2020 – konferencja ogólnopolska.

[27] Plakat naukowy „*Hyrdoxyapatite used in biomedicine – synthesis and characterization*”, International Conference UK-Russia Bioinspired Materials. Anglia, Lancaster, 02-03.02.2020 – konferencja międzynarodowa.

8. Działalność organizacyjna

[1] Opiekun naukowy studenckiego Koła Naukowego Materiałów Funkcjonalnych SMART-MAT, sekcji BioMat, 01.2023 – obecnie

[2] Koordynator Wydziałowy Forum Ekonomicznego w Karpaczu 2025

[3] Współorganizatorka pokazów naukowych popularyzujących naukę podczas trzeciego Ogólnopolskiego Dnia Inżynierii Materiałowej, 28 marzec 2025

[4] Organizacja wykładu pn. „Regeneracja kości to prosta sprawa” w ramach projektu #nauka4future (Program „Społeczna Odpowiedzialność Nauki”)

[5] Ambasadorka programu Dziewczyny do Nauki PERSPEKTYWY

[6] Komitet Organizacyjny Seminarium „Nauka i Przemysł – Wyzwania i możliwości w inżynierii materiałowej” oraz Jubileuszu 5-lecia Wydziału Inżynierii Materiałowej i Fizyki, 29 listopada 2024.

[7] Komitet Organizacyjny ogólnopolskiej konferencji "Zostań Badaczką 2024", 30 października 2024 r.

[8] Współorganizatorka pokazów naukowych popularyzujących naukę podczas Małopolskiej Nocy Naukowców, 27 września 2024

[9] Współorganizatorka pokazów naukowych popularyzujących naukę podczas pierwszego Ogólnopolskiego Dnia Inżynierii Materiałowej, 17 marzec 2023

[10] Współorganizatorka pokazów naukowych popularyzujących naukę podczas Małopolskiej Nocy Naukowców, 30 września 2022

9. Najważniejsze szkolenia i kursy

[1] PRINCE2® Foundation Certificate in Project Management, PeopleCert, 11.04.2023.

[2] Wymagania prawne i systemowe dla producentów wyrobów medycznych w świetle zapisów nowej ustawy o wyrobach medycznych, *CeCert*, 17.12.2022.

[3] Sekrety techniki ELISA, *Merck*, 12.10.2022.

[4] Przydatne techniki w prowadzeniu hodowli komórkowych, *Merck*, 05.10.2022.

[5] Cell Culture Fundamentals, *BrightTALK*, 31.08.2022.

[6] Zarządzanie projektami dla początkujących, *Polska Agencja Rozwoju Przedsiębiorczości*, 04.2022.

[7] Umiejętności kierownicze, *Polska Agencja Rozwoju Przedsiębiorczości*, 04.2022.

[8] Chromatografia cieczowa: przygotowanie układu pomiarowego, *Merck*, 27.04.2022.

[9] Zastosowanie metody FTIR w badaniach środowiskowych, *MS Specktrum*, 17.03.2022.

[10] Dobra Praktyka Laboratoryjna – zapewnienie jakości bada laboratoryjnych zgodnie z zasadami DPL, *Lab ISO Consulting*, 21.12.2021.

[11] Szkolenie dotyczące obsługi i użytkowania mikroskopu cyfrowego Keyence VHX Series, *Keyence International*, 18.10.2021.

[12] 3D printing in Regenerative Orthopedic, *BrightTALK*, 27.09.2021.

[13] Nano- and Microfabricated Hydrogels for Regenerative Engineerin, *BrightTALK*, 15.09.2021.

[14] Szkolenie dotyczące obsługi i konserwacji czytnika płytek 800TSI oraz programu Gen5, *BIOKOM*, 15.06.2021.

[15] Hodowle komórek w 3D, *Merck*, 23.04.2021.

[16] Szkolenie dotyczące pracy z systemem SHIMADZU HPLC Prominence oraz oprogramowaniem LabSolutions LC/GC, *SHIM-POL A.M. Borzymowski*, 22.03.2021.

[17] Szkolenie dotyczące obsługi i konserwacji dwuwiązkowego spektrofotometru UV-VIS GENESYS 180 UV-VIS Thermo Scientific, *Spectro-Lab*, 12.01.2021.

[18] Diagnosta laboratoryjny, *Studium Prawa Europejskiego i Uniwersytet Medyczny w Łodzi*, 10.05.2020.

[19] Potwierdzenie ważności wyników w laboratorium zgodnie z wymaganiami normy PN-EN ISO/IEC 17025:2018-02 – analiza trendów, karty kontrolne, interpretacja wyników programów PT/ILC, *CE2 Centrum Edukacji*, 7-8.04.2020.

[20] Metody laboratoryjne stosowane w diagnostyce serologicznej na przykładzie testów EUROIMMUN, *Akademia Euroimmun*, 27.03.2020.

[21] Badanie stabilności produktów leczniczych, *Biotechnologiczne Stowarzyszenie Edukacyjne „BIOMED-LUBLIN"*, 11.07.2019.

[22] Zasady Dobrej Praktyki Laboratoryjnej w farmacji przemysłowej, *Biotechnologiczne Stowarzyszenie Edukacyjne „BIOMED-LUBLIN"*, 20.07.2019.